
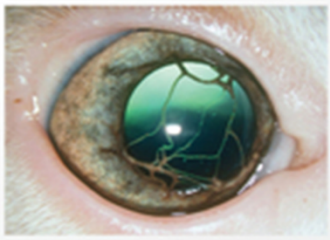
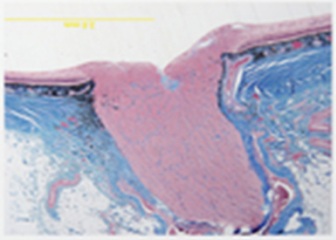
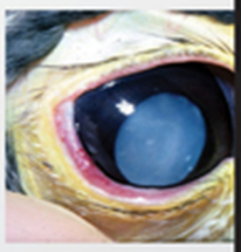

VETERINARY OPHTHALMOLOGY

EDITED BY **KIRK N. GELATT**

SIXTH EDITION

ASSOCIATE EDITORS

GIL BEN-SHLOMO

BRIAN C. GILGER

DIANE V.H. HENDRIX

THOMAS J. KERN

CARYN E. PLUMMER

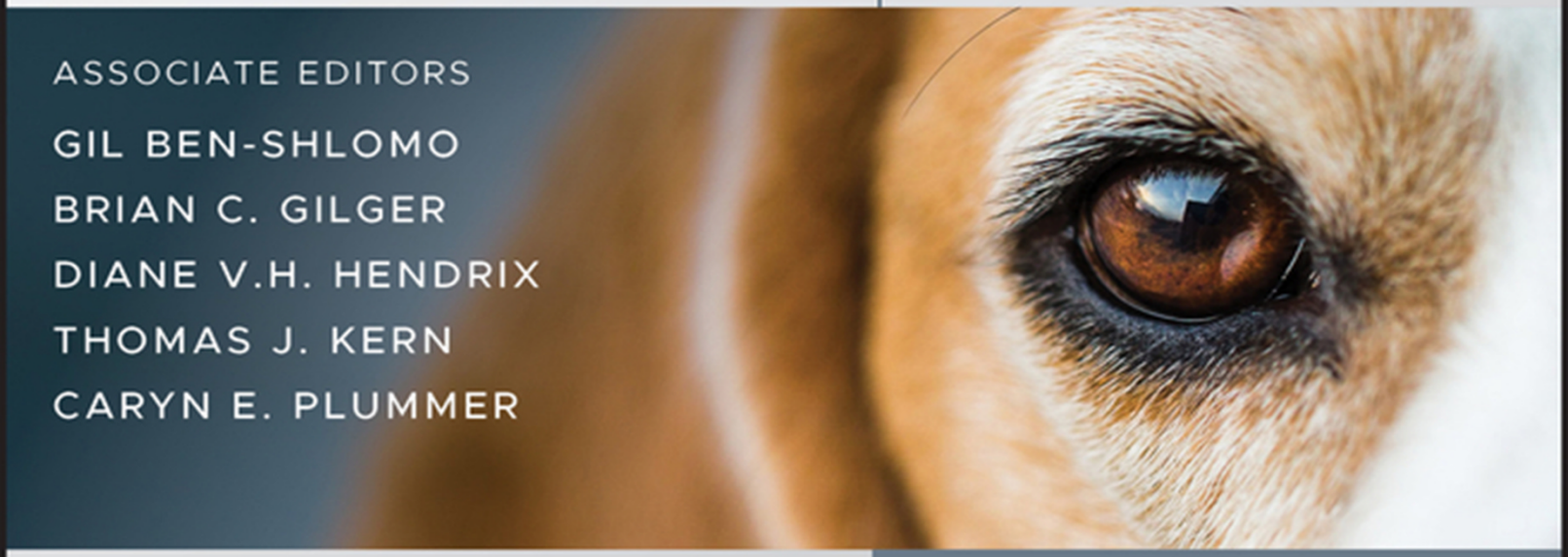

VOLUME ONE

with website

WILEY Blackwell

Veterinary Ophthalmology

Veterinary Ophthalmology

Volume I and Volume II

Editor
Kirk N. Gelatt

Associate Editors
Gil Ben-Shlomo
Brian C. Gilger
Diane V.H. Hendrix
Thomas J. Kern
Caryn E. Plummer

Sixth Edition

WILEY Blackwell

This edition first published 2021

Blackwell Publishing was acquired by John Wiley & Sons in February 2007. Blackwell's publishing program has been merged with Wiley's global Scientific, Technical and Medical business to form Wiley-Blackwell.

Registered Office
John Wiley & Sons, Inc., 111 River Street, Hoboken, NJ 07030, USA

Editorial Office
111 River Street, Hoboken, NJ 07030, USA

For details of our global editorial offices, customer services, and more information about Wiley products visit us at www.wiley.com.

Wiley also publishes its books in a variety of electronic formats and by print-on-demand. Some content that appears in standard print versions of this book may not be available in other formats.

Library of Congress Cataloging-in-Publication Data
Names: Gelatt, Kirk N., editor.
Title: Veterinary ophthalmology / editor, Kirk N. Gelatt ; associate
editors, Gil Ben-Shlomo, Brian C. Gilger, Diane V.H. Hendrix, Thomas J. Kern, Caryn E. Plummer.
Other titles: Textbook of veterinary ophthalmology
Description: Sixth edition. | Hoboken, NJ : Wiley-Blackwell, 2020. | Includes bibliographical references and index.
Identifiers: LCCN 2020010772 (print) | LCCN 2020010773 (ebook) | ISBN
9781119441830 (hardback) | ISBN 9781119441823 (adobe pdf) | ISBN 9781119441816 (epub)
Subjects: MESH: Eye Diseases–veterinary | Diagnostic Techniques,
Ophthalmological–veterinary | Ophthalmologic Surgical Procedures–veterinary
Classification: LCC SF891 (print) | LCC SF891 (ebook) | NLM SF 891 | DDC 636.089/77–dc23
LC record available at https://lccn.loc.gov/2020010772
LC ebook record available at https://lccn.loc.gov/2020010773

Cover image: Eye of a black horse © happylights / Shutterstock, Closeup of cat face. Fauna background © darkbird77 / Getty Images, Inquisitive Beagle Hound © bpretorius / Getty Images, Inset images courtesy of Kirk N. Gelatt.
Cover design by Wiley

Set in 9.5/12pt STIX TwoText by SPi Global, Pondicherry, India

10 9 8 7 6 5 4 3 2 1

This book is dedicated to the memory of Dr. Gil Ben-Shlomo, an exceptional scholar, teacher, father and friend. The veterinary ophthalmology community has lost a gentle doctor and a gentleman.

Contents

Contributors

Gil Ben-Shlomo, DVM, PhD
Diplomate ACVO, Diplomate ECVO
Associate Professor of Ophthalmology
Departments of Clinical Sciences
College of Veterinary Medicine
Cornell University
Ithaca, NY, USA

Ellison Bentley, DVM
Diplomate ACVO
Clinical Professor, Comparative Ophthalmology
Department of Surgical Sciences
School of Veterinary Medicine
University of Wisconsin-Madison
Madison, WI, USA

Michael H. Boevé, DVM, PhD
Diplomate ECVO
Staff Ophthalmologist
Department of Clinical Sciences of Companion Animals
Faculty of Veterinary Medicine
Utrecht University, The Netherlands

Alison Clode, DVM
Diplomate ACVO
Port City Veterinary Referral Hospital
Portsmouth, NH, USA

Cynthia S. Cook, DVM, PhD
Diplomate ACVO
Veterinary Vision
San Carlos and San Francisco, CA, USA

Cheryl L. Cullen, DVM
Diplomate ACVO
CullenWebb Animal Eye Specialists
Riverview, NB, Canada

Emma Dewhurst, MA, VetMB, MRCVS
Diplomate ECVCP, FRCPath
IDEXX Laboratories
Wetherby, West Yorkshire, UK

David Donaldson, BVSc(Hons), MRCVS, MANZCVS
Diplomate ECVO
European Specialist in Veterinary Ophthalmology
Senior Clinician in Ophthalmology
Langford Vets
University of Bristol Veterinary School
Langford, Bristol, UK

Seth Eaton, VMD
Diplomate ACVO
Clinical Assistant Professor, Comparative Ophthalmology
Department of Surgical Sciences
School of Veterinary Medicine
University of Wisconsin – Madison
Madison, WI, USA

Björn Ekesten, DVM, PhD
Diplomate ECVO
Professor of Ophthalmology
Department of Clinical Sciences
Faculty of Veterinary Medicine
Swedish University of Agricultural Science
Uppsala, Sweden

Robert English, DVM, PhD
Diplomate ACVO
Animal Eye Care of Cary
Cary, NC, USA

Heidi J. Featherstone, BVetMed, DVOphthal, MRCVS
Diplomate ECVO, Diplomate RCVS
Head of Ophthalmology
The Ralph Veterinary Referral Centre;
Honorary Associate Professor
Nottingham Veterinary School
Marlow, Buckinghamshire, UK

Kirk N. Gelatt, VMD
Diplomate ACVO
Emeritus Distinguished Professor of Comparative Ophthalmology
Department of Small and Large Animal Clinical Sciences
College of Veterinary Medicine
University of Florida
Gainesville, FL, USA

Brian C. Gilger, DVM, MS
Diplomate ACVO, Diplomate ACT
Professor of Ophthalmology
Department of Clinical Sciences
College of Veterinary Medicine
North Carolina State University
Raleigh, NC, USA

Juliet R. Gionfriddo, DVM
Diplomate ACVO
Professor Emeritus of Ophthalmology
Department of Clinical Sciences
College of Veterinary Medicine
Colorado State University
Fort Collins, CO, USA

Elizabeth A. Giuliano, DVM, MS
Diplomate ACVO
Associate Professor of Ophthalmology
Department of Veterinary Medicine and Surgery
College of Veterinary Medicine
University of Missouri
Columbia, MO, USA

Mary Belle Glaze, DVM
Diplomate ACVO
Gulf Coast Animal Eye Clinic
Houston, TX, USA

David Gould, BSc (Hons), BVM&S, PhD, DVOphthal, FRCVS
Diplomate ECVO
RCVS and European Specialist in Veterinary Ophthalmology
Head of Ophthalmology
Davies Veterinary Specialists
Manor Farm Business Park
Higham Gobion, Hertfordshire, UK

Bruce H. Grahn, DVM
Diplomate ACVO
Professor Emeritus of Veterinary Ophthalmology
Western College of Veterinary Medicine and
Prairie Ocular Pathology of Prairie Diagnostic Laboratories
University of Saskatchewan
Saskatoon, SK, Canada

Glenwood G. Gum, MS, PhD
Director of Ophthalmology
Absorption Systems
San Diego, CA, USA

Ralph E. Hamor, DVM, MS
Diplomate ACVO
Clinical Professor of Comparative Ophthalmology
Departments of Small and Large Animal Clinical Sciences
College of Veterinary Medicine
University of Florida
Gainesville, FL, USA

Claudia Hartley, BVSc, CertVOphthal, MRCVS
Diplomate ECVO
European Specialist in Veterinary Ophthalmology
Head of Ophthalmology
Langford Vets
University of Bristol Veterinary School
Langford, Bristol, UK

Christine L. Heinrich, DVOphthal, MRCVS
Diplomate ECVO
RCVS and European Specialist in Veterinary Ophthalmology
Eye Veterinary Clinic
Leominster, Herefordshire, UK

Diane V.H. Hendrix, DVM
Diplomate ACVO
Professor of Ophthalmology
Department of Small Animal Clinical Sciences
College of Veterinary Medicine
University of Tennessee
Knoxville, TN, USA

Ian P. Herring, DVM, MS
Diplomate ACVO
Associate Professor of Ophthalmology
Department of Small Animal Clinical Sciences
Virginia-Maryland College of Veterinary Medicine
Virginia Tech
Blacksburg, VA, USA

Allison R. Hoffman, DVM
Diplomate ACVO
Eye Care for Animals
Pasadena, CA, USA

Thomas J. Kern, DVM
Diplomate ACVO
Associate Professor of Ophthalmology
Department of Clinical Sciences
College of Veterinary Medicine
Cornell University
Ithaca, NY, USA

Patrick R. Kircher, Dr.Med.Vet., PhD
Diplomate ECVDI, Exec. MBA, UZH
Professor of Veterinary Diagnostic Imaging
Clinic for Diagnostic Imaging
Department of Clinical Diagnostics and Services
Vetsuisse Faculty, University of Zurich
Zurich, Switzerland

András M. Komáromy, DrMedVet, PhD
Diplomate ACVO, Diplomate ECVO
Professor of Ophthalmology
Department of Small Animal Clinical Science
College of Veterinary Medicine
Michigan State University
East Lansing, MI, USA

Marta Leiva, DVM, PhD
Diplomate ECVO
Professor Associate
Hospital Clinic Veterinari
Fundació Universitat Autònoma de Barcelona;
Departament de Medicina i Cirurgia Animal
Facultat de Veterinària
Universitat Autònoma de Barcelona
Bellaterra, Barcelona, Spain

David J. Maggs, BVSc
Diplomate ACVO
Professor of Ophthalmology
Department of Surgical and Radiological Sciences
School of Veterinary Medicine
University of California – Davis
Davis, CA, USA

Bianca C. Martins, DVM, MSc, PhD
Diplomate ACVO
Clinical Associate Professor of Ophthalmology
Department of Surgical and Radiological Sciences
School of Veterinary Medicine
University of California - Davis
Davis, CA, USA

Gillian J. McLellan, BVMS, PhD, DVOphthal, MRCVS
Diplomate ECVO, Diplomate ACVO
Associate Professor of Comparative Ophthalmology
Department of Surgical Sciences
School of Veterinary Medicine *and*
Department of Ophthalmology and Visual Sciences
School of Medicine and Public Health
University of Wisconsin-Madison
Madison, WI, USA

Richard J. McMullen, Jr., Dr.Med.Vet, CertEqOphth (Germany)
Diplomate ACVO, Diplomate ECVO
Associate Professor of Equine Ophthalmology
Department of Clinical Sciences
Auburn University
JT Vaughan Large Animal Teaching Hospital
Auburn, AL, USA

Jessica M. Meekins, DVM, MS
Diplomate ACVO
Associate Professor of Ophthalmology
Department of Clinical Sciences
Veterinary Health Center
College of Veterinary Medicine
Kansas State University
Manhattan, KS, USA

Tammy Miller Michau, DVM, MS, MSpVM
Diplomate ACVO
Vice President, Medical Affairs Operations
Mars Veterinary Health
Vancouver, WA, USA

Nicholas J. Millichamp, BVetMed, PhD, DVOphthal, MRCVS
Diplomate ACVO, Diplomate ECVO
Eye Care for Animals-Houston
Houston, TX, USA

Freya Mowat, BVSc, PhD
Diplomate ECVO, Diplomate ACVO
Assistant Professor of Ophthalmology
Department of Surgical Sciences
School of Veterinary Medicine
University of Wisconsin-Madison
Madison, WI, USA

Ron Ofri, DVM, PhD
Diplomate ECVO
Professor, Veterinary Ophthalmology
Koret School of Veterinary Medicine
Hebrew University of Jersualem
Rehovot, Israel

Kostas Papasouliotis, DVM, PhD, MRCVS
Diplomate RCPath (Vet.Clin.Path.), Diplomate ECVCP
EBVS® European Specialist in Veterinary Clinical Pathology
Senior Clinical Pathologist
IDEXX Laboratories
Wetherby, West Yorkshire, UK

Robert L. Peiffer, Jr., DVM, PhD
Diplomate ACVO
Professor Emeritus of Ophthalmology and Pathology
School of Medicine
University of North Carolina
Chapel Hill, NC, USA

Teresa Peña, DVM, PhD
Diplomate ECVO
Professor
Hospital Clinic Veterinari
Fundació Universitat Autònoma de Barcelona;
Departament de Medicina i Cirurgia Animal
Facultat de Veterinària
Universitat Autònoma de Barcelona
Bellaterra, Barcelona, Spain

Simon M. Petersen-Jones, DVetMed, PhD, DVOphthal, MRCVS
Diplomate ECVO
Myers-Dunlap Endowed Chair in Canine Health
Professor of Comparative Ophthalmology
Department of Small Animal Clinical Sciences
College of Veterinary Medicine
Michigan State University
East Lansing, MI, USA

Christopher G. Pirie, DVM
Diplomate ACVO
Associate Professor of Ophthalmology
Department of Small Animal Clinical Sciences
College of Veterinary Medicine
Michigan State University
East Lansing, MI, USA

Stefano Pizzirani, DVM, PhD
Diplomate ACVO, Diplomate ECVS-inactive
Associate Professor of Ophthalmology
Department of Clinical Science
Tufts Cummings School of Veterinary Medicine
North Grafton, MA, USA

Caryn E. Plummer, DVM
Diplomate ACVO
Professor of Comparative Ophthalmology
Departments of Small and Large Animal Clinical Sciences
College of Veterinary Medicine
University of Florida
Gainesville, FL, USA

Simon A. Pot, DVM
Diplomate ACVO, Diplomate ECVO
Ophthalmology Section
Equine Department
Vetsuisse Faculty, University of Zurich
Zurich, Switzerland

Amy J. Rankin, DVM, MS
Diplomate ACVO
Associate Professor of Ophthalmology
Department of Clinical Sciences
Veterinary Health Center
College of Veterinary Medicine
Kansas State University
Manhattan, KS, USA

Alain Regnier, Dr.Med.Vet, PhD
Emeritus Professor of Ophthalmology
Department of Clinical Sciences
School of Veterinary Medicine
Toulouse, France

Don A. Samuelson, PhD, MS
Professor of Comparative Ophthalmology (Retired)
Department of Small Animal Clinical Sciences
College of Veterinary Medicine
University of Florida
Gainesville, FL, USA

Lynne S. Sandmeyer, DVM, DVSc
Diplomate ACVO
Associate Professor of Ophthalmology (Retired)
Department of Small Animal Clinical Sciences
Western College of Veterinary Medicine
University of Saskatchewan
Saskatoon, SK, Canada

Erin M. Scott, VMD
Diplomate ACVO
Assistant Professor of Ophthalmology
Department of Small Animal Clinical Sciences
College of Veterinary Medicine and Biomedical Sciences
Texas A&M University
College Station, TX, USA

Frans C. Stades, DVM, PhD
Diplomate ECVO
Emeritus Professor of Veterinary Ophthalmology
Department of Clinical Sciences of Companion Animals
Faculty of Veterinary Medicine
Utrecht University
Utrecht, The Netherlands

Sara M. Thomasy, DVM, PhD
Diplomate ACVO
Professor of Comparative Ophthalmology
Department of Surgical and Radiological Sciences
School of Veterinary Medicine;
Department of Ophthalmology & Vision Science
School of Medicine
University of California
Davis, CA, USA

Samuel J. Vainisi, DVM
Diplomate ACVO
Animal Eye Clinic
Denmark, WI, USA

Lucien V. Vallone, DVM
Diplomate ACVO
Assistant Clinical Professor of Comparative Ophthalmology
Department of Small Animal Clinical Sciences
College of Veterinary Medicine
Texas A&M University
College Station, TX, USA

Alexandra van der Woerdt, DVM, MS
Diplomate ACVO, Diplomate ECVO
The Animal Medical Center
New York, NY, USA

Katrin Voelter, DVM, Dr.Med.Vet., PhD
Diplomate ECVO
Equine Department
Vetsuisse Faculty, University of Zurich
Zurich, Switzerland

Kenneth R. Waller III, DVM, MS
Diplomate ACVR
Clinical Associate Professor of Diagnostic Imaging
Department of Surgical Sciences
School of Veterinary Medicine
University of Wisconsin-Madison
Madison, WI, USA

Aubrey A. Webb, DVM, PhD
CullenWebb Animal Eye Specialists
Riverview, NB, Canada

R. David Whitley, DVM, MS
Diplomate ACVO
Gulf Coast Veterinary Specialists
Houston, TX;
Departments of Small and Large Animal
Clinical Sciences
College of Veterinary Medicine
University of Florida
Gainesville, FL, USA

David A. Wilkie, DVM, MS
Diplomate ACVO
Professor of Comparative Ophthalmology
Department of Veterinary Clinical Sciences
College of Veterinary Medicine
The Ohio State University
Columbus, OH, USA

David L. Williams, MA, VetMB, PhD, CertVOphthal, MRCVS
Senior Lecturer, Veterinary Ophthalmology
Department of Clinical Veterinary Medicine
University of Cambridge
Cambridge, UK

Joseph C. Wolfer, DVM
Diplomate ACVO
Toronto Animal Eye Clinic
Toronto, ON, Canada

Preface

In 1965 when I entered veterinary ophthalmology, it became very quickly apparent that there was a very limited information base or knowledge in veterinary ophthalmology. If this new clinical discipline was to grow and develop into a respected clinical specialty, we would need to develop our own scientific base, and compete with the other emerging clinical specialties in veterinary medicine. And we have! With our limited English-language books of *Veterinary Ophthalmology* by R.H. Smythe (1956), W.G. Magrane's first edition of *Canine Ophthalmology* (1965; Lea and Febiger), and *Diseases of the Canine Eye* by F.G. Startup (1969; Williams and Wilkins), and the chapter in *Advances in Veterinary Science* called 'Examination of the Eye' and 'Eye Operations in Animals' by Otto Überreiter (1959; Academic Press), we needed to "roll up our sleeves" and get to work big time!

We have available now (2021) a large number of veterinary ophthalmology books concentrating on the dog, cat, exotic animals, horses, ophthalmic pathology, and ophthalmic surgery. Two veterinary ophthalmology journals have proven invaluable to our success as a discipline. The first journal, *Veterinary and Comparative Ophthalmology*, was published by Fidia Research Foundation and Veterinary Practice Publishing (1991–1998), and our second journal was *Veterinary Ophthalmology* (published by Blackwell and Wiley-Blackwell, 1998 to present); they greatly assisted our development and proved critical for the distribution of new scientific information. In fact, the current journal provides more than 90% of animal ophthalmic literature annually worldwide.

In the late 1950s and extending into the 1970s, professional groups of budding veterinary ophthalmologists organized scientific societies to gather and exchange their knowledge and clinical experiences, which rapidly evolved to Colleges of Veterinary Ophthalmologists whose primary missions were to train new veterinary ophthalmologists (termed residents), and foster (and fund) research to "grow" the clinical discipline long term and worldwide. Nowadays these significant changes have greatly enriched veterinary ophthalmology, and markedly improved the quality of our ophthalmic animal patients.

The advances in this text, *Veterinary Ophthalmology*, have paralleled and documented the changes in veterinary ophthalmology, and has become our symbol of where we are today. In 1981, the first edition was released, consisting of 21 chapters (788 pages) by 22 authors, and was well received. As a result, subsequent editions followed: second edition (1991; 765 pages and 19 authors), and then in 1999 our last single-volume release (1544 pages, 37 chapters, and 44 authors). The third edition was markedly expanded and had color illustrations throughout the text.

The last two editions were two-volume sets: for 2007, volume one 535 pages, 9 chapters, and 45 authors, and for the second larger volume 1672 pages, 20 chapters, and 36 authors; and in 2012 for volume one 789 pages, 12 chapters, and 26 authors, and for the second volume 1479 pages, 22 chapters, and 39 authors. All editions were well referenced; in fact, a great value of this text is that it documents the advances in veterinary ophthalmology during the past half of the twentieth century, and the first two decades of the twenty-first century!

The sixth edition again consists of two volumes, 37 chapters, and 64 contributors. Like the last two editions, the first volume contains the basic science and foundations of clinical ophthalmology chapters and the first part of the third section on canine ophthalmology. Basic vision science courses in veterinary medical colleges are often an afterthought, and our veterinary ophthalmic basic sciences are frequently documented by veterinary ophthalmologists (rather than anatomists, physiologists, pharmacologists, etc.).

The first volume of the basic sciences and foundations of veterinary ophthalmology is designed to provide the base of those subjects that underpin the clinical sciences. They include embryology, anatomy, ophthalmology physiology, optics and physiology of vision, and fundamentals of vision in animals. In the foundations of clinical ophthalmology section, the chapters include immunity, microbiology, clinical pharmacology and therapeutics, ophthalmic pathology, ophthalmic examination and diagnostics, ophthalmic genetics and DNA testing, fundamentals of microsurgery, and photography. The third section starts with the chapters for

the first part of the canine ophthalmology including orbit, eyelids, nasolacrimal system, lacrimal secretory system, conjunctiva and nictitating membrane, cornea and sclera, and glaucoma.

The second volume focuses on clinical ophthalmology in the different species, and starts with the second part of canine ophthalmology (chapters- anterior uvea, lens and cataract formation, surgery of the lens, vitreous, ocular fundus, surgery of the posterior segment, and optic nerve), and continues with feline, equine, food and fiber-producing animals, avian, New World camelids, laboratory animals, pocket pet animals, and exotics, and concludes with comparative neuro-ophthalmology, ophthalmic manifestations of systemic diseases, and the index. The sixth edition more or less has devoted space relative to the amount of time based on different animal species encountered in veterinary ophthalmology practice.

Now, in 2021, the sixth edition of *Veterinary Ophthalmology* continues to document this discipline's advances. The magnitude of this edition has now required five associate editors, who devoted their time and expertise to make it happen. Like for me, I'm certain it was a learning experience! They are Drs. Brian C. Gilger, Diane V.H. Hendrix, Thomas J. Kern, Caryn E. Plummer, and Gil Ben-Shlomo. Each editor chose their authors and respective chapters, based on their expertise and preferences. A book like this is a huge undertaking, and all of us have devoted hundreds of hours to make it a successful product for the profession. Our 64 authors contributed hundreds of hours to this edition, taking time away from family and practice, and we thank them.

When all the chapters had been submitted and production had started, the COVID-19 pandemic spread across the world like a massive hurricane. Terms like "face masks," "social distancing," "isolation," and "quarantine or shelter at home" became common terms, and our daily personal and professional routines were markedly disrupted. But progress in the production of the sixth edition continued uninterrupted.

We thank Erica Judisch, Executive Editor, Veterinary Medicine and Dentistry, and Purvi Patel, Project Editor, of Wiley-Blackwell for their expertise and assistance in making the sixth edition of *Veterinary Ophthalmology* a reality. Our copyeditors, Jane Grisdale and Sally Osborn, and project manager Mirjana Misina were superb. And lastly, we thank and appreciate the continued support and encouragement of our spouses and family members who bear with us as we struggle to meet our time schedules and other life priorities.

Distinguished Professor of Comparative Ophthalmology, Emeritus

Kirk N. Gelatt, VMD, Diplomate, American College of Veterinary Ophthalmologists

About the Companion Website

This book is accompanied by a companion website:

www.wiley.com/go/gelatt/veterinary

The website includes:

- PowerPoints of all figures from the book for downloading
- References linked to CrossRef

Section I

Basic Vision Sciences

1

Ocular Embryology and Congenital Malformations

Cynthia S. Cook

Veterinary Vision, San Carlos and San Francisco, CA, USA

An understanding of normal and abnormal ocular development is essential to the broader subjects of anatomy, physiology, and pathology. Embryology provides both insight into the development of structures such as the cornea, iridocorneal angle, and retina and their normal and pathologic functions, as well as a means of understanding how congenital malformations occur.

Investigations of ocular development have often used rodents as animal models. Comparison with studies of humans and other animals demonstrates that the sequence of developmental events is very similar across species (Cook, 1995; Cook & Sulik, 1986; Hilfer, 1983; O'Rahilly, 1983). Factors that must be considered when making interspecies comparisons include duration of gestation, differences in anatomic end point (e.g., presence of a tapetum, macula, or Schlemm's canal), and when eyelid fusion breaks (during the sixth month of gestation in the human versus 2 weeks postnatal in the dog; Table 1.1).

This chapter describes normal events and abnormalities in this developmental sequence that can lead to malformations. Bearing in mind the species differences alluded to earlier, the mouse is a valuable model in the study of normal and abnormal ocular morphogenesis. In particular, studying the effects of acute exposure to teratogens during development has provided valuable information about the specific timing of events that lead to malformations.

Gastrulation and Neurulation

Cellular mitosis following fertilization results in transformation of the single-cell zygote into a cluster of 12–16 cells. With continued cellular proliferation, this morula becomes a blastocyst, containing a fluid-filled cavity. The cells of the blastocyst will form both the embryo proper and the extraembryonic tissues (i.e., amnion and chorion). At this early stage, the embryo is a bilaminar disc, consisting of hypoblast and epiblast. This embryonic tissue divides the blastocyst space into the amniotic cavity (adjacent to epiblast) and the yolk sac (adjacent to hypoblast; Fig. 1.1).

Gastrulation (formation of the mesodermal germ layer) begins during day 10 of gestation in the dog (day 7 in the mouse; days 15–20 in the human). The primitive streak forms as a longitudinal groove within the epiblast (i.e., future ectoderm). Epiblast cells migrate toward the primitive streak, where they invaginate to form the mesoderm. This forms the three classic germ layers: ectoderm, mesoderm, and endoderm. Gastrulation proceeds in a cranial-to-caudal progression; simultaneously, the cranial surface ectoderm proliferates, forming bilateral elevations called the neural folds (i.e., the future brain). The columnar surface ectoderm in this area now becomes known as the neural ectoderm (Fig. 1.2).

As the neural folds elevate and approach each other, a specialized population of mesenchymal cells, the neural crest, emigrates from the neural ectoderm at its junction with the surface ectoderm (Fig. 1.3). Migration and differentiation of the neural crest cells are influenced by the hyaluronic acid-rich extracellular matrix. This acellular matrix is secreted by the surface epithelium as well as by the crest cells, and it forms a space through which the crest cells migrate. Fibronectin secreted by the noncrest cells forms the limits of this mesenchymal migration (LeDouarin & Teillet, 1974). Interactions between the migrating neural crest and the associated mesoderm appear to be essential for normal crest differentiation (LeDouarin & Teillet, 1974; Noden, 1993). The neural crest cells migrate peripherally beneath the surface ectoderm to spread throughout the embryo, populating the region around the optic vesicle and ultimately giving rise to nearly all the connective tissue structures of the eye (Table 1.2; Hilfer & Randolph, 1993; Johnston et al., 1979; Noden, 1993). The patterns of neural crest emergence and migration correlate with the segmental disposition of the developing brain.

Veterinary Ophthalmology: Volume I, Sixth Edition. Edited by Kirk N. Gelatt, Gil Ben-Shlomo, Brian C. Gilger, Diane V.H. Hendrix, Thomas J. Kern, and Caryn E. Plummer.

Companion website: www.wiley.com/go/gelatt/veterinary

Table 1.1 Sequence of ocular development (Cook, 1995; O'Rahilly, 1983).

Human (Approximate Postfertilization Age)				Dog (Day Postfertilization)	
Month	**Week**	**Day**	**Mouse (Day Postfertilization)**	**Postnatal (P)**	**Developmental Events**
1	3	22	8	13	Optic sulci present in forebrain
	4	24	9	15	Optic sulci convert into optic vesicles
			10	17	Optic vesicle contacts surface ectoderm
					Lens placode begins to thicken
		26			Optic vesicle surrounded by neural crest mesenchyme
2	5	28	10.5		Optic vesicle begins to invaginate, forming optic cup
					Lens pit forms as lens placode invaginates
					Retinal primordium thickens, marginal zone present
		32	11	19	Optic vesicle invaginated to form optic cup
					Optic fissure delineated
					Retinal primordium consists of external limiting membrane, proliferative zone, primitive zone, marginal zone, and internal limiting membrane
					Oculomotor nerve present
		33	11.5	25	Pigment in outer layer of optic cup
					Hyaloid artery enters through the optic cup
					Lens vesicle separated from surface ectoderm
					Retina: inner marginal and outer nuclear zones
			11.5	29	Basement membrane of surface ectoderm intact
					Primary lens fibers form
					Trochlear and abducens nerves appear
					Lid folds present
	6	37	12		Edges of optic fissure in contact
			12	30	Tunica vasculosa lentis present
					Lens vesicle cavity obliterated
					Ciliary ganglion present
		41	12	32	Posterior retina consists of nerve fiber layer, inner neuroblastic layer, transient fiber layer of Chievitz, proliferative zone, outer neuroblastic layer, and external limiting membrane
			17	32	Eyelids fuse (dog)
	7				Anterior chamber beginning to form
			12.5	40	Secondary lens fibers present
		48	14	32	Corneal endothelium differentiated
	8	51			Optic nerve fibers reach the brain
					Optic stalk cavity is obliterated
					Lens sutures appear
					Acellular corneal stroma present
		54		30–35	Scleral condensation present
	9	57	17	40	First indication of ciliary processes and iris
					Extraocular muscles visible

Table 1.1 (Continued)

Human (Approximate Postfertilization Age)			Mouse (Day Postfertilization)	Dog (Day Postfertilization)	
Month	**Week**	**Day**		**Postnatal (P)**	**Developmental Events**
				—	Eyelids fuse (occurs earlier in the dog)
	10			45	Pigment visible in iris stroma
					Ciliary processes touch lens equator
					Rudimentary rods and cones appear
				45–1 P	Hyaloid artery begins to atrophy to the disc
3	12			—	Branches of the central retinal artery form
4				51	Pupillary sphincter differentiates
					Retinal vessels present
				56	Ciliary muscle appears
				—	Eye axis forward (human)
—				56	Tapetum present (dog)
				2–14 P	Tunica vasculosa lentis atrophies
					Short eyelashes appear
5				40	Layers of the choroid are complete with pigmentation
6				—	Eyelids begin to open, light perception
				1 P	Pupillary dilator muscle present
7				1–14 P	Pupillary membrane atrophies
				1–16 P	Rod and cone inner and outer segments present in posterior retina
				10–13 P	Pars plana distinct
9				16–40 P	Retinal layers developed
				14 P	Regression of pupillary membrane, tunica vasculosa lentis, and hyaloid artery nearly complete
					Lacrimal duct canalized

Data from Aguirre et al. (1972), Akiya et al. (1986), Cook (1995), and van der Linde-Sipman et al. (2003).

It is important to note that mesenchyme is a general term for any embryonic connective tissue. Mesenchymal cells generally appear stellate and are actively migrating populations surrounded by extensive extracellular space. In contrast, the term *mesoderm* refers specifically to the middle embryonic germ layer. In other parts of the body (e.g., the axial skeletal system), mesenchyme develops primarily from mesoderm, with a lesser contribution from the neural crest. In the craniofacial region, however, mesoderm plays a relatively small role in the development of connective tissue structures. In the eye, mesoderm probably gives rise only to the striated myocytes of the extraocular muscles and vascular endothelium. Most of the craniofacial mesenchymal tissue comes from neural crest cells (Johnston et al., 1979).

The neural tube closes initially in the craniocervical region with closure proceeding cranially and caudally. Once closure is complete, the exterior of the embryo is fully covered by surface ectoderm, and the neural tube is lined by neural ectoderm. Neural segmentation then occurs to form the specific parts of the brain: forebrain (i.e., prosencephalon), midbrain (i.e., mesencephalon), and hindbrain (i.e., rhombencephalon; see Fig. 1.3 and Fig. 1.4). The optic vesicles develop from neural ectoderm within the forebrain, with the ocular connective tissue derivatives originating from the midbrain neural crest.

Formation of the Optic Vesicle and Optic Cup

The optic sulci are visible as paired evaginations of the forebrain neural ectoderm on day 13 of gestation in the dog (see Fig. 1.3, Fig. 1.4, Fig. 1.5, Fig. 1.6, and Fig. 1.7). The transformation from optic sulcus to optic vesicle occurs

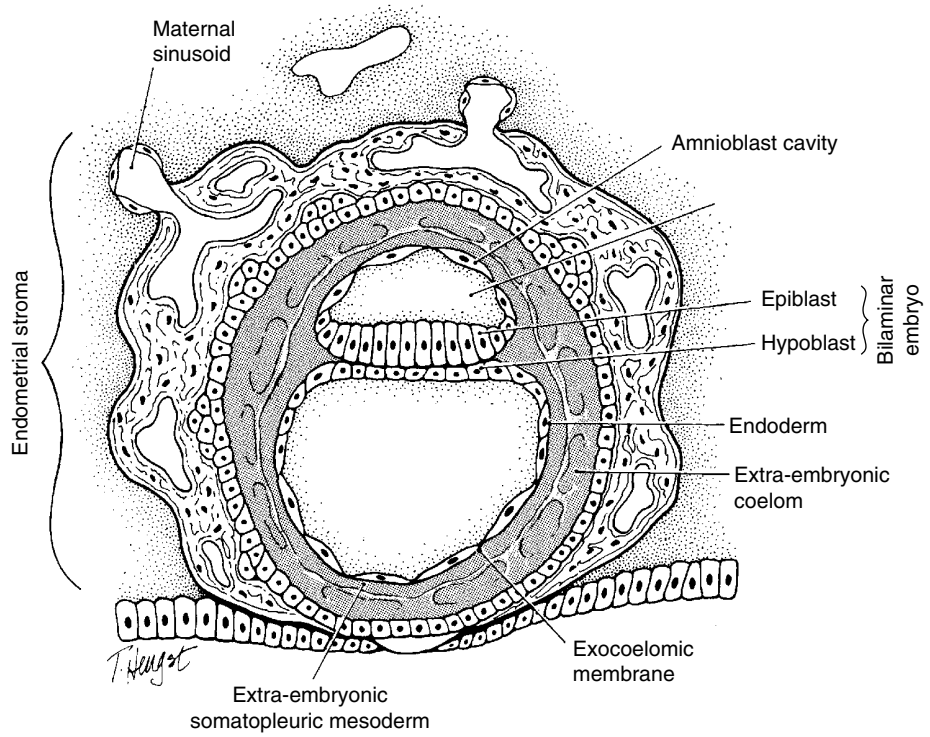

Figure 1.1 A blastocyst that has penetrated the maternal endometrium. An embryoblast has formed and consists of two cell layers: the epiblast above, and the hypoblast below. (Reprinted with permission from Cook, C., Sulik, K.K., & Wright, K.W. (2003) Embryology. In: *Pediatric Ophthalmology and Strabismus* (eds. Wright, K.W. & Spiegel, P.H.), pp. 3–38. New York: Springer.)

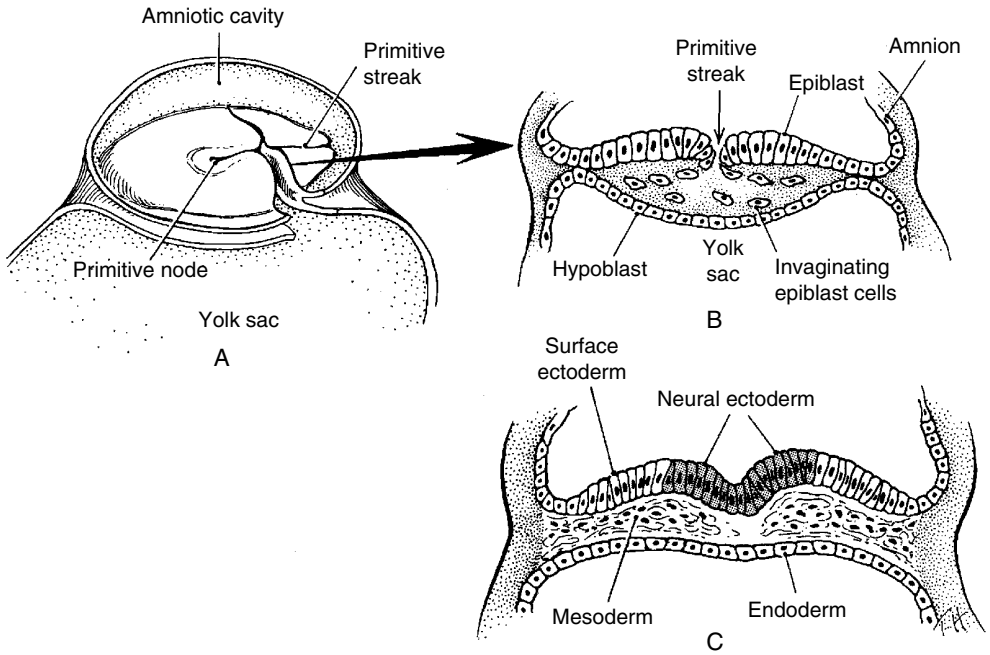

Figure 1.2 **A.** Dorsal view of an embryo in the gastrulation stage with the amnion removed. **B.** Cross-section through the primitive streak, representing invagination of epiblast cells between the epiblast and hypoblast layers. Note that the epiblast cells filling the middle area form the mesodermal layer. **C.** Cross-section through the neural plate. Note that the ectoderm in the area of the neural groove (shaded cells) has differentiated into neural ectoderm, whereas the ectoderm on each side of the neural groove is surface ectoderm (clear water cells). (Reprinted with permission from Cook, C., Sulik, K.K., & Wright, K.W. (2003) Embryology. In: *Pediatric Ophthalmology and Strabismus* (eds. Wright, K.W. & Spiegel, P.H.), pp. 3–38. New York: Springer.)

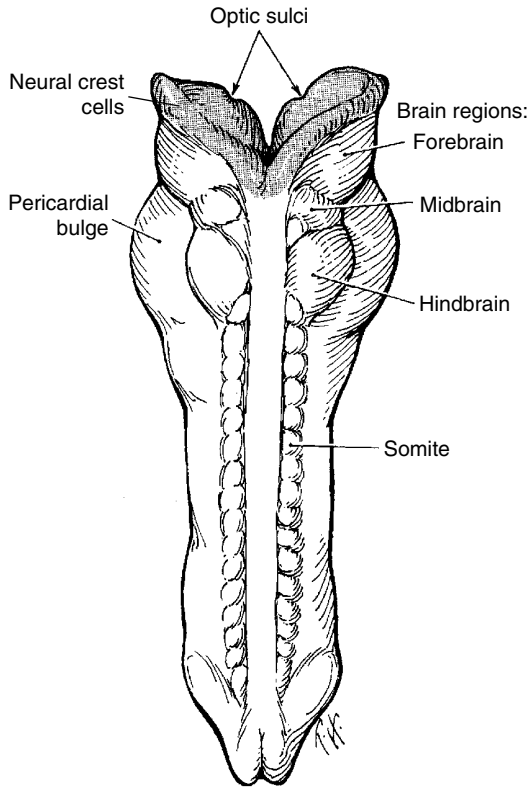

Figure 1.3 Dorsal view showing partial fusion of the neural folds to form the neural tube. Brain vesicles have divided into three regions: forebrain, midbrain, and hindbrain. The neural tube, groove, and facing surfaces of the large neural folds are lined with neural ectoderm (shaded cells), whereas surface ectoderm covers the rest of the embryo. Neural crest cells are found at the junction of the neural ectoderm and surface ectoderm. Neural crest cells migrate beneath the surface ectoderm, spreading throughout the embryo and specifically to the area of the optic sulci. Somites have formed along the lateral aspect of the closed cephalic neural tube. On the inside of both forebrain vesicles is the optic sulci. (Reprinted with permission from Cook, C., Sulik, K.K., & Wright, K.W. (2003) Embryology. In: *Pediatric Ophthalmology and Strabismus* (eds. Wright, K.W. & Spiegel, P.H.), pp. 3–38. New York: Springer.)

concurrent with the closure of the neural tube (day 15 in the dog). Intracellular filaments and microtubules within the cytoskeleton alter cell shape and allow for cell movement. In addition to the mechanical influences of the cytoskeleton and the extracellular matrix, localized proliferation and cell growth contribute to expansion of the optic vesicle (Fig. 1.5; Hilfer & Randolph, 1993; Hilfer et al., 1981).

The optic vesicle enlarges and, covered by its own basal lamina, approaches the basal lamina underlying the surface ectoderm (Fig. 1.5). The optic vesicle appears to play a significant role in the induction and size determination of the palpebral fissure and of the orbital and periocular structures (Jones et al., 1980). An external bulge indicating the presence of the enlarging optic vesicle can be seen at approximately day 17 in the dog.

Table 1.2 Embryonic origins of ocular tissues (Johnston et al., 1979; Noden, 1993; Yamashita & Sohal, 1987).

Neural Ectoderm	Neural Crest
Neural retina	Stroma of iris, ciliary body, choroid, and sclera
Retinal pigment epithelium	Ciliary muscles
Posterior iris epithelium	Corneal stroma and endothelium
Pupillary sphincter and dilator muscle (except in avian species)	Perivascular connective tissue and smooth muscle cells
	Striated muscles of iris (avian species only)
Bilayered ciliary epithelium	Meninges of optic nerve
	Orbital cartilage and bone
	Connective tissue of the extrinsic ocular muscles
	Endothelium of trabecular meshwork
Surface Ectoderm	**Mesoderm**
Lens	Extraocular myoblasts
Corneal and conjunctival epithelium	Vascular endothelium
Lacrimal gland	Schlemm's canal (human)
	Posterior sclera (?)

Data from Ashton (1966), Cook et al. (1991a), and Cook and Sulik (1986, 1988).

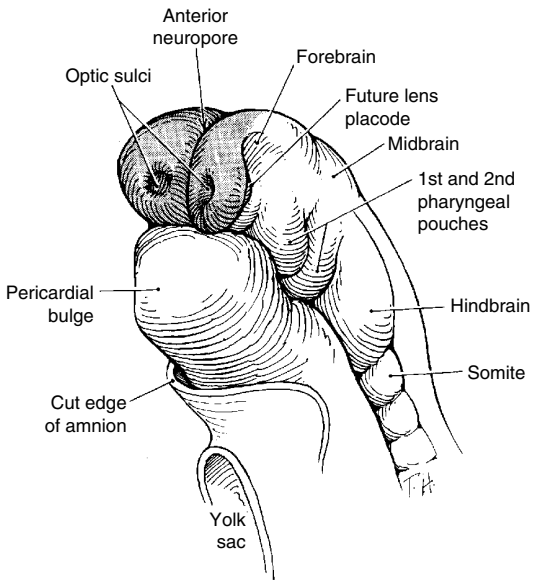

Figure 1.4 Development of the optic sulci, which are the first sign of eye development. Optic sulci on the inside of the forebrain vesicles consisting of neural ectoderm (shaded cells). The optic sulci evaginate toward the surface ectoderm as the forebrain vesicles simultaneously rotate inward to fuse. (Reprinted with permission from Cook, C., Sulik, K.K., & Wright, K.W. (2003) Embryology. In: *Pediatric Ophthalmology and Strabismus* (eds. Wright, K.W. & Spiegel, P.H.), pp. 3–38. New York: Springer.)

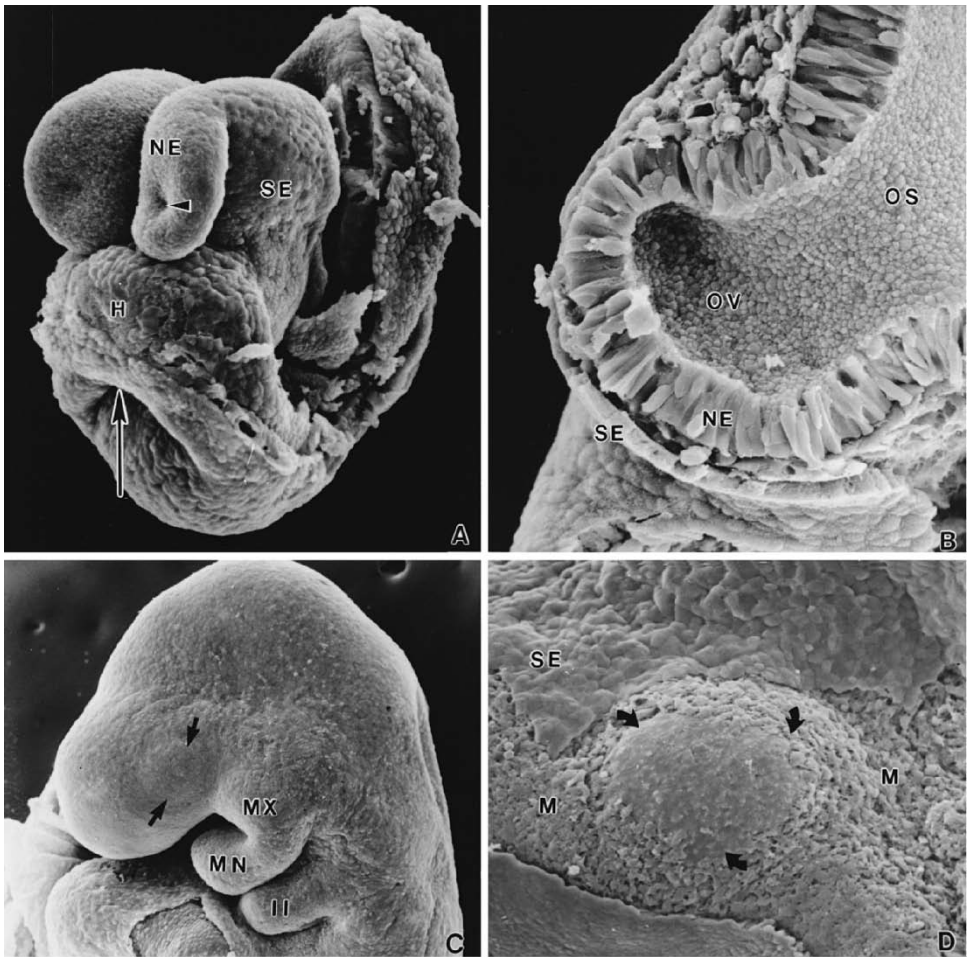

Figure 1.5 **A.** Scanning electron micrograph of a mouse embryo (six somite pairs) on day 8 of gestation, equivalent to day 13 of canine gestation. The amnion has been removed, and the neural folds have segmented into a forebrain region containing the optic sulci (arrowhead), which are evaginations of neural ectoderm (NE). The close proximity to the developing heart (H) can be seen. The area where the NE meets the surface ectoderm (SE) is where the neural fold will meet and fuse; this area also gives rise to the neural crest cells. The entrance to the foregut is indicated by the arrow. **B.** Scanning electron micrograph of the optic vesicle on day 9 of gestation in the mouse (day 15 in the dog). Expansion of the optic sulcus results in an optic vesicle (OV) that approaches the surface ectoderm (SE). A thin layer of mesenchyme is still present between the NE and the SE. The optic stalk (OS) is continuous with the ventricle of the forebrain. **C.** The bulge of the enlarging OV (arrows) can be seen externally. MN, mandibular prominence of the first visceral arch; MX, maxillary prominence of the first visceral arch; II, second visceral arch. **D.** Partial removal of the SE from an embryo of 25 somite pairs (day 17 in the dog; day 19 in the mouse) reveals the exposed basal lamina of the OV (arrows). Enlargement of the optic vesicle has displaced the adjacent mesenchyme (M) so that the basal lamina of the SE is in direct contact with that of the OV. (Reprinted with permission from Cook, C.S. & Sulik, K.K. (1986) Sequential scanning electron microscopic analyses of normal and spontaneously occurring abnormal ocular development in C57B1/6J mice. *Scanning Electron Microscopy*, **3**, 1215–1227.)

The optic vesicle and optic stalk invaginate through differential growth and infolding (Fig. 1.6 and Fig. 1.7). Local apical contraction (Wrenn & Wessells, 1969) and physiologic cell death (Schook, 1978) have been identified during invagination. The surface ectoderm in contact with the optic vesicle thickens to form the lens placode (Fig. 1.6, Fig. 1.7, and Fig. 1.8A, B), which then invaginates with the underlying neural ectoderm. The invaginating neural ectoderm folds onto itself as the space within the optic vesicle collapses, thus creating a double layer of neural ectoderm, the optic cup.

This process of optic vesicle/lens placode invagination progresses from inferior to superior, so the sides of the optic cup and stalk meet inferiorly in an area called the optic (choroid) fissure (Fig. 1.8F). Mesenchymal tissue (of primarily neural crest origin) surrounds and fills the optic cup, and by day 25 in the dog, the hyaloid artery develops from mesenchyme in the optic fissure. This artery courses from the optic stalk (i.e., the region of the future optic nerve) to the developing lens (Fig. 1.9 and Fig. 1.10). The two edges of the optic fissure meet and initially fuse anterior to the optic stalk, with fusion then progressing anteriorly and posteriorly.

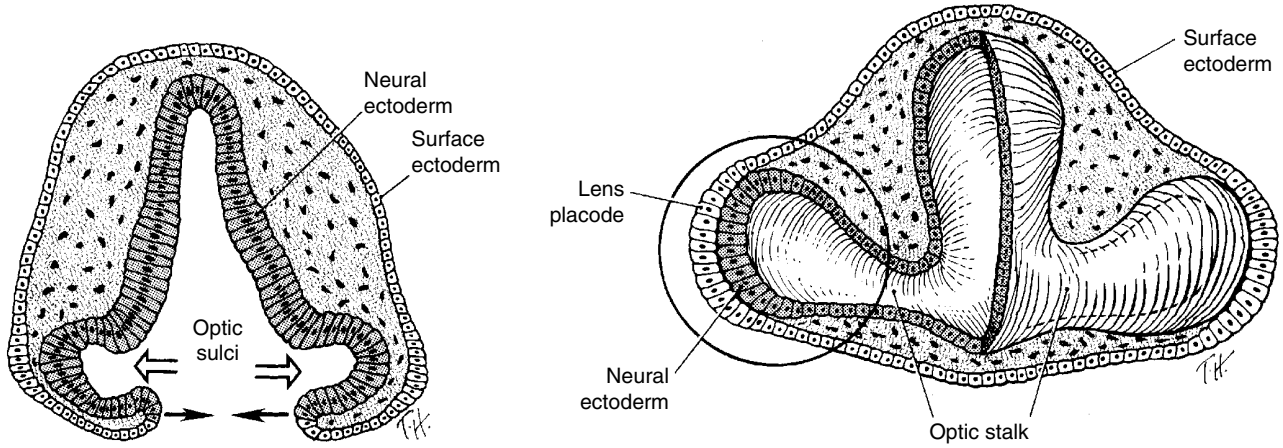

Figure 1.6 Cross-section at the level of the optic vesicle. Note that the neural tube is closed. The surface ectoderm now covers the surface of the forebrain, and the neural ectoderm is completely internalized. The surface ectoderm cells overlying the optic vesicles enlarge to form the early lens placode. (Reprinted with permission from Cook, C., Sulik, K.K., & Wright, K.W. (2003) Embryology. In: *Pediatric Ophthalmology and Strabismus* (eds. Wright, K.W. & Spiegel, P.H.), pp. 3–38. New York: Springer.)

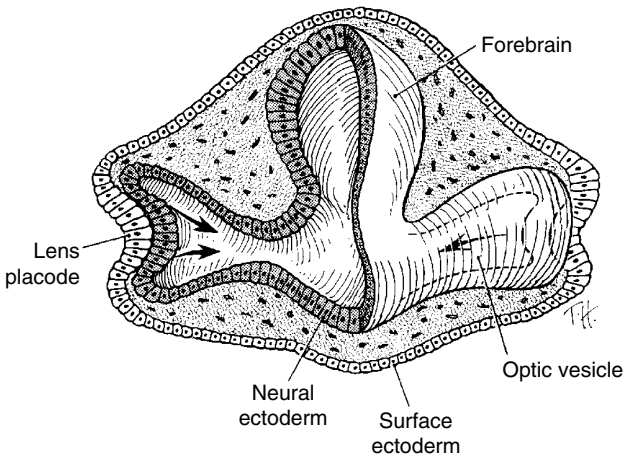

Figure 1.7 Transection showing invaginating lens placode and optic vesicle (arrows), thus creating the lens vesicle within the optic cup. Note the orientation of the eyes 180° from each other. (Reprinted with permission from Cook, C., Sulik, K.K., & Wright, K.W. (2003) Embryology. In: *Pediatric Ophthalmology and Strabismus* (eds. Wright, K.W. & Spiegel, P.H.), pp. 3–38. New York: Springer.)

This process is mediated by glycosaminoglycan-induced adhesion between the two edges of the fissure (Ikeda et al., 1995). Apoptosis has been identified in the inferior optic cup prior to formation of the optic fissure and, transiently, associated with its closure (Ozeki et al., 2000). Failure of this fissure to close normally may result in inferiorly located defects (i.e., colobomas) in the iris, choroid, or optic nerve. Colobomas other than those in the "typical" six o'clock location may occur through a different mechanism and are discussed later.

Closure of the optic cup through fusion of the optic fissure allows intraocular pressure (IOP) to be established. The protein in the embryonic vitreous humor (13% of plasma protein) is derived from plasma proteins entering the eye by diffusion out of permeable vessels in the anterior segment. After day 15, protein content in the vitreous decreases, possibly through dilution with aqueous humor produced by developing ciliary epithelium (Beebe et al., 1986).

Lens Formation

Before contact with the optic vesicle, the surface ectoderm first becomes competent to respond to lens inducers. Inductive signals from the anterior neural plate give this area of ectoderm a "lens-forming bias." Signals from the optic vesicle are required for complete lens differentiation, and inhibitory signals from the cranial neural crest may suppress any residual lens-forming bias in head ectoderm adjacent to the lens (Grainger et al., 1988, 1992). Adhesion between the optic vesicle and surface ectoderm exists, but there is no direct cell contact (Cohen, 1961; Hunt, 1961; Weiss & Jackson, 1961). The basement membranes of the optic vesicle and the surface ectoderm remain separate and intact throughout the contact period.

Thickening of the lens placode can be seen on day 17 in the dog. A tight, extracellular matrix-mediated adhesion between the optic vesicle and the surface ectoderm has been described (Aso et al., 1995; Cook & Sulik, 1988; Garcia-Porrero et al., 1979). This anchoring effect on the mitotically active ectoderm results in cell crowding and elongation and in formation of a thickened placode. This adhesion between the optic vesicle and lens placode also assures alignment of the lens and retina in the visual axis (Beebe, 1985). Abnormal orientation of the optic vesicle as it approaches the surface ectoderm may result in induction of a smaller lens vesicle,

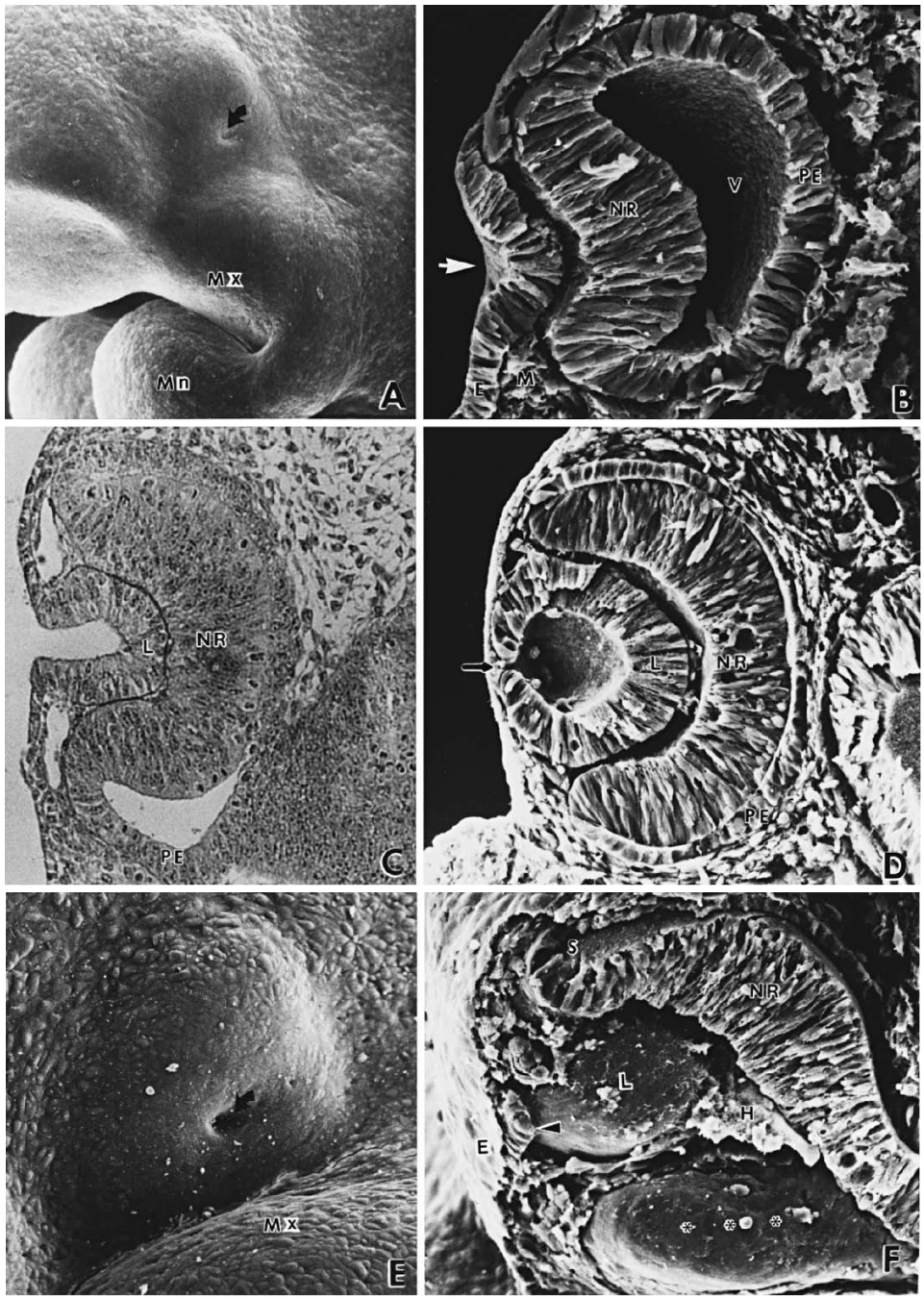

Figure 1.8 **A.** Mouse embryo on day 10 of gestation (29 somite pairs, equivalent to day 17 in the dog). On external examination, the invaginating lens placode can be seen (arrow). Note its position relative to the maxillary prominence (Mx) and mandibular (Mn) prominence of the first visceral arch. **B.** Frontal fracture through the lens placode (arrow) illustrates the associated thickening of the surface ectoderm (E). Mesenchyme (M) of neural crest origin is adjacent to the lens placode. As the precursor to the neural retina (NR), the distal portion of the optic vesicle concurrently thickens, whereas the proximal optic vesicle becomes a shorter, cuboidal layer that is the anlage of the retinal pigment epithelium (PE). The cavity of the optic vesicle (V) becomes progressively smaller. **C.** Light micrograph of the epithelium of the invagination lens placode (L). There is an abrupt transition between the thicker epithelium of the placode and the adjacent surface ectoderm, which is not unlike the transition between the future NR and PE. **D.** As the lens vesicle enlarges, the external opening of lens pore (arrow) becomes progressively smaller. The lens epithelial cells at the posterior pole of the lens elongate to form the primary lens fibers (L). NR, anlage of the neural retina; PE, anlage of the pigment epithelium (now a short cuboidal layer). **E.** External view of the lens pore (arrow) and its relationship to the Mx. **F.** Frontal fracture reveals the optic fissure (*) where the two sides of the invaginating optic cup meet. This forms an opening in the cup, allowing access to the hyaloid artery (H), which ramifies around the invaginating lens vesicle (L). The former cavity of the optic vesicle is obliterated except in the marginal sinus (S), at the transition between the NR and the PE. E, surface ectoderm. (Panels **B** and **F** reprinted with permission from Cook, C.S. & Sulik, K.K. (1986) Sequential scanning electron microscopic analyses of normal and spontaneously occurring abnormal ocular development in C57B1/6J mice. *Scanning Electron Microscopy,* **3**, 1215–1227; panels **C**, **D**, and **E** reprinted with permission from Cook, C. (1995) Embryogenesis of congenital eye malformations. *Veterinary and Comparative Ophthalmology*, **5**, 109–123.)

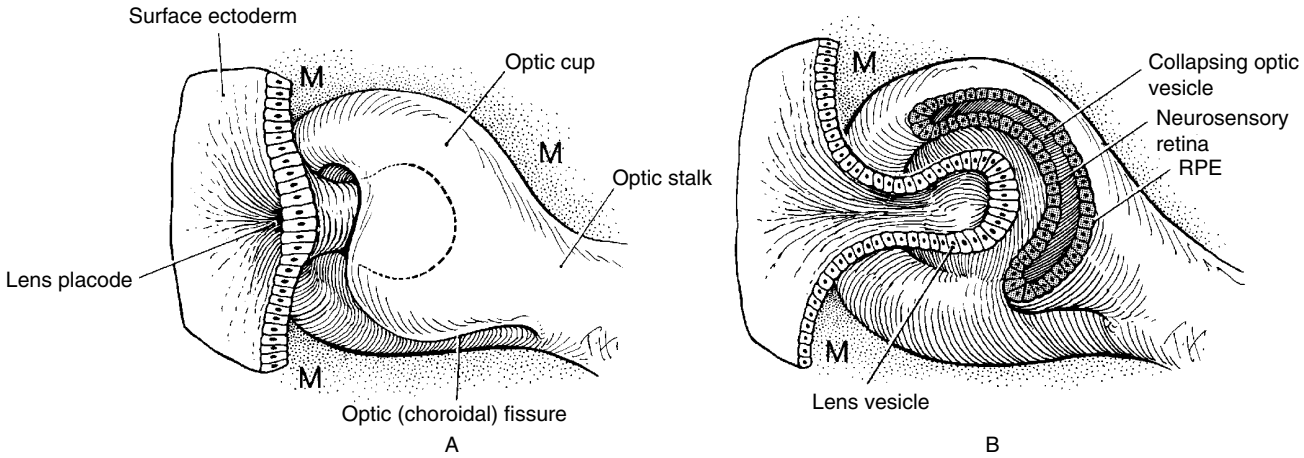

Figure 1.9 Formation of the lens vesicle and optic cup. Note that the optic fissure is present, because the optic cup is not yet fused inferiorly. **A.** Formation of lens vesicle and optic cup with inferior choroidal or optic fissure. Mesenchyme (M) surrounds the invaginating lens vesicle. **B.** Surface ectoderm forms the lens vesicle with a hollow interior. Note that the optic cup and optic stalk are of surface ectoderm origin. (Reprinted with permission from Cook, C., Sulik, K.K., & Wright, K.W. (2003) Embryology. In: *Pediatric Ophthalmology and Strabismus* (eds. Wright, K.W. & Spiegel, P.H.), pp. 3–38. New York: Springer.)

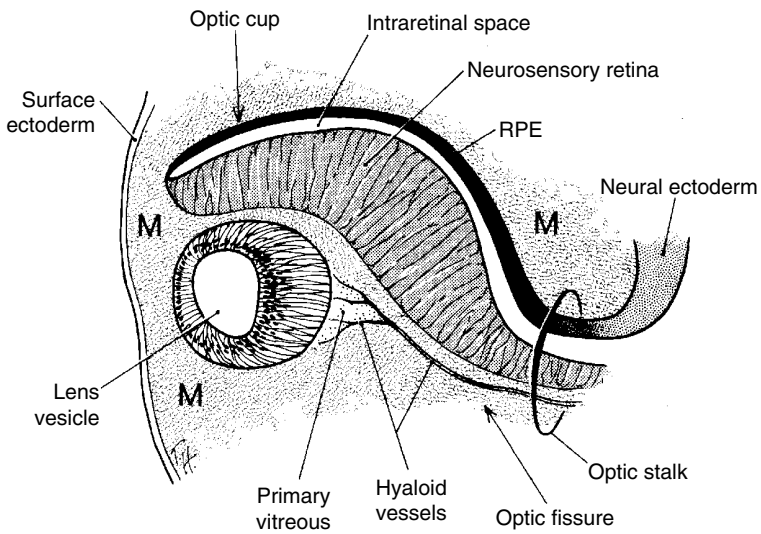

Figure 1.10 Cross-section through optic cup and optic fissure. The lens vesicle is separated from the surface ectoderm. Mesenchyme (M) surrounds the developing lens vesicle, and the hyaloid artery is seen within the optic fissure. (Reprinted with permission from Cook, C., Sulik, K.K., & Wright, K.W. (2003) Embryology. In: *Pediatric Ophthalmology and Strabismus* (eds. Wright, K.W. & Spiegel, P.H.), pp. 3–38. New York: Springer.)

which may assume an abnormal location within the optic cup (Cook & Sulik, 1988).

The lens placode invaginates, forming a hollow sphere, now referred to as a lens vesicle (Fig. 1.8C, D, Fig. 1.9, and Fig. 1.10). The size of the lens vesicle is determined by the contact area of the optic vesicle with the surface ectoderm and by the ability of the latter tissue to respond to induction. Aplasia may result from failure of lens induction or through later involutions of the lens vesicle, either before or after separation from the surface ectoderm (Aso et al., 1995).

Lens vesicle detachment is the initial event leading to formation of the chambers of the ocular anterior segment. This process is accompanied by active migration of epithelial cells out of the keratolenticular stalk, cellular necrosis, apoptosis, and basement membrane breakdown (Garcia-Porrero et al., 1979; Ozeki et al., 2001). Induction of a small lens vesicle that fails to undergo normal separation from the surface ectoderm is one of the characteristics of the teratogen-induced anterior segment dysgenesis described in animal models (Cook & Sulik, 1988). Anterior lenticonus and anterior capsular cataracts as well as anterior segment dysgenesis may result from faulty keratolenticular separation. Additional discussion of anterior segment dysgenesis occurs later in this chapter.

Following detachment from the surface ectoderm (day 25 in the dog), the lens vesicle is lined by a monolayer of cuboidal cells surrounded by a basal lamina, the future lens capsule. The primitive retina promotes primary lens fiber formation in the adjacent lens epithelial cells. Surgical rotation of the chick lens vesicle by 180° results in elongation of the lens epithelial

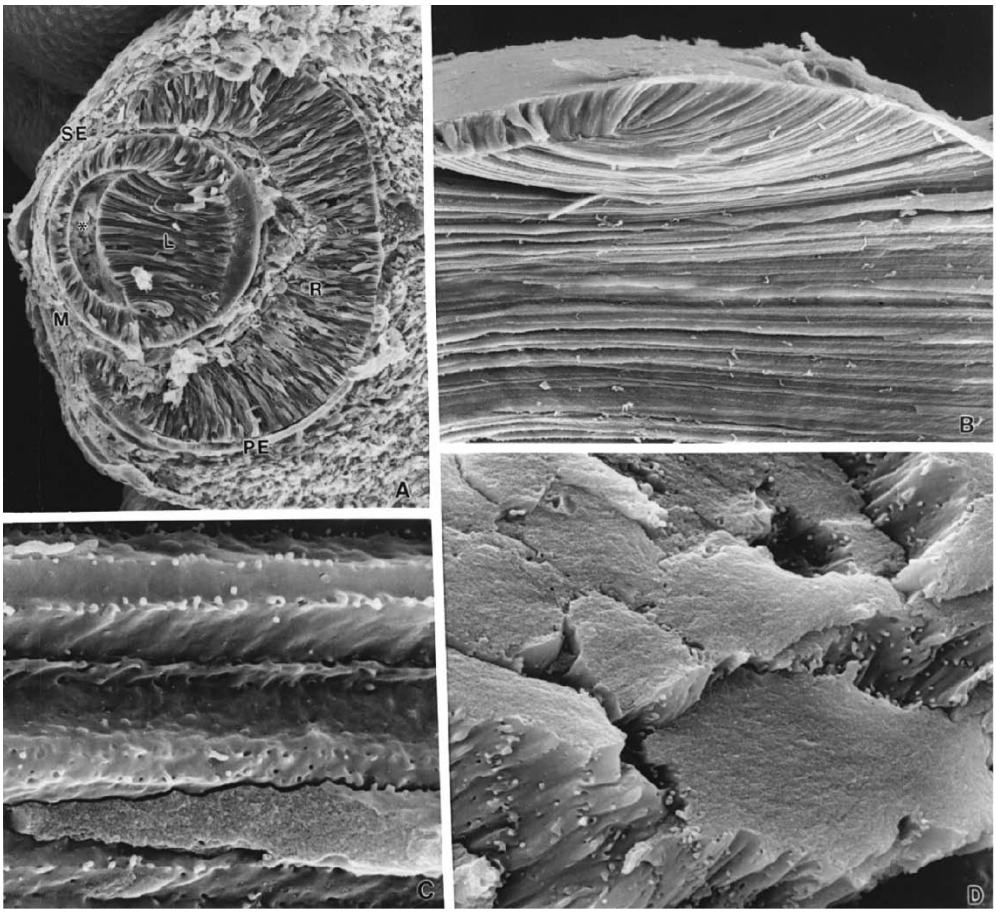

Figure 1.11 **A.** Following detachment of the lens vesicle from the surface ectoderm (SE), the posterior lens epithelial cells–primary lens fibers (L) elongate, obliterating the lens vesicle lumen (equivalent to day 29 of gestation in the dog). Invagination of the optic cup forms the inner neural retina (R) and the outer pigmented epithelium (PE). Mesenchyme of neural crest origin (M) surrounds the optic cup. **B.** Lens bow illustrating elongation of secondary lens fibers. **C** and **D.** Longitudinal view (**C**) and cross-section (**D**) of secondary lens fibers, illustrating the extensive interdigitations and the relative absence of extracellular space. (Reprinted with permission from Sulik, K.K. & Schoenwolf, G.C. (1985) Highlights of craniofacial morphogenesis in mammalian embryos, as revealed by scanning electron microscopy. *Scanning Electron Microscopy*, **4**, 1735–1752.)

cells nearest the presumptive retina, regardless of the orientation of the transplanted lens (Coulombre & Coulombre, 1969). Thus, while the retina develops independently of the lens, the lens appears to be dependent on the retinal primordium for its differentiation. The primitive lens filled with primary lens fibers is the embryonic lens nucleus. In the adult, the embryonic nucleus is the central sphere inside the "Y" sutures; there are no sutures within the embryonal nucleus (Fig. 1.11A, Fig. 1.12, and Fig. 1.13).

At birth, the lens consists almost entirely of lens nucleus, with minimal lens cortex. Lens cortex continues to develop from the anterior cuboidal epithelial cells, which remain mitotic throughout life. Differentiation of epithelial cells into secondary lens fibers occurs at the lens equator (i.e., lens bow; Fig. 1.11B). Lens fiber elongation is accompanied by a corresponding increase in cell volume and a decrease in intercellular space within the lens (Beebe et al., 1982). The lens fibers exhibit a hexagonal cross-sectional shape and extensive surface interdigitations (Fig. 1.11C, D). The secondary lens fibers course anteriorly and posteriorly around the embryonal nucleus to meet at the "Y" sutures (Fig. 1.13).

The zonule fibers are termed the *tertiary vitreous*, but their origin remains uncertain. The zonules may form from the developing ciliary epithelium or the endothelium of the posterior tunica vasculosa lentis (TVL). The embryonic TVL may produce fibrillin-2 and -3, providing a scaffold for zonule formation (Hubmacher et al., 2014). Abnormalities could result in congenital ectopia lentis. Congenitally displaced lenses are often small and are abnormally shaped (i.e., spherophakia), indicating a possible relationship between zonule traction and lens shape. Localized absence of zonules may result in a flattened lens equator; although not a true lens defect, this is often described inaccurately as a lens coloboma (see later Fig. 1.32).

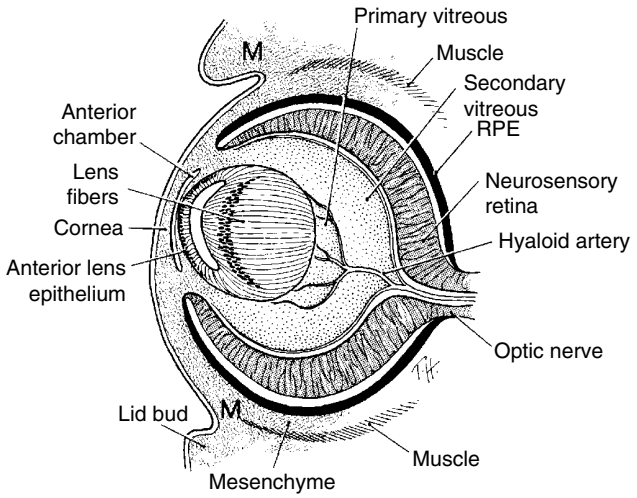

Figure 1.12 Overview of the developing eye surrounded by mesenchyme (M), which is mostly of neural crest origin. The hyaloid vasculature enters the optic cup through the optic fissure and surrounds the lens with capillaries that anastomose with the tunica vasculosa lentis. Axial migration of mesenchyme forms the corneal stroma and endothelium. RPE, retinal pigment epithelium. (Reprinted with permission from Cook, C., Sulik, K.K., & Wright, K.W. (2003) Embryology. In: *Pediatric Ophthalmology and Strabismus* (eds. Wright, K.W. & Spiegel, P.H.), pp. 3–38. New York: Springer.)

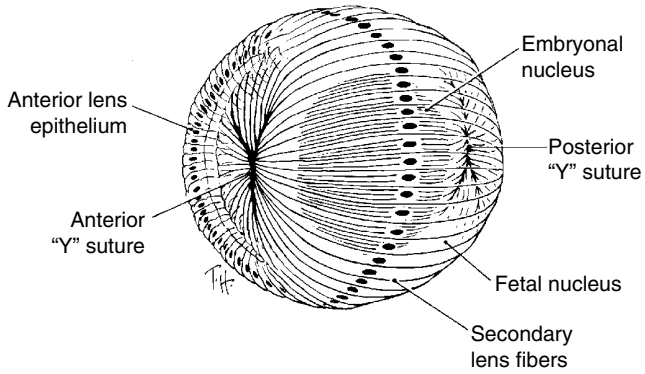

Figure 1.13 Secondary lens fibers and Y sutures. Secondary lens fibers elongate at the equator to span the entire lens, from the anterior to the posterior Y suture. The anterior Y suture is upright; the posterior Y suture is inverted. (Reprinted with permission from Cook, C., Sulik, K.K., & Wright, K.W. (2003) Embryology. In: *Pediatric Ophthalmology and Strabismus* (eds. Wright, K.W. & Spiegel, P.H.), pp. 3–38. New York: Springer.)

Vascular Development

The hyaloid artery is the termination of the primitive ophthalmic artery, a branch of the internal ophthalmic artery, and it remains within the optic cup following closure of the optic fissure. The hyaloid artery branches around the posterior lens capsule and continues anteriorly to anastomose with the network of vessels in the pupillary membrane (Fig. 1.14 and Fig. 1.15A, B; Schaepdrijver et al., 1989). The pupillary membrane consists of vessels and mesenchyme overlying the anterior lens capsule. This hyaloid vascular network that forms around the lens is called the anterior and posterior TVL. The hyaloid artery and associated TVL provide nutrition to the lens and anterior segment during its period of rapid differentiation. Venous drainage occurs via a network near the equatorial lens, in the area where the ciliary body will eventually develop. There is no discrete hyaloid vein (Schaepdrijver et al., 1989).

Once the ciliary body begins actively producing aqueous humor, which circulates and nourishes the lens, the hyaloid system is no longer needed. The hyaloid vasculature and

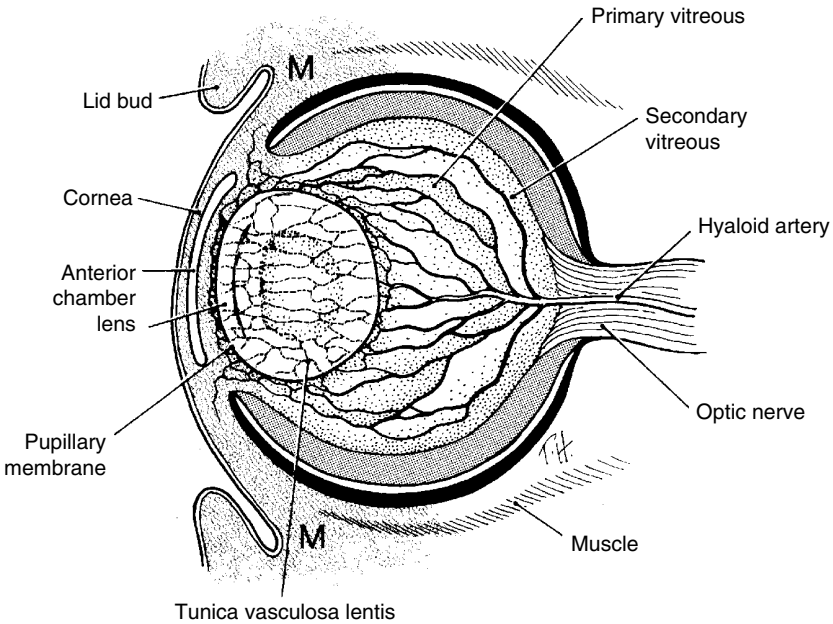

Figure 1.14 The hyaloid vascular system and tunica vasculosa lentis. (Reprinted with permission from Cook, C., Sulik, K.K., & Wright, K.W. (2003) Embryology. In: *Pediatric Ophthalmology and Strabismus* (eds. Wright, K.W. & Spiegel, P.H.), pp. 3–38. New York: Springer.)

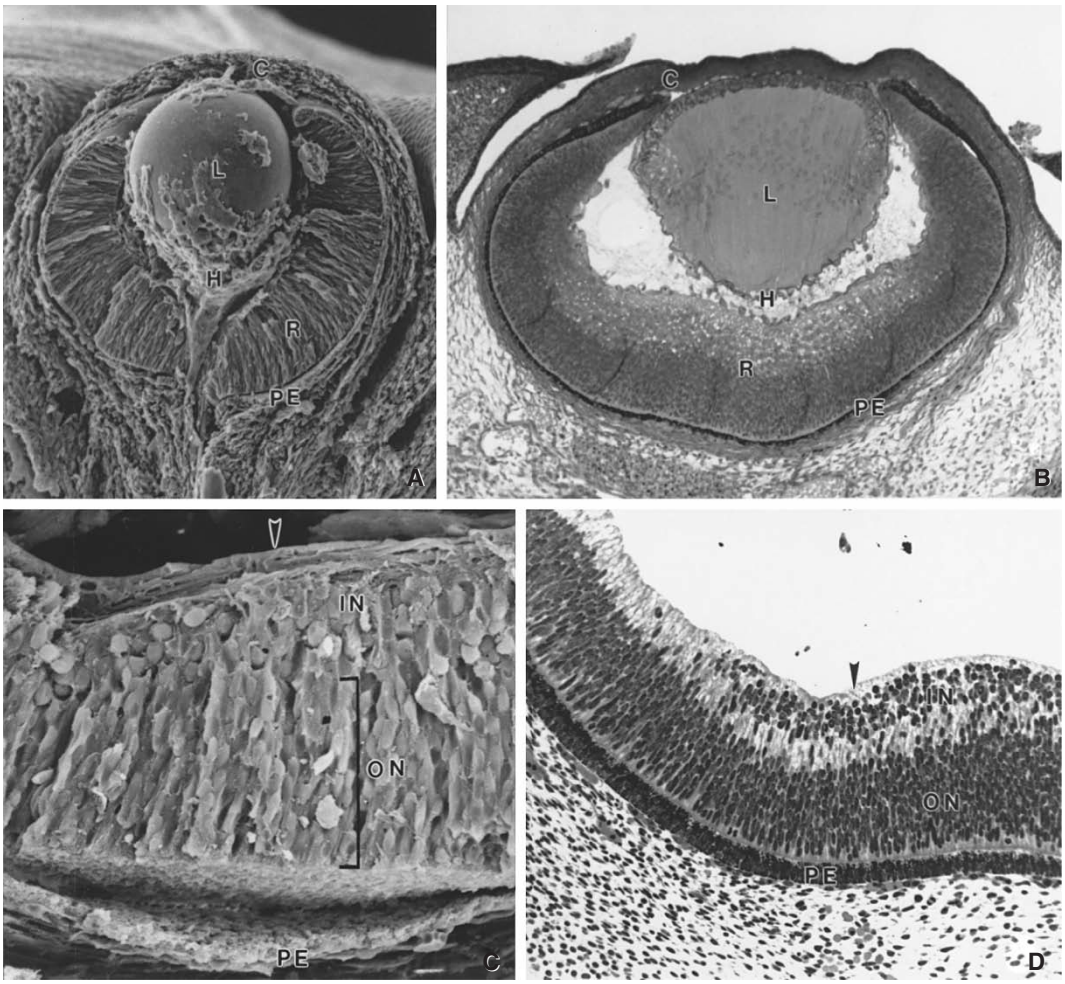

Figure 1.15 **A.** Scanning electron micrograph of a mouse embryo at 14 days of gestation (equivalent to day 32 in the dog). The hyaloid vasculature enters the optic cup through the optic stalk, and it surrounds the lens (L) with capillaries that anastomose with the tunica vasculosa lentis. Axial migration of mesenchyme forms the corneal stroma and endothelium (C). The retina (R) is becoming stratified, whereas the pigment epithelium (PE) remains cuboidal. **B.** The retina becomes stratified into an inner marginal zone and an outer nuclear zone. Note that the inner marginal zone is most prominent in the posterior pole. C, cornea; H, hyaloid artery; L, lens; R, retina. **C.** Segregation of the retina into inner (IN) and outer (ON) neuroblastic layers. The ganglion cells are the first to differentiate, giving rise to the nerve fiber layer (arrowhead). The PE has become artifactually separated in this specimen. **D.** Differentiation of the retina progresses from the central to the peripheral regions. Centrally, the inner (IN) and outer (ON) neuroblastic layers are apparent, with early formation of the nerve fiber layer (arrowhead). Peripherally, however, the retina consists of a single nuclear zone. Between the inner and outer neuroblastic layers is a clear zone, the transient fiber layer of Chievitz. This stage is equivalent to day 32 in the dog. (Panel **A** reprinted with permission from Sulik, K.K. & Schoenwold, G.C. (1985) Highlights of craniofacial morphogenesis in mammalian embryos, as revealed by scanning electron microscopy. *Scanning Electron Microscopy*, **4**, 1735–1752; panel **B** reprinted with permission from Cook, C.S. & Sulik K.K. (1986) Sequential scanning electron microscopic analyses of normal and spontaneously occurring abnormal ocular development in C57B1/6J mice. *Scanning Electron Microscopy*, **3**, 1215–1227; panels **C** and **D** reprinted with permission from Cook, C., Sulik, K.K., & Wright, K.W. (2003) Embryology. In: *Pediatric Ophthalmology and Strabismus* (eds. Wright, K.W. & Spiegel, P.H.), pp. 3–38. New York: Springer.)

TVL reach their maximal development by day 45 in the dog and then begin to regress.

As the peripheral hyaloid vasculature regresses, the retinal vessels develop. Vascular endothelial growth factor (VEGF)-A is a potent angiogenic peptide in the retina; antibody neutralization *in vivo* results in reduction in the hyaloid and retinal vasculature (Feeney et al., 2003). Spindle-shaped mesenchymal cells from the wall of the hyaloid artery at the optic disc form buds (*angiogenesis*) that invade the nerve fiber layer. In contrast, *vasculogenesis* refers to an assembly of dispersed angioblasts into solid cords of mesenchymal cells that later canalize (Fruttiger, 2002; Hughes et al., 2000). Controversy exists as to whether the process of retinal neovascularization occurs primarily through angiogenesis or vasculogenesis (Flower et al., 1985; Fruttiger, 2002; Hughes et al., 2000). Recent studies

indicate that spindle-shaped cells dispersed within the retina, previously thought to be angioblasts, may be immature retinal astrocytes, with retinal vascularization occurring primarily through angiogenesis (Hughes et al., 2000). The primitive capillaries have laminated walls consisting of mitotically active cells secreting basement membrane. Those cells in direct contact with the bloodstream differentiate into endothelial cells; the outer cells become pericytes. Zonulae occludens and gap junctions initially join adjacent cells, but later the capillary endothelium is continuous (Ashton, 1966; Mutlu & Leipold, 1964). The primitive capillary endothelial cells are multipotent and can redifferentiate into fibroblastic, endothelial, or muscle cells, possibly illustrating a common origin for these different tissue types (Ashton, 1966).

Branches of the hyaloid artery become sporadically occluded by macrophages prior to their gradual atrophy (Jack, 1972). Placental growth factor (PlGF) and VEGF appear to be involved in hyaloid regression (Feeney et al., 2003; Martin et al., 2004). Proximal arteriolar vasoconstriction at birth precedes regression of the major hyaloid vasculature (Browning et al., 2001). Atrophy of the pupillary membrane, TVL, and hyaloid artery occurs initially through apoptosis (Ito & Yoshioka, 1999) and later through cellular necrosis (Zhu et al., 2000), and is usually complete by the time of eyelid opening 14 days postnatally.

The clinical lens anomaly known as Mittendorf's dot is a small (1 mm) area of fibrosis on the posterior lens capsule, and it is a manifestation of incomplete regression of the hyaloid artery where it was attached to the posterior lens capsule. Bergmeister's papilla represents a remnant of the hyaloid vasculature consisting of a small, fibrous glial tuft of tissue emanating from the center of the optic nerve. Both are frequently observed as incidental clinical findings.

Development of the Cornea and Anterior Chamber

The anterior margins of the optic cup advance beneath the surface ectoderm and adjacent neural crest mesenchyme after lens vesicle detachment (day 25 in the dog). The surface ectoderm overlying the optic cup (i.e., the presumptive corneal epithelium) secretes a thick matrix, the primary stroma (Hay, 1980; Hay & Revel, 1969). This acellular material consists of collagen fibrils and glycosaminoglycans. Mesenchymal neural crest cells migrate between the surface ectoderm and the optic cup, using the basal lamina of the lens vesicle as a substrate. Proteolysis of collagen IX triggers hydration of the hyaluronic acid, creating the space for cellular migration (Fitch et al., 1998). Initially, this loosely arranged mesenchyme fills the future anterior chamber, and it gives rise to the corneal endothelium and stroma, anterior iris stroma, ciliary muscle, and most structures of the iridocorneal angle (Fig. 1.16A). The presence of an adjacent lens vesicle is required for induction of corneal endothelium, identified by their production of the cell adhesion molecule, n-cadherin (Beebe & Coats, 2000). Type I collagen fibrils and fibronectin secreted by the developing keratocytes form the secondary corneal stroma. Subsequent dehydration results in much of the fibronectin being lost and in a 50% reduction in stromal thickness (Allen et al., 1955; LeDouarin & Teillet, 1974). The endothelium also is important to the dehydration of the stroma. Patches of endothelium become confluent and develop zonulae occludens during days 30–35 in the dog, and during this period Descemet's membrane also forms. The cornea achieves relative transparency at the end of gestation in the dog. Following eyelid opening at approximately 14 days postnatal in the dog, there is an initial decrease in corneal thickness over 4 weeks, presumably as the corneal endothelium become functional. Then, a gradual increase in thickness occurs over the next 6 months (Montiani-Ferreira et al., 2003).

Neural crest migration anterior to the lens to form the corneal stroma and iris stroma also results in formation of a solid sheet of mesenchymal tissue, which ultimately remodels to form the anterior chamber. The portion of this sheet that bridges the future pupil is called the pupillary membrane (Fig. 1.16B, C, and D). Vessels within the pupillary membrane form the TVL, which surrounds and nourishes the lens. These vessels are continuous with those of the primary vitreous (i.e., hyaloid). The vascular endothelium is the only intraocular tissue of mesodermal origin; even the vascular smooth muscle cells and pericytes that originate from mesoderm in the rest of the body are of neural crest origin in the eye (Johnston et al., 1979; Smelser & Ozanics, 1971). In humans, the endothelial lining of Schlemm's canal, like the vascular endothelium elsewhere, is of mesodermal origin. In the dog, atrophy of the pupillary membrane begins by day 45 of gestation and continues during the first two postnatal weeks (Aguirre et al., 1972). Separation of the corneal mesenchyme (neural crest-cell origin) from the lens (surface ectoderm origin) results in formation of the anterior chamber.

In a microphthalmic or nanophthalmic globe, the cornea is correspondingly reduced in diameter. The term *microcornea* is used to describe a cornea that is proportionally smaller than normal for the size of the globe. As with lens induction, determination of the corneal diameter occurs at the time of contact by the optic vesicle with the surface ectoderm. This induction is also sensitive to timing; if the optic vesicle–ectoderm contact occurs earlier or later than normal, the ectoderm may not be fully capable of responding appropriately, resulting in microcornea.

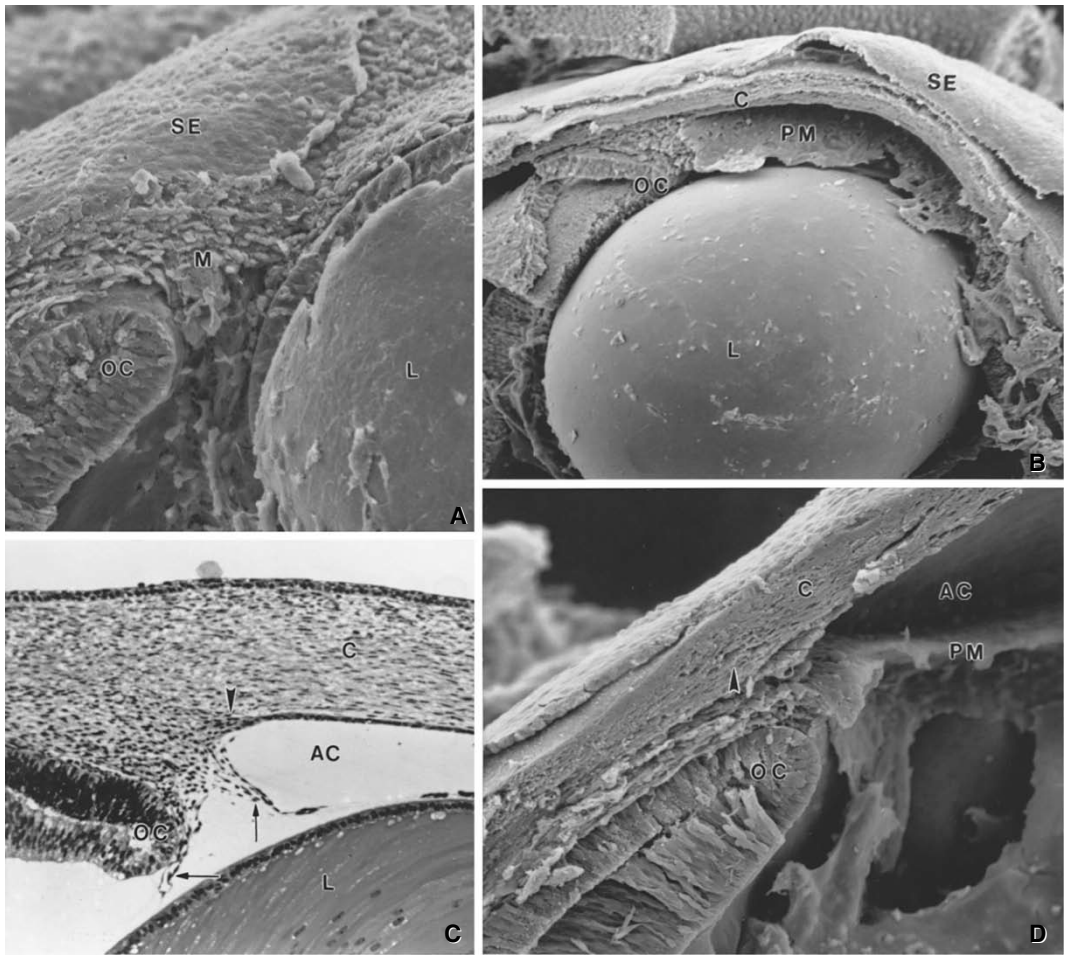

Figure 1.16 **A.** Scanning electron micrograph of a fetal human eye at approximately 42 days of gestation (equivalent to day 25 in the dog). The lens vesicle (L) has detached, and the neural crest–derived mesenchyme (M) is migrating axially between the optic cup (OC) and the surface ectoderm (SE). **B.** On day 54 in the human (day 32 in the dog), the pupillary membrane (PM) is seen within the anterior chamber. The corneal stroma (C) is apparent and is covered by the surface ectoderm (SE), which will become the corneal epithelium. OC, anterior margin of the optic cup, which will form the posterior epithelial layers of the iris, including the pupillary muscles. **C.** Light micrograph obtained at the same stage as in **B** illustrates the pupillary membrane and tunica vasculosa lentis (arrows) originating from the mesenchyme at the margin of the optic cup (OC). The limbal condensation that will become the scleral spur is indicated by the arrowhead. AC, anterior chamber; C, cornea; L, lens. **D.** Scanning electron micrograph of a fetal human eye at approximately 63 days of gestation. The AC is deeper and still bridged by the PM. Endothelialization of clefts within the neural crest–derived corneal stroma (C) by mesoderm will form Schlemm's canal (arrowhead) in the human eye. (Panels **A** and **D** reprinted with permission from Cook, C. (1989) Experimental models of anterior segment dysgenesis. *Ophthalmic Paediatrics and Genetics*, **10**, 33–46; panels **B** and **C** reprinted with permission from Cook, C., Sulik, K.K., & Wright, K.W. (2003) Embryology. In: *Pediatric Ophthalmology and Strabismus* (eds. Wright, K.W. & Spiegel, P.H.), pp. 3–38. New York: Springer.)

Development of the Iris, Ciliary Body, and Iridocorneal Angle

The two layers of the optic cup (neuroectoderm origin) consist of an inner, nonpigmented layer and an outer, pigmented layer. Both the pigmented and nonpigmented epithelium of the iris and the ciliary body develop from the anterior aspect of the optic cup; the retina develops from the posterior optic cup. The optic vesicle is organized with all cell apices directed to the center of the vesicle. During optic cup invagination, the apices of the inner and outer epithelial layers become adjacent. Thus, the cells of the optic cup are oriented apex to apex.

A thin, periodic acid–Schiff-positive basal lamina lines the inner aspect (i.e., vitreous side) of the nonpigmented epithelium and retina (i.e., inner limiting membrane). By approximately day 40 of gestation in the dog, both the pigmented and nonpigmented epithelial cells show apical cilia that project into the intercellular space. There also is increased prominence of Golgi complexes and associated vesicles within the ciliary epithelial cells. These changes, as well as the presence of "ciliary channels" between the

apical surfaces, probably represent the first production of aqueous humor.

The iris stroma develops from the anterior segment mesenchymal tissue (neural-crest cell origin), and the iris pigmented and nonpigmented epithelium originate from the neural ectoderm of the optic cup. The smooth muscle of the pupillary sphincter and dilator muscles ultimately differentiate from these epithelial layers, and they represent the only mammalian muscles of neural ectodermal origin. In avian species, however, the skeletal muscle cells in the iris are of neural crest origin, with a possible small contribution of mesoderm to the ventral portion (Nakano & Nakamura, 1985; Yamashita & Sohal, 1986, 1987).

Differential growth of the optic cup epithelial layers results in folding of the inner layer, representing early anterior ciliary processes (Fig. 1.16B). The ciliary body epithelium develops from the neuroectoderm of the anterior optic cup, and the underlying mesenchyme differentiates into the ciliary muscles. Extracellular matrix secreted by the ciliary epithelium becomes the tertiary vitreous and, ultimately, is thought to develop into lens zonules.

Three phases of iridocorneal angle maturation have been described (Reme et al., 1983a, 1983b). First is separation of anterior mesenchyme into corneoscleral and iridociliary regions (i.e., trabecular primordium formation), followed by differentiation of ciliary muscle and folding of the neural ectoderm into ciliary processes. Second is enlargement of the corneal trabeculae and development of clefts in the area of the trabecular meshwork, which is accompanied by regression of the corneal endothelium covering the angle recess. Third is postnatal remodeling of the drainage angle, associated with cellular necrosis and phagocytosis by macrophages, resulting in opening of clefts in the trabecular meshwork and outflow pathways.

This change in the relationship of the trabecular meshwork to the ciliary body and iris root during the last trimester of human gestation occurs through differential growth, with posterior movement of the iris and the ciliary body relative to the trabecular meshwork exposing the outflow pathways. This results in progressive deepening of the chamber angle and normal conformation of the ciliary muscle and ciliary processes (Anderson, 1981). This is in contrast to previous theories of cleavage of the iris root from the cornea or atrophy of angle tissue (Barishak, 1978; Smelser & Ozanics, 1971; Wulle, 1972).

In species born with congenitally fused eyelids (i.e., dog and cat), development of the anterior chamber continues during this postnatal period before eyelid opening. At birth, the peripheral iris and cornea are in contact. Maturation of pectinate ligaments begins by 3 weeks postnatal and rarefaction of the uveal and corneoscleral trabecular meshworks to their adult state occurs during the first 8 weeks after birth. There is no evidence of mesenchymal splitting, cell death, or phagocytic activity (Samuelson & Gelatt, 1984a, 1984b).

Retina and Optic Nerve Development

Infolding of the neuroectodermal optic vesicle results in a bilayered optic cup with the apices of these two cell layers in direct contact. Primitive optic vesicle cells are columnar, but by 20 days of gestation in the dog, they form an outer cuboidal layer containing the first melanin granules in the developing embryo within the future retinal pigment epithelium (RPE). The neurosensory retina develops from the inner, nonpigmented layer of the optic cup, and the RPE originates from the outer, pigmented layer. Bruch's membrane (the basal lamina of the RPE) is first seen during this time, and becomes well developed over the next week, when the choriocapillaris is developing. By day 45 in the dog, the RPE cells take on a hexagonal cross-sectional shape and develop microvilli that interdigitate with projections from photoreceptors of the nonpigmented (inner) layer of the optic cup.

At the time of lens placode induction, the retinal primordium consists of an outer, nuclear zone and an inner, marginal (anuclear) zone. Cell proliferation occurs in the nuclear zone, with migration of cells into the marginal zone. This process forms the inner and outer neuroblastic layers, separated by their cell processes that make up the transient fiber layer of Chievitz (Fig. 1.15C, D). Cellular differentiation progresses from inner to outer layers and, regionally, from central to peripheral locations. Peripheral retinal differentiation may lag behind that occurring in the central retina by 3–8 days in the dog (Aguirre et al., 1972). Retinal histiogenesis beyond formation of the neuroblastic layers requires induction by a differentiated RPE. There are several rodent models of RPE dysplasia resulting in failure of later retinal differentiation and subsequent degeneration (Bumsted & Barnstable, 2000; Cook et al., 1991b). Retinal ganglion cells develop first within the inner neuroblastic layer, and axons of the ganglion cells collectively form the optic nerve. Cell bodies of the Müller and amacrine cells differentiate in the inner portion of the outer neuroblastic layer. Horizontal cells are found in the middle of this layer; the bipolar cells and photoreceptors mature last, in the outermost zone of the retina (Greiner & Weidman, 1980, 1981, 1982; Spira & Hollenberg, 1973).

Significant retinal differentiation continues postnatally, particularly in species born with fused eyelids. Expression of extracellular matrix elements, chondroitin sulfate, and heparin sulfate occurs in a spatiotemporally regulated manner, with a peak of chondroitin sulfate occurring at the time of eyelid opening, This corresponds to the period of photoreceptor differentiation (Erlich et al., 2003). At birth, the canine retina has reached a stage of development equivalent to the human at 3–4 months of gestation (Shively et al., 1971). In the kitten, all ganglion cells and central retinal cells are present at birth, with continued proliferation in the peripheral retina continuing during the first 2–3 postnatal weeks in dogs and cats (Johns et al., 1979; Shively et al., 1971).

Possible means of retinal regeneration have become reality with the discovery of neural stem cells in the mature eye of warm-blooded vertebrates (Engelhardt et al., 2004; Fischer, 2005). These include cells at the retinal margin, pigmented cells in the ciliary body and iris, nonpigmented cells in the ciliary body, and Müller glia within the retina. Under the influence of growth factors, these neuroectodermal cells in the avian are capable of undergoing differentiation into retinal cells (Fischer, 2005).

Sclera, Choroid, and Tapetum

These neural crest–derived tissues are all induced by the outer layer of the optic cup (future RPE). Normal RPE differentiation is a prerequisite for normal development of the sclera and choroid. The choroid and sclera are relatively differentiated at birth, but the tapetum in dogs and cats continues to develop and mature during the first 4 months postnatally. The initially mottled, blue appearance of the immature tapetum is replaced by the blue/green to yellow/orange color of the adult. These color variations seen in immature dogs can prove a challenge to accurate funduscopic assessment.

Posterior segment uveoscleral colobomas most often result from a primary RPE abnormality. Subalbinotic animals have a higher incidence of posterior segment colobomas, with reduced RPE pigmentation being a marker for abnormal RPE development (Bertram et al., 1984; Cook et al., 1991a; Gelatt & McGill, 1973; Gelatt & Veith, 1970; Munyard et al., 2007; Rubin et al., 1991). The most common example is the choroidal hypoplasia of Collie eye anomaly (Barnett, 1979).

Vitreous

The primary vitreous forms posteriorly, between the primitive lens and the inner layer of the optic cup (see Fig. 1.10 and Fig. 1.12). In addition to the vessels of the hyaloid system, the primary vitreous also contains mesenchymal cells, collagenous fibrillar material, and macrophages. The secondary vitreous forms as the fetal fissure closes, and contains a matrix of cellular and fibrillar material, including primitive hyalocytes, monocytes, and hyaluronic acid (Akiya et al., 1986; Bremer & Rasquin, 1998). Identification of microscopic vascular remnants throughout the vitreous of adult rabbits has led to speculation for interactive remodeling of the primary vitreous to form secondary vitreous (Los et al., 2000a, 2000b). Plasma proteins enter and leave the vitreous and, in the chick, there is a concentration of 13% of that found in plasma, until a decline to 4% of plasma levels occurs during the last week prior to hatching (Beebe et al., 1986). Primitive hyalocytes produce collagen fibrils that expand the volume of the secondary vitreous.

The tertiary vitreous forms as a thick accumulation of collagen fibers between the lens equator and the optic cup. These fibers are called the marginal bundle of Drualt or Drualt's bundle. Drualt's bundle has a strong attachment to the inner layer of the optic cup, and it is the precursor to the vitreous base and lens zonules. The early lens zonular fibers appear to be continuous with the inner, limiting membrane of the nonpigmented epithelial layer covering the ciliary muscle. Elastin and emulin (elastin microfibril interface located protein) have been identified in developing zonules and Descemet's membrane (Bressan et al., 1993; Horrigan et al., 1992). Experimental exposure of chick embryos to homocysteine results in deficient zonule development and congenital lens luxation (Maestro De Las Casas et al., 2003). Traction of the zonules contributes to expansion of the lens and localized absence of zonules can lead to a corresponding area of the lens that is flattened and inaccurately referred to as a lens coloboma (see later Fig. 1.32).

Atrophy of the primary vitreous and hyaloid leaves a clear, narrow central zone, which is called Cloquet's canal. In the mouse, Doppler ultrasound biomicroscopy has been used to document *in vivo* the decrease in blood velocity associated with hyaloid regression between birth and postnatal day 13 (Brown et al., 2005). Most of the posterior vitreous gel at birth is secondary vitreous, with the vitreous base and zonules representing tertiary vitreous.

Optic Nerve

Axons from the developing ganglion cells pass through vacuolated cells from the inner wall of the optic stalk. A glial sheath forms around the hyaloid artery. As the hyaloid artery regresses, the space between the hyaloid artery and the glial sheath enlarges. Bergmeister's papilla represents a remnant of these glial cells around the hyaloid artery. Glial cells migrate into the optic nerve and form the primitive optic disc. The glial cells around the optic nerve and the glial part of the lamina cribrosa come from the inner layer of the optic stalk, which is of neural ectoderm origin. Later, a mesenchymal (neural crest origin) portion of the lamina cribrosa develops. Myelinization of the optic nerve begins at the chiasm, progresses toward the eye, and reaches the optic disc after birth.

Eyelids

The eyelids develop from surface ectoderm, which gives rise to the epidermis, cilia, and conjunctival epithelium. Neural crest mesenchyme gives rise to deeper structures, including the dermis and tarsus. The eyelid muscles (i.e., orbicularis and levator) are derived from craniofacial condensations of mesoderm called somitomeres. In the craniofacial region, presumptive connective tissue–forming mesenchyme derived from the neural crest imparts spatial patterning information

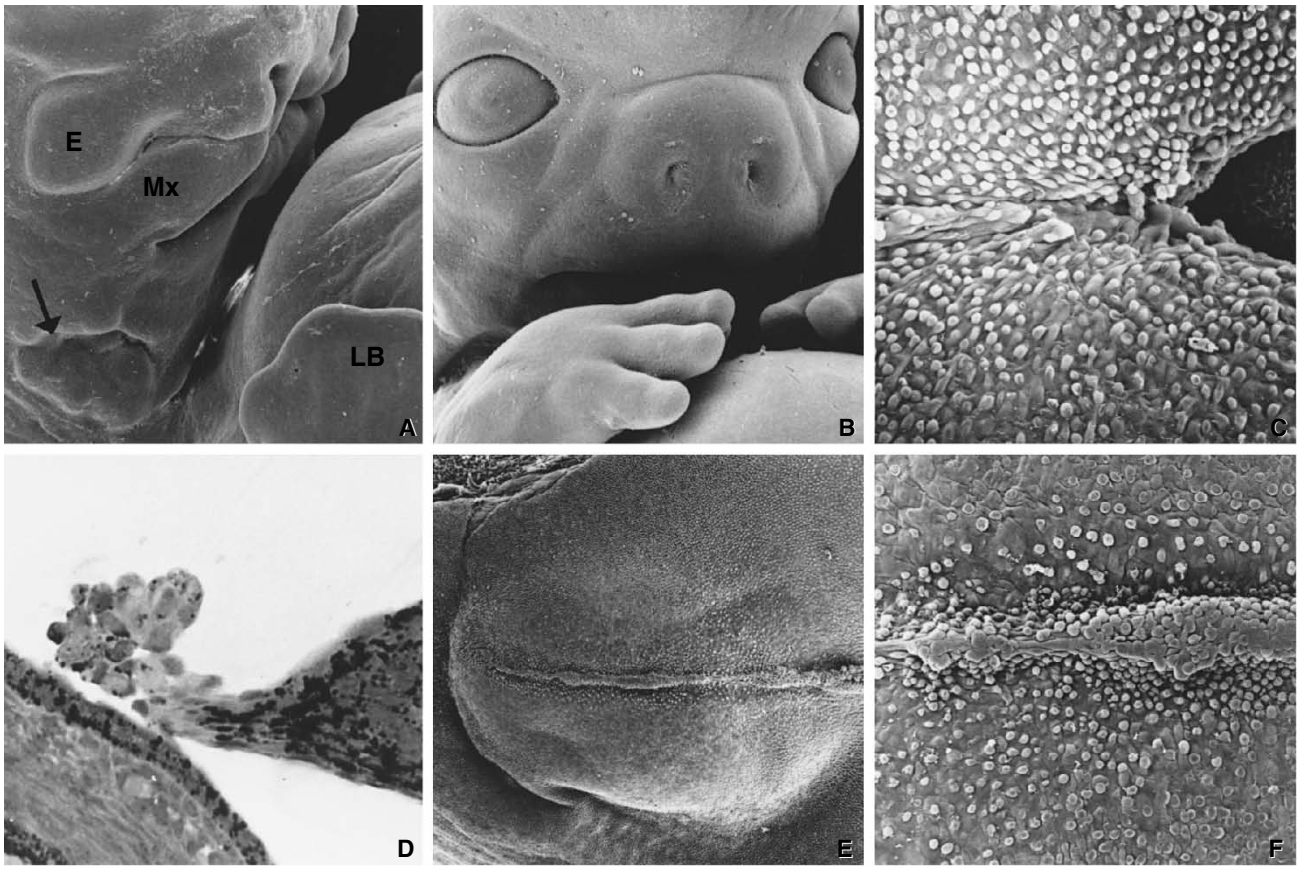

Figure 1.17 **A.** Lateral view of the head of a human embryo at 6 weeks of gestation. The individual hillocks that will form the external ear can be identified both cranial and caudal to the first visceral groove (arrow). The developing eye is adjacent to the maxillary prominence (Mx). LB, forelimb bud. **B.** Frontal view of the head of a human embryo at 8 weeks of gestation. Formation of the face is largely complete, and the eyelids are beginning to close. **C.** Eyelid closure begins at the medial and lateral canthi and progresses axially. **D.** Light micrograph of the eyelid marginal epithelium in a mouse at day 15 of gestation. The actively migrating epithelium forms a cluster of cells adjacent to the corneal epithelium. **E** and **F.** Surface view of the fused eyelids from a human embryo at 10 weeks of gestation. (Panels **A**, **B**, **E**, and **F** reprinted with permission from Sulik, K.K. & Schoenwolf G.C. (1985) Highlights of craniofacial morphogenesis in mammalian embryos, as revealed by scanning electron microscopy. *Scanning Electron Microscopy*, **4**, 1735–1752; panel **D** reprinted with permission from Cook, C.S. & Sulik, K.K. (1986) Sequential scanning electron microscopic analyses of normal and spontaneously occurring abnormal ocular development in C57B1/6J mice. *Scanning Electron Microscopy*, **3**, 1215–1227.)

upon myogenic cells that invade it (Noden, 1986). The upper eyelid develops from the frontonasal process; the lower eyelid develops from the maxillary process. The lid folds grow together and elongate to cover the developing eye (Fig. 1.17). The upper and lower lids fuse on day 32 of gestation in the dog. Separation occurs 2 weeks postnatally.

Extraocular Muscles

The extraocular muscles arise from mesoderm in somitomeres (i.e., preoptic mesodermal condensations; Jacobson, 1988; Meier, 1982; Meier & Tam, 1982; Packard & Meier, 1983; Tam, 1986; Tam et al., 1982; Tam & Trainor, 1994; Trainor & Tam, 1995). Spatial organization of developing eye muscles is initiated before they interact with the neural crest mesenchyme. Patterning of the segmental somitomeres follows that of the neural crest; that is, somitomere I (forebrain), somitomere III (caudal midbrain), and somitomeres IV and VI (hindbrain; Trainor & Tam, 1995). From studies of chick embryos, it has been shown that the oculomotor-innervated muscles originate from the first and second somitomeres, the superior oblique muscle from the third somitomere, and the lateral rectus muscle from the fourth somitomere (Wahl et al., 1994). The entire length of these muscles appears to develop spontaneously rather than from the orbital apex anteriorly, as had been previously postulated (Sevel, 1981, 1986). Congenital extraocular muscle abnormalities are rarely identified and reported in the dog (Martin, 1978). This may be a result of several factors, including the fact that the extraocular muscles are normally less well developed in domestic mammals compared with humans,

and the limited ability to assess minor abnormalities which would be manifest as impaired binocular vision.

Developmental Ocular Anomalies

Cyclopia and Synophthalmia

Formation of a single median globe (i.e., cyclopia) or two incompletely separated or fused globes (i.e., synophthalmia) may occur by two different mechanisms. The "fate maps," which have been produced for amphibian embryos, have revealed the original location of the neural ectodermal tissue that will form the globes as a single, bilobed area crossing the midline in the anterior third of the trilaminar embryonic disc. An early defect in separation of this single field could result in the formation of a single, or incompletely separated, median globe(s) (Fig 1.18A). After separation into bilateral optic vesicles, later loss of the midline territory in the embryo could result in fusion of the ocular fields. This loss of midline territory, prior to separation into two eye fields, is seen in holoprosencephaly, and the facial features characteristic of human fetal alcohol syndrome represent a mild end of the holoprosencephalic spectrum (Cohen & Sulik, 1992; Sulik & Johnston, 1982). Cases of cyclopia or synophthalmia are invariably associated with severe craniofacial malformations (Fig. 1.18A and B) and are usually nonviable.

Cyclopia is rarely identified in dogs (Njoku et al., 1978). However, in sheep, ingestion of the alkaloids (cyclopamine and jervine) from the weed *Veratrum californicum* by pregnant ewes on day 14 of gestation (total duration of gestation 150 days) is the best-documented example of teratogen-induced cyclopia and synophthalmia in domestic animals (Binns et al., 1959; Bryden et al., 1971; Cooper et al., 1998; Incardona et al., 1998; Keeler, 1990; Keeler & Binns, 1966; Saperstein, 1975). It has been shown that cyclopamine specifically blocks the Sonic hedgehog (Shh) signaling pathway (Cooper et al., 1998; Incardona et al., 1998, 2000). The specific timing for veratrum-induced cyclopia in sheep corresponds to the period of gastrulation and formation of the neural plate before separation of the optic fields. Exposure to the alkaloid earlier in gestation results in fetal death; later exposure causes skeletal malformation or has no effect, thus demonstrating the importance of narrow, sensitive periods in development.

Figure 1.18 **A.** Cyclopia in a Holstein calf, etiology unknown. Note the single median globe, palpebral fissure, cornea, and pupil. **B.** Cyclopia in a nonviable kitten. Note the narrow forebrain and midface regions. The limbs and axial skeleton are relatively normal, demonstrating limited effect on the forebrain region of the embryo. (Panel **A** courtesy of Brian Wilcock.)

Microphthalmia and Anophthalmia

Microphthalmia can occur early in development through a deficiency in the optic vesicle (Fig. 1.19A), or later through failure of normal growth and expansion of the optic cup (Fig. 1.19B). An early deficiency in the size of the globe as a

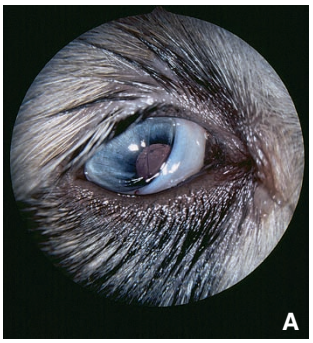

Figure 1.19 **A.** Microphthalmia and persistent pupillary membranes in a Chow Chow puppy. Note that the size of the palpebral fissure is proportional to the reduced size of the globe as a whole. This is consistent with microphthalmia induced at the optic vesicle stage. **B.** Microphthalmia induced at a later stage of gestation, possibly by delayed closure of the optic fissure, although this eye does not exhibit a coloboma. Note the larger size of the palpebral fissure relative to the small globe.

whole is often associated with a correspondingly small, palpebral fissure. The fissure size is determined by the optic vesicle size during its contact with the surface ectoderm, so this supports a malformation sequence beginning at formation of the optic sulcus, optic vesicle, or earlier. Results from studies of teratogen-induced ocular malformations have been helpful in identifying sensitive developmental periods. Acute exposure to teratogens before optic sulcus formation results in an overall deficiency of the neural plate, with subsequent reduction in the optic vesicle size. When microphthalmia originates during development of the neural plate/optic sulcus, it is often associated with multiple ocular malformations, including anterior segment dysgenesis, cataract, retinal dysplasia, and persistence of the hyaloid (Table 1.3).

Later initiation of microphthalmia can occur through failure to establish early IOP (Berman & Pierro, 1969; Hero et al., 1991). Placement of a capillary tube into the vitreous cavity of the embryonic chick eye reduces the IOP and markedly slows growth of the eye (Coulombre, 1956). Histologic examination of the intubated eyes demonstrates a proportional reduction in the size of all ocular tissues except the neural retina and the lens, which are normal in size for the age of the eye. The retina in these eyes is highly convoluted, filling the small posterior segment. Thus, it has been concluded that growth of the neural retina occurs independent of the other ocular tissues. Experimental removal of the lens does not alter retinal growth (Coulombre & Coulombre, 1964). Growth of the choroid and sclera appears to depend on IOP, as does folding of the ciliary epithelium (Bard et al., 1975; Cook, 1989, 1995; Cook & Sulik, 1988). Thus, failure of fusion of the optic fissure can result in microphthalmia and associated malformations (i.e., colobomatous microphthalmia). A delay in closure of this fissure during a critical growth period may result in inadequate globe expansion as well. If the fissure eventually closes, however, it may be difficult to distinguish between colobomatous and noncolobomatous microphthalmia. If the optic vesicle develops normally before abnormal (delayed) closure of the optic fissure, the palpebral fissure may not be reduced in size as much as the globe as a whole is reduced (Fig. 1.19B). In most cases, microphthalmia occurs through a combination of cellular deficiency within the optic vesicle/cup compounded by failure of the optic fissure to close on schedule.

Table 1.3 Anomalies associated with microphthalmia in dogs.

Anomaly	Breed	References
Anterior segment dysgenesis	Saint Bernard, Doberman	Arnbjerg & Jensen (1982); Bergsjo et al. (1984); Boroffka et al. (1998); Lewis et al. (1986); Martin & Leipold (1974); Peiffer & Fischer (1983); Stades (1980, 1983); van der Linde-Sipman et al. (1983)
Cataract	Old English Sheepdog	Barrie et al. (1979)
	Akita	Laratta et al. (1985)
	Miniature Schnauzer	Gelatt et al. (1983); Samuelson et al. (1987); Zhang et al. (1991)
	Chow Chow	Collins et al. (1992)
	Cavalier King Charles Spaniel	Narfstrom & Dubielzig (1984)
	English Cocker Spaniel	Strande et al. (1988)
	Irish Wolfhound	Kern (1981)
Retinal dysplasia	Saint Bernard	Martin & Leipold (1974)
	Doberman	Arnbjerg & Jensen (1982); Bergsjo et al. (1984); Lewis et al. (1986); Peiffer & Fischer (1983)

Anophthalmia represents an extreme on the spectrum of microphthalmia. In most cases, careful examination of the orbital contents will reveal primitive ocular tissue (i.e., actual microphthalmia). True anophthalmia results from a severe developmental deficiency in the primitive forebrain, at a stage before optic sulcus formation. This usually results in a nonviable fetus.

Microphthalmia in domestic animals occurs sporadically and is associated with multiple malformations (Table 1.3), including anterior segment dysgenesis, cataract, persistent hyperplastic primary vitreous (Bayon et al., 2001; Boeve et al., 1992; van der Linde-Sipman et al., 1983), and retinal dysplasia (Bayon et al., 2001; Bertram et al., 1984). In the Doberman Pinscher, microphthalmia, anterior segment dysgenesis, and retinal dysplasia are thought to be inherited as autosomal recessive traits (Bergsjo et al., 1984). Inherited microphthalmia in Texel sheep has as its primary event abnormal development with involution of the lens vesicle followed by proliferation of dysplastic mesenchyme, which develops into cartilage, smooth muscle, fat, and lacrimal gland (van der Linde-Sipman et al., 2003).

A similar spectrum of multiple ocular malformations has been described as a presumably inherited condition associated with central nervous system malformations in Angus (Rupp & Knight, 1984), Shorthorn (Greene & Leipold, 1974), and Hereford cattle (Blackwell & Cobb, 1959; Kaswan et al., 1987), as well as in nondomestic species, including raptors (Buyukmihci et al., 1988), camel (Moore et al., 1999), and white-tailed deer (Wyand et al., 1972). Colobomatous microphthalmia is initiated later in gestation.

In swine, congenital microphthalmia has been historically reported to be associated with maternal vitamin A deficiency (Hale, 1935; Manoly, 1951; Roberts, 1948). Conversely, maternal excess of vitamin A and its analogue, retinoic acid, has been demonstrated (Bayon et al., 2001) to result

in teratogenic ocular and craniofacial malformations in humans and laboratory animals (Cook, 1989; Cook & Sulik, 1988, 1990; Mulder et al., 2000).

Colobomatous Malformations

A coloboma refers broadly to any congenital (present at birth) tissue defect. Ocular colobomas most frequently involve the vascular tunic of the eye, namely the iris and choroid. The spectrum encompasses minor defects (i.e., dyscoria) as well as major defects (i.e., aniridia). Aniridia occurs rarely in animals (Irby & Aguirre, 1985; Saunders & Fincher, 1951), but is seen as a malformation in humans associated with genetic syndromes including Rieger syndrome (*PITX2* gene; Perveen et al., 2000) and *PAX6* gene mutations (Sonoda et al., 2000). The iris stroma develops from neural crest mesenchyme induced by the bilayered epithelium of the anterior optic cup. Thus, a complete and full-thickness defect in the iris most likely results from incomplete axial expansion of the anterior optic cup. Iris hypoplasia represents the mild spectrum of this type of coloboma and is seen frequently in dogs (particularly those breeds characterized by subalbinism) and has been recognized as a genetic syndrome in horses (Ewart et al., 2000).

The classic explanation for localized colobomatous malformations involves failure of the optic fissure to close. Such failure may result in secondary "colobomatous" microphthalmia (Fig. 1.20) and, in experimental models, there may be deviation of the fissure by 90° or more. When defects are located in any inferior location (particularly in a small globe), this is the most likely explanation. This defect in closure of the optic fissure (future RPE and ciliary and iris epithelium) results in failure of induction of the adjacent choroid and sclera. Any or all of these layers may be affected. The clinically apparent sequella to abnormal fissure closure may be only a subtle degree of dyscoria (Matsuura et al., 2013).

Figure 1.20 Microphthalmia and an inferior coloboma of the scleral and uveal tissue allowing vitreous prolapse into the subconjunctival space. In colobomatous microphthalmia, globe expansion is impaired by the inability to establish intraocular pressure because of the optic fissure failing to close. Both mechanisms of microphthalmia may occur in a single eye.

Many colobomatous defects, however, occur in other locations (Briziarelli & Abrutyn, 1975; Gelatt et al., 1969; Gwin et al., 1981). Differentiation of the neural crest–derived stroma of the choroid and iris is determined by the adjacent structures of the outer layer of the optic cup: anteriorly the iris and ciliary epithelium, and posteriorly the RPE. In sequential analyses of animals exhibiting primary abnormalities in differentiation of the outer layer of the optic cup, anterior and posterior segment colobomas are associated with uveal epithelium/RPE defects (Cook et al., 1991a, 1991b; Zhao & Overbeek, 2001).

Prenatal studies of colobomas in the Australian Shepherd dog have demonstrated a primary defect in the RPE, resulting in hypoplasia of the adjacent choroid and sclera (Fig. 1.21 and Fig. 1.22; Cook et al., 1991a). This condition is referred to as merle ocular dysgenesis (MOD) because of the correlation with the merle coat coloration (Bertram et al., 1984). A similar spectrum has been identified in cattle (Gelatt et al., 1969), Great Dane dogs, and cats (Gwin et al., 1981) exhibiting incomplete albinism. It is likely that the subalbinism is associated with abnormal RPE that fails to induce the overlying neural crest.

Choroidal hypoplasia in the Collie dog (i.e., "Collie eye anomaly" or CEA; Barnett, 1979) may represent a malformation sequence similar to that of MOD (Fig. 1.23 and Fig. 1.24). Differences between CEA and MOD are illustrated in Table 1.4. CEA has been widely described in the Collie, Border Collie, Shetland Sheepdog, and Australian Shepherd (Barnett, 1979; Barnett & Stades, 1979; Bedford, 1982a; Rubin et al., 1991). Variations of this congenital malformation, including scleral ectasia, sporadically occur in other breeds as well (Bedford, 1998). It has been demonstrated that choroidal hypoplasia associated with CEA segregates as an autosomal recessive trait with nearly 100% penetrance (Lowe et al., 2003).

Optic nerve coloboma as an isolated finding is likely caused by localized failure of closure of the optic fissure that begins to close at the level of the disc with progression anterior and posterior. Optic nerve coloboma is seen unassociated with genetically identifiable CEA mutation NHEJ1 in the Nova Scotia Duck Tolling Retriever (Brown et al., 2018).

Dermoid

The presence of aberrant tissue (e.g., skin, cartilage, bone) within the orbit may originate early in development through abnormal differentiation of an isolated group of cells. Arrest or inclusions of epidermal and connective tissues (i.e., surface ectoderm and neural crest) may occur during closure of

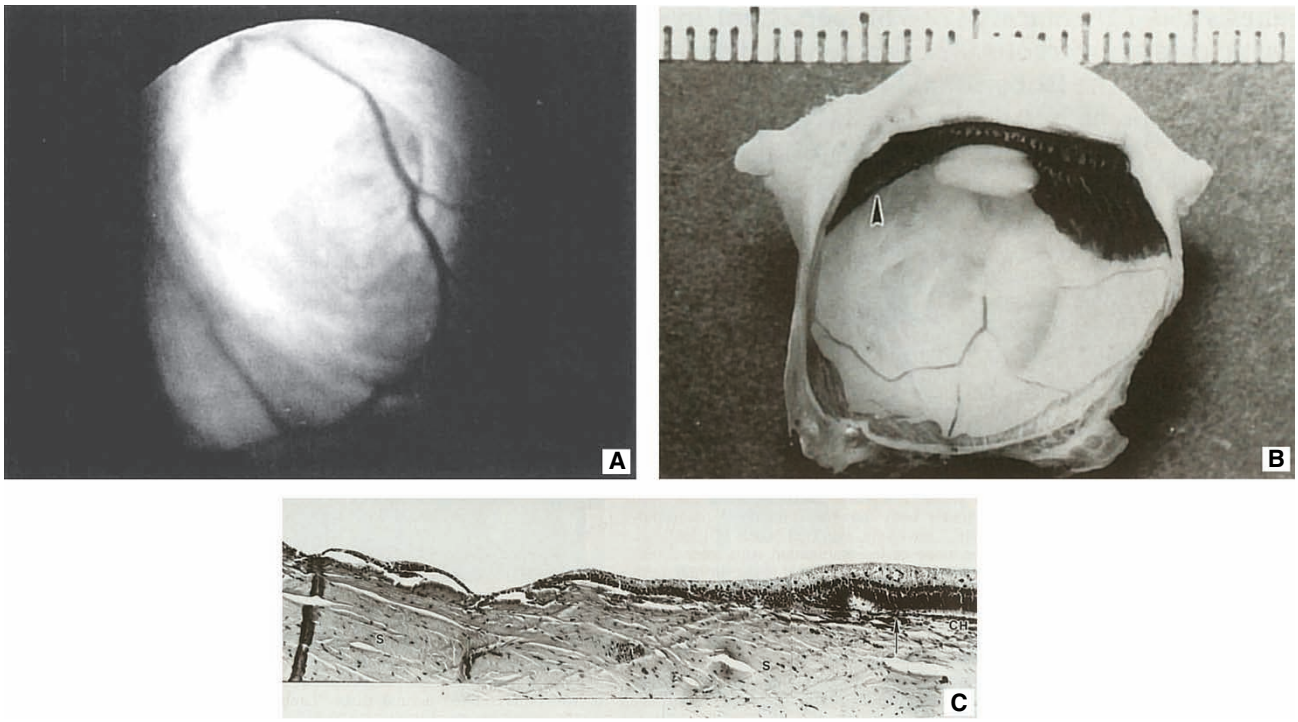

Figure 1.21 Clinical (**A**) and gross (**B**) photographs of the ocular fundus of an adult Australian Shepherd dog affected with merle ocular dysgenesis. Note the large excavation of the equatorial posterior segment. There is also a defect in the ciliary body (arrowhead), which was not apparent clinically. **C.** At the light microscopic level, defects such as this consist of a thin layer of sclera (S) lined by a glial membrane. Note the abrupt transition from normal retina, retinal pigment epithelium (RPE), and choroid seen on the right to the sudden loss of RPE and choroid at the level indicated by the arrow. (Reprinted with permission from Cook, C., Burling, K., & Nelson E. (1991) Embryogenesis of posterior segment colobomas in the Australian Shepherd dog. *Progress in Veterinary & Comparative Ophthalmology*, **1**, 163–170.)

the fetal clefts. Abnormal invagination of ectodermal tissue later in gestation may result in a pocket of well-differentiated dermal tissue. Eyelid dermoids may occur though isolation of an island of ectoderm later forming a nodule of tissue that is, strictly speaking, not abnormal in location, but in configuration, a nonneoplastic overgrowth of tissue disordered in structure (Fig. 1.25). These are termed *hamartomas* (i.e., benign tissue mass resulting from faulty development). Limbal dermoids represent *choristomas* (i.e., mass formed by tissue not normally found at this site; Fig. 1.26). Both eyelid epidermis and corneal epithelium originate from surface ectoderm, following induction by the optic vesicle, and there appears to be a narrow period during which the surface ectoderm can respond to inductive influences to produce a normal lens. The same may be true for induction of the cornea. Dermoids are seen in all species as an incidental finding, and they are seen as an inherited condition in cattle and some dog breeds (Adams et al., 1983; Barkyoumb & Leipold, 1984).

Anterior Segment Dysgenesis

The anterior segment dysgeneses identified in humans encompass a broad range of malformations, including Peters' anomaly, Axenfeld–Rieger syndrome, iridocorneal endothelium syndrome, posterior polymorphous dystrophy, and Sturge–Weber syndrome. Similar anomalies have been described in domestic animals, generally as sporadic occurrences (Irby & Aguirre, 1985; Peiffer, 1982; Rebhun, 1977; Swanson et al., 2001). Anterior segment dysgenesis is often associated with microphthalmia (Arnbjerg & Jensen, 1982; Bergsjo et al., 1984; Lewis et al., 1986; Martin & Leipold, 1974; Peiffer & Fischer, 1983).

In domestic animals, *persistent pupillary membranes* represent the most common manifestation of anterior segment dysgenesis. In the embryo, the pupillary membrane forms a solid sheet of tissue that is continuous with the iris at the level of the collarette (see Fig. 1.19). Regression occurs during the first two postnatal weeks, before eyelid opening in the dog. Persistence of some pupillary membrane strands was noted in 0.7% of 575 Beagles aged from 16 to 24 weeks (Bellhorn, 1974). Inherited persistent pupillary membranes occur in the Basenji dog (Bistner et al., 1971; Roberts & Bistner, 1968), and they may be associated with corneal or lens opacities (or both) at the site of membrane attachments. Complete persistence of a sheet of tissue bridging the pupil is rare and results in visual impairment. Persistent pupillary

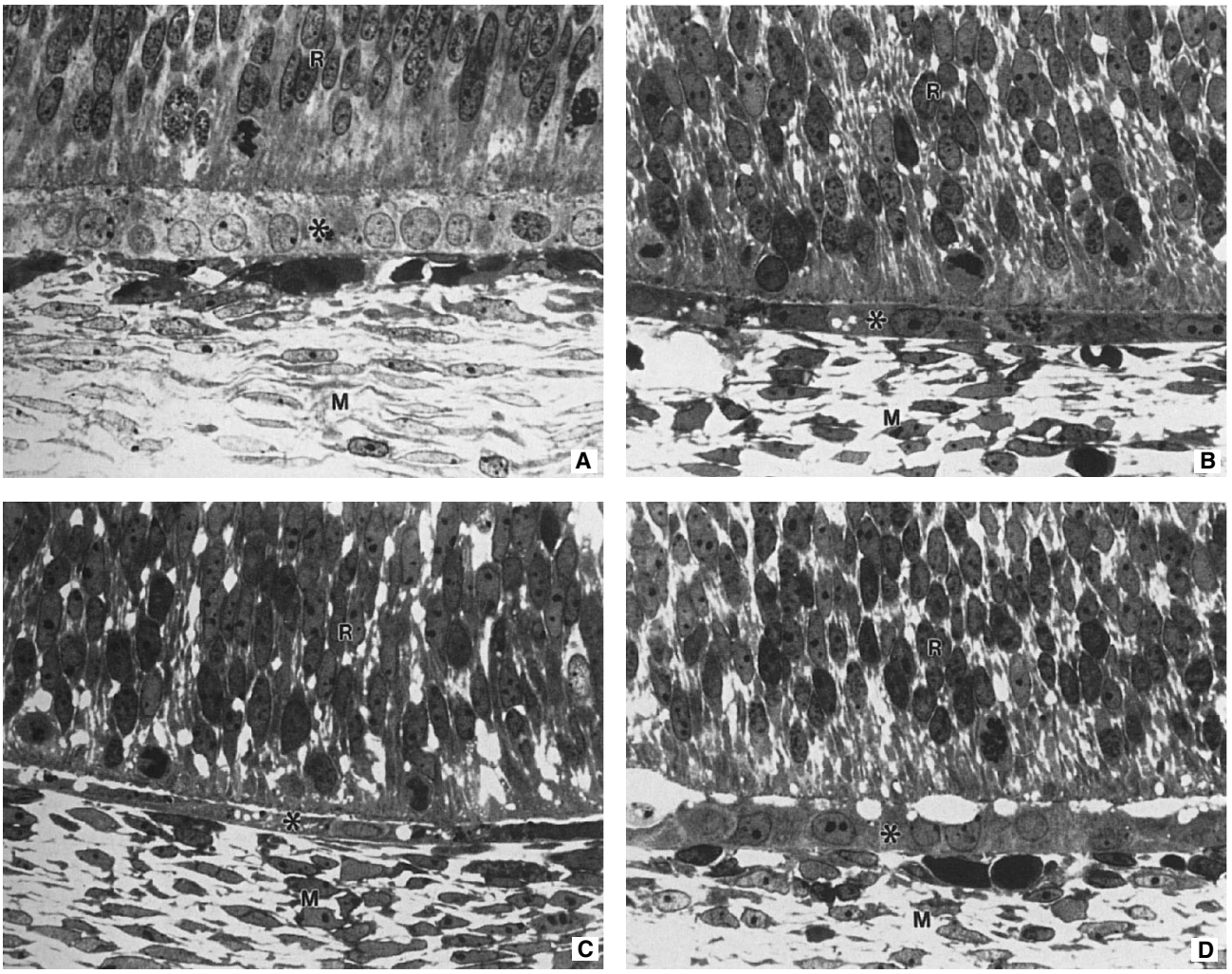

Figure 1.22 Sequential histology of merle ocular dysgenesis (MOD). **A.** Normal canine eye on day 30 of gestation. Note the cuboidal appearance of the nonpigmented retinal pigment epithelium (RPE; ·), which is closely apposed to the neural retina (R). The nuclei closest to the RPE are those of the outer neuroblastic layer. M, periocular mesenchyme—anlage of the choroid and sclera. **B.** MOD-affected eye on day 35 of gestation. The RPE (·) is shortened and contains a few intracytoplasmic vacuoles. **C** and **D.** MOD-affected eye on day 35 of gestation. The RPE (·) has become progressively thinner and exhibits a large number of vacuoles. Separation of the degenerating RPE from the neural retina also can be seen. (Reprinted with permission from Cook, C., Burling, K., & Nelson, E. (1991) Embryogenesis of posterior segment colobomas in the Australian shepherd dog. *Progress in Veterinary & Comparative Ophthalmology*, **1**, 163–170.)

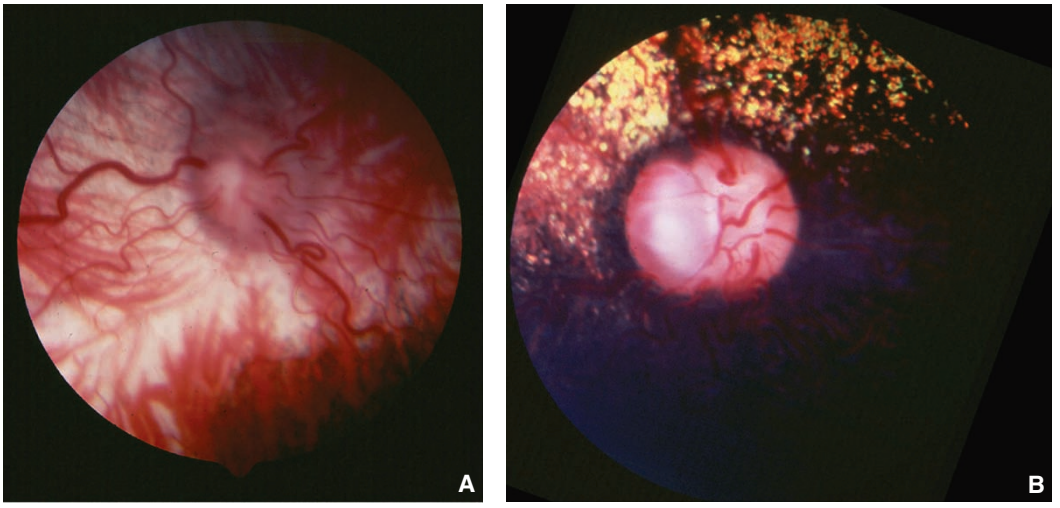

Figure 1.23 **A.** Fundus photograph of choroidal hypoplasia associated with Collie eye anomaly. Note the white sclera with superimposed choroidal and retinal vasculature. **B.** Optic nerve coloboma in a Collie affected with Collie eye anomaly. The coloboma is located temporally adjacent to an area of mild choroidal hypoplasia (identified by absence of tapetum and visible choroidal vasculature).

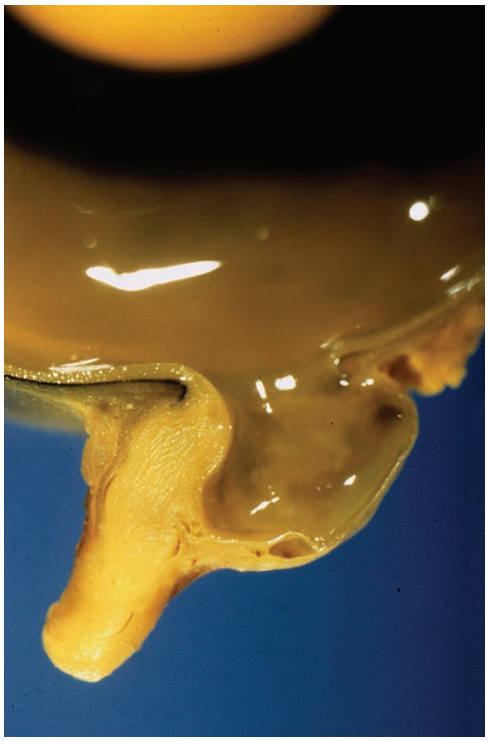

Figure 1.24 Gross photograph of an optic nerve coloboma in a Collie. Note the excavation of thinned sclera lined by glial tissue (neuroectoderm) continuous with retina. (Reprinted with permission from Wilcock, B. (2007) *Pathologic Basis of the Veterinary Disease*, 4th ed. (eds. McGavin, M.D. & Zachary, J.F.). St. Louis, MO: Elsevier.)

Table 1.4 Comparative features of merle ocular dysgenesis and Collie eye anomaly.

	Merle Ocular Dysgenesis	Collie Eye Anomaly
Coat color	Homozygous merle	No correlation
Microphthalmia	Frequent	Rare/mild
Choroidal hypoplasia	Extensive scleral/ retinal defects	Common, localized
Optic nerve coloboma	Rare	Frequent
Cataract	Frequent	Rare
Iris coloboma	Frequent	Rare

Reprinted with permission from Cook, C., Burling, K., & Nelson, E. (1991) Embryogenesis of posterior segment colobomas in the Australian Shepherd dog. *Progress in Veterinary & Comparative Ophthalmology*, **1**, 163–170.

membranes also occur sporadically in other breeds (Strande et al., 1988).

Because most structures of the ocular anterior segment are of neural crest origin, it is tempting in cases of anterior segment anomalies to incriminate this cell population as being abnormal in differentiation, migration, or both. This

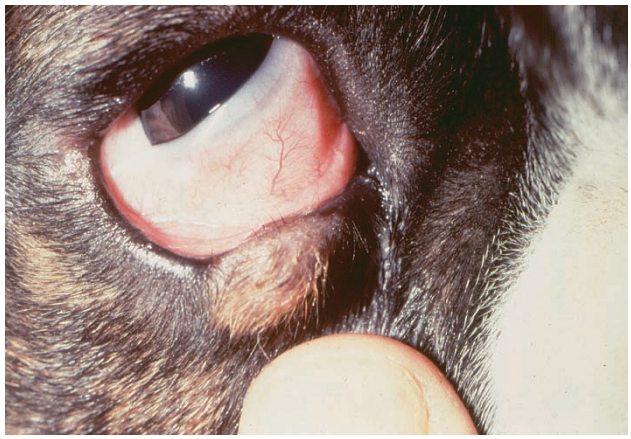

Figure 1.25 Eyelid dermoid in a Boxer dog. The tissue is histologically normal skin in a grossly normal location, but abnormal in configuration, representing a hamartoma. (Courtesy of Robert Peiffer.)

Figure 1.26 Limbal dermoid in a Lhasa Apso puppy. This is an example of a choristoma (histologically normal tissue in an abnormal location).

theory has resulted in labeling these conditions, when they occur in humans, as ocular neurocristopathies, particularly when other anomalies exist in tissues that are largely derived from the neural crest (e.g., craniofacial connective tissue, teeth; Bahn et al., 1984; Kupfer et al., 1975; Kupfer & Kaiser-Kupfer, 1978; Shields et al., 1985; Waring et al., 1975). When considering this theory, it is important to realize two concepts. First, the neural crest is the predominant cell population of the developing craniofacial region, particularly the eye. In fact, the list of ocular tissues *not* derived from neural crest is relatively small (see Table 1.2). Thus, the fact that most malformations of this region involve crest tissues may reflect their ubiquitous distribution rather than their common origin. The normal development of the choroid and sclera (also of neural crest origin) in most of these "neural crest syndromes" argues against a primary neural crest anomaly. Second, the neural crest is an actively migrating

population of cells and can be easily influenced by adjacent cell populations. Thus, the perceived anomaly of neural crest tissue may, in many cases, be a secondary effect.

Much of the maturation of the iridocorneal angle occurs late during gestation and during early postnatal life in the dog, but earlier events may influence development of the anterior segment. Anterior segment dysgenesis syndromes characterized primarily by axial defects in corneal stroma and endothelium, accompanied by corresponding malformations in the anterior lens capsule and epithelium (i.e., Peters' anomaly), most likely represent a manifestation of abnormal keratolenticular separation (Fig. 1.27 and Fig. 1.28). This spectrum of malformations that mimic Peters' anomaly can be induced by teratogen exposure in mice before optic sulcus invagination (Fig. 1.29 and Fig. 1.30; Cook, 1989; Cook & Sulik, 1988; Cook et al., 1987). Similar syndromes of anterior segment dysgenesis have been identified in humans following ethanol exposure (Miller et al., 1984; Stromland et al., 1991).

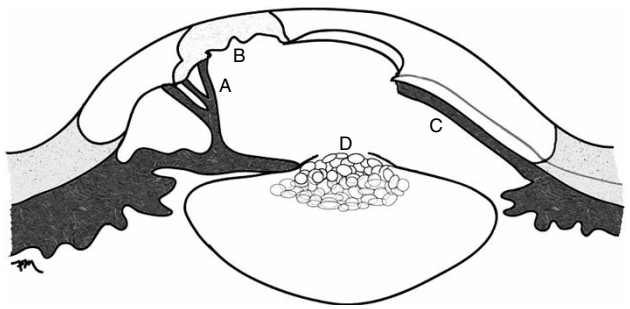

Figure 1.27 Clinical features of Peters' anomaly (anterior segment dysgenesis) resulting from abnormal separation of the lens vesicle from the surface ectoderm. **A.** Persistent pupillary membranes. **B.** Corneal opacity associated with defect in corneal endothelium, Descemet's membrane, and corneal stroma (neural crest). **C.** Iris hypoplasia. **D.** Anterior lenticonus and anterior polar cataract associated with partial defect in anterior lens capsule. (Drawing by Farid Mogannam.)

The size of the lens vesicle is determined by the area of contact between the optic vesicle and the surface ectoderm. Thus, factors influencing the size of the optic vesicle or the angle at which the optic vesicle approaches the surface ectoderm may affect the ultimate size of the lens vesicle. Microphakia resulting from optic vesicle deficiencies may be initiated very early in gestation (i.e., during formation of the neural plate). Microphakia associated with lens luxation has been described in two unrelated Siamese kittens (Molleda et al., 1995); as the globes were apparently otherwise normal, a primary abnormality in the lens placode ectoderm can be postulated. Aphakia is much more rare, and may occur through failure of contact between the optic vesicle and the surface ectoderm during the period when the surface ectoderm can respond to its inductive influences. As the anterior lens epithelium is required for induction of the corneal endothelium, this early initiation of aphakia would be associated with dysgenesis of the cornea and (likely) anterior uvea. Alternatively, normal induction of a lens vesicle followed by later involution would be expected to result in an eye with more normal anterior segment morphology. The lens aplasia (lap) mouse demonstrates faulty lens basement membrane formation associated with apoptosis and involution of the rudimentary lens vesicle (Aso et al., 1995, 1998). Sporadic cases of aphakia have been described in domestic animals, including a cat with associated retinal detachment but apparently normal iridocorneal structures (histopathology not available; Peiffer, 1982), and a litter of Saint Bernard puppies with multiple ocular malformations (Martin & Leipold, 1974). In humans, *in utero* exposure to rubella or parvovirus B can result in aphakia; anterior segment structures are variably affected (Hartwig et al., 1988). Abnormalities in lens shape (e.g., spherophakia, lens coloboma) may actually represent a primary abnormality in the ciliary processes, zonular fibers, or both, resulting in a lack of tension on the lens (Fig. 1.31 and Fig. 1.32). Thus, the term *coloboma* may be inaccurate when used in reference to a flattened equatorial portion of the lens that is not a true lens defect.

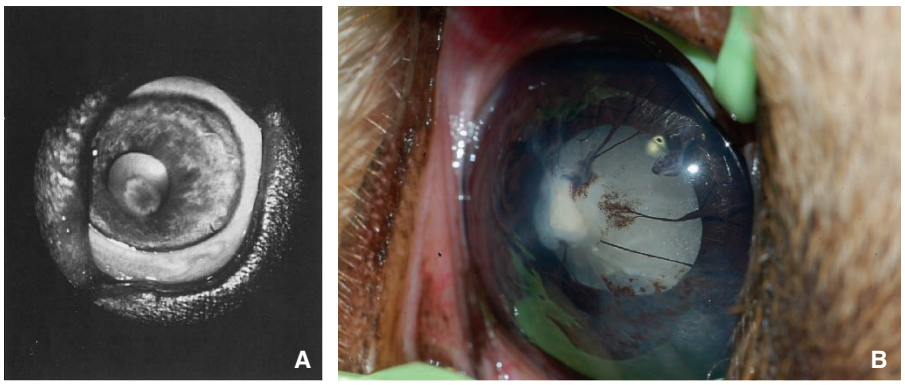

Figure 1.28 **A.** Clinical photograph of a puppy with Peters' anomaly exhibiting microphthalmia, a central corneal opacity, anterior axial cataract, and persistent pupillary membranes. **B.** A more severe form of anterior segment dysgenesis with visible lens material trapped within the axial cornea, accompanied by persistent pupillary membranes leading to the corneal defect.

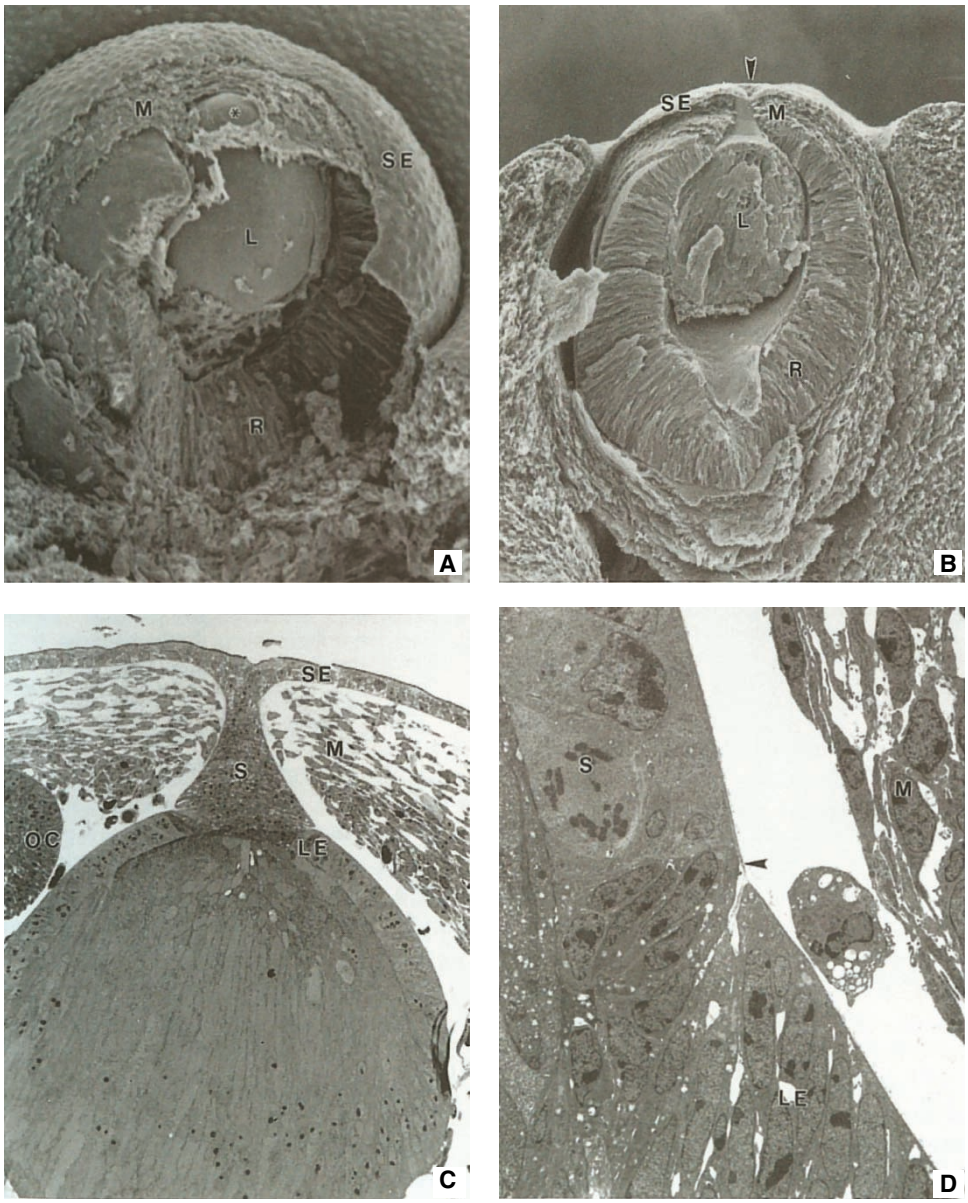

Figure 1.29 Keratolenticular dysgenesis induced by teratogen exposure in mice. **A.** Mouse embryo following acute exposure to ethanol during gastrulation. Delay in separation of the lens vesicle (L) from the surface ectoderm (SE) results in an anterior lenticonus (*) and failure of the mesenchyme (M) to complete its axial migration to form the corneal stroma, endothelium, and iris stroma. R, retinal primordium. Original magnification, 166×. **B**, **C**, and **D.** Mouse embryo following acute exposure to 13-*cis*-retinoic acid during gastrulation. A large keratolenticular stalk (S) persists and is continuous axially with the SE. The arrow in **B** indicates the incompletely closed lens pore. **D** is a transmission electron microscopic view of the stalk seen in **C.** There is discontinuity between the lens epithelium (LE) and the stalk epithelium (S). Adjacent neural crest mesenchyme (M) is visible, and two layers of basement membrane can be seen in **D**, bridging the lens–stalk junction as well as dividing the two zones. Mechanical interference with the axial migration of neural crest cells is responsible in this model for malformations, which mimics Peters' anomaly in the human. OC, optic cup. (Reprinted with permission from Cook, C. (1995) Embryogenesis of congenital eye malformations. *Veterinary and Comparative Ophthalmology*, **5**, 109–123.)

Uveal Cysts

Uveal cysts occur through failure of adhesion of the inner and outer layers of the optic cup. In the dog, they are most commonly identified as single or multiple spherical pigmented masses within the pupil or free-floating within the anterior chamber (Fig. 1.33 and Fig. 1.34). They appear to have a genetic predilection. In the cat, they are more often thick-walled and remain attached to the posterior iris surface, causing anterior displacement of the iris and shallowing of the anterior chamber, and may result in secondary glaucoma (Gemensky-Metzler et al., 2004). In cats they also

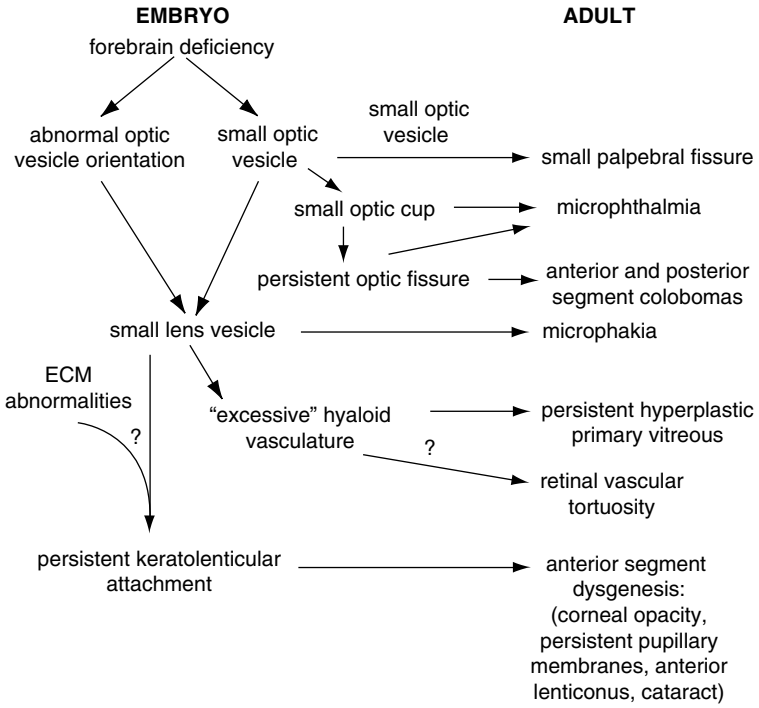

Figure 1.30 The relationship between microphthalmia and associated ocular malformations. An early embryonic insult (during gastrulation) leads to a deficiency in the forebrain and its derivatives, the optic sulci. The subsequently small optic vesicle often exhibits an abnormal relationship to the surface ectoderm, which is programmed (by the underlying neural crest) to form the lens. The result is a spectrum of malformations in the adult, including microphthalmia, microphakia, colobomas, persistent hyperplastic primary vitreous, and anterior segment dysgenesis. ECM, extracellular matrix. (Reprinted with permission from Cook, C. (1995) Embryogenesis of congenital eye malformations. *Veterinary and Comparative Ophthalmology*, **5**, 109–123.)

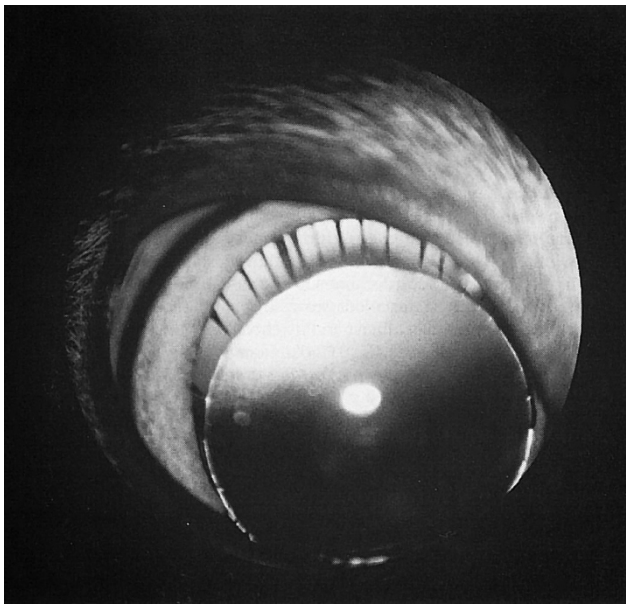

Figure 1.31 Microphakia and spherophakia in a cat. Note the elongated ciliary processes. The globe was not microphthalmic, and this most likely represented a primary abnormality in the surface ectoderm destined to become lens placode.

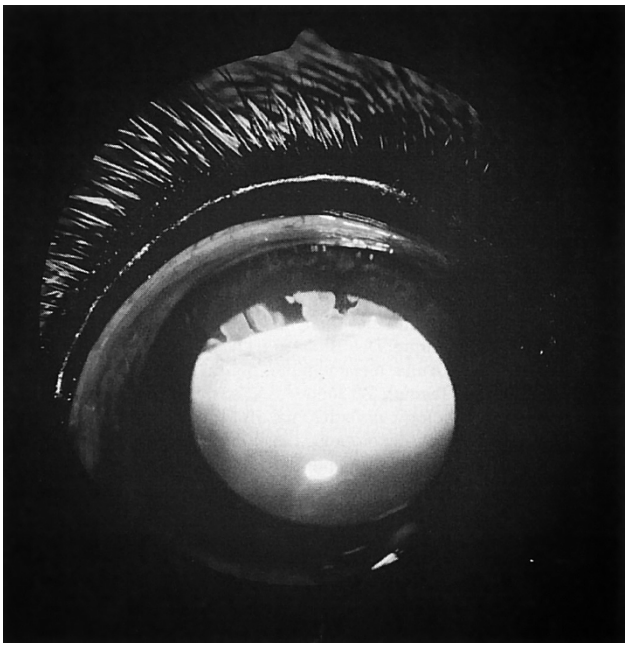

Figure 1.32 Nonpigmented ciliary body cysts in a cat. Note the flattened lens equator, which would incorrectly be called a lens coloboma. In this case, a medulloepithelioma of the ciliary body resulted both in the cysts and in the localized absence of zonules. Failure of normal traction by the zonule on the lens equator resulted in this flattened appearance. (Courtesy of Kristina Burling.)

appear to have a genetic predisposition, with Burmese cats overrepresented (Blacklock et al., 2016). When uveal cysts originate within the ciliary body, they can be nonpigmented (see Fig. 1.32).

Uveal cysts are often seen associated with pigmentary uveitis or pigmentary and cystic glaucoma in Golden Retriever dogs and other breeds. There has been a great deal of speculation about whether the cysts may play a causal role in the inflammatory disease process (Pumphrey et al., 2013; Townsend & Gornik, 2013). Uveal cysts seen in dogs affected

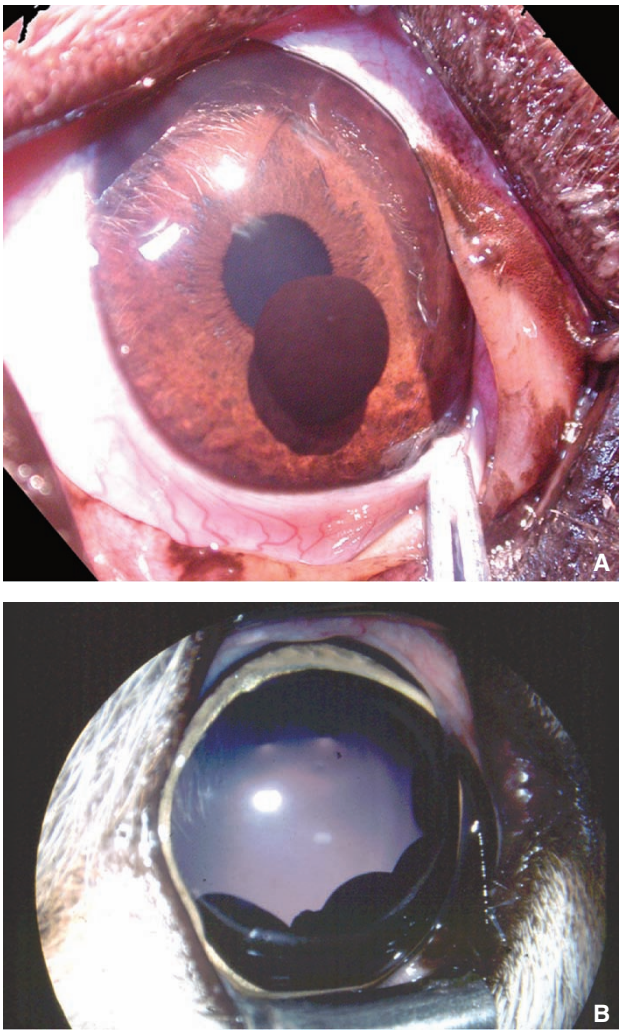

Figure 1.33 Iris cysts. **A.** Single iris cyst in a dog. **B.** Multiple iris cysts in a cat. In cats, these cysts are often thick-walled and remain attached to the posterior iris surface, causing anterior displacement of the iris and a shallow anterior chamber.

Figure 1.34 Histologic appearance of a uveal cyst on the posterior iris surface. These cysts form beneath the posterior pigmented epithelium and frequently separate to become free-floating spheres within the anterior chamber. (Courtesy of Robert Peiffer.)

with uveitis have a unique clinical appearance, being more translucent, irregularly shaped, and often adherent to the lens or cornea. This is in distinct contrast to the cysts commonly seen in other canine breeds with complete lack of inflammation.

Congenital Ocular Anomalies in Horses

A syndrome of multiple congenital ocular anomalies (MCOA) has been identified as a bilaterally symmetrical, inherited condition in several breeds of horses, most notably the Rocky Mountain breed, silver mutant ponies, and miniature horses (Andersson et al., 2011; Komaromy et al., 2011; Plummer & Ramsey, 2011; Ramsey et al., 1999a, 1999b; Fig. 1.35). Affected individuals most often have a silver coat color, and correlation with the Silver Dapple locus is suspected. The condition in the heterozygote is characterized by cysts of the posterior iris, ciliary body, and peripheral retina, indicating failure of adhesion of the inner and outer layers of the optic cup. These cysts are consistently located temporally, not associated with the optic fissure. Areas of current or previous retinal detachment were further manifestations of abnormal cup invagination and adhesion. The spectrum of anterior segment malformations seen in homozygous individuals included megalocornea, deep anterior chamber, iris hypoplasia, and cataract. Increased thickness of the central and peripheral corneas was noted and increased with age. Intraocular pressures were normal (Ramsey et al., 1999b). The syndrome in Rocky Mountain horses appears to exhibit codominant inheritance (Ewart et al., 2000). Cataracts have been identified in Exmoor ponies, with a suspected sex-linked mode of inheritance (Pinard & Basrur, 2011). Other congenital anomalies appear to occur rarely in horses, with occasional neonatal diagnosis of retinal and conjunctival hemorrhages thought to be due to injury during parturition (Barsotti et al., 2013).

Congenital Cataracts

Congenital cataracts resulting from abnormal formation of primary or secondary lens fibers would be expected to be localized to the nuclear region, and be nonprogressive. However, an early effect on the primary lens fibers may extend to involve the secondary fibers, resulting in a congenital cataract that progresses to involve the entire lens.

Abnormal lens vesicle invagination, separation, or defects in the lens epithelium or capsule would result in a cataract (with or without anterior or posterior lenticonus; Ori et al., 2000) that would remain associated with the peripheral portion of the lens, with the secondary lens fibers forming underneath (e.g., Old English Sheepdog, Barrie et al., 1979; Cavalier King Charles Spaniel, Narfstrom & Dubielzig, 1984). Congenital cataracts associated with mild microphthalmia (Miniature Schnauzer, Gelatt et al., 1983; Monaco

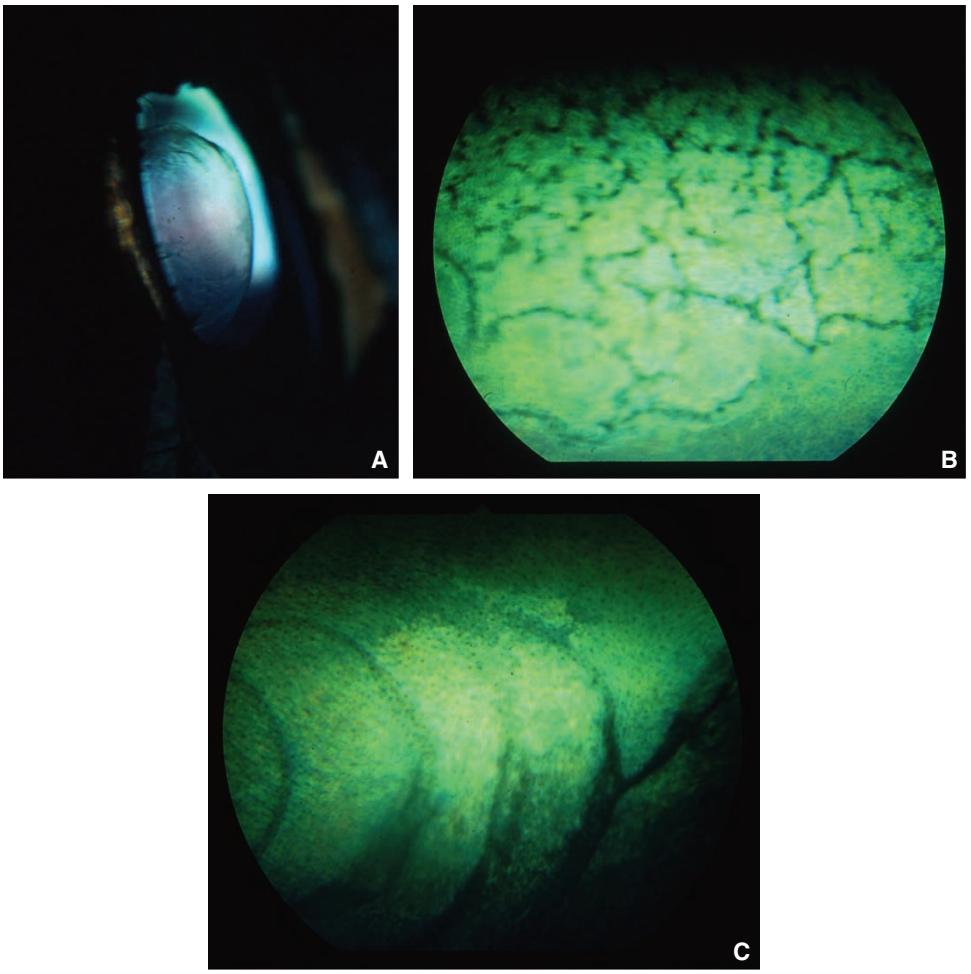

Figure 1.35 Spectrum of ocular lesions seen in Rocky Mountain horses. **A.** A large translucent cyst arising from the lateral part of the ciliary body extends into the vitreous cavity and occupies part of the temporal pupillary axis of the right eye. **B.** Retinal dysplasia is characterized by numerous pigmented folds located in the superior peripapillary neurosensory retina. **C.** Multiple, well-delineated, darkly pigmented curvilinear streaks of retinal pigment epithelium are present in the peripheral right tapetal fundus. These streaks originate and terminate at the ora ciliaris retinae and extend toward the optic papilla. They represent demarcation lines from previous retinal detachments and are referred to clinically as "high-water markers." (Reprinted with permission from Ramsey, D.T., Ewart, S.L., Render, J.A., et al. (1999) Congenital ocular abnormalities of Rocky Mountain horses. *Veterinary Ophthalmology*, **2**, 47–59.)

et al., 1985; Samuelson et al., 1987) may result from early abnormalities in the lens placode/epithelium, and they may involve the lens nucleus, cortex, or both. In the Miniature Schnauzer, these lesions are recessively inherited, typically bilateral, and initially involve the posterior subcapsular region with rapid progression (Gelatt et al., 1983; Zhang et al., 1991).

Congenital Glaucoma

Malformations of the iridocorneal angle (i.e., goniodysgenesis) have been described in several breeds, including the Basset Hound (Martin & Wyman, 1968; Wyman & Ketring, 1976) and the Bouvier des Flandres (van Rensburg et al., 1992). The iridocorneal angles of affected animals are malformed at birth, but the IOP often remains normal until middle age. Thus, the relationship between angle conformation and glaucoma is unclear. In English Springer Spaniels, a correlation was observed between pectinate ligament dysplasia and glaucoma (Bjerkas et al., 2002). Although pectinate ligament dysplasia is a congenital malformation, it may appear to clinically progress over time, as assessed by sequential gonioscopic evaluations in Flat-Coated Retrievers (Pearl et al., 2015).

Goniodysgenesis is characterized by abnormal tissue bridging the ciliary cleft. During normal development, this sheet undergoes rarefaction to form the pectinate ligament during the first three postnatal weeks (Martin, 1974; Samuelson & Gelatt, 1984a). Failure of this membrane to undergo normal atrophy is thought to result in goniodysgenesis. Congenital

glaucoma associated with presumed primary iridoschisis (i.e., degeneration of the anterior iris) has been described in a cat (Brown et al., 1994).

Persistent Hyperplastic Primary Vitreous/ Persistent Hyperplastic Tunica Vasculosa Lentis

Variable persistence of the hyaloid occurs in association with many other types of malformations, including microphthalmia, microphakia, cataract, and retinal dysplasia (Fig. 1.36; Bayon et al., 2001; Boeve et al., 1992). Persistent hyperplastic primary vitreous/persistent hyperplastic tunica vasculosa lentis (PHPV/PHTVL) may occur secondary to other malformations or as a primary, spontaneous failure of vascular regression. This condition has been described as an inherited trait in the Doberman (Stades, 1980; van der Linde-Sipman et al., 1983) and the Bouvier des Flandres (van Rensburg et al., 1992), and has been identified in two cats (Allgoewer & Pfefferkorn, 2001). In the Doberman, the genetics appear to be something more than simple recessive (Stades, 1983).

The mechanism involved is failure of normal vascular regression and hyperplasia of the persistent tissue. Normal vitreous may have antiangiogenic properties, and it may be essential for initiating regression of the hyaloid. Expression of the Arf tumor suppressor gene in perivascular cells may repress VEGF expression, thus promoting hyaloid regression in mice (Martin et al. 2004). Thus, the primary abnormality in PHPV/PHTVL may rest with the product of the ciliary epithelium (i.e., secondary vitreous).

Figure 1.36 Persistent hyperplastic primary vitreous in a puppy associated with a posterior subcapsular cataract. This eye is also microphthalmic.

Retinal Dysplasia

Abnormal retinal differentiation results in rosettes and multifocal disorganization known as retinal dysplasia. Retinal folds without rosette formation may result from inequity in the relative growth rates of the inner (i.e., retinal) and outer (i.e., RPE) layers of the optic cup (Fig. 1.37 and Fig. 1.38). This is a particularly likely pathogenesis in cases in which the folds resolve as the animal matures; this is seen most commonly among Collies. These folds do not represent abnormal differentiation and thus are not

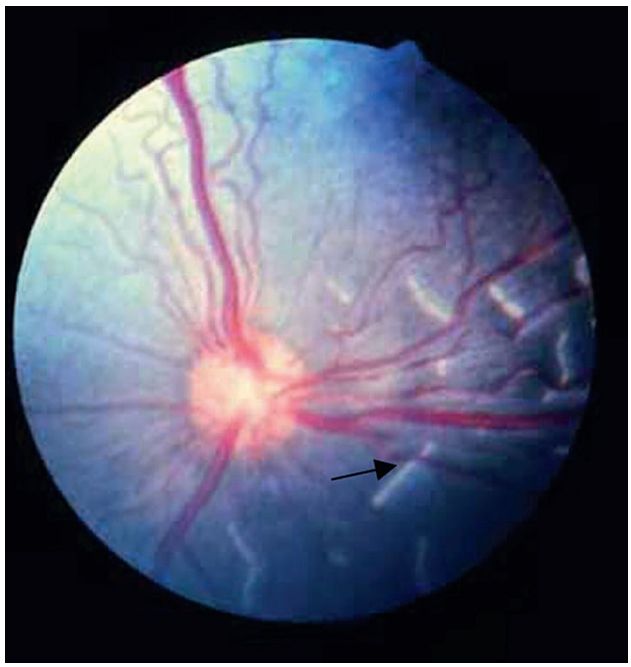

Figure 1.37 Fundus photograph of retinal folds in a young American Cocker Spaniel. These appear as single or multiple white curvilinear streaks. Elevation of a retinal vessel crossing a fold (arrow) can be seen.

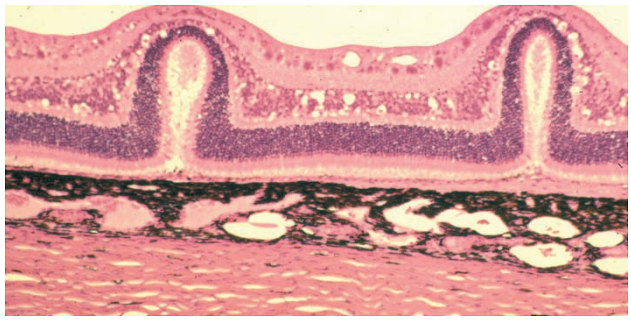

Figure 1.38 Histologic appearance of retinal folds. Note the normal stratification of the retinal layers and the mechanical distortion caused by disparate growth of the neural retina (inner optic cup) and the underlying RPE (outer optic cup). (Courtesy of Robert Peiffer.)

accurately referred to as dysplasia. Simple folding in the retina has been described in the American Cocker Spaniel (MacMillan & Lipton, 1978) and the Beagle (Heywood & Wells, 1970; Schiavo & Field, 1974). The genetic relationship between simple folds and true retinal dysplasia is undetermined.

True retinal dysplasia is characterized by disorganized development, the hallmark of which is the rosette. Abnormal or incomplete contact between the inner and outer layers of the optic cup during embryogenesis can result in dysplasia, with the most severe form associated with complete retinal nonattachment. This usually occurs in eyes that are microphthalmic with multiple ocular anomalies (e.g., Bedlington terrier, Rubin, 1963, 1968; Sealyham terrier, Ashton et al., 1968; and American Pit Bull terrier, Rodarte-Almeida et al., 2016). In the Labrador Retriever, retinal dysplasia genetically associated with skeletal anomalies is inherited as an autosomal dominant trait (Barnett et al., 1970; Carrig et al., 1988; Nelson & Macmillan, 1983). A similar form of inherited skeletal-ocular dysplasia is seen in the Samoyed dog (Aroch et al., 1996; Meyers et al., 1983).

Multifocal retinal rosettes in a retina that is partially attached to the underlying RPE represent the most common form of retinal dysplasia (Fig. 1.39 and Fig. 1.40). This condition has been described extensively in the English Springer Spaniel (Lavach et al., 1978; O'Toole et al., 1983). Retinal dysplasia occurs sporadically in other breeds (Bedford, 1982b) and species (Murphy et al., 1985). Multifocal, "geographic" retinal dysplasia most likely represents a later initiation of retinal disorganization. The dysplastic changes are first apparent at 45–50 days of gestation. Focal loss of cell junctions of the external limiting membrane is seen, with proliferation of neuroblasts in the retina forming rosettes (Whiteley, 1991). Retinal differentiation and maturation in the dog continue during the first 40 days postnatal. In addition, maturation of the tapetum during the first 6 months results in an inconsistent ability to detect mild forms of retinal dysplasia in puppies less than 10 weeks of age (Holle et al., 1999).

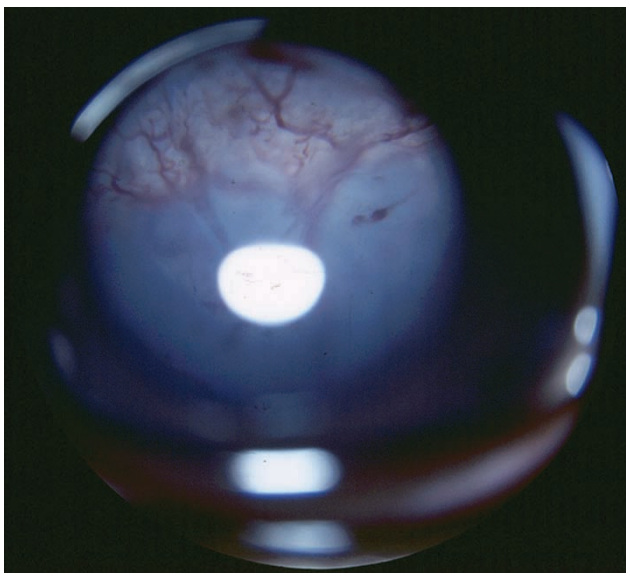

Figure 1.39 Geographic retinal dysplasia in an English Springer Spaniel. The retina is detached and lies just posterior to the lens; there are many folds visible.

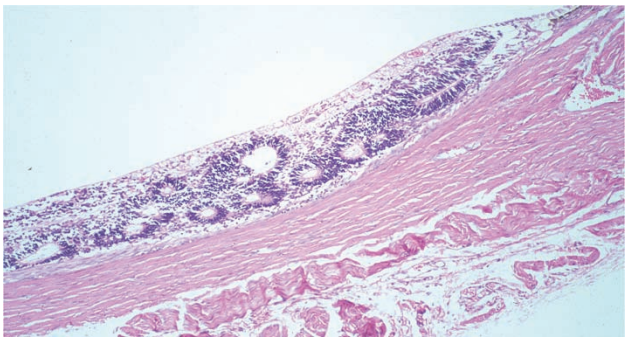

Figure 1.40 Histologic appearance of geographic retinal dysplasia. The retina exhibits disorganization and classic rosette formation. Note also the hypoplastic choroid. (Courtesy of Robert Peiffer.)

An unusual form of RPE dysplasia with duplication of neural retina in the outer layer of the optic cup has been described in several mutant mouse strains (Bumsted & Barnstable, 2000; Cook et al., 1991b). Large colobomas of the choroid and sclera in the areas adjacent to the dysplastic RPE illustrate the importance of this layer in coordinating differentiation of the neural crest.

Viral-induced "retinal dysplasia" has been associated with early postnatal exposure to canine herpesvirus and prenatal exposure to bovine viral diarrhea virus (Bistner et al., 1970; Brown et al., 1975; Kahrs et al., 1970), bluetongue virus in lambs (Silverstein & Al, 1971), and feline panleukopenia virus (Percy et al., 1975). Histopathologically, affected retinas are characterized by early inflammatory cell infiltrate and, later, by necrosis, gliosis, and diffuse disorganization of cell layers. Similar postnatal retinal disorganization can be induced in the dog by radiation exposure (Shively et al., 1970, 1972). These conditions are more accurately classified as teratogen-induced necrosis and degeneration rather than as dysplasia.

Optic Nerve Hypoplasia

Though difficult to document experimentally, optic nerve hypoplasia most likely results from a primary abnormality in the number or ultimate differentiation of the retinal ganglion cells (Fig. 1.41). Hypovitaminosis A in cattle can result

Figure 1.41 Optic nerve hypoplasia in an 8-week-old Alsatian puppy. This was a unilateral lesion and the pup presented with anisocoria. (Courtesy of Robert Peiffer.)

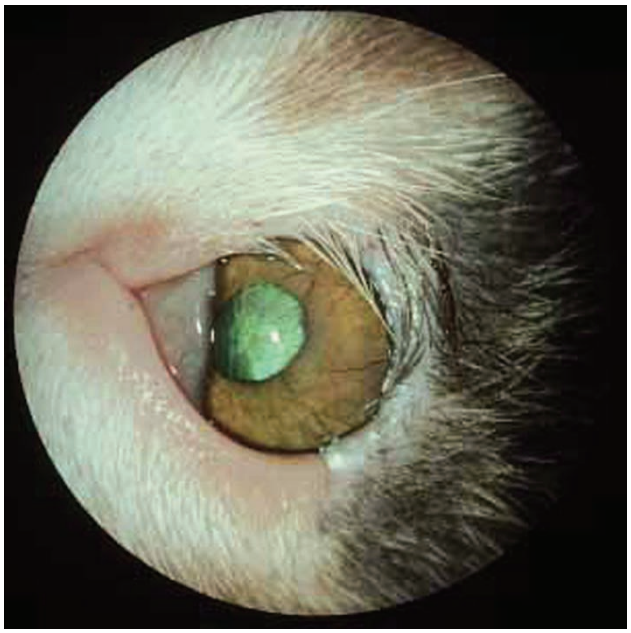

Figure 1.42 Eyelid coloboma in a kitten. The eyelid margin is absent from the temporal two-thirds of the upper lid. There is keratitis due to exposure and trichiasis. The eye also exhibits microphthalmia, dyscoria, and persistent pupillary membranes.

in stenosis of the optic foramen with secondary optic nerve degeneration, incorrectly labeled hypoplasia. Colobomas of the optic nerve result from failure of the optic fissure to close, as described for "typical" colobomas. Myelination of the optic nerve progresses from the brain to the eye during the first 3 weeks postnatal (Fox, 1963). Reduction in the amount of myelinization leads to a small optic disc that can mimic hypoplasia but is unassociated with vision deficits (termed micropapilla).

Eyelid Coloboma

The eyelids and palpebral fissure are initially induced at the time of contact of the optic vesicle with the surface ectoderm. This is also the time of induction of the lens placode. Eyelid agenesis (coloboma) occurs in domestic cats, often with concurrent persistent pupillary membranes, keratolenticular dysgenesis, and subtle to severe microphthalmia (Fig. 1.42; Glaze, 2005; Koch, 1979; Martin et al., 1997; Narfstrom, 1999). Eyelid colobomas occur less commonly in dogs (Fig. 1.43) and a case of upper eyelid agenesis has also been described in a Peregrine Falcon (Aguirre et al., 1972; Murphy et al., 1985) and in two sibling snow leopards (Hamoudi et al., 2013). The snow leopards also exhibited microphthalmia, typical anterior segment dysgenesis, and persistent hyaloid.

The receptivity of the surface ectoderm to the inductive influences of the optic vesicle is highly spatiotemporally

Figure 1.43 A Cavalier King Charles Spaniel with bilateral lower eyelid colobomas and dermoids. Note the notch defects in the central portion of the lower lids and the abnormal hair growth adjacent to the defects.

specific. The fairly consistent location of the defect in the temporal upper eyelid leads to suspicion of an abnormal orientation of the optic vesicle as it approaches the surface ectoderm, possibly eccentrically contacting the surface ectoderm in an area that is only partially receptive.

References

Adams, S.B., Horstman, L., & Hoerr, F.J. (1983) Periocular dermoid cyst in a calf. *Journal of the American Veterinary Medical Association*, **182**, 1255–6.

Aguirre, G., Rubin, L., & Bistner, S. (1972) Development of the canine eye. *American Journal of Veterinary Research*, **33**, 2399.

Akiya, S., Uemura, Y., Tsuchiya, S., et al. (1986) Electron microscopic study of the developing human vitreous collagen fibrils. *Ophthalmic Research*, **18**, 199–202.

Allen, L., Burian, H., & Braley, A. (1955) A new concept of the development of the anterior chamber angle: Its relationship to developmental glaucoma and other structural anomalies. *Archives of Ophthalmology*, **53**, 783–798.

Allgoewer, I. & Pfefferkorn, B. (2001) Persistent hyperplastic tunica vasculosa lentis and persistent hyperplastic primary vitreous (PHTVL/PHPV) in two cats. *Veterinary Ophthalmology* **4**, 161–164.

Anderson, D. (1981) The development of the trabecular meshwork and its abnormality in primary infantile glaucoma. *Transactions of the American Ophthalmology Society*, **79**, 458–485.

Andersson, L.S., Lyberg, K., Cothran, G., et al. (2011) Targeted analysis of four breeds narrows equine multiple congenital ocular anomalies locus to 208 kilobases. *Mammalian Genome*, **22**, 353–360.

Arnbjerg, J. & Jensen, O. (1982) Spontaneous microphthalmia in two Doberman puppies with anterior chamber cleavage syndrome. *Journal of the American Animal Hospital Association*, **18**, 481–484.

Aroch, I., Ofri, R., & Aizenberg, I. (1996) Haematological, ocular and skeletal abnormalities in a Samoyed family. *Journal of Small Animal Practice*, **37**, 333–339.

Ashton, N. (1966) Oxygen and the growth and development of retinal vessels. *American Journal of Ophthalmology*, **62**, 412–435.

Ashton, N., Barnett, K., & Sachs, D. (1968) Retinal dysplasia in the Sealyham terrier. *Journal of Pathology and Bacteriology*, **96**, 269–272.

Aso, S., Horiwaki, S., & Noda, S. (1995) Lens aplasia: A new mutation producing lens abnormality in the mouse. *Laboratory Animal Science*, **45**, 41–46.

Aso, S., Tashiro, M., Baba, R., et al. (1998) Apoptosis in the lens anlage of the heritable lens aplastic mouse (lap mouse). *Teratology*, **58**, 44–53.

Bahn, C.F., Falls, H.F., Varley, G.A., et al. (1984) Classification of corneal endothelial disorders based on neural crest origin. *Ophthalmology*, **91**, 558–563.

Bard, J., Hay, E., & Meller, S. (1975) Formation of the endothelium of the avian cornea: A study of cell movement *in vivo*. *Developmental Biology*, **42**, 334.

Barishak, Y. (1978) The development of the angle of the anterior chamber in vertebrate eyes. *Documenta Ophthalmologica*, **45**, 329–360.

Barkyoumb, S. & Leipold, H. (1984) Nature and cause of bilateral ocular dermoids in Hereford cattle. *Veterinary Pathology*, **21**, 316–324.

Barnett, K. (1979) Collie eye anomaly. *Journal of Small Animal Practice*, **20**, 537–542.

Barnett, K., Bjorck, G., & Kock, E. (1970) Hereditary retinal dysplasia in the Labrador Retriever in England and Sweden. *Journal of Small Animal Practice*, **10**, 755–759.

Barnett, K.C. & Stades, F.C. (1979) Collie eye anomaly in the Shetland Sheepdog in the Netherlands. *Journal of Small Animal Practice*, **20**, 321–329.

Barrie, K., Peiffer, R., Gelatt, K., et al. (1979) Posterior lenticonus, microphthalmia, congenital cataracts and retinal folds in an Old English Sheepdog. *Journal of the American Animal Hospital Association*, **15**, 715–717.

Barsotti, G., Sgorbini, M., Marmorini, P., & Corazza, M. (2013) Ocular abnormalities in healthy Standardbred foals. *Veterinary Ophthalmology* **16**, 245–250.

Bayon, A., Tovar, M.C., Fernandez Del Palacio, M.J., et al. (2001) Ocular complications of persistent hyperplastic primary vitreous in three dogs. *Veterinary Ophthalmology*, **4**, 35–40.

Bedford, P.G. (1982a) Collie eye anomaly in the Border Collie. *Veterinary Record*, **111**, 34–35.

Bedford, P.G. (1982b) Multifocal retinal dysplasia in the Rottweiler. *Veterinary Record*, **111**, 304–305.

Bedford, P.G. (1998) Collie eye anomaly in the Lancashire Heeler. *Veterinary Record*, **143**, 354–356.

Beebe, D. (1985) Ocular growth and differentiation factors. In: *Growth and Maturation Factors* (ed. Guroff, G.), Vol. **3**, pp. 39–76. New York: Wiley.

Beebe, D.C. & Coats, J.M. (2000) The lens organizes the anterior segment: Specification of neural crest cell differentiation in the avian eye. *Developmental Biology*, **220**, 424–431.

Beebe, D.C., Compart, P.J., Johnson, M.C., et al. (1982) The mechanism of cell elongation during lens fiber cell differentiation. *Developmental Biology*, **92**, 54–59.

Beebe, D.C., Latker, C.H., Jebens, H.A., et al. (1986) Transport and steady-state concentration of plasma proteins in the vitreous humor of the chicken embryo: Implications for the mechanism of eye growth during early development. *Developmental Biology*, **114**, 361–368.

Bellhorn, R.W. (1974) A survey of ocular findings in eight- to ten-month-old Beagles. *Journal of the American Veterinary Medical Association*, **164**, 1114–1116.

Bergsjo, T., Arnesen, K., Heim, P., et al. (1984) Congenital blindness with ocular developmental anomalies, including retinal dysplasia, in Doberman Pinscher dogs. *Journal of the American Veterinary Medical Association*, **184**, 1383–1386.

Berman, M. & Pierro, L. (1969) Lens detachment and choroid fissure closure in the embryonic mouse eye. *American Zoologist*, **9**, 365.

Bertram, T., Coignoul, F., & Cheville, N. (1984) Ocular dysgenesis in Australian Shepherd dogs. *Journal of the American Animal Hospital Association*, **20**, 177.

Binns, W., Thacker, E.J., James, L.F., et al. (1959) A congenital cyclopian-like malformation in lambs. *Journal of the American Veterinary Medical Association*, **134**, 180–183.

Bistner, S., Rubin, L., & Roberts, S. (1971) A review of persistent pupillary membranes in the Basenji dog. *Journal of the American Animal Hospital Association*, **7**, 143–157.

Bistner, S., Rubin, L., & Saunders, L. (1970) The ocular lesions of bovine viral diarrhea-mucosal disease. *Veterinary Pathology*, **7**, 275.

Bjerkas, E., Ekesten, B., & Farstad, W. (2002) Pectinate ligament dysplasia and narrowing of the iridocorneal angle associated with glaucoma in the English Springer Spaniel. *Veterinary Ophthalmology*, **5**, 49–54.

Blacklock, B. T., Grundon, R.A., Meehan, M., et al. (2016) Uveal cysts in domestic cats: A retrospective evaluation of thirty-six cases. *Veterinary Ophthalmology*, **19**, 56–60.

Blackwell, R. & Cobb, E. (1959) A hydrocephalus lethal in Hereford cattle. *Journal of Heredity*, **50**, 143–147.

Boeve, M.H., Stades, F.C., Linde-Sipman, J.S.V.D., et al. (1992) Persistent hyperplastic tunica vasculosa lentis and primary vitreous (PHTVL/PHPV) in the dog: A comparative review. *Progress in Veterinary & Comparative Ophthalmology*, **2**, 163.

Boroffka, S.A., Verbruggen, A.M., Boeve, M.H., et al. (1998) Ultra-sonographic diagnosis of persistent hyperplastic tunica vasculosa lentis/persistent hyperplastic primary vitreous in two dogs. *Veterinary Radiology and Ultrasound*, **39**, 440–444.

Bremer, F.M. & Rasquin, F. (1998) Histochemical localization of hyaluronic acid in vitreous during embryonic development. *Investigative Ophthalmology & Visual Science*, **39**, 2466–2469.

Bressan, G.M., Daga-Gordini, D., Colombatti, A., et al. (1993) Emilin, a component of elastic fibers preferentially located at the elastin–microfibrils interface. *Journal of Cell Biology*, **121**, 201–212.

Briziarelli, G. & Abrutyn, D. (1975) Atypical coloboma in the optic disc of a Beagle. *Journal of Comparative Pathology*, **85**, 237–240.

Brown, A., Munger, R., & Peiffer, R. (1994) Congenital glaucoma and iridoschisis in a Siamese cat. *Veterinary & Comparative Ophthalmology*, **4**, 121–124.

Brown, A.S., Leamen, L., Cucevic, V., et al. (2005) Quantitation of hemodynamic function during developmental vascular regression in the mouse eye. *Investigative Ophthalmology & Visual Science*, **46**, 2231–2237.

Brown, E.A., Thomasy, S.M., Murphy, C.J., & Bannasch, D.L. (2018) Genetic analysis of optic nerve head coloboma in the Nova Scotia Duck Tolling Retriever identifies discordance with the NHEJ1 intronic deletion (Collie eye anomaly mutation). *Veterinary Ophthalmology*, **21**, 144–150.

Brown, T., Delahunta, A., Bistner, S., et al. (1975) Pathogenetic studies of infection of the bovine fetus with bovine viral diarrhea virus: II. Ocular lesions. *Veterinary Pathology*, **12**, 394–404.

Browning, J., Reichelt, M.E., Gole, G.A., et al. (2001) Proximal arterial vasoconstriction precedes regression of the hyaloid vasculature. *Current Eye Research*, **22**, 405–411.

Bryden, M.M., Evans, H.E., & Keeler, R.F. (1971) Cyclopia in sheep caused by plant teratogens. *Journal of Anatomy*, **110**, 507–510.

Bumsted, K.M. & Barnstable, C.J. (2000) Dorsal retinal pigment epithelium differentiates as neural retina in the microphthalmia (mi/mi) mouse. *Investigative Ophthalmology & Visual Science*, **41**, 903–908.

Buyukmihci, N.C., Murphy, C.J., & Schulz, T. (1988) Developmental ocular disease of raptors. *Journal of Wildlife Diseases*, **24**, 207–213.

Carrig, C.B., Sponenberg, D.P., Schmidt, G.M., et al. (1988) Inheritance of associated ocular and skeletal dysplasia in Labrador Retrievers. *Journal of the American Veterinary Medical Association*, **193**, 1269–1272.

Cohen, A.I. (1961) Electron microscopic observations of the developing mouse eye: I. Basement membranes during early development and lens formation. *Developmental Biology*, **3**, 297–316.

Cohen, M.M. & Sulik, K.K.(1992) Perspectives on holoprosencephaly: Part II. Central nervous system, craniofacial anatomy, syndrome commentary, diagnostic approach, and experimental studies. *Journal of Craniofacial Genetics and Developmental Biology*, **12**, 196–244.

Collins, B.K., Collier, L.L., Johnson, G.S., et al. (1992) Familial cataracts and concurrent ocular anomalies in Chow Chows. *Journal of the American Veterinary Medical Association*, **200**, 1485–1491.

Cook, C. (1989) Experimental models of anterior segment dysgenesis. *Ophthalmic Paediatrics and Genetics*, **10**, 33–46.

Cook, C. (1995) Embryogenesis of congenital eye malformations. *Veterinary & Comparative Ophthalmology*, **5**, 109–123.

Cook, C., Burling, K., & Nelson, E. (1991a) Embryogenesis of posterior segment colobomas in the Australian Shepherd dog. *Progress in Veterinary & Comparative Ophthalmology*, **1**, 163–170.

Cook, C. & Sulik, K. (1986) Sequential scanning electron microscopic analyses of normal and spontaneously abnormal ocular development in C57b1/6j mice. *Scanning Electron Microscopy*, **3**, 1215–1227.

Cook, C. & Sulik, K. (1988) Keratolenticular dysgenesis (Peters' anomaly) as a result of acute embryonic insult during gastrulation. *Journal of Pediatric Ophthalmology and Strabismus*, **25**, 60–66.

Cook, C.S., Generoso, W.M., Hester, D., et al. (1991b) RPE dysplasia with retinal duplication in a mutant mouse strain. *Experimental Eye Research*, **52**, 409–415.

Cook, C.S., Nowotny, A.Z., & Sulik, K.K. (1987) Fetal alcohol syndrome: Eye malformations in a mouse model. *Archives of Ophthalmology*, **105**, 1576–1581.

Cook, C.S. & Sulik, K.K. (1990) Laminin and fibronectin in retinoid induced keratolenticular dysgenesis. *Investigative Ophthalmology & Visual Science*, **31**, 751–757.

Cooper, M.K., Porter, J.A., Young, K.E., et al. (1998) Teratogen mediated inhibition of target tissue response to shh signaling. *Science*, **280**, 1603–1607.

Coulombre, A. (1956) The role of intraocular pressure in the development of the chick eye. *Journal of Experimental Zoology*, **133**, 211–225.

Coulombre, A.J. & Coulombre, J.L. (1964) Lens development: I. Role of the lens in eye growth. *Journal of Experimental Zoology*, **156**, 39–47.

Coulombre, J. & Coulombre, A. (1969) Lens development: IV. Size, shape and orientation. *Investigative Ophthalmology & Visual Science*, **8**, 251–257.

Engelhardt, M., Wachs, F.P., Couillard-Despres, S., et al. (2004) The neurogenic competence of progenitors from the postnatal rat retina *in vitro*. *Experimental Eye Research*, **78**, 1025–1036.

Erlich, R.B., Werneck, C.C., Mourao, P.A.S., et al. (2003) Major glycosaminoglycan species in the developing retina: Synthesis, tissue distribution and effects upon cell death. *Experimental Eye Research*, **77**, 157–165.

Ewart, S.L., Ramsey, D.T., Xu, J., et al. (2000) The horse homolog of congenital aniridia conforms to codominant inheritance. *Journal of Heredity*, **91**, 93–98.

Feeney, S.A., Simpson, D.A.C., Gardiner, T.A., et al. (2003) Role of vascular endothelial growth factor and placental growth factors during retinal vascular development and hyaloid regression. *Investigative Ophthalmology & Visual Science*, **44**, 839–847.

Fischer, A.J. (2005) Neural regeneration in the chick retina. *Progress in Retinal and Eye Research*, **24**, 161–182.

Fitch, J., Fini, M.E., Beebe, D.C., et al. (1998) Collagen type IX and developmentally regulated swelling of the avian primary corneal stroma. *Developmental Dynamics*, **212**, 27–37.

Flower, R.W., McLeod, D.S., Lutty, G.A., et al. (1985) Postnatal retinal vascular development of the puppy. *Investigative Ophthalmology & Visual Science*, **26**, 957–968.

Fox, M. (1963) Postnatal ontogeny of the canine eye. *Journal of the American Veterinary Medical Association*, **143**, 968–974.

Fruttiger, M. (2002) Development of the mouse retinal vasculature: Angiogenesis versus vasculogenesis. *Investigative Ophthalmology & Visual Science*, **43**, 522–527.

Garcia-Porrero, J., Collado, J. & Ojeda, J. (1979) Cell death during detachment of the lens rudiment from ectoderm in the chick embryo. *Anatomical Record*, **193**, 791–804.

Gelatt, K., Huston, K., & Leipold, H. (1969) Ocular anomalies of incomplete albino cattle: Ophthalmoscopic examination. *American Journal of Veterinary Research*, **30**, 1313–1316.

Gelatt, K., Samuelson, D., Barrie, K., et al. (1983) Biometry and clinical characteristics of congenital cataracts and microphthalmia in the Miniature Schnauzer. *Journal of the American Veterinary Medical Association*, **183**, 99–102.

Gelatt, K.N. & McGill, L.D. (1973). Clinical characteristics of microphthalmia with colobomas of the Australian Shepherd Dog. *Journal of the American Veterinary Medical Association*, **162**, 393–396.

Gelatt, K.N. & Veith, L.A. (1970) Hereditary multiple ocular anomalies in Australian shepherd dogs. (preliminary report). *Veterinary Medicine, Small Animal Clinician*, **65**, 39–42.

Gemensky-Metzler, A.J., Wilkie, D.A., & Cook, C.S. (2004) The use of semiconductor diode laser for deflation and coagulation of anterior uveal cysts in dogs, cats and horses: A report of 20 cases. *Veterinary Ophthalmology*, **7**, 360–368.

Glaze, M.B. (2005) Congenital and hereditary ocular abnormalities in cats. *Clinical Techniques in Small Animal Practice*, **20**, 74–82.

Grainger, R., Henry, J., & Henderson, R. (1988) Reinvestigation of the role of the optic vesicle in embryonic lens induction. *Development*, **102**, 517–526.

Grainger, R.M., Henry, J.J., Saha, M.S., et al. (1992) Recent progress on the mechanisms of embryonic lens formation. *Eye*, **6**, 117–122.

Greene, H. & Leipold, H. (1974) Hereditary internal hydrocephalus and retinal dysplasia in Shorthorn calves. *Cornell Veterinarian*, **64**, 367–375.

Greiner, J.V. & Weidman, T.A. (1980) Histogenesis of the cat retina. *Experimental Eye Research*, **30**, 439–453.

Greiner, J.V. & Weidman, T.A. (1981) Histogenesis of the ferret retina. *Experimental Eye Research*, **33**, 315–332.

Greiner, J.V. & Weidman, T.A. (1982) Embryogenesis of the rabbit retina. *Experimental Eye Research*, **34**, 749–765.

Gwin, R., Wyman, M., Lim, D., et al. (1981) Multiple ocular defects associated with partial albinism and deafness. *Journal of the American Animal Hospital Association*, **17**, 401.

Hale, F. (1935) The relation of vitamin A to anophthalmos in pigs. *American Journal of Ophthalmology*, **18**, 1087–1093.

Hamoudi, H., Rudnick, J.-C., Prause, J.U., et al. (2013) Anterior segment dysgenesis (Peters' anomaly) in two snow leopard (Panthera uncia) cubs. *Veterinary Ophthalmology*, **16**, 130–134.

Hartwig, N.G., Vermeij-Keers, C., & Versteeg, J. (1988) The anterior eye segment in virus-induced primary congenital aphakia. *Acta Morphologica Neerlando-Scandinavica*, **26**, 283–292.

Hay, E. (1980) Development of the vertebrate cornea. *International Review of Cytology*, **63**, 263–322.

Hay, E. & Revel, J. (1969) Fine structure of the developing avian cornea. In: *Monographs in Developmental Biology* (eds Wolsky, A. & Chen, P.S.), Vol. **1**, pp. 1–144. Basel: Karger.

Hero, I., Farjah, M., & Scholtz, C.L. (1991) The prenatal development of the optic fissure in colobomatous microphthalmia. *Investigative Ophthalmology & Visual Science*, **32**, 2622–2635.

Heywood, R. & Wells, G. (1970) A retinal dysplasia in the Beagle dog. *Veterinary Record*, **87**, 178–180.

Hilfer, S. (1983) Development of the eye of the chick embryo. *Scanning Electron Microscopy*, **III**, 1353–1369.

Hilfer, S., Brady, R., & Yank, J. (1981) Intracellular and extracellular changes during early ocular development in the chick embryo. In: *Ocular Size and Shape: Regulation during Development* (eds Hilfer, S. & Sheffield, J.), pp. 47–78. New York: Springer-Verlag.

Hilfer, S.R. & Randolph, G.J. (1993) Immunolocalization of basal lamina components during development of chick otic and optic primordia. *Anatomical Record*, **235**, 443–452.

Holle, D.M., Stankovics, M.E., Sarna, C.S., et al. (1999) The geographic form of retinal dysplasia in dogs is not always a congenital abnormality. *Veterinary Ophthalmology*, **2**, 61–66.

Horrigan, S.K., Rich, C.B., Streeten, B.W., et al. (1992) Characterization of an associated microfibril protein through recombinant DNA techniques. *Journal of Biological Chemistry*, **267**, 10087–10095.

Hubmacher, D., Reinhardt, D.P., Plesec, T., et al. (2014) Human eye development is characterized by coordinated expression of fibrillin isoforms. *Investigative Ophthalmology & Visual Science*, **55**, 7934–7944.

Hughes, S., Yang, H.J., & Chan-Ling, T. (2000) Vascularization of the human fetal retina: Roles of vasculogenesis and angiogenesis. *Investigative Ophthalmology & Visual Science*, **41**, 1217–1228.

Hunt, H.H. (1961) A study of the fine structure of the optic vesicle and lens placode of the chick embryo during incubation. *Developmental Biology*, **3**, 175–209.

Ikeda, K., Shirai, S., Majima, A., et al. (1995) Histological and histochemical studies of normal and faulty closure of the embryonic fissure in the eye of ICR mouse. *Japanese Journal of Ophthalmology*, **39**, 20–29.

Incardona, J.P., Gaffield, W., Kapur, R.P., et al. (1998) The teratogenic veratrum alkaloid cyclopamine inhibits sonic hedgehog signal transduction. *Development*, **125**, 3553–3562.

Incardona, J.P., Gaffield, W., Lange, Y., et al. (2000) Cyclopamine inhibition of Sonic hedgehog signal transduction is not mediated through effects on cholesterol transport. *Developmental Biology*, **224**, 440–452.

Irby, N.L. & Aguirre, G.D. (1985) Congenital aniridia in a pony. *Journal of the American Veterinary Medical Association*, **186**, 281–283.

Ito, M. & Yoshioka, M. (1999) Regression of the hyaloid vessels and pupillary membrane of the mouse. *Anatomy and Embryology*, **200**, 403–411.

Jack, R. (1972) Regression of the hyaloid vascular system: An ultrastructural analysis. *American Journal of Ophthalmology*, **74**, 261–272.

Jacobson, A.G. (1988) Somitomeres: Mesodermal segments of vertebrate embryos. *Development*, **104** (Suppl.), 209–220.

Johns, P.R., Rusoff, A.C., & Dubin, M.W. (1979) Postnatal neurogenesis in the kitten retina. *Journal of Comparative Neurology*, **187**, 545–555.

Johnston, M.C., Noden, D.M., Hazelton, R.D., et al. (1979) Origins of avian ocular and periocular tissues. *Experimental Eye Research*, **29**, 27–43.

Jones, K., Higginbottom, M. & Smith, D. (1980) Determining the role of the optic vesicle in orbital and periocular development and placement. *Pediatric Research*, **14**, 703–708.

Kahrs, R., Scott, F., & De Lahunta, A. (1970) Congenital cerebellar hypoplasia and ocular defects in calves following bovine virus diarrhea-mucosal disease infection in pregnant cattle. *Journal of the American Veterinary Medical Association*, **156**, 1443.

Kaswan, R.L., Collins, L.G., Blue, J.L., et al. (1987) Multiple hereditary ocular anomalies in a herd of cattle. *Journal of the American Veterinary Medical Association*, **191**, 97–99.

Keeler, R.F. (1990) Teratogenic compounds of *Veratrum californicum* (durand): X. Cyclopia in rabbits produced by cyclopamine. *Teratology*, **3**, 175–180.

Keeler, R.F. & Binns, W. (1966) Teratogenic compounds of *Veratrum californicum* (durand): II. Production of ovine fetal cyclopia by fractions and alkaloid preparations. *Canadian Journal of Biochemistry*, **44**, 829–838.

Kern, T.J. (1981) Persistent hyperplastic primary vitreous and microphthalmia in a dog. *Journal of the American Veterinary Medical Association*, **178**, 1169–1171.

Koch, S.A. (1979) Congenital ophthalmic abnormalities in the Burmese cat. *Journal of American Veterinary Medical Association*, **174**, 90–91.

Komaromy, A.M., Rowlan, J.S., La Croix, N.C., et al. (2011) Equine multiple congenital ocular anomalies (MCOA) syndrome in PMEL17 (Silver) mutant ponies: Five cases. *Veterinary Ophthalmology*, **14**, 313–320.

Kupfer, C. & Kaiser-Kupfer, M.I. (1978) New hypothesis of developmental anomalies of the anterior chamber associated with glaucoma. *Transactions of the Ophthalmology Society of the United Kingdom*, **98**, 213–215.

Kupfer, C. Kuwabara, T., & Stark, W.J. (1975) The histopathology of Peters' anomaly. *American Journal of Ophthalmology*, **80**, 653–660.

Laratta, L.J., Riis, R.C., Kern, T.J., et al. (1985) Multiple congenital ocular defects in the Akita dog. *Cornell Veterinarian*, **75**, 381–392.

Lavach, D.D., Murphy, J.M., & Severin, G.A. (1978) Retinal dysplasia in the English Springer Spaniel. *Journal of the American Animal Hospital Association*, **14**, 192–199.

LeDouarin, N. & Teillet, M. (1974) Experimental analysis of the migration and differentiation of neuroblasts of the autonomic nervous system and of neurectodermal mesenchymal derivatives, using a biological cell marking technique. *Developmental Biology*, **41**, 162–184.

Lewis, D., Kelly, D., & Sansom, J. (1986) Congenital microphthalmia and other developmental ocular anomalies in the Dobermann. *Journal of Small Animal Practice*, **27**, 559–566.

Los, L.I., van Luyn, M.J.A., Eggli, P.S., et al. (2000a) Vascular remnants in the rabbit vitreous body: II. Enzyme digestion and immunohistochemical studies. *Experimental Eye Research*, **71**, 153–165.

Los, L.I., van Luyn, M.J.A., & Nieuwenhuis, P. (2000b) Vascular remnants in the rabbit vitreous body: I. Morphological characteristics and relationship to vitreous embryonic development. *Experimental Eye Research*, **71**, 143–151.

Lowe, J.K., Kukekova, A.V., Kirkness, E.F., et al. (2003) Linkage mapping of the primary disease locus for Collie eye anomaly. *Genomics*, **82**, 86–95.

MacMillan, A. & Lipton, D. (1978) Heritability of multifocal retinal dysplasia in American Cocker Spaniels. *Journal of the American Veterinary Medical Association*, **172**, 568–572.

Maestro De Las Casas, C., Epeldegui, M., Tudela, C., et al. (2003) High exogenous homocysteine modifies eye development in early chick embryos. *Birth Defects Research. Part A, Clinical and Molecular Teratology*, **67**, 35–40.

Manoly, R. (1951) Blindness in newborn pigs. *Veterinary Record*, **63**, 398.

Martin, A.C., Thornton, J.D., Liu, J., et al. (2004) Pathogenesis of persistent hyperplastic primary vitreous in mice lacking the Arf tumor suppressor gene. *Investigative Ophthalmology & Visual Science*, **45**, 3387–3396.

Martin, C. (1974) Development of the pectinate ligament structure of the dog. *American Journal of Veterinary Research*, **35**, 1433.

Martin, C. (1978) Strabismus associated with extraocular muscle agenesis in a dog. *Journal of the American Animal Hospital Association*, **14**, 486–489.

Martin, C. & Wyman, M. (1968) Glaucoma in the Basset Hound. *Journal of the American Veterinary Medical Association*, **153**, 1320–1327.

Martin, C.L. & Leipold, H.W. (1974) Aphakia and multiple ocular defects in Saint Bernard puppies. *Veterinary Medicine, Small Animal Clinician*, **69**, 448–453.

Martin, C.L., Stiles, J., & Willis, M. (1997) Feline colobomatous syndrome. *Veterinary & Comparative Ophthalmology*, **7**, 39–43.

Matsuura, T., Tsuji, N., Kodama, Y., et al. (2013) Iridal coloboma induces dyscoria during miosis in FLS mice. *Veterinary Ophthalmology*, **16**, 186–191.

Meier, S. (1982) The development of segmentation in the cranial region of vertebrate embryos. *Scanning Electron Microscopy,* **Pt 3**, 1269–1282.

Meier, S. & Tam, P.P. (1982) Metameric pattern development in the embryonic axis of the mouse: I. *Differentiation of the cranial segments. Differentiation*, **21**, 95–108.

Meyers, V.N., Jezyk, P.F., Aguirre, G.D., et al. (1983) Short-limbed dwarfism and ocular defects in the Samoyed dog. *Journal of the American Veterinary Medical Association*, **183**, 975–979.

Miller, M.T., Epstein, R.J., Sugar, J., et al. (1984) Anterior segment anomalies associated with the fetal alcohol syndrome. *Journal of Pediatric Ophthalmology and Strabismus*, **21**, 8–18.

Molleda, J.M., Martin, E., Ginel, P.J., et al. (1995) Microphakia associated with lens luxation in the cat. *Journal of the American Animal Hospital Association*, **31**, 209–212.

Monaco, M., Samuelson, D., & Gelatt, K. (1985) Morphology and postnatal development of the normal lens in the dog and congenital cataract in the Miniature Schnauzer. *Lens Research*, **2**, 393–433.

Montiani-Ferreira, F., Petersen-Jones, S., Cassotis, N., et al. (2003) Early postnatal development of central corneal thickness in dogs. *Veterinary Ophthalmology*, **6**, 19–22.

Moore, C.P., Shaner, J.B., Halenda, R.M., et al. (1999) Congenital ocular anomalies and ventricular septal defect in a Dromedary camel (*Camelus dromedarius*). *Journal of Zoo and Wildlife Medicine*, **30**, 423–430.

Mulder, G.B., Manley, N., Grant, J., et al. (2000) Effects of excess vitamin A on development of cranial neural crest-derived structures: A neonatal and embryologic study. *Teratology*, **62**, 214–226.

Munyard, K.A., Sherry, C.R., & Sherry, L. (2007) A retrospective evaluation of congenital ocular defects in Australian Shepherd dogs in Australia. *Veterinary Ophthalmology*, **10**, 19–22.

Murphy, C.J., Kern, T.J., Loew, E., et al. (1985) Retinal dysplasia in a hybrid falcon. *Journal of the American Veterinary Medical Association*, **187**, 1208–1209.

Mutlu, F. & Leipold, I. (1964) The structure of the fetal hyaloid system and tunica vasculosa lentis. *Archives of Ophthalmology*, **71**, 102–110.

Nakano, K.E. & Nakamura, H. (1985) Origin of the irideal striated muscle in birds. *Journal of Embryology and Experimental Morphology*, **88**, 1–13.

Narfstrom, K. (1999) Hereditary and congenital ocular disease in the cat. *Journal of Feline Medicine Surgery*, **1**, 135–141.

Narfstrom, K. & Dubielzig, R. (1984) Posterior lenticonus, cataracts and microphthalmia in the Cavalier King Charles Spaniel. *Journal of Small Animal Practice*, **25**, 669–677.

Nelson, D. & Macmillan, A. (1983) Multifocal retinal dysplasia in field trial Labrador Retrievers. *Journal of the American Animal Hospital Association*, **19**, 388–392.

Njoku, C.O., Esievo, K.A., Bida, S.A., et al. (1978) Canine cyclopia. *Veterinary Record*, **102**, 60–61.

Noden, D. (1993) Periocular mesenchyme: Neural crest and mesodermal interactions. In: *Duane's Foundations of Clinical Ophthalmology* (eds Tasman, W. & Jaeger, E.), pp. 1–23. Hagerstown, MD: Lippincott.

Noden, D.M. (1986) Patterning of avian craniofacial muscles. *Developmental Biology*, **116**, 347–356.

O'Rahilly, R. (1983) The timing and sequence of events in the development of the human eye and ear during the embryonic period proper. *Anatomy and Embryology*, **168**, 87–99.

Ori, J.I., Yoshikai, T., Yoshimur, S., et al. (2000) Posterior lenticonus with congenital cataract in a Shih Tzu dog. *Journal of Veterinary Medical Science*, **62**, 1201–1203.

O'Toole, D., Young, S., Severin, G.A., et al. (1983) Retinal dysplasia of English Springer Spaniel dogs: Light microscopy of the postnatal lesions. *Veterinary Pathology*, **20**, 298–311.

Ozeki, H., Ogura, Y., Hirabayashi, Y., et al. (2000) Apoptosis is associated with formation and persistence of the embryonic fissure. *Current Eye Research*, **20**, 367–372.

Ozeki, H., Ogura, Y., Hirabayashi, Y., et al. (2001) Suppression of lens stalk cell apoptosis by hyaluronic acid leads to faulty separation of the lens vesicle. *Experimental Eye Research*, **72**, 63–70.

Packard, D.S. & Meier, S. (1983) An experimental study of the somitomeric organization of the avian segmental plate. *Developmental Biology*, **97**, 191–202.

Pearl, R., Gould, D., & Spiess, B. (2015) Progression of pectinate ligament dysplasia over time in two populations of Flat-Coated Retrievers. *Veterinary Ophthalmology*, **18**, 6–12.

Peiffer, R. (1982) Bilateral congenital aphakia and retinal detachment in a cat. *Journal of the American Animal Hospital Association*, **18**, 128–130.

Peiffer, R. & Fischer, C. (1983) Microphthalmia, retinal dysplasia and anterior segment dysgenesis in a litter of Doberman Pinschers. *Journal of the American Veterinary Medical Association*, **183**, 875.

Percy, D., Scott, F., & Albert, D. (1975) Retinal dysplasia due to feline panleukopenia virus infection. *Journal of the American Veterinary Medical Association*, **167**, 935–937.

Perveen, R., Lloyd, I.C., Clayton-Smith, J., et al. (2000) Phenotypic variability and asymmetry of Rieger syndrome associated with PITX2 mutations. *Investigative Ophthalmology & Visual Science*, **41**, 2456–2460.

Pinard, C.L. & Basrur, P.K. (2011) Ocular anomalies in a herd of Exmoor ponies in Canada. *Veterinary Ophthalmology*, **14**, 100–108.

Plummer, C.E. & Ramsey, D.T. (2011) A survey of ocular abnormalities in miniature horses. *Veterinary Ophthalmology*, **14**, 239–243.

Pumphrey, S.A., Pizzirani, S., Pirie, C.G., & Needle, D.B. (2013) Glaucoma associated with uveal cysts and goniodysgenesis in American Bulldogs: A case series. *Veterinary Ophthalmology*, **16**, 377–385.

Ramsey, D.T., Ewart, S.L., Render, J.A., et al. (1999a) Congenital ocular abnormalities of Rocky Mountain horses. *Veterinary Ophthalmology*, **2**, 47–59.

Ramsey, D.T., Hauptman, J.G., & Petersen-Jones, S.M. (1999b) Corneal thickness, intraocular pressure, and optical corneal diameter in Rocky Mountain horses with cornea globosa or clinically normal corneas. *American Journal of Veterinary Research*, **60**, 1317–1321.

Rebhun, R. (1977) Congenital anterior staphyloma with rudimentary lens in a calf. *Journal of the American Veterinary Medical Association*, **171**, 440–442.

Reme, C., Urner, U., & Aeberhard, B. (1983a) The development of the chamber angle in the rat eye. *Graefe's Archive for Clinical and Experimental Ophthalmology*, **220**, 139–153.

Reme, C., Urner, U., & Aeberhard, B. (1983b) The occurrence of cell death during the remodelling of the chamber angle recess in the developing rat eye. *Graefe's Archive for Clinical and Experimental Ophthalmology*, **221**, 113–121.

Roberts, L. (1948) Microphthalmia in swine. *Journal of Heredity*, **39**, 146.

Roberts, S.R. & Bistner, S.I. (1968) Persistent pupillary membrane in Basenji dogs. *Journal of the American Veterinary Medical Association*, **153**, 533–542.

Rodarte-Almeida, A.C.V., Petersen-Jones, S., Langohr, I.M., et al. (2016) Retinal dysplasia in American Pit Bull terriers – phenotypic characterization and breeding study. *Veterinary Ophthalmology*, **19**, 11–21.

Rubin, L. (1963) Hereditary retinal detachment in Bedlington Terriers: A preliminary report. *Veterinary Medicine, Small Animal Clinician*, **3**, 387–389.

Rubin, L. (1968) Heredity of retinal dysplasia in Bedlington Terriers. *Journal of the American Veterinary Medical Association*, **152**, 260–262.

Rubin, L., Nelson, E., & Sharp, C. (1991) Collie eye anomaly in Australian Shepherd dogs. *Progress in Veterinary & Comparative Ophthalmology*, **1**, 105–108.

Rupp, G. & Knight, A. (1984) Congenital ocular defects in a crossbred beef herd. *Journal of the American Veterinary Medical Association*, **184**, 1149–1150.

Samuelson, D. & Gelatt, K. (1984a) Aqueous outflow in the Beagle: Postnatal development of the pectinate ligament and trabecular meshwork. *Current Eye Research*, **3**, 783.

Samuelson, D. & Gelatt, K. (1984b) Aqueous outflow in the Beagle: II. Postnatal morphologic development of the iridocorneal angle: Corneoscleral trabecular meshwork and angular aqueous plexus. *Current Eye Research*, **3**, 795–807.

Samuelson, D., Das, N., Bauer, J., et al. (1987) Prenatal morphogenesis of the congenital cataracts in the Miniature Schnauzer. *Lens Research*, **180**, 231–250.

Saperstein, G. (1975) Congenital defects in sheep. *Journal of the American Veterinary Medical Association*, **167**, 314.

Saunders, L. & Fincher, M. (1951) Hereditary multiple eye defects in grade Jersey calves. *Cornell Veterinarian*, **41**, 351–366.

Schaepdrijver, L.D., Simoens, P., Lauwers, H., et al. (1989) The hyaloid vascular system of the pig. *Anatomy and Embryology*, **1989**, 549–554.

Schiavo, D.M. & Field, W.E. (1974) Unilateral focal retinal dysplasia in Beagle dogs. *Veterinary Medicine, Small Animal Clinician*, **69**, 33–34.

Schook, P. (1978) A review of data on cell actions and cell interactions during the morphogenesis of the embryonic eye. *Acta Morphologica Neerlando-Scandinavica*, **16**, 267–286.

Sevel, D. (1981) Reappraisal of the origin of human extraocular muscles. *Ophthalmology*, **88**, 1330.

Sevel, D. (1986) The origins and insertions of the extraocular muscles: Development, histologic features, and clinical significance. *Transactions of the American Ophthalmological Society*, **84**, 488–526.

Shields, M., Buckley, E., Klintworth, G., et al. (1985) Axenfeld–Rieger syndrome. A spectrum of developmental disorders. *Survey of Ophthalmology*, **29**, 387–409.

Shively, J., Phemister, R., Epling, G., et al. (1970) Pathogenesis of radiation-induced retinal dysplasia. *Investigative Ophthalmology & Visual Science*, **9**, 888–900.

Shively, J., Phemister, R., Epling, G., et al. (1972) Dose relationships of pathologic alterations in the developing retina of irradiated dogs. *American Journal of Veterinary Research*, **33**, 2121–2134.

Shively, J.N., Epling, G.P., & Jensen, R. (1971) Fine structure of the postnatal development of the canine retina. *American Journal of Veterinary Research*, **32**, 383–392.

Silverstein, A. & Al, E. (1971) An experimental virus-induced retinal dysplasia in the fetal lamb. *American Journal of Ophthalmology*, **72**, 22.

Smelser, G. & Ozanics, V. (1971) The development of the trabecular meshwork in primate eyes. *American Journal of Ophthalmology*, **71**, 366.

Sonoda, S., Isashiki, Y., Tabata, Y., et al. (2000) A novel PAX6 gene mutation (P118R) in a family with congenital nystagmus associated with a variant form of aniridia. *Graefe's Archive for Clinical and Experimental Ophthalmology*, **238**, 552–558.

Spira, A.W. & Hollenberg, M.J. (1973) Human retinal development: Ultrastructure of the inner retinal layers. *Development Biology*, **31**, 1–21.

Stades, F. (1980) Persistent hyperplastic tunica vasculosa lentis and persistent hyperplastic primary vitreous (PHTVL/PHPV) in 90 closely related Doberman Pinschers: Clinical aspects. *Journal of the American Animal Hospital Association*, **16**, 739–751.

Stades, F. (1983) Persistent hyperplastic tunica vasculosa lentis and persistent hyperplastic primary vitreous in Doberman Pinschers: Genetic aspects. *Journal of the American Animal Hospital Association*, **19**, 957–964.

Strande, A., Nicolaissen, B., & Bjerkas, I. (1988) Persistent pupillary membrane and congenital cataract in a litter of English Cocker Spaniels. *Journal of Small Animal Practice*, **29**, 257–260.

Stromland, K., Miller, M., & Cook, C. (1991) Ocular teratology. *Survey of Ophthalmology*, **35**, 429–446.

Sulik, K.K. & Johnston, M.C. (1982) Embryonic origin of holoprosencephaly: Interrelationship of the developing brain and face. *Scanning Electron Microscopy*, **Pt 1**, 309–322.

Swanson, H.L., Dubielzig, R.R., Bentley, E., et al. (2001) A case of Peters' anomaly in a Springer Spaniel. *Journal of Comparative Pathology*, **125**, 326–330.

Tam, P.P. (1986) A study of the pattern of prospective somites in the presomitic mesoderm of mouse embryos. *Journal of Embryology and Experimental Morphology*, **92**, 269–285.

Tam, P.P. & Trainor, P.A.A. (1994) Specification and segmentation of the paraxial mesoderm. *Anatomy and Embryology (Berlin)*, **189**, 275–305.

Tam, P.P., Meier, S., & Jacobson, A.G. (1982) Differentiation of the metameric pattern in the embryonic axis of the mouse: II. Somitomeric organization of the presomitic mesoderm. *Differentiation*, **21**, 109–122.

Townsend, W. M. & Gornik, K.R. (2013) Prevalence of uveal cysts and pigmentary uveitis in Golden Retrievers in three Midwestern states. *Journal of the American Veterinary Medical Association*, **243**, 1298–1301.

Trainor, P.A. & Tam, P.P. (1995) Cranial paraxial mesoderm and neural crest cells of the mouse embryo: Co-distribution in the craniofacial mesenchyme but distinct segregation in branchial arches. *Development*, **121**, 2569–2582.

van der Linde-Sipman, J., Stades, F., & De Wolff-Rouendaal, D. (1983) Persistent hyperplastic tunica vasculosa lentis and persistent hyperplastic primary vitreous in the Doberman Pinscher: Pathological aspects. *Journal of the American Animal Hospital Association*, **19**, 791–802.

van der Linde-Sipman, J.S., van den Ingh, T.S.G.A.M., & Vellema, P. (2003) Morphology and morphogenesis of hereditary microphthalmia in Texel sheep. *Journal of Comparative Pathology*, **128**, 269–275.

van Rensburg, I.B.J., Petrick, S.W., van der Lugt, J., et al. (1992) Multiple inherited eye anomalies including persistent hyperplastic tunica vasculosa lentis in Bouvier des Flandres. *Veterinary & Comparative Ophthalmology*, **2**, 133–139.

Wahl, C.M., Noden, D.M., & Baker, R. (1994) Developmental relations between sixth nerve motor neurons and their targets in the chick embryo. *Developmental Dynamics*, **201**, 191–202.

Waring, G., Rodriques, M., & Laibson, P. (1975) Anterior chamber cleavage syndrome: A stepladder classification. *Survey of Ophthalmology*, **20**, 3–33.

Weiss, P. & Jackson, S.F. (1961) Fine structural changes associated with lens determination in the avian embryo. *Developmental Biology*, **3**, 532–554.

Whiteley, H. (1991) Dysplastic canine retinal morphogenesis. *Investigative Ophthalmology & Visual Science*, **32**, 1492–1498.

Wrenn, J. & Wessells, N. (1969) An ultrastructural study of lens invagination in the mouse. *Journal of Experimental Zoology*, **171**, 359–368.

Wulle, K. (1972) The development of the productive and draining system of the aqueous humor in the eye. *Advances in Ophthalmology*, **26**, 296–355.

Wyand, D., Lehav, M., Albert, D., et al. (1972) Intraocular lacrimal gland tissue with other ocular abnormalities occurring in a white-tailed deer. *Journal of Comparative Pathology*, **82**, 219–221.

Wyman, M. & Ketring, K. (1976) Congenital glaucoma in the Basset Hound: A biologic model. *Transactions. Section on Ophthalmology. American Academy of Ophthalmology and Otolaryngology*, **81**, OP645–OP652.

Yamashita, T. & Sohal, G. (1986) Development of smooth and skeletal muscle cells in the iris of the domestic duck, chick and quail. *Cell and Tissue Research*, **244**, 121–131.

Yamashita, T. & Sohal, G. (1987) Embryonic origin of skeletal muscle cells in the iris of the duck and quail. *Cell and Tissue Research*, **249**, 31–37.

Zhang, R.L., Samuelson, D.A., Zhang, Z.G., et al. (1991) Analysis of eye lens-specific genes in congenital hereditary cataracts and microphthalmia of the Miniature Schnauzer dog. *Investigative Ophthalmology & Visual Science*, **32**, 2662–2665.

Zhao, S. & Overbeek, P.A. (2001) Regulation of choroid development by the retinal pigment epithelium. *Molecular Vision*, **7**, 277–282.

Zhu, M.D., Madigan, M.C., van Driel, D., et al. (2000) The human hyaloid system: Cell death and vascular regression. *Experimental Eye Research*, **70**, 767–776.

2

Ophthalmic Anatomy

Jessica M. Meekins[1], Amy J. Rankin[1], and Don A. Samuelson[2]

[1] *Department of Clinical Sciences, Veterinary Health Center, College of Veterinary Medicine, Kansas State University, Manhattan, KS, USA*
[2] *Department of Small Animal Clinical Sciences, College of Veterinary Medicine, University of Florida, Gainesville, FL, USA*

Introduction

A thorough understanding of normal ophthalmic anatomy is an integral part of the foundational knowledge of a veterinary ophthalmologist. It is important to be able to differentiate normal anatomic structures from abnormal structures during ophthalmic examinations, histopathologic examinations, or during surgical procedures. The veterinary ophthalmologist examines eyes from a wide variety of animal species. During vertebrate evolution, the eye has largely retained the same basic components, but important and clinically relevant differences do exist. This chapter will primarily present the normal ophthalmic anatomy of dogs, cats, horses, livestock species, and birds. The anatomy of selected exotic species is covered in Section IV, but there is also a tremendous amount of literature elsewhere for reference.

Orbit

The orbit is the bony fossa that surrounds and protects the eye while separating it from the cranial cavity. Through numerous foramina, the orbit also provides pathways for various blood vessels and nerves involved in the function of the eye. The size, shape, and position of the orbit are closely associated with time of visual activity and feeding behavior (Table 2.1). In domestic carnivores such as the cat and dog, the orbital axes are set rostrolaterally, approximately 10° and 20° from midline, respectively (Prince et al., 1960). As a result, these animals possess enhanced binocular vision, which serves to improve predatory feeding behavior. In horses and ruminants, the orbits are positioned more laterally than carnivores, being approximately 40° (i.e., horses) and 50° (i.e., cattle) from midline. Monocular vision in these and other ungulate species is enhanced, providing a strong panoramic line of vision that allows for scanning the horizon to search for potential predators. In the rabbit, the axis of each eye extends as much as 85° from the midline; this orbit placement also occurs among the majority of lizards, some snakes, and in certain fish. In these latter instances where binocular vision has become greatly reduced, there is a tendency for the eyes to protrude so that the visual axis of the eye can expand what the optic axis of the skull has provided (Prince et al., 1960).

In addition to size, shape, and position, all vertebrate orbits are one of two kinds: the enclosed orbit, which is completely encompassed by bone; or the open or incomplete orbit, which is only partially surrounded by bone (Fig. 2.1, Fig. 2.2, and Fig. 2.3). Among domestic animals, horses, sheep, cattle, and goats have enclosed orbits. Pigs and carnivores (i.e., dogs and cats) have open orbits. The enclosed orbit of large herbivorous prey species is theorized to be essential for protection, whereas the open orbit gives animals such as carnivores the ability to open their jaws widely during consumption of prey (Prince, 1956).

The bony orbit typically consists of five to seven bones, depending on the species (Table 2.2). The canine orbit is composed of five, and sometimes six, bones, the supraorbital ligament that extends from the frontal to the zygomatic bone, and the periosteum (Fig. 2.1). The orbital rim is formed by the frontal, lacrimal, and zygomatic bones. Laterally, the orbit is formed by the supraorbital ligament which is contiguous with a fibroelastic connective tissue sheath for much of the floor of the orbit. The orbital floor is incomplete, being partially formed by the sphenoid and palatine bones. In the feline orbit, the processes of the frontal and zygomatic bones extend a great deal more toward one another, resulting in a shortened supraorbital ligament (Fig. 2.1). In animals with enclosed orbits, closure of the temporal side of the orbit is accomplished by union of the zygomatic process of the frontal bone with the frontal process of the zygomatic bone

Veterinary Ophthalmology: Volume I, Sixth Edition. Edited by Kirk N. Gelatt, Gil Ben-Shlomo, Brian C. Gilger, Diane V.H. Hendrix, Thomas J. Kern, and Caryn E. Plummer.

Companion website: www.wiley.com/go/gelatt/veterinary

(see Fig. 2.2 and Fig. 2.3). In the horse, the zygomatic process of the temporal bone intervenes between these two and completes the orbital rim (see Fig. 2.3).

Within the orbit, various foramina and fissures provide osseous pathways for blood vessels and nerves to pass from the cranial cavity and alar canal into the orbital region. Those foramina of rather constant position in domestic animals are the rostral alar, ethmoidal, lacrimal, orbital, ovale, optic, rotundum, and supraorbital. Other foramina closely related to the orbital structures are within the pterygopalatine region, and these are the maxillary, caudal palatine, and sphenopalatine (Table 2.3). The orbital foramen is elongated in most domestic animals except the horse; therefore, it is referred to as the orbital fissure. In cattle, the orbital fissure and foramen rotundum are typically fused to form the foramen orbitorotundum (see Fig. 2.2).

Orbital Fascia

The orbital fascia consists of a thin, tough connective tissue lining that envelops all the structures within the orbit, including the bony fossa itself. This fascia consists of three anatomic components: the periorbita, Tenon's capsule or fascia bulbi, and the extraocular muscle (EOM) fascial sheaths (Fig. 2.4).

The periorbita is a conically shaped, fibrous membrane that lines the orbit and encloses the globe, EOMs, blood vessels, and nerves. The apex of the periorbita is located where the optic nerve exits the orbit. At this point, it is continuous with the dural sheath of the optic nerve. In the orbit, it is thin, attaches firmly to the orbital bones, and forms their periosteum. In the dog, the periorbita does not always fuse with the periosteum of the frontal and the sphenoid bones (Constantinescu & McClure, 1990). Instead, the periosteum and periorbita often remain distinct and separate in these orbital regions. In animals with an incomplete lateral orbital

Table 2.1 Orbital dimensions.

Dimension	Feline (mm)	Canine (mm)	Bovine (mm)	Equine (mm)
Width	24	29	65	62
Height	26	28	64	59
Depth	—	49	120	98
Distance between orbits	23	36	151	173

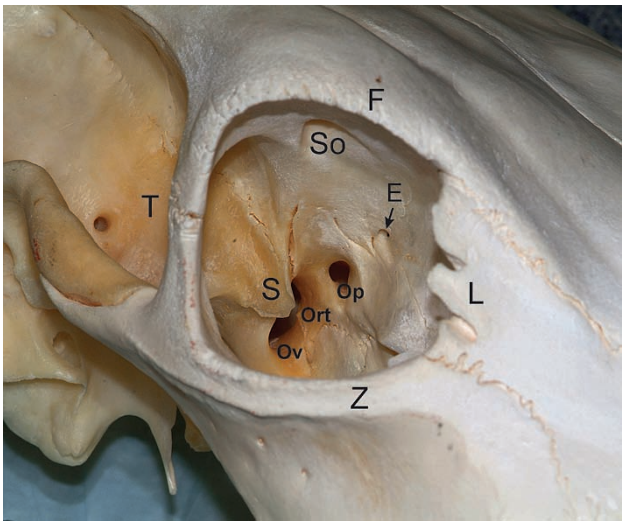

Figure 2.2 Bovine orbit. Bones of the orbit: frontal (F), lacrimal (L), sphenoid (S), temporal (T), zygomatic (Z). Orbital foramina: ethmoidal (E), optic (Op), orbitorotundum (Ort), ovale (Ov), supraorbital (So).

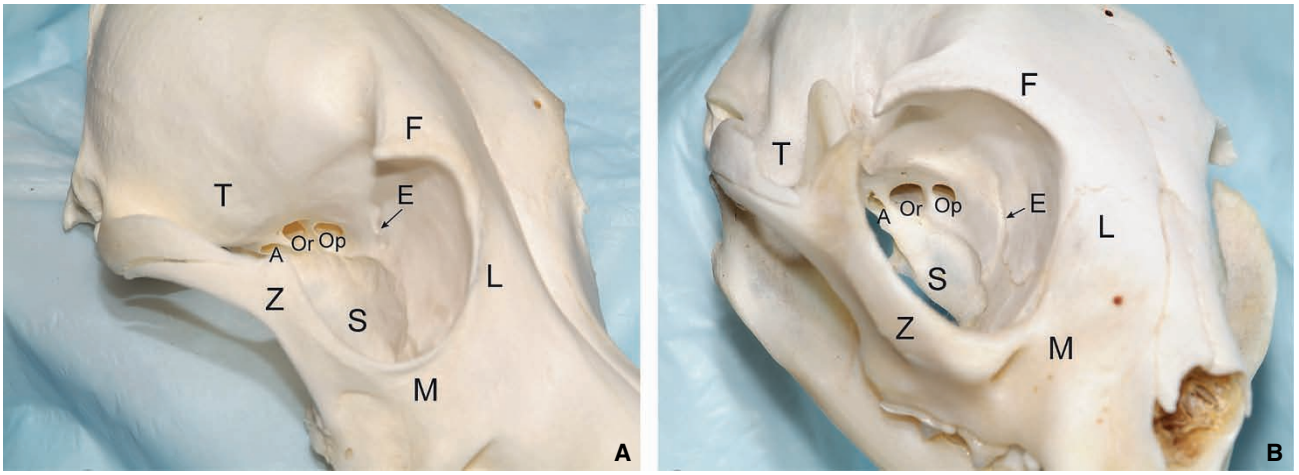

Figure 2.1 **A.** Canine orbit. **B.** Feline orbit. Bones of the orbit: frontal (F), lacrimal (L), maxilla (M), sphenoid (S), temporal (T), zygomatic (Z). Orbital foramina: rostral alar (A), ethmoidal (E), optic (Op), orbital fissure (Or).

wall, the periorbita is thicker laterally next to the orbital ligament. Anteriorly, in the dorsolateral part of the orbit, the periorbita separates and surrounds the lacrimal gland. At the orbital rim, it divides again, one part becoming continuous with the periosteum of the facial bones and the other, that is, the septum orbitale, merging with the eyelids and becoming continuous with the tarsal plates (the fibrous sheet in the eyelids). Within the periorbital tissue of carnivores (dogs and cats), smooth muscle has been observed along the lateral wall of the orbit, portions of the roof and floor of the orbit, and next to the periosteal lining of orbital bones (Brunton, 1938). The smooth muscle is oriented circularly so that when observed in the coronal plane, the muscle fibers are seen longitudinally. Contraction of the muscle has been produced by stimulation of the cervical sympathetic nerve trunk and results in forward movement of the globe. Although the function of this fibromuscular tissue remains unknown, it may facilitate repositioning the eye within the orbit during relaxation of the retractor oculi muscle.

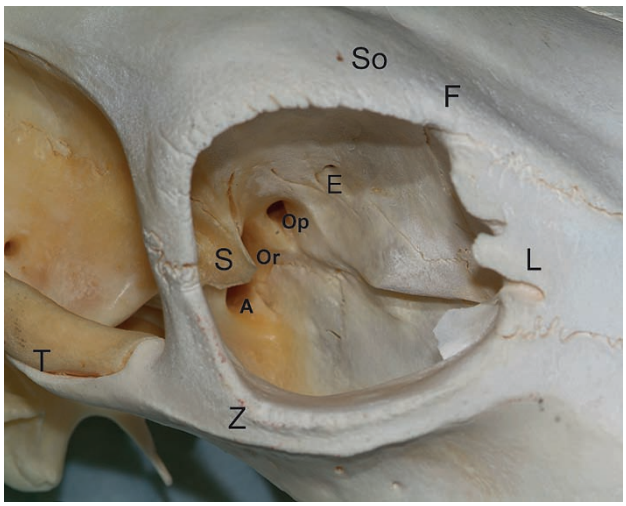

Figure 2.3 Equine orbit. Bones of the orbit: frontal (F), lacrimal (L), sphenoid (S), temporal (T), zygomatic (Z). Orbital foramina: rostral alar (A), ethmoidal (E), optic (Op), orbital fissure (Or), supraorbital (So).

Tenon's capsule (fascia bulbi) is connective tissue on the outer aspect of the sclera. Tenon's capsule is separated from the sclera by a narrow, cleft-like space filled with loose connective tissue, Tenon's space. Tenon's capsule is attached to the sclera near the corneoscleral junction (i.e., limbus), and it becomes continuous with the fascia surrounding the EOMs.

The fascial sheaths of the EOMs are dense, fibrous membranes loosely attached to the muscles with fine trabeculae of connective tissue. These sheaths are continuous with, or reflections of, Tenon's capsule, but they are not always considered part of it.

In the dog, the muscular fasciae consist of three layers. A superficial, thick layer extends caudally from the orbital septum and is penetrated by blood vessels and nerves. A middle layer consists of superficial and deep sheets that anteriorly attach to the outer junction of the sclera and cornea. A deep layer next to the surface of the EOMs separates the recti muscles from the retractor oculi muscles (Constantinescu & McClure, 1990).

Extraocular Muscles and Orbital Fat

The three sheets of orbital fascia are separated by orbital fat. Orbital fat fills the dead space in the orbit and acts as a protective cushion for the eye. The amount of orbital fat varies between individuals and to a greater extent between species. The color of orbital fat ranges from white to yellow. The yellow coloration is attributed to higher levels of lutein, beta-carotene, retinol, and other unidentified carotenoids (Sires et al., 2001). Some animals, including birds and many reptiles, have very little orbital fat (Duke-Elder, 1958). When the retractor oculi muscle contracts, orbital fat can displace the glandular tissue associated with the nictitating membrane, resulting in its passive movement over the cornea. In the dog, orbital fat surrounds the optic nerve and forms a

Table 2.2 Orbital bones.

Animal	Lacrimal	Zygomatic	Frontal	Sphenoid	Palatine	Maxillary	Ethmoid	Temporal
Dog	X	X	X	X	X	X		
Cat	X	X	X	X	X	X		
Horse	X	X	X	X	X			X
Ox	X	X	X	X	X	X		
Sheep	X	X	X	X	X	X		
Goat	X	X	X	X	X			
Pig	X	X	X	X	X		X	
Rabbit	X	X	X	X	X			X
Human	X	X	X	X	X	X	X	

Table 2.3 Foramina and associated nerves and vessels.

Foramen or fissure	Species	Associated nerves and vessels
Alar, rostral	Canine, equine, feline	Maxillary artery and nerve
Ethmoidal (one or more)	All species	Ethmoidal vessels and nerve
Orbital	Canine, equine, feline	Abducens, oculomotor, ophthalmic, and trochlear nerves
Orbitorotundum	Bovine	Cranial nerves III–IV, retinal, and internal maxillary arteries
Optic	All species	Optic nerve, internal ophthalmic artery
Rotundum	Canine, equine, feline	Maxillary nerve
Supraorbital	Bovine, canine, equine (feline variable)	Supraorbital vessels and nerve
Caudal palatine	All species	Major palatine vessels and nerve
Maxillary	All species	Infraorbital vessels and nerve
Sphenopalatine	All species	Sphenopalatine vessels and pterygopalatine nerve

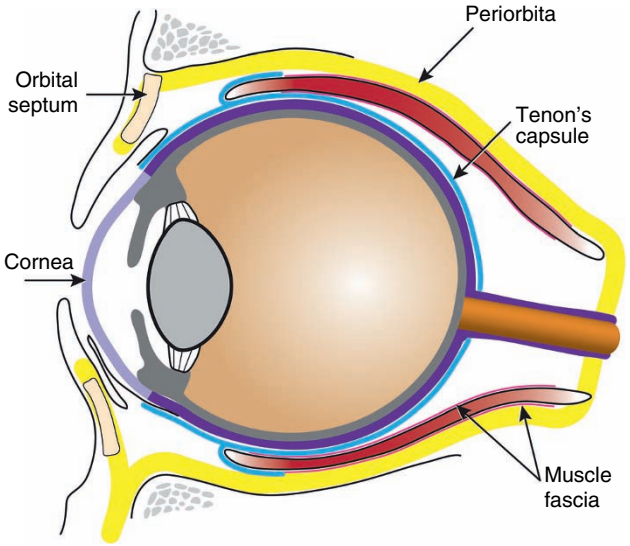

Figure 2.4 Divisions of orbital fascia.

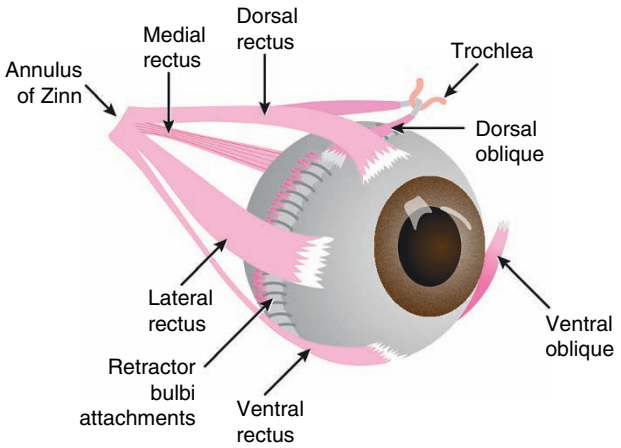

Figure 2.5 Arrangement of the orbital muscles of domestic animals.

cone that separates the optic nerve from the retractor oculi muscle (Murphy et al., 2012).

The EOMs suspend the globe in the orbit and provide ocular motility. There are four rectus muscles: the dorsal, ventral, medial, and lateral recti (Fig. 2.5 and Fig. 2.6). They originate from the orbital apex (i.e., annulus of Zinn) and insert, in the dog, approximately 5 mm posterior to the limbus medially, 6 mm ventrally, 7 mm dorsally, and 9 mm laterally (see Fig. 2.5, Fig. 2.6, and Fig. 2.7). They move the eye in the direction of their names (Table 2.4). The dorsal (superior) oblique originates from the medial orbital apex, continuing forward dorsomedially to pass through a trochlea located near the medial canthus. It then turns acutely, passing dorsolaterally to the globe. It pulls the dorsal aspect of the globe medially and ventrally (intorsion). The ventral (inferior) oblique originates from the anterolateral margin of the palatine bone on the medial orbital wall and passes beneath the eye, crossing the ventral rectus tendon. The muscle divides as it reaches the lateral rectus, with the anterior portion covering the insertion of the lateral rectus and the posterior portion inserting beneath the rectus. The ventral oblique moves the globe medially and dorsally (extorsion) (Prince et al., 1960).

The EOM of birds vary among species. For example, the superior oblique in hawks can produce forces greater than those of owls allowing for greater globe torsion which corresponds with globe shape. Hawks have more globular-shaped eyes and keep their heads facing forwards when tracking prey in contrast with owls that have tubular eyes and utilize head movement to direct field of view (Plochocki et al., 2018).

The retractor oculi (retractor bulbi) muscle originates at the orbital apex and continues forward to form a cone surrounding the optic nerve and inserting posterior and deep to the recti muscles (see Fig. 2.5, Fig. 2.6, and Fig. 2.7). The retractor oculi muscle retracts the globe into the orbit.

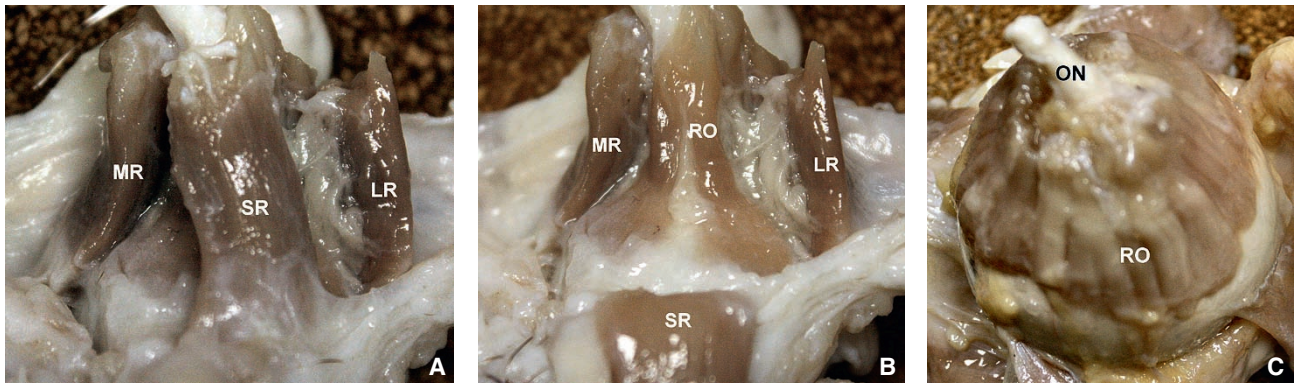

Figure 2.6 Superior lateral view of the canine extraocular musculature. **A.** Lateral rectus muscle (LR), medial rectus muscle (MR), superior rectus muscle (SR). **B.** Same view as seen in **A** but with the superior rectus muscle retracted. RO, retractor oculi muscle. **C.** Posterior view of the equine extraocular musculature. RO, retractor oculi muscle; ON, optic nerve.

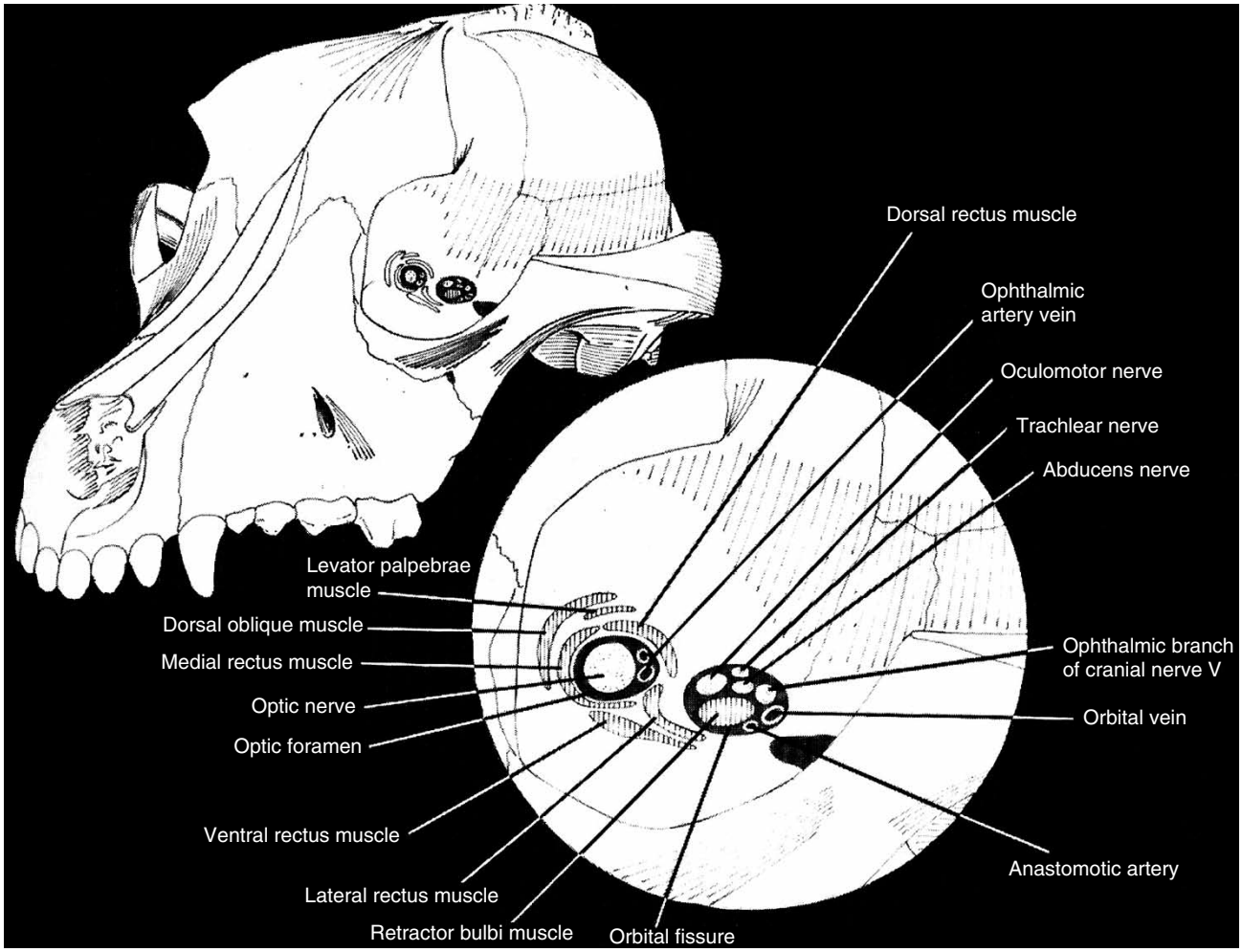

Figure 2.7 Orbital apex of the dog, illustrating structures passing through the optic foramen and orbital fissure as well as the extraocular muscle attachments. (*Source:* Modified from Evans, H. & Christensen, G. (1979) *Miller's Anatomy of the Dog.*, 2nd ed. Philadelphia, PA: W.B. Saunders. Reproduced with permission of Elsevier.)

Table 2.4 Muscles of the eye and eyelids.

Muscle	Function	Nerve supply
Dorsal (superior) rectus	Rotates globe upward	Oculomotor
Ventral (inferior) rectus	Rotates globe downward	Oculomotor
Medial rectus	Rotates globe medially	Oculomotor
Lateral rectus	Rotates globe laterally	Abducens
Dorsal (superior) oblique	Rotates dorsal part of globe medially and ventrally	Trochlear
Ventral (inferior) oblique	Rotates ventral part of globe medially and dorsally	Oculomotor
Retractor oculi (bulbi)	Retracts globe	Abducens
Levator palpebrae superioris	Raises upper eyelid	Oculomotor
Orbicularis oculi	Closes palpebral fissure	Facial
Retractor anguli oculi	Lengthens lateral palpebral fissure	Facial

The retractor oculi muscle is ubiquitous among mammals, but it is absent in various nonmammalian groups, including birds and snakes. The dorsal, ventral, and medial recti as well as the ventral oblique muscles are innervated by the oculomotor nerve (cranial nerve [CN] III), whereas the lateral rectus and retractor oculi muscles are innervated by the abducens nerve (CN VI), and the dorsal oblique muscle is innervated by the trochlear nerve (CN IV) (see Table 2.4).

Eyelids

The eyelids, or palpebrae, are thin folds of skin continuous with the facial skin. The upper (superior) and lower (inferior) eyelids meet to form the lateral and medial canthi (singular canthus). The opening formed by the upper and lower eyelids is the palpebral fissure. This fissure is prevented from assuming a circular shape by the medial (nasal) and lateral (temporal) palpebral ligaments that attach each canthus to the orbital wall. The medial ligament inserts into the periosteum of the nasal bones, whereas the lateral ligament inserts into the temporal fascia and bones associated with the lateral orbit. In the dog, the lateral ligament is essentially replaced by the retractor anguli oculi muscle and its tendon. Closure of the eyelids is achieved by contraction of the orbicularis oculi muscle located deep in the eyelids. Opening the eyelids is accomplished by relaxation of the orbicularis oculi muscle and contraction of the levator palpebrae superioris muscle, which inserts into the upper tarsus.

In the dog the upper eyelid has two to four rows of eyelashes (i.e., cilia) that usually begin near the medial quarter or third

Figure 2.8 Canine eye: medial canthus (A), lateral canthus (B), cilia (C), nictitating membrane (D), ciliary zone of iris (E), pupillary zone of iris (F), collarette (G). *Insert:* Arrows indicate meibomian gland openings.

and either extend across to the lateral canthus or end shortly before the canthus (Fig. 2.8). The lower eyelid has no cilia and has a hairless region approximately 2 mm wide adjacent to the eyelid margin extending the length of the lower eyelid and around the lateral canthus. The medial canthus, unlike the lateral canthus, has variable amounts of facial hair.

In the cat neither lid has cilia, but the leading row of hair from the medial third laterally on the upper eyelid is distinct enough in most cats to be considered cilia (accessory cilia or eyelashes).

In the horse a protuberance of variable size and pigmentation (i.e., the lacrimal caruncle) is present at the medial canthus (Fig. 2.9). The lateral canthus is more rounded than that of the dog, and small amounts of bulbar conjunctiva and sclera are visible both medially and laterally. The exposed lateral conjunctiva is often pigmented. The cilia are well developed on the upper eyelid but absent on the lower eyelid. The cilia begin near the junction of the medial third and the middle third of the eyelid, and they extend almost to the lateral canthus. The facial hair is sparse adjacent to the lower eyelid margins at both the medial and lateral canthi and often at the medial upper eyelid. Horizontal folds are present in both the upper and lower eyelids. Vibrissae (long, specialized tactile hairs) are present on the base of the lower eyelid and on the medial aspect of the upper eyelid.

The eyelids protect the eyes from light, produce part of the tear film, spread the tear film across the cornea, and remove debris from the cornea and conjunctival surfaces. Through closure in a 'zipper-like' fashion from lateral to medial, the eyelids also direct the preocular tear film into the nasolacrimal drainage system.

Histologically, the eyelids consist of four parts: the outermost layer contiguous with adjacent skin, the subjacent orbicularis oculi muscle layer, followed internally by a tarsus and stromal layer, and the innermost layer, the palpebral conjunctiva (Fig. 2.10).

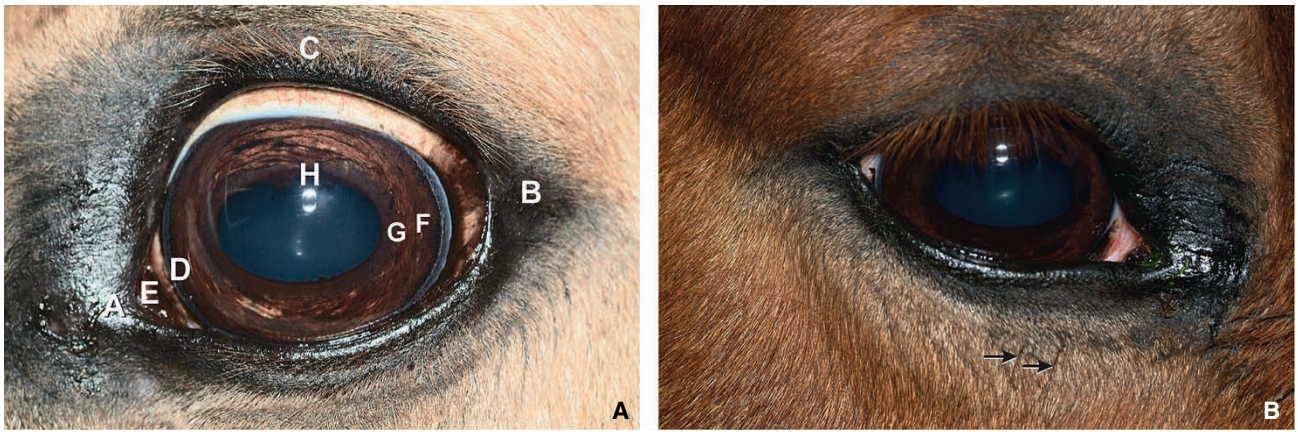

Figure 2.9 Equine eye. **A**. Medial canthus (A), lateral canthus (B), cilia (C), nictitating membrane (D), lacrimal caruncle (E), ciliary zone of iris (F), pupillary zone of iris (G), granula iridica (H). **B**. Arrows indicate vibrissae.

The outer layer of the eyelid is skin covered by a dense coat of hairs with associated sebaceous and tubular glands. In dogs and cats, the hair follicles might be compound. Tactile hairs (pili supraorbitales), similar to the eyebrows of humans, may be present on or near the upper eyelids. Bundles of smooth muscle fibers, arrectores ciliorum, extend from the follicles of the eyelashes toward the tarsus. These muscle bundles are absent in carnivores and humans, but they are common in ruminants (Prince, 1956). The roots of the large cilia are in close association with prominent sebaceous glands (glands of Zeis) and modified apocrine sweat glands (glands of Moll, ciliary glands). The epithelium near the terminus of the gland consists of an outer myoepithelial layer and an inner layer of flattened glandular cells. The structure and location of the glands of Moll are similar in all domestic species (Adam et al., 1970). In primates, including humans, these glands contain a variety of antimicrobial proteins (Stoeckelhuber et al., 2004). These apocrine glands may provide host defense at the margin of the eyelids and possibly in the tears.

Deep to the eyelid skin, there is dense collagenous stroma and bundles of striated muscle fibers that comprise the orbicularis oculi muscle. The orbicularis oculi muscle is arranged in parallel rows that extend nearly the full length of each eyelid. In humans, nearly 90% of the orbicularis oculi muscle fibers consist of the fast type (Hwang et al., 2011).

In the upper eyelid, the levator palpebrae superioris muscle, which originates from the orbital apex, fans out along the dorsal half of the midstroma. The muscle extends toward the inner connective tissue boundary of the orbicularis oculi muscle ending in individual small tendons. The eyelid muscles are separated from the posterior epithelial lining of the eyelids (i.e., the palpebral conjunctiva) by a narrow layer of dense connective tissue. This tissue is well developed in humans and is referred to as the cartilaginous tarsal plate; in most veterinary species, it is less developed (fibrous tissue) and referred to as the tarsus.

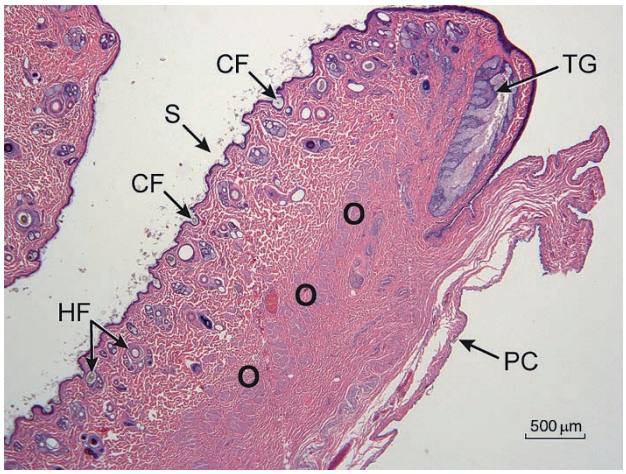

Figure 2.10 Photomicrograph of the eyelid of a dog: hair follicle (HF), cilia follicle (CF), palpebral conjunctiva (PC), tarsal gland (TG), skin (S), orbicularis oculi muscle fibers (O).

The meibomian (tarsal) glands (see Fig. 2.8 and Fig. 2.10) are located in the distal portion of the tarsus near the eyelid margins and contribute to the outer, oily component of the preocular tear film. There are typically 20–40 glands present in each eyelid in the dog (Pollock, 1979), and they are usually more developed in the upper eyelid, especially in cats. These holocrine, modified sebaceous glands form parallel rows of lobules, which have their duct openings on the eyelid margins. The meibomian gland ducts are lined by a keratinized stratified squamous epithelium (Jester et al., 1981). Each gland is made of a number of holocrine acini, which are arranged in vertical columns and open into a central duct. Individual acini have an associated plexi of nerve fibers, which are believed to stimulate their secretion (Chung et al., 1996; Seifert & Spitznas, 1996). The nerve fibers, which are largely parasympathetic in origin, closely appose the basement membrane of each acinus. The eyelids of the

Asian elephant, rock hyrax, and birds are devoid of meibomian glands.

In addition to the meibomian glands, there are accessory lacrimal glands associated with the eyelids. In humans they are referred to as the glands of Krause and Wolfring. The glands of Wolfring are found along the posterior lining of the eyelids whereas the glands of Krause are located at the conjunctival fornix. In domestic species, these accessory glands are most commonly located in the conjunctiva and have been referred to as conjunctival glands. Their contribution to the volume of tear film in cats is negligible (McLaughlin et al., 1988).

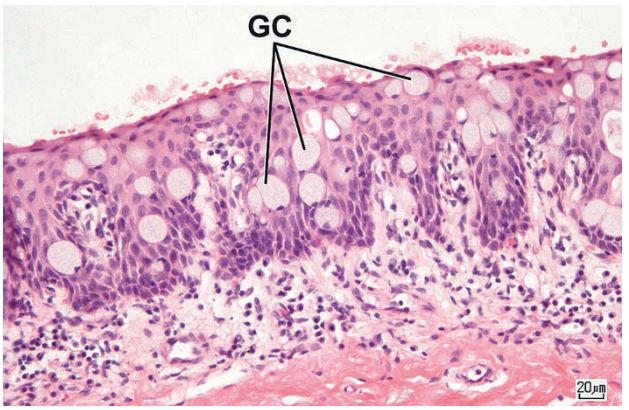

Figure 2.11 Palpebral conjunctiva of a porcine eyelid is externally lined by a stratified to pseudostratified columnar epithelium possessing numerous goblet cells (GC) near the fornix.

Conjunctiva

The conjunctiva is a mucous membrane that lines the inner aspect of the eyelids, the anterior and posterior surfaces of the nictitating membrane (NM), and the exposed sclera. The conjunctiva consists of a thin layer of loose connective tissue beneath a simple to stratified squamous epithelium that becomes consistently stratified toward the eyelid margin. The palpebral conjunctiva lines the inner aspect of the eyelids. As the conjunctiva reflects onto the globe, it is called the bulbar conjunctiva and becomes continuous with the limbal and corneal epithelium. The conjunctiva on the anterior and posterior surfaces of the nictitating membrane is contiguous with the palpebral and bulbar conjunctiva mucosa, respectively. The junction between the palpebral and bulbar conjunctiva is the conjunctival fornix, and the epithelial lining in this region varies according to species, ranging from pseudostratified columnar to stratified cuboidal (Goller & Weyrauch, 1993).

Ventrally, an additional fold is formed by reflection of the conjunctiva over the NM. The reflections at the conjunctival fornix and NM form the conjunctival sac. All parts of the conjunctiva are continuous, but for descriptive purposes, it is divided into the palpebral, bulbar, and fornix conjunctiva and further referenced to specific eyelids. The distribution of goblet cells in the conjunctiva is heterogeneous in the dog (Moore et al., 1987). The highest densities occur along the lower nasal and middle fornix and the lower tarsal portion of the palpebral conjunctiva (Fig. 2.11). In cats the conjunctival goblet cell density varies widely by region but is highest in the anterior surface of the NM and the conjunctival fornices (Sebbag et al., 2016). Additionally, in most domestic species, the bulbar conjunctiva has been reported to either essentially lack goblet cells or has a much lower population of these mucus-forming cells (Bourges-Abella et al., 2007; Doughty, 2002; Grahn et al., 2005). At the fornix, the conjunctiva is arranged into small folds that contain protruding goblet cells and, dorsolaterally, the openings of the lacrimal gland's ducts (Goller & Weyrauch, 1993).

The substantia propria of the conjunctiva is composed of two layers: a superficial adenoid layer, which in the dog and cat contains a variable presence of lymphatic follicles and glands; and a deep, fibrous layer that contains the conjunctival nerves and vessels. The arteries of the conjunctiva arise from the anterior ciliary arteries, which are branches of the external ophthalmic artery, and from branches of the superior and inferior palpebral and malar arteries (Murphy et al., 2012).

The lymphatics of the conjunctiva, called the conjunctiva-associated lymphatic tissue (CALT), are arranged in two plexuses: a superficial and a deep system. CALT is generally diffuse with intermittent nodules or follicles. Often the diffuse component of CALT infiltrates and is adjacent to tear-secreting glands, especially those associated with the NM. Variations in the size and distribution of nodules occur between the upper and lower eyelids and are influenced by exposure to various foreign substances including potentially infectious microorganisms (Fix & Arp, 1991). Cells such as CD8-positive suppressor/cytotoxic effector cells are generally more prevalent (Knop & Knop, 2005). CALT of domestic and wildlife species can have follicle-associated conjunctival epithelium where goblet cells are characteristically absent, being replaced by antigen-absorptive cells called M (i.e., microfold) cells (Samuelson et al., 2011). The ultrastructural appearance of these cells is not identical to those described in mucosa-associated lymphoid tissues throughout the body (Chodosh et al., 1998). The lymphatic drainage of the conjunctiva is toward both commissures, where the drainage joins the lymphatics of the eyelids. Drainage from the lateral commissure is to the parotid lymph nodes, whereas the medial regions drain to the mandibular lymph nodes.

The conjunctiva at the fornix is very thin and translucent, and it lies loosely on the underlying connective tissue. In the domestic carnivore, approximately 3 mm from the limbus, the bulbar conjunctiva, Tenon's capsule, and sclera become closely united. The connective tissue is much more abundant in this location in the dog than in humans and other species.

The primary functions of the conjunctiva are to prevent desiccation of the cornea, to allow mobility of the eyelids and the globe, and to provide a physical and physiological barrier against microorganisms and foreign bodies. This latter role is most important considering that conjunctival sacs house considerable microbial flora, including many potential pathogens (Samuelson et al., 1984a).

Nictitating Membrane

The NM (membrana nictitans, third eyelid, or *plica semilunaris*) protrudes from the medial canthus in the ventromedial anterior orbit (see Fig. 2.8). It contains a cartilaginous, T-shaped plate, the horizontal part of which is parallel with the free or leading edge of the membrane (Fig. 2.12). In many animal species, the free edge is pigmented. The stroma consists of loose to dense connective tissue that supports glandular and lymphoid tissue (Fig. 2.13). The distal portion of the anterior (i.e., palpebral) and posterior (i.e., bulbar) surfaces is usually covered with nonkeratinized stratified squamous epithelium. The NM possesses a prominent accessory lacrimal gland often referred to as the NM gland (nictitans gland) or gland of the NM (Murphy et al., 2012). In many species, the gland surrounds much of the vertical base of the cartilaginous plate. This gland is serous in horses and cats, mixed (seromucous) in cattle and dogs, and mostly mucous in pigs (Aughey & Frye, 2001; Murphy et al., 2012).

The cartilage of the NM is predominately elastic in horses, cats, and pigs and hyaline in ruminants and dogs (Banks, 1993). The three-dimensional shape of the cartilage varies considerably among domestic species (Schlegel et al., 2001). The horizontal portion of the T cartilage appears as a reverse S-shape in the cat, a crescent-shape in the dog, and a hook-shape in the horse.

The Harderian gland (Harder's gland) when present, is usually located posterior to the NM, and appears grossly and histologically to be an extension of the NM gland. This glandular tissue in some animals can be considerably larger than the NM gland. The anatomical presence of the Harderian gland among mammals has been found mostly in rodents (mouse, rat, Guinea-pig, Mongolian gerbil, golden hamster, wood mouse, Plains mouse, various squirrel species, chipmunk, and deer mouse), with only the Mongolian gerbil having the nictitans gland as well. Other mammals that possess the Harderian gland exclusively include members of Insectivora (hedgehog and shrews), species of deer (red deer, fallow deer), nine-banded armadillo, cottontail rabbit, and

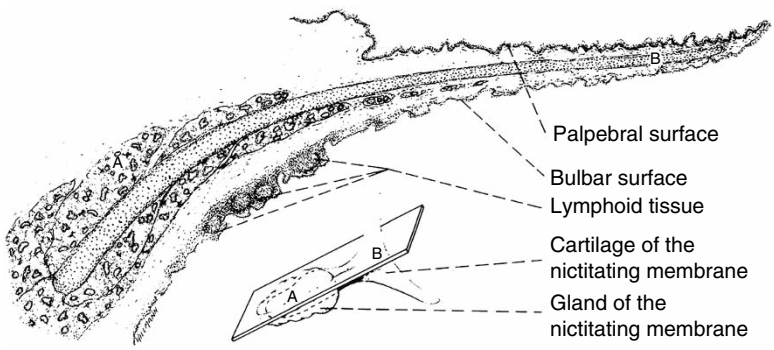

Figure 2.12 Drawing of a histologic section of the mammalian nictitating membrane. (*Source:* Modified from Evans, H. & Christensen, G. (1979) *Miller's Anatomy of the Dog*, 2nd ed. Philadelphia, PA: W.B. Saunders. Reproduced with permission of Elsevier.)

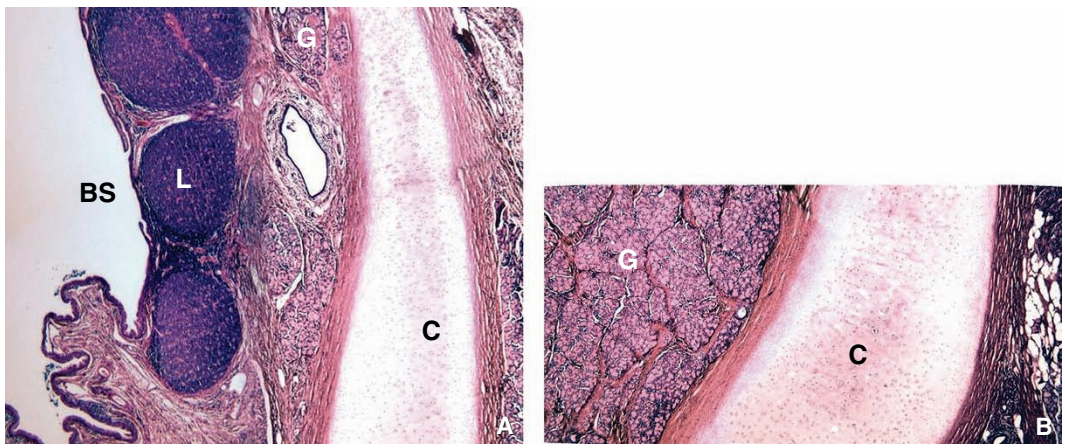

Figure 2.13 **A**, **B**. Nictitating membrane of the horse contains both glandular (G) and lymphoid (L) tissues, with the latter being superficially located within the stroma next to the bulbar surface (BS). C, cartilage. (Original magnification, 10×.)

Afghan pika. Besides the Mongolian gerbil, mammals with both nictitans and Harderian glands are the pig and rabbit (Sakai, 1992).

In mammals, the secretory cells of the Harderian glands are columnar and lined by myoepithelium. The adenomeres are generally tubular or tubuloalveolar and secrete lipid materials in addition to seromucous products. In rodents, the lipids are released uniquely in an exocytotic (merocrine) manner (Payne, 1994). Most importantly, their secretions contain unusual compounds including porphyrins and melatonin (Menendez-Pelaez & Buzzel, 1992; Spike et al., 1992).

Harderian glands contain autonomically controlled nerves and are also under the control of gonadal, thyroid, and pituitary hormones. The functions of this gland remain speculative, but they may include immunologic defense, photoprotection, provision for thermoregulatory lipids, osmoregulation, reproductive influences, and pheromone production.

In most domestic animals, the movement of the NM is indirect, resulting from contraction of the retractor oculi muscle, which retracts the globe into the orbital space and causes passive elevation of the NM. However, in the domestic cat, the retractor oculi muscle is less well developed, and small bundles of smooth muscle have been found in the NM that most likely contribute to its more rapid movements. Specifically, there are nine strands of smooth muscle fibers that extend into the feline's NM and are believed to be involved with its protrusion and retraction (Nuyttens & Simoens, 1995). Each strand is discrete, much like the erector pili muscle associated with hair follicles of skin, but more developed. These smooth muscle bundles or strands contribute to forward movement of the NM, quite possibly in response to an endocrine signal (fight or flight). In birds and other nonmammalian species that lack a retractor oculi muscle, movement of the NM is controlled by the pyramidalis and quadratus muscles, attached to the posterior surface of the sclera (Duke-Elder, 1958). The pyramidalis and the quadratus muscles are skeletal muscles controlled by the oculomotor nucleus that moves the NM anteriorly (Bravo & Inzunza, 1985; Maier et al., 1972).

Lacrimal and Nasolacrimal System

An adequate precorneal tear film (PTF) is necessary for optical integrity, maintenance of the cornea, and normal ocular function. The PTF serves several functions, including the following

1) maintenance of an optically uniform corneal surface
2) removal of foreign material and debris from the cornea and conjunctival sac
3) delivery of an oxygen source to the avascular cornea, and
4) provision of antimicrobial substances.

The PTF is trilaminar, although all three layers are intricately mingled. The outer, thin, oily layer is produced by the meibomian glands and sebaceous glands of Zeis. This layer reduces evaporation of the underlying aqueous layer and forms a barrier along the lid margins that prevents tear overflow.

The middle layer is the aqueous layer and is secreted by the orbital lacrimal gland (61.7%), the accessory glands (3.1%), and the gland of the NM (35.2%) (Gelatt et al., 1975). This layer delivers oxygen and other nutrients to the avascular cornea and provides a volume of fluid to 'flush' the ocular surface and remove debris.

The innermost layer is the mucin layer and is produced predominately by the conjunctival goblet cells. The glycocalyx, produced by the corneal epithelial cells, also contributes to the mucin layer. The mucin produced by lacrimal and lacrimal-accessory glands that have mucus-secreting cells, contributes to the mucin layer as well. The mucin is adsorbed to the corneal epithelial surface and is distributed evenly during normal blinking. This layer provides a hydrophilic surface over which the aqueous tear fluid spreads evenly and lubricates the corneal and conjunctival surfaces.

Excess lacrimal fluid collects by gravity in the lower conjunctival sac and is mechanically 'pumped' through the upper and lower lacrimal puncta located approximately 1–2 mm inside the margin of the medial eyelid. Each punctum is surrounded by smooth muscle that works in coordination with eyelid blinking to remove excess lacrimal fluid and prevent its backflow. The puncta continue as the upper and lower canaliculi, which pass slightly vertically away from the eyelid margins and turn toward the medial canthus, pass through the periorbita, and meet at a dilation, the lacrimal sac, located in the lacrimal fossa of the lacrimal bone (Fig. 2.14). This sac empties into the nasolacrimal duct, which passes through a short, bony canal and opens into the nasal cavity, where it continues as a duct until it reaches an opening at the floor of the nostril approximately 1 cm from the end of the nares. Approximately 40% of dogs have an

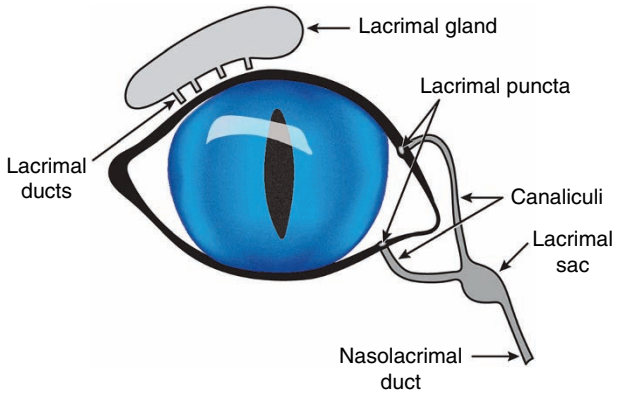

Figure 2.14 The nasolacrimal system.

accessory opening in the canal as it passes by the root of the upper canine tooth (Michel, 1955). For a comprehensive review of the nasolacrimal system anatomy and disorders, the reader is referred to Ali et al. (2019).

The lacrimal gland is a diamond-shaped structure in the dorsolateral aspect of the orbit underneath the orbital ligament (Park et al., 2016). The mean length, width, thickness, and weight of the lacrimal gland in three different breeds of dogs were ~17 ± 0.7 mm, ~13 ± 0.4 mm, ~3 ± 0.1 mm, and ~316 ± 21 mg, respectively (Park et al., 2016). Fifteen to 20 small ductules drain into the superior conjunctival fornix. Histologically, the gland is a tubuloalveolar type. The lacrimal gland produces the majority of the aqueous portion of the preocular tear film. In rats and rabbits, mucous components are also secreted from the lacrimal gland (Ding et al., 2011; Draper et al., 1998). The innervation to the lacrimal gland is not fully understood, but the lacrimal branch of CN V, sympathetic, and parasympathetic nerves are all involved in its function. Clinically, certain cholinergic drugs (e.g., pilocarpine) stimulate tear secretion, whereas other drugs (i.e., anticholinergics) decrease tear secretion.

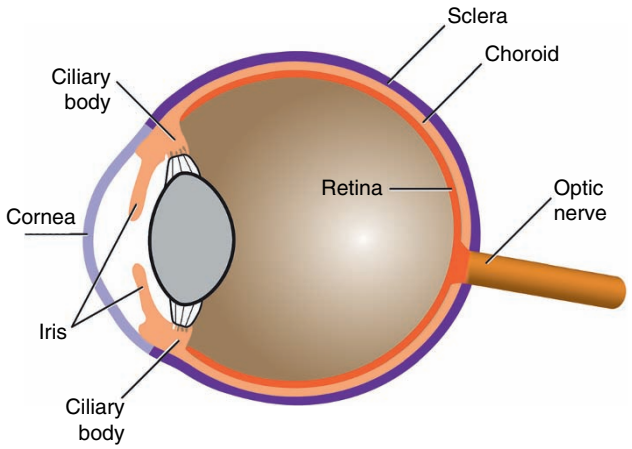

Figure 2.15 The three tunics that comprise the mammalian globe. Outermost fibrous tunic (light and dark purple), consisting of the cornea and sclera; the middle tunic called the uvea (light orange), consisting of the iris, ciliary body and choroid; and the nervous tunic (dark orange) consisting of the retina and optic nerve.

Globe

Components

The globe is composed of three basic layers or coats (Fig. 2.15). The outer layer is the fibrous tunic which is further divided into the cornea and sclera. The fibrous tunic provides shape to the eye. In addition, the anterior portion of the fibrous tunic (i.e., the cornea) is transparent, thus enabling light to pass through, and is shaped in a manner that makes it a powerful lens that refracts light rays centrally, toward the visual axis of the eye. The middle layer is the vascular tunic, called the uvea (meaning "grape"). The uvea is further divided into the iris, ciliary body, and choroid and is heavily pigmented and vascularized. It functions to restrict the amount of light entering the eye and to provide nourishment and remove waste products. The innermost layer is the nervous tunic, which consists of the retina and optic nerve. The three tunics embrace the large, inner, transparent media of the eye: the aqueous humor, lens, and vitreous humor, which collectively function to transmit and refract light to the retina and provide an internal pressure that keeps the globe firmly distended.

Size, Shape, and Topography

The eyes in domestic animals are quite variable in size, but their shapes are comparatively uniform, being spherical in most instances, in which the three axes of the globe (anteroposterior, horizontal or transverse, and vertical) are nearly identical in dimensions (see Table 2.5 and Table 2.6). Some of the larger ungulates, including the cow and horse, possess globes that are relatively flattened in the anteroposterior axis (Fig. 2.16). The geometric axis of the eye is positioned from the center of the cornea (i.e., anterior pole) to the posterior center of the sclera (i.e., posterior pole). Two principal planes, the equatorial and meridional, are traditionally used

Table 2.5 External globe dimensions.

Animal	Meridional A–P axis of the eye, A (mm)	Equatorial axis, V (mm)	Horizontal, T (mm)	Ratio of A/V/T	Ratio of V/T
Horse	43.68	47.63	48.45	1:1.09:1.10	1:1.10
Cow	35.34	40.82	41.90	1:1.15:1.18	1:1.02
Sheep	26.85	30.02	30.86	1:1.11:1.15	1:1.02
Pig	24.60	26.53	26.23	1:1.08:1.06	1:0.99
Dog	21.73	21.34	21.17	1:0.98:0.97	1:0.99
Cat	21.30	20.60	20.55	1:0.97:0.96	1:0.99

Source: Translated from Bayer, J. (1914) *Angenheilkunde*. Vienna: Braumueller.

Table 2.6 Globe dimensions.

Animal	Axial globe length (mm)	Anterior chamber depth (mm)	Axial lens thickness (mm)	Vitreous chamber depth (mm)	Reference
Horse	39.23 ± 1.26	5.63 ± 0.86	11.75 ± 0.80		McMullen & Gilger, 2006
	40.4 ± 1.8	6.8 ± 0.5	11.7 ± 0.6	21.8 ± 1.3	Mouney et al., 2012
Dog	20 ± 1.6	3.8 ± 0.1	6.7 ± 1.0		Williams, 2004
Cat	19.75 ± 1.59	4.66 ± 0.86		7.92 ± 0.86	Konrade et al., 2012
	20.91 ± 0.53	5.07 ± 0.36	7.77 ± 0.23		Gilger et al., 1998

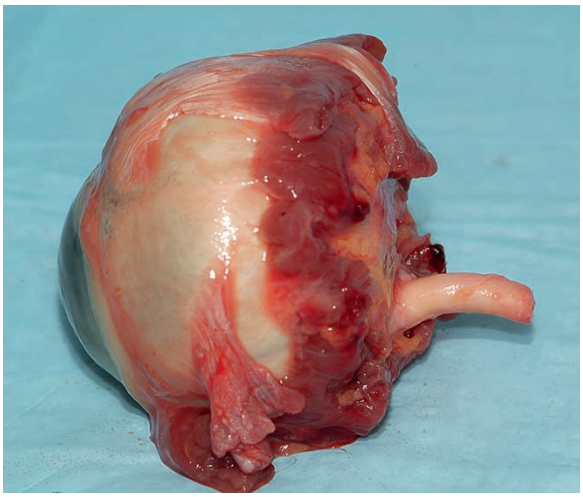

Figure 2.16 Lateral view of an equine globe. Note the marked flattening in the anteroposterior axis and the marked ventral exit of the optic nerve from the posterior pole.

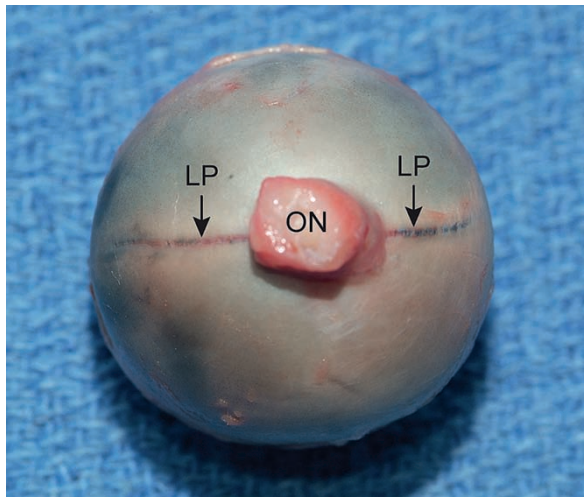

Figure 2.18 Posterior view of a canine globe. LP, long posterior ciliary artery; ON, optic nerve.

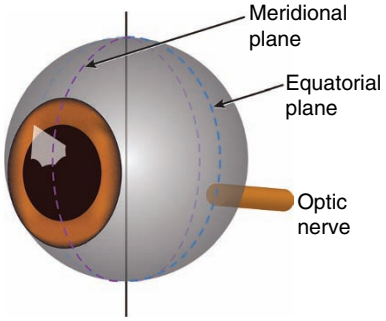

Figure 2.17 The equatorial and meridional planes of the eye.

in references to the three axes (Fig. 2.17). The equatorial plane bisects the anterior and posterior poles and is perpendicular to the meridional plane. Any plane that runs parallel to the equatorial plane is called the frontal, coronal, radial, or transverse plane. The meridional plane moves along the anteroposterior axis of the eye, vertically dividing it into medial and lateral halves, even though meridional planes can be horizontal or oblique. Planes that run parallel to the meridional plane are described as sagittal planes.

The optic nerve in most domestic animals lies inferior and lateral to the posterior pole. Surrounding the optic nerve are many ciliary nerves and short posterior ciliary arteries. In normal dogs, the mean number of short posterior ciliary arteries is 12 (~7 dorsally and ~5 ventrally) (Frick & Dubielzig, 2016). The posterior ciliary nerves pursue a long intrascleral course (up to 12 mm) before entering the suprachoroidal space to reach the iris, ciliary body, and limbus. In the dog, the long posterior ciliary arteries enter the sclera approximately 3–5 mm from the optic nerve in the horizontal meridian (Fig. 2.18). In the cat, these arteries can enter the sclera immediately adjacent to the optic nerve. These vessels are visible on the nasal and temporal sides of the eye within the sclera at least as far as the equator before entering the choroidal space. At this point, each artery accompanies the long ciliary nerve to the iris and ciliary body. Recurrent vascular branches enter the choroid, but the main vessel trunk continues to be the major supply to the iris. A variable number of vortex veins (usually four) emerge from the sclera posterior to the equator; typically, two vortex veins are present dorsally and two ventrally.

Several topographic features help establish the proper anatomic positions of an enucleated globe. For example,

observation of the long posterior arteries and the longer horizontal dimension of the cornea determines the horizontal meridian. Location of the ventral exit of the optic nerve and the dorsal oblique muscle tendon establish the dorsoventral aspect of the globe. Remnants of the NM and the lateral placement of the optic nerve to the posterior pole determine the medial and lateral aspects.

Cornea

The cornea is the transparent, anterior portion of the fibrous tunic of the globe. Like the lens, the cornea is normally clear and transmits and refracts light (40–42 diopters in dogs). The avascular cornea relies on both the aqueous humor and tear film for nourishment and on the eyelids and NM for protection from the external environment.

The cornea is elliptical in shape, with a horizontal diameter greater than the vertical. In the dog and the cat, the difference between these diameters is small, thus making their corneas appear almost circular (see Fig. 2.8). In most ungulates, this difference is much more pronounced, allowing for a remarkable horizontal field of view (Fig. 2.19) that is further complemented by the lateral positioning of the orbits. The combination of the exaggerated corneal dimensions and orbital positions in these grazing animals appears to be the adaptive result of their feeding behavior, affording them greater protection from predators.

Corneal thickness varies between species, breeds, individuals, and location (i.e., central vs. peripheral cornea). In most domestic animals, it is less than 1 mm thick. Table 2.7 lists the central corneal thickness in dogs, cats, and horses using selected noninvasive diagnostic imaging modalities. One study using ultrasonic pachymetry in cats found there is no significant difference in mean corneal thickness between the central and peripheral cornea (Gilger et al., 1993). However, another study using the same modality found that the feline cornea is not uniform in thickness; when compared with the axial cornea, the superior nasal area is thinner, and the temporal area is thicker (Schoster et al., 1995). In dogs, the superior peripheral and temporal peripheral cornea are significantly thicker than the central cornea (Gilger et al., 1991).

Corneal thickness is also influenced by age and time of day. Corneal thickness increases significantly with age in the dog, cat, and horse (Gilger et al., 1991, 1993; Herbig & Eule, 2015). Additionally, central corneal thickness and intraocular pressure (IOP) in healthy Beagles are significantly lower

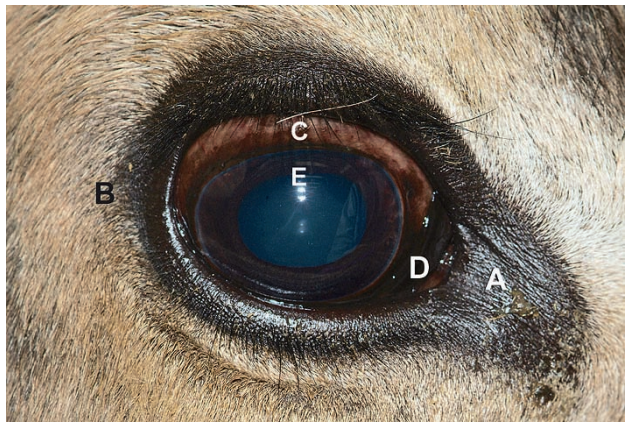

Figure 2.19 The globe of the cow viewed anteriorly. Note the horizontally elongated ellipse of the cornea. A, medial canthus; B, lateral canthus; C, cilia; D, nictitating membrane; E, granula iridica.

Table 2.7 Corneal thickness.*

	SD-OCT (μm)	Scheimpflug (μm)	Confocal (μm)	Ultrasound pachymetry (μm)	High resolution ultrasound biomicroscopy (μm)
Dog	610.56 ± 57.48[d] 587.72 ± 32.44[f] 611.2 ± 40.3[j] 497.54 ± 29.76[n] 606.83 ± 39.5[s]	629.73 ± 64.57[d] 606.83 ± 39.45[h]	585 ± 79[k]	560 ± 5.2[a] 554.95 ± 72.41[c] 598.54 ± 32.28[f] 555.49 ± 17.19[n] 545.6 ± 21.7[q]	689.77+55.93[d]
Cat	584.93 ± 39.05[e] 629.08 ± 47.05[g]	606.41 ± 44.18[e]	592 ± 80[k]	578 ± 64[b] 546 ± 48[r]	
Horse	812.0 ± 44.1[i] 800 ± 50[l]		835[m]	770.0 ± 7.5[o] 785.6 ± 2.98[p] (Miniature Horse)	

* Most data is from the central cornea, but not all papers stated measurement location.
SD-OCT, spectral-domain optical coherence tomography.
[a] Gilger et al., 1991; [b] Gilger et al., 1993; [c] Garzon-Ariza et al., 2017; [d] Wolfel et al., 2017; [e] Cleymaet et al., 2016; [f] Alario & Pirie, 2014b; [g] Alario & Pirie, 2013a; [h] Alario & Pirie, 2013b; [i] Pirie et al., 2014; [j] Alario & Pirie, 2014a; [k] Kafarnik et al., 2007; [l] Pinto & Gilger, 2014; [m] Ledbetter & Scarlett, 2009; [n] Strom et al., 2016a; [o] Ramsey et al., 1999; [p] Plummer et al., 2003; [q] Martin-Suarez et al., 2014; [r] Schoster et al., 1995; [s] Alario & Pirie, 2013b

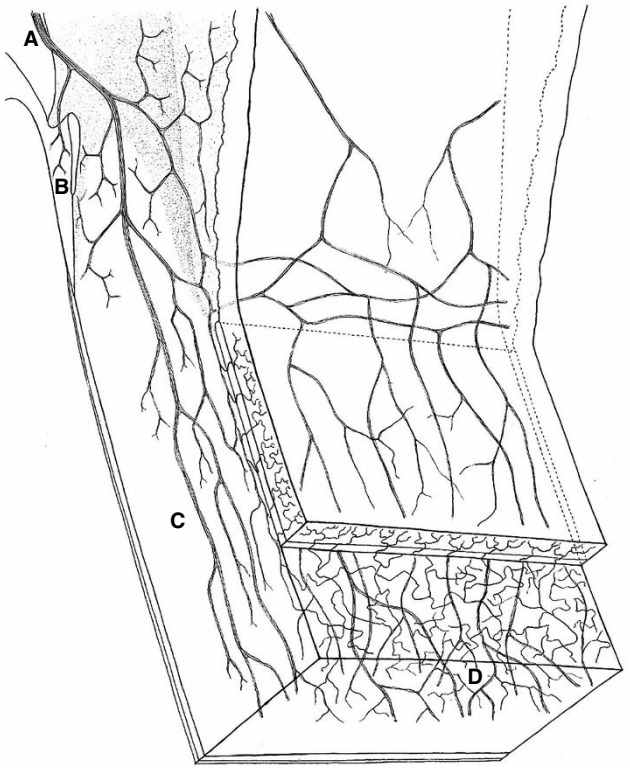

Figure 2.20 Innervation of the limbus and cornea. The long ciliary nerve (A) supplies the limbal region, then sends branches into the cornea. Nerves also supply the trabecular meshwork (B) and the region of the canal of Schlemm (i.e., angular aqueous plexus in nonprimates). Note the paucity of nerves in the deep cornea (C) and their absence in the region of Descemet's membrane as compared with a multitude of branched endings of nerves within the anterior stroma (D) and epithelium. (*Source:* Modified from Hogan, M.J., Alvarado, J.A. & Weddell, J.E. (1971) *Histology of the Human Eye*. Philadelphia, PA: W.B. Saunders. Reproduced with permission of Elsevier.)

in the afternoon/evening than in the morning (Garzon-Ariza et al., 2017; Martin-Suarez et al., 2014).

The cornea is richly supplied with sensory nerves, particularly pain receptors, and this sensitivity provides protection to the cornea and helps maintain transparency (Fig. 2.20). The cornea is innervated by the long ciliary nerves, which are derived from the ophthalmic branch of the trigeminal nerve (Mawas, 1951). The epithelial cell layers are richly innervated, and these nerve endings are unsheathed among the epitheliae. Use of immunohistochemical localization of neuropeptides associated with the ciliary ganglion in the dog has revealed the presence of a well-developed pattern of epithelial innervation consisting of numerous horizontally oriented leash formations at the level of the epithelial basal cells (Marfurt et al., 2001). These formations comprise anastomotic networks of variously sized nerve fascicles that course circumferentially along the limbus, becoming oblique to eventually radial in orientation centrally. By comparison, stromal innervations, which exist superficially, consist of main bundles that repetitively branch in a dichotomous manner to create elaborate axonal arborizations. In general, the most superficial layers are primarily innervated with pain receptors, whereas more pressure receptors are found in the stroma. This explains why a superficial corneal injury is often more painful than a deeper wound.

The following anatomic factors contribute to the transparency of the cornea

1) lack of blood vessels
2) nonkeratinized surface epithelium maintained by a PTF
3) lack of pigmentation
4) relative dehydration (deturgescence), and
5) size and organization of stromal collagen fibrils.

The cornea comprises four (sometimes five) layers. From superficial to deep, the layers are the epithelium, Bowman's layer (in some species), stroma, Descemet's membrane, and endothelium (Fig. 2.21).

Corneal Epithelium

The corneal epithelium is a nonkeratinized, stratified squamous epithelium that covers the anterior corneal surface. The epithelium is approximately 25–40 µm thick in the domestic carnivore and two to four times thicker in the ungulate. In the dog, cat, and bird, the anterior epithelium consists of a single layer of basal cells that lie on a thin basement membrane; two or three layers of polyhedral (i.e., wing) cells and two or three layers of nonkeratinized squamous cells (Fig. 2.21 and Fig. 2.22). In larger animals, the layers of polyhedral and squamous cells are more numerous. The cells are arranged to provide orderly replacement of the surface cells during desquamation. In normal Beagles, the superficial epithelial cell diameter is 43.3 ± 6.6 µm

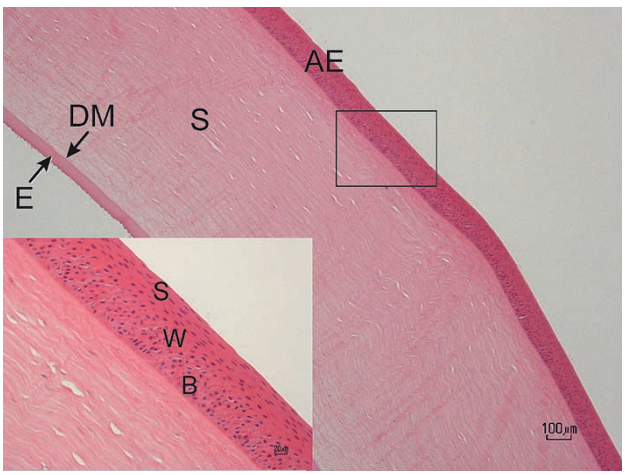

Figure 2.21 Histologic view of the four layers in the equine cornea: anterior epithelium (AE), stroma (S), Descemet's membrane (DM), and endothelium (E). *Insert*: Basal cells (B), wing cells (W), squamous cells (S).

and the basal cell diameter is 4.4 ± 0.7 µm as examined via *in vivo* confocal microscopy (Strom et. al., 2016b).

The basal cells are tall, columnar cells with a flattened base and domed apex. They are crowded together, and as a result, the nuclei, which are located in the apical region, are often forced into two or alternating layers. Mitosis is confined to the basal cells or those cells immediately superficial to the basal cells (i.e., stratum germinativum). Adjacent cell surfaces have small infoldings with numerous desmosomal attachments (Hogan et al., 1971; Shively & Epling, 1970). Occasional lymphocytes are present in the basal epithelium and more superficial layers.

Wing cells are polygonal-shaped cells superficial to the basal cells. Wing cells vary from two or three layers in thickness to several layers, depending on the species and the location in the cornea. These layers form a transition zone between the columnar basal cells and the more superficial squamous cells.

There are several layers of flattened superficial squamous cells. The cells appear to be flat and polygonal with straight borders on scanning electron microscopy (SEM) (Fig. 2.23 and Fig. 2.24). Both light and dark cell types can be identified. The light cells contain more microvillae and microplicae. These numerous projections scatter electrons and, as a result, produce a lighter appearance of the cell. The darker cells are older and are occasionally seen to be desquamating

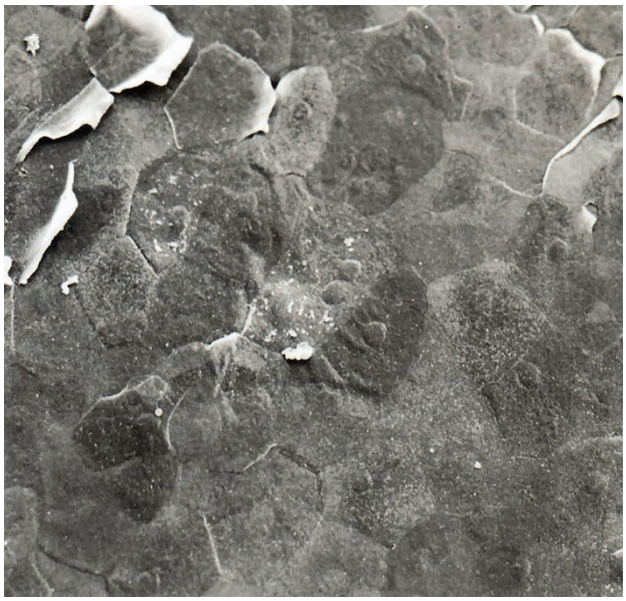

Figure 2.23 SEM shows the surface of the anterior epithelium of a bovine cornea. The surface cells can be light or dark. Note the round bulges, where the nuclei lie within each cell. Note also that some cells appear to be desquamating. (Original magnification, 400×.)

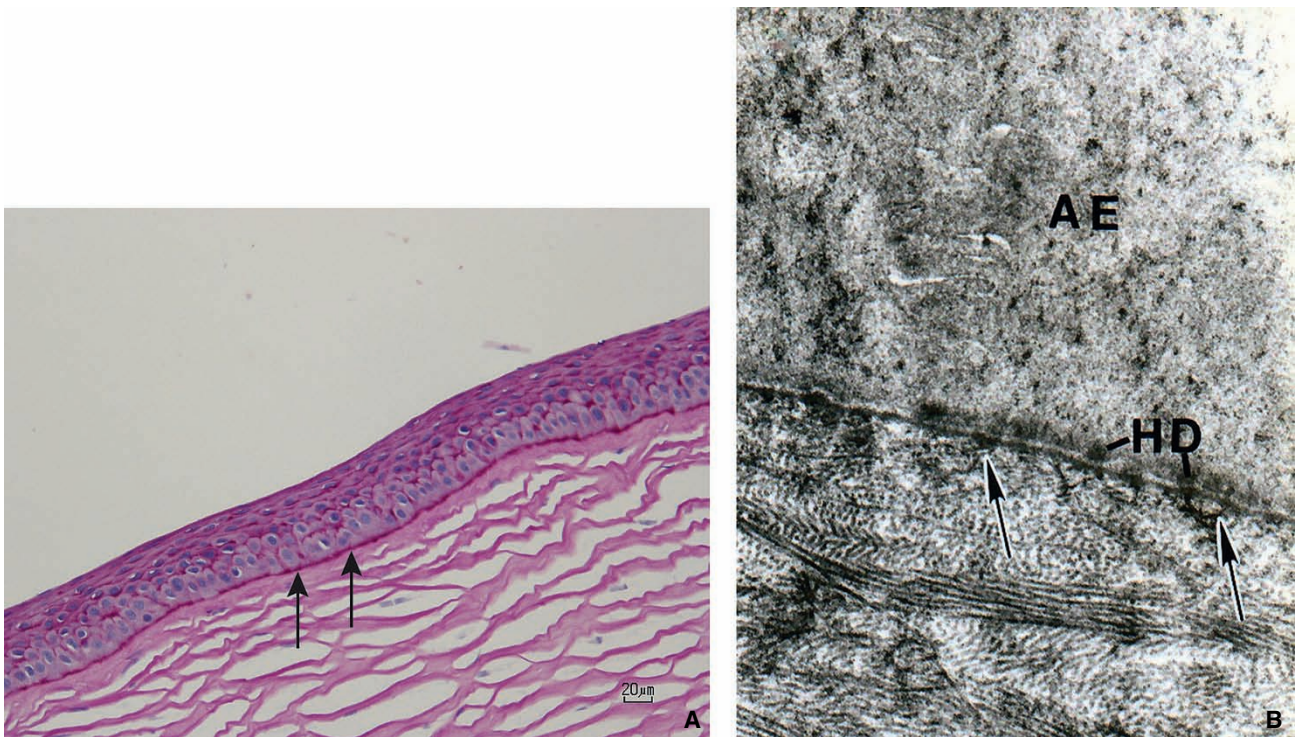

Figure 2.22 Basement membrane (arrows) of the anterior epithelium of the canine cornea viewed light microscopically with the aid of PAS stain (**A**) and ultrastructurally (**B**). AE, anterior epithelium; HD, hemidesmosomes. (Original magnification, 18,000×.)

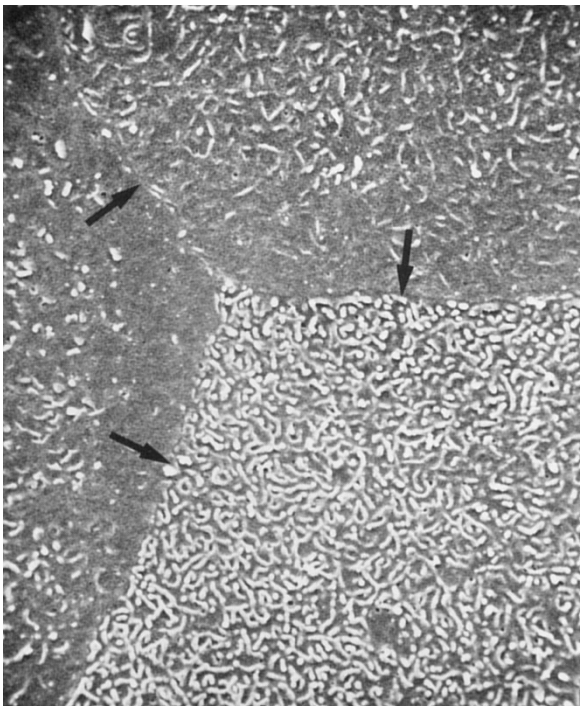

Figure 2.24 SEM shows the corneal epithelial surface of a horse. Junction of a light cell with two dark cells (arrows) illustrates the increased numbers of microplicae and microvillae in the light cell. (Original magnification, 3888×.)

(see Fig. 2.23). Cells in the central cornea have more projections (i.e., microplicae and microvillae) than those in the periphery. It has been proposed that the fine microplicae and microvillae that considerably expand the cells' surface area enable movement of oxygen, potential nutrients, and various metabolic products across the exposed cell membranes of the outermost squamous epithelial cells (Collin & Collin, 2006). However, it is unlikely that the surface expansion would facilitate that process significantly among terrestrial mammals. More than likely, the microprojections of the squamous epithelial cells, which can be sometimes intricate in their patterns, allow mucin of the PTF to adhere firmly to the anterior epithelium which aids in stabilizing the tear film on the corneal surface (Blumcke & Morgenroth, 1976; Harding et al., 1974).

The cytoplasm of the superficial cells contains numerous tonofilaments and vesicles but generally lacks the mitochondria, rough endoplasmic reticulum, and ribosomes that are present in the basal and wing cells. Cytokeratins have been demonstrated in the corneal epithelium of several species (Nautscher et al., 2016). Numerous desmosomal attachments are present, and the surface cells have a zonula occludentes on their lateral membranes.

The corneal epithelium is thicker at the periphery of the cornea than in the center. With the junction of the bulbar conjunctiva, however, it abruptly thins, and pigmented cells

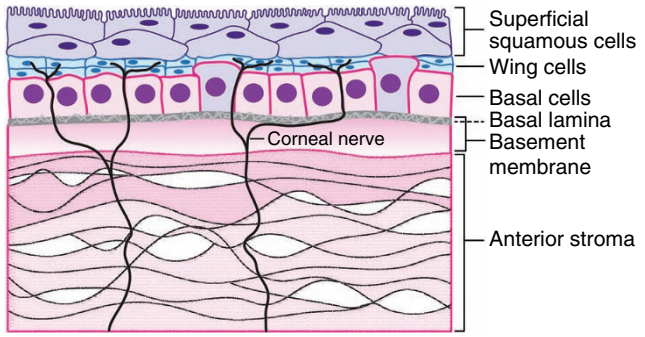

Figure 2.25 The corneal epithelium and anterior stroma. Nonkeratinized squamous cells (2–3 layers), wing cells (2–3 layers) basal cells (single layer), basal lamina, and corneal nerves.

are observed. At the limbus, pigment is scattered in all layers except the superficial squamous cells. Nerves enter the epithelium and terminate among the wing cells (Fig. 2.25; Hogan et al., 1971).

Beneath the epithelium is a basement membrane, which stains positively with periodic acid–Schiff (PAS) (see Fig. 2.22A). The basal cells are firmly attached to the basal lamina of the basement membrane (i.e., anterior limiting lamina) by hemidesmosomes, anchoring collagen fibrils, and the glycoprotein laminin. Various types of collagen are found within the different layers of the cornea (Table 2.8). Interestingly, evidence of type IV collagen, which is ubiquitous throughout basement membranes of the body, is weak (Nakamura et al., 1994a, 1994b). Hyaluronan and fibronectin also have been associated with corneal epithelial attachment (Nakamura et al.,1994a). Ultrastructurally, the basement membrane consists of a 30–55 nm thick osmiophilic layer that is separated from the basal cell plasma membrane by a 25 nm wide, electron-lucent zone (see Fig. 2.22B). Hemidesmosomes attach the basal cells to the basement membrane, which in turn anchors the epithelium to the stroma. The arrangement of hemidesmosomes varies among different animals, being linear among mammals and amphibians, in rosettes among birds and reptiles, and punctate without arrangement, or completely absent, among fish (Buck, 1983). The epithelial cells have strong regenerative abilities (basal cell turnover time is approximately 7 days), but after removal of the basal lamina, weeks to months may be necessary for it to completely reestablish; until the basement membrane is completely reformed, the epithelium can be easily removed from the stroma (Gelatt & Samuelson, 1982; Khodadoust et al., 1968).

Stroma

The corneal stroma (i.e., the substantia propria) constitutes 90% of the corneal thickness. It consists of transparent lamellae of collagenous tissue, and these lamellae lie in sheets and separate easily into planes (Fig. 2.26A).

Table 2.8 Location of glycans and collagen types in the cornea.

Location	Types of collagen	Glycans[a]	References
Anterior epithelium/ basement membrane	IV, VI, and VII	Laminin, fibronectin, hyaluronans	Nakamura et al., 1994b; Smolek & Klyce, 1993
Bowman's layer/ anterior stroma	I, III, V, and VI	Heparan sulfate	Gordon et al., 1994
Stroma	I, III, V, VI, and XII	Chondroitin 6- and 4-sulfates, dermatan sulfate	Cintron & Covington, 1990; Doane et al., 1992; Linsenmayer et al., 1993; Nakamura et al., 1994b; Takahashi et al., 1993
Descemet's membrane	I, III, IV, V, VI, and VIII	Laminin, fibronectin tenascin, P component, heparan sulfate	Tamura et al., 1991

[a] Includes glycoproteins and glycosaminoglycans.

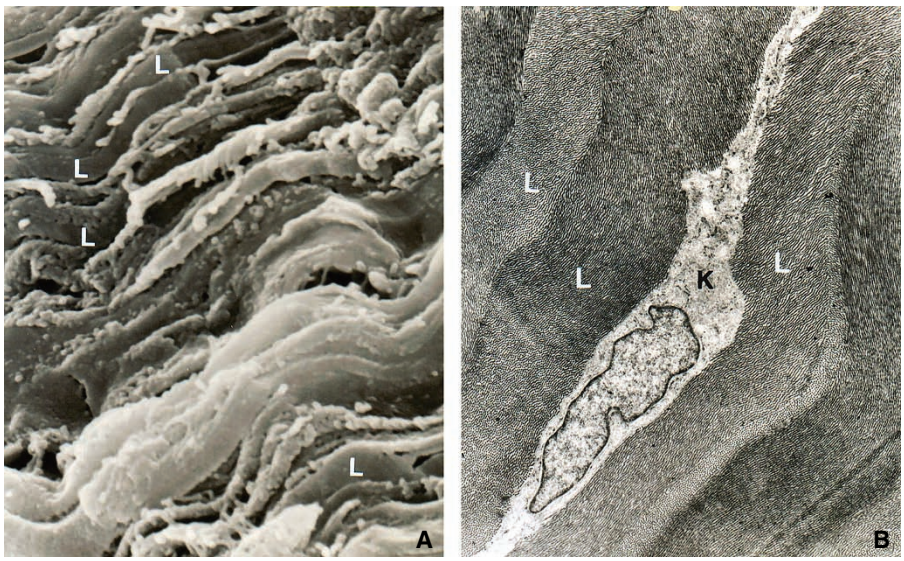

Figure 2.26 **A.** SEM of corneal stroma in the dog. (Original magnification, 7,400×.) **B.** TEM of corneal stroma in the horse consists of layers or lamellae (L) of collagen, which are sparsely interspersed with keratocytes (K). (Original magnification, 10,000×.)

Between the lamella are fixed cells and infrequent wandering cells. The fixed cells are fibrocytes, which are called keratocytes, and their extensions contribute to the formation and maintenance of the stromal lamellae. The keratocytes have thin nuclei, ill-defined borders, and delicate cell membranes (Fig. 2.26B). Similar to lens fibers, these cells possess crystallins, which are believed to facilitate tissue transparency (Jester, 2008). Keratocytes can transform into myofibroblasts when deep corneal injury occurs, and they can form scar tissue that is not transparent. In normal Beagles the keratocyte density in the anterior and posterior stroma is ~993 ± 134 cells/mm^2 and ~789 ± 87 cells/mm^2, respectively. Cell density is significantly greater and nuclei size is significantly smaller in the anterior stroma in comparison with the posterior stroma (Strom et al., 2016b).

The lamellae are parallel bundles of collagen fibrils, with each lamella running the entire diameter of the cornea. All the collagen fibrils within a lamella are parallel, but between lamellae, they vary greatly in direction (Fig. 2.26). The lamellae of the posterior stroma are more regular in arrangement than those of the anterior third of the stroma. The anterior lamellae are more oblique to the surface, and they have more branching and interweaving.

The precise organization of the corneal stroma is the most important factor in maintaining corneal clarity, which involves the select integration of collagen and amorphous ground matrix, consisting of select proteoglycans such as lumican, keratocan, osteoglycin, and decorin (Hassell & Birk, 2010). The collagen in the human cornea has a periodicity of 100 nm (Dawson et al., 2011). This special arrangement of the collagen in the stroma is believed to permit 99%

of the light entering the cornea to pass without scatter (Hogan et al., 1971). The stroma is comprised of at least five types of collagen (see Table 2.8). Of these five, collagen type I is by far the most prevalent, forming the small, evenly sized, striated fibrils. Type VI is associated only with the interfibrillar matrix that forms a network around the fibrils. Evidence from adult mice suggests that type VI is connected with type I through chondroitin/dermatan sulfate glycosaminoglycans (GAGs). Type VI, which is associated with the fibrils and keratocytes, appears to play a role in cell–matrix interactions, which would be especially important during development and repair (Doane et al., 1992). In comparison, type V is combined or coassembled with type I, and it is believed to be responsible for the formation of the small, uniform diameter of the striated fibril, which is approximately 25 nm in most species (Linsenmayer et al., 1993). Types III and XII are both suspected to be developmental forms, with type III being the more common; their importance during wound repair is unknown.

Collagen fibrils, along with the proteoglycans and their associated GAGs and glycoproteins, constitute 15%–25% of the stroma, and they are the principal support structure of the cornea. These collagen fibrils form the matrix for a specialized population of proteoglycans within the corneal stroma (Borcherding et al., 1978; Hassell & Birk, 2010). The cornea is 75%–85% water, and it is relatively dehydrated compared with other tissues. This state of dehydration is termed deturgescence and is, in part, a function of the endothelium and epithelium. These cells move water out of the stroma via energy-dependent Na^+/K^+ adenosine triphosphatase (ATPase) pumps, being most active in the endothelium. Other "pumps" for deturgescence might also exist, including carbonic anhydrase. These cells pump Na^+ and HCO^{3-} ions outward, into the aqueous humor and tears. An osmotic gradient is established, and water flows down the gradient from the corneal stroma into the aqueous humor. Experimentally, removal of the epithelium produces an increase of 200% in corneal thickness after 24 hours because of the influx of water. Removal of the endothelium produces an increase of 500% or more in thickness as the permeability increases sixfold, so the endothelium appears to be more important in maintenance of corneal deturgescence (Watsky et al., 1995). Figure 2.27 illustrates the primary roles the endothelium plays, both as a pump and as a barrier. The barrier component is provided by the tight junctions occurring apically along the lateral faces of adjoining cells next to the anterior chamber. These tight junctions are sensitive to calcium exposure, and they break down when excess free Ca^{++} exists in the aqueous humor. The Na^+/K^+ ATPase pump is located along the lateral membranes of neighboring cells (see Fig. 2.27). A breakdown of the pump, the barrier, or both will result in rapid movement of water into the highly hydrophilic stroma, causing corneal edema to develop.

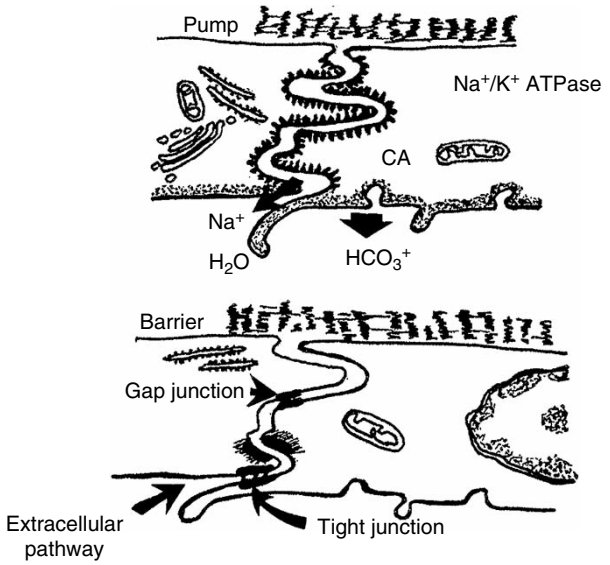

Figure 2.27 Location of the corneal endothelial metabolic pump (Na^+/K^+ ATPase along the lateral membranes and carbonic anhydrase along the apical margins) and barrier (apical tight junctions along the lateral membranes). (*Source:* Redrawn from Watsky, M.A., Olsen, T.W. & Edelhauser, H.F. (1995) Cornea and sclera. In: *Duane's Foundation of Clinical Ophthalmology* (eds Tasman, W. & Jaeger, E.A.), Vol. 2. Philadelphia, PA: J.B. Lippincott.)

The presence of GAGs in the cornea allows the pumps to be effective. Thus, any change in the population of the GAGs, any significant damage to the epithelium or endothelium, or any pressure exerted on the cornea causes a physical rearrangement of the precise collagen organization, which in turn results in opacification of the cornea. GAGs in the cornea consist of heparan sulfates, hyaluronic acid, undersulfated chondroitin sulfates, chondroitin 6-sulfate, chondroitin 4-sulfate, keratan sulfates, and dermatan sulfates (see Table 2.8). The most abundant of these is keratan sulfate, followed by dermatan sulfate (Cintron & Covington, 1990). Nearly all keratan sulfates are derived from stromal fibroblasts (i.e., keratocytes), whereas heparan sulfates are largely derived from the corneal epithelium, particularly as individuals mature. Hyaluronic acids, however, are formed to a fair degree by the corneal endothelium. Each corneal cell type contributes its own specific array of distinct GAG classes as well as other glycoconjugates to the extracellular matrix of the cornea. Corneal keratan sulfate, which differs from that in cartilage by length, branching, and cross-linkage within the polymer, will absorb two to three times more water than chondroitin sulfates, but the latter will retain water eight to nine times more effectively than keratan sulfate. Because of the different water-binding ability of GAGs, keratan sulfate is concentrated within the posterior bovine cornea, where it facilitates movement of water from the aqueous humor into the cornea (Castoro et al., 1988). Dermatan sulfate is concentrated within the anterior stroma.

In addition to the differential concentration of GAGs within the corneal stroma, the relative amount of keratan sulfate is lower toward the limbus, whereas the level of dermatan sulfate increases (Borcherding et al., 1978). As the amount of keratan sulfate decreases towards the limbus, a corresponding increase in collagen fiber size and lack of organization, as seen in the sclera, occurs.

The anterior-most stroma has a thin, cell-free zone corresponding in location with the anterior-limiting membrane, also known as Bowman's layer (anterior lamina), in humans and nonhuman primates. Bowman's layer is also present in birds, giraffes, dolphins, some whales, and large herbivores (Fig. 2.28; Hayashi et al., 2002; Murphy et al., 1991; Samuelson et al., 2005). In avian and human corneas, Bowman's layer is 10–15 µm thick, relatively acellular, and composed of collagen fibrils of various types (see Fig. 2.28; Table 2.8). Bowman's layer fibrils are smaller in diameter and less uniform than those of the stroma (Gordon et al., 1994). The anterior epithelium produces the majority of the collagen associated with this modified, acellular zone of the cornea. Bowman's layer is not elastic, and when damaged it is replaced with scar tissue. Bowman's layers of the land-based species share similarities in size, morphology, and histochemistry, differing substantially from that of marine mammals, which may reflect a variation of roles that this structure plays. Among whales, Bowman's layer is not thought to exist in deep-diving species, suggesting that its presence may be more closely associated with ocular function near or at the surface of the water.

Descemet's Membrane

Descemet's membrane is a PAS-positive, homogenous, acellular membrane that is the basement membrane of the posterior endothelium. Descemet's membrane is produced throughout life, thus becoming thicker as individuals age. Clinically, the membrane shows elasticity, but it contains only fine collagen fibrils (Jakus, 1956). Descemet's membrane is normally under some tension and when ruptured it tends to curl like a scroll. Descemet's membrane ends at the

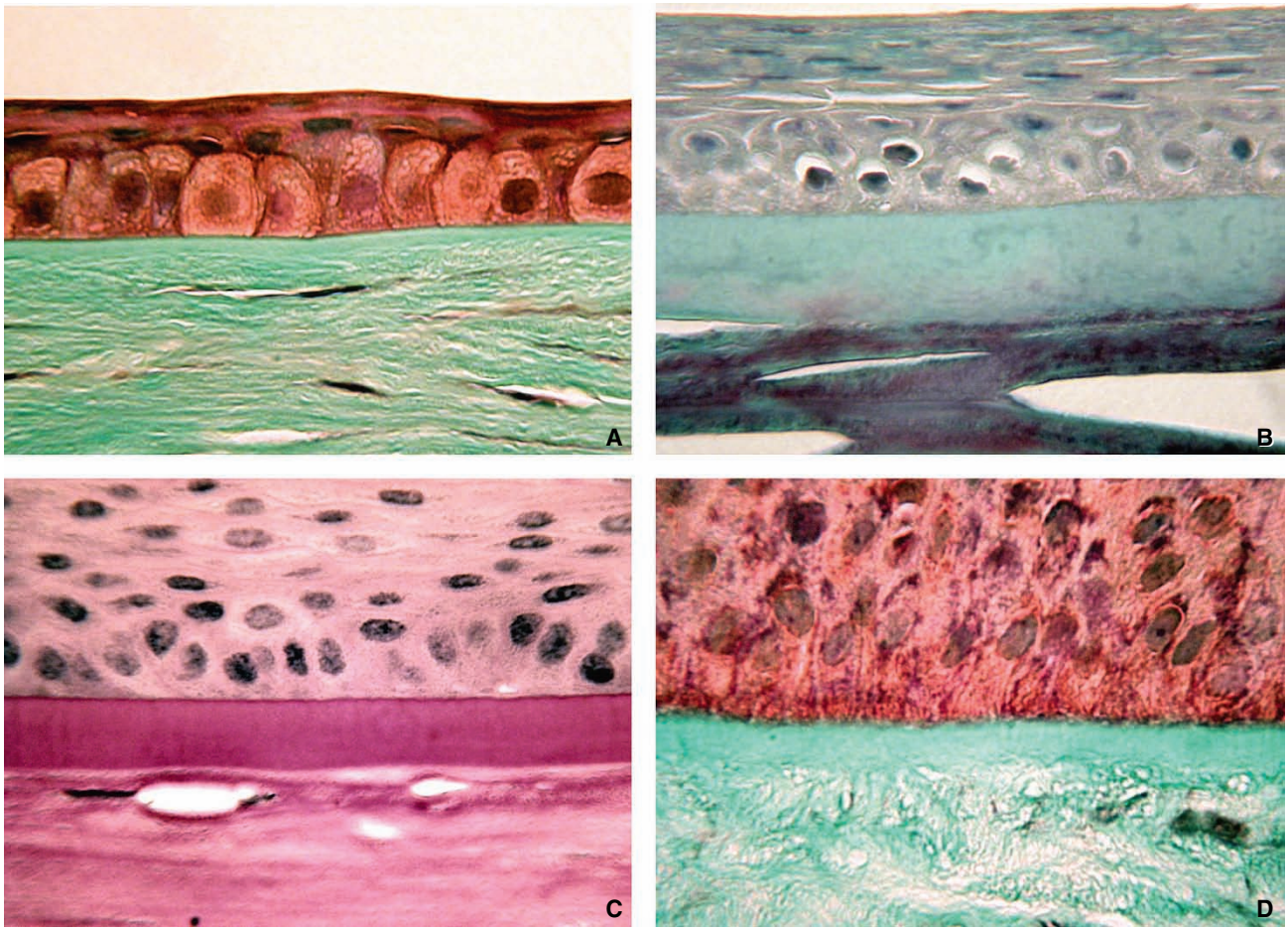

Figure 2.28 Bowman's layer among mammalian species. **A.** Rhesus monkey. (Original magnification, 400×; Masson trichrome stain.). **B.** Bottle-nosed dolphin. (Original magnification, 400×; Masson trichrome stain.). **C.** Pilot whale. (Original magnification, 400×; PAS stain.). **D.** Giraffe (Original magnification, 400×; Masson trichrome stain.). (Courtesy of AZ Zivotofsky and D Zivotofsky.)

apex of the trabecular meshwork in the limbal region. To some degree, its composition is similar to that of the trabeculae of the iridocorneal angle (ICA). Descemet's membrane is comprised of a number of collagen types, including type VIII, which is found in the ICA but not elsewhere in the cornea (see Table 2.8) (Tamura et al., 1991). Ultrastructurally, Descemet's membrane is distinctly layered in most animals, usually having a relatively thin anterior, unbanded zone next to the stroma, followed by a broad-banded zone and then by another broad, posterior unbanded zone located next to the endothelium. Collagen types III and IV comprise the posterior unbanded zone, types IV and VIII the anterior banded zone, and types V and VI the anterior unbanded zone (Smolek & Klyce, 1993).

Corneal Endothelium

The corneal endothelium is a single layer of flattened cells lining the inner cornea (Fig. 2.21). The regenerative ability of the endothelium varies with species and age. In most species active mitosis of the endothelium occurs primarily in the immature animal (Chi et al., 1960; Laing et al., 1976; MacCallum et al., 1983; Oh, 1963; von Sallman et al., 1961). Specular microscopy and SEM of adult eyes reveal that the cells are usually hexagonally shaped (Fig. 2.29). Closer inspection by SEM reveals that the surface is spotted with small microvillae and pores, and that the lateral edges of one cell interdigitate with another (Fig. 2.29B). In young canines (i.e., 1–4 weeks of age), many of the cells do not have the typical hexagonal shape. Pronounced pleomorphism has also been observed in kittens and rabbits (MacCallum et al., 1983).

Transmission electron microscopy (TEM) reveals the extensive, lateral, convoluted interdigitations between adjacent cells in the dog (Fig. 2.30). The cell junctions, including zonulae occludentes and maculae adherentes, are located at the lateral cell margins. The abundance of mitochondria, smooth and rough endoplasmic reticulum, and a variety of vesicles, indicates these cells are metabolically active. There is gradual loss of the hexagonal shape in older animals caused by a gradual decrease in the overall cell density of the

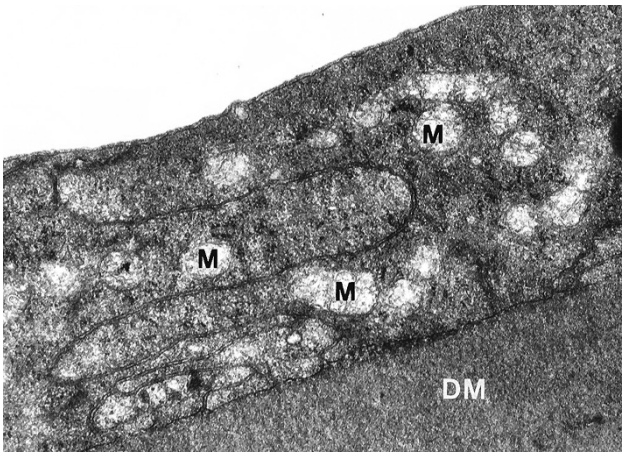

Figure 2.30 The lateral interdigitations observed between endothelial cells along the surface continue throughout the entire thickness of adjacent cells in the canine cornea. Numerous mitochondria (M) are associated with these interdigitations. DM, Descemet's membrane. (Original magnification, 16,000×.)

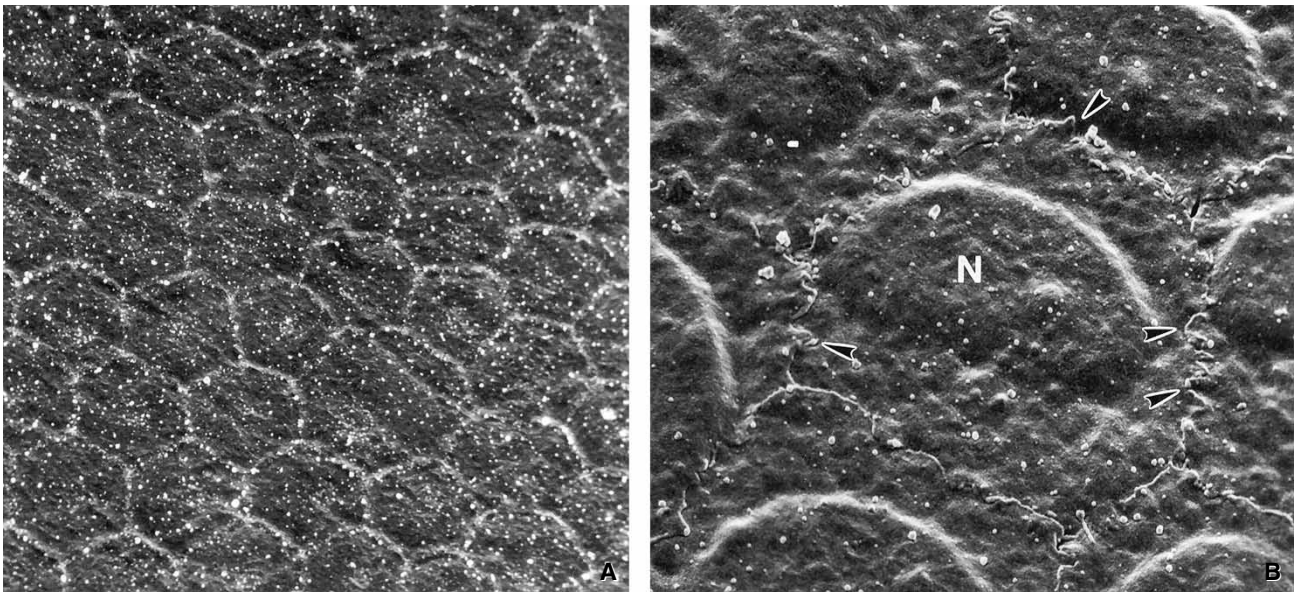

Figure 2.29 SEM of a 4-year-old canine corneal endothelium reveals occasional variability in cell size (**A**) and the lateral surface interdigitations (arrows) between cells (**B**). The most prominent feature of the endothelial cell is the nucleus (N), which bulges slightly into the anterior chamber. (Original magnification: **A**, 960×; **B**, 3500×.)

endothelium. In young dogs, endothelial density is greater than 3000 cells/mm^2 with approximately 3600 cells/mm^2 in dogs younger than 1 year (Kafarnik et al., 2007). As animals age, endothelial density can gradually decrease to 50% or less of that number.

With a smaller population of cells, the endothelial cells spread out and produce more pump sites to compensate for increasing leakage. An age-related decrease in the density of corneal endothelial cells results in little change in overall corneal thickness (Andrew et al., 2001). If the cell density continues to decrease, however, the cells become too attenuated, resulting in the pumps being unable to withstand the increasing leakage with concomitant corneal thickening and loss of optical clarity. This point is known as corneal decompensation, and it usually occurs when the endothelial cell density decreases to between 500 and 800 cells/mm^2.

Sclera

The sclera comprises the remainder of the fibrous tunic of the globe. Anteriorly, it merges with the peripheral cornea and the bulbar conjunctiva to form a transition zone, the limbus (Fig. 2.31). At the limbus, the sclera is variably pigmented, and the overlying epithelium is thicker, with pigmented epithelial cells. The stroma loses the regular arrangement characteristic of the cornea and takes on a less organized appearance of irregular, dense connective tissue. Numerous blood vessels (i.e., the anastomosing branches of the anterior ciliary arteries) terminate in the loops of the marginal plexus, then drain back into the conjunctival venules.

Along the outer portion of the scleral stroma is an interconnecting network of veins, the intrascleral plexus, which receives aqueous humor from the veins that drain the angular aqueous plexus (AAP) (Fig. 2.32). In domestic animals the intrascleral plexus is variably connected with the choroidal venous system, the vortex system (Fig. 2.33; Smith et al., 1988; Van Buskirk, 1979). The intrascleral plexus is variable in size and depth within the sclera (Natiello et al., 2005; Sharpnack et al., 1984; Troncoso, 1942b; Ujiie & Bill, 1984). For example, in rabbits and primates, the plexus is formed on the outer side of circumferentially coursing canals, and it is composed of small vessels deep in the sclera. In carnivores, the intrascleral plexus is prominent and composed of

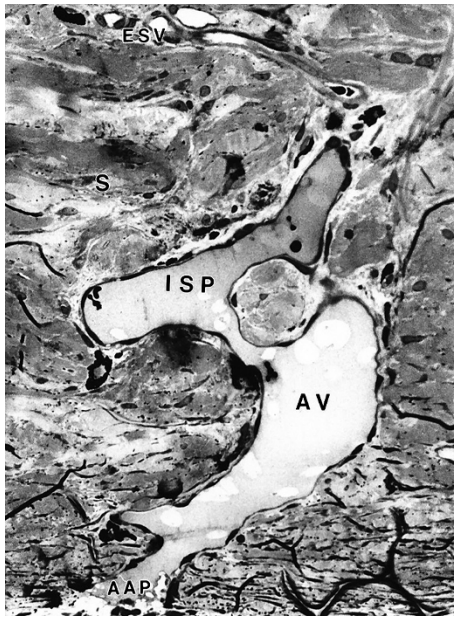

Figure 2.32 The intrascleral plexus (ISP) of a dog is located within the midsclera (S), and is interconnected to the angular aqueous plexus (AAP) by aqueous veins (AV). ESV, episcleral veins. (Original magnification, 125×.)

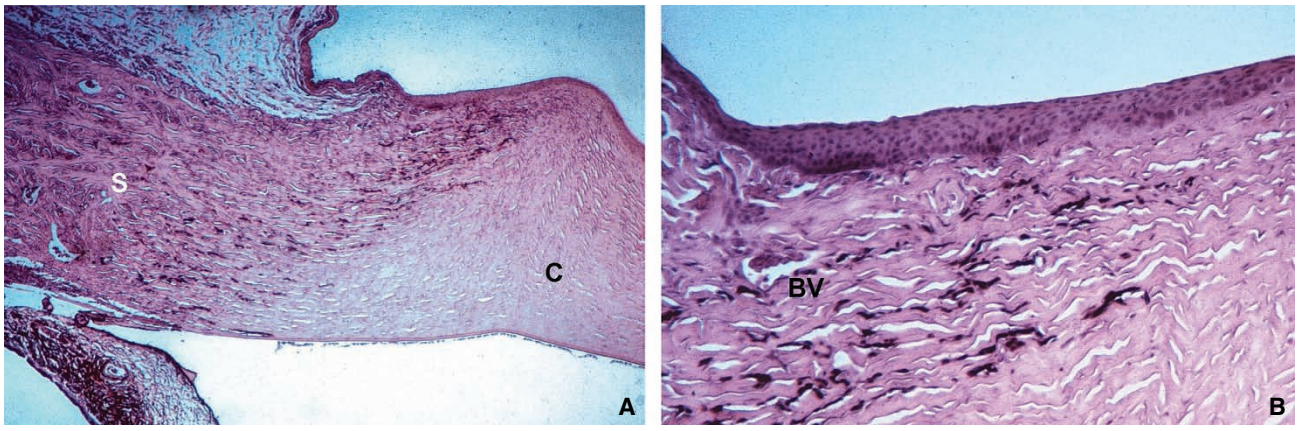

Figure 2.31 Photomicrographs of canine limbus. **A.** The irregular connective tissue of the sclera (S) merges with the highly organized connective tissue of the cornea (C). **B.** Close-up of the outer limbus reveals an anterior epithelium that is markedly thickened, and contains small blood vessels (BV), and melanocytes. (Original magnification, 250×.)

two to four large, anastomosing vessels in the midsclera. The intrascleral plexus also receives afferent channels superficially via the episcleral network at the limbus. In the horse, the plexus, which is less prominent, collateralizes entirely with the anterior vortex system, because it is oriented radially to facilitate unidirectional flow outward from the angle region toward the vortex veins; in carnivores and primates, the reservoirs receiving aqueous humor are circumferentially oriented.

The color of the sclera depends on the thickness of its stroma, appearing blue when thin (less than 0.2 mm) or yellow with increased fat content (carotenoids). The inner surface, which is referred to as the lamina fusca, is brown because of the adherent suprachoroidal pigment. The sclera contains elastic fibers that are interlaced among the collagen fibers, as are melanocytes (anteriorly) and fibrocytes. The collagen fibers, fibrocytes, and occasional melanocytes are arranged meridionally, obliquely, and radially in an irregular fashion. Its rigidity provides resistance to intraocular fluid pressure, and several channels, or emissaria, are present for the passage of blood vessels and nerves. The most notable emissaria accommodate the optic nerve, long and short ciliary nerves, long posterior ciliary arteries, vortex veins, and anterior ciliary vessels.

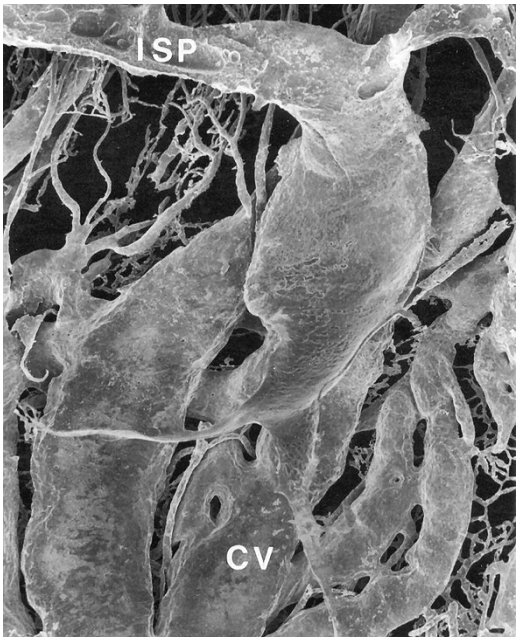

Figure 2.33 Corrosion cast of the canine ocular microvasculature demonstrates collateralization of the intrascleral plexus (ISP) with choroidal veins (CV) of the vortex system. (Original magnification, 410×.)

Scleral thickness varies considerably among species and in different areas of the globe. The sclera is thinnest near the equator, posterior to the insertions of the EOMs, and in the dog is only 0.12 mm thick (Table 2.9). By comparison, in the pig it thins to 0.43 mm, then nearly doubles its thickness for much of the posterior portion of the eye, being comparable to that of the human eye (Olsen et al., 2002). The region of the intrascleral venous plexus is the thickest area in animals with a well-developed plexus (e.g., the dog and cat), whereas in ungulates, the region of the optic nerve entrance or posterior pole is the thickest. At the point where the optic nerve passes through the sclera, it becomes sieve-like in the area known as the lamina cribrosa.

In most cetaceans the sclera increases to thicknesses not found elsewhere among vertebrate species. The posteriorly broadened sclera likely maintains the widened and flattened shape of the retina and choroid, which is observed in the large eyes of most cetaceans and of many terrestrial species (Murphy et al., 1991; Walls, 1942).

The episclera is a collagenous, vascular, and elastic tissue that is between the sclera and the conjunctiva and attaches to Tenon's capsule. Tenon's capsule consists of small, compact bundles of collagen that lie parallel to the surface of the episclera.

Besides dense connective tissue, the sclera can be largely composed of cartilage, as in fish, lizards, chelonians, some

Table 2.9 Thickness of the sclera.

Animal	Center of fundus (mm)	Optic nerve entry point (mm)	Globe equator (mm)	Limbus (mm)
Horse	1.5–2.2	1.35	0.5–0.3	1.1
	1.9		0.4	
Cow	1.9	2.20	1.0	1.2–1.5
Sheep	1.0–1.2	No increase in thickness	0.25–0.30	0.4–0.5
Pig	1.0–1.2	Thicker	0.5–0.8	
Cat	0.09–0.20	0.13–0.60	0.09–0.20	1.1, in the form of a ring 5–7 mm wide
Dog	Similar to the cat, only thinner	0.3–0.4	0.12–0.20	0.6

Source: Translated from Bayer, J. (1914) *Angenheilkunde*. Vienna: Braumueller; and from Donovan, R.H., et al. (1974) Histology of the normal collie eye. *Annals of Ophthalmology*, **6**, 257.

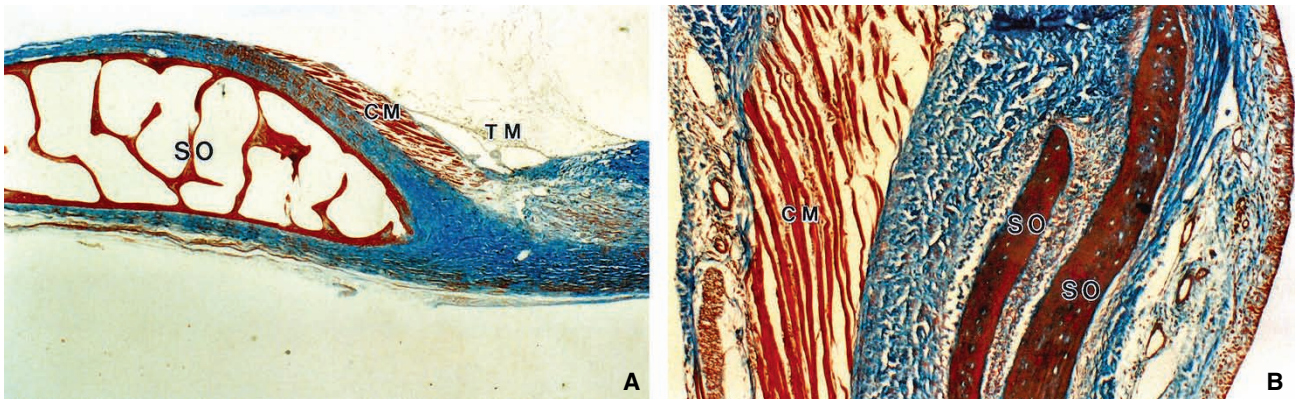

Figure 2.34 Scleral ossicles (SO) in birds vary in size and shape. **A.** Screech owl with large intraosseous spaces. (Original magnification, 40×.) **B.** Chicken with smaller scleral ossicles and considerable overlap between adjacent ossicles (Original magnification, 100×). CM, ciliary body musculature (Crampton's muscle); TM, trabecular meshwork.

amphibians, and birds. When cartilage is found in the sclera, it usually forms a complete cup that extends to the margin of the cornea or, in birds and lizards, to a ring of bony plates or ossicles. Scleral ossicles are located external to the ciliary body (Fig. 2.34). Though birds and reptiles possess this structure, the ossicle is believed to have originated from fish and was eventually passed on to amphibians. Birds with the greatest range of accommodation, such as the kingfisher and other diving birds, have larger ossicles than those species tending to be more confined to land (Curtis & Miller, 1938). Ossicles are believed to have evolved for retaining ocular rigidity. The number of ossicles that comprise a ring can vary within the same species; in individual eyes with fewer ossicles the single ossicle area increases, resulting in a constant scleral ring area (Canavese et al., 1994).

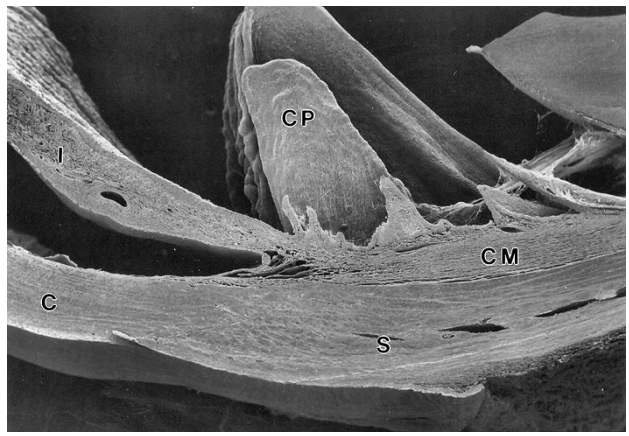

Figure 2.35 SEM of the canine anterior uvea: cornea (C), ciliary processes (CP), ciliary body musculature (CM), iris (I), sclera (S). (Original magnification, 25×.)

Uvea

The iris, ciliary body, and choroid form the uvea. Unlike the fibrous coat, the uveal coat is highly vascular and usually pigmented. The ciliary body and choroid are attached to the internal surface of the sclera (Fig. 2.35). The iris originates from the anterior portion of the ciliary body, and it extends centrally to form a diaphragm anterior to the lens. The iris and ciliary body are the anterior uvea, and the choroid is the posterior uvea.

Iris

The iris is a diaphragm that extends centrally from the ciliary body to cover the anterior surface of the lens, except for a central opening, the pupil. It divides the anterior ocular compartment into anterior and posterior chambers, which communicate through the pupil. The shape of the pupil varies among species. Among mammals, it is round in primates, canines, most large felines (cougar, leopard, lion, and tiger) and pigs; it is vertical when constricted in the smaller felines (bobcat, lynx, and domestic cat); and it is oval in a horizontal plane in herbivores (horses, cattle, sheep, and goats) (Fig. 2.8, Fig. 2.9, and Fig. 2.19). In herbivores, along the upper and lower margin of the pupil are several round dark brown 'masses' referred to as granula iridica (corpora nigra) (see Fig. 2.9 and Fig. 2.36). Camelids have a pupillary ruff along the dorsal and ventral pupillary margins. These pigmented masses are extensions of the posterior pigmented epithelium that augment the effectiveness of pupillary constriction. Occasional myocytes of the sphincter muscle are present in the basal portion of the granula iridica of goats and horses. The presence of these cells indicates that the granula iridica probably plays more than a passive role during changes of pupillary size and shape. Eyes of animals with pupils that constrict to a slit are believed, in most instances, to be more sensitive to light than those with circular pupils (Prince, 1956).

Figure 2.36 Equine iris (I) and anterior ciliary body (CB). The arrow points to the granula iridica, which continues posteriorly as the posterior pigment epithelium (PE).

The iris has a central pupillary zone and a peripheral ciliary zone. The demarcation between these two zones is the collarette, which is best demonstrated with moderate pupillary constriction. The portion of the pupillary zone adjacent to the pupil is sometimes more pigmented than the rest of the iris.

The function of the iris is to control the quantity of light entering the posterior segment through a central pupil. Constriction of the pupil reduces the amount of light entering the eye. Narrowing the pupil also eliminates the peripheral portion of the refractive system, which diminishes lenticular spherical and chromatic aberrations. During periods of reduced light, the pupil dilates allowing maximal stimulation of photoreceptor cells.

The iris is composed of an anterior border layer, stroma and sphincter muscle, and posterior epithelial layers (see Fig. 2.36). The anterior border layer consists of two cell types: fibroblasts and melanocytes. Results of electron microscopic studies indicate these cells are fibrocytic in nature rather than forming an epithelial sheet (Donovan et al., 1974a; Rohen, 1961; Tousimis & Fine, 1959). The anterior cells, which lack a basement membrane, form an almost continuous layer with their cellular processes, but frequent small openings with large intercellular spaces and extension of underlying melanocyte processes break the continuity. This anterior fibrocytic layer can be exquisitely thin and easily overlooked histologically. Particles measuring up to 200 µm in diameter can diffuse into the iris stroma through the anterior portion of the iris (Rodriques et al., 1988; Smith et al., 1986). One or more layers of melanocytes are deep to the single layer of fibroblasts and compose the remainder of the anterior border layer. For the most part, the melanocytes are oriented parallel to the iris surface, and their processes intermingle with other melanocytes and anterior fibroblasts with no intercellular junctions. The shape of the melanin granules in the stroma varies between species and with the maturity of the granules. The pigment granules in the cat and dog are lanceolate to ovoid in shape, whereas they are round to ovoid in the horse (Sharpnack et al., 1984; Tousimis, 1963). In addition to the scattered melanocytes in the anterior stroma of many dog irides, a dense band of melanocytes can be present in the ciliary zone anterior to the dilator muscle, extending centrally to the sphincter muscle. The granules are generally smaller and more rod-like than the pigmented granules of the posterior epithelium. Particularly in the horse and the dog, large cells containing pigment are associated with capillaries and venules near the sphincter muscle (Tousimis & Fine, 1959; Woberman & Fine, 1972). These are thought to be macrophages of hematogenous origin. In humans, these cells are known as the clump cells of Koganei (Woberman & Fine, 1972).

The iris stroma is composed of fine collagenous fibers, chromatophores, and fibroblasts. The stroma is loosely arranged except around blood vessels and nerves, where it can form dense sheaths. The collagen fibrils are organized to some extent in overlapping, wide arcades running from the pupil to the ciliary body (Shively & Epling, 1969). Despite the dense histologic appearance, considerable extracellular space is evident ultrastructurally.

Iridal color varies considerably among individuals, breeds, and species. The variation of iridal color results from the amount and type of pigmentation present. The coloration of irides in most domestic animals is dark brown, golden brown, gold, blue, or blue–green. Several avian species have brightly colored irides. Historically, these bright colors were thought to result from the presence of carotenoids, an idea based on a single study of the yellow iris of chickens performed over 50 years ago. Carotenoid-bearing cells are referred to as xanthophores, and their presence certainly has been demonstrated to produce brightly colored irides. However, purines and pteridines are also major iridal pigments in a variety of avian species, including doves and great-horned owls (Oliphant, 1988). Combinations of purines, pteridines, and carotenoids probably occur. Development of these pigments within an individual has been known to take a considerable amount of time, even as long as several years (Oliphant, 1988).

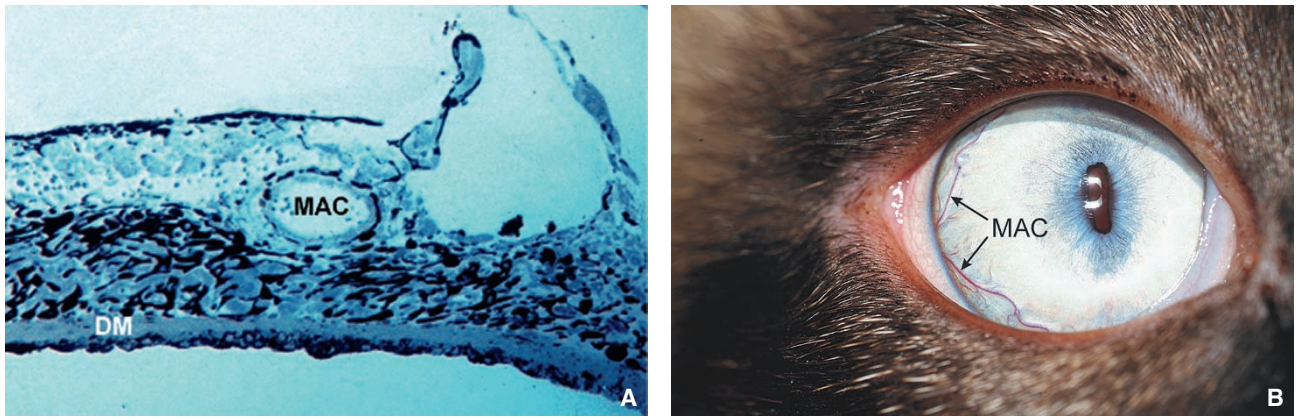

Figure 2.37 **A.** In many canine irides, melanocytes are concentrated in a wide band anterior to the dilator muscle (DM), as seen in the lower half of this iris. MAC, major arterial circle. (Original magnification, 100×.) **B**. The major arterial circle (MAC) in the peripheral iris of a cat.

The major arterial circle is located at the peripheral iris root or the anterior ciliary body (Fig. 2.37). The arteries enter at the nine- and three-o'clock positions as terminations of the medial and lateral branches of the long posterior ciliary arteries. Each artery branches dorsally and ventrally to pass circumferentially toward the opposite artery and forms an incomplete arterial circle in most species. In primates, the major arterial circle forms a completely enclosed ring. The major arterial circle gives rise to numerous radial arteries that end either in a capillary bed near the pupillary margin (i.e., in the dog and cat) or in a minor arterial circle of the iris (i.e., in primates and pigs). There is some debate over the presence of secondary arterial circles in the equine iris (Anderson & Anderson, 1977; Smith et al., 1988).

The arteries radial to the pupil are tortuous in most animals. The degree of tortuosity might reflect differences in pupil mobility between species. The radial arteries lose the internal elastic membrane that is present in the major arterial circle artery, and they have only one layer of smooth muscle cells, compared with two to four in the arteries of the major arterial circle. A thick basement membrane is present externally, which also surrounds the smooth muscle cells, but this membrane is interrupted by frequent myoepithelial junctions.

A capillary network near the pupillary margin connects the terminal arterioles with the venules, which pass to the base of the iris behind the arterioles in the posterior stroma. The capillary endothelium is not fenestrated, but the type of intercellular junctions varies with species. Mice, monkeys, and humans have tight junctions (zonula occludens), but rats, cats, and pigs have 4 nm gap junctions between desmosomes (maculae occludentes) (Szalay et al., 1975).

Venous drainage of the iris occurs through tortuous, radial vessels that empty directly into the anterior choroidal veins and out the vortex veins (Fig. 2.38). These vessels typically

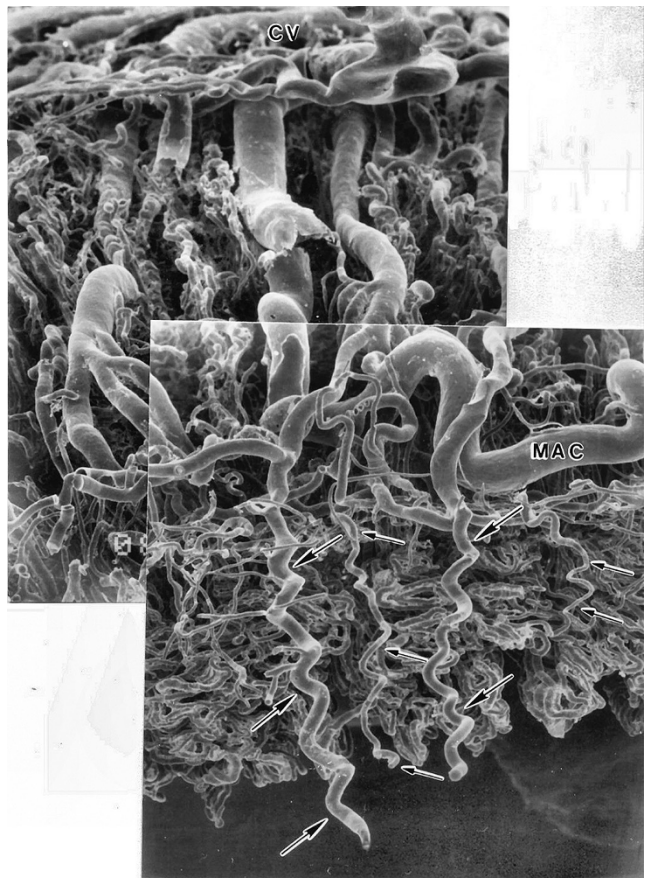

Figure 2.38 SEM corrosion cast of the anterior microvasculature of the equine eye. The iridal arteries (small arrows) and veins (large arrows) have a tortuous appearance as they progress toward the pupil. Note the iridal veins eventually empty posteriorly, into the anterior choroidal venous system (CV). MAC, major arterial circle. (Original magnification, 40×.)

number four in humans, pigs, and cats, but may vary in other species (Anderson & Anderson, 1977; Risco & Nopanitaya, 1980; Van Buskirk, 1979). In horses, a unique variation of iridal venous drainage exists where branches of the intrascleral venous plexus empty into the bases of the iridal veins, which in turn empty into the anterior choroidal venous circulation (Smith et al., 1988).

The iridal sphincter muscle, which is a flat band of thin, circular bundles of smooth muscle fibers in mammals and striated muscle fibers in nonmammalian species, is located in the iris stroma near the pupil. In the dog and cat, it lies in the posterior stroma, separated from the pigmented epithelium and subjacent dilator muscle by a thin layer of connective tissue (Fig. 2.39A). In the horse, the sphincter occupies the main portion of the central stroma and is capped by the granula iridica when present (Fig. 2.39B). The shape of the sphincter muscle varies among species according to the pupillary shape (Fig. 2.40; Prince, 1956). The sphincter muscle is innervated primarily by parasympathetic nerve fibers.

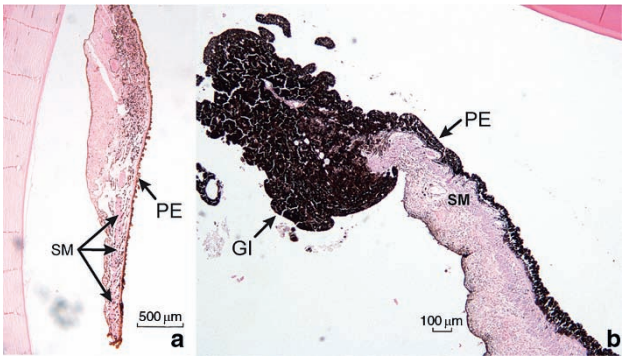

Figure 2.39 Sphincter muscle (SM) location in the dog (**A**) and in the horse (**B**). The sphincter muscle in the horse is capped by the granula iridica (GI), which is a proliferation of the posterior epithelium (PE). (Original magnification, 200×.)

The iridal dilator muscle is a single layer of smooth muscle fibers in the posterior iridal stroma extending from the iris sphincter to the iris periphery. These muscle fibers apically (i.e., posteriorly) contain pigment around their nuclei and are innervated by sympathetic nerve fibers. The basal regions of each cell, which contain the myofilaments, overlap one another in a shingle-like fashion. This cell layer could be considered as a highly developed, pigmented myoepithelium. The size of the dilator muscle varies between species, being well developed in the dog and involving the full circumference of the iris. In the horse, it is less developed, and in species with elongated pupils, it is poorly developed adjacent to the long axis of the pupil (Prince et al., 1960).

The posterior iridal surface is covered by two layers of epithelium. The anterior layer, which forms the dilator muscle, is continuous with the pigmented epithelium of the ciliary body, whereas the posterior layer, which is densely pigmented, is continuous with the nonpigmented epithelium of the ciliary body.

The basal aspect of the posterior epithelium of the iris faces the posterior chamber and has numerous surface projections (Fig. 2.41). The posterior surface of the iris contains folds that extend to the base of the ciliary processes. These folds are radially oriented, but the pigmented epithelial cells are oriented with their long axis running circumferentially in the iris, thus giving rise to two patterns on the posterior surface (Donovan et al., 1974a). A basement membrane separates the cells from the posterior chamber but does not follow all the invaginations of the cell surface. The lateral cell surfaces of the posterior epithelium have numerous slender cell processes with scattered desmosomes. In general, large spaces occur between the lateral cell membranes, which allow free access to the posterior chamber. The nuclei of the iridal posterior epithelium in the dog are oval and moderately indented, whereas the nuclei in the horse are often bizarre-shaped, being indented by adjacent pigment granules.

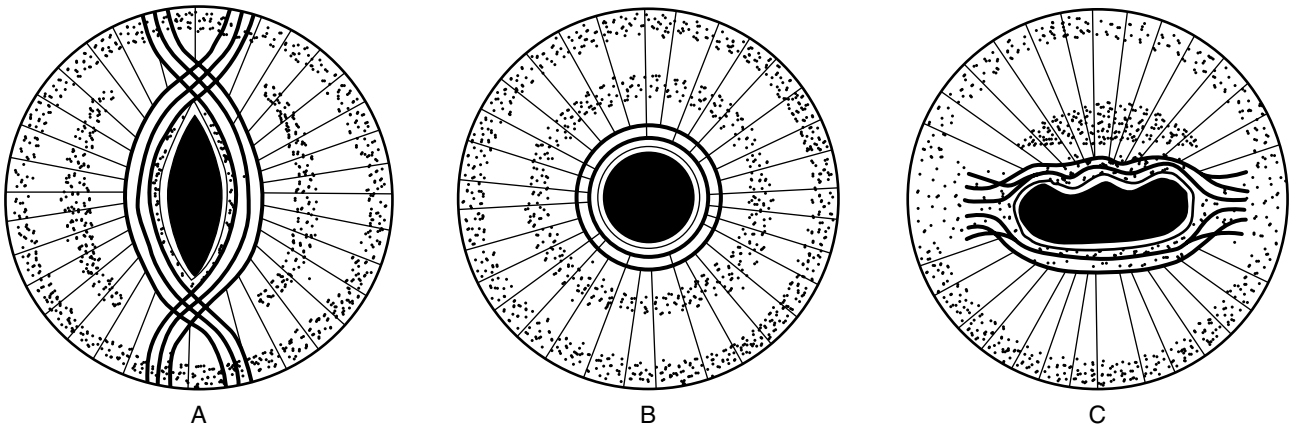

Figure 2.40 **A.** Iris sphincter muscles that create a slit pupil when the pupil is constricted found in domestic cats, bobcats, and lynx. **B.** The circular iris sphincter muscle as found in primates, birds, dogs, and pigs. **C.** Iris sphincter muscle in an ungulate with a horizontal pupil. (*Source:* Redrawn from Prince, J.H. (1956) *Comparative Anatomy of the Eye*. Springfield, IL: Charles C. Thomas.)

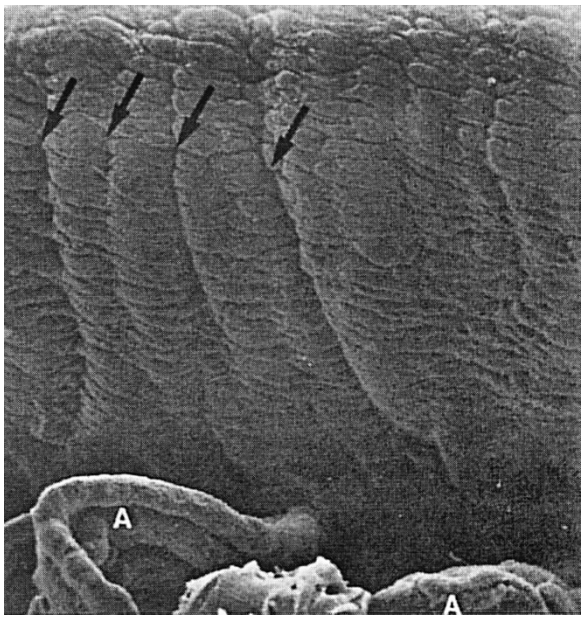

Figure 2.41 SEM of the posterior iris surface of a cat. Arrows point to radial folds. Tips of ciliary processes (A). Note circumferential orientation of clumps of posterior epithelium with small bumps from melanin granules. (Original magnification, 81×.)

The apical portion of the cells of the anterior epithelium (iris dilator muscle) contains the nucleus and is located adjacent to the apical portion of the posterior epithelium. Melanin granules are predominately present in the apical portion of the cell. The myoepithelial (basal) portion has scattered melanin granules, forms irregular projections into the stroma, and is covered by a basement membrane. In the horse, basement membrane material fills much of the intercellular space between projections of the myoepithelium.

In avian species and other lower vertebrates, the iris muscles are striated. In addition to controlling the amount of light that enters the back of the eye, the iris of birds is thought to contribute to lenticular accommodation. Changes in the pupil diameters of chickens and pigeons result in changes in the positioning of their lenses (Glasser & Howland, 1995). In some birds and other animals, for example, American alligators, the sphincter and dilator muscles are both striated and smooth. Specifically, in great-horned owls, pupillary constriction occurs mostly by skeletal muscle and pupillary dilation mostly by the radial myoepithelium, which contains smooth muscle myofilaments (Oliphant, 1983).

The iris contains numerous myelinated and nonmyelinated nerves for autonomic innervation. The myelinated fibers do not specifically follow the iris vessels, but they have a similar pattern as they follow the collagen fibers of the stroma. Upon entering the iris, each long ciliary nerve forms a dorsal and a ventral branch, to form a circular nerve in the ciliary zone and also to meet their counterparts from the opposite side dorsally and ventrally. Radial nerve bundles from the circular nerve pass centrally to the pupil with a corkscrew shape, presumably to accommodate pupillary constriction. A circular plexus is formed near the collarette, from which branches continue toward the pupil, then divide, and intersect to form a rhomboid-shaped mesh (Saari, 1971).

The belief that reflex constriction of the mammalian pupil in response to light depends exclusively on neural pathways between the eye and central nervous system may not be true (Lau et al., 1992). In both golden hamsters and hooded rats, effective constriction of the pupil in response to light occurred after a variety of interventions, including bilateral intraorbital optic nerve transection and unilateral intracranial optic nerve transection with enucleation of the contralateral eye, combined in some cases with bilateral removal of the superior cervical ganglia, pinealectomy, or both. The constrictions that occurred after these different interventions were considerably slower than the usual, neuronally driven reflex but present. Interestingly, the slow, nonneural pupillary reflex was not observed in albino animals, which suggests a possible melanin-mediated component to the slow pupillary light reflex.

Ciliary Body

The ciliary body is a heavily pigmented structure that provides nourishment for and removes wastes from the cornea and lens and participates in lens accommodation. The ciliary body is divided into the anterior pars plicata (corona ciliaris) and the posterior pars plana. The pars plicata consists of a ring of 70–100 ciliary processes, depending on the species, with intervening valleys (Fig. 2.42; Prince et al., 1960). The

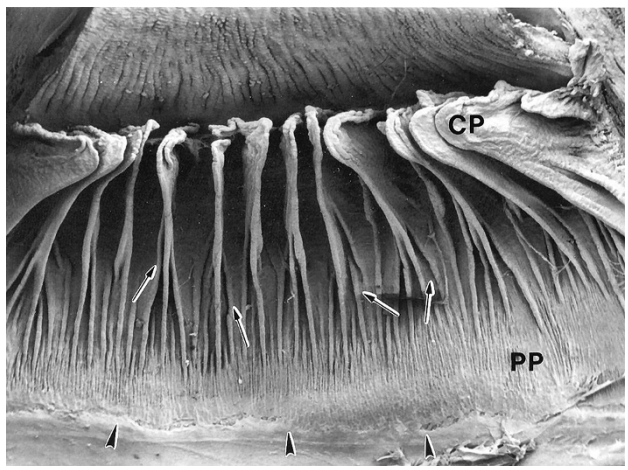

Figure 2.42 Inner surface of the ciliary body of a dog treated with α-chymotrypsin to remove the lenticular zonules. Note the thin ciliary processes (CP), which posteriorly give rise to smaller secondary folds (small arrows). These folds flatten and disappear in the region called the pars plana (PP), which ends posteriorly at the adjoining retina, forming a line known as the ora ciliaris retinae (arrowheads). (Original magnification, 18×.)

processes are generally more prominent and numerous in animals with larger anterior chambers (the cow and horse have 100 and 102 processes, respectively) than in animals with smaller anterior chambers (carnivores and primates have 74–76 processes) (Prince et al., 1960). Ciliary body processes are often absent in lower vertebrates (most fish, lizards, and snakes) (Duke-Elder, 1958; Prince, 1956; Prince et al., 1960). In anurans, birds, and some reptiles, the ciliary body processes are attached to the lens and participate directly in accommodation. In mammals, the ciliary body processes are attached to the lenticular zonules, which connect to the lens equator.

The appearance of individual ciliary body processes varies among species. In carnivores, the processes are thin and bladelike, with rounded tips that are invested with zonular fibers. Between the major ciliary processes, wide valleys with smaller, secondary folds are present. Many of the smaller secondary folds originating near the pars plana merge with the major processes at their base. The surface of each process has numerous convolutions, but most of it is obscured by the attachments of the zonular fibers (Fig. 2.43; Troncoso, 1942a).

In some ungulates, the ridge of the ciliary processes is capped by a broad, convoluted surface that overhangs the main body of the processes (Troncoso, 1942a). Numerous zonular fibers extend from a firm attachment on the sides of the processes to the lens. These fibers also run circumferentially, connecting the broad ridges together (Fig. 2.44). The cap of broad convolutions stops before the anterior tips of the ciliary processes, which are free of fibers.

Each ciliary process consists of a central core of stroma and blood vessels covered by a double layer of epithelium: an inner, nonpigmented, cuboidal epithelium, and an outer, pigmented, cuboidal epithelium (Fig. 2.45). In ungulates, the double-layered epithelium is more columnar than cuboidal. The nonpigmented ciliary body epithelium is confluent posteriorly with the neurosensory retina at the ora ciliaris retinae and anteriorly with the posterior pigmented epithelium of the iris. The basal surfaces of these cells face the posterior chamber and can be irregular. The basement membrane of this epithelial layer follows the general contour, but it does not pass down into the small irregularities or into the intercellular spaces. The basement membrane helps to anchor the lenticular zonular fibers and vitreous base.

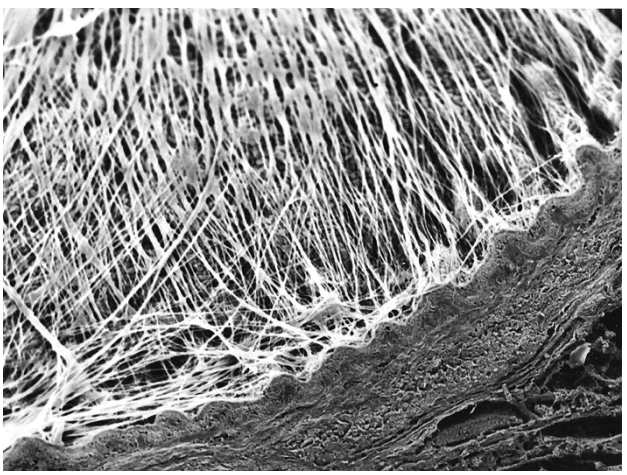

Figure 2.43 SEM (sagittal view) of the inner ciliary body of a dog reveals numerous zonular fibers attached along the epithelial surface. (Original magnification, 130×.)

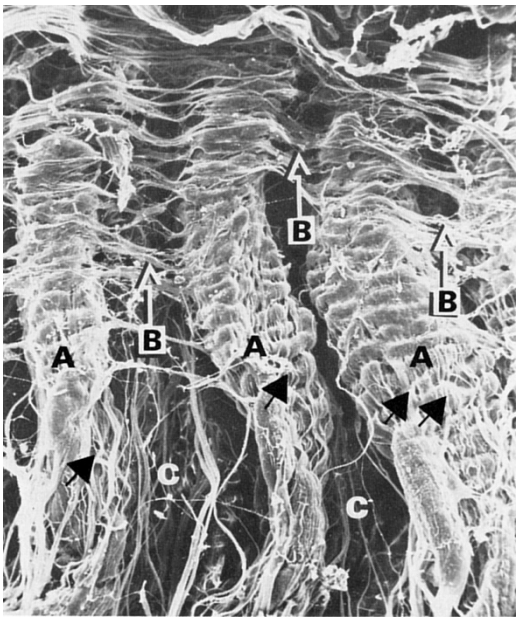

Figure 2.44 SEM of the ciliary processes and zonular fibers in a horse. Ciliary process (A). White arrows point in the direction of the lens equator as well as to the horizontal fiber network joining adjacent process (B). Zonular fibers in valleys between processes (C). Note also the zonular fiber ensheathment of the ciliary processes (black arrows). (Original magnification, 41×.)

The lateral cell surfaces of the nonpigmented epithelium have numerous villous processes along the bottom one-half to two-thirds. Cystic intercellular spaces in this region and in the pars plana are filled with material that has the staining characteristics of GAGs. The base of the cells also reacts positively for the same material. The nonpigmented epithelium most likely produces the GAGs of the vitreous humor. These cells secrete the GAGs, which consist mostly of hyaluronans, laterally into the cystic intercellular spaces, which then communicate with the vitreous base (Fine & Yanoff, 1979). The enzyme carbonic anhydrase has been cytochemically localized at or in the nonpigmented epithelium (Streeten, 1988).

The types of cellular junctions between the nonpigmented and pigmented epithelium of the ciliary processes consist of many gap junctions interspersed with desmosomes and

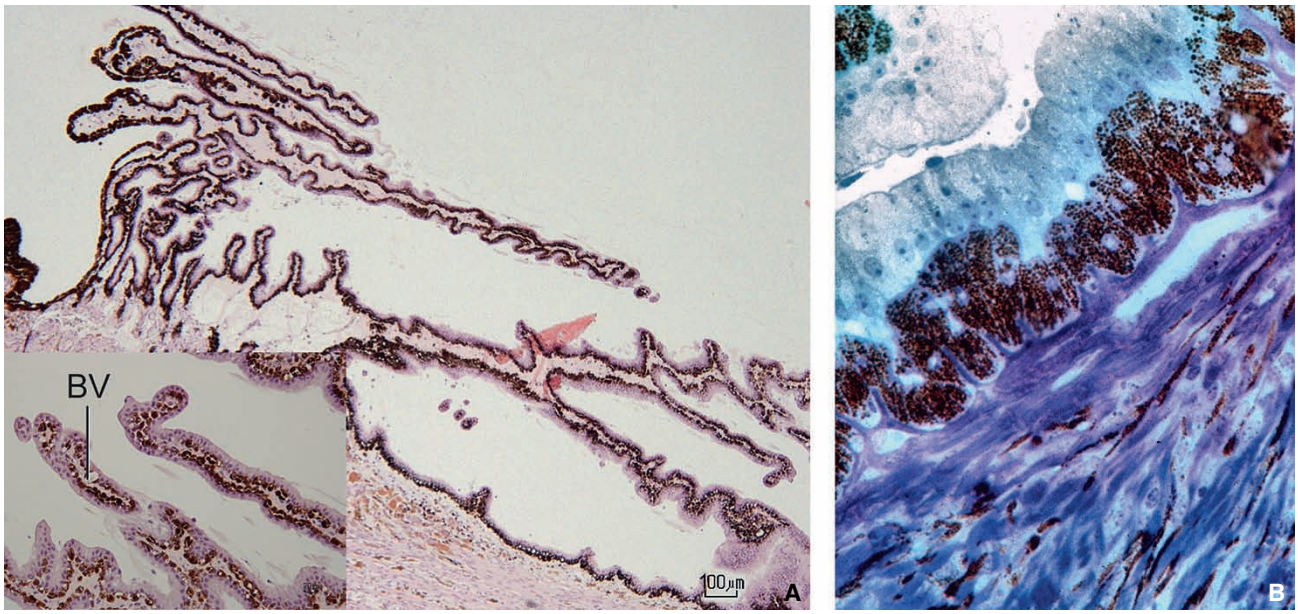

Figure 2.45 The bilayered ciliary epithelium that lines the ciliary processes and intervening valleys. The outer layer is pigmented; the inner layer is nonpigmented. **A.** Feline ciliary processes. *Insert:* Cross-section of ciliary processes. The bilayered epithelium, which is cuboidal, lines blood vessels (BV), which together form a blood–aqueous barrier. **B.** Longitudinal section of an equine ciliary epithelium at the base of a process. Both layers are considerably more columnar than those in the dog and cat. (Original magnification, 400×.)

unusual junctions termed puncta adherentes, which resemble desmosomes but lack the larger tonofilaments and associated intercellular central band (Streeten, 1988). The lateral intercellular junctions of the nonpigmented epithelium consist of desmosomes, except at the apical end (Fig. 2.46). The apical ends possess gap junctions, zonula adherens, and zonula occludens, which represent the anatomic site of the blood–aqueous barrier (Fig. 2.46; Shabo et al., 1976; Smith, 1971; Smith & Raviola, 1983; Smith & Rudt, 1973; Streeten, 1988). There are also dilated portions of the apical intercellular spaces with villous cytoplasmic processes protruding into them. These dilations are termed ciliary channels, and they are usually near the apical termination of two adjacent cells.

The ciliary process pigmented epithelium is confluent with the retinal pigment epithelium. Anteriorly, it continues as the anterior pigmented epithelial layer of the iris, which forms the dilator muscle. The pigmented epithelium is generally cuboidal and heavily laden with round-to-oval melanin granules. The basal aspect of the pigmented epithelium faces the ciliary body stroma and is covered by a basement membrane. In some instances, the basement membrane of adjacent capillaries in the ciliary processes comes into contact with the basement membrane of the pigmented epithelium to form a thickened, irregular, common basement membrane. The lateral cell surfaces of the pigmented epithelium are joined by desmosomes, and the basal cell surfaces have no specialized junctions. The nuclei of both pigmented and nonpigmented epithelia are located apically. The cytoplasm

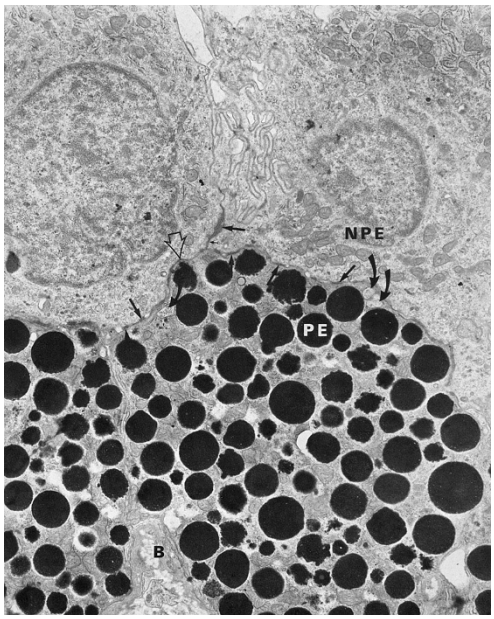

Figure 2.46 Apical junctions of nonpigmented (NPE) and pigmented (PE) ciliary epithelium in a cat. The nonpigmented epithelial nuclei are located apically; the wide intercellular spaces and villi can be seen in the basilar aspect of the intercellular spaces of the nonpigmented epithelium. The apical aspect of the nonpigmented intercellular space is the anatomic site of the blood–aqueous barrier and contains a fascia occludens (small arrow) and fascia adherentes (large arrow). The apical cell surfaces contain a fascia adherentes, gap junctions (open arrows), and arch-shaped gap junctions (curved arrows). The basement membrane (B) of the pigmented epithelium. (Original magnification, 9800×.)

of the pigmented epithelium contains melanin granules, rough endoplasmic reticulum, smooth endoplasmic reticulum, free ribosomes (polysomes), and mitochondria.

A thin layer of loose connective tissue with blood vessels and nerves lies under the ciliary epithelium, separating the ciliary body epithelium from the underlying ciliary body musculature. The vascular plexus within the stroma of the ciliary process is leaky, being lined with a fenestrated endothelium. Fibrocytes and melanocytes are sparsely populated within the stroma, being more concentrated near the ciliary body muscle (CBM).

The pars plana is the flat, posterior portion of the ciliary body that extends from the posterior termination of the processes to the retina (ora ciliaris retinae) (see Fig. 2.42). The width of the pars plana varies because the retina extends more anteriorly in the inferior and medial quadrant in most species, enhancing peripheral vision. Therefore, the pars plana is usually widest superiorly and laterally. In the dog, the ora ciliaris retinae is 8 mm behind the limbus dorsally and laterally but only 4 mm ventrally and medially (Donovan et al., 1974a).

Ciliary Body Musculature

The CBM is comprised of smooth muscle fibers in mammals. Contraction of the CBM draws the ciliary processes and body both forward and inward, thus relaxing the lenticular zonules (suspensory ligament of the lens) and altering the shape and refraction of the lens. This muscle is often weakly developed in many nonprimate species and as a result, offers poor accommodative ability.

On the basis of ciliary body musculature development, the placental mammalian ICA has been categorized into three main groups: the herbivorous, the carnivorous, and the anthropoid (Henderson, 1926; Tripathi, 1974). The categorization depicted in Fig. 2.47 was originally inspired from observations of the ciliary regions of the dog, pig, and ape (Duke-Elder, 1958).

The herbivorous type has been characterized as the most common and primitive in orders of mammals up to and including ungulates. This type of angle consists of an inner layer of connective tissue that forms a baseplate of the ciliary body and extends from the root of the iris to the ora ciliaris retinae. It also consists of an outer layer of smooth muscle that presses against the sclera externally and runs meridionally from the corneoscleral junction toward the ora ciliaris retinae (Fig. 2.47A and Fig. 2.48A). The two layers are often referred to as "leaves" that separate anteriorly and form the ciliary cleft. The ciliary cleft is then a triangular area that varies both in depth (i.e., length) and height, and functionally may be considered a posterolateral extension of the anterior chamber into the ciliary body. Historically, this region was called the ciliioscleral sinus, but because it neither separates the ciliary body from the sclera nor is a part of the ciliary venous sinus,

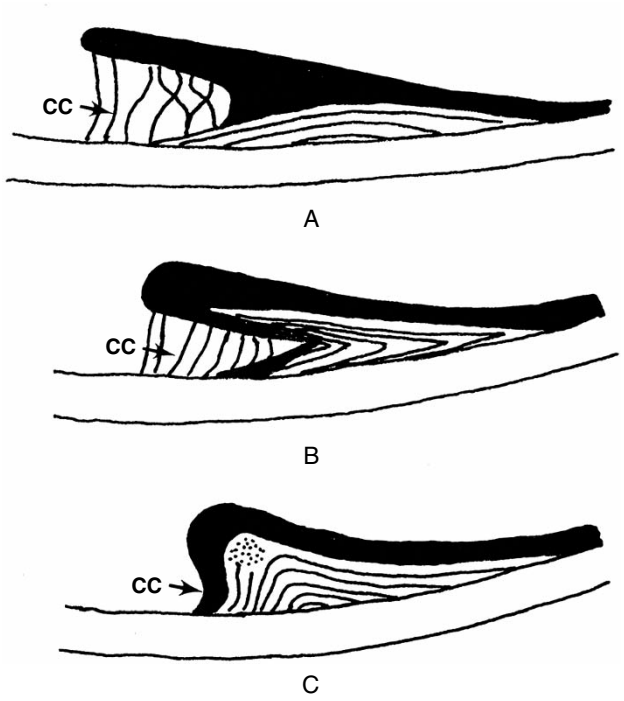

Figure 2.47 Degree of development of the ciliary body musculature among mammalian iridocorneal angles in the ungulate (**A**), carnivore (**B**), and ape (**C**). The ciliary body musculature is most pronounced in primates and least developed in ungulates. The size of the iridocorneal angle and its cilioscleral cleft or sinus (CC) is inversely large or most pronounced in the ungulate. (*Source:* Redrawn from Duke-Elder, S. (1958) *System of Ophthalmology. Vol. I. The Eye in Evolution*. London: Henry Kimpton.)

the term cilioscleral sinus has been replaced with ciliary cleft (Duke-Elder, 1958; Tripathi, 1974; Troncoso, 1938).

The ciliary cleft is an area containing wide spaces filled with aqueous humor and interspersed with cell-lined cords of connective tissue. The spaces between the fibrous cords were initially described in cattle and horses, and they have been often referred to as Fontana's spaces (Samuelson, 1996).

The carnivorous type possesses a bi-leaflet configuration as well, but the fibrous inner leaf or layer is usually replaced by meridionally oriented smooth muscle and some radially oriented muscle fibers (see Fig. 2.47 and Fig. 2.48B) (Duke-Elder, 1958). Similar to the herbivorous type, the two leaves separate anteriorly and hold a wide, deep ciliary cleft. In both the herbivorous and carnivorous types, the ciliary cleft offers little support to properly anchor the iris. Compensation for wide and deep ciliary clefts is provided by a series of pectinate ligaments attaching the anterior iridal root and inner ciliary baseplate to the limbal cornea.

The anthropoid type differs sharply in its configuration compared with the other types (see Fig. 2.47C and Fig. 2.48C). The ciliary body musculature of primates is believed to be the most highly developed among mammals. The muscle, which has three components (i.e., radial, meridional, and circular),

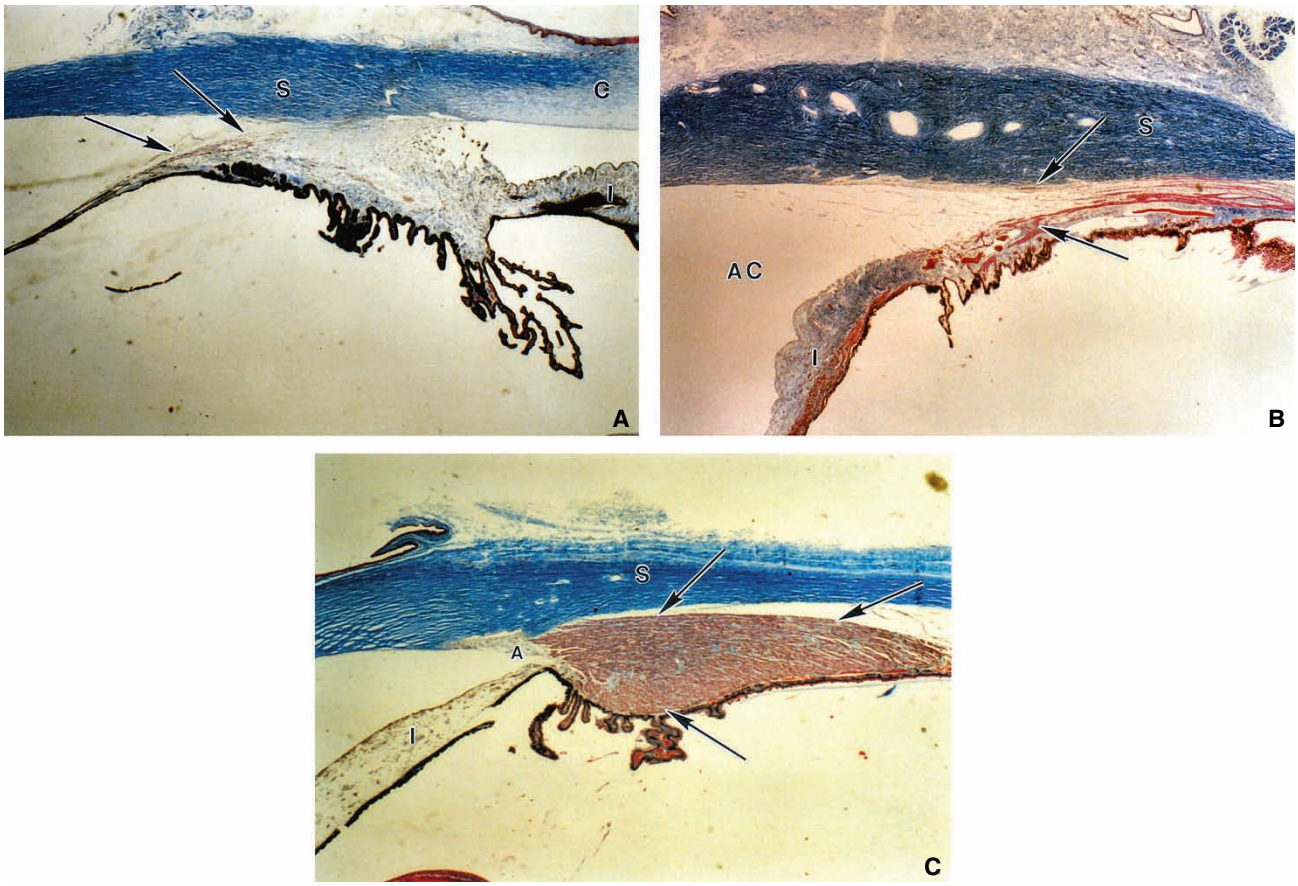

Figure 2.48 **A.** The deer has the traditional herbivorous type of iridocorneal angle and associated ciliary body musculature, which forms a single outer "leaf" (arrows) as it lines the outer, posterior portion of the iridocorneal angle. C, cornea; I, iris; S, sclera. (Original magnification, 20×.) **B.** The cat possesses the traditional carnivorous type of iridocorneal angle, which forms a "bileaflet" anteriorly (arrows). I, iris; S, sclera; AC, anterior chamber. (Original magnification, 25×.) **C.** The Rhesus monkey has the anthropoid type, which consists of small iridocorneal angle and a well-developed ciliary body musculature (*arrows*). I, iris; S, sclera; A, iridocorneal angle. (Original magnification, 20×.)

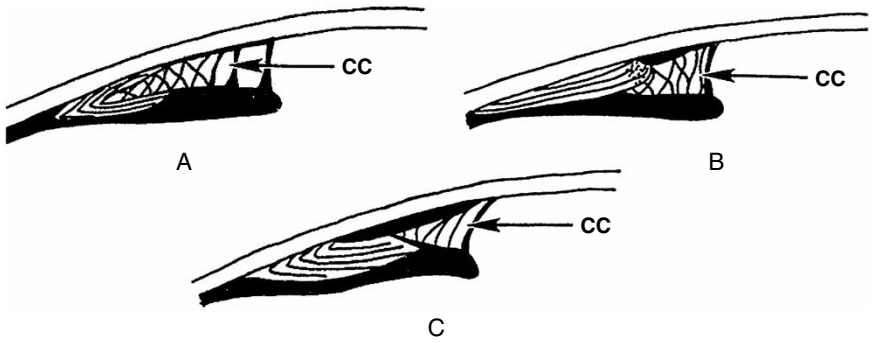

Figure 2.49 Three additional configurations of the eutherian nonprimate iridocorneal angle. Ciliary body musculature is indicated by linear shading. Ciliary cleft (CC). **A.** Small diurnal herbivore. **B.** Large diurnal herbivore. **C.** "High" accommodative carnivore. (Samuelson, D.A. (1996) A reevaluation of the comparative anatomy of the Eutherian iridocorneal angle and associated ciliary body musculature. *Veterinary & Comparative Ophthalmology*, **6**, 153–172.)

forms a large, anterior pyramidal structure that provides a strong baseplate for iridal attachment. The anterior portion of the CBM has replaced both the ciliary cleft, which barely exists in the anthropoid angle, and the pectinate ligaments, which vestigially consist of scattered iridal processes.

In addition to the three basic forms of CBM and ICA, three more configurations have been described among nonprimate mammals (Fig. 2.49; Samuelson, 1996). Among herbivores, two other types have been identified: the small diurnal herbivore and the large diurnal herbivore. In the

small diurnal herbivore, such as the squirrel, a deep ciliary cleft is lined by inner and outer leaves of fibrous tissue and smooth muscle of the ciliary body. In the large diurnal herbivore, such as the pig, there is a well-developed ciliary cleft and outer leaf of ciliary muscle, which anteriorly includes circularly oriented muscle embedded within a scleral spur. The scleral spur is a small ridge of dense connective tissue that separates the muscle fibers from the posterior ICA. TEM of different ungulates has revealed that many of the muscle fibers, especially those located anteriorly, course more circumferentially than meridionally (Samuelson & Lewis, 1995). This difference in orientation of the musculature is most evident in the pig and water buffalo. In these animals, circular muscle fibers are located near the innermost portion of the posterior end of the ciliary cleft.

A third type occurs in "high" accommodative carnivores, such as raccoons and ferrets. In this configuration, the anterior CBM is highly developed but not as an outer leaflet. Instead, the anterior musculature extends as a single leaflet either internally (i.e., raccoons) or intermediately (i.e., ferrets) (Fig. 2.49C and Fig. 2.50).

In birds and other nonmammalian species, the CBM consists of skeletal muscle cells that are primarily meridional. At least two distinct muscle bundles are located in this region of the avian eye: an anterior bundle, which is known as the muscle of Crampton, arises near the corneal margin; and a posterior bundle, which is known as Brücke's muscle. In birds such as the hawk, Brücke's muscle is well developed and sometimes is referred to as two muscles: Müller's (anterior) and Brücke's (Duke-Elder, 1958). Contraction of Brücke's muscle causes the ciliary body to push against or compress the lens, thus deforming it, whereas contraction of Crampton's muscle alters the shape of the cornea by shortening its radius of curvature.

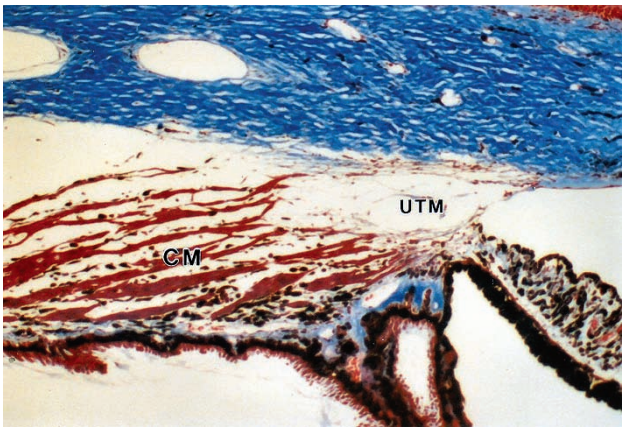

Figure 2.50 The mongoose has the "high" accommodative type of iridocorneal angle. CM, ciliary body musculature; UTM, trabecular meshwork. (Original magnification, 100×.)

Ciliary Body Vasculature

The blood supply of the ciliary body derives from the two long posterior ciliary arteries and the anterior ciliary arteries. As the long posterior arteries pass into the suprachoroidal space equatorially along the lateromedial horizontal plane, they undergo several divisions. These divisions anastomose anteriorly with branches of the anterior ciliary arteries to form the major arterial circle, which is located either in the base of the iris or the anterior ciliary body (see Fig. 2.37 and Fig. 2.38). The anterior ciliary arteries, which arise from branches of the ophthalmic artery, typically enter the globe at the attachment sites for the recti muscles and help to supply the ciliary muscles (Streeten, 1988). The major arterial circle is the primary vasculature supply of the ciliary processes.

Numerous anatomic variations of this vasculature have been found among mammals (Funk & Rohen, 1990; Matsuo, 1973; Morrison & Van Buskirk, 1983; Morrison et al., 1987a, 1987b; Natiello & Samuelson, 2005). In primates and rabbits, two types of arterioles supply the major and minor processes, whereas in other species, a single type of arteriole originates from the major arterial circle and supplies the ciliary process vasculature (Morrison & Van Buskirk, 1983; Morrison et al., 1987a, 1987b; Natiello & Samuelson, 2005). Discrete interspecies variations occur in the angioarchitecture of the ciliary processes (Fig. 2.51). Rodents, rats and Guinea pigs have extensive interprocess connections and concentrically parallel capillaries that are irregularly dilated and travel posteriorly, emptying into the anteriormost choroidal veins. Carnivores such as dogs and cats have processes supplied by one arteriole that is directed posteriorly throughout its length, with capillary arcades that extend to each process margin, from which they empty into venous sinuses.

The mammalian CBM is supplied by parasympathetic fibers from the oculomotor nerve and by sympathetic nerve fibers. The parasympathetic fibers leave the oculomotor nerve, penetrate the ventral oblique muscle, and synapse in the ciliary ganglion. From the ciliary ganglion, short ciliary nerves penetrate the sclera around the optic nerve to pass into the sclera and suprachoroidal space innervating the ciliary muscle and iris muscles. The sympathetic fibers arrive via the long ciliary nerves from the dorsal or superior cervical ganglia in a similar manner (Gum et al., 2007).

Iridocorneal Angle

Aqueous humor is produced by the ciliary body epithelium and enters the posterior chamber before flowing through the pupil into the anterior chamber. In the conventional outflow pathway, aqueous humor exits the eye through the corneoscleral trabecular meshwork.

The anatomy of the aqueous humor outflow system has been extensively studied in humans, nonhuman primates,

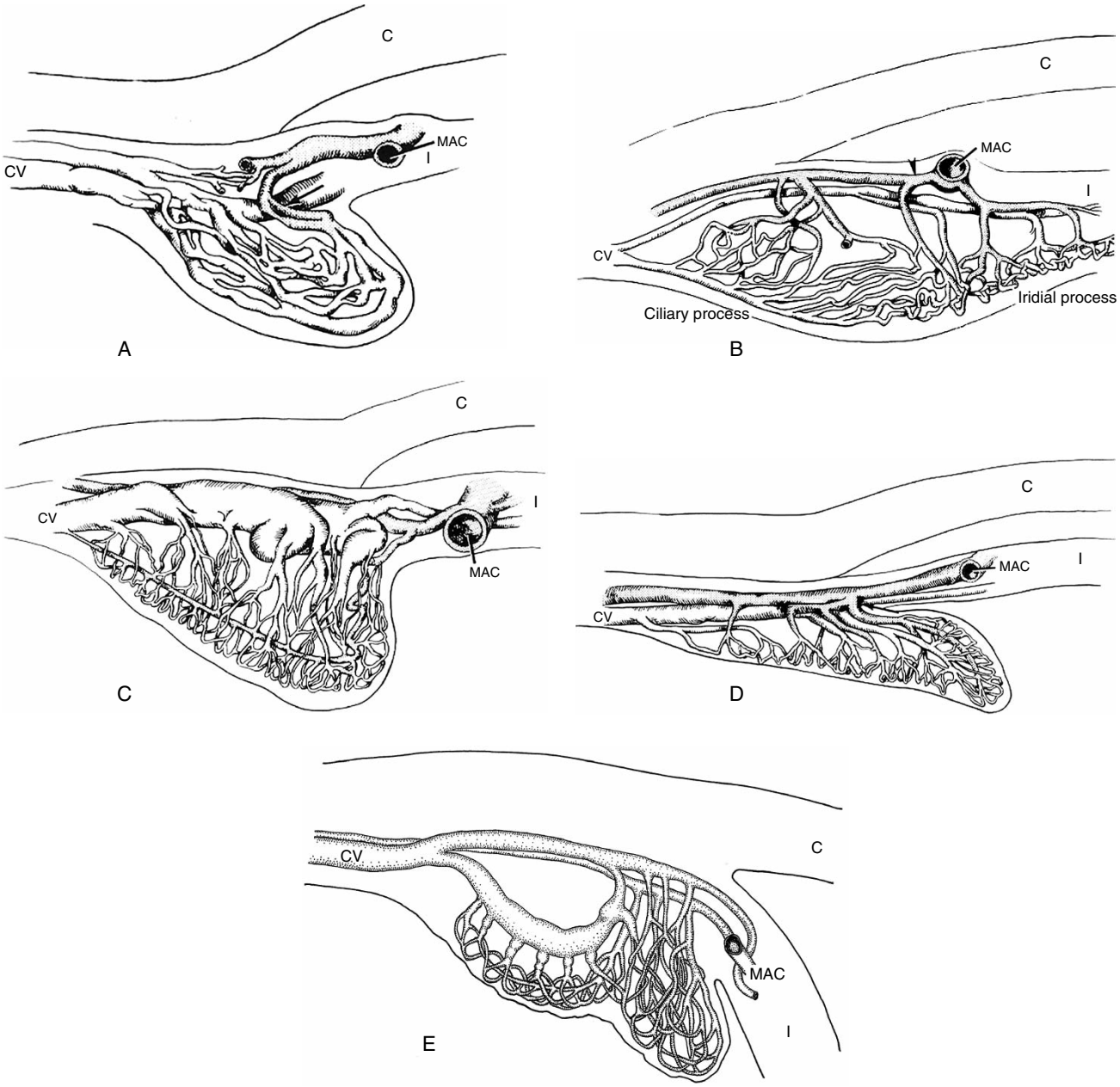

Figure 2.51 Comparative angioarchitecture of the ciliary processes. **A.** Rodents, **B.** Rabbit, **C.** Carnivores, **D.** Ungulates, **E.** Manatee. C, cornea; CV, choroidal vein; I, iris; MAC, major arterial circle. (*Source:* Modified from Morrison, J.C., DeFrank, M.P. & Van Buskirk, E.M. (1987) Comparative microvascular anatomy of mammalian ciliary processes. *Investigative Ophthalmology Visual Science*, **28**, 1325–1340; Morrison, J.C., DeFrank, M.P. & Van Buskirk, E.M. (1987) Regional microvascular anatomy of the rabbit ciliary body. *Investigative Ophthalmology Visual Science*, **28**, 1314–1324; Natiello, N. & Samuelson, D. (2005) Three-dimensional reconstruction of the angioarchitecture of the ciliary body of the West Indian Manatee (*Trichechus manatus*). *Veterinary Ophthalmology*, **8**, 367–373.)

dogs, cats, rabbits, horses, and other ungulate species (Bedford & Grierson, 1986; Bill, 1975b; Inomata et al., 1972; Martin, 1975; McMaster & Macri, 1968; Samuelson & Gelatt, 1984a, 1984b; Samuelson & Lewis, 1995; Samuelson et al., 1989; Sharpnack et al., 1984; Smith & Rudt, 1973; Smith et al., 1986, 1988; Tripathi, 1971a, 1974; Troncoso, 1938, 1942a). This system primarily consists of the ICA, which is bounded anteriorly by the peripheral cornea and perilimbal sclera, and posteriorly by the peripheral iris and anterior CBM. From amphibians to higher mammals, the ICA consists of an irregular, reticular network of connective tissue beams called trabeculae that are lined partially or entirely by a single layer of cells (Samuelson, 1996; Tripathi, 1971a, 1974). The size of the ICA varies among species. In dogs of

different ages and breeds that had undergone cataract surgery, the size of the ICA as determined by the angle opening distance (the distance between the internal limbus and the base of the iris) using ultrasound biomicroscopy was found to vary considerably (Crumley et al., 2009). At the expense of the CBM, a proportionally larger sinus is found in most domestic animals than in humans.

The pectinate ligaments consist of long strands anchoring the anterior base of the iris to the inner peripheral cornea (Fig. 2.52 and Fig. 2.53). In the dog and cat, these strands are usually slender and widely separated from each other, thus making it difficult to visualize histologically an intact pectinate ligament fiber for its entire length. In the rabbit and pig, the strands are somewhat shorter and thicker than those of domestic carnivores (Simones et al., 1996). In contrast, most ungulates possess moderately broad to very stout pectinate ligaments (Fig. 2.54). The pectinate ligaments are entirely lined by cells that are confluent with the anterior surface of the iris. In ICAs with stout pectinate ligaments, the anterior chamber freely communicates with the ICA through pores that lead into a collection of small channels surrounded by cords of densely packed collagen. Posteriorly, the pectinate ligament anastomoses with anterior beams of the trabecular meshwork. In mammals, the network of

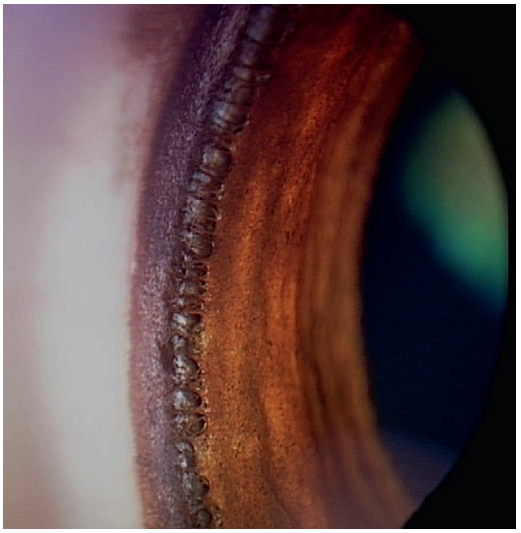

Figure 2.52 Gonioscopic view of the anterior ciliary body shows the fibrous strands, known as the pectinate ligaments, that attach the anterior base of the iris to the limbus.

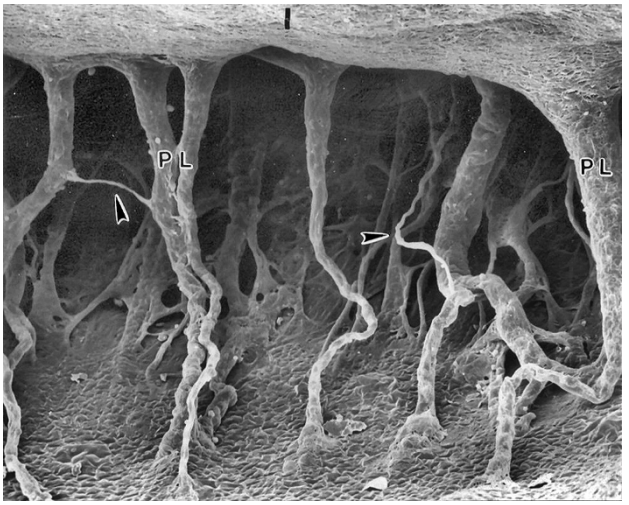

Figure 2.53 Frontal view SEM of the canine iridocorneal angle. Fibrous pillars that attach the iris (I) to the limbus form the pectinate ligaments (PL). Arrows indicate smaller fibrous connections between these pillars and uveal trabeculae located behind the pectinate ligament. (Original magnification, 160×.)

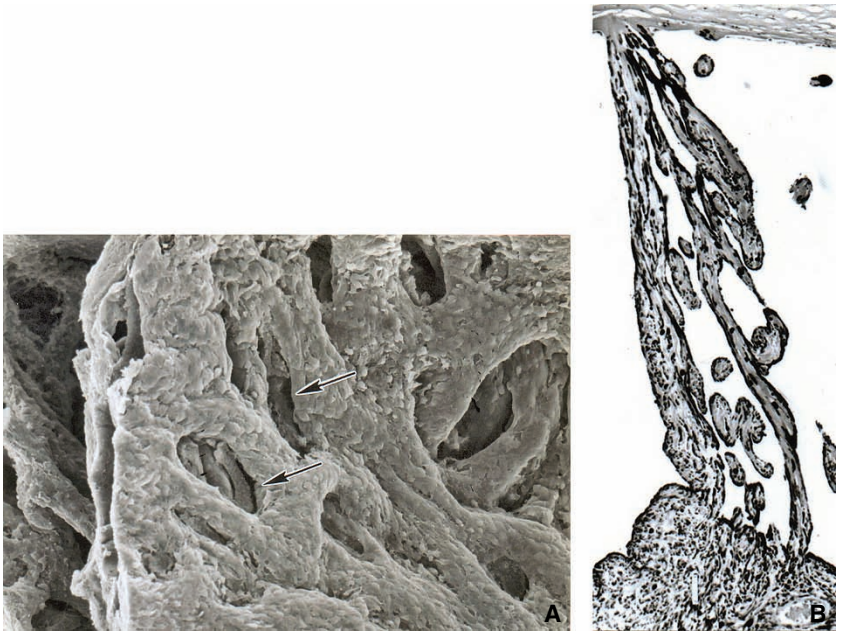

Figure 2.54 Frontal view SEM (**A**) and sagittal view light micrograph (**B**) of the equine pectinate ligament. Anteriorly pores (arrows) form openings that permit the aqueous humor to move from the anterior chamber into the iridocorneal angle. (Original magnification: **A**, 200×; **B**, 100×.)

trabeculae is usually subdivided into two regions. The uveal trabecular meshwork, which in most animals comprises most of the inner ICA area, thus forming the ciliary cleft, and the corneoscleral trabecular meshwork, which is similar in construction to the uveal meshwork but smaller both in size of the trabecular beams and the channels or spaces between the cell-lined beams.

The uveal meshwork interconnects the inner, anterior CBM with the pectinate ligament. For the most part, the uveal trabeculae are oriented meridionally. In most animals, these beams are completely encased by an endothelium referred to as trabecular cells. The beams branch increasingly toward the CBM in radial and circular directions. As a result, the posterior uveal trabeculae are smaller, with smaller intertrabecular spaces separating them. The posterior uveal meshwork often merges imperceptibly with the posterior, innermost regions of the corneoscleral trabecular meshwork.

The corneoscleral trabecular meshworks of domestic animals are characterized mainly by small trabeculae separated by small intertrabecular spaces. In carnivores, these trabeculae are incompletely lined by trabecular cells (Fig. 2.55). By comparison, in certain ungulates, including horses, bison, and water buffalo, each trabecula is completely lined by trabecular cells. In ruminants and pigs, individual trabeculae can be completely lined, whereas others are incompletely lined.

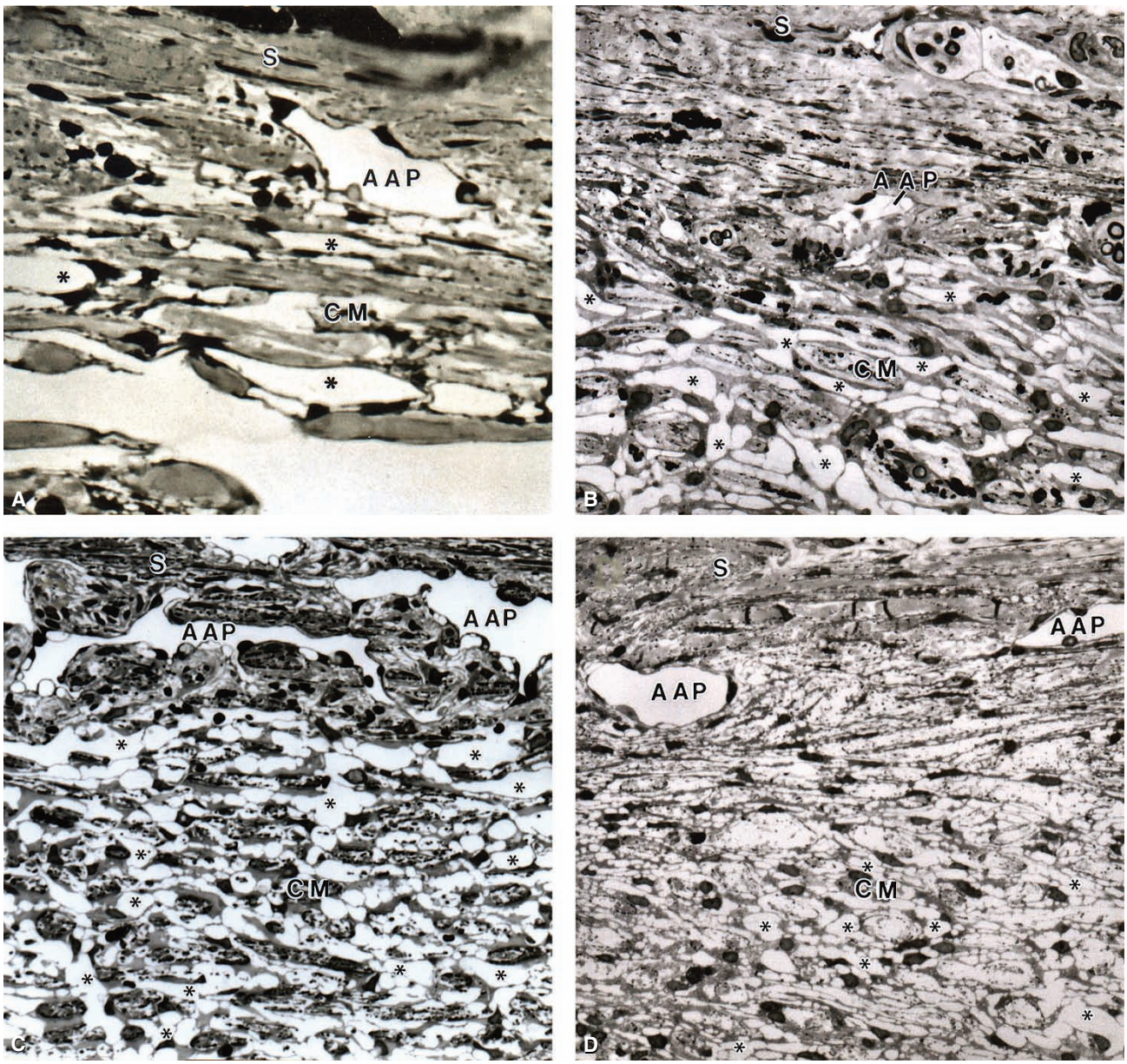

Figure 2.55 **A–D.** The corneoscleral trabecular meshwork (CM), sclera (S) and adjacent angular aqueous plexus (AAP) in the dog (asterisks indicate intertrabecular spaces). (Original magnification: All, 400×.) **B.** Bison, **C.** Horse, **D.** Pig.

Composition of the trabeculae varies very little among species (Bedford & Grierson, 1986; Samuelson, 1996; Samuelson & Gelatt, 1984a, 1984b; Samuelson et al., 1989; Tripathi, 1971a). The core, or center, of each beam is made up of circularly and meridionally oriented collagen fibers interspersed with a modified elastin (Gong et al., 1989). The core is usually enveloped by a cortical zone consisting of amorphous, granular material surrounded by basement membrane-like material. In cats, horses, and water buffalo, the larger corneoscleral trabeculae and smaller uveal trabeculae have multiple layers of basement membrane-like material within the cortical zone (Samuelson et al., 1989; Tripathi, 1974). In horses, a narrow zone of thickened, rounded, corneoscleral trabeculae is present between the outflow veins of the ICA and the pectinate ligament. These trabeculae possess no basement membrane-like material; instead, they have long-spacing collagen.

Trabecular cells are similar across species, being fibroblast-like with slender cell processes that attach to adjacent cells and their processes. These processes allow the corneoscleral trabecular meshwork to act as a sieve, thus reducing the size of the particles that can move into the meshwork (Garcia et al., 1986; Johnson et al., 1990; Samuelson et al., 1985; Smith et al., 1986). The degree of meshwork porosity varies between species, with the dog having a more porous meshwork when compared with the horse. The trabecular cell also has the ability to ingest a wide variety of particles, which can range greatly in size (Samuelson et al., 1984b). The phagocytic-like quality of the trabecular cell provides the ICA with an indigenous clearance mechanism for debris, thus reducing possibilities for an inflammatory response (Grierson & Lee, 1973; Sherwood & Richardson, 1981).

An operculum is located within the canine corneoscleral trabecular meshwork (Samuelson et al., 2001). The operculum comprises much of the nonfiltering portion of the trabecular meshwork in the anterior portion of the ICA (Rohen & Lutjen-Drecoll, 1989). It consists of the peripheral extension of the corneal endothelium (and its subjacent basement membrane, i.e., Descemet's membrane) and the underlying, anteriormost portion of the corneoscleral trabecular meshwork. The operculum is especially well developed in dogs, rabbits, and nonhuman primates (Fig. 2.56; Samuelson, 1996). The peripheral termination of the corneal endothelium and its basement membrane leads to what is referred to as the cribriform ligament because it branches both posteroexternally, into the corneoscleral trabecular meshwork, and posterointernally, joining with the anterior uveal trabeculae. The function of the operculum is unknown; however, cells intimately associated with the operculum (i.e., Schwalbe's line cells) are secretory in nature, able to form and release certain enzymes, including enolase and hyaluronans synthase, and phospholipid surfactant-like material (Fig. 2.57; Allen et al., 1955; Lutjen-Decoll & Rohen, 1992; Raviola,

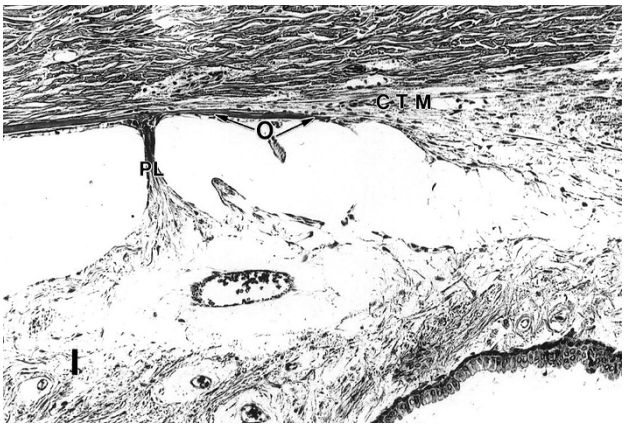

Figure 2.56 In the rabbit, as in most carnivores and monkeys, the peripheral corneal endothelium and its basement membrane extend posteriorly at variable lengths beyond the pectinate ligaments (PL) and form the operculum (O). In turn, the operculum forms a lid-like cover over the anteriormost corneoscleral trabecular meshwork (CTM). I, iris. (Original magnification, 100×.)

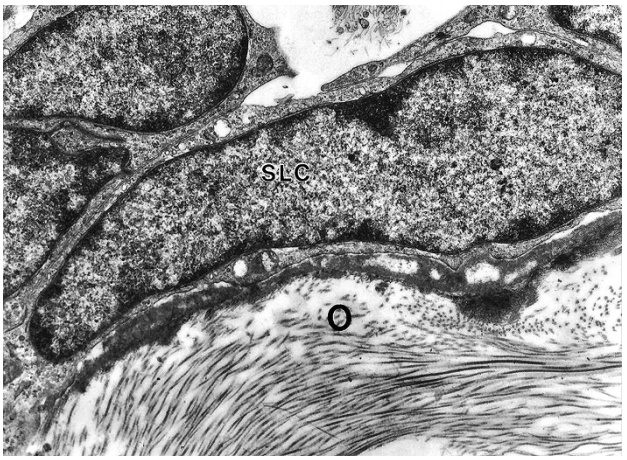

Figure 2.57 Cells associated with the operculum in the dog form clusters and can be linearly arranged (SLC, Schwalbe's line cells) within the anteriormost regions of the corneoscleral trabecular meshwork. O, operculum. (Original magnification, 9800×.)

1982; Samuelson et al., 2001; Stone et al., 1984). Although the role these cells play in the mature ICA has yet to be determined, Schwalbe's line cells represent a distinct subpopulation within most mammalian ICAs.

The external boundary of the corneoscleral trabecular meshwork is formed by the sclera and a plexus of aqueous humor collector vessels. In mammals and most lower vertebrates, the aqueous humor chiefly exits the eye through the trabecular meshworks into these vessels (see Fig. 2.55). In most mammals, these vessels consist of a small network of veins collectively termed the AAP (Tripathi, 1971a, 1974). These vessels have radially oriented lumens, differing from the circumferentially coursing canal of Schlemm in primates (Grierson et al., 1977; Kayes, 1967; Tripathi,

1971b). The plexiform nature of the drainage vessels in most mammals allows removal of a substantial amount of aqueous humor. The single canal in primates most likely represents an evolutionary adaptation for removal of aqueous humor from a relatively small anterior chamber through a small, compact ICA bordered by a large and highly developed CBM essential for accommodation. Adjacent to the meshwork are aqueous collecting channels, which in turn empty into the intrascleral venous plexus and then the vortex veins.

The size of the individual collector vessels (i.e., trabecular veins) and the tissue immediately adjacent to the AAP varies considerably among mammals. The trabecular veins in cattle, sheep, and water buffalo are large and extensive. Those associated with dogs, cats, pigs, and horses are less prominent but are still extensive.

The manner by which aqueous humor flows into the trabecular veins of the AAP or canal of Schlemm is not completely understood (Allingham et al., 1989; Grierson et al., 1977; Kayes, 1967; Lee & Grierson, 1975; Samuelson, 1996; Tripathi, 1971b). Most of the aqueous humor is thought to move through large, vacuole-like structures of the inner endothelial cells (see Fig. 2.55).

The area adjacent to the trabecular veins typically consists of a zone of cellular elements intermixed with irregularly arranged elastin, collagen, and basement membrane-like material. These elements are much more compact in the horse than in other mammals, except for humans. They constitute a separate zone, called the juxtacanalicular zone that is readily distinguished from the rest of the outer corneoscleral trabecular meshwork. The function of this zone has yet to be determined, but it may contribute substantially to aqueous humor outflow resistance.

In some species, including dogs, rats, rabbits, and humans, smooth muscle-like cells (myofibroblastic cells) have been observed in the trabecular meshwork, especially adjacent to the aqueous humor outflow channels and along the distal or outer walls of the AAP and Schlemm's canal (de Kater et al., 1990; Ryland et al., 2003). In the dog, the presence of myofibroblastic cells within the ICA suggests that these cells and the smooth muscle cells of the ciliary body along the same plane of orientation function to facilitate the removal of aqueous humor and are likely to be influenced by vascular mediators. Whether all myofibroblastic cells play a significant role in regulation of aqueous humor outflow is unknown.

GAGs form an integral component of trabeculae within the ICA and the area adjacent to the AAP (and canal of Schlemm). Treatment with hyaluronidase results in lowering of the IOP. GAGs appear to regulate IOP via their state of polymerization, which controls hydration capacity and swelling or shrinking (Grierson & Lee, 1975; Gum et al., 1992; Knepper et al., 1996; Samuelson & Gelatt, 1998; Samuelson et al., 1987b).

Uveoscleral Outflow

Aqueous humor is not entirely removed by a plexus of collector vessels via the ICA. Some aqueous humor drains either posteriorly into the vitreous humor, anteriorly within the iridal stroma and across the cornea, or exteroposteriorly along a supraciliary–suprachoroidal space into the adjacent sclera (Fig. 2.58; Bill, 1985; Bill & Phillips, 1971; McMaster & Macri, 1968; Smith et al., 1988). The lattermost pathway is called the uveoscleral, or unconventional, outflow pathway. The degree of uveoscleral outflow varies remarkably between species, with cats experiencing the least drainage (3%), followed by humans (4%–14%), rabbits (13%), dogs (15%), and nonhuman primates (30%–65%) (Barrie et al., 1985; Bill & Phillips, 1971). In the horse, the uveoscleral pathway may be just as important as the conventional route for aqueous humor removal. Large spaces of the outer uveal meshwork become confluent posteriorly, with a uniquely wide and well-defined meshwork between the CBM and the sclera (i.e., the supraciliary space). This region, which has been found only in the horse, is called the supraciliary meshwork, and most likely represents a major pathway for aqueous humor removal (Fig. 2.59; Samuelson et al., 1989).

In pigs, cattle, dogs, cats, and horses, the outer anterior CBM forms longitudinal and circumferential attachments to trabeculae of the ICA (Samuelson & Birkin-Streit, 2011; Sedacca et al., 2011). Spaces between the endings of the CBM form avenues for the beginning of the uveoscleral pathway (Fig. 2.60). In pigs, the corneoscleral trabecular meshwork is anchored by a scleral spur, which in turn anchors much of the outer CBM. As a result, the uveoscleral pathway is limited to small intertrabecular spaces of the

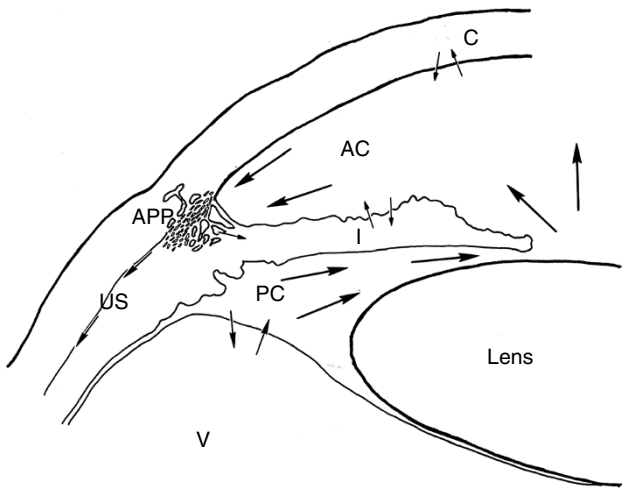

Figure 2.58 The majority of aqueous humor flows from the posterior chamber (PC) into the anterior chamber (AC), where it is removed via the iridocorneal angle by the trabecular meshwork and angular aqueous plexus (AAP). Other drainage routes include exchange across the vitreous face (V), iris vessels (I), and corneal endothelium (C), and via the uveoscleral (US) pathway.

posterior ICA that interface with the anterior CBM. Within the outer ciliary body, there are blood vessels in close proximity to the sclera. More posteriorly, the supraciliary space contains occasional collagenous trabeculae (Sedacca et al., 2011).

In cattle and domestic carnivores, outer anterior muscle bundles attach the CBM to the sclera with an anterior elastic sheath, which is especially well developed in dogs. Initially, the uveoscleral pathway consists of small intercellular spaces lying between the attachments of the anterior smooth muscle bundles of the ciliary body and the posterior uveal trabecular meshwork. Within the supraciliary space, slender trabeculae are most numerous anteriorly extending from the ciliary body obliquely and radially.

In horses, the outer anterior muscle bundles of the ciliary body are connected to branching connective tissue trabeculae within the uveoscleral pathway that are attached radially to the sclera (Samuelson et al., 1989; Sedacca et al., 2011). An elastic sheath lines this portion of the uveoscleral pathway. Trabeculae within the supraciliary space are extensive, consisting of either collagen or muscle. Both types of trabeculae are often branched and lined by melanocytes, becoming less numerous, narrower, and less branched posteriorly.

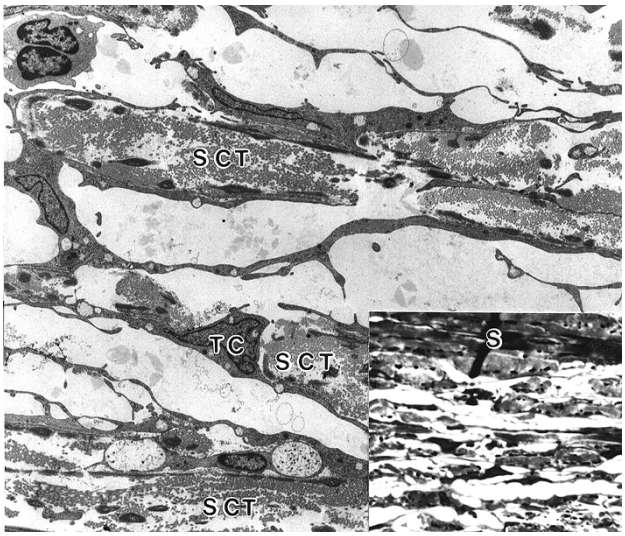

Figure 2.59 Located between the ciliary body meshwork and the sclera (i.e., supraciliary space), the supraciliary meshwork likely represents a major pathway for aqueous humor drainage in the horse via uveoscleral outflow. SCT, supraciliary trabecula; TC, trabecular cell. (Original magnification, 3500×.) *Insert*: Light micrograph of the meshwork. S, sclera. (Original magnification, 200×.)

Aging

A number of age-related changes occur in the ciliary body. As the nonpigmented epithelium grows older, its basement membrane thickens greatly, becoming multilaminar (Streeten, 1988). The pigmented epithelial basement membrane similarly thickens with age, producing a nearly identical multilaminar appearance. The nonpigmented epithelium thins irregularly. The stroma of the ciliary body concomitantly thickens because of increased amounts of collagen and other extracellular materials. The degree of pigmentation in the ciliary body lessens with age, particularly in the pigmented epithelium along the crests of the ciliary processes (Streeten, 1988).

Age-related changes associated with the ICA are well documented in humans and dogs (Bedford & Grierson, 1986; Hogan et al., 1971; Samuelson & Gelatt, 1984a, 1984b, 1998). The cortical zone within the trabecula broadens in older individuals. This thickening is caused by the presence of additional basement membrane-like material and additional amorphous material. The thickened cortical zone could contribute to increased thickening of the corneoscleral

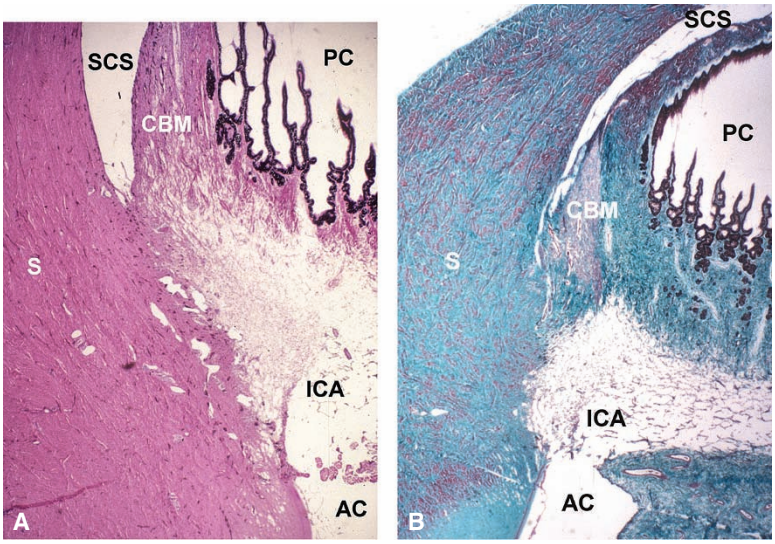

Figure 2.60 Anterior uveoscleral outflow pathway viewed tangentially. **A.** Bovine anterior uvea. (Original magnification, 20×.) **B.** Porcine anterior uvea. (Original magnification, 20×.) AC, anterior chamber; CBM, ciliary body musculature; ICA, iridocorneal angle; PC, posterior chamber; S, sclera; SCS, supraciliary space; UTM, uveal trabecular meshwork.

trabeculae within the canine ICA. Use of PAS stain, which reacts strongly with basement membrane material, on normal laboratory-quality Beagle ICAs of different ages (from 3 months to 8 years) demonstrates positive reactions within the corneoscleral trabecular meshwork, especially along the posterior extension of Descemet's membrane. The apparent increase in PAS staining with age occurs mostly within the anteriormost portion of the corneoscleral trabecular meshwork. No age-related changes have been observed or reported within the uveal trabeculae of the canine ICA (Bedford & Grierson, 1986).

Perhaps the most discernable alterations of the canine ICA with regard to age are those associated with the extracellular fibers comprising the bulk of each trabecula. When comparing the average diameter of the collagen fibril as well as the distribution of diameter size within the inner and outer regions of the corneoscleral trabecular meshwork and subjacent sclera next to the aqueous plexus at different ages, several changes are recognized (Gelatt & Samuelson, 1986). The average diameter of collagen fibrils within the outer corneoscleral trabecular meshwork increases by approximately 25% during the second and third years of life compared with the latter half of the first year (Samuelson & Gelatt, 1998). On the other hand, collagen fibrils within the inner corneoscleral trabecular meshwork and adjacent outer uveal trabecular meshwork become progressively thinner during the first 3 years of life. Early age-related changes in collagen fibrillar size are most remarkable within the sclera forming the outermost lining of the ICA, increasing nearly 100% in average diameter over a 2.5-year period. The increase of collagen fibrillar size within the inner scleral wall of the limbal region occurs unevenly, with some fibrils remaining small and others attaining considerable widths.

The appearance of the trabecular (i.e., endothelial) cells in both the uveal and corneoscleral meshworks changes mostly during the first year of life. As the cells become more separated spatially, they elongate and possess less clustered cytoplasmic processes. In older animals (>4 years of age), fewer cells are observed in both meshworks compared with those in younger animals (<1 year of age). By the end of the first year, the average cellular density of both meshworks has dropped by nearly 30% (Samuelson & Gelatt, 1998). The lowering of cellular density during this period undoubtedly results from the overall increase in ICA size during the first year of life in dogs (Samuelson & Gelatt, 1984a, 1984b). A further substantial decrease in cellular density is not observed for another 5 years, until the seventh and eighth years of age. The size of the ICAs in older dogs (7–8 years of age) is, in fact, slightly smaller than that in the younger mature dogs (1–6 years of age), which may be attributed to the age-related increase in lens size. These changes appear to reduce the area available for aqueous humor outflow.

Innervation

As mentioned previously, the ciliary musculature is innervated both sympathetically and parasympathetically (Gum et al., 2007; Murphy et al., 2012). Cholinergic and adrenergic nerve endings have been observed in the various components of the ciliary body, including the trabecular meshwork and within the ICA. In the dog, cholinergic activity is most intense in the musculature, ciliary processes, and epithelium. Dense adrenergic innervation, however, is located in the subepithelial portions of the ciliary body (Gwin et al., 1979). Species differences in the distribution of these nerves among many lower mammals have been demonstrated (Ehinger, 1966a), but the function of the cholinergic and adrenergic nerves within the ciliary body remains speculative (Ehinger, 1966b; Nomura & Smelser, 1974).

Choroid

The choroid is the posterior portion of the uveal coat. It is composed primarily of blood vessels (mainly thin-walled veins) and pigmented support tissues. It is the main source of nutrition for the outer layers of the retina. In most domestic animals, the anterior margin of the choroid joins the ciliary body along a regular, nonserrated junction called the ora ciliaris retinae. In primates, the junction is irregular and serrated and termed the ora serrata. The choroid tends to thicken along the posterior pole, becoming thinner toward the globe equator.

For morphologic discussions, the choroid is divided externally to internally, as shown in Fig. 2.61, into

1) the suprachoroidea
2) the large-vessel layer
3) the medium-sized vessel and tapetum layer, and
4) the choriocapillaris.

The tapetal layer varies among species, and it is absent in pigs, squirrels, rodents, rabbits, kangaroos, llamas, alpacas, and many nonhuman primates.

Suprachoroidea

The suprachoroidea consists of elastic, heavily pigmented connective tissue that forms a transition between the sclera and the choroid. Branching collagen lamellae traverse the potential suprachoroidal space to fasten the choroid to the lamina fusca of the inner sclera (see Fig. 2.61). During processing for histologic examination, the choroid frequently separates from the sclera. The suprachoroidea also functions as the posterior component for uveoscleral outflow. Aqueous humor that has moved along this narrow junction of the sclera and choroid diffuses into the sclera and, subsequently, the systemic circulation. The layers of melanocytes and fibrocytes and the interspersing collagen and elastic fibers may produce resistance to uveoscleral drainage, even though

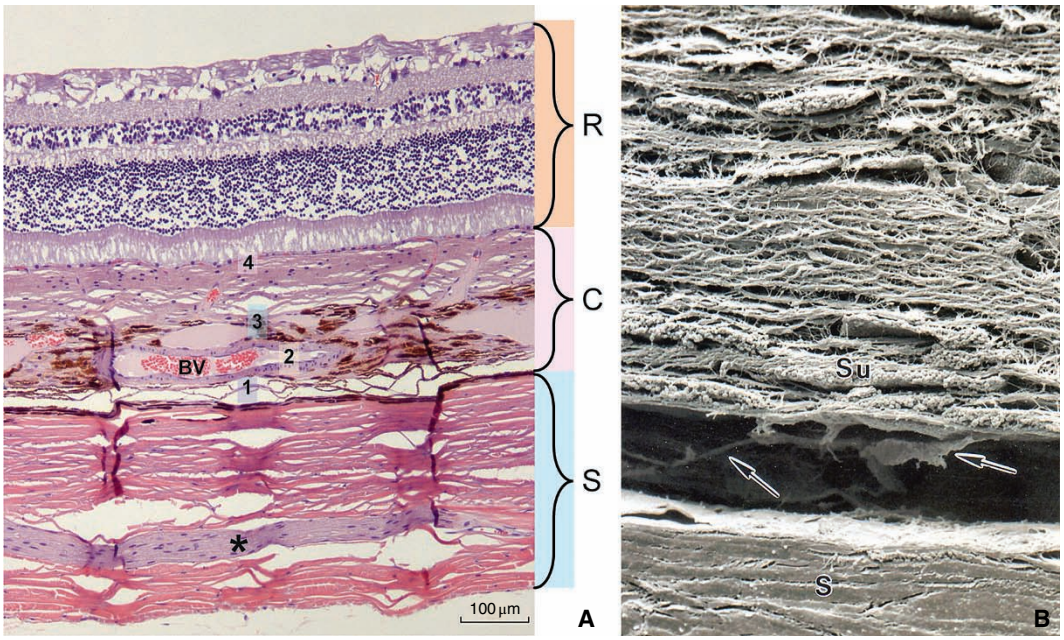

Figure 2.61 **A.** The canine choroid (C) consists of the suprachoroidea (1), large-vessel layer (2), medium-sized vessel and tapetum layer (3), and choriocapillaris (4). R, retina; BV, blood vessel. * denotes a nerve within the sclera (S). **B.** SEM shows a close-up view of the outer choroid, where the suprachoroidea (Su) forms fine collagenous attachments (arrows) with lamina fusca of the sclera (S). (Original magnification, 850×.)

a cellular barrier has not been found (Koseki, 1992). The long posterior ciliary nerves and arteries course their way anteriorly in the suprachoroidea along the horizontal meridian (Castro-Correia, 1967).

In birds, this region also contains a layer of nonvascular smooth muscle cells (DeStefano & Mugnaini, 1997). This layer is believed to be innervated by somatostatin-expressing neurons located within the avian choroid. The function of this band or layer of smooth muscle within the suprachoroidea is unknown, but its location suggests that it could play a significant role in uveoscleral outflow and IOP regulation.

Large-Vessel Layer

Immediately internal to the suprachoroidea is a vascular plexus embedded in loose connective tissue containing melanocytes and fibrocytes. This plexus is composed mostly of large veins and scattered arteries (Fig. 2.62). These veins merge centripetally into four or more prominent vortex veins located obliquely near the globe equator between the horizontal and vertical meridians. In cross section, the veins are cavern-like, occupying 50% or more of the total volume of the choroid (see Fig. 2.61 and Fig. 2.63). They frequently collateralize with each other and communicate anteriorly with anterior ciliary veins, the intrascleral venous plexus, and the iridal veins (Natiello et al., 2005; Wong & Macri, 1964). The large arteries, which are much fewer in number, are mostly branches of the short posterior ciliary arteries,

Figure 2.62 SEM corrosion cast of the choroidal vasculature in the dog. Large arrows indicate collateralization of the intrascleral plexus (ISP) with the large choroidal veins (V). Small arrows indicate choroidal arteries. (Original magnification, 10×.)

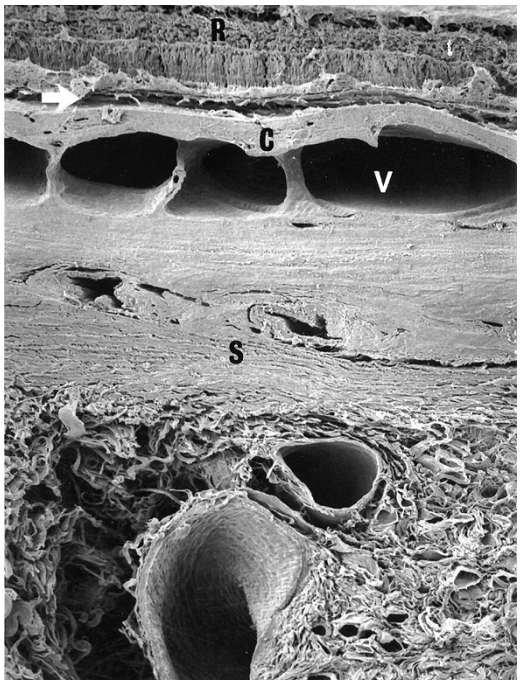

Figure 2.63 SEM of the posterior canine eye shows the choroid (C) is composed mostly of large, cavernous veins (V) that drain the choriocapillaris (arrow), which nourishes the outer retina (R). S, sclera. (Original magnification, 25×.)

which enter the globe in the vicinity of the optic nerve and supply the retina, optic nerve, and choroid. To a lesser extent, the choroid also receives blood from the long posterior ciliary arteries and the anterior ciliary arteries (Torczynski, 1988).

In addition to providing the major source of oxygen and nutrients for the retina, the large vessels may act as a "cooling system," dissipating the heat produced from light absorption (Auker et al., 1982; Parver et al., 1982). The osmotic pressure created by high levels of plasma proteins in the choroidal tissue fluid might also assist in keeping the retina attached to the retinal pigment epithelium (RPE), by allowing retinal fluids to pass into the choroid, then subsequently into the suprachoroidea, sclera, and episcleral tissues (Bill, 1968, 1975a, 1985).

In the avian eye, the large veins are directly associated with another bed of vessels, which have been referred to as sinusoids, lacunae, or most recently, lymphatic vessels (DeStefano & Mugnaini, 1997; Meriney & Pilar, 1987; Walls, 1942). These vessels comprise a major portion of the choroidal volume, and they serve as a large reservoir that may assist in IOP regulation by removal of fluid from the blood vessels (DeStefano & Mugnaini, 1997; Meriney & Pilar, 1987). Morphologically, the vessels are similar to lymphatic vessels, with a fenestrated endothelium but no innervation or defined, basal lamina-associated smooth muscle. These vessels are mostly located next to the suprachoroidea, and a

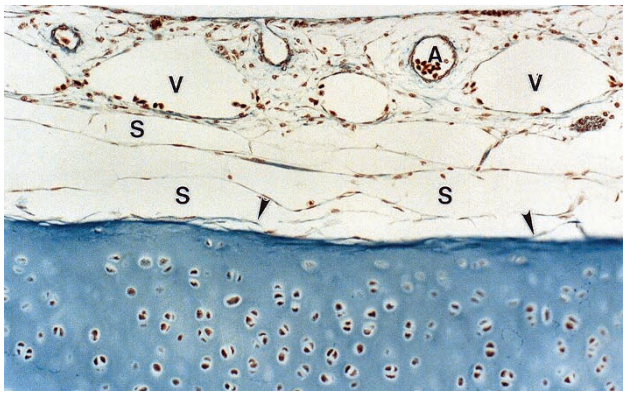

Figure 2.64 The outer choroid in the avian (i.e., chicken) eye consists of sinusoids (S) that extend to the suprachoroidea (arrows) and adjacent "cup" of hyaline cartilage. A, arteries; V, veins. (Original magnification, 200×.)

portion of them extends into adjacent large veins as the latter exit the choroid (Fig. 2.64). The combination of these accessory vessels in the outer choroid and the previously discussed thin band of smooth muscle within the suprachoroidea distinguishes the avian from the mammalian choroid.

Medium-Sized Vessel and Tapetum Layer

A small layer of medium-sized vessels and pigmented reticular connective tissue lies internal to the large-vessel layer. These vessels are emissaries between a single sheet of capillaries and the layer of large blood vessels. The medium-sized vessels, especially the arteries, dichotomously branch, radiating slightly inward in a fanlike manner from the larger vessels. The cells surrounding these vessels consist of melanocytes and fibrocytes. In heavily pigmented individuals, the melanocyte is the predominant cell type. In most domestic animals, the melanocyte possesses characteristically oval-to-round melanin granules ranging from 0.1 to 4.0 μm in diameter. The extracellular space consists of loosely arranged bundles of collagen interspaced with numerous elastic fibers.

Nonmyelinated nerve fibers in the choroid are predominantly associated with the vascular system, and most of the nerves are associated with the arterial system. They arrive in the choroid as short ciliary nerves around the optic nerve and provide numerous collaterals in the posteroanterior route. They follow the short posterior ciliary artery branches, and they give off anastomotic branches. Most of the nerve endings provide motor input to the smooth muscles of the arteries.

In most domestic animals, the dorsal portion of the choroid at the medium-sized vessel layer contains a layer of reflective tissue called the tapetum lucidum. The tapetum is roughly triangular in shape when viewed funduscopically, and it varies in color (Fig. 2.65). It reflects light that has

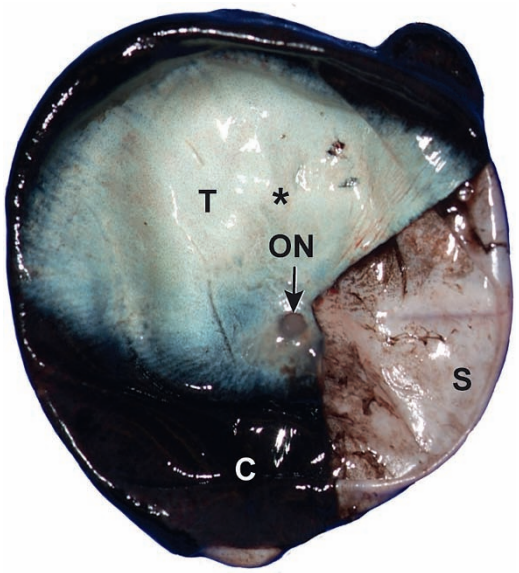

Figure 2.65 The tapetum lucidum (T), which is always located dorsally, usually ends along the horizontal plane next to or including the optic nerve head (ON). In this specimen, a portion of the retina and choroid (*) have been removed to demonstrate the posterior eyewall, the sclera (S). Feline globe.

passed through the retina and thus restimulates the photoreceptor cells. The tapetum lucidum is responsible both for the "eyeshine" seen at night when the eye is illuminated and for the variable background color of the ocular fundus when viewed ophthalmoscopically during fundic examination. Animals without a tapetum lucidum have diurnal habits and red or orange to pale gray (depending on the amount of choroidal pigmentation) fundic reflections (Young & Braekevelt, 1993). The red-to-orange backgrounds result from reflection of light from choroidal blood vessels in less pigmented individuals.

The tapetal layer is composed of regularly arranged collagenous fibers in herbivores (i.e., the tapetum fibrosum in horses, cattle, sheep, and goats) and of specific polyhedral cells, or iridocytes, containing reflecting crystals in carnivores (i.e., the tapetum cellulosum in the dog and cat). Animals with a tapetum show great color variation depending on species, breed, age, and amount of pigmentation. Microscopically, the tapetum is interposed between the branching vessels in the choroid and the single layer of the choriocapillaris beneath the retina. The thickness of the tapetum varies, being multilayered at its center and thinning to a single cell (or lamella) at its periphery and adjacent to the optic nerve. The tapetum develops late in animals born with immature eyes (e.g., dogs and cats); it is usually completely developed by 4 months of age. Animals born with mature eyes (e.g., ungulates and equines) have a well-developed tapetum at birth.

Histologically, the tapetum cellulosum is composed of rectangular-shaped cells, iridocytes, with a species-dependent

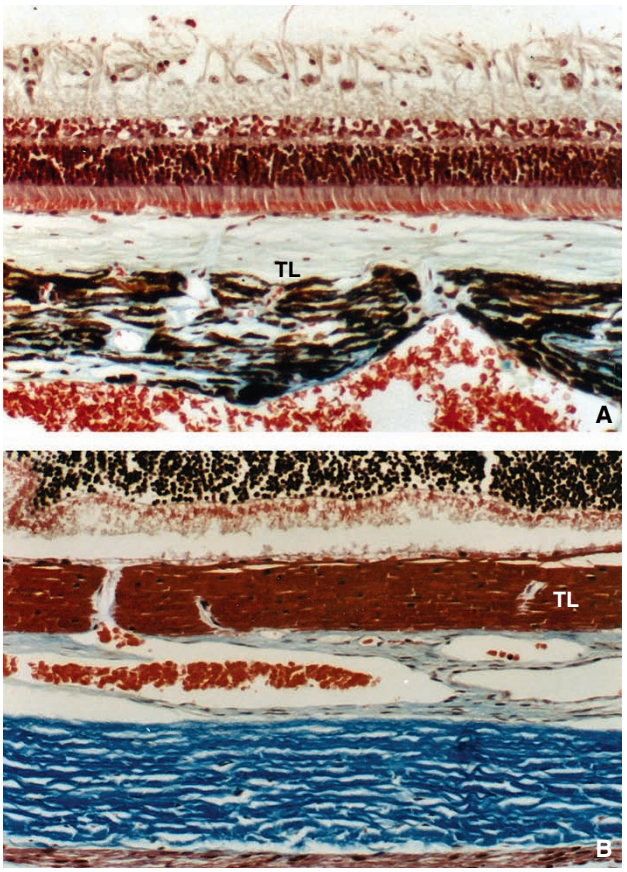

Figure 2.66 The carnivorous tapetum lucidum (TL) consists of layers of cells, called iridocytes, which vary in number, size, and composition. **A.** The dog. **B.** The cat. (Original magnification: 200×.)

variability in number of cell layers (Fig. 2.66; Table 2.10). The tapetal layer is thickest centrally and thins toward the periphery until the tapetum cellulosum is replaced by regular choroidal stroma. From the underlying choroidal stroma, numerous small vessels penetrate the tapetal layer to form a single-layered capillary bed, known as the choriocapillaris network, on the inner surface of the tapetum. Iridocytes have a round nucleus with a prominent nucleolus; in tangential sections, the tapetal cells are polygonal.

The most striking ultrastructural feature of tapetal cells in the dog and cat is the presence of numerous slender, electron-dense rods in the cytoplasm. These rods in the cat are densely packed, uniform in size, circular in cross section, and circumferentially arranged into highly organized groups (Fig. 2.67). The sides of adjacent tapetal cells have a wider intercellular space, separated by collagen and elastic fibrils, than the ends of the cells, which are in closer apposition to each other. Within each cell, there may be several groups of rods, often oriented at right angles to each other but still maintaining their long axis parallel to the retinal surface. The rods are membrane-bound and pack the cytoplasm so that the remaining organelles are limited to the perinuclear

Table 2.10 Choroidal tapeta among selected vertebrates.

Classification	Type of tapetum	Reflective material	Thickness	Size of fibrils or rodlet dimensions
Fish (Elasmobranchs)	Occlusible	Guanine	60–80 µm	12–20 superposed crystals
Dog	Cellulosum	Zinc cysteine	9–20 layers	Length: 4 µm Diameter: 0.14–0.18 µm Spacing: 0.20 µm
Cat	Cellulosum	Riboflavin, zinc	10–30 layers	Length: 0.10–6 µm Diameter: 0.10–10 µm Spacing: 0.08–0.20 µm
Cow	Fibrosum			Diameter: 0.15–0.20 µm Spacing: 0.20 µm
Sheep	Fibrosum	Collagen	9-16 layers	Diameter: 0.15 µm Spacing: 0.08–0.2 µm

Source: From Ollivier, F.J., et al. (2004) Comparative morphology of the tapetum lucidum (among selected species). *Veterinary Ophthalmology*, **1**, 11–23. Reproduced with permission of John Wiley & Sons.

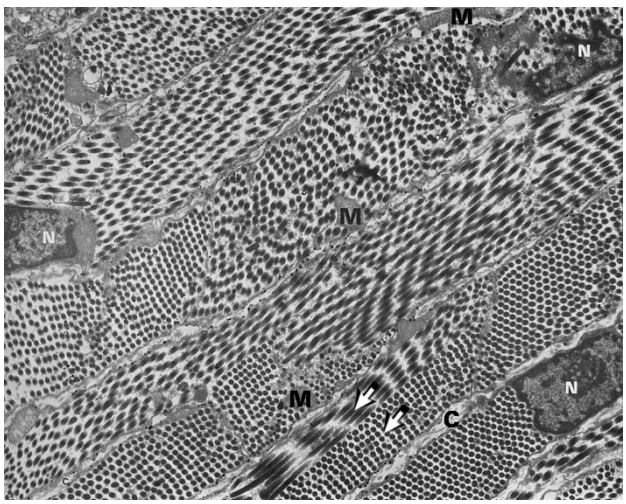

Figure 2.67 Tapetal cells of a cat. The main cytoplasmic components are the rods; mitochondria (M) are infrequent. The rods are uniform in a group concerning spatial orientation, but more than one group is often present within a cell (arrows). The sides of adjacent cells have wide intercellular spaces with scattered collagen fibrils (C), whereas the ends of the cells are in close apposition. N, nucleus of tapetal cell. (Original magnification, 7750×.)

region and the cell periphery. Melanin granules are present in small numbers in the tapetal cells on the scleral side of the tapetum (Chijiiwa et al., 1990; Pedler, 1963), and tapetal rods have the ability to bind calcium at a similar level to melanin; this suggests that, in all likelihood, the iridocyte is a modified melanocyte. The chemical composition of the tapetal layer varies among species. A high level of zinc (zinc cysteine) is present in canine iridocytes, whereas feline iridocytes contain abundant riboflavin and zinc (Braekevelt, 1993a). The tapetal rods are believed to contain high concentrations of these substances (Pirie, 1966).

In ungulates, closely and regularly arranged collagen fibers comprise the tapetum, which is often referred to as a fibrous tapetum. The fibrous tapetum is basically acellular, except for an occasional fibrocyte. The collagen fibrils are organized into well-ordered lamellae that branch and interconnect with adjacent lamellae at the same level, parallel with the retinal surface. The collagen fibrils within each layer vary little in diameter (approximately 80 nm) and have a regular spatial arrangement similar to that seen in the corneal stroma (see Fig. 2.26).

Small blood vessels, typically capillaries, penetrate the tapetum at right angles to the long axis of the iridocytes in carnivores, and to the collagen lamellae in herbivores, directly interconnecting the medium-sized blood vessels with the choriocapillaris (Fig. 2.68). When observed ophthalmoscopically, these end-on vessels are sometimes called the "stars of Winslow." In the dog and cat, these vessels are separated from the iridocytes by a small amount of loose connective tissue and a lining of fibrocytes (see Fig. 2.68).

In nonmammalian species, the tapetum lucidum is either located within the retina (teleosts and some reptiles) or within the choroid (elasmobranches). The tapetum lucidum is consistently absent in birds (Pirie, 1966). With a retinal tapetum lucidum, either lipid- or guanine-laden material lies within the cytoplasm of the RPE (Ollivier et al., 2004; Schwab et al., 2002). Among teleosts, movement of melanin granules within the RPE occurs depending on the environmental illumination, with the melanin granules migrating toward the vitreous humor (forward) during illumination or toward the sclera (backward) during dim light or darkness. The movement of melanin granules causes the reflective material within the RPE to become masked or occluded. Consequently, these retinal tapeta lucida are referred to as occlusible. In elasmobranchs, the tapetum lucidum is also occlusible, but not because of melanin movement. In a

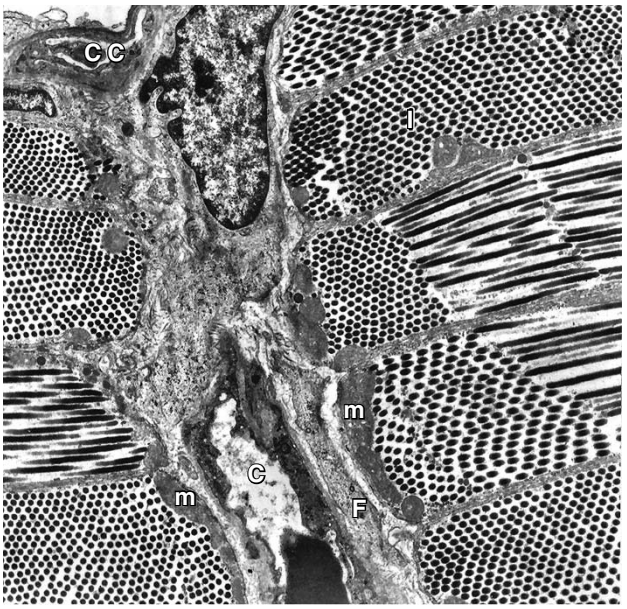

Figure 2.68 Capillaries (C) vertically interconnect medium-sized blood vessels with the choriocapillaris (CC) in the cat. The iridocytes (I), or tapetal cells, line up evenly next to these capillaries. The end of each iridocyte is bordered by mitochondria (m). F, fibrocyte. (Original magnification, 7200×.)

phenomenon termed retinomotor movement, RPE cell processes and the photoreceptors experience positional rearrangements based on changes in ambient lighting. The RPE processes move between and over the reflective cells within the tapetum during illumination, masking the reflective material. Then in low light conditions, this movement is reversed, exposing the reflective material and enhancing the ability of the photoreceptors to process light.

Choriocapillaris

The choriocapillaris is the innermost layer of choroidal vessels, forming a thin layer of capillaries separated from the RPE by a basement membrane complex known as Bruch's membrane (Fig. 2.69). The lumen of the choriocapillaris is fairly wide, allowing red blood cells to pass through two to three abreast. The endothelial lining of the choriocapillaris possesses numerous circular fenestrations, which are often arranged in rows. External to the endothelium is a basement membrane forming the external layer of Bruch's membrane. Bruch's membrane is poorly developed in many domestic animals when compared to primates. In most diurnal species that lack a tapetum lucidum, including pigs and primates, Bruch's membrane is pentalaminated, consisting of basal laminae of the RPE and choriocapillaris endothelia, two adjacent layers of collagen, and an intervening band of elastic fibers. In animals with tapeta, and especially with

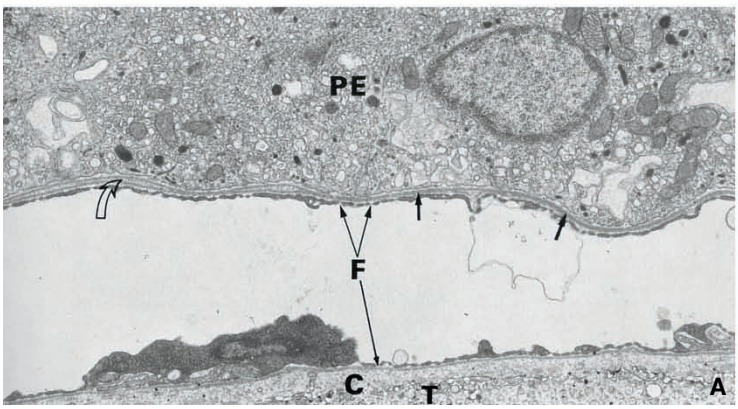

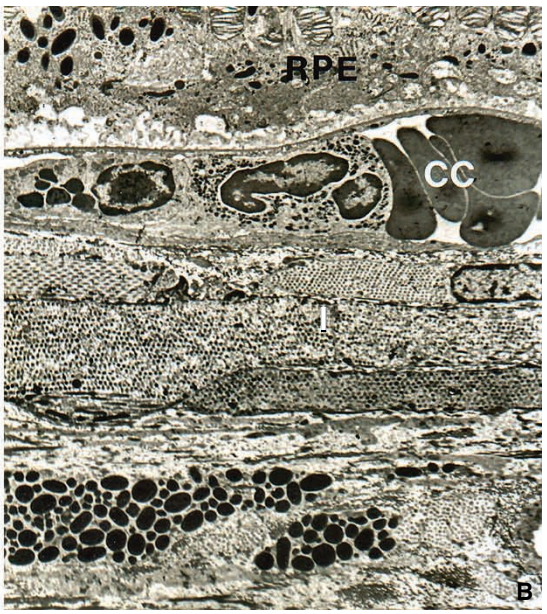

Figure 2.69 Choriocapillaris in the dog. **A.** Note the numerous fenestrations (F) in the endothelium. Bruch's membrane in most places consists of only the fusion of the pigment epithelium (PE) and the endothelial basal lamina (dark arrows), but small amounts of the collagenous zone are visible when they separate (open arrow). Note how the tapetum (T) is buffered from the capillary by a layer of collagenous tissue (C). Note also the lack of pigment in the PE over the area of the tapetum. (Original magnification, 12,400×.) **B.** The choriocapillaris (CC) forms the innermost layer of the choroid, being a wide capillary bed intimately associated with the RPE. I, iridocyte. (Original magnification, 3000×.)

cellular tapeta, Bruch's membrane is reduced to a trilaminated structure consisting of two basal laminae and a layer of collagen.

Lens

The crystalline lens is a transparent, avascular structure that focuses light onto the retina. It is suspended within the eye by zonules arising from the ciliary body epithelium (i.e., pars plicata) and attaching circumferentially to the lens capsule at the lens equator. The lens is also held in place posteriorly within a shallow depression in the anterior vitreous (i.e., the patella fossa), and the iris rests against it anteriorly. In many mammals, birds, and reptiles, the lens is biconvex; the degree of convexity (i.e., shape) is able to change during accommodation because of the elasticity of the capsule and the pliability of the lens fibers. In young mammals, the lens is quite soft, with only a small, central, denser nucleus. The lens grows throughout life, with newly formed fibers added continuously to the outermost cortex, causing compression of the central, older zone of lens fibers. This results in a hardening of the central nucleus (i.e., nuclear sclerosis), which reduces accommodation ability as the lens ages.

The refractive power of the lens is less than the cornea because the change of refractive index is much greater at the air–cornea interface than at the aqueous–lens and lens–vitreous interfaces. Contraction of the CBM reduces tension on the lenticular zonules, thereby changing the shape of the lens resulting in an alteration of the dioptric power. Of the roughly 60 diopters of total refractive power of the eye, the lens contributes approximately 13–16 diopters in humans. In dogs, the dioptric power of the lens contributes approximately 40 diopters. The remaining refraction is provided by the cornea. Some mammals, including monotremes, marsupials, some herbivores, aquatic (primarily marine), placentals, and many nocturnal types such as mice and rats, have no known accommodative mechanism (Prince, 1956). Others, such as ungulates, accommodate weakly, having poor near vision; as a result, they rely more on other senses to detect near objects.

The lens is proportionately larger in domestic animals than in humans. The dog lens has a volume of approximately 0.5 mL and averages 7 mm in thickness at the anteroposterior axis, with a 10-mm equatorial diameter. The proportion of lens volume to entire globe volume ranges from 1 : 8 to 1 : 10. The equine lens, on the other hand, has a volume of approximately 3 mL, 12–15 mm average anteroposterior axis thickness, an approximately 21-mm equatorial diameter, and a lens–globe ratio of 1 : 20. Lens volumes of sheep, cattle, and pigs fall between these volumes, thicknesses, and diameters (Table 2.11). The lens consists of an enveloping basement membrane called the lens capsule, an anterior epithelium, and lens fibers occupying two main zones: the nucleus and the cortex (Fig. 2.70).

Table 2.11 Lens measurements in domestic animals.

Animal	Volume (mL)	Anteroposterior axis (mm)	Diameter (mm)
Dog	0.5	7	10
Cat	0.5	7.5–7.8	9–10.4
Horse	3.0	12–15	18–22
Cow	2–2.3	12–14.9	17.2–19.5
Sheep	0.9–1.2	8–12	12–15
Pig	0.5–0.8	7.5–8.1	9.5–11

Source: Translated from Bayer, J. (1914) *Angenheilkunde*. Vienna: Braumueller.

Table 2.12 Lens capsule measurements in the dog.

Age	Anterior pole (μm)	Equator (μm)	Posterior pole (μm)
Neonatal	1.9	3.8	1.9
1 week	2.9	4.8	1.9
4 weeks	6.7	7.6	3.8
8 weeks	10.5	7.6	3.8
12 weeks	20.9	7.6	3.8
16 weeks	21.9	7.6	3.8
1 year	48.5	7.6	3.8

Source: Monaco, M.A., Samuelson, D.A. & Gelatt, K.N. (1985) Morphology and postnatal development of the normal lens in the dog and congenital cataract in the Miniature Schnauzer. *Lens Research*, **2**, 393–433.

Lens Capsule

The lens fibers are completely enclosed within a thick, PAS-positive capsule, which is the exaggerated basement membrane of the lens epithelium. It has elastic properties but no elastic fibers (Hogan et al., 1971). The thickness of the capsule varies by region, with the thinnest being the posterior pole. The canine lens capsule thickness is 8–12 μm at the equator, 50–70 μm anteriorly, and only 2–4 μm posteriorly. Most of the capsule thickening occurs during the first year of life (Table 2.12; Monaco et al., 1985). As in most basement membranes, the main component of the lens capsule is type IV collagen.

Anterior Epithelium

Lining the anterior capsule is a monolayer of lens epithelial cells that continuously produce new basement membrane (i.e., capsule material). The cells are cuboidal to squamous axially at the anterior pole of the lens, become columnar near the equator, then elongate into slender hexagonal lens fibers. Nuclei are lost as lens fibers mature and move centrally. The lens epithelium lines only the interior aspect of the anterior surface of the capsule postnatally. The cell apices face the outer lens fibers, being attached to the underlying

cortical fibers by tight junctions (zonula occludens) and macula adherens (Benedetti et al., 1976; Hogan et al., 1971; Monaco et al., 1985; Rafferty & Esson, 1974; Samuelson et al., 1987a). The posterior lens epithelium forms the embryonic primary lens fibers and, thus, is absent under the posterior lens capsule later in life.

Mature lens fibers become dependent on the anterior epithelium for maintaining a critical level of dehydration, which allows the soluble proteins to be functionally effective, and for providing a healthy level of reduced glutathione. The lens epithelium is highly susceptible to damage caused by factors such as changes in local oxygen concentration, exposure to toxins, X-ray irradiation, and ultraviolet (UV) light damage. Nocturnal (and arrhythmic) animals might be less able to compensate for exposure to bright light, as free-radical scavenging and other defense mechanisms might differ between species.

Lens Fibers

Immediately anterior to the lens equator is a proliferative zone within the epithelium, referred to as the lens bow (Fig. 2.70 and Fig. 2.71). The cells within this zone begin to mitose at approximately the same time the primary lens fibers form during early fetal development. This zone of mitosis continues throughout life. The most recently formed cells elongate, with the apical portion of the cell extending forward beneath the epithelium and the basal portion posteriorly along the capsule (Fig. 2.72). As these cells transform into lens fibers, small ball-and-socket interdigitations begin to develop (Fig. 2.73) and the lens fibers become roughly hexagonal in shape. The ball-and-socket junctions, which are present along the length of the fibers, are formed only at the six angular regions; in this way, any particular lens fiber is tightly coupled to six other lens fibers, including two older fibers, two of the same generation, and two younger fibers. In addition to these cytoplasmic interdigitations are many gap junctions, or nexi (Philipson et al., 1975). The nucleus of each developing lens fiber retains its central location, and the difference in the degree of elongation between younger and older developing lens fibers creates the lens bow configuration of nuclei at the equator (see Fig. 2.70, Fig. 2.72, and Fig. 2.74).

The lens fibers elongate toward the anterior and posterior poles, forming a U-shaped cell. The fibers do not reach the full distance from one pole to the next, much less the entire circumference of the lens; rather, they meet fibers from the opposite side to form the anterior and posterior lens sutures. The sutures are simply the junctions from opposite fibers at

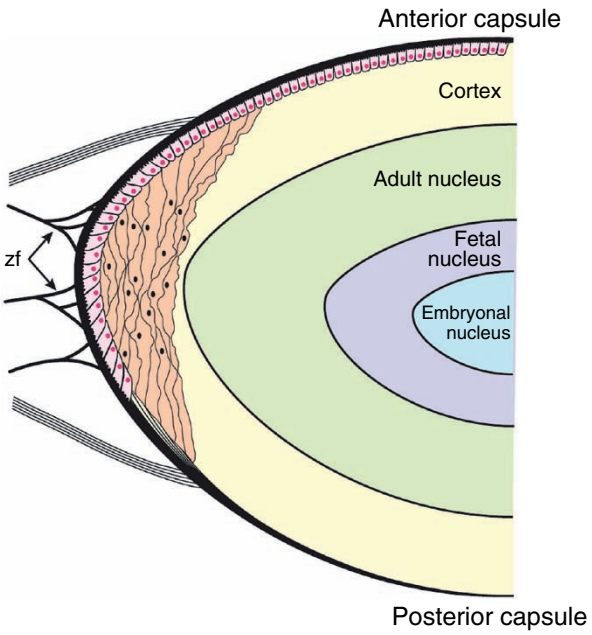

Figure 2.70 Composite drawing of the lens, capsule, attachments, and nuclear zones. The lens epithelial cells line the anterior capsule. At the equator, these dividing cells elongate to form lens cortical cells (fibers). As they elongate anteriorly and posteriorly toward the sutures, their nuclei migrate somewhat anterior to the equator and form the lens bow. Zonular fibers (zf) attach to the anterior and posterior lens capsule and to the equatorial capsule, forming pericapsular or zonular lamellae of the lens. (*Source:* Modified from Hogan, M.J., Alvarado, J.A. & Weddell, J.E. (1971) *Histology of the Human Eye*. Philadelphia, PA: W.B. Saunders. Reproduced with permission of Elsevier.)

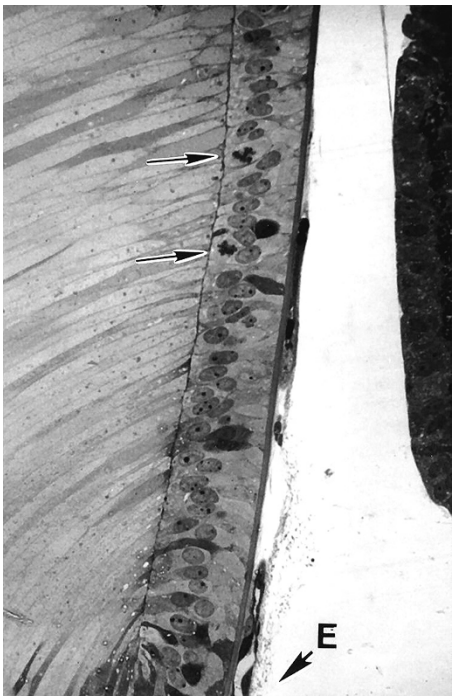

Figure 2.71 The anterior epithelium of a neonatal canine lens near the equator (E) has a proliferative zone at which cells undergo mitosis (arrows) and, subsequently, are pushed toward the equator. (Original magnification, 400×.)

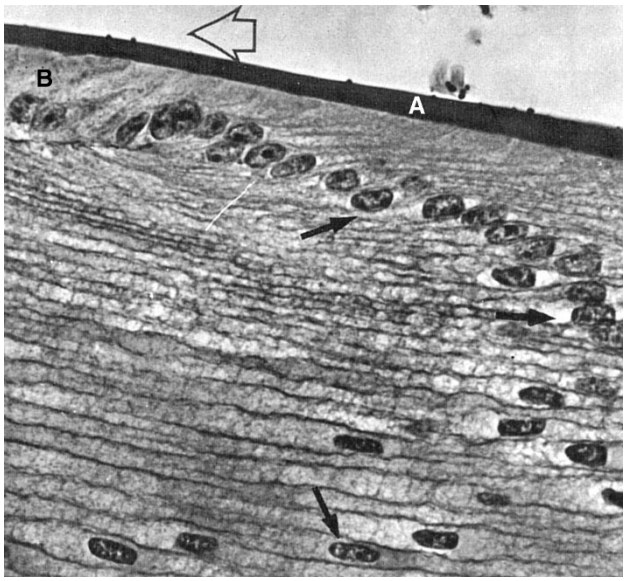

Figure 2.72 Young horse lens near the equator. Lens capsule (A) and columnar lens epithelium (B) at equator. Arrows delineate the formation of the lens bow by the nuclei of the newly formed fibers. Open arrow points rostrally. (Original magnification, 500×.)

a given level in the lens. They vary in configuration among species and at different levels within the lens.

The sutures usually form a Y-shaped pattern near the center of the lens, but in older eyes, they become more complex, with branching arms in the more superficial layers (Fig. 2.75). The suture patterns extend throughout the depth of the lens, but they are apparent *in vivo* only at optical interfaces. The sutures in the anterior half are typically in an upright Y-shaped pattern, whereas those on the posterior half are an inverted Y-shaped pattern. Figure 2.76 illustrates how inversion of the suture pattern develops and how a fiber attaches to opposite sites on a suture arm at its anterior and posterior limits (Hogan et al., 1971). At the lens sutures, the fibers markedly interdigitate with each other (Fig. 2.77). The interdigitations can affect optical quality to some degree by varying the focal length of light in this region of the lens, especially in the presence of nuclear sclerosis, lens pathology, or both (Kuszak et al., 1991). Overall, the combination of these well-developed regions for cell attachment, including the ball-and-socket and gap junctions, make the lens a remarkably unified structure. Lens fibers that become attached at the suture have fully matured; these cells lie in the deep bow zone and eventually lose their nuclei and organelles (Kuwabara & Imaizumi, 1974).

The mammalian adult lens consists of lens fibers formed chronologically throughout life. The oldest portion, formed during embryonic development, is in the center of the lens and known as the embryonic nucleus. It is a small, dark, lucent zone. Extending outwardly, the fetal nucleus, adult nucleus, and cortex are respectively encountered. These portions are frequently subdivided clinically into anterior and posterior divisions to further localize lesions (Daniel et al., 1984; Martin, 1969).

The surface of lens fibers varies according to the location within the lens. In newly mature fibers (i.e., the outer cortex), the ball-and-socket junctions are the dominant feature along each hexagonal edge (see Fig. 2.73). This feature is notably reduced in the lens fibers in the inner cortex next to the adult nucleus. The reduction in size of these interdigitations and the undulating appearance of the fibers undoubtedly result from the increasing compression this region undergoes. This change is even more remarkable in the nucleus, in which lens fibers have lost their ball-and-socket

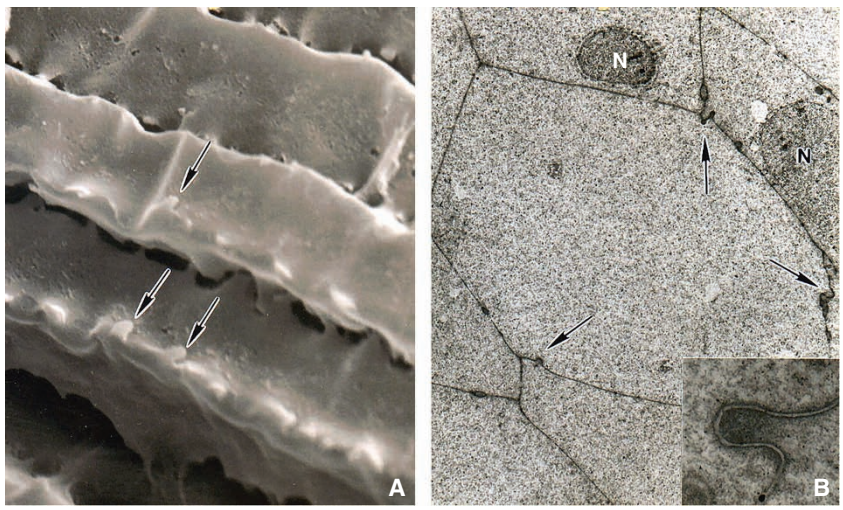

Figure 2.73 Newly formed canine secondary lens fibers are evenly hexagonal in cross-section. They form small ball-and-socket junctions (arrows) along their six angular edges. **A.** SEM. (Original magnification, 6,600×.) **B.** TEM. (Original magnification, 8,000×.) *Insert*: Close-up of one of the ball-and-socket junctions. N, nucleus. (Original magnification, 30,000×.)

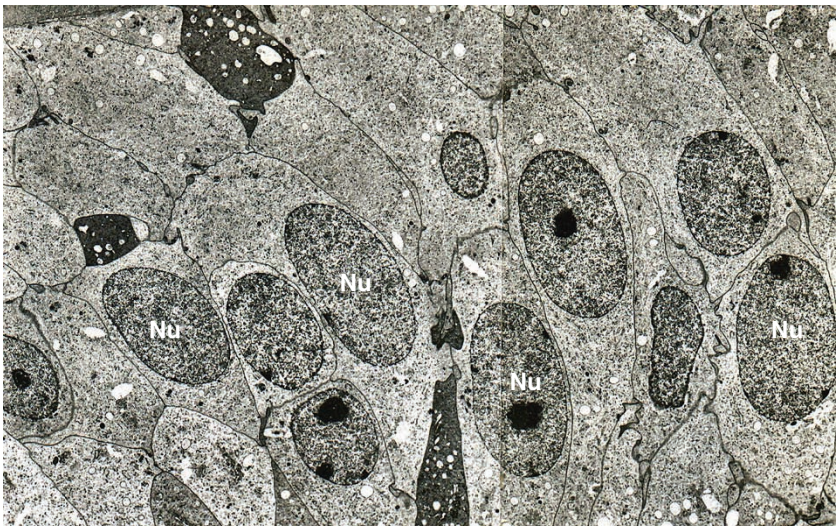

Figure 2.74 At the equator of a dog lens, the nuclei (Nu) of the newly forming secondary lens fibers are arranged linearly, taking up a central location within each cell. As these fibers mature, their nuclei are more rostrally or anteriorly located, achieving a bow-like configuration. These cells possess a great deal of free ribosomes and rough endoplasmic reticulum. (Original magnification, 3000×.)

Figure 2.75 Stereoscopic view of the posterior pole in an adult bovine lens demonstrates the distinct, Y-shaped suture pattern where lens fibers attach to each other. Branching arms (arrowheads) of the Y-shaped sutures occur more superficially, representing the attachment of younger cells. (Original magnification, 40×.)

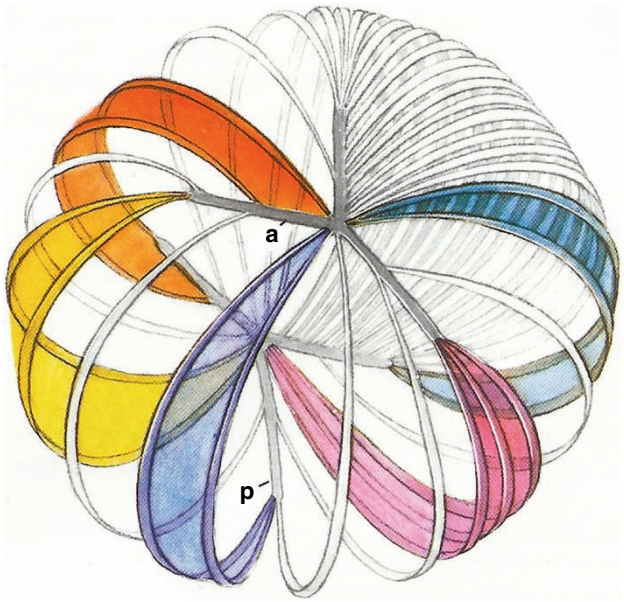

Figure 2.76 Drawing of the embryonal lens (i.e., nucleus) shows the anterior (a) Y suture, posterior (p) Y suture, and arrangement of the lens cells. The lens cells are depicted as wide, shaded bands. Those that attach to the tips of the Y sutures at one pole of the lens (a) attach to the fork of the Y at the opposite pole (p). (*Source:* Revised from Hogan, M.J., Alvarado, J.A. & Weddell, J.E. (1971) *Histology of the Human Eye*. Philadelphia: WB Saunders. Reproduced with permission of Elsevier.)

junctions entirely and instead possess tongue-and-groove junctions.

To a greater extent than in mammals, lenticular accommodation in birds depends on the ability of the lens to change shape. The avian lens is generally softer and more flexible than the mammalian lens, and consequently is more readily deformed during contraction of the ciliary body and peripheral iris musculature (Glasser et al., 1995). As the anterior uveal muscles contract, it is theorized that the ciliary body pushes against the mid-equatorial region of the lens while the peripheral edge of the iris presses against the anterior equatorial surface (Fig. 2.78). As an evolutionary adaptation to this activity, the avian lens has an annular pad (i.e., 'ringwulst'), which consists of lens fibers that are relatively enlarged and arranged radially instead of

concentrically (Fig. 2.79). The size of the annular pad appears to relate directly to the degree of accommodative ability. In both birds and reptiles, the ciliary processes directly contact the lens equator, and zonules are not present.

Between the annular pad and the main lens body exists a space called the cavum lenticuli, which separates these two distinct zones of the avian lens (Willekens & Vrensen, 1985). Annular pad fibers have a hexagonal circumference and are similar to young developing mammalian lens fibers. The annular pad fibers are smooth-surfaced, lacking any anchoring cellular processes (as in the chicken, song thrush, and kestrel), or they may be studded with edge protrusions, including ball-and-socket junctions (Willekens & Vrensen, 1985). At the transition between the annular pad and the main lens body, the cells become considerably elongated, and their nuclei appear to be oval before they disappear. The germinative epithelial cells differentiate in two phases: first

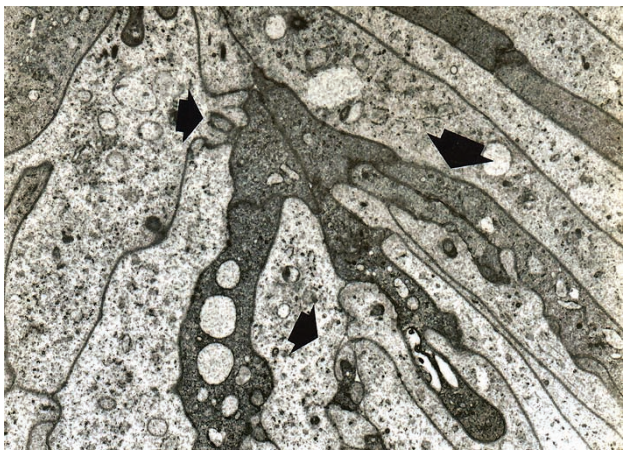

Figure 2.77 Close-up of a suture line in a dog lens reveals the great amount of cellular interdigitation (arrows) between adjacent lens fibers. (Original magnification, 5,000×.)

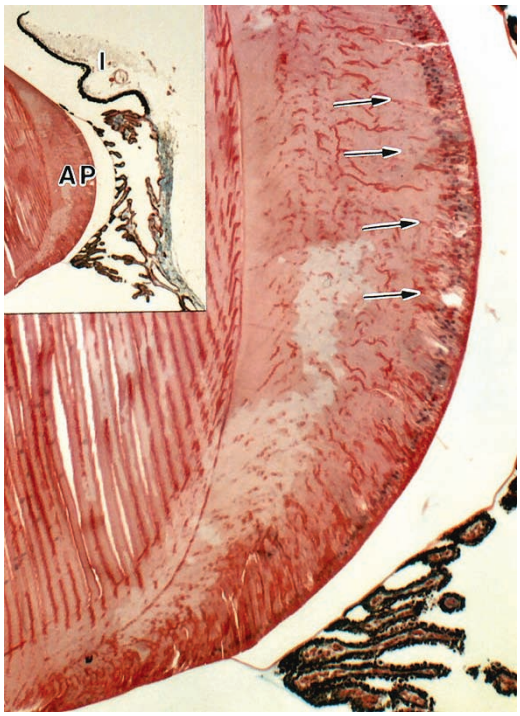

Figure 2.79 The "ringwulst," or annular pad (AP), of a screech owl's lens consists of radially arranged cells (arrows) that can withstand direct pressure. (Original magnification, 200×.) *Insert*: Overview of the annular pad. I, iris. (Original magnification, 20×.)

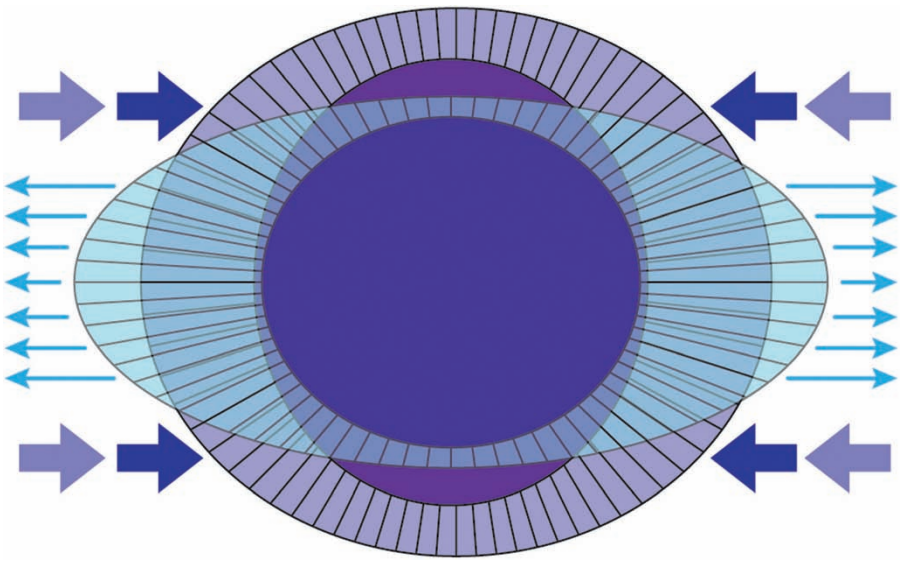

Figure 2.78 The avian lens is capable of dramatic changes in shape during accommodation, because it can be physically compressed (broad arrows) into a more rounded shape by the adjacent ciliary processes. By comparison, the lens "at rest" is stretched by zonules (small arrows) into a biconvex form.

into annular pad fibers that are elongated horizontal to the anteroposterior axis of the lens, and then into main lens body fibers, which continue to elongate further and eventually lose their organelles.

Zonular Attachment

The mammalian lens is circumferentially suspended from the ciliary body by fibers called zonules. Zonular attachment is achieved by a complex arrangement of fibers that insert onto the lens capsule in a zone encompassing the equator and a short distance both anterior and posterior to the equator (Fig. 2.80A, B; Farnsworth et al., 1976). Each zonular fiber is made of numerous small fibrils, which are visible under SEM as they attach to the lens capsule (Fig. 2.80C). The zonular fibers spread out near the equator and terminate into smaller bundles. Each of these bundles also fan out and form a network that ramifies over the surface of the lens capsule, approximately 1.5–2.0 mm away from the lens equator. As each smaller bundle of fibrils blends into the outer capsule, it is interwoven with an adjacent bundle, thus providing added strength for its insertion.

It was once believed that the zonular fibrils consisted of collagen and were perhaps a condensation of vitreous; zonules are therefore referred to as the tertiary vitreous. However, the fibrils are composed in part of a noncollagenous glycoprotein, fibrillin-1, that is also found in elastin (Cain et al., 2006; Dische & Murty, 1974; Streeten & Licari, 1981). Zonular fibers are believed to originate from the ciliary body, specifically the nonpigmented epithelium (Gloor, 1974). At the level of the ciliary body nonpigmented epithelium, the fibrils do not penetrate the basement membrane entirely, but rather intermix with the inner folds of the basement membrane. At the level of the lens, the zonules insert

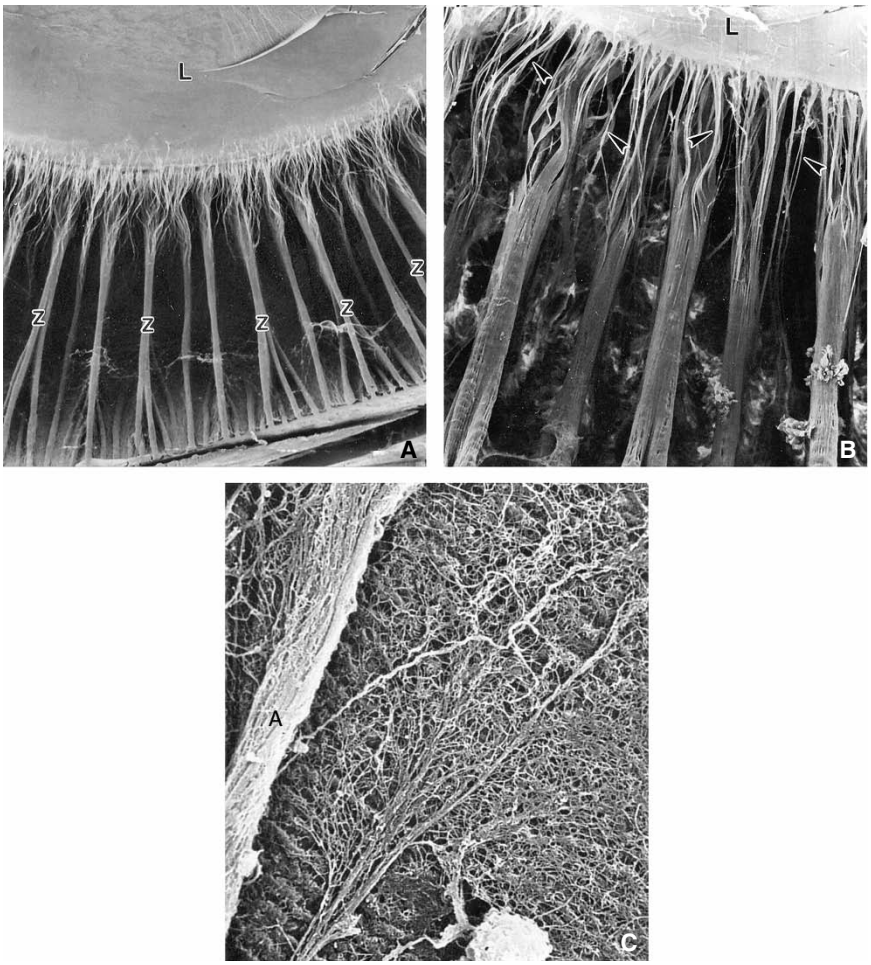

Figure 2.80 Zonular attachments to the lens in a dog. **A.** SEM shows zonules (Z) extend from the ciliary body onto the equator of the lens (L) in a ring-like manner, covering each ciliary process. (Original magnification, 30×.) **B.** SEM shows that each zonule consists of bundles (arrowheads) of fibrils, which are most apparent next to the lens (L). (Original magnification, 78×.) **C.** SEM shows termination of zonular fibrils, which unravel to form a dense meshwork over the capsule that greatly increases the surface area of attachment. A, zonular fiber. (Original magnification, 1600×.)

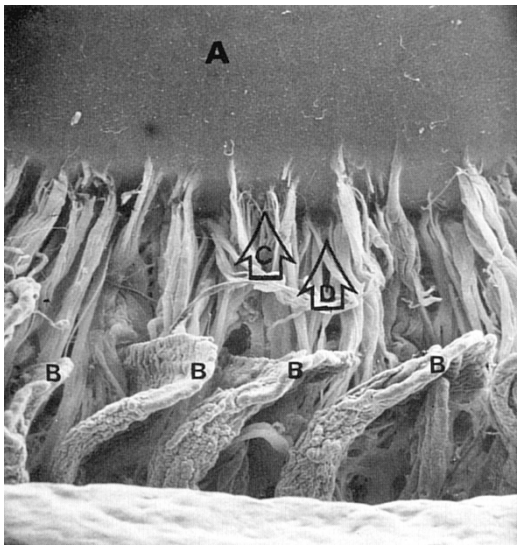

Figure 2.81 Caudal-view SEM of ciliary processes and zonular attachments to the lens in a cat. A, Posterior lens. B, Ciliary processes. C, Posterior zonular fibers. D, Anterior zonular fibers. Note the zonular fibers extending from the valleys and producing a cluster of fibers at their lenticular insertion with gaps between bundles. (Original magnification, 40×.)

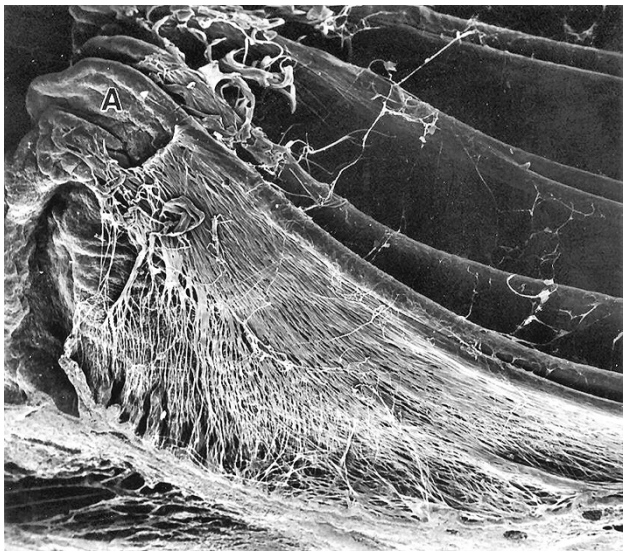

Figure 2.82 SEM shows that the apical portion (A) of each ciliary process in the dog is not intimately associated with zonular fibers. (Original magnification, 50×.)

intracapsularly, mixing with the type IV collagen of the lens capsule (Hiraoka et al., 2010).

The relationship of the zonules to ciliary processes varies to some extent among species. In primates, the zonular fibers originate largely from the pars plana, within 1 mm anterior to the ora serrata (Raviola, 1971; Rohen, 1979; Streeten, 1992). As the zonules course anteriorly, almost all have a close attachment to ciliary processes, adhering strongly to the valleys between the folds and along the sides of the processes.

In the cat, the zonular fibers largely appear to bypass the ciliary processes and insert in the valleys (Fig. 2.81). In the dog, tips of the ciliary processes are free of zonular fibers, but the remaining process is ensheathed very intimately with the zonules (see Fig. 2.43 and Fig. 2.82; Gelatt & Samuelson, 1998). The fibers as a group can be followed to the base of the ciliary process. As the fibers insert into the lens capsule, they can fan out over a breadth of 300 µm, and as a result overlap considerably with fibers arising from adjacent processes. The horse (see Fig. 2.44) has numerous fibers both ensheathing the processes and in the valleys, and both types continue down to the pars plana. In addition, an extensive network of fibers runs horizontally, joining the ridges of the processes.

Vitreous

The vitreous humor is a transparent hydrogel that comprises a portion of the clear ocular media and accounts for up to two-thirds of globe volume. Vitreous volumes in selected species are listed in Table 2.13. Anteriorly, the vitreous provides support for the lens as it rests in a shallow concavity (i.e., the patella fossa), whereas posteriorly, the vitreous abuts the neurosensory retina. As a result, the vitreous functions to transmit light, to maintain the shape of the eye, and to help maintain the normal position of the lens and retina (Jaffe, 1969).

Table 2.13 Vitreous humor volume in selected species.

Animal	Vitreous volume (mL)
Dog[a]	1.7
Horse[a]	26.15
Calf	10
Pig	3.5
Rabbit	1
Human	4

Source: Modified from Jaffe, N. (1969) *The Vitreous in Clinical Ophthalmology*. St Louis.
[a] Gilger et al., 2005.

Embryologically, the vitreous is composed of three components

1) the primary vitreous (containing the hyaloid artery system)
2) the secondary (definitive, or adult) vitreous, and
3) the tertiary vitreous (lens zonules, discussed earlier).

The primary, or primitive, vitreous develops first, as the hyaloid artery system courses through it to provide a blood supply to the avascular developing lens. The secondary

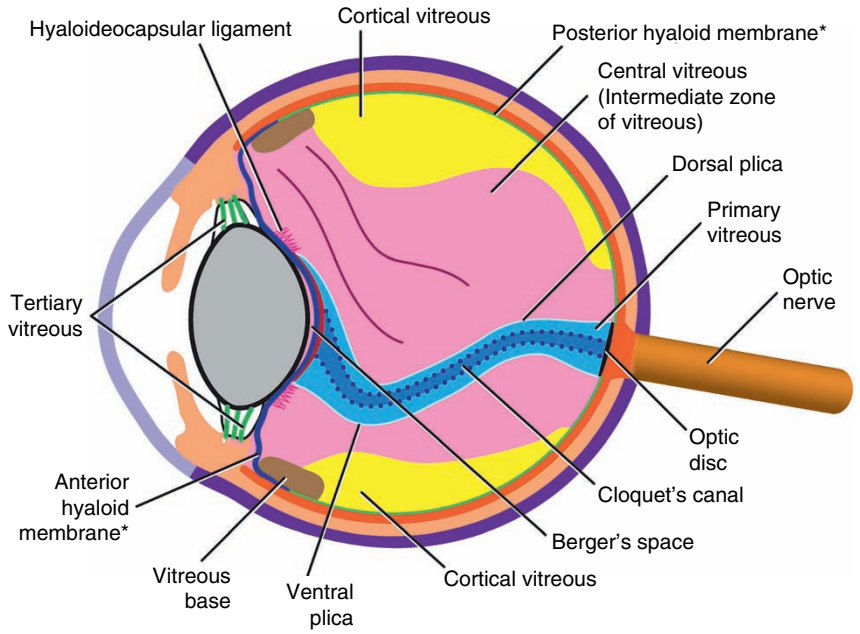

Figure 2.83 The various components of and spaces within the vitreous. The secondary, or adult, vitreous is composed of the cortical and central (intermediate zone) components. (*Not a true 'membrane'.)

vitreous then forms around the primary vitreous, leaving the primary vitreous at the central core of the vitreal compartment. The secondary vitreous becomes the definitive, or adult, vitreous.

Within the adult vitreous exist several anatomic structures, potential spaces, and connection points between the vitreous and adjacent tissues (Fig. 2.83). The core of the primary vitreous around which the adult vitreous develops is occupied by Cloquet's canal (i.e., the hyaloid canal), a potential space that contained the hyaloid artery in the embryonic eye. The remnant of the anterior insertion of the hyaloid artery appears as a dense, white, small dot (i.e., Mittendorf's dot) with a variable "corkscrew" tail extending from the posterior pole of the lens. The anterior and posterior surfaces of the vitreous are lined by the anterior and posterior hyaloid membranes, respectively; though, no true 'membrane' exists in an ultrastructural sense at either location. The peripheral portion of the vitreous next to the retina is referred to as the cortex. Here, the collagen fibrils of the cortex join the basement membranes of Müller and glial retinal cells.

A potential space, sometimes referred to as Berger's space, exists between the posterior lens capsule and the anterior hyaloid membrane. The anterior hyaloid membrane curves forward from the region of the ora ciliaris retinae (i.e., vitreous base) to blend in with the peripheral posterior lens capsule, where a strong circumferential attachment forms (i.e., the hyaloideocapsular ligament). The adult vitreous attaches firmly to the area around the optic disc, the region of the ora ciliaris retinae (i.e., vitreous base), and at the hyaloideocapsular ligament.

The central portion of the vitreous consists of tracts, which are layers of funnel-shaped sheets or plicae fitted one into another (see Fig. 2.83). Between the cortex and central vitreous exists a border layer composed of many compacted lamella, with each lamella consisting of a meshwork of collagen fibrils (Faulborn & Bowald, 1982).

The vitreous is 99% water; the remaining 1% is a network of polygonal, hydrated fibrils consisting of type II collagen and hyaluronic acid (McLaughlin & McLaughlin, 1986; Snowden & Swann, 1980). The collagen fibrils interconnect with the hyaluronic acid by associated GAGs, consisting principally of chondroitin sulfate IV and VI and heparan sulfate (Goes et al., 2005; Noulas et al., 2002). A number of proteins are also part of the vitreal extracellular matrix; these proteins are produced primarily by the posterior half of the nonpigmented ciliary epithelium and appear to be in a continuous state of turnover (Bishop et al., 2002).

The vitreous has a relatively low cell density, with most cells found in the cortex near the vitreous base. The main cell type is the hyalocyte, which is a histiocyte with a poorly developed lysosomal system. Hyalocytes can produce hyaluronic acid *in vitro* and are thought to contribute to formation of the vitreous humor, along with the nonpigmented ciliary body epithelium and the non-neuronal cells of the retina (Jacobson, 1976). However, the possibility that these cells play a role in remodeling events in the vitreous, rather than in hyaluronic acid production, is plausible. In addition to the hyalocyte, fibrocytes and glial cells, found next to the ciliary body and the optic disc, comprise roughly one-tenth of the total population of vitreal cells (Balazs et al., 1964).

The consistency of the vitreous is quite variable, because of the different proportions of gel to liquid that occur among species and at different ages. In the cat and dog, the cortex is fluid, and the center is dense. In cattle, pigs, and sheep, the entire vitreous is nearly homogenous in structure and of high density. Like ruminants, the pig and the horse do not show a separation into cortical and central zones, but the vitreous is of comparatively low optical density. The rabbit vitreous is of such low optical density that it could hardly be examined (Eisner, 1975, 1988; Eisner & Bachmann, 1974a, 1974b, 1974c, 1974d). The consistency of the vitreous is also influenced by aging. In most species, holes and liquefaction (i.e., syneresis) occur in older individuals, particularly in the central region.

Retina

The retina and optic nerve are derivatives of the forebrain; consequently, their morphology and physiology are similar to that of the brain. The neurosensory retina is connected to the brain by the optic nerve and the optic tracts. The rods and cones, the primary retinal photoreceptors, comprise a complex layer of specialized cells, which contain photopigments that convert light energy into a series of biochemical events. The RPE furnishes important metabolites to the photoreceptors; it also actively phagocytizes the outermost photoreceptor segments as they are shed during normal outer-segment renewal. The retina has one of the highest rates of metabolism of any tissue in the body and receives almost all its nutrition from the retinal and choroidal capillaries.

The function of the retina is to turn light stimuli from the external environment into nervous impulses and transmit this information accurately to the brain, where it is then interpreted as vision. Stimulation of the photoreceptors by light alters the release of a neurotransmitter; this response is received and modified by cells with nuclei located in the inner nuclear layer (i.e., amacrine, bioplar, and horizontal cells) (Fig. 2.84). The modified message is then relayed to ganglion cells, with axons that form the nerve fiber layer and extend through the optic nerve to targets in the brain (including the lateral geniculate nucleus and occipital cortex) (see Chapter 4).

Classically, 10 layers are described in retinal histology. The neurosensory retina contains nine, and the supportive pigmented epithelium is the tenth layer (Fig. 2.85). The

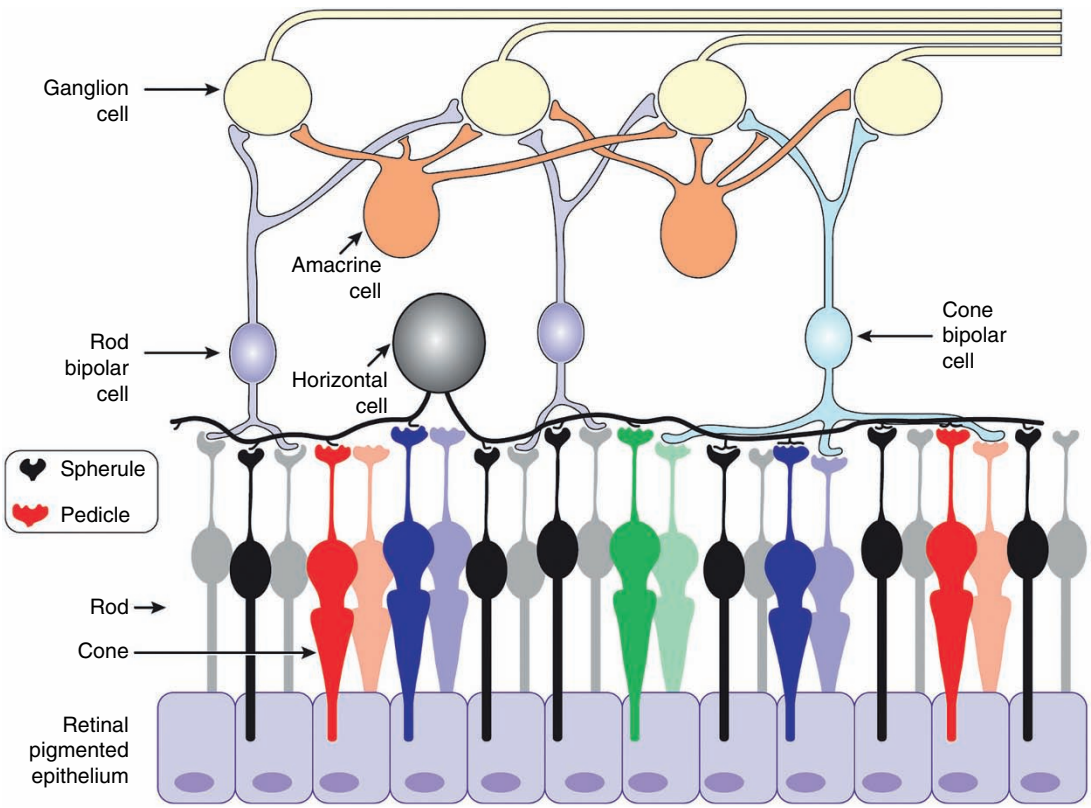

Figure 2.84 Relationship between different neuronal cells within the retina. The amacrine cell has a reciprocal inhibitory response onto the bipolar cell from which the information originated and acts to adjust the sensitivity of the ganglion cell synapse after receiving a signal. Horizontal cells interconnect laterally to integrate and regulate input from multiple photoreceptors.

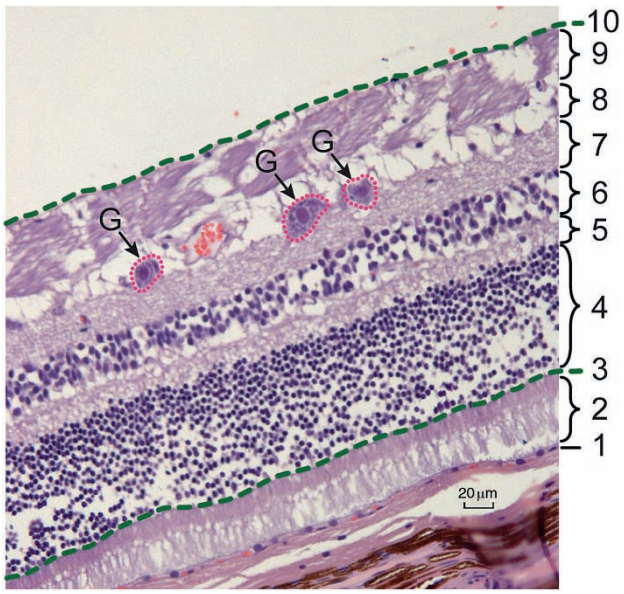

Figure 2.85 The retina consists of nine discrete layers and a supportive pigmented epithelium that forms an outer, tenth layer, as demonstrated by light microscopy in the dog. G, ganglion cell; 1, retinal pigment epithelium; 2, photoreceptor layer; 3, outer limiting membrane; 4, outer nuclear layer; 5, outer plexiform layer; 6, inner nuclear layer; 7, inner plexiform layer; 8, ganglion cell layer; 9, nerve fiber layer; 10, inner limiting membrane. The outer and inner limiting membranes are denoted by dashed lines.

10 identifiable layers are considered, sclerad to vitread, in the following order:

1) RPE
2) photoreceptor layer (rod and cone layer)
3) outer limiting membrane
4) outer nuclear layer
5) outer plexiform layer
6) inner nuclear layer
7) inner plexiform layer
8) ganglion cell layer
9) nerve fiber layer, and
10) inner limiting membrane.

Retinal Pigment Epithelium

The RPE is a monolayer of flat, polygonal cells that forms the outermost layer of the retina. It is the continuation of the outer pigmented epithelial layer of the ciliary body. The RPE is more adherent to the choroid than to the rest of the retinal tissue, and it serves an important role in nutrient transport from the choriocapillaris to the outer layers of the retina. Each cell sends cytoplasmic processes inward to surround the photoreceptor outer segments, which help to filter out excessive amounts of light and increase the photoreceptors' individual sensitivity. The cells also phagocytize the outer segments of photoreceptors as they are continuously shed.

The RPE cells are usually densely pigmented, but there is some variability in the intensity of pigmentation amongst individual animals. This variability is largely based on hair color and the relative amount of pigmentation in other areas of the eye; for instance, RPE cells might contain light, rust-colored pigment in a tan or red colored animal, or pigment could be virtually absent in an animal with a blue iris (i.e., subalbinotic). Additionally, RPE cells overlying the tapetum lucidum, when present, are devoid of pigment. The absence of melanin permits light to pass through the RPE to the tapetum and then reflect back to the light-sensitive photoreceptors.

On flat preparations, the RPE of most species forms a mosaic of hexagonal cells, which is most uniform in the posterior pole and in young animals. In most species, except the rat and rabbit, these cells are generally mononucleate. In general, the cells are larger and have more binucleate forms near the ora ciliaris retinae (Tso & Friedman, 1967).

The morphology and location of RPE melanosomes varies to some degree among different animals. The shape of melanosomes is typically oval, but they can be more elliptical in diurnal species such as birds and various reptiles (Kuwabara, 1979). The elliptical to nearly lanceolate melanosomes are frequently positioned within apical microvilli, which are cytoplasmic projections of the RPE cells that lie between and surround the photoreceptors. These microvilli offer substantial shielding for the photoreceptors against scattered light. Melanosomes within the RPE of arrhythmic and nocturnal species, such as the rat, hamster, mouse, and bat, tend to be rounder, fewer in number, and less frequently located within the microvilli.

In addition to providing protection against light scatter, the apical microvilli surround the outermost and oldest portion of the photoreceptor outer segments. No cell membrane attachments exist between the RPE and the photoreceptors, but a viscous ground substance of GAGs surrounds the photoreceptor outer segments (Fine & Yanoff, 1979; Spitznas & Hogan, 1970; Weale, 1963). On SEM examination, the apical microvilli are quite numerous, being clustered next to outer segments that have fractured and adhered to the RPE during routine cryopreparation, as shown in Fig. 2.86. Microvilli are especially large and long in the RPE of many nonmammalian animals (Kuwabara, 1979). The lateral RPE cell surfaces near the apical end have a well-defined junctional complex, including zonular occludens and zonular adherens.

The basal aspect of the RPE rests on Bruch's membrane, a basal complex in the capillary zone over the choriocapillaris. Marked basal infoldings of the cell membrane contrast sharply with the basement membrane, which is relatively smooth (Fig. 2.87). The size and organization of the basal infoldings vary to some degree among mammals (Braekevelt, 1986, 1990a, 1990b). In birds, the basal infoldings are especially developed and tightly packed as opposed to those in mammals, which tend to be smaller and irregularly

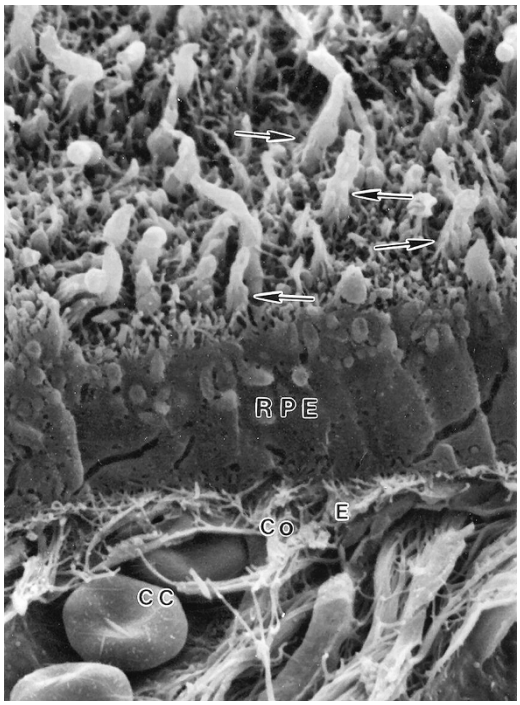

Figure 2.86 SEM shows cryofractured RPE and the underlying choriocapillaris (CC) of a sheep. Arrows indicate photoreceptor outer segments that remain fastened to apical villi. Note the strands of collagen (Co) and elastic fibers (E) that make up much of Bruch's membrane. (Original magnification, 6,000×.)

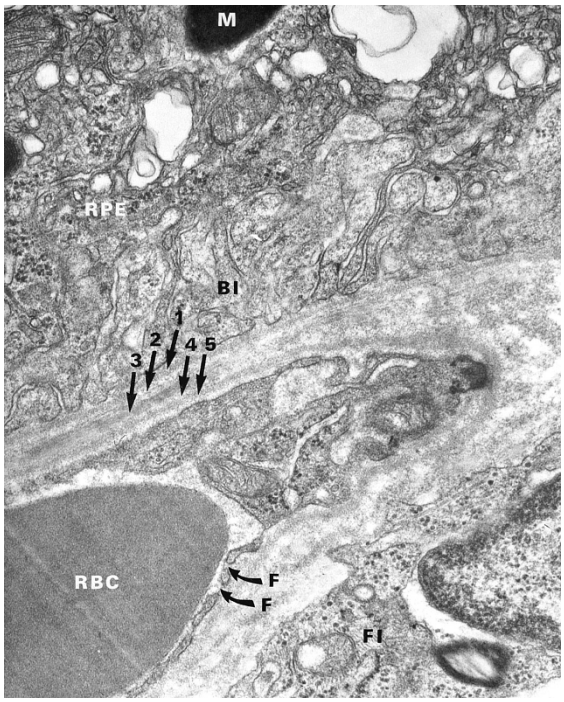

Figure 2.87 TEM shows the basal complex (i.e., Bruch's membrane) in the capillary zone over the non-tapetal region of a dog. Note the RPE with melanin (M) granules and basal infoldings (BI) of the RPE. The basal complex consists of: 1, basal lamina of RPE; 2, inner collagenous zone; 3, elastic layer; 4, outer collagenous zone; 5, basal lamina of choriocapillaris. F, fenestrations in choriocapillary endothelium; FI, fibroblast in anterior choroid; RBC, erythrocyte in choriocapillaris. (Original magnification, 43,600×.)

positioned (Braekevelt, 1990b, 1998a; Braekevelt & Thorlakson, 1993). In animals with a cellular tapetum, the basement membrane of the pigment epithelium and the basement membrane of the choriocapillaris occasionally fuse, thus reducing the pentalaminated structure to a single layer. More often, however, the basement membrane of both epithelia remains, with a shared collagenous zone of variable thickness.

Neurosensory Retina

The neurosensory retina varies in thickness (Table 2.14), being thickest near the optic disc and tapering toward the ora ciliaris retinae. The width of all layers decreases, but the nerve fiber layer contributes the most to the variation in thickness. Most domestic animals have a central retina of approximately 200–240 µm and a peripheral retina of 100–190 µm (Brown, 1968; Donovan et al., 1974b; Prince et al., 1960). In animals with poorly vascularized or avascular retinas, retinal thickness rarely exceeds 140 µm, which is the proposed oxygen diffusion maximum for retinal tissue (Buttery et al., 1991; Chase, 1982; Dollery et al., 1969).

The retinal photoreceptors are the primary visual cells of the eye and are the first-order neurons (see Fig. 2.84). Rods function in dim or reduced illumination, and cones function

Table 2.14 Retinal thickness measured by optical coherence tomography.

Animal	Retinal thickness (µm)	Retinal location	Reference
Dog[a]	198.7	Dorsal/superior	Hernandez-Merino et al., 2011
	164.4	Ventral/inferior	
Cat	245	Peripapillary	Gekeler et al., 2007
	204	Peripheral	
	182	Area centralis	
Horse[b]	239	Dorsal	Pinto & Gilger, 2014
	133	Ventral	
	276	Nasal	
	263	Temporal	
Cow[c]	235	Tapetal (dorsal)	Chauhan & Marshall, 1999
	120	Non-tapetal (ventral)	
Human	160	Foveola[d]	Chauhan & Marshall, 1999
	258	Clivus[e]	

[a] Female Beagle dogs.
[b] Measurements taken 1.0 mm from optic disc.
[c] Cadaveric globes.
[d] Central depression within fovea.
[e] Sloping wall of fovea.

in bright light. The rods allow detection of shapes and motion, while the cones provide sharp visual acuity and color sensitivity. Primates and many avian and reptilian species possess cone-rich regions completely free of rods. These regions are called foveae (i.e., fovea centralis) and are responsible for the perception of different hues of color, high resolution, binocular fixation, and depth perception. Domestic animals do not have foveal pits, but dogs have been shown to have a small fovea-like structure, a fovea plana (Beltran et al., 2014). Other domestic animals instead possess an area of high cone density called the area centralis. The area centralis, which surrounds the fovea plana, frequently occurs in a location 1.5 mm temporal and 0.6 mm superior to the optic disc in the dog, which corresponds to a location 1.2 disc diameters temporal and 0.6 disc diameters superior to the optic disc for purposes of clinical ophthalmoscopy (Mowat et al., 2008). The visual streak is a region of the retina with increased ganglion cell density that occurs in a horizontal band, dorsal to the optic disc. The area centralis resides within the visual streak, and these terms are sometimes used synonymously. Often, the two regions are nearly identical, or even topographically identical. Instances do occur, however, in which peak ganglion-cell densities do not topographically match peak cone densities (Rapaport & Stone, 1984). Instead, a specific subpopulation of ganglion cells might be associated with the area centralis (Enroth-Cugell & Robson, 1966; Provis, 1979).

Photoreceptor cell densities have been measured in a variety of species, including the dog and cat (Table 2.15; Beltran et al., 2014; Koch & Rubin, 1972; Mowat et al., 2008; Østerberg, 1935; Steinberg et al., 1973). In the cat, the cones in the area centralis are approximately six to seven times more numerous than in the periphery (26,000–27,000 cells/mm^2 vs. 4,000 cells/mm^2). By comparison, the rods of the cat are similar in density when comparing the peripheral retina (250,000 cells/mm^2) to the area centralis (275,000 cells/mm^2); however, the density of the rods nearly doubles (460,000 cells/mm^2) along a zone surrounding the area centralis (Steinberg et al., 1973).

In general, animals with foveae and well-developed areas centrales or visual streaks, including fish, reptiles, birds, squirrels, ungulates, carnivores, and primates, are essentially diurnal or arrhythmic (Duke-Elder, 1958). True nocturnal species possess rod-dominant retinas lacking cone-rich centers. Diurnal predaceous birds can have two foveae, a principal "deep" central fovea and a shallower temporal fovea. The central fovea provides enhanced lateral viewing for these animals, whereas the temporal fovea provides straight-ahead projection, enhancing the binocular field (Fig. 2.88; Meyer, 1977; Tucker, 2000). The bi-foveate condition in diurnal raptors is closely associated with orbit orientation and amount of eye movement (O'Rourke et al., 2010). There appear to be strong relationships between depth of field, optimal range of stereopsis and motion parallax, and selective prey detection.

Photoreceptor Layer (Rod and Cone Layer)

The photoreceptor layer contains only the outer parts of the photoreceptor cells known as the inner and outer segments; the photoreceptor nuclei are contained in the outer nuclear layer. These segments are cylindrically to conically shaped and closely packed together, with a radial orientation parallel to incoming light as it passes through the pupil (Fig. 2.89). The segments are stimulated by incoming light to initiate the conversion of light to a nerve signal (i.e., phototransduction) that will ultimately be relayed to the brain, which eventually forms a visual image.

Table 2.15 Photoreceptor densities and ratios.

Animal	Photoreceptor density (cells/mm^2)	Location	Rod-cone ratio	Reference
Dog	23,000 cones/mm^2	Area centralis	23:1	Mowat et al., 2008
	501,000 rods/mm^2			Mowat et al., 2008
	127,000 cones/mm^2	Fovea-like area		Beltran et al., 2014
	7,500 cones/mm^2	Inferior periphery	41:1	Mowat et al., 2008
	305,000 rods/mm^2			Mowat et al., 2008
	200,000 rods/mm^2	Ora ciliaris retinae		Yamaue et al., 2015
Cat	487,000	Area centralis	11:1	Steinberg et al., 1973
	279,000	Periphery	65:1	
	253,000	Ora ciliaris retinae	100:1	
Sheep	120,000–298,000	Dorsotemporal	20:1	Shinozaki et al., 2010
	203,000	Area centralis	6:1	
Pig	138,500	Entire retina	8:1	Chandler et al., 1999
Human	5,000 cones/mm^2	Ora serrata	50:1	Østerberg, 1935
	40,000 rods/mm^2	Ora serrata		

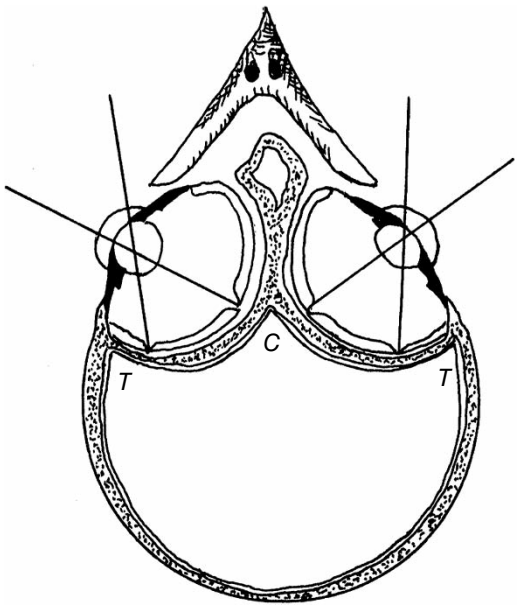

Figure 2.88 The foveal arrangement in the swallow, which possesses two foveae within each eye: one located temporally (T) for binocular vision, and one located centrally (C) for panoramic vision. (*Source:* Redrawn from Duke-Elder, S. (1958) *System of Ophthalmology. Vol I. The Eye in Evolution*. London: Henry Kimpton.)

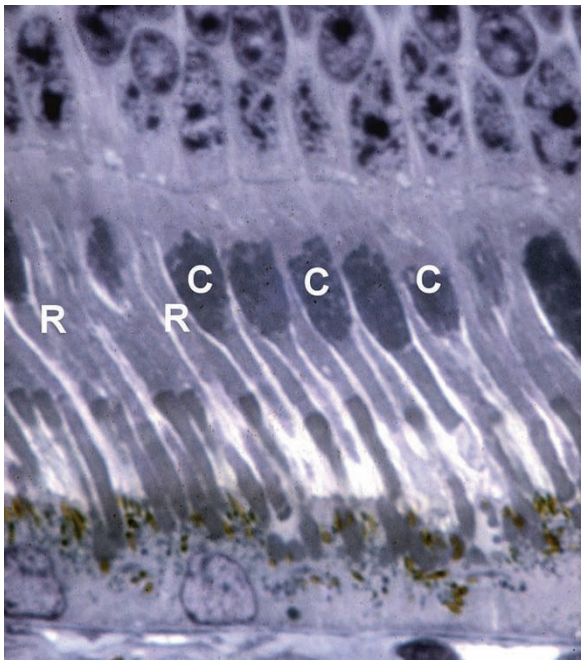

Figure 2.89 The photoreceptor layer of the pig contains many cones (C) among the rods (R) within the area centralis, making this animal well suited for day vision. Note that the rods are uniform in width throughout their length, while the cones are conically shaped due to variation in disc width at one end.. (Original magnification, 400×.)

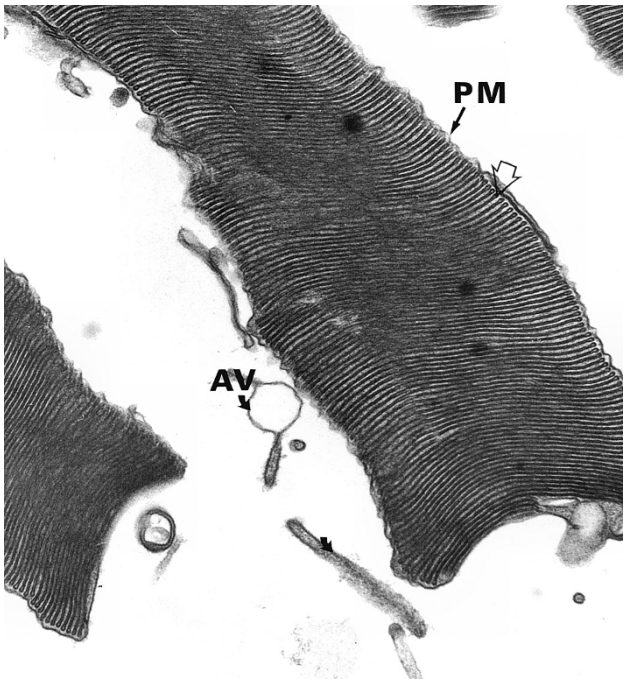

Figure 2.90 Tip of the outer segment discs in a rod of a young dog. Note that the discs or lamellae are separated from each other as well from as the plasma membrane (PM). The intralamellar space is slightly dilated at their periphery (arrow). Apical villi (AV) of pigmented epithelium are found between outer segments. (Original magnification, 54,000×.)

The outer segments of the rods and cones are composed of stacks of membranous discs surrounded by the cell membrane. The rods form stacks of discs of uniform width throughout their length and are longer than the cone outer segments (Fig. 2.89 and Fig. 2.90; see Fig. 4.26). The cones form stacks of discs wider at one end, producing a conical shape (Fig. 2.89; see Fig. 4.26). In the area centralis, the cones are longer and more slender; nevertheless, they remain easily distinguished from the rods (see Fig. 2.89). The invaginations of the photoreceptor cell membrane, which form the disc lamellae, constitute the major morphologic difference between cones and rods (Cohen, 1969). In cones, which are the most ancestral photoreceptors, the discs remain connected to the cell membrane, whereas with rods, the discs are detached and fill the outer segment like a 'stack of coins' (Fig. 2.90) (Hogan et al., 1971; Rodieck, 1973).

The discs contain visual photopigments that are sensitive to different wavelengths of light. Cones contain a more diverse array of photopigments compared with rods, as cones are traditionally responsible for color vision. Retinal physiology is covered in detail in Chapter 4 and fundamentals of animal vision is covered in Chapter 5.

The photoreceptor outer segments are connected to the inner segments by a nonmotile cilium (Fig. 2.91A). The inner segments carry the cellular machinery necessary to meet the high metabolic demands of each photoreceptor cell. The outer portion of the inner segment is called the ellipsoid, and it is filled with long, tubular mitochondria that produce ATP (see Fig. 2.91B and Fig. 2.92). The cone ellipsoid

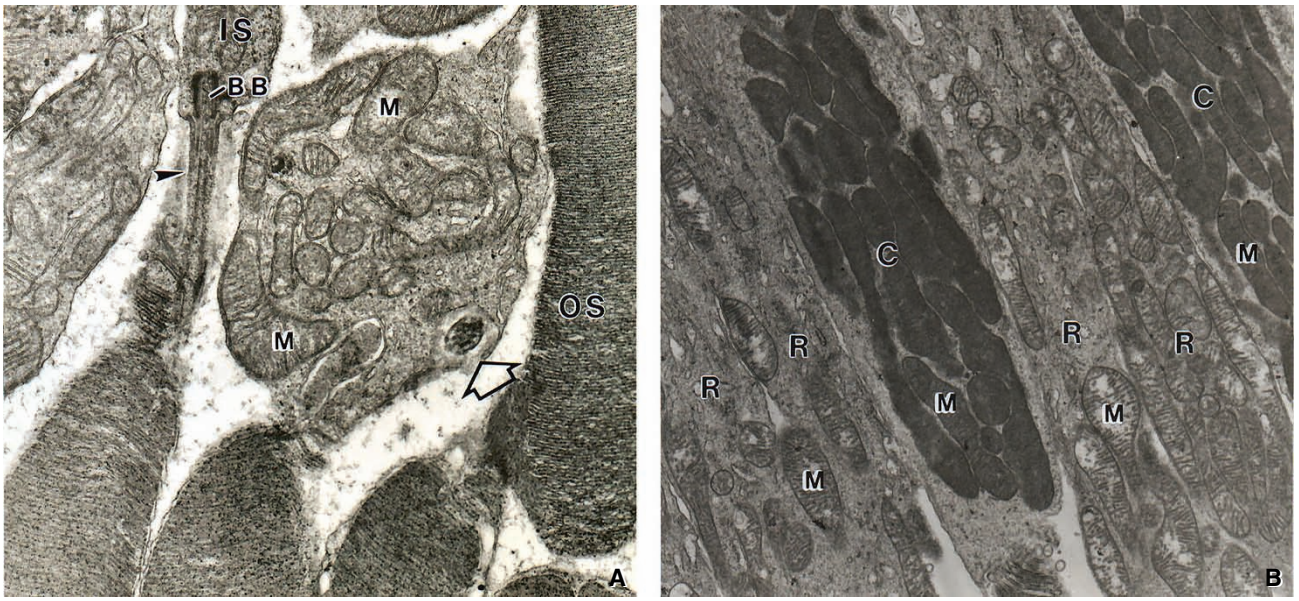

Figure 2.91 **A.** The outer portion of a rod inner segment (IS) of a dog contains a basal body (BB) that gives rise to the connecting cilium (arrowhead). Note the oblique plane of an adjacent inner segment reveals the peripheral placement (open arrow) of these basal bodies and confluent cilia. M, mitochondria; OS, outer segment. (Original magnification, 18,000×.) **B.** The ellipsoids of rods (R) and cones (C) in the central retina of a sheep. The cone ellipsoids possess more mitochondria (M) than the rod ellipsoids. (Original magnification, 11,000×.)

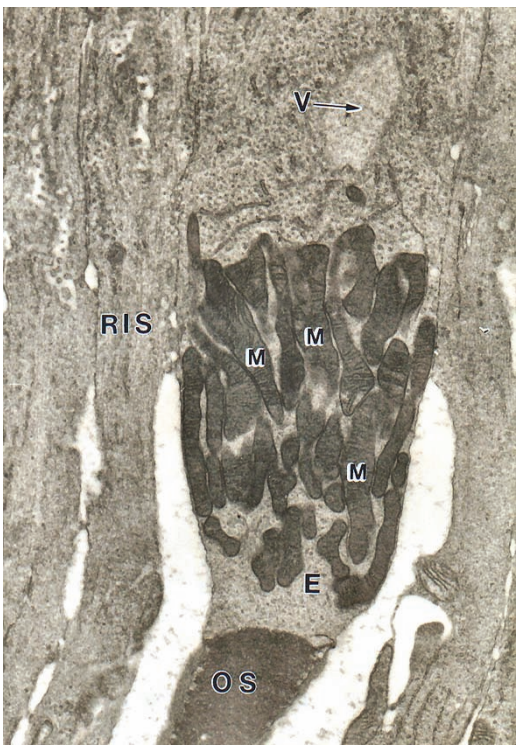

Figure 2.92 Inner portion of the outer segment (OS) and adjacent inner segment of a porcine cone. E, ellipsoid; M, mitochondria; RIS, rod inner segment; V, vesicle. (Original magnification, 10,000×.)

is more broad and conical, and contains more mitochondria, than the rod ellipsoid. In a number of vertebrates, including birds, reptiles, amphibians, and nonplacental mammals, the cone ellipsoid contains an oil droplet that separates the numerous mitochondria from the connecting cilium (Prince et al., 1960). The appearance of this droplet varies according to the species and type of cone (Braekevelt, 1993b, 1993c). The function of the oil droplet has undergone considerable speculation, and since the 19th century, it has been thought to serve as a light filter, allowing only specific wavelengths to be transmitted to the outer segments (King-Smith, 1969; Schultze, 1866).

The vitread or inner portion of the inner segment is called the myoid, and it is the principal site of protein synthesis. The myoid contains ribosomes, rough and smooth endoplasmic reticulum, Golgi bodies, and rare mitochondria. In the pig, the cone myoid may also contain a fairly prominent vesicle (see Fig. 2.91). In the avian myoid, there is an area filled with glycogen, called the paraboloid, that is best recognized with light microscopy through use of histochemical localization.

Rod and cone inner segments are separated from each other by long, villous extensions of Müller cells called fiber baskets (Fig. 2.93). The fiber baskets are virtually identical morphologically among the vertebrate species, but they are less numerous in retinas with intraretinal vasculature (Uga & Smelser, 1973). It is hypothesized that these cell

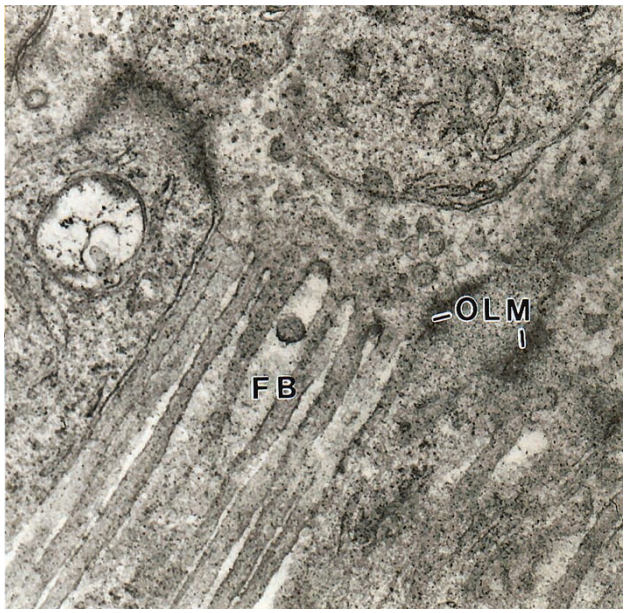

Figure 2.93 Long, villous extensions of Müller cells, known as fiber baskets (FB), occur ubiquitously in the vertebrate eye, as shown here in the dog. OLM, outer limiting membrane. (Original magnification, 35,000×.)

processes serve to keep the extracellular portion of the photoreceptor layer dehydrated and thus help to maintain proper alignment of the outer segments (Sigelman & Ozanics, 1988). These processes are also likely involved in the exchange of metabolites with the RPE, thereby helping to provide a homeostatic environment for the outer segments (Magalhaes, 1976).

In addition to the rod and cone photoreceptors, there is a third class of primary photoreceptors known as the double-cone photoreceptor, which is found in all vertebrate groups except placental mammals. The double-cone consists of two closely associated, but separated, cone photoreceptors that differ in size, shape, and structure (Fig. 2.94). The significance of the double-cone has yet to be determined, but it is the dominant photoreceptor in diurnal animals, occupying up to 82% of the retina at the inner segment level (Meyer, 1977; Walls, 1942). The chief cone of the double-cone pair is the longer of the two, and it possesses an oil droplet. The accessory cone, on the other hand, lacks an oil droplet, having instead a conspicuous paraboloid (i.e., barrel-shaped body of glycogen).

Outer Limiting Membrane

An extremely thin limiting membrane composed of the junctional complexes between Müller cells, as well as between Müller and photoreceptor cells, forms a lateral intercellular border between the inner segments of the photoreceptor layer and their nuclei (Fig. 2.93). The function of the outer limiting membrane is somewhat speculative.

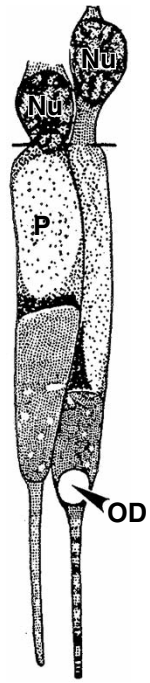

Figure 2.94 An avian double-cone photoreceptor. Nu, nucleus; OD, oil droplet; P, paraboloid. (*Source:* Modified from Duke-Elder, S. (1958) *System of Ophthalmology. Vol I. The Eye in Evolution*. London: Henry Kimpton. Reproduced with permission of Elsevier.)

In addition to holding the outer retina together, the outer limiting membrane most likely forms a barrier between the photoreceptor layer extracellular spaces and the rest of the neurosensory retina. It might also help to maintain the location of the photoreceptor nuclei away from the highly metabolic inner segments, thus reducing the potential for oxidative injury.

Outer Nuclear Layer

The soma, or cell bodies, of the photoreceptors are contained within this layer. The number of rows of nuclei varies greatly according to species and location within the retina. In the central retina, the dog and cat possess the greatest depth of rows (10–15 and 12–18, respectively), whereas ungulates have fewer rows (five in the horse and pig, 10 in the cow) (Table 2.16). The outer nuclear layer gradually thins as it approaches the peripheral retina where the density of rods and cones decreases. Cone nuclei are universally situated next to the outer limiting membrane. In mammals, they are usually larger, oval, and more histologically euchromatic (i.e., more lightly staining) than the rod nuclei (Fig. 2.95). Rod nuclei are smaller, round to oval, darker, and more heterochromatic (i.e., more darkly staining).

Additional structures in the outer nuclear layer include rod and cone connecting fibers, rod and cone axons, and Müller cell processes. The rod and cone connecting fibers link the photoreceptor nuclei to their respective inner

Table 2.16 Rows of nuclei in the outer nuclear layer.

		Peripheral retina	
Animal	**Central retina**	**Dorsal**	**Ventral**
Dog	10–15	8–9[a]	8–10[a]
Cat	12–18	8–10[a]	8–10[a]
Horse	4–6	3–4[b]	3[b]
Cow	8–10	3–4[b]	3–4[b]
Pig	5–6	3–4[a]	3–4[a]

[a] Measurements taken 1.0 mm from ora ciliaris retinae.
[b] Measurements taken 2.0 mm from ora ciliaris retinae.

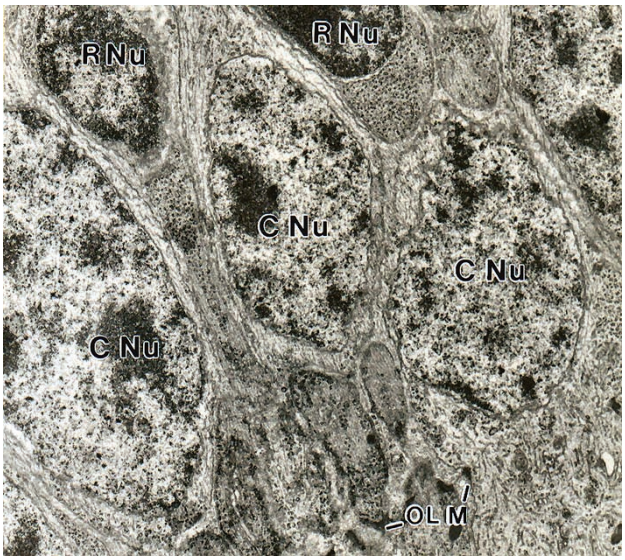

Figure 2.95 Within the outer nuclear layer of a sheep, cone nuclei (CNu) form a single layer next to the outer (i.e., external) limiting membrane (OLM). The rod nuclei (RNu) are typically smaller and more heterochromatic. (Original magnification, 6,500×.)

segments, while the axons of the rod and cone nuclei extend into the outer plexiform layer to synapse with horizontal and bipolar cells.

Outer Plexiform Layer

The axons of the photoreceptors and their synaptic connections are the two components of the outer plexiform layer. The photoreceptors of the outer nuclear layer form connections with the horizontal and bipolar cells of the inner nuclear layer (see Fig. 2.84 and Fig. 2.85). The rod axons typically terminate in pear-shaped spherules, whereas cone axons end in larger, broader pedicles (see Fig. 2.84). The rod spherule has one or more invaginations at which ribbon synapses occur, whereas the cone pedicle has numerous, more shallow invaginations of ribbon synapses (see Fig. 2.84). The cone pedicles usually extend further vitread into the outer plexiform layer (Hogan et al., 1971; Kaas et al., 1972; Rodieck, 1973; Shively et al., 1970).

Two distinct types of synapses occur in the outer plexiform layer, and each is specific to the rod spherule or the cone pedicle. The invagination of each rod spherule synaptic expansion contains two deeply inserted, horizontal cell processes laterally and one or more bipolar cell process centrally (see Fig. 2.84; Fig. 4.22B). Within the presynaptic spherule at the site of synaptic expansion is a dense lamellar structure, the synaptic ribbon, which is oriented perpendicularly and close to the cytoplasmic invaginations (Fig. 2.96). A specific horizontal cell will contact a spherule only once, but each spherule may be contacted by several horizontal cells as well as by the dendritic processes from one to four bipolar cells.

The shallow, broad invaginations of each cone pedicle synaptic expansion contain flat bipolar cell processes. Horizontal cell processes may have conventional synaptic contacts between bipolar cell processes, and they can have both pre- and postsynaptic sites along their length. In the cat, the horizontal cell processes synapse only to cones, and the axon terminal connects exclusively to rods (Kolb, 1974; Kolb & Famiglietti, 1974). Thus, rods and cones are interconnected primarily by horizontal cells. Direct contact through gap junctions (connexin channels) also exists between adjacent cones and between rods and cones (Bloomfield & Völgyi, 2009; Park et al., 1994; Witkovsky, 1992).

Inner Nuclear Layer

The inner nuclear layer is composed of the soma of horizontal, bipolar, amacrine, interplexiform (in some retinas), and Müller cells. The neurons in this layer maintain connections

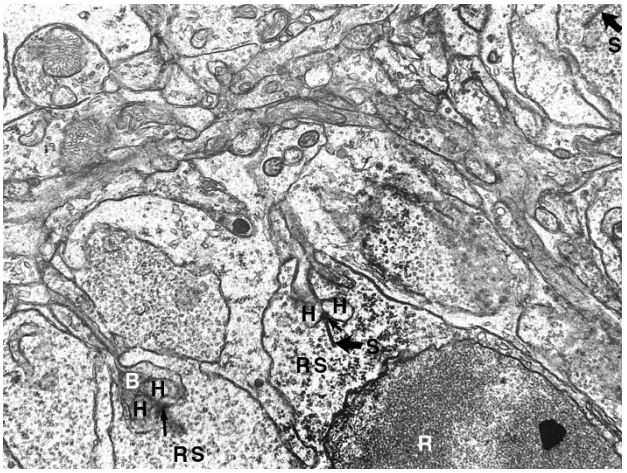

Figure 2.96 Outer plexiform layer of the cat. Synaptic vesicles fill spherules, and the small arrows point to an arciform density. B, bipolar cell process; H, horizontal cell process; R, rod nuclei; RS, rod spherules; S, ribbon synapse in rod spherule with synaptic ribbon. (Original magnification, 22,500×.)

between the photoreceptor layer and the ganglion cell layer and are involved in modification and integration of the neural responses elicited by the stimuli. Specifically, horizontal and bipolar cells are second-order neurons that connect with photoreceptors (first-order neurons) and ganglion cells (third-order neurons). Amacrine cells are inhibitory cells that interact with bipolar cells and ganglion cells, and Müller cells are the main glial cell of the retina. Little is known about the function of interplexiform cells, but they increase the gain in the photoreceptor-to-bipolar synapses, at least in some species (Jiang et al., 2014).

The horizontal cell nuclei are positioned along the outermost margin of the inner nuclear layer (near the outer plexiform layer), whereas the amacrine cells are positioned along the innermost margin (near the inner plexiform layer) (Fig. 2.97). These two cell types have ramifying branches in their respective plexiform layers and act as integrating units. The bipolar cell nuclei and Müller cell nuclei comprise the intermediate zone of the inner nuclear layer (Hogan et al., 1971; Shively et al., 1970; Sigelman & Ozanics, 1988).

The nuclei of horizontal cells are large, with a single, prominent nucleolus. The cells are also characterized by their wide, horizontally oriented cell processes. There are different kinds of horizontal cells: axonless and those with axons (Boycott et al., 1987; Gallego, 1986; Kolb, 1974; Kolb et al., 1992). They have been studied in several species, including cats, horses (Guo & Sugita, 2002; Macneil et al., 2009; Sandmann et al., 1996b), some even-toed ungulates (Sandmann et al., 1996a), rabbits (Mills & Massey, 1992; Strettoi & Masland, 1995), and tree shrews (Müller & Peichl, 1993).

In horses and related species, type B horizontal cells outnumber type A from 5:1 to 10:1. The type A horizontal cells are unusual among mammals in that they have very large dendritic fields. These dendrites, which are fine and sparsely branched, appear to contact cones selectively, specifically blue cones, which comprise 10%–25% of the cone population. Type B cell densities range between 500 and 900 cells/mm^2 within the visual streak, being greater than 1000 cells/mm^2 in the area centralis at the temporal end of the visual streak. The density of type B cells drops sharply away from the visual streak to between 100 and 300 cells/mm^2. By comparison, type A cell density is between 50 and 100 cells/mm^2 within the visual streak and from 15 to 45 cells/mm^2 peripherally (Sandmann et al., 1996b).

The bipolar cell is the second most numerous neuron in the retina of most domestic animals, and it constitutes the radial connection between the photoreceptors and the ganglion cells. In cone-rich retinas, the numbers of bipolar cells increase remarkably, as do those of amacrine cells. Bipolar cell dendritic processes in the outer plexiform layer synapse with photoreceptors and horizontal cells. Axonal processes then terminate in the inner plexiform layer, synapsing with amacrine and ganglion cells. Among mammalian retinas, the inner nuclear layer houses the somata of a single type of rod bipolar cell and a variety of cone bipolar cell types.

Cone bipolar cells can be divided into many types, consisting of 11 in the cat (Cohen & Sterling, 1990; Kolb & Nelson, 1996). Flat, diffuse bipolar cells synapse with several cones, whereas midget bipolar cells synapse with single cones. All cone bipolar cells can synapse with ganglion cells and amacrine cells in the internal plexiform layer. For the most part, cone bipolar cells have narrow dendritic and

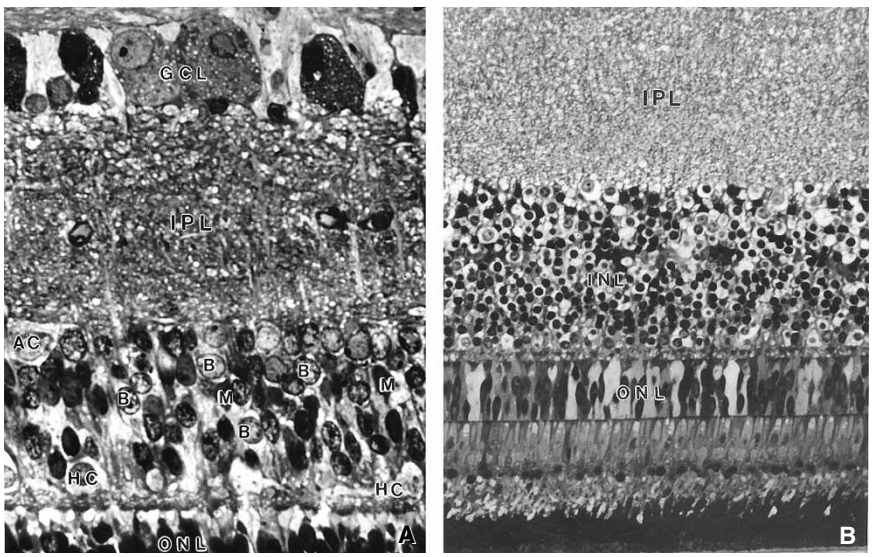

Figure 2.97 Inner nuclear layer (INL) and inner plexiform layer (IPL) of a pig (**A**) and a chicken (**B**). AC, amacrine cell; B, bipolar cell; GCL, ganglion cell layer; HC, horizontal cell; M, Müller cell; ONL, outer nuclear layer. (Original magnification: **A**, 100×; **B**, 200×.)

axonal fields, which would be expected in radial transmission of information for high-spatial resolution.

Amacrine cells do not have recognizable axons, and their processes terminate in the region of the inner plexiform layer (Rodieck, 1973). Ultrastructural studies have demonstrated that these neurons are of the pseudounipolar type, having axons with the characteristic synaptic vesicles but also having features in common with dendrites (Sigelman & Ozanics, 1988). Amacrine cells are located vitread in the inner nuclear layer, and they often have indented euchromatic nuclei. Their cytoplasm is more copious than that of bipolar cells, being filled with polysomes and rough endoplasm reticulum, mitochondria, neurofilaments, and tubules. Collectively, amacrine cells provide horizontal integration in the inner plexiform layer between bipolar cell terminals, ganglion cell dendrites, and other amacrine cells.

Another type of amacrine cell is located in the ganglion cell layer and appropriately named the displaced amacrine cell (Chang & Straznicky, 1992; Vaney et al., 1991). Most amacrine cells of the peripheral cat retina consist of this type (White & Chalupa, 1991).

In addition to the horizontal cell, bipolar cell, and amacrine cell, there is a fourth neuron of the inner nuclear layer, called the interplexiform cell, that is not found in all retinas (Iuvone, 1986; Linberg et al., 1996; Park et al., 1994). This neuron, which is observed in the innermost zone of the inner nuclear layer, has both pre- and postsynaptic processes in the inner plexiform layer and presynaptic connections with horizontal and bipolar cells via a long horizontal process extending to the outer plexiform layer. As a result, it provides a feedback mechanism from the inner retina to the outer synaptic layer (Jiang et al., 2014).

Müller cells (radial glial cells) are the principal nonneuronal cell of the vertebrate retina and serve as support cells for most neurons in the retina. In teleost fish, Müller cells can obtain stem cell characteristics after retinal damage and play an important role in the regeneration of the retina, whereas they can both be protective and harmful to the damaged retina in mammals (Goldman, 2014). They tend to have more cytoplasm and to lie in the outer portion of the inner nuclear layer. Müller cells are elongated, branching cells that extend from the internal limiting membrane to beyond the external limiting membrane. They are important for internal structural support as well as for retinal nutrition. Müller cell fibers fill almost all the extracellular space between neural cells. In both the outer nuclear and ganglion cell layers, Müller cells form close contacts to the neuronal somata, entirely encasing them, compared with the neuronal somata of the inner nuclear layer, which are only partially wrapped (Distler & Dreher, 1996; Robinson et al., 1989). Their nuclei are angular and have denser chromatin than other nuclei in the inner nuclear layer. The vitread ends of the Müller cells possess end feet, which have the ability to phagocytize foreign substances and consequently may play an important role in normal retinal function (Nishizono et al., 1993). The lateral sides of the end feet contain gap junctions, thus allowing these cells to transmit information throughout the retina.

As a cell type within the vertebrate retina, the Müller cell is unique in that it consists of a single morphologic class or type. These cells do vary in length according to the overall thickness of the retina, being shortest peripherally and longest centrally. Müller cells have a neuronal-like distribution with densities highest parafoveally and in the visual streak (Distler & Dreher, 1996; Robinson et al., 1989).

Inner Plexiform Layer

The inner plexiform layer comprises the cell processes of the inner nuclear and ganglion cell layers, at which synapses between bipolar, amacrine, and ganglion cells occur. The bipolar cells synapse in ribbon synapses with two postsynaptic elements, and hence are termed a dyad. The postsynaptic elements of the dyad consist of: (1) a ganglion cell dendrite and an amacrine cell process, or (2) two amacrine cell processes (see Fig. 2.84 and Fig. 2.98).

In addition to the ribbon synapses, abundant conventional synapses are present on amacrine cells. These synapses involve bipolar cells, ganglion cells, and other amacrine cells. Some act as reciprocal synapses back onto a bipolar cell after participating in a dyad synapse (see Fig. 2.98); thus, a single amacrine cell might connect presynaptically and

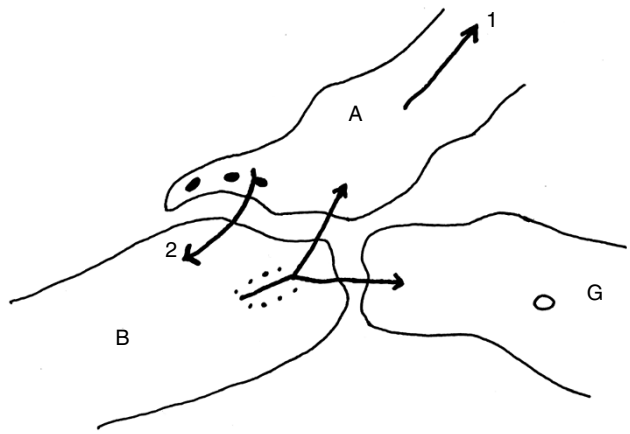

Figure 2.98 The bipolar–amacrine–ganglion cell interaction. The bipolar cell (B) projects onto both the ganglion (G) and the amacrine (A) cells. The amacrine cell controls or adjusts the bipolar cell in a negative feedback arrangement. 1, further interactions; 2, reciprocal inhibition. (*Source:* Redrawn from Records, R.E., et al. (1988) Electrical signals of the retinal microcircuitry and the visual cortex. In: *Biomedical Foundations of Ophthalmology* (eds Duane, T.D. & Jaeger, E.A.), Vol. 2. Philadelphia, PA: J.B. Lippincott.)

postsynaptically to different areas of the same bipolar cell. In addition, serial synapses between two or more adjacent amacrine cell processes have been observed (Dowling & Werblin, 1971; Kolb, 1997; Masland, 2012).

The bipolar cell axons contain numerous synaptic vesicles and mitochondria. The ganglion cell axons are the only processes in the inner plexiform layer without synaptic vesicles. They are pale, with smooth and rough endoplasmic reticulum, small mitochondria, and microtubules. The amacrine cell processes, which also are pale and possess large mitochondria and synaptic vesicles, are the most numerous because of the extensive arborization of their axons.

Functionally, the outer plexiform layer is organized to enhance static or spatial aspects so as to accentuate contrast in the retinal image. The inner plexiform layer appears to be involved in temporal or dynamic activities, enhancing motion and direction responses (Dowling & Werblin, 1971).

Ganglion Cell Layer

This layer contains different types of ganglion cells, neuroglial cells, and retinal blood vessels. It is the innermost cell layer of the retina and consists of a single layer of cells, except in the area centralis and visual streak, where it can be two or three cell layers thick (see Fig. 2.85 and Fig. 2.97). In primates and various nonmammalian species, the ganglion cell layer can be six to nine cell layers thick.

With measurement of retinal ganglion cell isodensity lines, the location of the visual streak and associated area centralis has been determined in many vertebrate species. The ganglion cell density of those species of greatest veterinary importance are in Table 2.17 (Henderson, 1985; Peichl, 1992; Silveira et al., 1989; Wong, 1989). In most instances, isodensity measurements of the ganglion cells reveal a streak along the horizontal axis that often extends more temporally than nasally. Some variations of the shape and location of the visual streak do occur. In the dog and cat, the visual streak is more concentric than elongated (Gonzalez-Soriano et al., 1995). In the horse, which has a narrow, elongated visual streak, the highest ganglion cell density occurs within its temporal portion, at which optimal resolution is believed to be restricted (Timney & Keil, 1992). In the elephant, in addition to a concentration of ganglion cells along the horizontal plane inferior to the optic disc, is another concentration of ganglion cells in the dorsal temporal retina, which may be an evolutionary adaptation enabling the animal to monitor its trunk (Stone & Halasz, 1989). In sloths, the visual streak is oriented vertically in the ventral temporal retina. The location of the visual streak may be an adaptation allowing the three-toed sloth to rotate uniquely its head 180° while climbing upside down along horizontal branches (Costa et al., 1987). Giraffes, like other artiodactyls, have both a horizontal streak and a temporal area which improve resolution along the horizon and in the frontal visual field, respectively. Giraffes also have a dorsal arch related to their head height that affords enhanced resolution in the inferior visual field. Additionally, the alpha ganglion cell distribution pattern is unique to the giraffe, and it enhances acquisition of motion information for the control of tongue movement during foraging and the detection of predators (Coimbra et al., 2013).

Three basic forms of ganglion cells have been described in the cat, and extensive research has related the morphology of these cells to their neurophysiology (see Chapter 4; Henderson, 1985). Boycott and Wassle described α-, β-, and

Table 2.17 Ganglion cell densities in various species.

Animal	Ganglion cell density (per mm^2)	Total ganglion cells	Reference
Dog	5,300–14,400 (area centralis)	109,000	Gonzalez-Soriano et al., 1995
		115,000	Peichl, 1992
	1,500 (area centralis)	75,000[a]	McGreevy et al., 2004
Cat	9,000–10,000		Hughes, 1975
Horse	6,500 (area centralis)		Hebel, 1976
	3,000 (area centralis)		Evans & McGreevy, 2007
		440,000	Guo & Sugita 2000
Cow	5,000 (area centralis)		Hebel, 1976
	600–2,400 (peripherally)		Hebel & Holländer, 1979
Rabbit	4,700–5,400		Robinson et al., 1989
			Vaney, 1980;
Human	32,000–38,000		Curcio et al., 1990

[a] Only large and medium size cells were counted in this study.

γ-ganglion cells in the retina on the basis of dendritic fields, and these morphologic types correspond with the three physiologic types of ganglion cells (Y, X, and W) (Boycott & Wassle, 1974; Levick, 1975). The size of the dendritic fields for each of the three morphologic types varies with location in the retinal field. All three are represented throughout the retina, including the visual streak and area centralis, but the proportions vary.

Alpha- or Y-cells have rather sparsely branching dendrites and a large perikaryon and are found primarily within the peripheral retina. In the canine retina, the density of the α-cell varies by location, and they comprise between 3% and 14% of the total ganglion cell population in the dog (Peichl, 1992).

Beta or X ganglion cells are smaller than α-cells and have more branches. They are also more numerous than α-cells, being more concentrated within the area centralis and visual streak than peripherally.

Gamma- or W-cells, which have a small perikaryon with a few thin, infrequently branching dendrites, are also numerous and mostly concentrated in the central retina. They are most often directly connected with midget bipolar cells, which synapse solely with cones. These ganglion cells are involved in high-resolution vision and project mostly to the superior colliculus (Stone & Keens, 1980). In the cat, the γ-cells comprise nearly one-half the ganglion cells in most of the nasal retina but only one-third of those in the temporal retina and area centralis (Stein & Berson, 1995).

Ultrastructurally, the types of ganglion cells have not been differentiated. In general, they have abundant cytoplasm containing rough endoplasmic reticulum, ribosomes, a smooth-surfaced endoplasmic reticulum, dense membrane-bound bodies, and mitochondria (Beauchemin, 1974; Hogan et al., 1971; Shively et al., 1970).

Nerve Fiber Layer

Axons of ganglion cells gather in the nerve fiber layer, converging to turn at right angles and course to the posterior pole at which the optic nerve exits the globe. To maintain transparency of the retina, the axons lack myelin sheaths. Some neuroglial cells and the cellular processes of Müller cells are also present among the axons. Large retinal vessels occur in the nerve fiber layer as well as in the ganglion cell and inner plexiform layers.

The nerve fiber layer increases in thickness as it approaches the optic disc. The axons, which do not branch, pass radially to the optic nerve, except in the area centralis, where the concentration of axons arising from this region causes the more peripheral axons to take an altered course around this area to reach the optic disc. Axonal diameters within the optic nerve may be as much as 30% greater than those within the nerve fiber layer (Fitzgibbon & Funke, 1994).

The neurons of the nerve fiber layer are mainly centripetal (i.e., afferent) fibers carrying impulses from the retina to the brain. The axons are of various sizes, and the large axons originate from the large ganglion cells (Y- or a-cells). In some species, centrifugal (i.e., efferent) fibers carrying impulses from the brain to the retina have been described. In birds, the presence of centrifugal fibers is well established, but in other animals, the existence of these fibers is controversial (Brooks et al, 1999; Matsuyama, 1973; Rodieck, 1973).

In addition to Müller cells, glial cells are present in the inner retina, being found in the inner plexiform, ganglion cell, and nerve fiber layers. Astrocytes have long, branching processes found along the retinal blood vessels in vascular retinas, but these cells are not present in avascular retinas. Astrocytes play a supportive role structurally, and perhaps nutritionally, around blood vessels and nerve axons and are the main producers of vascular endothelial growth factor (VEGF) under both normal conditions and in disease (Ozaki et al, 2000; Rodieck, 1973). Furthermore, they are an essential part of the blood–retinal barrier.

Inner Limiting Membrane

The inner limiting membrane is a true basement membrane formed by the fused terminations of Müller cells. Vitreal fibrils insert into the membrane, effectively establishing a 'fusion' between the neurosensory retina and the vitreous body.

Retinal Vasculature

Classically, variations in the retinal vasculature have been categorized into four basic patterns: holangiotic, merangiotic, paurangiotic, and anangiotic. Most mammals possess the holangiotic pattern, in which the majority of the neurosensory retina receives a direct blood supply. The merangiotic pattern consists of blood vessels localized to a region of the retina medial and lateral to the optic disc. Examples of animals with this retinal vascular pattern are lagomorphs (rabbits and pika). In the paurangiotic pattern, blood vessels within the retina occur only circumferentially near the optic disc (peripapillarily). This pattern can be found in certain ungulates, such as horses, elephants, and rhinoceroses, and in some marsupials such as kangaroos. The anangiotic pattern is characterized by an absence of any vasculature within the neurosensory retina, and it occurs in sugar gliders, Guinea pigs, chinchillas, and nonmammalian species such as birds. In general, the retinal arterial supply in domestic animals comes from the short posterior ciliary arteries, which are termed cilioretinal arteries, rather than via a central retinal artery origin as in higher primates, rats, and mice (Henkind, 1966; Matlu & Leopold, 1964; Michaelson, 1954; Prince et al., 1960).

In the holangiotic pattern of the cat, three major pairs of cilioretinal arterioles and venules are present, originating

around the optic disc margin. They consist of a dorsomedial pair that curves laterally, a ventromedial pair, and a ventrolateral pair. These vessels arc around the area centralis, leaving what appears clinically as a vessel-free zone; however, a capillary network exists in intercommunicating nets within the nerve fiber and inner nuclear layers. Adjacent to arterioles is a 100–200-µm capillary-free zone (Matlu & Leopold, 1964). In the dog, approximately 20 cilioretinal arterioles and three to four major venules radiate from the optic disc. Additional smaller venules join the larger venules on the optic disc and form a very short central retinal vein. The capillary network is extensive and similar to that of the cat in its depth, having a capillary-free zone around arterioles and a capillary network over the area centralis.

Histologically, the larger vessels of holangiotic retinas lie within the nerve fiber, ganglion cell, and inner plexiform layers. Capillaries, however, lie mostly within the inner nuclear layer and, to a lesser extent, within the ganglion cell and nerve fiber layers. Ultrastructurally, one to four endothelial cells line a capillary lumen. A basement membrane covers the endothelium as well as divides the surrounding mural cells (i.e., pericytes) and their processes (Shively et al., 1970). Adjacent endothelial cells are attached by desmosomes and tight junctions (Sigelman & Ozanics, 1988).

Around the optic disc, the paurangiotic retina of the horse contains approximately 30 fine arterioles and 30 venules of approximately 25 and 35 µm diameter, respectively (Michaelson, 1954). Ophthalmoscopically, they cannot be distinguished from each other, and they radiate 360 degrees outward from the disc for 6 mm horizontally and 3–4 mm vertically. The arterioles do not form a capillary network at their terminations; rather, they pass directly into the venules, which have arteriolar annuli at the point of side-arm branching (Michaelson, 1954; Prince et al., 1960).

In the merangiotic rabbit retina, there is a horizontal band of vessels confluent with medullated nerve fibers, emanating medially and laterally from each side of the optic disc. The vessels branch in a side-branch manner rather than dichotomously, which is usually the case in most mammals (Hyvarinen, 1967). Four capillary areas are located within the horizontal band, including superficial net capillaries, deep capillaries of the nerve fiber layer, peripheral capillaries, and peripapillary capillaries.

In the anangiotic avian retina, vasculature is restricted to a structure called the pecten (pecten oculi), which lies vitread to the optic nerve. The pecten is a highly pigmented, pleated structure reminiscent of ciliary processes, and it contains a rich plexus of small blood vessels (Fig. 2.99). The plexus is supplied by tributaries of the ophthalmotemporal artery and lacks any direct connections with the neighboring choroidal circulation (Iskandar et al., 1988). The main function of the pecten is to provide nourishment for the inner retina (Duke-Elder, 1958; Meyer, 1977). When viewed grossly, the pecten can be divided into three types: the pleated type seen in most birds; the conical type found in kiwi; and the vaned type reported in the ostrich (Meyer, 1977; Sillman, 1973). Among the pleated pecten, the number of pleats and the size vary considerably within avian species. The variations appear to be associated with the general activity of the species, including its visual capability. The size of the pecten and

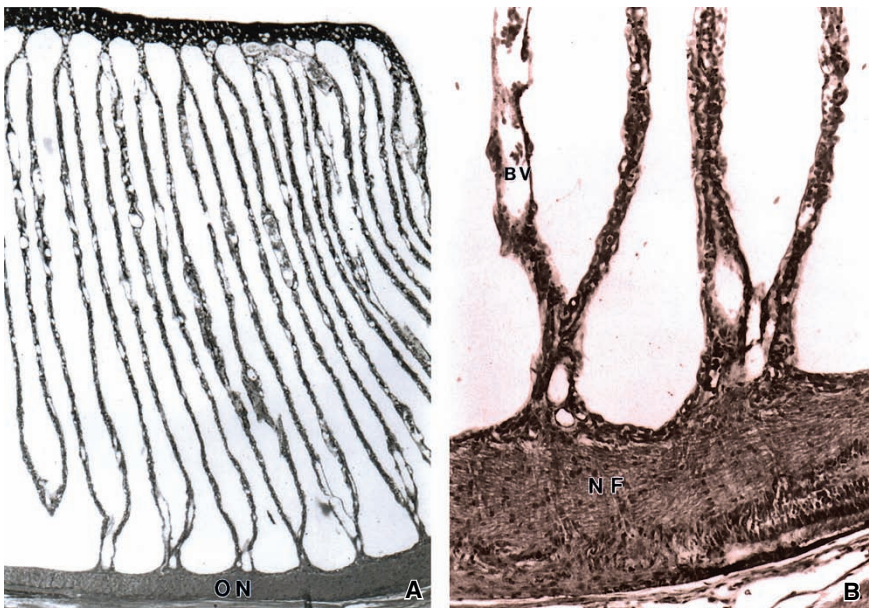

Figure 2.99 **A.** The avian pecten, as seen here in the chicken, consists of a pleated vascular plexus that lies vitread atop the optic nerve head (ON). (Original magnification, 50×.) **B.** Close-up of the base of the pecten as it internally lines the nerve fibers (NF) that form the optic nerve head. BV, blood vessels of the pecten. (Original magnification, 250×.)

its number of folds are indicative of its role in transport of substances to the avascular retina (Braekevelt, 1991, 1994, 1998b).

The amount of pigmentation varies among pecten of different birds, but melanin is especially located along the apical portion, which may protect the blood vessels against exposure to UV light (Kiama et al., 1994). The amount of UV light the retina and pecten receive has not been determined in birds; however, evidence indicates that at least some avian retinas use UV light for visual detection (Bennett & Cuthill, 1994). In addition to providing protection against the damaging influence of UV light, the extensive population of melanocytes may also offer structural support to the pecten (Braekevelt, 1991, 1993d; Smith et al., 1996).

Aging

In aging eyes, the inner limiting membrane becomes thickened and increasingly vacuolated. The inner and outer plexiform layers can have cystoid spaces. The layers of the sensory retina, especially the outer nuclear layer of the peripheral retina, progressively thin (Gao & Hollyfield, 1992). A displacement or migration of photoreceptor nuclei into the photoreceptor layer also occurs with age in humans and rats (Gartner & Henkind, 1981; Lai, 1980). RPE cells decrease in number and, concomitantly, fill with residual bodies, including aging pigment (lipofuscin) (Feeney-Burns et al., 1984; Fite & Bengston, 1989; Gao & Hollyfield, 1992).

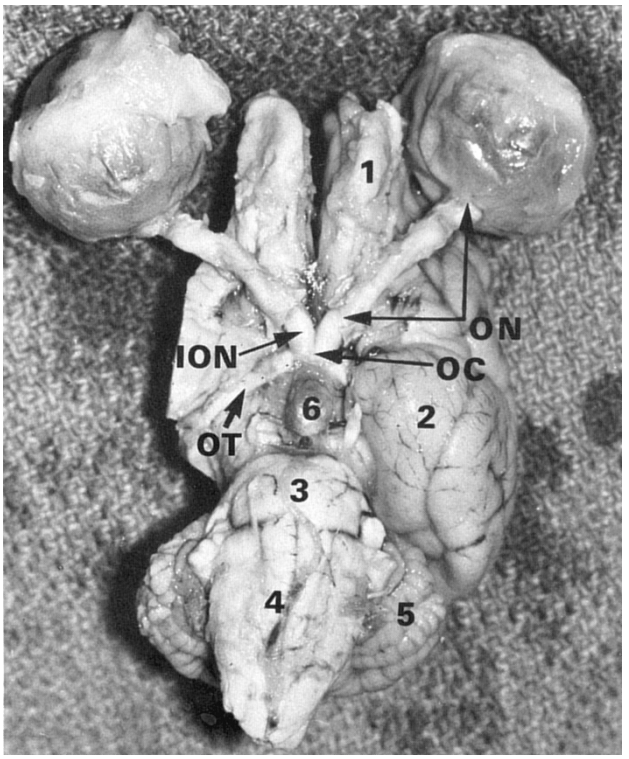

Figure 2.100 Ventral view of the dog brain–eye relationship. The right cerebral hemisphere has been removed; note how physically close the eyes are to the brain. ION, intracranial optic nerve; OC, optic chiasm; ON, orbital optic nerve; OT, optic tracts; 1, olfactory tract; 2, piriform lobe; 3, pons; 4, medulla; 5, cerebellum; 6, pituitary.

Optic Nerve

Retinal ganglion cell axons leave the nerve fiber layer and form the optic disc. From this area, they pass through the choroid and sclera and into the orbit as the optic nerve. In addition to ganglion cell axons, the optic nerve is composed of glial cells and septae, which arise from the pia mater. The visual axons synapse in the lateral geniculate nucleus, whereas the pupillomotor fibers synapse in the nucleus of CN III.

The optic nerve extends from the globe to the optic chiasm, and it consists of four regions: intraocular, intraorbital, intracanalicular, and intracranial (Fig. 2.100; Brooks et al., 1999). Because of similar anatomic properties, the optic nerve is considered to be more of a nerve fiber tract of the brain than a peripheral nerve (Hogan et al., 1971). The intraocular optic nerve consists of retinal, choroidal, and scleral portions.

The terms optic disc, papilla, and optic nerve head are interchangeable and include the retinal and choroidal portions of the optic nerve. Optic papilla refers to an elevation of the nerve head, and its presence and development vary among and within species (Hogan et al., 1971). Within the optic papilla is a central depression called the physiologic cup. The cup is lined by a plaque of astrocytes known as the central supporting tissue meniscus of Kuhnt (Fig. 2.101). An exaggeration of this tissue is Bergmeister's papilla, which is the remnant of the hyaloid artery on the disc's surface.

Converging nerve fibers of the retina cluster into fascicles or bundles as they become lined by glial (fibrous astrocytes) and collagenous (lamina cribrosa) elements. The astrocytes are oriented perpendicularly to the length of the bundle, thus separating the nerve fibers from all non-neuronal components, that is, extracellular fibers of connective tissue, blood vessels, and microglia. Vitread, the astrocytes and associated loose connective tissue form capillary-bearing trabeculae that support the nerve bundles as they turn 90° into the scleral canal from the nerve fiber layer (Fig. 2.102; Hayreh, 1974). This region is referred to as the choroidal or the anterior lamina cribrosa portion of the optic nerve.

Two morphologic types of fibrous astrocytes are present throughout the optic nerve: thin-bodied and thick-bodied (Trivino et al., 1996). Thin-bodied astrocytes are located more anteriorly, both accompanying and contacting axons. Thick-bodied astrocytes are located throughout the optic nerve head and the prelaminar, laminar, and postlaminar regions. Within the posterior prelaminar region, these cells

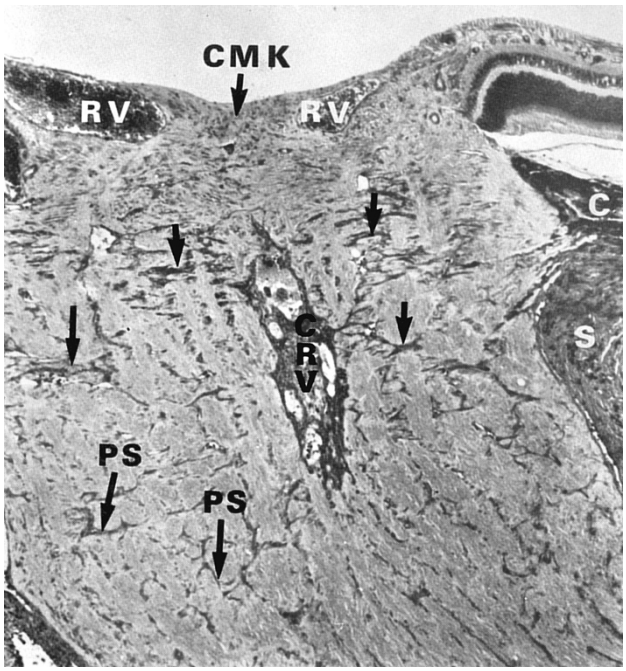

Figure 2.101 The optic nerve head and bulbar optic nerve of a dog. Arrows indicate lamina cribrosa; note the number of astrocytes anterior to it. C, choroid; CMK, central meniscus of Kuhnt (accumulation of astrocytes in physiologic cup); CRV, central retinal vein; RV, retinal veins; S, sclera; PS, pial septa. (Original magnification, 720×.)

Figure 2.102 Trypsin digest of a canine optic nerve shows the network of collagen beams that make up the lamina cribrosa (LC). These beams, which are largely a continuation of the fibrous tunic, are interconnected externally to pial septa (PS). (Original magnification, 25×.) (Courtesy of D.E. Brooks.)

form glial tubes, which guide axons into the lamina cribrosa (Trivino et al., 1996).

Sclerad, the posterior region of the lamina cribrosa consists of meridional extensions of the sclera. In turn, these extensions consist of successive laminar sheets with radially aligned perforations (see Fig. 2.102). Each lamina possesses a capillary in its center. As in the retina, the optic nerve capillaries are nonfenestrated, having tight junctions (i.e., zonula adherens) (Anderson & Baverman, 1976; Brooks et al., 1989). The lamina cribrosa of cats, dogs, horses, squirrels, and monkeys is well developed, having prominent collagenous laminae (Brooks et al., 1989; Tansley, 1956). By comparison, the lamina cribrosa of mice, rats, and rabbits is poorly developed, lacking substantial amounts of collagen within the lamina. Among rodents, the lamina cribrosa in the rat optic nerve is least developed, consisting of only one or two beams of sparse connective tissue (Johanssen, 1987); however, the lamina cribrosa of guinea pigs is considerably more developed, consisting of three or more beams of abundant connective tissue. Of the different types of collagen within the lamina cribrosa, type VI predominates.

The axons within the optic nerve are easily distinguished by their tubular processes, which contain evenly dispersed neurofilaments and neurotubules, and occasional vesicles and mitochondria. The vesicles, mitochondria, lipids, proteins, and other cytoplasmic materials are continuously transported within the axon either toward the synaptic ending (orthograde) or toward the cell body (retrograde), in a movement called axonal flow. Axonal flow within the optic nerve is normally unimpeded throughout the life of the ganglion cell; however, at the lamina cribrosa axonal flow is susceptible to blockage, which usually results from elevated IOP (Samuelson et al., 1983; Williams et al., 1983a). As the IOP rises, the laminar perforations lose their proper alignment, and axonal flow is interrupted (Brooks et al., 1989, 1994; Quigley & Addicks, 1981; Samuelson et al., 1983). Partial constriction of axoplasmic flow, however, has been found at the lamina cribrosa of normotensive eyes among a wide range of mammals, including humans, cats, rabbits, rats, Guinea pigs, sheep, cattle, and pigs (Hollander et al., 1995). This constriction may result from the pressure gradient across the lamina cribrosa and could play a role in normotensive glaucoma. In dogs, each axon is myelinated by oligodendrocytes throughout the entire optic nerve, including the optic disc. In cats, horses, cattle, and humans, myelination begins posterior to the lamina cribrosa and is responsible for the marked increase in optic nerve diameter after exiting the lamina cribrosa (Prince et al., 1960).

The number of optic nerve fibers, their density and size, vary considerably among species (Fig. 2.103; Table 2.18; Ashton, 1960; Beazley & Dunlop, 1983; Brooks et al., 1995a, 1995b; Bruesch & Arey, 1942; Do Nascimento et al., 1991; Fischer & Kirby, 1991; Fitch et al., 1991; Flocks, 1956; Flugel et al., 1991; Fritz, 1906; Fukuda et al., 1982; Geri et al., 1982; Henderson, 1985; Jonas et al., 1990, 1992; Kirby et al., 1982; Krinkle et al., 1985; Levy et al., 1996; Novokhatshii & Reshetniak, 1987; Qijiu et al., 1981; Sanchez et al., 1986; Shen et al., 1985; Silveira et al., 1989; Vaney & Hughes, 1976; Virchow, 1910; Wakakuwa et al., 1987; Williams et al., 1983a). Animals with poorly developed eyes, such as mole

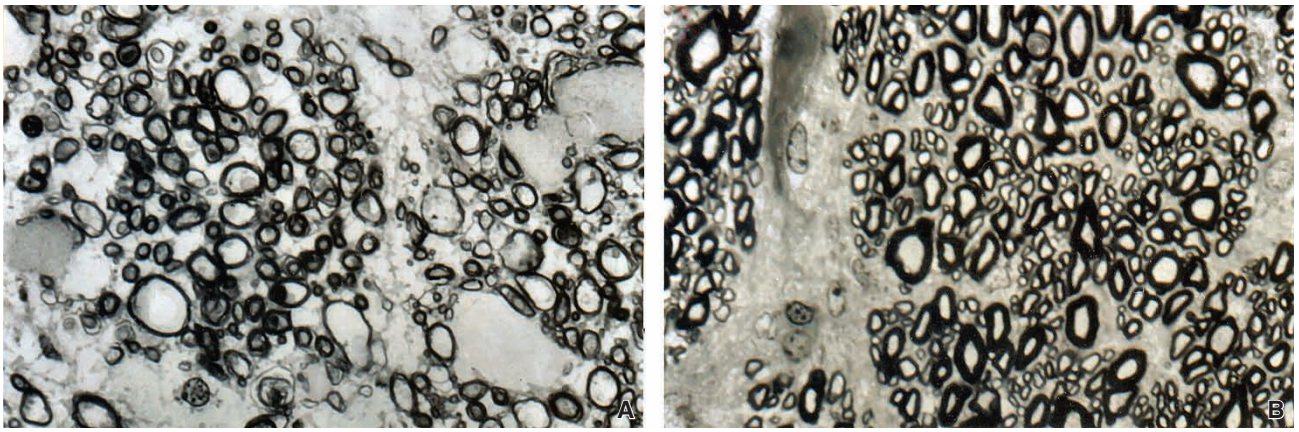

Figure 2.103 Cross-section of the optic nerve in a dog (**A**) and a horse (**B**) posterior to the laminar cribrosa. In both species, the widths of individual nerve fibers vary a great deal within a nerve fiber bundle. The myelin sheaths of the nerve fibers in the horse are generally thicker than those in the dog, reflecting the longer distances they extend in that species. (Original magnification, 1,000×.)

Table 2.18 Axon count and density of the optic nerve.

Animal	Total axon count	Axon density (per mm^2)	Mean fiber diameter (μm)	Reference
Dog	145,000–165,000	~50,000	1.5	Brooks et al., 1995a; Bruesch & Arey, 1942; Krinkle et al., 1985; Novokhatshii & Reshetniak, 1987; Williams et al., 1983b
Cat	193,000	78,000	1.6	Williams et al., 1983b
Horse	1.08 million	62,800	1.9	Brooks et al., 1995b
Rat	102,085	568,000	0.6–0.83	Fukuda et al., 1982
Rabbit	394,000	354, 395	1.0	Vaney & Hughes, 1976
Human	1.1–1.2 million	150,000	~100	Jonas et al., 1990, 1992

rats, contain approximately 900–1800 nerve fibers, whereas those with highly developed eyes, such as various primates, have 100–150 times that number. Interestingly, the size of the eye often does not correlate with the total number of nerve fibers within the optic nerve.

The orbital portion of the optic nerve is covered by the three meningeal sheaths of the central nervous system: the dura mater, the arachnoid sheath, and the pia mater. The outermost sheath is the thick dura mater, which fuses with the sclera anteriorly. Posteriorly, at the optic foramen, it divides into two layers. The outermost of these layers reflects onto orbital periosteum, and the innermost is continuous with the dura of the cranial vault (Fig. 2.104). The collagenous fibers of the dura run longitudinally on the external surface and circumferentially internally. The principal cell type is the fibroblast (Donovan et al., 1974b; Prince et al., 1960). The arachnoid sheath is internal to the dural sheath, and it is composed of collagen trabeculae covered by fibroblastic meningothelial cells. The pia mater is closely apposed to the nerve and sends septa radially into the nerve, thus dividing it into columns (Fig. 2.105). Small blood vessels accompany the pial septae into the optic nerve.

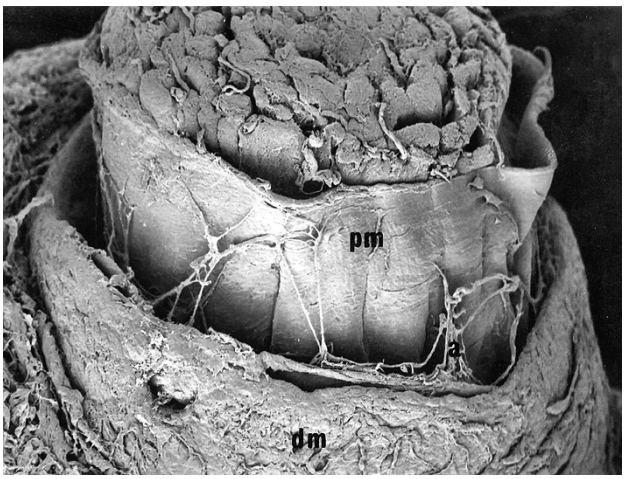

Figure 2.104 SEM shows how the orbital optic nerve is protected by the three meningeal layers, or sheaths, of the central nervous system; the thick dura mater (dm), which is internally lined by the arachnoid and its trabeculae; and the pia mater (pm). (Original magnification, 33×.)

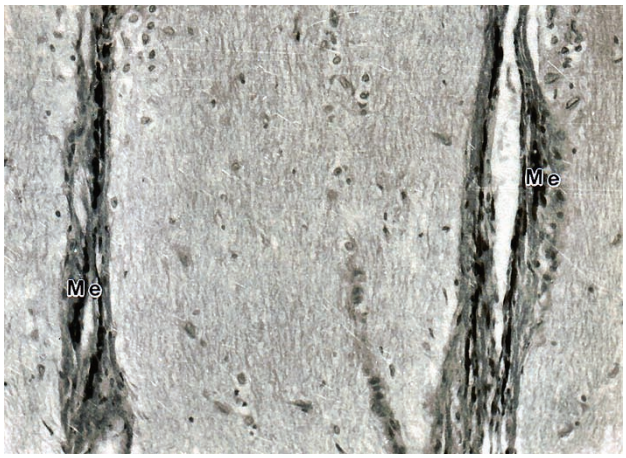

Figure 2.105 Pial septae within the pig orbital optic nerve can contain melanocytes (Me) and separate the nerve fiber bundles into long columns. (Original magnification, 200×.)

Vasculature of the Eye and Orbit

Among domestic animals, the main supply of blood to the eye and orbit is via the internal maxillary artery (a branch of the external carotid artery), which after passing through the alar canal, branches to give rise to the external ophthalmic artery. By comparison, in primates, the entire microcirculation of the eye and most of the orbital circulation is supplied via the internal carotid artery, which gives rise to the internal ophthalmic artery (Prince et al., 1960).

Domestic animals possess both internal and external ophthalmic arteries, but the external ophthalmic artery provides most of the circulation to the eye. Both the long and short posterior ciliary arteries as well as the lacrimal, muscular, and supraorbital arteries derive from the external ophthalmic artery. The internal ophthalmic artery, which is relatively small, provides the blood supply for the optic nerve and anastomoses with the external ophthalmic artery or one of its branches (Fig. 2.106); this anastomosis is especially prominent in the dog.

The blood vessels of the retina and choroid arise from both the long and short posterior ciliary arteries. Domestic animals generally have a number of small arteries entering the retinal layers from around the optic disc; a single central retinal artery does not exist.

In the horse, the choroidal vasculature is fed by short posterior ciliary arteries, which originate from the four posterior ciliary arteries, including the lateral and medial posterior arteries that continue anteriorly. Additionally, choroidoretinal

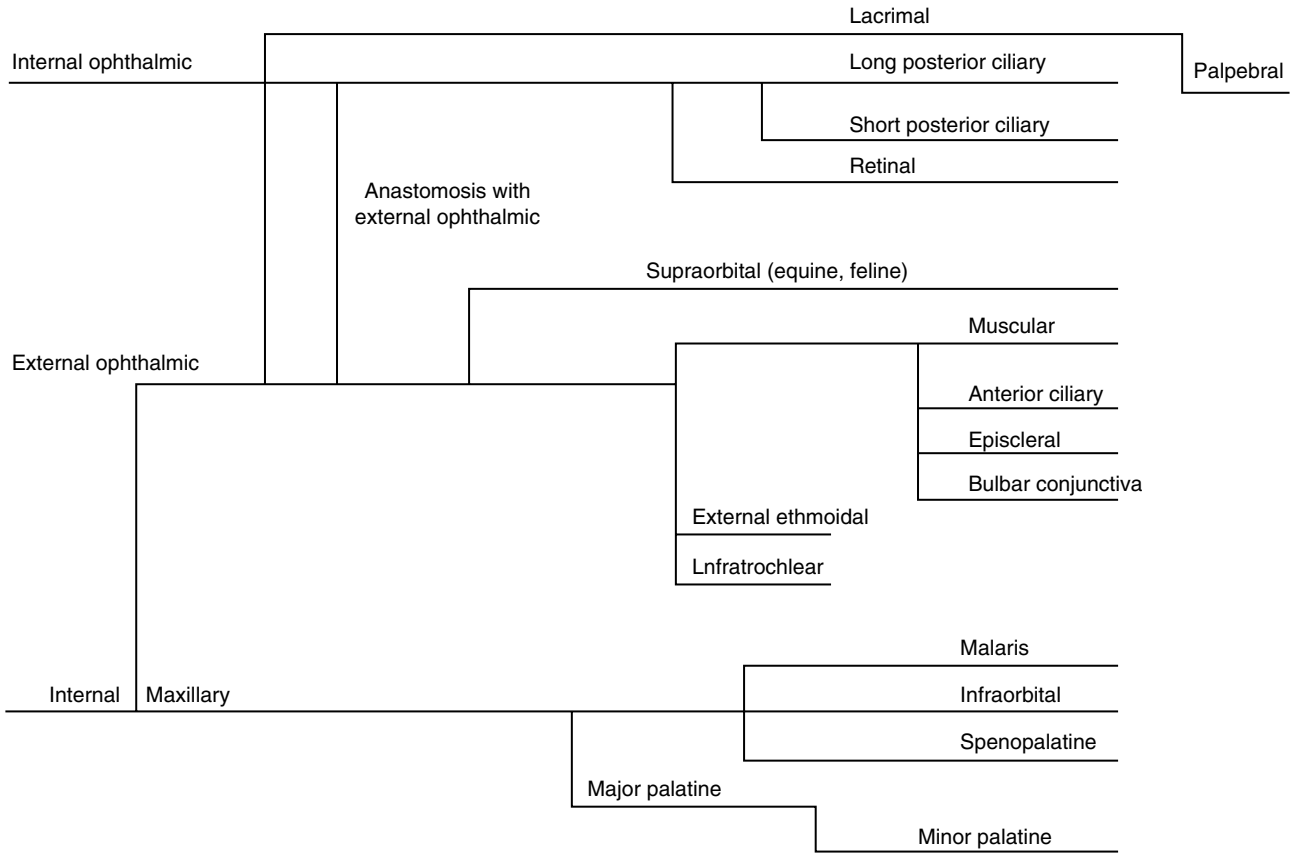

Figure 2.106 Arterial system of the mammalian orbit. Note that variations exist in different animals.

arteries form a network around the optic nerve, giving rise to small retinal arterioles that characterize the paurangiotic fundus of this species as well as giving rise to peridiscal choroidal branches (Simoens et al., 1996).

In small mammals, the arterial supply to the eye is comparable but can be understandably reduced. In the hamster, the primary blood supply for the eye is derived from the long posterior ciliary artery, which initially enters the optic nerve head region and separates into three branches, consisting of the medial and lateral long posterior ciliary arteries and the central retinal artery (Ninomiya & Inomata, 2005). The central retinal artery, in turn, branches into six radiating arterioles, which characterize the holangiotic fundus of this animal.

Venous drainage of the eye varies considerably among domestic animals (Fig. 2.107; Prince et al., 1960). In the dog, the two main venous channels within the orbit are the supraorbital and the inferior orbital veins. The lacrimal, superior vortex, ethmoidal, and several muscular veins empty into a large dilation of the supraorbital vein. The inferior vortex and malaris veins empty into the inferior orbital veins, which anastomose anteriorly and join the supraorbital dilation at the apex of the orbit posteriorly. Two prominent veins drain the supraorbital dilation: the orbital vein, which enters the intracranial system; and an internal maxillary vein, which connects to the external jugular vein (Prince et al., 1960).

The cat has an external rete or vascular network that is more venous than arterial (Prince et al., 1960). The anterior ciliary veins, four vortex veins, and a pair of fine long posterior veins empty into the rete (Tousimis, 1963). The inferior vortex vein and anterior ciliary veins initially join the inferior orbital veins, and the superior vortex vein drains initially into the superior orbital veins. The rete is drained by a large ophthalmic vein, which passes into the external jugular. The supraorbital vein also empties anteriorly into the facial vein via the angular and inferior orbital veins, which eventually empty into the internal jugular vein (Prince et al., 1960).

In the horse, the principal venous channels of the eye consist of the ophthalmic, orbital, supraorbital, and reflex veins. The dorsal ophthalmic vein receives blood from the superior vortex, palpebral, and lacrimal veins (Fig. 2.108). The dorsal ophthalmic vein is joined posteriorly by the anterior ciliary,

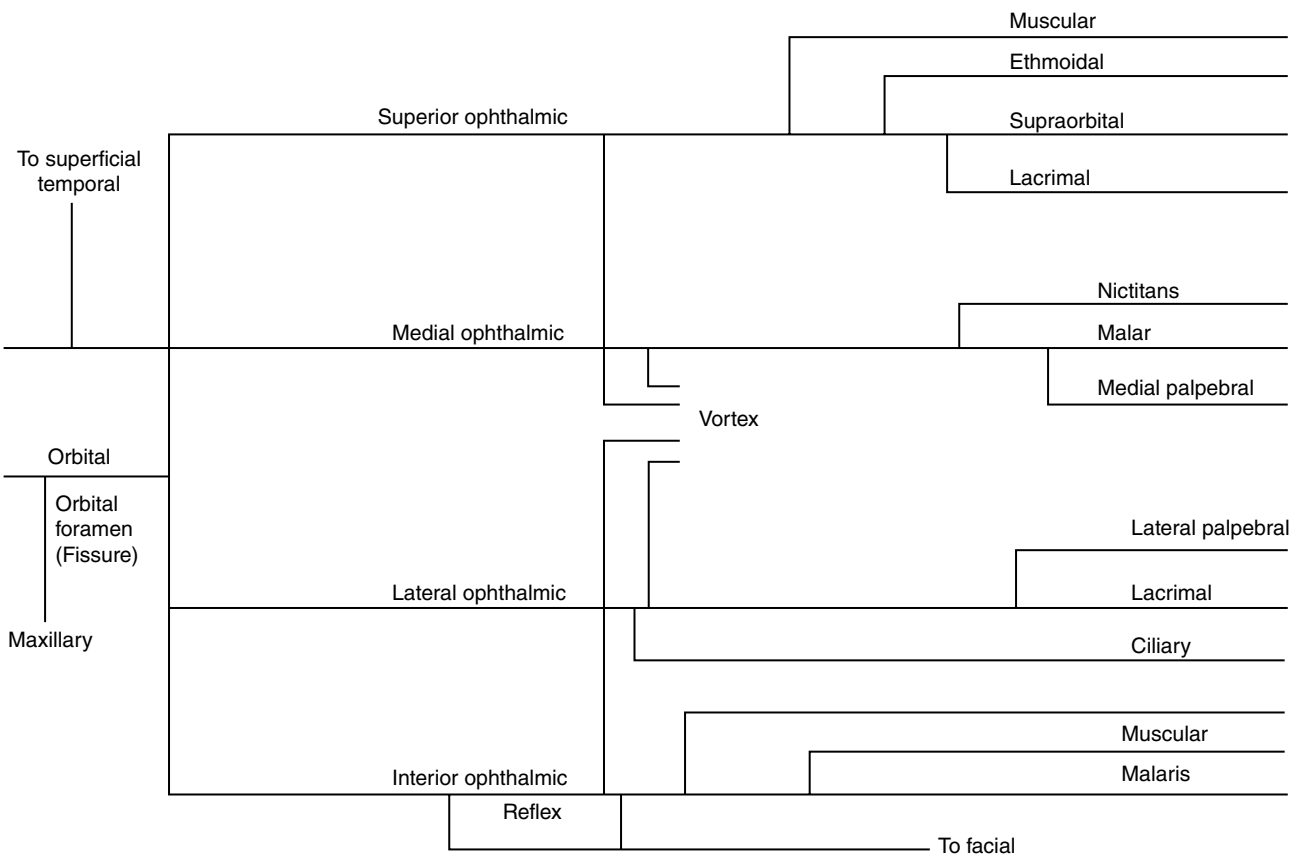

Figure 2.107 Venous system of the mammalian orbit. (*Source:* Modified from Prince, J.H., Diesen, C.D., Eglitis, I. & Ruskell, G.L. (1960) *Anatomy and Histology of the Eye and Orbit in Domestic Animals*. Springfield, IL: Charles C. Thomas. Reproduced with permission of Charles C. Thomas Publisher.)

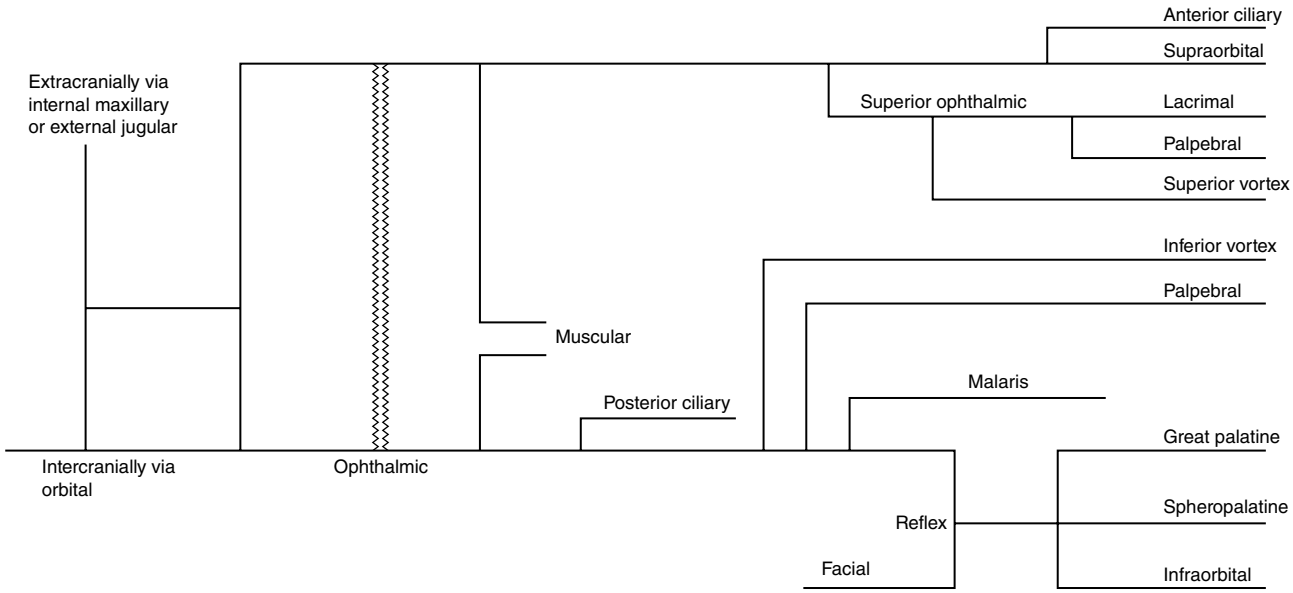

Figure 2.108 Venous system of the equine orbit. (*Source:* Modified from Prince, J.H., Diesen, C.D., Eglitis, I. & Ruskell, G.L. (1960) *Anatomy and Histology of the Eye and Orbit in Domestic Animals*. Springfield, IL: Charles C. Thomas. Reproduced with permission of Charles C. Thomas Publisher.)

supraorbital, muscularis, infratrochlear veins, and ultimately, the ophthalmic vein at the apex of the orbit, at which point blood is then drained intracranially by the orbital vein and extracranially by the internal maxillary vein. The ophthalmic vein also passes anteriorly to become the reflex vein after first receiving the inferior vortex veins via muscular veins, posterior ciliary veins, inferior vortex veins, and palpebral veins (Prince et al., 1960). The reflex vein receives the great palatine, sphenopalatine, and infraorbital veins before joining the facial vein.

References

Adam, W.S., Calhoun, M.L., Smith, E.M. & Stinson, A.W. (1970) *Microscopic Anatomy of the Dog: A Photogr* Springfield, IL: Charles C. Thomas.

Alario, A.F. & Pirie, C.G. (2013a) Intra and inter-user reliability of central corneal thickness measurements obtained in healthy feline eyes using a portable spectral-domain optical coherence tomography device. *Veterinary Ophthalmology*, **16**, 446–450.

Alario, A.F. & Pirie, C.G. (2013b) A spectral-domain optical coherence tomography device provides reliable corneal pachymetry measurements in canine eyes. *Veterinary Record*, **172**, 605–608.

Alario, A.F. & Pirie, C.G. (2014a) Reliability of manual measurements of corneal thickness obtained from healthy canine eyes using spectral-domain optical coherence tomography (SD-OCT). *Canadian Journal of Veterinary Research*, **78**, 221–225.

Alario, A.F. & Pirie, C.G. (2014b) Central corneal thickness measurements in normal dogs: a comparison between ultrasound pachymetry and optical coherence tomography. *Veterinary Ophthalmology*, **17**, 207–211.

Ali, M.J., Rehorek, S.J. & Paulsen, F. (2019) A major review on disorders of the animal lacrimal drainage systems: Evolutionary perspectives and comparisons with humans. *Annals of Anatomy*, **224**, 102–112.

Allen, L., Burian, H.M. & Braley, A.E. (1955) The anterior border ring of Schwalbe and the trabecular zone. *A.M.A. Archives of Ophthalmology*, **53**, 799–806.

Allingham, R.R., de Kater, A.W., Anderson, P.J., et al. (1989) Relationship between outflow facility and inner wall pores and vacuoles in Schlemm's canal. *Investigative Ophthalmology & Visual Science*, **30**(Suppl.), 222.

Anderson, B.G. & Anderson, W.D. (1977) Vasculature of the equine and canine iris. *American Journal of Veterinary Research*, **38**, 1791–1799.

Anderson, D.R. & Baverman, S. (1976) Reevaluation of the optic disk vasculature. *American Journal of Ophthalmology*, **82**, 165–174.

Andrew, S., Ramsey, D.T., Hauptman, J.G. & Brooks, D.E. (2001) Density of corneal endothelial cells and corneal thickness in eyes of euthanized horses. *American Journal of Veterinary Research*, **62**, 479–482.

Ashton, N. (1960) The exit of the aqueous. *Transactions of the Ophthalmological Societies of the United Kingdom*, **80**, 379–421.

Aughey, E. & Frye, F.L. (2001) Special senses. In: *Comparative Veterinary Histology with Clinical Correlates* (eds Aughey, E. & Frye, F.L.), p. 228. Ames, IA: Iowa State University Press.

Auker, C.R., Parver, L.M., Doyle, T. & Carpenter, D.O. (1982) Choroidal blood flow. I. Ocular tissue temperature as a measure of flow. *Archives of Ophthalmology*, **100**, 1323–1326.

Balazs, E.A., Toth, L.Z., Eckl, E.A. & Mitchell, A.P. (1964) Studies on the structure of the vitreous body: XII. Cytological and histochemical studies on the cortical tissue layer. *Experimental Eye Research*, **3**, 57–71.

Banks, W.J. (1993) Eye and ear. In: *Applied Veterinary Histology*. (ed. Banks, W.J.), pp.484–488. St Louis, MO: Mosby–Year book Inc.

Barrie, K.P., Gum, G.G., Samuelson, D.A. & Gelatt, K.N. (1985) Quantitation of uveoscleral outflow in normotensive and glaucomatous Beagles by H-labeled dextran. *American Journal of Veterinary Research*, **46**, 84–88.

Beauchemin, M.L. (1974) The fine structure of the pig's retina. *Albrecht von Graefes Archiv fur klinische und experimentelle Ophthalmologie*, **190**, 27–45.

Beazley, L.D. & Dunlop, S.A. (1983) The evolution of an area centralis and visual streak in the marsupial, *Setonix brachyurus*. *Journal of Comparative Neurology*, **216**, 211–231.

Bedford, P.C.G. & Grierson, I. (1986) Aqueous drainage in the dog. *Research in Veterinary Science*, **41**, 172–186.

Beltran, W.A., Cideciyan, A.V., Guziewicz, K.E., et al. (2014) Canine retina has a primate fovea-like bouquet of cone photoreceptors which is affected by inherited macular degenerations. *PLoS One*, **9**, e90390.

Benedetti, E.L., Dunia, I., Bentzel, C.J., et al. (1976) A portrait of plasma membrane specializations in eye lens epithelium and fibers. *Biochimica et biophysica Acta*, **157**, 353.

Bennett, A.T. & Cuthill, I.C. (1994) Ultraviolet vision in birds: what is its function? *Vision Research*, **34**, 1471–1478.

Bill, A. (1968) A method to determine osmotically effective albumin and gamma globulin concentrations in tissue fluids, its application to the uvea and a note on the effects of capillary "leaks" on tissue fluid dynamics. *Acta Physiologica Scandinavica*, **73**, 511–522.

Bill, A. (1975a) Blood circulation and fluid dynamics in the eye. *Physiological Reviews*, **55**, 383–417.

Bill, A. (1975b) The drainage of aqueous humor. *Investigative Ophthalmology*, **14**, 1–6.

Bill, A. (1985) Some aspects of the ocular circulation. *Investigative Ophthalmology & Visual Science*, **26**, 410–424.

Bill, A. & Phillips, C.I. (1971) Uveoscleral drainage of aqueous humor in human eyes. *Experimental Eye Research*, **12**, 275–281.

Bishop, P.N., Takanosu, M., Le Goff, M. & Mayne, R. (2002) The role of the posterior ciliary body in the biosynthesis of vitreous humor. *Eye*, **16**, 454–460.

Bloomfield, S.A. & Völgyi, B. (2009) The diverse functional roles and regulation of neuronal gap junctions in the retina. *Nature Reviews Neuroscience*, **10**, 495–506.

Blumcke, S. & Morgenroth, K. (1976) The stereo ultrastructure of the external and internal surface of the cornea. *Journal of Ultrastructure Research*, **18**, 502–518.

Borcherding, M.S., Blacik, L.J., Sittig, R.A., et al. (1978) Proteoglycans and collagen fibre organization in human corneoscleral tissue. *Experimental Eye Research*, **21**, 59–70.

Bourges-Abella, N., Raymond-Letron, I., Diquelou, A., et al. (2007) Comparison of cytologic and histologic evaluations of conjunctiva in normal equine eye. *Veterinary Ophthalmology*, **10**, 12–18.

Boycott, B.B., Hopkins, J.M. & Sperling, H.G. (1987) Cone connections of the horizontal cells of the Rhesus monkey's retina. *Proceedings of the Royal Society of London. Series B. Biological Sciences*, **229**, 345–379.

Boycott, B.B. & Wassle, H. (1974) The morphological types of ganglion cells of the domestic cat's retina. *Journal of Physiology*, **226**, 397–400.

Braekevelt, C.R. (1986) The retinal epithelial fine structure in the grey seal. *Acta Anatomica*, **127**, 255–261.

Braekevelt, C.R. (1990a) The retinal epithelial fine structure in the domestic cat. *Anatomia, Histologia, Embryologia*, **19**, 58–66.

Braekevelt, C.R. (1990b) Retinal pigment epithelial fine structure in the red-tailed hawk (*Buto jamaicensis*). *Anatomia, Histologia, Embryologia*, **21**, 48–56.

Braekevelt, C.R. (1991) Fine structure of the pecten oculi of the red-tailed hawk *(Buteo jamaicensis)*. *Anatomia, Histologia, Embryologia*, **20**, 354–362.

Braekevelt, C.R. (1993a) Fine structure of the tapetum lucidum of the paca Cuniculus paca. *Acta Anatomica* (Basel), **146**, 244–50.

Braekevelt, C.R. (1993b) Fine structure of the retinal photoreceptors of the great horned owl (*Bubo virginianus*). *Histology and Histopathology*, **8**, 25–34.

Braekevelt, C.R. (1993c) Retinal photoreceptor fine structure in the red-tailed hawk (*Buteo jamaicensis*). *Anatomia, Histologia, Embryologia*, **22**, 222–232.

Braekevelt, C.R. (1993d) Fine structure of the pecten oculi in the great horned owl (*Bubo virginianus*). *Histology and Histopathology*, **8**, 9–15.

Braekevelt, C.R. (1994) Fine structure of the pecten oculi in the American crow *(Corvus brachyrhynchos)*. *Anatomia, Histologia, Embryologia*, **23**, 357–366.

Braekevelt, C.R. (1998a) Fine structure of the retinal pigment epithelium (RPE) of the emu (*Dromaius novaehollandiae*). *Tissue and Cell*, **30**, 149–156.

Braekevelt, C.R. (1998b) Fine structure of the pecten oculi of the emu (*Dromaius novaehollandiae*). *Tissue and Cell*, **30**, 157–165.

Braekevelt, C.R. & Thorlakson, I.J. (1993) Fine structure of the retinal pigment epithelium of the great horned owl *(Bubo virginianus)*. *Histology and Histopathology*, **8**, 17–23.

Bravo, H. & Inzunza, O. (1985) The oculomotor nucleus, not the abducent, innervates the muscles which advance the nictitating membrane in birds. *Acta Anatomica*, **122**, 99–104.

Brooks, D.E., Blocker, TL, Samuelson, DA, et al. (1995b) Histomorphometry of the optic nerves of normal horses and horses with glaucoma. *Veterinary & Comparative Ophthalmology*, **5**, 193–210.

Brooks, D.E., Komaromy, A.M. & Kallberg, M.E. (1999) Comparative retinal ganglion cell and optic nerve morphology. *Veterinary Ophthalmology*, **2**, 3–11.

Brooks, D.E., Samuelson, D.A. & Gelatt, K.N. (1989) Morphologic changes in the lamina cribrosa of Beagle dogs with primary open angle glaucoma. *American Journal of Veterinary Research*, **50**, 908–914.

Brooks, D.E., Strubbe, D.T., Kubilis, P.S., et al. (1995a) Histomorphometry of the optic nerves of normal dogs and dogs with hereditary glaucoma. *Experimental Eye Research*, **60**, 71–89.

Brooks, D.E., Strubbe, DT, Myrick, T, et al. (1994) Histomorphometry of the equine scleral lamina cribrosa. *Veterinary & Comparative Ophthalmology*, **4**, 184–192.

Brown, K.T. (1968) The electroretinogram: its components and their origins. *Vision Research*, **l8**, 633–677.

Bruesch, S. & Arey, L. (1942) The number of myelinated and unmyelinated fibers in the optic nerve of vertebrates. *Journal of Comparative Neurology*, **77**, 631–665.

Brunton, C.E. (1938) Smooth muscle of the periorbita and the mechanism of exophthalmos. *British Journal of Ophthalmology*, **22**, 257–268.

Buck, R.C. (1983) Ultrastructural characteristics associated with the anchoring of corneal epithelium in several classes of vertebrates. *Journal of Anatomy*, **137**, 743–756.

Buttery, R.G., Hinrichsen, C.F.L., Weller, W.L., et al. (1991) How thick should a retina be? A comparative study of mammalian species with and without intraretinal vasculature. *Vision Research*, **31**, 169–187.

Cain, S.A., Morgan. A., Sherratt, M.J., et al. (2006) Proteomic analysis of fibrillin-rich microfibrils. *Proteomic*, **6**, 111–122.

Canavese, B., Fazzini, U. & Colitti, M. (1994) Morphometric analysis of the scleral bony ring with different numbers of ossicles in the eye of *Coturnix japonica*. *Anatomia, Histologia, Embryologia*, **23**, 128–136.

Castoro, J.A., Bettelheim, A.A. & Bettelheim, F.A. (1988) Water concentration gradients across bovine cornea. *Investigative Ophthalmology & Visual Science*, **29**, 963–968.

Castro-Correia, J. (1967) Studies on the innervation of the uveal tract. *Ophthalmologica*, **154**, 497–520.

Chandler, M.J., Smith, P.J., Samuelson, D.A., et al. (1999) Photoreceptor density of the domestic pig retina. *Veterinary Ophthalmology*, **2**, 179–184.

Chang, S.K. & Straznicky, C. (1992) The generation and changing retinal distribution of displaced amacrine cells in *Bufo marinus* from metamorphosis to adult. *Anatomy and Embryology*, **186**, 175–181.

Chase, J. (1982) The evolution of retinal vascularization in mammals: a comparison of vascular and avascular retinae. *Ophthalmology*, **89**, 1518–1525.

Chauhan, D.S. & Marshall, J. (1999) The interpretation of optical coherence tomography images of the retina. *Investigative Ophthalmology & Visual Science*, **40**, 2332–2342.

Chi, H.H., Teng, C.C. & Katzin, H.M. (1960) Healing process in the mechanical denudation of the corneal endothelium. *American Journal of Ophthalmology*, **49**, 693–703.

Chijiiwa, T., Ishibashi, T. & Inomata, H. (1990) Histological study of choroidal melanocytes in animals with tapetum lucidum cellulosum. *Graefe's Archive for Clinical and Experimental Ophthalmology*, **228**, 161–168.

Chodosh, J., Nordquist, R.E. & Kennedy, R.C. (1998) Comparative anatomy of mammalian conjunctival lymphoid tissue: a putative mucosal immune site. *Developmental and Comparative Immunology*, **22**, 621–630.

Chung, C.W., Tigges, M. & Stone, R.A. (1996) Peptidergic innervation of the primate meibomian gland. *Investigative Ophthalmology & Visual Science*, **37**, 238–245.

Cintron, C. & Covington, H.I. (1990) Proteoglycan distribution in developing rabbit cornea. *Journal of Histochemistry and Cytochemistry*, **38**, 675–680.

Cleymaet, A.M., Hess, A.M. & Freeman, K.S. (2016) Comparison between Pentacam-HR and optical coherence tomography central corneal thickness measurements in healthy feline eyes. *Veterinary Ophthalmology*, **19**, 105–114.

Cohen, A.I. (1969) Rods and cones and the problem of visual excitation. In: *The Retina-Morphology, Function and Clinical Characteristics* (eds Straatsma, B.R., Hall, M.O. & Allen, R.A.), pp. 31–62. Los Angeles, CA: University of California Press.

Cohen, E. & Sterling, P. (1990) Convergence and divergence of cones onto bipolar cells in the central area of cat retina. *Philosophical transactions of the Royal Society of London. Series B. Biological Sciences*, **330**, 323–328.

Coimbra, J.P., Hart, N.S., Collin, S.P. & Manger, P.R. (2013) Scene from above: retinal ganglion cell topography and spatial resolving power in the giraffe (*Giraffa camelopardalis*). *Journal of Comparative Neurology*, **15**, 2042–2057.

Collin, S.P. & Collin, H.B. (2006) The corneal epithelial surface in the eyes of vertebrates: environmental and evolutionary influences on structure and function. *Journal of Morphology*, **267**, 273–291.

Constantinescu, G.M. & McClure, R.C. (1990) Anatomy of the orbital fasciae and third eyelid in dogs. *American Journal of Veterinary Research*, **51**, 260–263.

Costa, B.L., Pessoa, V.F., Bousfield, J.D., et al. (1987) Unusual distribution of ganglion cells in the retina on the three-toed sloth *(Bradypus variegatus). Brazilian Journal of Medical and Biological Research*, **20**, 741–748.

Crumley, W., Gionfriddo, J.R. & Radeki, S.V. (2009) Relationship of the iridocorneal angle, as measured using ultrasound biomicroscopy, with post-operative increases in intraocular pressure post-phacoemulsification in dogs. *Veterinary Ophthalmology*, **12**, 22–27.

Curcio, C.A. & Allen, K.A. (1990) Topography of ganglion cells in human retina. *Journal of Comparative Neurology*, **300**, 5–25.

Curtis, E.L. & Miller, R.C. (1938) The sclerotic ring of North American birds. *The Auk*, **55**, 225–243.

Daniel, W.J., Noonan, N.E. & Gelatt, K.N. (1984) Isolation and characterization of the crystallins of the normal and cataractous canine lens. *Current Eye Research*, **3**, 911–922.

Dawson, D. G., Ubels, J.L. & Edelhauser, H.F. (2011) Cornea and Sclera. In: *Adler's Physiology of the Eye* (eds Levin, L.A.,

Nilsson, S.F.E., Ver Hoeve, J. & Wu, S.M.), 11th ed., p. 83. New York: Saunders Elsevier.
de Kater, A.W., Spurr-Michand, S.J. & Gibson, I.K. (1990) Localization of smooth muscle myosin-containing cells in the aqueous outflow pathway. *Investigative Ophthalmology & Visual Science*, **31**, 347–353.
DeStefano, M.E. & Mugnaini, E. (1997) Fine structure of the choroidal coat of the avian eye. *Investigative Ophthalmology & Visual Science*, **38**, 1241–1260.
Ding, C., Huang, J., Macveigh-Aloni, M., et al. (2011) Not all lacrimal epithelial cells are created equal-heterogeneity of the rabbit lacrimal gland and differential secretion. *Current Eye Research*, **36**, 971–978.
Dische, Z. & Murty, V.L.N. (1974) An insoluble structural glycoprotein: a major constituent of the zonula zinni. *Investigative Ophthalmology & Visual Science*, **13**, 991.
Distler, C. & Dreher, Z. (1996) Glial cells of the monkey retina. II. Müller cells. *Vision Research*, **36**, 2381–2394.
Doane, K.J., Yang, G. & Birk, D.E. (1992) Corneal cell-matrix interactions: type VI collagen promotes adhesion and spreading of corneal fibroblasts. *Experimental Eye Research*, **200**, 490–499.
Dollery, C.T., Bulpitt, C.J. & Kohner, E.M. (1969) Oxygen supply to the retina and choroidal circulation at normal and increased arterial oxygen tensions. *Investigative Ophthalmology*, **8**, 588–594.
Do Nascimento, J.L., Do Nascimento, R.S., Damasceno, B.A., et al. (1991) The neurons of the retinal ganglion cell layer of the Guinea pig: quantitative analysis of their distribution and size. *Brazilian Journal of Medical and Biological Research*, **24**, 199–214.
Donovan, R.H., Carpenter, R.L., Schepens, C.L. & Tolentino, F.I. (1974a) Histology of the normal Collie eye. II. Uvea. *Annals of Ophthalmology*, **6**, 1175–1189.
Donovan, R.H., Carpenter, R.L., Schepens, C.L. & Tolentino, F.I. (1974b) Histology of the normal Collie eye. III. Lens, retina and optic nerve. *Annals of Ophthalmology*, **6**, 1299–1307.
Doughty, M.J. (2002) Surface features and morphology of bulbar conjunctival cells of bovine eyes obtained from a slaughterhouse: a scanning electron microscope and impression cytology study. *Current Eye Research*, **24**, 341–353.
Dowling, J.E. & Werblin, F.S. (1971) Synaptic organization of the vertebrate retina. *Vision Research*, **3**(Suppl. 3), 1–15.
Draper, C.E., Adeghate, E., Lawrence, P.A., et al. (1998) Age-related changes in morphology and secretory responses of male rat lacrimal gland. *Journal of Autonomic Nervous System*, **69**, 173–183.
Duke-Elder, S. (1958) *System of Ophthalmology. Vol. I. The Eye in Evolution*. London: Henry Kimpton.
Ehinger, B. (1966a) Adrenergic nerves to the eye and to related structures in man and the Cynomolgus monkey *(Macaca irus)*. *Investigative Ophthalmology*, **5**, 42–52.
Ehinger, B. (1966b) Distribution of adrenergic nerves in the eye and some related structures in the cat. *Acta Physiologica Scandinavica*, **66**, 123–128.
Eisner, G. (1975) Zue anatomie des glaskorpers. *Albrecht von Graefes Archiv fur klinische und experimentelle Ophthalmologie*, **193**, 33–56.
Eisner, G. (1988) Clinical anatomy of the vitreous. In: *Biomedical Foundations of Ophthalmology* (eds Duane, T.D. & Jaeger, E.A.), Vol. **1**, Chapter 16, pp. 1–34. Philadelphia, PA: J.B. Lippincott.
Eisner, G. & Bachmann, E. (1974a) Vergleichend morphologische spaltlampenuntersuchung des glaskorpers beim rind. *Albrecht von Graefes Archiv fur klinische und experimentelle Ophthalmologie*, **191**, 329–342.
Eisner, G. & Bachmann, E. (1974b) Vergleichend morphologische spaltlampuntersuchung des glaskorpers beim pferd. *Albrecht von Graefes Archiv fur klinische und experimentelle Ophthalmologie*, **192**, 1–8.
Eisner, G. & Bachmann, E. (1974c) Vergleichend morphologische spaltlampenuntersuchung des glaskorpers von schaf, schwein, hund, affen und kaninchen. *Albrecht von Graefes Archiv fur klinische und experimentelle Ophthalmologie*, **192**, 9–17.
Eisner, G. & Bachmann, E. (1974d) Vergleichend morphologische spaltlempenuntersuchung des glaskorpers bei der katze. *Albrecht von Graefes Archiv fur klinische und experimentelle Ophthalmologie*, **191**, 343–350.
Enroth-Cugell, C. & Robson, J.G. (1966) The contrast sensitivity of retinal ganglion cells of the cat. *Journal of Physiology*, **187**, 517–522.
Evans, K.E. & McGreevy, P.D. (2007) The distribution of ganglion cells in the equine retina and its relationship to skull morphology. *Anatomia, Histologia, Embryologia*, **36**, 151–156.
Farnsworth, P.N., Mauriello, J.A., Burke-Gadomski, P., et al. (1976) Surface ultrastructure of the human lens capsule and zonular attachments. *Investigative Ophthalmology & Visual Science*, **15**, 36–40.
Faulborn, J. & Bowald, S. (1982) Combined macroscopic light microscopic, scanning, and transmission electron microscopic investigation of the vitreous body. II. The anterior vitreous cortex. *Ophthalmic Research*, **14**, 117–123.
Feeney-Burns, L., Hilderbrand, E.S. & Eldridge, S. (1984) Aging human RPE: morphometric analysis of macular, equatorial, and peripheral cells. *Investigative Ophthalmology & Visual Science*, **25**, 195–200.
Fine, B.S. & Yanoff, M. (1979) *Ocular Histology*. 2nd ed. New York: Harper & Row.
Fischer, Q.S. & Kirby, M.A. (1991) Number and distribution of retinal ganglion cells in anubis baboons (*Papio anubis*). *Brain, Behavior and Evolution*, **37**, 189–203.
Fitch, J.M., Birk, D.E., Linsenmayer, C., et al. (1991) Stromal assemblies containing collagen types IV and VI and fibronectin in the developing embryonic avian cornea. *Developmental Biology*, **144**, 379–391.
Fite, K.V. & Bengston, L. (1989) Aging and sex-related changes in the outer retina of Japanese quail. *Current Eye Research*, **8**, 1039–1048.

Fitzgibbon, T. & Funke, K. (1994) Retinal ganglion cell axon diameter spectrum of the cat: mean axon diameter varies according to retinal position. *Visual Neuroscience*, **11**, 425–439.

Fix, A.S. & Arp, L.H. (1991) Morphologic characterization of conjunctiva-associated lymphoid tissue in chickens. *American Journal of Veterinary Research*, **52**, 1852–1859.

Flocks, M. (1956) The anatomy of the trabecular meshwork as seen in tangential sections. *A.M.A. Archives of Ophthalmology*, **56**, 708–718.

Flugel, C., Tamm, E. & Lutjen-Drecoll, E. (1991) Different cell populations in bovine trabecular meshwork: an ultrastructural and immunocytochemical study. *Experimental Eye Research*, **52**, 681–690.

Frick, C.M. & Dubielzig, R.D. (2016) Short posterior ciliary artery anatomy in normal and acutely glaucomatous dogs. *Veterinary Ophthalmology*, **19**, 43–49.

Fritz, W. (1906) Uber die membrana descemets und das ligamentum pectinatum iridis bei den saugtieren und menschen. *Sitzungsberichte der Akademie der Wissenschaften zu Wien*, **115**, 485–568.

Fukuda, Y., Sugimoto, T. & Shirokawa, T. (1982) Strain differences in quantitative analysis of the rat optic nerve. *Experimental Neurology*, **75**, 525–532.

Funk, R. & Rohen, J.W. (1990) Scanning electron microscopic study on the vasculature of the human anterior eye segment. *Experimental Eye Research*, **51**, 651–661.

Gallego, A. (1986) Studies on horizontal cells and a note on microglial cells. *Progress in Retinal Research*, **5**, 165–206.

Gao, H. & Hollyfield, J.G. (1992) Aging of the human retina. Differential loss of neurons and retinal pigment epithelial cells. *Investigative Ophthalmology & Visual Science*, **33**, 1–17.

Garcia, G.A., Whitley, R.D., Samuelson, D.A., et al. (1986) Microsphere evaluation of aqueous outflow in the chicken eye. *Investigative Ophthalmology & Visual Science*, **27**(Suppl), Abstract 200.

Gartner, S. & Henkind, P. (1981) Aging and degeneration of the human macula. 1. Outer nuclear layer and photoreceptors. *British Journal of Ophthalmology*, **65**, 23–28.

Garzon-Ariza, A., Guisado, A., Galan, A., et al. (2017) Diurnal variations in intraocular pressure and central corneal thickness and the correlation between these factors in dogs. *Veterinary Ophthalmology*, **20**, 1–7.

Gekeler, F., Gmeiner, H., Volker, M., et al. (2007) Assessment of the posterior segment of the cat eye by optical coherence tomography (OCT). *Veterinary Ophthalmology*, **10**, 173–178.

Gelatt, K.N., Peiffer, R.L. Jr., Erickson, J.L. & Gum, G.G. (1975) Evaluation of tear formation in the dog, using a modification of the Schirmer tear test. *Journal of the American Veterinary Medical Association*, **166**, 368–370.

Gelatt, K.N. & Samuelson, D.A. (1982) Recurrent corneal erosions and epithelial dystrophy in the Boxer dog. *Journal of the American Animal Hospital Association*, **18**, 453–460.

Gelatt, K.N. & Samuelson, D.A. (1986) Collagen fiber organization in the iridocorneal angle of Beagles with inherited glaucoma. *Investigative Ophthalmology & Visual Science*, **27**(Suppl.), 310.

Gelatt, K.N. & Samuelson, D.A. (1998) The role of lens luxation in inherited glaucoma in the Beagle. *Animal Eye Research*, **17**, 1–8.

Geri, G.A., Kimsey, R.A. & Dvorak, C.A. (1982) Quantitative electron microscopic analysis of the optic nerve of the turtle, *Pseudemys*. *Journal of Comparative Neurology*, **207**, 99–103.

Gilger, B.C., Davidson, M.G. & Howard, P.B. (1998) Keratometry, ultrasonic biometry, and prediction of intraocular lens power in the feline eye. *American Journal Veterinary Research*, **59**, 131–134.

Gilger, B.C., Reeves, K.A. & Salmon, J.H. (2005) Ocular parameters related to drug delivery in the canine and equine eye: aqueous and vitreous humor volume and scleral surface area and thickness. *Veterinary Ophthalmology*, **8**, 265–269.

Gilger, B.C., Whitley, R.D., McLaughlin, S.A., et al. (1991) Canine corneal thickness measured by ultrasonic pachymetry. *American Journal of Veterinary Research*, **52**, 1570–1572.

Gilger, B.C., Wright, J.C., Whitley, R.D. & McLaughlin, S.A. (1993) Corneal thickness measured by ultrasonic pachymetry in cats. *American Journal of Veterinary Research*, **54**, 228–230.

Glasser, A. & Howland, H.C. (1995) *In vitro* changes in back vertex distance of chick and pigeon lenses: Differences and the effects of aging. *Vision Research*, **35**, 1813–1824.

Glasser, A., Murphy, C.J., Troilo, D. & Howland, H.C. (1995) The mechanism of lenticular accommodation in chicks. *Vision Research*, **35**, 1525–1540.

Gloor, B.P. (1974) Zur entwicklung des glaskorpers undder zonule: VI. Autoradiographische untersuchurgen zur entwicklung der zonule der maus mit ^{3}H-markeirten aminoauren und ^{3}H-glucose. *Albrecht von Graefes Archiv fur klinische und experimentelle Ophthalmologie*, **189**, 99–104.

Goes, R.M., Nader,H.B., Porcionatto, M.A., et al. (2005) Chondroitin sulfate proteoglycans are structural renewable constituents of the rabbit vitreous body. *Current Eye Research*, **30**, 405–413.

Goldman, D. (2014) Müller glial cell reprogramming and retina regeneration. *Nature Reviews Neuroscience*, **15**, 431–442.

Goller, T. & Weyrauch, K.D. (1993) Das Konjunktivalepithel des hundes. Licht- und elektronenmikroskopische untersuchungen. *Anatomischer Anzeiger*, **175**, 127–134.

Gong, H., Trinkaus-Randall, V. & Freddo, T.F. (1989) Ultrastructural localization of elastin in normal infant and adult trabecular meshwork using atropoelastin antibody. *Investigative Ophthalmology & Visual Science*, **30**(Suppl.), 204.

Gonzalez-Soriano, J., Rodriguez-Veiga, E, Maitinez-Sainx, P., et al. (1995) A quantitative study of ganglion cells in the German Shepherd dog retina. *Anatomia, Histologia, Embryologia*, **24**, 61–65.

Gordon, M.K., Foley, J.W., Birk, D.E., et al. (1994) Type V collagen and Bowman's membrane. Quantitation of mRNA

in corneal epithelium and stroma. *Journal of Biological Chemistry*, **269**, 2459–2466.
Guo, X. & Sugita, S. (2000) Topography of ganglion cells in the retina of the horse. *Journal of Veterinary Medical Science*, **62**, 1145–1150.
Guo, X. & Sugita, S. (2002) Quantitative analysis of the organization of the inner nuclear layer of the horse retina. *Journal of Veterinary Medical Science*, **64**, 847–849.
Grahn, B.H., Sisler, S. & Storey, E. (2005) Quantitative tear film and conjunctival goblet cell assessment of cats with corneal sequestra. *Veterinary Ophthalmology*, **8**, 167–170.
Grierson, I. & Lee, W.R. (1973) Erythrocyte phagocytosis in the human trabecular meshwork. *British Journal of Ophthalmology*, **57**, 400–415.
Grierson, I. & Lee, W.R. (1975) Acid mucopolysaccharides in the outflow apparatus. *Experimental Eye Research*, **21**, 417–431.
Grierson, I., Lee, W.R. & Abraham, S. (1977) Pathways for drainage of aqueous humor into Schlemm's canal. *Transactions of the Ophthalmological Societies of the United Kingdom*, **97**, 719–725.
Gum, G.G., Gelatt, K.N. & Esson, D. (2007) Ophthalmic physiology. In: *Veterinary Ophthalmology* (ed. Gelatt, K.N.), 4th ed., pp. 149–181. Ames, IA: Blackwell.
Gum, G.G., Samuelson, D.A. & Gelatt, K.N. (1992) Effect of hyaluronidase on aqueous outflow resistance in normal and glaucomatous dogs. *American Journal of Veterinary Research*, **53**, 767–770.
Gwin, R.M., Gelatt, K.N. & Chiou, C.Y. (1979) Adrenergic and cholinergic innervation of the anterior segment of the normal and glaucomatous dog. *Investigative Ophthalmology & Visual Science*, **18**, 674–682.
Harding, C., Baqchi, M., Weingieder, A., et al. (1974) A comparative study of corneal epithelial cell surfaces utilizing the scanning electron microscope. *Investigative Ophthalmology*, **13**, 906–912.
Hassell, J.R. & Birk, D.E. (2010) The molecular basis of corneal transparency. *Experimental Eye Research*, **91**, 326–335.
Hayashi, S., Osawa, T. & Tohyama, K. (2002) Comparative observations on corneas with special reference to Bowman's layer and Descemet's membrane in mammals and amphibians. *Journal of Morphology*, **254**, 247–258.
Hayreh, S.H. (1974) Anatomy and physiology of the optic nerve head. *Transactions—American Academy of Ophthalmology and Otolaryngology*, **78**, 240.
Hebel, R. (1976) Distribution of retinal ganglion cells in five mammalian species (pig, sheep, ox, horse, dog). *Anatomy and Embryology*, **150**, 45–51.
Hebel, R. & Holländer, H. (1979) Size and distribution of ganglion cells in the bovine retina. *Vision Research*, **19**, 667–674.
Henderson, T. (1926) The anatomy and physiology of accommodation in Mammalia. *Transactions of the Ophthalmological Societies of the United Kingdom*, **46**, 280–308.
Henderson, Z. (1985) Distribution of ganglion cells in the retina of adult pigmented ferret. *Brain Research*, **358**, 221–228.
Henkind, P. (1966) The retinal vascular system of the domestic cat. *Experimental Eye Research*, **5**, 10–20.
Herbig, L.E. & Eule, C.J. (2015) Central corneal thickness measurements and ultrasonographic study of the growing equine eye. *Veterinary Ophthalmology*, **18**, 462–471.
Hernandez-Merino, E., Kecova, H., Jacobson, S.J., et al. (2011) Spectral domain optical coherence tomography (SD-OCT) of the healthy female canine retina and optic nerve. *Veterinary Ophthalmology*, **14**, 400–405.
Hiraoka, M., Inoue, K., Ohtaka-Maruyama, C., et al. (2010) Intracapsular organization of ciliary zonules in monkey eyes. *Anatomical Record (Hoboken, N.J.: 2007)*, **293**, 1797–1804.
Hogan, M.J., Alvarado, J.A. & Weddell, J.E. (1971) *Histology of the Human Eye*. Philadelphia, PA: WB Saunders.
Hollander, H., Marakov, F., Stefani, F.H., et al. (1995) Evidence of constriction of optic nerve axons at the lamina cribrosa in the normotensive eye in humans and other mammals. *Ophthalmic Research*, **27**, 296–309.
Hughes, A. (1975) A quantitative analysis of the cat retinal ganglion cell topography. *Journal of Comparative Neurology*, **163**, 107–128.
Hwang, K., Huan, F. & Kim, D.J. (2011) Muscle fiber types of human orbicularis oculi muscle. *Journal of Craniofacial Surgery*, **22**, 1827–1830.
Hyvarinen, L. (1967) Vascular structures of the rabbit retina. *Acta Ophthalmologica*, **45**, 852–861.
Inomata, H., Bill, A. & Smelzer, G. (1972) Aqueous humor pathways through the trabecular meshwork and into Schlemm's canal in the cynomolgous Cynomolgous monkey (*Macaca irus*). *American Journal of Ophthalmology*, **73**, 760–798.
Iskandar, L.A., Samuelson, D.A. & Whitley, R.D. (1988) The pecten and the posterior circulation in the avian eye. *Investigative Ophthalmology & Visual Science Supplement*, **29**, 381.
Iuvone, P.M. (1986) Neurotransmitters and neuromodulators in the retina-regulation, interaction, and cellular effects. In: *The Retina—A Model for Cell Biology Studies. Part II* (eds Adler, R. & Farber, D.). Orlando, FL: Academic Press.
Jacobson, B. (1976) Biosynthesis of hyaluronic acid in the vitreous: V. Studies on a particular hyalocyte glycosyl transferase. *Experimental Eye Research*, **27**, 247–249.
Jaffe, N.S. (1969) *The Vitreous in Clinical Ophthalmology*, 1st ed. St. Louis, MO: CV Mosby.
Jiang, Z., Yang, J., Purpura, L.A., et al. (2014) Glycinergic feedback enhances synaptic gain in the distal retina. *Journal of Physiology*, **592**, 1479–1492.
Jakus, M.A. (1956) Studies on the cornea. II: the fine structure of Descemet's membrane. *Journal of Biophysical and Biochemical Cytology*, **2**, 243–250.
Jester, J.V. (2008) Corneal crystallins and the development of cellular transparency. *Seminars in Cell & Developmental Biology*, **19**, 82–93.
Jester, J.V., Nicolaides, N. & Smith, R.E. (1981) Meibomian gland studies: Histologic and ultrasound investigations. *Investigative Ophthalmology & Visual Science*, **20**, 537–547.

Johanssen, J.O. (1987) The lamina cribrosa in the eyes of rats, hamsters, gerbils and Guinea pigs. *Acta Anatomica*, **128**, 55–62.

Johnson, M., Johnson, D.H., Kamm, R.D., et al. (1990) The filtration characteristics of the aqueous outflow system. *Experimental Eye Research*, **50**, 407–418.

Jonas, J., Müller-Bergh, J., Schlotzer-Schrehardt, U., et al. (1990) Histomorphometry of the human optic nerve. *Investigative Ophthalmology & Visual Science*, **31**, 736–744.

Jonas, J., Schmidt, A.M., Müller-Bergh, J.A., et al. (1992) Human optic nerve fiber count and optic disc size. *Investigative Ophthalmology & Visual Science*, **33**, 2012–2018.

Kaas, J.H., Hall, W.C., Kilackey, H., et al. (1972) Receptor pedicle density in the cat's retina. *Brain Research*, **42**, 496–497.

Kafarnik C., Fritsche, J. & Reese, S. (2007) *In vivo* confocal microscopy in the normal corneas of cats, dogs and birds. *Veterinary Ophthalmology*, **10**, 222–230.

Kayes, J. (1967) Pore structure of the inner wall of Schlemm's canal. *Investigative Ophthalmology*, **6**, 381–394.

Khodadoust, A.A., Silverstein, A.M., Kenyon, D.R. & Dowling, J.E. (1968) Adhesion of regeneration corneal epithelium: the role of basement membrane. *American Journal of Ophthalmology*, **65**, 339–348.

Kiama, S.G., Bhattacharjee, J., Maina, J.N., et al. (1994) A scanning electron microscope study of the pecten oculi of the black kite *(Milvus migrans)*: possible involvement of melanosomes in protecting the pecten against damage by ultraviolet light. *Journal of Anatomy*, **185**, 637–642.

King-Smith, P.E. (1969) Absorption spectra and function of coloured oil drops in the pigeon retina. *Vision Research*, **9**, 1391–1399.

Kirby, M.A., Clift-Fornsberg, L., Wilson, P.D., et al. (1982) Quantitative analysis of the optic nerve of the North American opossum *(Didelphis virginiana)*: an electron microscopic study. *Journal of Comparative Neurology*, **211**, 318–327.

Knepper, P.A., Goosens, W., Hvizd, M., et al. (1996) Glycosaminoglycans of the human trabecular meshwork in primary open angle glaucoma. *Investigative Ophthalmology & Visual Science*, **37**, 1360–1367.

Knop, E. & Knop, N. (2005) The role of eye-associated lymphoid tissue in corneal immune protection. *Journal of Anatomy*, **206**, 272–285.

Koch, S.A. & Rubin, L.F. (1972) Distribution of cones in retina of the normal dog. *American Journal of Veterinary Research*, **33**, 361–363.

Kolb, H. (1974) The connections between horizontal cells and photoreceptors in the retina of the cat: electron microscopy of Golgi preparations. *Journal of Comparative Neurology*, **155**, 1–14.

Kolb, H. (1997) Amacrine cells of the mammalian retina: neurocircuitry and functional roles. *Eye*, **11**, 904–923.

Kolb, H. & Famiglietti, E.V. (1974) Rods and cone pathways in the inner plexiform layer of cat retina. *Science*, **186**, 47–49.

Kolb, H., Linberg, K.A. & Fisher, S.K. (1992) Neurons of the human retina—a Golgi study. *Journal of Comparative Neurology*, **318**, 147–187.

Kolb, H. & Nelson, R. (1996) Hyperpolarizing, small-field, amacrine cells in cone pathways of cat retina. *Journal of Comparative Neurology*, **371**, 415–436.

Konrade, K.A. Hoffman, A.R., Ramey, K.C., et al. (2012) Refractive states of eyes and associations between ametropia and age, breed, and axial globe length in domestic cats. *American Journal of Veterinary Research*, **73**, 279–284.

Koseki, T. (1992) Ultrastructural studies of the lamina suprachoroidea in the human eye. *Nippon Ganka Gakkai Zasshi*, **96**, 757–766.

Krinkle, A., Frohlich, E. & Krinkle, G. (1985) An analysis of the distribution of the myelinated nerve fibers in the optic fascicles of a Beagle dog. *Experientia*, **41**, 464–465.

Kuszak, J.R., Sivak, J.G. & Weerheim, J.A. (1991) Lens optical quality is a direct function of lens sutural architecture. *Investigative Ophthalmology & Visual Science*, **32**, 2119–2129.

Kuwabara, T. (1979) Species differences in the retinal pigment epithelium. In: *The Retinal Pigment Epithelium* (eds Zinn, G.M. & Marmor, M.F.), pp. 58–82. Cambridge, MA: Harvard Press.

Kuwabara, T. & Imaizumi, M. (1974) Denucleation process of the lens. *Investigative Ophthalmology*, **13**, 973–981.

Lai, Y.L. (1980) Outward movement of photoreceptor cells in normal rat retina. *Investigative Ophthalmology & Visual Science*, **19**, 849–856.

Laing, R.A., Sanstrom, M.M., Berruspi, A.R., et al. (1976) Changes in the corneal endothelium as a function of age. *Experimental Eye Research*, **22**, 587–594.

Lau, K.C., So, K.F., Campbell, G. & Lieberman, A.R. (1992) Pupillary constriction in response to light in rodents, which does not depend on central neural pathways. *Journal of the Neurological Sciences*, **113**, 70–79.

Ledbetter E.C. & Scarlett J.M. (2009) *In vivo* confocal microscopy of the normal equine cornea and limbus. *Veterinary Ophthalmology*, **12**, 57–64.

Lee, W.R. & Grierson, I. (1975) Pressure effects on the endothelium of the trabecular wall of Schlemm's canal: a study by scanning electron microscopy. *Albrecht von Graefes Archiv fur klinische und experimentelle Ophthalmologie*, **196**, 255–265.

Levick, W.R. (1975) Form and function of cat retinal ganglion cells. *Nature*, **254**, 659–662.

Levy, S.G., Moss, J., Sawada, H., et al. (1996) The composition of wide-spaced collagen in normal and diseased Descemet's membrane. *Current Eye Research*, **15**, 45–52.

Linberg, K.A., Suemune, S. & Fisher, S.K. (1996) Retinal neurons of the California ground squirrel, *Spermophilus beecheyi*: a Golgi study. *Journal of Comparative Neurology*, **365**, 173–216.

Linsenmayer, T.F., Gibney, E., Igoe, F., et al. (1993) Type V collagen: molecular structure and fibrillar organization of the chicken alpha 1 (V) NH2-terminal domain, a putative

regulator of corneal fibrillogenesis. *Journal of Cell Biology*, **121**, 1181–1189.
Lutjen-Decoll, E. & Rohen, J.W. (1992) Functional morphology of the trabecular meshwork. In: *Biomedical Foundations of Ophthalmology* (eds Tasman, W. & Jaeger, E.A.), Vol. **1**, pp. 1–33. Philadelphia, PA: J.B. Lippincott.
MacCallum, D.K., Bahn, C.F., Lillie, J.H., et al. (1983) Evidence for corneal endothelial cell hypertrophy during postnatal growth of the cat cornea. *Investigative Ophthalmology & Visual Science*, **24**, 247–250.
MacNeil, M.A., Purrier, S. & Rushmore, R.J. (2009) The composition of the inner nuclear layer of the cat retina. *Visual Neuroscience*, **26**, 365–374.
Magalhaes, M.M. (1976) Functional cytoarchitecture of the retina Müller cell. In: *The Structure of the Eye* (eds Yamada, E. & Mishima, S.). Tokyo: Japanese Journal of Ophthalmology.
Maier, A., Eldred, E. & Edgerton, V.R. (1972) Types of muscle fibers in extraocular muscles of birds. *Experimental Eye Research*, **13**, 261–265.
Marfurt, C.F., Murphy, C.J. & Florczak, J.L. (2001) Morphology and neurochemistry of canine corneal innervation. *Investigative Ophthalmology & Visual Science*, **42**, 2241–2251.
Martin, C. (1969) Slit lamp examination of the normal canine anterior ocular segment. Part II: description. *Journal of Small Animal Practice*, **10**, 151–162.
Martin, C.L. (1975) The normal canine iridocorneal angle as viewed with the scanning electron microscope. *Journal of the American Animal Hospital Association*, **11**, 180–192.
Martin-Suarez, Mollleda, C., Tardon, R., et al. (2014) Diurnal variations of central corneal thickness and intraocular pressure in dogs from 8:00 am to 8:00 pm. *Canadian Veterinary Journal*, **55**, 361–365.
Masland, R.H. (2012) The tasks of amacrine cells. *Vision Neuroscience*, **29**, 3–9.
Matlu, F. & Leopold, I.H. (1964) Structure of the retinal vascular system of the dog, monkey, rat, mouse, and cow. *American Journal of Ophthalmology*, **58**, 261–270.
Matsuo, N. (1973) Scanning electron microscopic studies on the corrosion casts of the blood vessels of the ciliary body. *Acta Society Ophthalmology, Japan*, **77**, 928.
Matsuyama, M. (1973) Peculiar patterns of nerve fibers in the retina. I. Normal animal eye. *Journal of Pediatric Ophthalmology*, **10**, 77.
Mawas, J. (1951) The innervation of the human cornea. *Bulletin des societes d'ophtalmologie de France*, **2**, 162–168.
McGreevy, P., Grassi, D. & Harman AM. (2004) A strong correlation exists between the distribution of retinal ganglion cells and nose length in the dog. *Brain, Behavior and Evolution*, **63**, 13–22.
McLaughlin, P.S. & McLaughlin, B.G. (1986) A comparison of the chemical constituents of vitreous humor in four species. *Proceedings of the Annual Meeting of the American Association for Veterinary Laboratory Diagnostics*, Madison WI, 183–184.
McLaughlin, S.A., Brightman, A.H., Helper, L.C., et al. (1988) Effect of removal of lacrimal and third eyelid glands in Schirmer tear test results in cats. *Journal of the American Veterinary Medical Association*, **193**, 820–822.
McMaster, P.R.B. & Macri, F.J. (1968) Secondary aqueous humor outflow pathways in the rabbit, cat, and monkey. *Archives of Ophthalmology*, **79**, 297–303.
McMullen, R.J. & Gilger, B.C. (2006) Keratometry, biometry and prediction of intraocular lens power in the equine eye. *Veterinary Ophthalmology*, **9**, 357–360.
Menendez-Pelaez, A. & Buzzel, G.R. (1992) Harderian gland indoles. In: *Harderian Glands* (eds Webb, S.M., Hoffman, R.A., Puig-Domingo, M.L. & Reiter, R.J.), pp. 219–234. Berlin: Springer-Verlag.
Meriney, S.D. & Pilar, G. (1987) Cholinergic innervation of the smooth muscle cells in the choroid coat of the chick eye and its development. *Journal of Neuroscience*, **7**, 3827–3839.
Meyer, D.B. (1977) The avian eye and its adaptations. In: *Handbook of Sensory Physiology* (ed. Crescitelli, F.), pp. 559–566. Berlin: Springer-Verlag.
Michaelson, I.C. (1954) *Retinal Circulation in Man and Animals*. Springfield, IL: Charles C. Thomas.
Michel, G. (1955) Beitrag zur Anatomie der Traenenorgane von Hund und Katze. *Deutsche Tieraerztliche Wochenschrift*, **2**, 347–349.
Mills, S.L. & Massey, S.C. (1992) Morphology of bipolar cells labeled by DAPI in the rabbit retina. *Journal of Comparative Neurology*, **321**, 133–149.
Monaco, M.A., Samuelson, D.A. & Gelatt, K.N. (1985) Morphology and postnatal development of the normal lens in the dog and congenital cataract in the Miniature Schnauzer. *Lens Research*, **2**, 393–433.
Moore, C.T., Wilman, N.J., Nordheim, E.V., et al. (1987) Density and distribution of canine conjunctival goblet cells. *Investigative Ophthalmology & Visual Science*, **28**, 1925–1932.
Morrison, J.C., DeFrank, M.P. & Van Buskirk, E.M. (1987a) Comparative microvascular anatomy of mammalian ciliary processes. *Investigative Ophthalmology & Visual Science*, **28**, 1325–1340.
Morrison, J.C., DeFrank, M.P. & Van Buskirk, E.M. (1987b) Regional microvascular anatomy of the rabbit ciliary body. *Investigative Ophthalmology & Visual Science*, **28**, 1314–1324.
Morrison, J.C. & Van Buskirk, E.M. (1983) Anterior collateral circulation in the primate eye. *Ophthalmology*, **90**, 707–715.
Mouney, M.C., Townsend, W.M. & Moore, G.E. (2012) Association of height, body weight, age, and corneal diameter with calculated intraocular lens strength of adult horses. *American Journal of Veterinary Research*, **73**, 1977–1982.
Mowat, F.M., Petersen-Jones, S.M., Williamson, H., et al. (2008) Topographical characterization of cone photoreceptors and the area centralis of the canine retina. *Molecular Vision*, **14**, 2518–2527.
Müller, B. & Peichl, L. (1993) Horizontal cells in the cone-dominated tree shrew retina: morphology, photoreceptor

contacts, and topographical distribution. *Journal of Neuroscience*, **13**, 3628–3646.
Murphy, C.J., Kern, T.J. & Howland, H.C. (1991) Refractive state, corneal curvature, accommodative range and ocular anatomy of the Asian Elephant *(Elephas maximus)*. *Vision Research*, **32**, 2013–2121.
Murphy, C.J., Samuelson, D.A. & Pollock, R.V. (2012) The eye. In: *Miller's Anatomy of the Dog* (eds Evans, H.E. & Christensen, G.C.), 4th ed., p. 765. Philadelphia, PA: WB Saunders.
Nakamura, M., Kohayashi, M., Hirano, R., et al. (1994b) Glycosaminoglycan and collagen fibrillar interactions in the mouse corneal stroma. *Matrix Biology*, **14**, 283–286.
Nakamura, M., Mishima, H., Nishida, T., et al. (1994a) Binding of hyaluron to plasma fibronectin increases the attachment of corneal epithelial cells to a fibronectin matrix. *Journal of Cellular Physiology*, **159**, 415–422.
Natiello, M., Lewis, P. & Samuelson, D. (2005) Comparative anatomy of the ciliary body of the West Indian manatee (*Trichechus manatus*) and selected species. *Veterinary Ophthalmology*, **8**, 375–385.
Natiello, N. & Samuelson, D. (2005) Three-dimensional reconstruction of the angioarchitecture of the ciliary body of the West Indian manatee (*Trichechus manatus*). *Veterinary Ophthalmology*, **8**, 367–373.
Nautscher, N., Bauer, A., Steffl, M., et al. (2016) Comparative morphological evaluation of domestic animal cornea. *Veterinary Ophthalmology*, **19**, 297–304.
Ninomiya, H. & Inomata, T. (2005) Microvasculature of the hamster eye: scanning electron microscopy of vascular corrosion casts. *Veterinary Ophthalmology*, **8**, 7–12.
Nishizono, H., Murata, Y., Tanaka, M., et al. (1993) Evidence that Müller cells can phagocytize egg-lecithin-coated silicone particles. *Tissue and Cell*, **25**, 305–310.
Nomura, T. & Smelser, G. (1974) The identification of adrenergic and cholinergic nerve endings in the trabecular meshwork. *Investigative Ophthalmology*, **13**, 525–532.
Noulas, A.V., Theocharis, A.D., Ferelis, R., et al. (2002) Pig vitreous gel: macromolecular composition with particular reference to hyaluronan-binding proteoglycans. *Biochimie*, **84**, 295–302.
Novokhatshii, A. & Reshetniak, V. (1987) Quantitative characteristics of degeneration of the fibers of the optic nerve after section. *Arkhiv anatomii, gistologii i embriologii*, **93**, 55–58.
Nuyttens, J.J. & Simoens, P.J. (1995) Morphologic study of the musculature of the third eyelid in the cat (*Felix catus*). *Laboratory Animal Science*, **45**, 561–563.
Oh, J.O. (1963) Changes with age in the corneal endothelium of normal rabbits. *Acta Ophthalmologica*, **41**, 568–573.
Oliphant, L. (1983) The musculature and pupillary response of great horned owl iris. *Experimental Eye Research*, **37**, 583–595.
Oliphant, L.W. (1988) Cytology and pigments of non-melanophore chromatophores in the avian iris. In: *Advances in Pigment Cell Research* (ed. Bagnara, J.T.), pp. 65–82. New York: Alan R. Liss.
Ollivier, F.J., Samuelson. D.A., Brooks, D.E., et al. (2004) Comparative morphology of the tapetum lucidum (among selected species). *Veterinary Ophthalmology*, **7**, 11–22.
Olsen, T.W., Sanderson, S., Feng, X., et al. (2002) Porcine sclera: thickness and surface area. *Investigative Ophthalmology & Visual Science*, **43**, 2529–2532.
O'Rourke, C.T., Hall, M.I., Pitlik, T., et al. (2010) Hawk eyes I: diurnal raptors differ in visual fields and degree of eye movement. *PLoS ONE*, **95**, e12802. doi:10.1371/journal.pone.0012802.
Osterberg, G. (1935) Topography of the layer of rods and cones in the human retina. *Acta Ophthalmology* (Kbh) suppl VI; Thesis.
Ozaki, H., Seo, M.S., Ozaki, K., et al. (2000) Blockade of vascular endothelial cell growth factor receptor signaling is sufficient to completely prevent retinal neovascularization. *American Journal of Pathology*, **156**, 679–707.
Park, S.A., Taylor, K.T., Zwingenberger, A.L., et al. (2016) Gross anatomy and morphometric evaluation of the canine lacrimal and third eyelid glands. *Veterinary Ophthalmology*, **19**, 230–236.
Park, S.S., Sigelman, J. & Gragoudas, E.S. (1994) The anatomy and cell biology of the retina. In: *Duane's Foundations of Clinical Ophthalmology* (eds Tasman, W. & Jaeger, E.A.), Vol. **1**, Chapter 19, pp. 1–63. Philadelphia, PA: Lippincott-Raven.
Parver, L.M., Auker, C.R., Carpenter, D.O., et al. (1982) Choroidal blood flow. II. Reflexive control in the monkey. *Archives of Ophthalmology*, **100**, 1327–1330.
Payne, A.P. (1994) The Harderian gland: a tercentennial review. *Journal of Anatomy*, **185**, 1–49.
Pedler, C. (1963) The fine structure of the tapetum cellulosum. *Experimental Eye Research*, **2**, 189–195.
Peichl, L. (1992) Topography of ganglion cells in the dog and wolf retina. *Journal of Comparative Neurology*, **324**, 603–620.
Philipson, B.T., Hanninen, L. & Balazs, E.A. (1975) Cell contacts in human and bovine lenses. *Experimental Eye Research*, **21**, 505–519.
Pinto, N.I. & Gilger, B.C. (2014) Spectral-domain optical coherence tomography evaluation of the cornea, retina, and optic nerve in normal horses. *Veterinary Ophthalmology*, **17**, 140–148.
Pirie, A. (1966) The chemistry and structure of the tapetum lucidum in animals. In: *Aspects of Comparative Ophthalmology* (ed. Graham-Jones, O.), pp. 57–68. New York: Pergamon Press.
Pirie, C.G., Alario, A.F., Barysauskas, C.M., et al. (2014) Manual corneal thickness measurements of healthy equine eyes using a portable spectral-domain optical coherence tomography device. *Equine Veterinary Journal*, **46**, 631–634.
Plochocki, J.H., Segev, T., Grow, W., et al. (2018) Extraocular muscle architecture in hawks and owls. *Veterinary Ophthalmology*, **21**, 595–600.
Plummer, C.E., Ramsey, D.T. & Hauptman, J.G. (2003) Assessment of corneal thickness, intraocular pressure,

optical corneal diameter, and axial globe dimensions in Miniature Horses. *American Journal of Veterinary Research*, **64**, 661–665.
Pollock, R.V.H. (1979) Eyelids. In: *Anatomy of the Dog* (eds Evans, H.E. & Christensen, G.C.). Philadelphia, PA: WB Saunders.
Prince, J.H. (1956) *Comparative Anatomy of the Eye*. Springfield, IL: Charles C. Thomas.
Prince, J.H., Diesen, C.D., Eglitis, I., et al. (1960) *Anatomy and Histology of the Eye and Orbit in Domestic Animals*. Springfield, IL: Charles C. Thomas.
Provis, J.M. (1979) The distribution and size of ganglion cells in the retina of the pigmented rabbit: a quantitative analysis. *Journal of Comparative Neurology*, **185**, 121–137.
Qijiu, W., Junfeng, L. & Yumei, X. (1981) The numbers and diameter spectra of bats *(Pipistrellus abramus)*. *Acta Zoologica Sinica*, **27**, 337–342.
Quigley, H.A. & Addicks, E.M. (1981) Regional differences in the structure of the lamina cribrosa and their relation to glaucomatous optic nerve damage. *Archives of Ophthalmology*, **99**, 137–143.
Rafferty, N.S. & Esson, E.A. (1974) An electron-microscope study of adult mouse lens: some ultrastructural specializations. *Journal of Ultrastructure Research*, **46**, 239–253.
Ramsey, D.T., Hauptman, J.G. & Petersen-Jones, S.M. (1999) Corneal thickness, intraocular pressure, and optical corneal diameter in Rocky Mountain Horses with cornea globose or clinically normal corneas. *American Journal of Veterinary Research*, **60**, 1317–1321.
Rapaport, D.H. & Stone, J. (1984) The area centralis of the retina in the cat and other mammals: focal point for function and development of the visual system. *Neuroscience*, **11**, 289–301.
Raviola, G. (1971) The fine structure of the ciliary zonule and ciliary epithelium with special regard to the organization and insertion of the zonular fibrils. *Investigative Ophthalmology & Visual Science*, **10**, 851–869.
Raviola, G. (1982) Schwalbe's line cells: a new cell type in the trabecular meshwork of *Macaca mulatta*. *Investigative Ophthalmology & Visual Science*, **22**, 45–56.
Risco, J.M. & Nopanitaya, W. (1980) Ocular microcirculation: scanning electron microscopy. *Investigative Ophthalmology & Visual Science*, **19**, 5–12.
Robinson, S.R., Dreher, B. & McCall, M.J. (1989) Non-uniform retinal expansion during the formation of the rabbit's visual streak: implications for the ontogeny of mammalian retinal topography. *Visual Neuroscience*, **2**, 201–219.
Rodieck, R.W. (1973) *The Vertebrate Retina: Principles of Structure and Function*. San Francisco, CA: W.H. Freeman.
Rodriques, M.M., Hackett, J. & Donohoo, P. (1988) Iris. In: *Biomedical Foundations of Ophthalmology* (eds Duane, T.D. & Jaeger, E.A.), Vol. **1**, pp. 1–18. Philadelphia, PA: J.B. Lippincott.
Rohen, J. (1961) Comparative and experimental studies on the iris of primates. *American Journal of Ophthalmology*, **52**, 384–396.
Rohen, J.W. (1979) Scanning electron microscopic studies of the zonular apparatus in human and monkey eyes. *Investigative Ophthalmology & Visual Science*, **18**, 133–144.
Rohen, J.W. & Lutjen-Drecoll, E. (1989) Morphology of aqueous outflow pathways in normal and glaucomatous eyes. In: *The Glaucomas* (eds Ritch, R., Shields, M.B. & Krupin, T.), pp. 41–74. St. Louis, MO: CV Mosby.
Ryland, T.R., Lewis, P.A., Chisholm, M., et al. (2003) Localization of smooth muscle actin in the iridocorneal angle of normal and spontaneous glaucomatous Beagle dogs. *Veterinary Ophthalmology*, **6**, 205–209.
Saari, M. (1971) Myelinated nerves of the pig iris. *Acta Ophthalmologica*, **49**, 921–937.
Sakai, T. (1992) Comparative anatomy of mammalian Harderian glands. In: *Harderian Glands* (eds Webb, S.M., Hoffman, R.A., Puig-Domingo, M.L. & Reiter, R.J.), pp. 7–23. Berlin: Springer-Verlag.
Samuelson, D.A. (1996) A reevaluation of the comparative anatomy of the Eutherian iridocorneal angle and associated ciliary body musculature. *Veterinary & Comparative Ophthalmology*, **6**, 153–172.
Samuelson, D.A., Andresen, T.L. & Gwin, R.M. (1984a) Conjunctival fungal flora in horses, cattle, dogs and cats. *Journal of the American Veterinary Medical Association*, **184**, 1240–1242.
Samuelson, D.A. & Birkin-Streit, A. (2011) Microanatomy of the anterior uveoscleral outflow pathway in normal and primary open-angle glaucomatous dogs. *Veterinary Ophthalmology*, **15**(Suppl. 1), 47–53.
Samuelson, D.A., Das, N.D., Bauer, J.E., et al. (1987a) Prenatal morphogenesis of the congenital cataracts in the Miniature Schnauzer. *Lens Research*, **4**, 231–250.
Samuelson, D.A., Ganesh, K.C., Miles, S.M., et al. (2005) Morphology and histochemistry of Bowman's layer in selected vertebrates. *Investigative Ophthalmology & Visual Science, ARVO Supplement*, **45**, 2181.
Samuelson, D.A. & Gelatt, K.N. (1984a) Aqueous outflow in the Beagle. I. Postnatal morphologic development of the iridocorneal angle: pectinate ligament and uveal trabecular meshwork. *Current Eye Research*, **6**, 783–794.
Samuelson, D.A. & Gelatt, K.N. (1984b) Aqueous outflow in the Beagle. II. Postnatal morphologic development of the iridocorneal angle: corneoscleral trabecular meshwork and angular aqueous plexus. *Current Eye Research*, **6**, 795–807.
Samuelson, D.A., Gelatt, K.N. & Gum, G.G. (1984b) Kinetics of phagocytosis in the normal canine iridocorneal angle. *American Journal of Veterinary Research*, **45**, 2359–2366.
Samuelson, D., Smith, P. & Brooks, D. (1989) Morphologic features of the aqueous humor drainage pathways in horses. *American Journal of Veterinary Research*, **50**, 720–727.
Samuelson, D.A. & Gelatt, K.N. (1998) The aging iridocorneal angle and glaucoma. In: *Pathobiology of the Aging Dog* (ed. Mohr, U.). Ames, IA: ILSI Press.
Samuelson, D.A., Gum, G.G., Gelatt, K.N. et al. (1985) Aqueous outflow in the beagle: unconventional outflow, using

different-sized microspheres. *American Journal of Veterinary Research*, **46**, 242–248.
Samuelson, D.A., Gum, G.G. & Gelatt, K.N. (1987b) Action of hyaluronidase on aqueous outflow resistance in normal and glaucomatous dogs. *Investigative Ophthalmology & Visual Science*, **28**(Suppl.), 131.
Samuelson, D.A. & Lewis, P.A. (1995) Comparative morphology of the iridocorneal angle of selected artiodactyls (ungulates). *Veterinary & Comparative Ophthalmology*, **5**, 89–103.
Samuelson, D.A., McGee, J.L., Levitt, J., et al. (2011) Ultrastructural characterization of the conjunctiva and associated lymphoid tissue (CALT) in the Florida manatee. 42nd Proceedings of the Annual Conference of the International Association for Aquatic Animal Medicine, pp. 73–74.
Samuelson, D.A., Plummer, C. & Gelatt, K. (2001) Schwalbe line's cell in the normal and glaucomatous dog. *Veterinary Ophthalmology*, **4**, 47–53.
Samuelson, D.A., Williams, l.W., Gelatt, K.N., et al. (1983) Orthograde rapid axoplasmic transport and ultrastructural changes of the optic nerve. Part II. Beagles with primary open-angle glaucoma. *Glaucoma*, **5**, 189–196.
Sanchez, R., Dunkelberger, G. & Quigley, H. (1986) The number and diameter distribution of axons in the monkey optic nerve. *Investigative Ophthalmology & Visual Science*, **27**, 1342–1350.
Sandmann, D., Boycott, B.B. & Peichl, L. (1996a) The horizontal cells of artiodactyls retinae: comparison with Cajal's descriptions. *Visual Neuroscience*, **13**, 735–746.
Sandmann, D., Boycott, B.B. & Peichl, L. (1996b) Blue-cone horizontal cells in the retinae of horses and other equidae. *Journal of Neuroscience*, **16**, 3381–3396.
Schlegel, T., Brehm, H. & Amselgruber, W.M. (2001) The cartilage of the third eyelid: a comparative macroscopic and histological study in domestic animals. *Annals of Anatomy*, **183**, 165–169.
Schoster, J.V., Wickman, L. & Stuhr, C. (1995) The use of ultrasonic pachymetry and computer enhancement to illustrate the collective corneal thickness profiles of 25 cats. *Veterinary & Comparative Ophthalmology*, **5**, 68–73.
Schultze, M. (1866) Zur anatomie und physiologie der retina. *Archiv fur Mikroskopische Anatomie*, **3**, 215–244.
Schwab, I.R., Yuen, C.K., Buyukmihci, N.C., et al. (2002) Evolution of the tapetum. *Transactions of the American Ophthalmological Society*, **100**, 187–199.
Sebbag, L., Reilly, C.M., Eid, R., et al. (2016) Goblet cell density and distribution in cats with clinically and histologically normal conjunctiva. *Veterinary Ophthalmology*, **19**, 38–43.
Sedacca, K.K., Samuelson, D.A. & Lewis, P.A. (2011) Examination of the anterior uveoscleral pathway in domestic species. *Veterinary Ophthalmology*, **15**(Suppl. 1), 1–7.
Seifert, P. & Spitznas, M. (1996) Immunocytochemical and ultrastructural evaluation of the distribution of nervous tissue and neuropeptides in the meibomian gland. *Graefe's Archive for Clinical and Experimental Ophthalmology*, **234**, 648–656.
Shabo, A.L., Maxwell, D.S. & Kreiger, A.D. (1976) Structural alterations in the ciliary process and the blood-aqueous barrier of the monkey after systemic urea injections. *American Journal of Ophthalmology*, **81**, 162–172.
Sharpnack, D.D., Wyman, M., Anderson, B.G., et al. (1984) Vascular pathways of the anterior segment of the canine eye. *American Journal of Veterinary Research*, **45**, 1287–1294.
Shen, J.Y., Kelly, D.E., Hyman, S., et al. (1985) Intraorbital cerebrospinal fluid outflow and posterior uveal component of the hamster eye. *Cell and Tissue Research*, **240**, 77–87.
Sherwood, M. & Richardson, T.M. (1981) Kinetics of the phagocytic process in the trabecular meshwork of cats and monkeys. *Investigative Ophthalmology & Visual Science*, **20**(Suppl.), 65.
Shinozaki, A., Hosaka, Y., Imgawa, T., et al. (2010) Topography of ganglion cells and photoreceptors in the sheep retina. *Journal of Comparative Neurology*, **518**, 2305–2315.
Shively, J.N. & Epling, G.P. (1969) Fine structure of the canine eye: iris. *American Journal of Veterinary Research*, **30**, 13–25.
Shively, J.N., Epling, G.P. & Jensen, R. (1970) Fine structure of the canine eye: retina. *American Journal of Veterinary Research*, **31**, 1339–1359.
Sigelman, J. & Ozanics, V. (1988) Retina. In: *Biomedical Foundations of Ophthalmology* (eds Duane, T.D. & Jaeger, E.A.), Vol. **1**, Chapter 19, pp. 1–63. Philadelphia, PA: J.B. Lippincott.
Sillman, A.J. (1973) Avian vision. In: *Avian Biology* (eds Farmer, D.A., King, J.K. & Parkes, K.C.), pp. 349–387. New York: Academic Press.
Silveira, L.C., Picanço-Diniz, C.W. & Oswaldo-Cruz, E. (1989) Distribution and size of ganglion cells in the retinae of large Amazon rodents. *Visual Neuroscience*, **2**, 221–235.
Simoens, P., Muylle, S. & Lauwers, H. (1996) Anatomy of the ocular arteries in the horse. *Equine Veterinary Journal*, **28**, 360–367.
Simones, P., DeGeest, J.P. & Lauwers, H. (1996) Comparative morphology of the pectinate ligaments of domestic mammals, as observed under the dissecting microscope and the scanning electron microscope. *Journal of Veterinary Medical Science*, **58**, 977–982.
Sires, B.S., Saan, J.C., Garwin, G.G., et al. (2001) The color difference in orbital fat. *Archives of Ophthalmology*, **119**, 868–871.
Smith, B.J., Smith, S.A. & Braekevelt, C.R. (1996) Fine structure of the pecten oculi in the barred owl (*Strix varia*). *Histology and Histopathology*, **11**, 89–96.
Smith, P.J., Samuelson, D.A., Brooks, D.E., et al. (1986) Unconventional aqueous humor outflow of microspheres perfused into the equine eye. *American Journal of Veterinary Research*, **47**, 2445–2453.
Smith, P., Samuelson, D. & Brooks, D. (1988) Aqueous drainage paths in the equine eye: scanning electron microscopy of corrosion cast. *Journal of Morphology*, **198**, 33–42.
Smith, R.L. & Raviola, G. (1983) The structural basis of the blood-aqueous barrier in the chicken eye. *Investigative Ophthalmology & Visual Science*, **24**, 326–338.

Smith, R.S. (1971) Ultrastructural studies of the blood-aqueous barrier. I. Transport of an electron-dense tracer in the iris and ciliary body of the mouse. *American Journal of Ophthalmology*, **71**, 1066–1077.

Smith, R.S. & Rudt, L.A. (1973) Ultrastructural studies of the blood-aqueous barrier. II. The barrier to horseradish peroxidase in primates. *American Journal of Ophthalmology*, **76**, 937–947.

Smolek, M.K. & Klyce, S.D. (1993) Cornea. In: *Biomedical Foundations of Ophthalmology* (eds Wasman, W. & Jaeger, E.A.), Vol. **1**, pp. 1–20. Philadelphia, PA: J.B. Lippincott.

Snowden, J. & Swann, D. (1980) Vitreous structure: V. The morphology and thermal stability of vitreous collagen fibers and comparison to articular cartilage (type II) collagen. *Investigative Ophthalmology & Visual Science*, **19**, 610–618.

Spike, R.C., Payne, A.P. & Moore, M.R. (1992) Porphyrins and their possible significance in Harderian glands. In: *Harderian Glands* (eds Webb, S.M., Hoffman, R.A., Puig-Domingo, M.L. & Reiter, R.J.), pp. 165–194. Berlin: Springer-Verlag.

Spitznas, M. & Hogan, M.J. (1970) Outer segments of photoreceptors and the retinal pigment epithelium: interrelationship in the human eye. *Archives of Ophthalmology*, **84**, 810–819.

Stein, J.J. & Berson, D.M. (1995) On the distribution of gamma cells in the cat retina. *Visual Neuroscience*, **12**, 687–700.

Steinberg, R.H., Reid, M. & Lacy, P.L. (1973) The distribution of rods and cones in the retina of the cat. *Journal of Comparative Neurology*, **148**, 229–235.

Stoeckelhuber, M., Stoeckelhuber, B.M. & Welsch, U. (2004) Apocrine glands in the eyelid of primates contribute to the ocular host defense. *Cells, Tissues, Organs*, **176**, 187–194.

Stone, J. & Halasz, P. (1989) Topography of the retina in the Elephant, *Loxodonta africana*. *Brain, Behavior and Evolution*, **34**, 84–95.

Stone, J. & Keens, J. (1980) Distribution of small and medium-sized ganglion cells in the cat's retina. *Journal of Comparative Neurology*, **192**, 235–246.

Stone, R.A., Kuwayama, Y., Laties, A.M. & Marangos, P.J. (1984) Neuron-specific enolase-containing cells in the Rhesus monkey trabecular meshwork. *Investigative Ophthalmology & Visual Science*, **25**, 1332–1334.

Streeten, B. (1988) Cilary body. In: *Biomedical Foundations of Ophthalmology* (eds Duane, T.D. & Jaeger, E.A.), Vol. **1**, pp. 1–38. Philadelphia, PA: J.B. Lippincott.

Streeten, B.W. (1992) Zonular apparatus. In: *Biomedical Foundations of Ophthalmology* (eds Duane, T.D. & Jaeger, E.A.), Vol. **1**. Philadelphia, PA: J.B. Lippincott.

Streeten, B.W. & Licari, P. (1981) Immunohistochemical comparison of zonular fibrils and elastic tissue microfibrils. *Investigative Ophthalmology & Visual Science*, **21**, 130–135.

Strettoi, E. & Masland, R.H. (1995) The organization of the inner nuclear layer of the rabbit retina. *Journal of Neuroscience*, **15**, 875–888.

Strom, A.R., Cortes, D.E., Rasmussen, C.A., et al. (2016a) *In vivo* evaluation of the cornea and conjunctiva of the normal laboratory Beagle using time- and Fourier-domain optical coherence tomography and ultrasound pachymetry. *Veterinary Ophthalmology*, **19**, 50–56.

Strom, A.R., Cortes, D.E., Thomasy, S.M., et al. (2016b) *In vivo* ocular imaging of the cornea of the normal female laboratory Beagle using confocal microscopy. *Veterinary Ophthalmology*, **19**, 63–67.

Szalay, J., Nunziata, B. & Henkind, P. (1975) Permeability of iridal blood vessels. *Experimental Eye Research*, **21**, 531–543.

Tamura, Y., Konomi, H., Sawada, H., et al. (1991) Tissue distribution of type VIII collagen in human adult and fetal eyes. *Investigative Ophthalmology & Visual Science*, **32**, 2636–2644.

Tansley, K. (1956) Comparison of the lamina cribrosa in mammalian species with good and indifferent vision. *British Journal of Ophthalmology*, **40**, 178–182.

Takahashi, T., Cho, H., Kublin, C.L., et al. (1983) Keratan sulfate and dermatan sulfate proteoglycans associate with type VI collagen in fetal rabbit cornea. *Journal of Histochemistry and Cytochemistry*, **41**, 1447–1457.

Timney, B. & Keil, K. (1992) Visual acuity in the horse. *Vision Research*, **32**, 2289–2293.

Torczynski, E. (1988) Choroid and suprachoroid. In: *Biomedical Foundations of Ophthalmology* (eds Duane, T.D. & Jaeger, E.A.), Vol. **1**, Chapter 22, pp. 1–33. Philadelphia, PA: J.B. Lippincott.

Tousimis, A. (1963) Pigment cells of the mammalian iris. *Annals of the New York Academy of Sciences*, **100**, 447–466.

Tousimis, A. & Fine, B. (1959) Ultrastructure of the iris: an electron microscopic study. *American Journal of Ophthalmology*, **48**, 397–417.

Tripathi, R.C. (1971a) Ultrastructure of the exit pathway of the aqueous in lower mammals. *Experimental Eye Research*, **12**, 311–314.

Tripathi, R.C. (1971b) Mechanism of the aqueous outflow across the trabecular wall of Schlemm's canal. *Experimental Eye Research*, **11**, 116–121.

Tripathi, R.C. (1974) Comparative physiology and anatomy of aqueous humor outflow pathway. In: *The Eye* (ed. Davson, H.), Vol. **5**, pp. 163–272. New York: Academic Press.

Trivino, A., Ramirez, J.M., Salazar, J.J., et al. (1996) Immunohistochemical study of human optic nerve head astroglia. *Vision Research*, **36**, 2015–2028.

Troncoso, M.U. (1938) Comparative anatomy, physiology and evolution of the angle of the anterior chamber in Mammalia. *XV International Congress of Ophthalmology Cairo*, **4**, pp. 98–119.

Troncoso, M.U. (1942a) Microanatomy of the eye with the slit lamp microscope. II. Comparative anatomy of the ciliary body, zonula and related structures in mammalia. *American Journal of Ophthalmology*, **25**, 1–30.

Troncoso, M.U. (1942b) The intrascleral vascular plexus and its relations to the aqueous outflow. *American Journal of Ophthalmology*, **65**, 1153–1162.

Tso, M.O. & Friedman, E. (1967) The retinal pigment epithelium. I. Comparative histology. *Archives of Ophthalmology*, **78**, 641–649.

Tucker, V. (2000) The deep fovea, sideways vision and spiral flight paths in raptors. *Journal of Experimental Biology*, **203**, 3745–3754.

Uga, S. & Smelser, G.K. (1973) Comparative study of the fine structure of retinal Müller cells in various vertebrates. *Investigative Ophthalmology*, **12**, 434–448.

Ujiie, K. & Bill, A. (1984) The drainage routes for aqueous humor in monkeys as revealed by scanning electron microscopy of corrosion casts. *Scanning Electron Microscopy*, **2**, 84A.

Van Buskirk, E.M. (1979) The canine eye: the vessels of aqueous drainage. *Investigative Ophthalmology & Visual Science*, **18**, 223–230.

Vaney, D.I. (1980) A quantitative comparison between the ganglion cell populations and axonal outflows of the visual streak and periphery of the rabbit retina. *Journal of Comparative Neurology*, **189**, 215–233.

Vaney, D.I. & Hughes, A. (1976) The rabbit optic nerve: fiber diameter spectrum, fibre count, and comparison with retinal ganglion cell count. *Journal of Comparative Neurology*, **170**, 241–252.

Vaney, D.I., Young, H.M. & Gynther, I.C. (1991) The rod circuit in the rabbit retina. *Visual Neuroscience*, **7**, 141–154.

Virchow, H. (1910) Die kammerbucht und das gerustwerk der selben. In: *Graefe-Saemisch: Handbuch der Geramten Augenheilk*, 2nd ed., Vol. **1**. Leipzig.

von Sallman, L., Caravaggio, L.L. & Grimes, P. (1961) Studies on the corneal endothelium of the rabbit. I. Cell division and growth. *American Journal of Ophthalmology*, **51**, 955–969.

Wakakuwa, K., Watanake, M., Sugimoto, T., et al. (1987) An electron microscopic analysis of the optic nerve of the eastern Chipmunk *(Tasmias sibiricusasiaticus)*: total fiber count and retinoptic organization. *Vision Research*, **27**, 1891–1901.

Walls, G.L. (1942) *The Vertebrate Eye and Its Adaptive Radiation*. Bloomfield Hills, MI: Cranebrook Press.

Watsky, M.A., Olsen, T.W. & Edelhauser, H.F. (1995) Cornea and sclera. In: *Duane's Foundation of Clinical Ophthalmology* (eds Tasman, W. & Jaeger, E.A.), Vol. **2**, pp. 1–29. Philadelphia, PA: J.B. Lippincott.

Weale, R.A. (1963) *The Aging Eye*. London: Lewis.

White, C.A. & Chalupa, L.M. (1991) Subgroup of alpha ganglion cells in the adult cat retina is immunoreactive for somatostatin. *Journal of Comparative Neurology*, **304**, 1–13.

Willekens, B. & Vrensen, G. (1985) Lens fiber organization in four avian species: a scanning electron microscopic study. *Tissue and Cell*, **17**, 359–377.

Williams, D.L. (2004) Lens morphometry determined by B-mode ultrasonography of the normal and cataractous canine lens. *Veterinary Ophthalmology*, **7**, 91–95.

Williams, L.W., Gelatt, K.N, Gum, G.G., et al. (1983a) Orthograde rapid axoplasmic transport and ultrastructural changes of the optic nerve. Part I. Normotensive and acute hypertensive Beagles. *Glaucoma*, **5**, 177–188.

Williams, R.W., Bastiani, M.J. & Chalupa, L.M. (1983b) Loss of axons in the cat optic nerve following fetal unilateral enucleation: an electron microscopic analysis. *Journal of Neuroscience*, **3**, 133–144.

Witkovsky, P. (1992) Functional anatomy of the retina. In: *Foundations of Clinical Ophthalmology* (eds Tasman, W. & Jaeger, E.A.), Vol. **1**, Chapter 20, pp. 1–29. Philadelphia, PA: Lippincott-Raven.

Woberman, P. & Fine, B. (1972) The clump cells of Koganei. The light and electron microscopic study. *American Journal of Ophthalmology*, **73**, 90–101.

Wolfel, A.E. Pederson, S.L., Claymaet, A.M., et al. (2017) Canine central corneal thickness measurements via Pentacam-HR®, optical coherence tomography (Optovue iVue®), and high-resolution ultrasound biomicroscopy. *Veterinary Ophthalmology*, 1–9.

Wong, R.O. (1989) Morphology and distribution of neurons in the retina of the American garter snake, *Thamnophis sitalis*. *Journal of Comparative Neurology*, **283**, 587–601.

Wong, V.G. & Macri, F.J. (1964) Vasculature of the cat eye. *Archives of Ophthalmology*, **72**, 351–358.

Yamaue, Y., Hosaka, Y.Z. & Uehara, M. (2015) Spatial relationships among the cellular tapetum, visual streak and rod density in dogs. *Journal of Veterinary Medical Science*, **77**, 175–179.

Young, D.L. & Braekevelt, C.R. (1993) Fine structure of the retinal epithelial regions of the red kangaroo *(Macropus rufus)*. *Anatomischer Anzeiger*, **175**, 299–303.

3

Physiology of the Eye

Diane V.H. Hendrix[1], Sara M. Thomasy[2], and Glenwood G. Gum[3]

[1] *Department of Small Animal Clinical Sciences, College of Veterinary Medicine, University of Tennessee, Knoxville, TN, USA*
[2] *Department of Surgical and Radiological Sciences, School of Veterinary Medicine; Department of Ophthalmology & Vision Science, School of Medicine, University of California, Davis, CA, USA*
[3] *Absorption Systems, San Diego, CA, USA*

Functional knowledge of ocular physiology in animal species provides a critical foundation for clinicians practicing comparative and veterinary ophthalmology. Diagnostic procedures, interactions of ocular tissues and drugs, ophthalmic diseases, and surgical procedures require a thorough understanding of the normal physiology as well as the pathophysiology of the eye and its associated structures. This chapter presents the physiology of the eye, especially regarding the adnexa, anterior segment, ocular circulation, aqueous humor dynamics, lens, and vitreous. The optics and physiology of vision are presented in Chapter 4.

The rate at which both relatively simple and complex ocular physiological mechanisms are being studied is incredible. This chapter presents the fundamental physiological phenomena of the eye required by the clinical veterinary ophthalmologist. Other resources should be referenced for the newest and most detailed information and that associated with less commonly seen species.

Anterior Eye Structures

Eyelids

The eyelids of domestic animals are designed to protect the eye, particularly the cornea. All domestic animal species have a superior (upper) and inferior (lower) eyelid; most have a nictitating membrane (NM, third eyelid). The eyelids contain the meibomian glands; these are large sebaceous glands that secrete the outer, oily layer of the precorneal tear film (PTF). The conjunctiva which lines the inside of the eyelids and reflects onto the globe contains goblet cells that contribute the mucin to the PTF; accessory lacrimal glands are also present in some species. The normal blinking of the eyelids maintains the physiologic thickness of the preocular tear film, aids movement of the tears both to and within the nasolacrimal system, and helps eliminate small particles from the corneal and conjunctival surfaces. Reflex closure of the eyelids protects the anterior segment from external trauma.

The eyelids determine the shape and width of the palpebral fissure, along with the associated medial and lateral canthal ligamentous and muscle attachments. For example, a wide, round palpebral fissure is normal among brachycephalic breeds, and a narrow, almond-shaped palpebral fissure is normal among dolichocephalic breeds. The shape of the palpebral fissure also depends on the relationship of the globe to the orbit. A small globe in a deep orbit allows a narrow palpebral fissure; the opposite occurs with a large globe in a shallow orbit. The NM aids in protection of the conjunctiva and cornea by moving, either passively or actively, over the cornea when the globe is retracted. The NM contains one or more important accessory, tear-producing glands that contribute to the aqueous portion of the PTF. The NM also helps to support the position of the lower eyelid through its mass in the ventromedial cul-de-sac, and it forms part of the lacrimal lake in the medial canthus. In all animals, if the globe is retracted by the retractor bulbi muscles or decreases in size, the membrane passively begins to cover the eye.

Eyelid closure is mediated by the efferent fibers of the facial nerve (CN VII) and their effects on the orbicularis oculi muscles. The oculomotor (CN III) innervates the *levator palpebral superioris*, which is responsible for opening the upper eyelid.

Eyelid closure is the end result of three eyelid reflexes, the corneal, palpebral, and dazzle reflexes, and the menace response (Table 3.1). The corneal and palpebral reflexes are primitive reflexes with a purely subcortical course. Both are

Veterinary Ophthalmology: Volume I, Sixth Edition. Edited by Kirk N. Gelatt, Gil Ben-Shlomo, Brian C. Gilger, Diane V.H. Hendrix, Thomas J. Kern, and Caryn E. Plummer.

Companion website: www.wiley.com/go/gelatt/veterinary

elicited by touch, with the afferent pathway being the ophthalmic branch of the trigeminal nerve (corneal) or the ophthalmic and maxillary branches of the trigeminal nerve (palpebral). The efferent pathway of these two reflexes as well as the menace response is the facial nerve stimulating the orbicularis oculi muscles, resulting in a blink. These reflexes are present immediately following birth or eyelid opening. By contrast, the menace response is cortically mediated and is initiated by a threatening gesture. The visual input results in a blink closure via the facial nerve or globe retraction via the abducens nerve. This response requires integration and interpretation and is a learned response (see Chapter 36).

Blinking and blink rates have been studied in many species under varying circumstances and methodologies, making comparisons and generalized statements difficult (Table 3.2). However, a few generalizations can be made. Blinking does not occur randomly, and blinks are often associated with gaze shifts and saccades. One of the theories for this timing is that blinking temporarily blocks visual information, and blinking during gaze shifts and saccades takes advantage of blocking vision when the images are already degraded from movement (Yorzinski, 2016). Diurnal primates and birds have higher blink rates than nocturnal primates and birds (Kirsten & Kirsten, 1983; Tada et al., 2013). A large comparative study showed that in general, larger mammals and primates blink more often than smaller mammals (Blount, 1927).

Eyelids in the Dog

In dogs, the upper eyelid, which contains the cilia or eyelashes, is more mobile than the lower eyelid. When the eyelids are closed, most of the ambient light is prevented from entering the eyes. Restrained dogs blink 10–20 times/min in comparison to unrestrained dogs (Table 3.2; Gum & MacKay, 2013). Some 50% of dogs' blinks are incomplete (Harmer & Williams, 2003). Puppies normally open their eyelids between 10 and 15 days of age (Glaze, 2011).

Eyelids in the Cat

In cats, both eyelids lack cilia. The eyelids of pigmented cats allow no more than 5% of light at longer wavelengths to be transmitted (Crawford & Marc, 1976). Kittens normally open their eyelids between 10 and 15 days of age; however, both eyes do not always open on the same day (Blakemore & Cummings, 1975).

The NM of the feline species is large and active and may passively or actively cover part of the cornea or be drawn into the medial canthus. It can extend at least two-thirds of the way across the cornea and contains nine smooth muscles which lead to active retraction or protrusion (Nuyttens & Simoens, 1995). The smooth muscle that draws the membrane into the medial canthus is innervated exclusively by postganglionic adrenergic sympathetic nerve fibers, with cell bodies located in the anterior cervical ganglion. Their axons follow the oculomotor nerve. Normally, the NM shows no spontaneous activity, because the smooth muscle lacks tight junctions like that of the visceral smooth muscle. Each muscle cell is innervated by one or more axons, thus confirming that activation of the smooth muscle in the NM is neurogenic and that the myogenic conduction normally found in visceral smooth muscles does not occur (Marshall, 1974). Cats are the only common domestic animal in which sympathetic stimulation will cause the NM to move slightly. The NM permits ~10% of applied light to pass in this species (Crawford & Marc, 1976).

Other Species

Horse

In horses, the cilia are long and numerous on the upper eyelid, except near the medial canthus. While horses blink at 19 blinks/minute, approximately 33% each of the blinks are minimal incomplete, moderate incomplete, or complete, with only 6% of the blinks having a complete squeeze. Lid

Table 3.1 Reflexes involving the blink response.

	Cornea Reflex	Palpebral Reflex	Menace Response[a]	Dazzle Reflex
Stimulus	Corneal touch	Eyelid touch	Menacing gesture	Bright light
Receptors	Somesthetic	Somesthetic	Photoreceptors	Photoreceptors
Afferent pathway	Trigeminal nerve (ophthalmic)	Trigeminal nerve (ophthalmic & maxillary)	Optic nerve	Optic nerve
Interneuron	Subcortical	Subcortical	Cortical, cerebellum	Subcortical
Efferent pathway	Facial nerve	Facial nerve	Facial nerve, VI, IX	Facial nerve
Effectors	Orbicularis oculi muscle	Orbicularis oculi muscle	Orbicularis oculi muscle, retractor bulbi muscle	Orbicularis oculi muscle
Response	Blink	Blink	Blink, retract globe[b]	Blink

[a] If sufficient cortex of one cerebral hemisphere is damaged, the menace reaction cannot be elicited in the contralateral eye of the dog. Pathology of the cerebellar cortex can also affect the menace reaction.
[b] The menace response can also involve turning the head or moving away from the stimulus.

Table 3.2 Blinking rates of domestic animals.

Species	Blinks/Minute	Interblink Period	Concurrent Blinks
Dog	3–5[a]	20–30 seconds[b,c]	85%[a]
Cat	1–5 per 5 min[a]	18.5 seconds[b]	70%[a]
Horse	19[d]		77%[d]
Cattle	5[e]		60%[e]
Pigs	10 [e]		90%[e]

[a] Gum & MacKay (2013).
[b] Blount (1927).
[c] Dogs have partial blinks every few seconds between complete blinks.
[d] Best et al. (2018).
[e] Gum (1991).

closure is approximately twice as rapid as lid opening (Best et al., 2018). Eyelids are open at birth.

Long tactile hairs, or vibrissae, are present on both the dorsal brow and lower eyelid. The vibrissae are long, stout, single shafts of hair that are usually thicker than adjacent skin hair; they may provide additional sensation for the eyelids.

Cattle, Sheep, and Pigs

In cattle, sheep, and pigs, the upper eyelid is the most mobile, and the majority of cilia are present on the upper eyelid. Pigs, rabbits, rodents, and some ruminants have a deeper structure, the Harder's gland or harderian gland, in addition to the superficial gland of the NM. This gland secretes lipids, porphyrins, indoles, and growth factors and is thus also important for lubrication of the eye.

In the pig, the meibomian glands are poorly developed, and the primary eyelid glands are sweat glands. Eyelids are open at birth.

Birds and Reptiles

In birds and certain reptiles, the lower eyelid is larger and more mobile than the upper eyelid. There are no feathers corresponding to eyelashes on the lids. The superciliary line refers to feathers that correspond to the eyebrow and are often different colors than surrounding feathers. The superciliary or supraorbital ridge refers to the unfeathered bony protuberance just dorsal to the orbital rim that is seen in many raptors, such as eagles and hawks. This ridge is thought to provide shade to the eye. Birds blink with both eyelids or the NM alone. In contrast to mammals, the nearly transparent NM of birds is under direct skeletal muscular control. Two muscles extraneous to the lid pull the NM over the entire cornea as many as 15–20 times per minute, even with the other eyelids closed (Gum & MacKay, 2013). Blinks in peacocks are strongly associated with gaze shifts (Yorzinski, 2016). The NM also contains a superficial tear gland, and some species have a deeper harderian gland. Chicks hatch with their eyes open.

Tear Production and Drainage

Both the optical and normal functions of the cornea depend on the integrity of the lacrimal system. The PTF maintains an optically uniform corneal surface by smoothing out minor irregularities, removing foreign matter from the cornea and conjunctiva, lubricating the conjunctiva and cornea, providing nutrients to the avascular cornea, and controlling the local bacterial flora. The PTF also undergoes constant evaporation and formation of transient "dry spots." Hence, the rate of tear evaporation appears to be directly related to the rate of blinking, since the rate of blinking is faster than the development of these dry spots (Milder & Weil, 1983). Actual tear flow rates are difficult to measure in most species; however, in the horse, the tear flow rate was estimated to be 34 µL/min with a tear volume of 234 µL, which indicates a tear volume turnover rate of approximately 7 minutes (Chen & Ward, 2010). By comparison, tear turnover and tear evaporation rates in humans are ~1 ± 0.4 µL/min and 0.14 ± 0.07 µL/min, respectively (Tomlinson et al., 2009).

In all species studied, the PTF can be loosely divided into three layers that intermix (Fig. 3.1). The outer layer (~0.1 µm) is a very thin, oily layer that forms a reversible, noncollapsible, multilayer film with the primary purpose of stabilizing the air–tear interface (Eftimov et al., 2017). The primary constituent of this lipid layer is the meibomian gland secretions (MGS), or meibum, a composite lipid-rich mixture. Up to 22 wt% comprises nonlipid components (proteins, salts, and polysaccharides; McMahon et al., 2013). The main lipid classes found in canine MGS (cMGS) are very long-chain cholesteryl esters, wax esters, (O-acyl)-omega-hydroxy fatty acids (OAHFA), and cholesteryl esters of OAHFA (Butovich et al., 2011). The lipidomes of cMGS and human MGS are

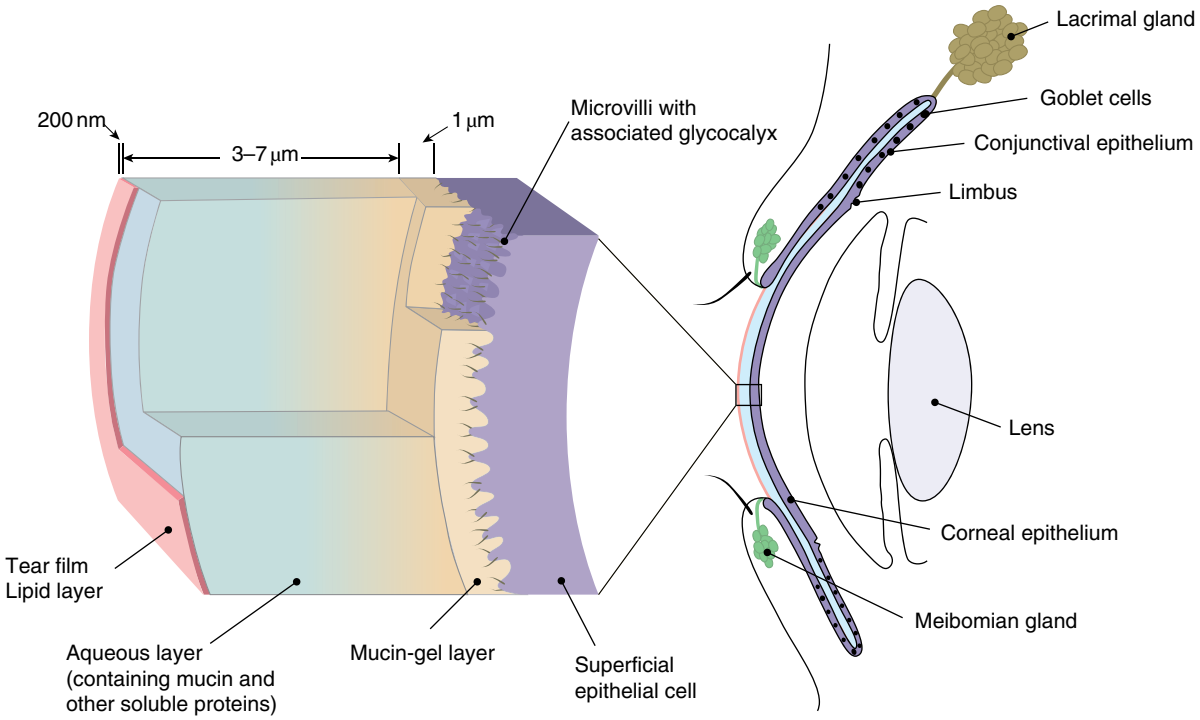

Figure 3.1 The tear film is a complex multilayered fluid phase. This figure represents the classic three-layered model, composed of a mucin-gel layer adjacent to the epithelial surface, an aqueous layer containing mucin, and other soluble proteins and a thin lipid film on the outermost surface. (Reproduced with permission from Yanez-Soto, B., Mannis, M.J., Schwab, I.R., et al. (2014) Interfacial phenomena and the ocular surface. *Ocular Surface*, **12**, 178–201.)

similar, implying similar biosynthetic and biodegradation pathways. However, dogs have a relatively larger proportion of OAHFA than humans, which could be related to a higher tear film stability and lower blink rate in dogs versus humans (Butovich et al., 2011). The same types of molecules are found in the MGS of cattle, rodents, and marsupials (Butovich et al., 2011; Nicolaides & Santos, 1985). This outer lipid layer prevents evaporation of the underlying layers and overflow of tear film onto the eyelids, spreads over the aqueous subphase, imparts stability to the tear film, thickens the aqueous subphase, provides a smooth optical surface for the cornea, constitutes a barrier against foreign particles, provides some antimicrobial activity, and seals the lid margins during prolonged closure. Additionally, it prevents maceration of the lid skin by the tears (Bron et al., 2004).

The lipid layer is produced by sebaceous glands (i.e., tarsal or meibomian glands) of the eyelids. These glands undergo holocrine secretion (release of the entire cell and its contents). Androgens as well as neurotransmitters are likely involved in the regulation of MGS. Androgen receptor mRNA and protein have been isolated from rat, rabbit, and human meibomian acinar epithelial cells. Additionally, the neuropeptides, calcitonin gene-related peptide, substance P, neuropeptide Y, and vasoactive intestinal peptide have been identified in association with meibomian glands in humans and guinea pigs (Davidson & Kuonen, 2004). A lipid layer may not be present in all species, as one was not detected in sea lions (Kelleher Davis et al., 2013).

The middle aqueous layer (~7 µm) is the thickest (>60% of the total tear film thickness) and performs the primary functions of the tear film. This layer is composed of ~98% water and ~2% solids, comprising predominantly proteins. The aqueous layer contains inorganic salts, glucose, urea, proteins, glycoproteins, and soluble mucins (Butovich et al., 2008; Hicks & Carrington, 1997; Hicks et al., 1998). The lacrimal gland, gland of the NM, harderian gland, and accessory lacrimal glands in the conjunctiva all contribute to its formation. Destruction or excision of the lacrimal gland or NM gland results in a variable reduction in aqueous tear production (Gelatt et al., 1975; Helper et al., 1974; McLaughlin et al., 1988; Saito et al., 2001). These studies indicate that approximately two-thirds of the aqueous tear production is produced by the lacrimal gland, approximately one-third by the gland of the third eyelid, and a very minor amount by the accessory lacrimal glands in the conjunctiva; however, there is variability between dogs. The aqueous portion is evaluated clinically primarily through use of the Schirmer tear test (STT), but the phenol red thread test can be used in very small animals.

The deep, or mucin, layer (~1 µm) is composed of tear mucins produced by the apocrine conjunctival goblet cells, as well as an underlying glycocalyx which is associated with the corneal and conjunctival microvilli. The distribution of goblet cells varies among species. The fornix is rich in goblet cells in dogs, cats, and horses (Bourges-Abella et al., 2007; Eördögh et al., 2017; Moore et al., 1987; Sebbag et al., 2016), whereas the highest density in chinchillas and guinea pigs is in the palpebral conjunctiva (Gasser et al., 2011; Voigt et al., 2012). All species have lower concentrations of goblet cells in the bulbar conjunctiva. In rats and mice, the goblet cells occur in clusters, while in rabbits, cats, dogs, and humans, they appear as single cells (Huang et al, 1988). Mucin is produced by goblet cells in response to mechanical, immune, histamine, antigenic, or (direct or indirect) neural stimulation (Davidson & Kuonen, 2004). The gel-forming mucin layer contains glycoproteins (20–40 million daltons and classified as MUC1-21), which are carbohydrate–protein complexes characterized by the presence of hexosamines, hexoses, and sialic acid.

The glycocalyx comprises polysaccharides that are produced by the stratified squamous epithelial cells of the cornea and conjunctiva and project from the surface microvilli of those cells. They are considered membrane-spanning mucins versus secreted mucins that are described above (Dartt, 2011). In dogs, MUC16 is expressed at a higher level than MUC1 and MUC4, whereas rabbits have relatively equal expression of all three mucins. Additionally, the peripheral corneal epithelium has higher MUC1, MUC4, and MUC16 mRNA expression when compared with the central corneal epithelium (Leonard et al., 2016). Roles specific to these membrane-associated mucins include promotion of water retention, provision of a dense barrier to pathogens and debris, participation in signal transduction, and direct interaction with the actin cytoskeleton (Gipson & Argueso, 2003). Mucins from the goblet cells and the corneal epithelial cells both play a critical role in lubricating the corneal surface, thus making its hydrophobic surface more hydrophilic (to permit spreading), and in stabilizing the PTF (Van Haeringen, 1981). The mucin layer as well as the integrity of the outermost layer of corneal epithelium are necessary for retention of the tear film on the cornea (Mishima, 1965).

Tears are a clear and slightly alkaline solution, with a mean pH of 8.3, 8.1, and 7.8 in cattle, dogs, and horses, respectively (Beckwith-Cohen et al., 2014). In humans, horses, cattle, and rabbits, tear electrolyte concentration is similar to that of plasma, except for potassium, which is three to six times more abundant in tears, thus indicating an active transport mechanism (Best et al., 2015; Maidment et al., 1985; Mircheff, 1989). Tear film osmolarity/osmolality is influenced by the rate of tear secretion, evaporation, and composition. It is similar in cats (329 mOsm/L), dogs (356 mOsmol/L), and rabbits (376 mmol/kg; Davis & Townsend, 2011; Korth et al., 2010; Wei et al., 2012), whereas humans (283 mmol/kg) and horses (284 mmol/kg) have a lower osmolarity (Best et al., 2015; Wei et al., 2012). Even though the units are different, osmolarity and osmolality are interchangeable parameters in aqueous solutions such as the tear film.

In human patients, increased osmolarity is correlated with a faster tear film break-up time and greater surface tension. Additionally, hyperosmolarity induces expression and production of inflammatory cytokines and activates several signaling pathways that activate inflammatory cells (Davis & Townsend, 2011). Mean total solids concentration in the PTF of horses, cattle, and dogs is ~2 ± 1.3 g/dL, ~1 ± 0.6 g/dL, and ~0.3 ± 0.2 g/dL, respectively (Beckwith-Cohen et al., 2014). The glucose concentration is lower in human tears than in plasma, but its concentration parallels that in plasma. However, in human patients with diabetes, the elevated glucose concentrations in tears appear to be related to the tissue fluids and are not from the lacrimal gland secretions (Zhang et al., 2011). Normal horses have measurable cortisol in their tears that approximates serum cortisol following adrenocorticotropic hormone (ACTH) stimulation. The results of this study raise the question of whether this cortisol could hinder corneal healing in this species (Monk et al., 2014).

The PTF contains both nonspecific and specific antimicrobial substances. Nonspecific substances include lysozyme, lactoferrin, α-lysine, and complement. Specific antimicrobial substances include secretory immunoglobulins A, G, and M. Toll-like receptors that play a role in the defense against many types of microbial infections are expressed by the corneal and conjunctival epithelial cells in humans and horses (Gornik et al., 2011; Kumar & Yu, 2006). Protein concentrations in canine tears average 0.35 g/dL, with 93% globulin, 4% albumin, and 3% lysozyme, which is a ubiquitous antibacterial enzyme that hydrolyzes bacterial cell walls (Roberts & Erickson, 1962). Lysozyme is produced by the conjunctival goblet cells and has antibacterial and antifungal properties; its concentration increases with conjunctivitis (Roberts & Erickson, 1962). Relative to humans and nonhuman primates, domestic animals have very low amounts of lysozyme (e.g., the horse has one-half to one-fourth that of human tears) and the cat has none (Bonavida et al., 1968; Erickson et al., 1956; Luchter & Gurisatti, 1974; Marts et al., 1977). Lysozyme activity has not been detected in cattle, but it has been detected in sheep and goats (Daubs, 1976). Lactoferrin has been identified in the PTF of humans, dogs, cats, cattle, and other mammals, and reversibly binds the iron that would be available for bacterial metabolism and growth (Holmberg et al., 2004). Immunoglobulin A (IgA) contributes to ocular defenses by coating bacterial and viral microorganisms leading to agglutination, neutralization, and lysis. IgA is present in greater concentrations in the PTF than immunoglobulins G and M (Davidson & Kuonen, 2004). Cat tears have a 6.6 mg/mL total protein concentration with 9.7% IgA (Petznick et al., 2012).

The lacrimal nerve, a branch of the trigeminal nerve, is primarily sensory but also provides the lacrimal gland with its parasympathetic (release ACh and VIP neurotransmitters) and sympathetic (release norepinephrine and neuropeptide Y neurotransmitters) fibers (Elsby & Wilson, 1967; Powell & Martin, 1989). Both adrenergic and cholinergic distribution patterns around the acini and blood vessels of the canine lacrimal gland are similar; however, the cholinergic fibers appear to be greater in number than the adrenergic fibers (Powell & Martin, 1989). The acinar cells are primarily responsible for secretion of proteins in lacrimal gland fluid. These proteins are synthesized in the endoplasmic reticulum, modified in the Golgi apparatus, and stored in secretory granules. Stimulation of the cholinergic and adrenergic fibers in the lacrimal gland initiates release of these proteins into the lacrimal fluid. This process requires a series of separate cellular pathways that use secondary messengers and is controlled by signal transduction (Dartt, 1989).

Lacrimation is stimulated by painful irritants, eye diseases, mechanical or olfactory stimuli of the nasal mucous membranes, and sinus diseases. Tear production as assessed with the external ocular surfaces anesthetized and the lower conjunctival fornix dried by Dacron swabs (STT II) measures ~50% of that measured without manipulation (STT I) in the cat and dog. Larger dogs also have greater wetting per minute than smaller dogs as measured with the STT I (Berger & King, 1998; Gelatt et al., 1975). Additionally, canine neonates have lower tear production than adults (da Silva et al., 2013; Verboven et al., 2014). In one litter of puppies, both the STT I and STT II increased significantly until 9 and 10 weeks of age, respectively (Verboven et al., 2014). Clinical estimation of the rate of evaporation (and, indirectly, of the mucus component of the PTF) is performed through determining the time (in seconds) for the tear film to break up (Carrington et al., 1987a, 1987b, 1987c). While somewhat subjective, this has been studied in dogs and cats and is covered in Chapter 10.

The nasolacrimal drainage system eliminates used tear film and any excessive tears. The PTF accumulates along the palpebral margin of each eyelid and is forced by blinking to move medially into the lacrimal puncta. When the tears are in the lacrimal pool and the facial muscles relax, the tears flow into the canaliculi by capillary action. Normal breathing movements also facilitate this flow into the canaliculi. Reflex blinking of the eyelids closes the lacrimal sac, which acts as a passive pump. Pseudoperistaltic motion of the nasolacrimal duct allows movement of the tears into the nasal cavity (François & Neetens, 1973). Autoregulation of the lacrimal system with receptors in the excretory portion has been suggested in studies of human tear flow (François & Neetens, 1973). Evaluation of canalicular function in humans suggests that destruction of either canaliculus alone does not affect excretion of tears; in domestic animals, the lower canaliculus is considered to be the more important for tear drainage (Jones et al., 1972).

Cornea

The clear cornea serves as a window for the eye with two critical optical properties, transparency and refractive power, both of which are essential for vision. The cornea, with the sclera, protects the inner components of the eye from injury through its exquisite structure, biomechanics, and sensitivity.

Transparency

The cornea serves as the most powerful refractive structure of the eye. To fulfill this role, it must remain transparent. Corneal clarity is a result of the lattice-like organization of the stromal collagen fibrils as well as the transparency of the cells within the cornea. The state of relative dehydration, hypocellularity, unmyelinated nerve fibers, a nonkeratinized epithelium, and absence of blood vessels and pigment also contribute to corneal transparency. For further details on how the cornea refracts light, see Chapter 4.

The corneal stroma comprises the bulk of the cornea and is responsible for 90% of its thickness. It is predominantly composed of water that is stabilized by an organized network of collagens, glycosaminoglycans (GAGs), and glycoproteins. Cellular and nerve components are also present. Type 1 collagen is the most abundant form in the cornea; it aggregates into structural, banded fibrils with a uniform diameter of 25 nm in the central cornea that gradually increase to 50 nm at the limbus (Meek, 2008; White et al., 1997). Correspondingly, interfibrillar spacing is relatively constant in the central cornea at 20 nm and gradually increases in the paraxial cornea, before rapidly increasing at the limbus (Meek, 2008). The GAGs are important for maintaining this regular spacing between fibrils. The uniform-thickness, small collagen fibrils arrange into parallel lamellae running at oblique angles to each other, and are separated by less than a wavelength of light (Fig. 3.2; Maurice, 1960). This formation results in a highly ordered lattice-like arrangement whereby short-range order results in corneal transparency via destructive interference. However, it lacks the precise arrangement of a true crystalline lattice. The parallel arrangement of the corneal collagen fibers extends from the center of the cornea to its periphery, where the fibrils develop a concentric configuration to form a "weave" at the limbus, which in turn provides strength and helps to maintain its curvature. For further details on the constituents and structure of the cornea, see Chapter 2.

Quiescent keratocytes lie between collagenous lamellae to form a closed, exquisitely structured syncytium (Nishida et al., 1988). These three-dimensional, stellate-shaped cells comprise a cell body with multiple, extensive dendritic processes that interact with other keratocytes. Abundant corneal crystallins (~25–30% of the intracellular soluble protein), such as aldehyde dehydrogenase and transketolase,

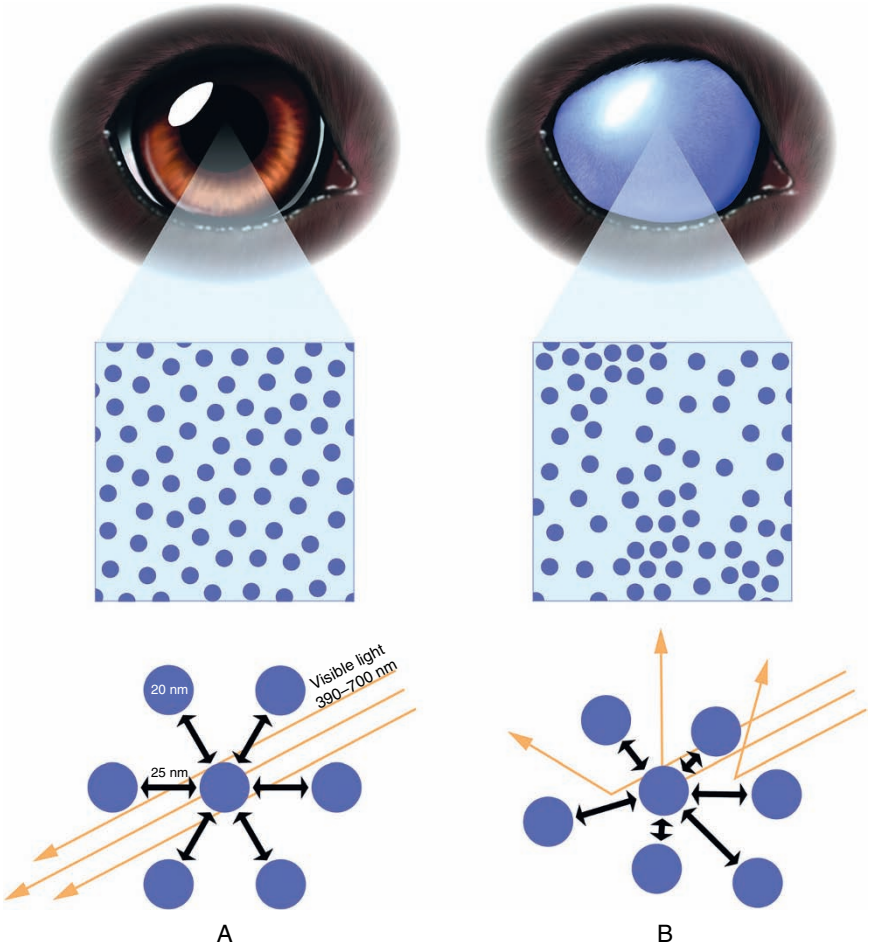

Figure 3.2 In the normal cornea (**A**), a cross-section of the corneal fibrils demonstrates a nearly perfect lattice arrangement, with equidistant collagen fibrils permitting light transmission and concomitant transparency. By contrast, swelling of the cornea with edema (**B**) disrupts this highly ordered arrangement, resulting in light diffraction and an opaque, blue cornea.

minimize refractive differences in the keratocyte cytoplasm, thus ensuring transparency of these cells. Furthermore, the dendritic cellular processes of normal keratocytes demonstrate negligible backscatter of light (Jester et al., 1999). The thinness and even spacing of keratocytes in a clockwise circular arrangement throughout the stroma also minimize light scatter. Upon corneal wounding, transformation of keratocytes to activated fibroblasts and myofibroblasts results in a dramatic increase in cell volume and subsequent dilution of corneal crystallins with a concomitant increase in light scatter (Jester et al., 2012). Corneal scarring is now thought to be due to alterations in the light-scattering properties of keratocytes, in addition to changes to the extracellular matrix (Jester, 2008).

The epithelium and endothelium are responsible for maintaining the cornea in a relatively dehydrated state. Specifically, loss of the corneal epithelium or endothelium results in a 200% or 500% increase in corneal thickness, respectively, due to stromal edema (Maurice & Giardini, 1951). Anatomic integrity of the epithelium and endothelium provides two-way, physical barriers against the influx of tears and aqueous humor (AH), respectively. However, the multiple-layered epithelium provides a relatively impermeable barrier versus the leaky, single-layered endothelium. The endothelium primarily maintains stromal deturgescence via active transport that is energetically maintained by sodium potassium–activated adenosine triphosphatases (Na^+-K^+-ATPases; Dikstein & Maurice, 1972). A summary of the molecular mechanisms that contribute to the corneal endothelial pump was provided by Bonanno (2012).

Metabolism

Steady-state hydration in the cornea occurs when the endothelial leak and pump rates are equivalent; this process is termed the "pump-leak" mechanism (Maurice, 1960). The leaky barrier function of the endothelium may at first seem counterintuitive, but most nutrients for the cornea, except

oxygen, come from the AH. Thus, leakiness of the endothelium is essential to providing bulk fluid flow through a tissue that lacks blood and lymphatic vessels. Glucose transporters are found on both the apical and basolateral endothelial cell membranes that face the AH and stroma, respectively, to ensure transcellular glucose flux (Kumagai et al., 1994). The corneal epithelium converts glucose to glucose-6-phosphate, where it is subsequently metabolized to pyruvate via glycolysis. Most of this pyruvate is then metabolized into lactate, but some is diverted into the tricarboxylic acid cycle to produce ATP. Glucose is also stored in the epithelium as glycogen, which can be used for energy under stressful conditions such as corneal injury.

The corneal epithelium and keratocytes in the anterior stroma obtain oxygen for aerobic glycolysis from the precorneal tear film, while the endothelium and keratocytes in the posterior stroma receive their oxygen from the AH. Upon eyelid closure, oxygenation of the anterior cornea is achieved by exposure to the palpebral conjunctiva and its vasculature. However, the palpebral conjunctiva has approximately one-third the atmospheric oxygen concentration, resulting in reduced corneal oxygenation (Chhabra et al., 2009). Consequently, the corneal epithelium will rely on anaerobic glycolysis for energetic needs in the absence of oxygen. If excessive lactate is produced by this process, corneal hydration occurs (Forrester et al., 1996; Maurice, 1960). Glucose is also metabolized by the corneal epithelium via the pentose phosphate shunt, which produces nicotinamide-adenine dinucleotide phosphate (NADPH), an important free radical scavenger. Other metabolites from this pathway are ribose-5-phosphate (ribose-P) and reduced triphosphatepyridine nucleotide. Ribose-P is used in nucleic acid synthesis of DNA or RNA, whereas triphosphate-pyridine nucleotide is used by the corneal epithelium for lipid synthesis. Keratocytes primarily metabolize glucose via the pentose phosphate shunt as their metabolic needs are limited, and primarily relate to maintenance of the collagen fibrils and GAGs within the stroma. By contrast, the corneal endothelium has immense glucose needs (~5 times that of the epithelium) to sustain its pump mechanism. It uses similar glycolytic pathways as the epithelium: mainly anaerobic glycolysis, with the pentose phosphate and tricarboxylic acid pathways also making substantial contributions.

Biomechanics

The cornea is a thick-walled, pressurized, partially intertwined, unidirectionally fibril-reinforced laminate biocomposite, which imparts stiffness, strength, and extensibility to withstand both inner and outer forces that may alter its shape or integrity (Dawson et al., 2011; US Department of Defense, 1997; Hayes et al., 2007; Thomasy et al., 2014). A soft, fibrous connective tissue, like the cornea, usually is much stronger in the parallel versus perpendicular direction to the collagen fibrils (Fung, 1981). Consequently, the collagen fibrils are arranged into complex hierarchic structures, which give the cornea its anisotropic mechanical properties (Silver et al., 1992). The collagen lamellar architecture of the cornea varies dramatically between vertebrate species, with nonmammalian vertebrates exhibiting an orthogonal-rotational arrangement with a marked increase in lamellar branching in species such that birds >> reptiles > amphibians > fish; by contrast, the mammalian species exhibit a random pattern (Winkler et al., 2015). In mammals without a Bowman's membrane, the biomechanical behaviors of the cornea from the macro- to nanoscale are primarily due to the collagen architecture in three composite-like regions: anterior stroma, posterior stroma, and Descemet's membrane (Fig 3.3; Boyce et al., 2007; Bron, 2001; Elsheikh et al., 2008; Jue & Maurice, 1986; Meek & Newton, 1999; Winkler et al., 2015).

Tissues are biomechanically characterized by measuring the elastic modulus, a property that defines a material's ability to resist deformation under an applied stress, which approximates its stiffness. The elastic moduli of the layers of the cornea have been reported and the values can differ markedly depending on methods of measurement and/or sample preparation (McKee et al., 2011). In thin, heterogenous tissues such as the cornea, atomic force microscopy (AFM) is optimal for determining the micron-scale deformations that cells and their adjacent matrix experience. The elastic moduli of the corneal layers as measured by AFM have been reported in the human and the rabbit (Table 3.3); all layers of the human cornea were stiffer than those of the rabbit (Last et al., 2009, 2012; Thomasy et al., 2014). The variability in corneal collagen fiber organization and matrix properties observed between species likely contributes to their diverse mechanical properties (Thomasy et al., 2014; Worthington et al., 2014). For more information on corneal biomechanics, we direct the reader to these excellent summaries: Dawson et al. (2011), Kling and Hafezi (2017), Pinero and Alcon (2015), and Ruberti et al. (2011).

Sensitivity and Innervation

The cornea is an exquisitely sensitive tissue, and this sensitivity provides a critical protective function. Upon stimulation of the cornea, involuntary blinking occurs via intermediate relays from the ophthalmic branch of the trigeminal nerve to orbicularis oculi innervation from the facial nerve – a fundamental reaction termed the corneal or blink reflex. Concomitant with the blink reflex is reflex tearing from parasympathetic innervation to the lacrimal gland. During extreme pain, the corneal reflex is exaggerated, and blepharospasm sometimes occurs such that the eyelids cannot be opened voluntarily. Corneal sensitivity varies by species, region of the cornea, and, in the dog and cat, skull conformation (Barrett et al., 1991; Blocker & van der Woerdt,

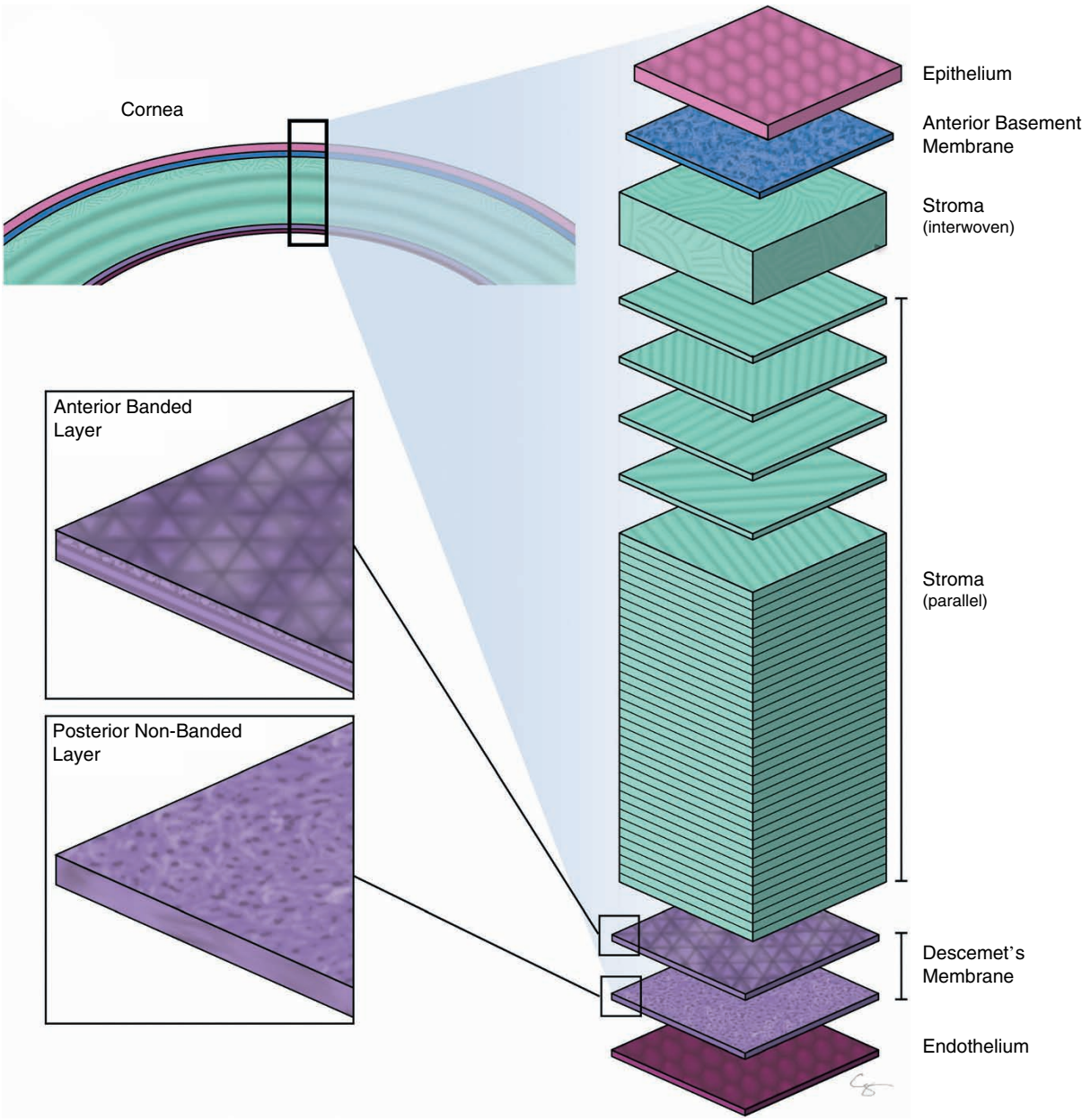

Figure 3.3 Schematic of collagen fiber organization in the canine cornea. The epithelium produces an anterior basement membrane with a complex surface topography consisting of a meshwork of fibers and holes. The anterior 10% of the cornea comprises unidirectional, interwoven collagen lamellae, while the posterior 90% consists of unidirectional, nonwoven collagen lamellae with a random orientation. Descemet's membrane, the specialized basement membrane of the endothelium, can be divided into the anterior banded and posterior non-banded layers. The anterior banded layer is dominated by collagen VIII, which appears as a hexagonal network en face and parallel bands in transverse section. The surface topography posterior non-banded layer has a rich network of intertwined fibers, but with a smaller pore size in comparison to the anterior basement membrane.

2001; Good et al., 2003). For example, corneal sensitivity in dogs, as measured by the Cochet–Bonnet esthesiometer and histology of the corneal nerves, was highest, intermediate, and lowest in the dolichocephalic, mesatocephalic, and brachycephalic skull types, respectively (Barrett et al., 1991). Similarly, the central cornea is less sensitive in brachycephalic cats than Domestic Shorthair (DSH) cats (Blocker & van der Woerdt, 2001). Corneal sensitivity is greatest in the central cornea and lower in the peripheral cornea (Barrett et al., 1991; Good et al., 2003). For more detailed information on corneal esthesiometry, see Chapter 10.

The cornea is one of the most richly innervated tissues in the body. Most corneal nerve fibers are sensory in origin and respond to mechanical, chemical, and thermal stimuli via

Table 3.3 Elastic moduli of layers of the cornea as determined by atomic force microscopy in rabbits and humans.

	Elastic Modulus (kPa)	
Corneal Layer	**Rabbit (Thomasy et al., 2014)**	**Human (Last et al., 2009, 2012)**
Epithelium	0.6 ± 0.3	Not assessed
Anterior basement membrane	4.5 ± 1.2	7.5 ± 4.2
Bowman's layer	Absent	110 ± 13
Stroma	1.1 ± 0.6 (anterior) 0.4 ± 0.2 (posterior)	33 ± 6 (anterior)
Descemet's membrane	12 ± 7.4	50 ± 18
Endothelium	4.1 ± 1.7	Not assessed

the ophthalmic branch of the trigeminal nerve. However, a small proportion of nerves are sympathetic or parasympathetic in origin and derive from the superior cervical ganglion or ciliary ganglion, respectively. Corneal nerve organization is similar across mammalian species, with only minor interspecies differences. All mammalian corneas contain a dense limbal plexus, multiple radially directed stromal nerve bundles, a dense highly anastomotic subepithelial plexus, and a richly innervated epithelium (Fig. 3.4; Marfurt et al., 2001).

In the dog, corneal innervation arises from the corneal limbal plexus, which comprises a 0.8–1 mm wide, ring-like band, surrounding the peripheral cornea. Morphologically, this plexus can be further subdivided into a predominantly perivascular, outer, periscleral zone and a denser and more highly branched inner, pericorneal zone. From the limbal plexus, nerve fibers enter into the stroma as 14–18 prominent, radially directed, superficial stromal bundles that are

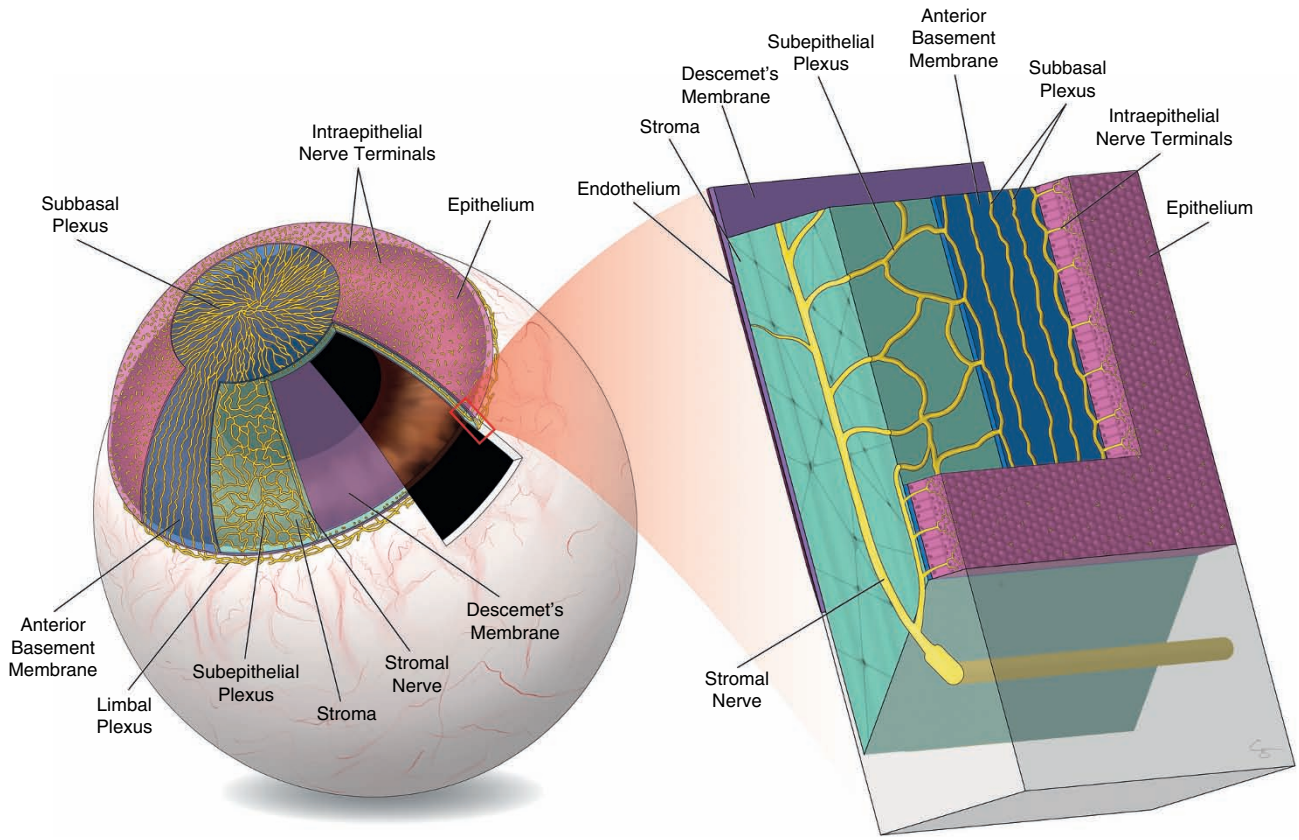

Figure 3.4 Schematic of corneal innervation. The limbal plexus is a ring-like band of predominantly myelinated fibers in the sclera adjacent to the cornea. From the limbal plexus, nerve fibers enter into the corneal stroma as nerve bundles and lose their myelin as they traverse to the central cornea. The subepithelial plexus is a dense, anastomosing network of thin axons immediately underlying the anterior basement membrane. The subepithelial plexus gives rise to the subbasal plexus, a whorl-shaped network of axons between the anterior basement membrane and basal epithelium where nerve fibers run horizontally as long parallel nerves, termed leashes. The axons of the subbasal plexus then vertically ascend to terminate in various layers of the epithelium.

evenly distributed around the limbus (Marfurt et al., 2001). The number of stromal bundles varies among mammals, with 6–8 and ~60 bundles in the rat and human, respectively (Muller et al., 1996; Sasaoka et al., 1984). Any myelinated axons included in stromal nerve bundle will lose their myelin as they traverse toward the central cornea. Each bundle in the canine cornea contains approximately 30 to 40 axons which undergo repetitive dichotomous branching to form complex axonal trees that innervate the anterior cornea (Marfurt et al., 2001). Immediately beneath the anterior basement membrane is a dense, anastomosing network of exceptionally thin, preterminal axons that comprise the subepithelial nerve plexus. The subbasal plexus arises from subepithelial nerve fibers entering the basal epithelium to form unique, preterminal arborizations termed epithelial leashes which exhibit a highly ordered distribution and give rise to a profusion of smaller, ascending branches (Marfurt et al., 2001). The subbasal nerve plexus of dogs, cats, and humans has a centripetal whorl-like pattern, whereas cattle and rabbits exhibit a horizontal pattern that is directed nasally (He et al.,2019; Marfurt et al., 2019). The innervation of the epithelium is denser than any other surface epithelium such that injury to a single epithelial cell may be sufficient to stimulate nociception (Marfurt, 2000). While the anterior cornea is densely innervated, only sparse nerve fibers are present in the posterior cornea and are typically adjacent to the corneal endothelium (Marfurt et al., 2001). Thus, superficial corneal ulcers are typically more painful than deep stromal ulcers.

The majority of sensory fibers that innervate the cornea are activated by a variety of exogenous mechanical, chemical, and thermal stimuli, as well as endogenous factors released by tissue injury, and are thus termed polymodal nociceptors (Belmonte & Giraldez, 1981; Belmonte et al., 1991; Gallar et al., 1993). The remainder of the sensory fibers innervating the cornea comprise mechano-nocireceptors and cold thermal receptors, which are only activated in response to mechanical forces or changes in temperature, respectively (Gallar et al., 1993; Tanelian & Beuerman, 1984). Furthermore, electrophysiologic recordings of impulses from corneal nerve fibers of anesthetized cats demonstrated that different types of stimuli evoked variable responses from the three aforementioned sensory receptors (Acosta et al., 2001).

In addition to their contributions to corneal protection via the blink reflex and reflex tearing, corneal nerves maintain corneal epithelial health through the secretion of trophic factors and maintenance of basal tear secretions (Lawrenson, 1997; Muller et al., 2003). Specifically, corneal nerves secrete a variety of neurotransmitters, including acetylcholine, vasoactive intestinal peptide (VIP), and neurotensin, as well as neuropeptides such as substance P and calcitonin gene-related protein (CGRP), which are critical to corneal epithelial proliferation and function (Belmonte et al., 2004; Muller et al., 2003). Thus, impairment of corneal sensory innervation, termed neurotrophic keratitis, causes decreased corneal healing, increased epithelial permeability, and recurrent corneal ulcers (Beuerman & Schimmelpfennig, 1980; Bonini et al., 2003; Muller et al., 2003; Scott & Bistner, 1973). The neuropeptides CGRP and substance P also act as neurogenic mediators of inflammatory responses by inducing vasodilatation, plasma extravasation, and cytokine release following their release from depolarized nociceptor endings (Bynke et al., 1984; Keen et al., 1982). This neurogenic inflammation impacts both the injured cornea and the noninjured conjunctiva, iris, and ciliary body, as nerve impulses from stimulated nociceptors travel not only centripetally through the axon to the central nervous system, but also to nonstimulated peripheral axon branches of the trigeminal nerve. This reflex is likely responsible for the clinical signs of conjunctival hyperemia and anterior uveitis, including miosis, ocular hypotension, and aqueous flare associated with an isolated corneal lesion (Belmonte et al., 2004).

Iris and Pupil

Pupillary functions include regulating light entering the posterior segment of the eye, increasing the depth of focus for near vision, and minimizing optical aberrations by the lens. The iris muscles consist of both a constrictor (sphincter) that encircles the pupil and radial dilator muscle. The sphincter muscle is an annular band of smooth muscles near the pupillary margin of the iris and is derived from neural ectoderm. The dilator muscle, also derived from neural ectoderm, consists of a series of myoepithelial cells that extend from near the pupillary margin to the base of the iris and are contiguous posteriorly with the pigmented epithelium of the ciliary body. Pupil size varies on the basis of the balance between these two muscle groups. The constrictor muscle, which is the stronger of the two, is innervated by the oculomotor nerve (CN III) which provides primarily parasympathetic control; by contrast, the dilator muscle is innervated primarily by sympathetic nerves. The constrictor muscle causes miosis, and the dilator muscle is responsible for mydriasis. Bright light decreases pupil size. The sympathetic activity in the iridal dilator muscle and ciliary body musculature (discussed later) is mediated by a combination of β-receptors (β_1 and β_2) and α-receptors (α_1 and α_2; Yoshitomi & Ito, 1986). Components of the pupillary light reflex (PLR) are listed in Table 3.4.

Species differences of the α- and β-receptors have been demonstrated among humans, rabbits, nonhuman primates, cats, and dogs, and they are summarized in Table 3.5 (Bartlett & Jaanus, 1989; Colasabti & Trotter, 1981; Jones & Studdert, 1975; Lee & Wang, 1975; Loewy et al., 1973; Macri & Cevario, 1974; Murphy & Howland, 1986; Neufeld & Sears, 1974; Ogidigben & Potter, 1993; Piccone et al., 1988; Potter & Rowland,

1978; Shields, 1992; Toyoshima et al., 1980; van Alphen et al., 1965; Vareilles et al., 1977b; Wallenstein & Wang, 1979; Yoshitomi & Ito, 1986, 1988; Zimmerman, 1993). These receptors alter the effects of drugs on the eye. For example, feline pupils constrict with the use of timolol, a nonselective β-adrenergic antagonist, because the feline iris sphincter muscle has primarily β-adrenergic nerve fibers (van Alphen et al., 1965). Because β-adrenergic nerve fibers are inhibitory to the sphincter muscle, the miosis in response to topically applied timolol is suspected to be the result of its antagonism of inhibitory input to the sphincter muscle (Kiland et al., 2016). Most synapses in the ciliary ganglion are involved in relaying impulses that result in accommodation; the remainder are concerned with constriction of the pupil. Pure mu opioid agonists such as morphine act on subcortical cells (i.e., oculomotor nuclear complex) to cause constriction of the canine pupil and dilation of the feline pupil because of the release of catecholamines from the adrenal glands (Lee & Wang, 1975; Wallenstein & Wang, 1979). Endogenous prostaglandin F2α appears to be involved in maintaining muscle tone in the sphincter muscle of the iris. Prostaglandins most likely act directly on these muscles, and they appear to act to a lesser extent on the dilator muscles of the canine iris (Yoshitomi & Ito, 1988). Exogenous prostaglandin analogues cause miosis in cats, dogs, and horses, and the receptors have been detected in the iris and ciliary body of several mammals (Bhattacherjee & Paterson, 1994; Bhattacherjee et al., 1997; Gum et al., 1991; Willis et al., 2001). Additionally, biologically active peptides have been isolated in the nerve supply of the intraocular muscles. For example, neuropeptide Y has a modulatory role on the iris dilator muscles that enhances adrenergic-induced contractions. By itself, however, neuropeptide Y does not have any potent contractile qualities (Piccone et al., 1988).

Iridal color and pupil size vary widely among species, and the irides of the young are often a different color than those of the adult. Iris color, or the amount of melanin, influences the effects of many drugs, as melanin can bind drugs, increasing their time to onset and duration (Ogidigben & Potter, 1993).

Pupil shape also varies among species. Vertical pupils are most commonly seen in terrestrial mammals and reptiles that are ambush predators and are diurnal. Prey species tend to have horizontally elongated pupils. These respective variations are thought to keep images on the vertical and horizontal contours sharp. In domesticated cats, the constricted pupil is a vertical slit, whereas in the larger, wild felidae, it is circular. On dilation, the vertical sides of the domestic feline pupil expand to produce a circular pupil. The constrictor muscle fibers are vertically oriented, and therefore contraction leads to a vertically oriented slit pupil. Additionally, in prey with horizontal pupils, changing head pitch causes torsional movement of the eye, such that the pupil's long axis maintains rough alignment with the horizon (Banks et al., 2015).

In young horses, the pupil is more circular than in adults. Under illumination, the ends of the oval pupil of mature horses do not constrict, but the dorsal and ventral borders do. In bright daylight, the superior granula iridica occludes the central papillary opening, resulting in two apertures and assisting with focusing through the creation of Scheiner's disc phenomenon (Murphy & Howland, 1986). With very low illumination or administration of a mydriatic, the dorsal and ventral borders of the pupil dilate, thereby forming a circular pupil. The equine pupil responds relatively slowly to a light stimulus in comparison to that of cats and dogs.

Table 3.4 Components of the pupillary light reflex.

Stimulus	Illumination of the Retina
Receptors	Photoreceptors (rods and cones)
Afferent pathway	Optic nerve–optic tract to pretectal area (ipsi- and contralateral via posterior commissure)
Efferent pathway	Pretectal area to the parasympathetic nucleus of CN III (ipsi- and contralateral), and then parasympathetic fibers to ciliary ganglion (via CN III)
	Postganglionic fibers to the iris
Effector	Sphincter muscle of the iris
Response	Miosis (constriction of the pupil both direct and consensual reflex)

Table 3.5 Adrenergic receptors in the iris and ciliary body.

Species	Iris Sphincter	Iris Dilator	Ciliary Muscles
Human	α and β equally	Mainly α, very few or no β	Mainly β, very few α
Rabbit	Mainly β, few α	Mainly α, few β	Mainly α, few β
Monkey	Mainly α, perhaps β	Mainly α, few β	Only β, no α
Cat	Mainly β, some α	Mainly α, some β	Mainly β, some α
Dog	α and β	α And β	?

The avian pupil is circular and highly motile. The consensual pupillary reflex is usually absent (because of total decussation of nerve fibers at the optic chiasm), but occasionally a strong beam of light may traverse the posterior ocular layers and the thin medial orbital bones to stimulate the opposite retina. As the constrictor and dilator muscles are mainly striated with varying amounts of nonstriated fibers, the pupil is not affected by traditional mydriatic agents, but it can be dilated by various neuromuscular-blocking drugs.

When dogs are under combined injectable and inhalation anesthesia, the pupil reaches a steady baseline size. In this state, light stimulation causes a rapid pupil constriction, an initial redilation phase, and a slower secondary recovery to baseline. As light intensity increases, the amplitude of pupil constriction increases, and the latency decreases. Average constriction velocity and initial redilation velocity increase with increasing stimulus intensities, but then gradually decline with intensities greater than 11 log photons/cm^2/s. Similar to humans, dogs demonstrate intrinsically photosensitive retinal ganglion cells (ipRGC) that contribute to the PLR. Melanopsin, the ipRGC photopigment, has peak sensitivity at 480 nm. The ipRGCs are slow to activate and have a high threshold. Below the ipRGC threshold, PLRs to blue and red stimuli are similar. However, when the ipRGCs are strongly activated with a blue stimulus at 14.5 log photons/cm^2/s intensity, pupil constriction persists for at least 60 seconds after the stimulus is removed. Additionally in dogs, the stimulus intensity required to elicit a threshold PLR is approximately 10-fold lower than that required to elicit a scotopic threshold ERG response in the dark-adapted state (Whiting et al., 2013).

Nutrition of Intraocular Tissues

While allowing light transmission through the eye, nutrients are provided and waste is removed by two systems of blood vessels (i.e., retinal vessels, uveal vessels), the formation and egress of AH, and the vitreous body. Intraocular tissues lack a typical lymphatic system, and the uveal tract (i.e., iris, ciliary body, and choroid) provides this function.

Ocular Circulation

The choroid, ciliary body, and iris are supplied by the uveal vessels. The outer retina in some animals (e.g., dogs, cats, ruminants, and pigs) and almost all or the entire retina in others (e.g., horses, guinea pigs) is nourished by diffusion from the uveal vessels in the choroid. The inner retina is supplied by retinal vessels in many species. Blood vessels supplying the cornea and lens in the embryo regress before birth or shortly thereafter, leaving the AH as the primary source of nutrients for the cornea and lens.

Birds have a unique structure, the *pecten oculi*, which is a heavily pigmented, highly vascularized, and usually fanlike structure projecting from the surface of the optic nerve into the vitreous. A similar structure occurs in reptiles, termed the *conus papillaris*. The avian pecten likely functions as an important source of nutrients for the inner retina (Bellhorn & Bellhorn, 1975; Wingstrand & Munk, 1965). This assumption is based on the observations that the avian retina is thicker than oxygen could perfuse from the choroid and that the pectinate artery resistive and pulsatility indices are low (Chase, 1982; de Moraes et al., 2017; Ferreira et al., 2016). The pecten may also control the intraocular pH, which is affected by acidic retinal waste products (Brach, 1975). Several marine mammals, the bottlenose dolphin (*Tursiops truncatus*), spotted seal (*Phoca largha*), and California sea lion (*Zalophus californianus*), have an ophthalmic rete from which the retinal and choroidal arteries are derived. A higher degree of thermal emission in this area than adjacent areas of the skin suggests that the rete might conserve ocular heat so that photoreceptor and ocular muscle function can be maintained in a cold ambient temperature. Additionally, the rete may have a flow-damping effect by maintaining resistance to blood flow in the orbit (Ninomiya, 2017; Ninomiya et al., 2014).

Ocular Blood Flow

The vascular pressure promoting flow, the resistance of blood vessels, and the viscosity of the blood all influence the blood flow through all tissues, including the eye. The pressure head for blood flow (i.e., perfusion pressure) is the difference in pressure between the arteries and the veins. In the eye, the intraocular pressure (IOP) approximates the venous pressure, so the perfusion pressure is the difference in pressure between the small arteries entering the eye and the IOP (Bill, 1963). Of clinical importance is that the perfusion pressure to the eye is reduced by lowering the blood pressure or raising the IOP, as occurs in glaucoma. Studies of hemodynamics in the rabbit ophthalmic artery demonstrate that autoregulation maintains normal blood velocity and resistance when the IOP is below 40 mmHg. However, at higher pressures the autoregulatory capacity is limited (Yang et al., 2011)

Anterior Uveal Blood Flow

In most species, the major arterial circle of the iris is formed by the nasal and temporal long posterior ciliary arteries. The iris and ciliary body receive approximately 1% and 10%, respectively, of the ocular blood flow (Bill, 1975). In humans and rabbits, additional iridal blood flow occurs from the anterior ciliary arteries via the extraocular muscles (EOM). Blood flow to the ciliary body in most species that have been studied is provided by the iridal major arterial circle,

branches of the anterior ciliary arteries, and branches of the long posterior ciliary arteries. The cat and monkey iris and ciliary body have autoregulation of their blood flow. Carbon dioxide dilates the anterior uveal vessels, and sympathetic α-adrenergic receptors cause vasoconstriction in the anterior uvea. Parasympathetic muscarinic receptors and prostaglandins, however, cause vasodilation (Alm & Bill, 1972). Prostaglandins E_1 and $F_{2\alpha}$ appear to cause a two- to threefold increase in blood flow to the anterior uvea when applied topically (Green et al., 1985).

Choroidal Blood Flow

The outer retina (and the entire retina in some species) depends on choroidal blood flow for nutrients and waste removal. In the animal species studied, most of the blood supply to the choroid is supplied by the short posterior ciliary arteries, but some of the peripheral choroid receives blood from the major arterial circle of the iris. The choroidal capillaries are fenestrated and large (diameter 15–50 μm). These vessels are highly permeable and permit glucose, proteins, and other substances in the blood to enter the choroid.

Within the choroid, these proteins create a high osmotic pressure gradient that assists in removal of fluids from the retina. The short posterior ciliary arteries appear to supply well-defined territories within the choroid. As a result, these "watershed zones" can develop with marked elevations of IOP, and appear in the dog as pyramidal-shaped areas of choroidal and retinal degeneration extending from the optic nerve head.

The rate of uveal blood flow is rapid (1.2 mL/min in the cat), with a mean combined retinal and choroidal circulation time of 3–4 seconds (Bill, 1962; Freidman & Smith, 1965). In monkeys, 95% of the ocular blood flows through the uveal tract, of which 85% is through the choroid. With this high rate of blood flow, oxygen extraction from each millimeter of blood is low (~5%–10%). The oxygen content of choroidal venous blood is 95% of that in arterial blood. Reduced flow rates result in higher oxygen extraction, so that total extraction is reached. This protects the oxygen supply to the retina, and it also protects the eye from light-generated thermal damage (Bill, 1975). Choroidal vessels have little to no autoregulatory mechanism, but carbon dioxide is a potent vasodilator of choroidal vessels (Kiel & Shepherd, 1992; Mann et al., 1995; Yu et al., 1988). Choroidal vessels are under the strong influence of sympathetic stimulation, which can result in a 60% reduction of choroidal blood flow. Parasympathetic fibers have been found in the choroid of monkeys, but no studies concerning the relationship of these fibers to blood flow have been conducted. The α-adrenergic drugs cause vasoconstriction of choroidal vessels, but β-adrenergic drugs have no effect (Bill, 1975). In rabbits, α- and β-adrenergic blockade causes choroidal vasodilation and vasoconstriction, respectively (Kiel & Shepherd, 1992).

Retinal Blood Flow

The retina receives 4% of the ocular blood flow in the monkey (Bill, 1975). In cats, 20% of the oxygen consumed by the retina is delivered through the retinal circulation and the remaining 80% is via the choroidal circulation (Alm & Bill, 1972). Similar data are not available for other domestic animals.

Blood flow in the innermost retina is practically unaffected by moderate changes in perfusion pressure. Autoregulation of retinal blood flow is extensive in the cat, monkey, and pig, and protects the retinal circulation from large variations in perfusion pressure (Alm & Bill, 1972; Attariwala et al., 1994). Both metabolic and myogenous autoregulation are present in the eye. Metabolic control of retinal blood flow is similar to that of blood flow to the brain. In the brain, increased PO_2 and decreased PCO_2 cause vasoconstriction, and decreased PO_2 and increased PCO_2 cause vasodilation. In the cat, maximum retinal vasodilation occurs with an increased PCO_2 of 75–80 mmHg, so as to increase flow from 15 to 50 mL/min (Alm & Bill, 1972). Interestingly, retinopathy of prematurity occurs when immature eyes with developing blood vessels are exposed to higher oxygen concentrations than the normal physiologic *in utero* hypoxia. The increased oxygen causes vasoconstriction and inhibition of vascular development, with obliteration of vessels. With the hypoxic injury is a concomitant, rebound release of angiogenic factors that lead to pathologic angiogenesis. Signs include vasoproliferation, retinal edema, hemorrhages, and possible retinal detachment (Dogra et al., 2017).

Neural control of retinal blood flow is limited to those vessels indirectly affecting retinal blood flow. Retinal vessels have α-adrenergic-binding sites that, when stimulated, cause vasoconstriction, thus increasing retinal vascular resistance (Forster et al., 1987; Hoste et al., 1989). Retinal arteries most likely autoregulate through a myogenic mechanism, which is activated based on stretch. During sympathetic stimulation, myogenic autoregulatory responses appear to increase (Hoste et al., 1989). Opening and closing of capillary beds in many tissues occur with varying metabolic needs. Spontaneous contractions and dilations of small retinal arterioles have been observed in kittens, but are rare in adult cats (Bill, 1975). In general, it is believed that choroidal blood flow is constant through all capillary beds; however, regional blood flow in the retina decreases from the optic disc to the periphery (Laatikairen, 1976).

The vascular endothelial cells may produce nitric oxide, endothelins, prostaglandins, and renin-angiotensin products in response to chemical stimuli (e.g., acetylcholine, brachykinin), changes in blood pressure and blood vessel wall stress, changes in local oxygen levels, and other stimuli (Brown & Jampol, 1996). As the mechanisms of local autoregulation become better understood, pharmacologic modulation of these processes may become possible.

The theoretical oxygen diffusion maximum of 143 μm plays a significant role in animal species with avascular retinas; as a result, avascular retinas are usually very thin and have short photoreceptors, no tapeta, high glycogen levels in the Müller cells, and no retinal taper (Chase 1982).

Blood Flow of the Optic Nerve Head

Blood flow of the optic nerve head is usually provided primarily by branches from the short posterior ciliary arteries. In humans, cats, and rabbits, optic nerve head blood flow possesses autoregulation over a wide range of IOPs (~30–75 mmHg), but in humans, this autoregulation is most efficient when IOP is 6–30 mmHg (Shonat et al., 1992; Weinstein et al., 1983). Ocular perfusion pressure, the relationship between systemic blood pressure and IOP, determines blood flow in the optic nerve head. The autoregulatory capacity of optic nerve head blood flow is more susceptible to an ocular perfusion pressure decrease induced by lowering the blood pressure, compared with that induced by increasing the intraocular pressure (Wang et al., 2015).

Studies of blood flow in the optic nerve head have been limited by the small tissue mass involved. The optic nerve head is subjected to several different pressures as well as to the tissue stress at the level of the scleral lamina cribrosa. Axons from the retinal ganglion cells exit the eye under the effect of IOP, passing through the lamina scleral cribrosa at progressively decreasing tissue pressures to become the optic nerve. The retrolaminar pressure for these axons in the dog is approximately 7 mmHg and relates directly to the cerebrospinal pressure (Morgan et al., 1995). Both short- and long-term elevations in IOP also produce tissue changes within the lamina cribrosa that influence blood flow and axon vitality.

Ocular Barriers

The blood–ocular barriers contain endothelial and epithelial tight junctions with varying degrees of "leakiness." These barriers prevent nearly all protein movement and are effective against low-molecular-weight solutes such as fluorescein and sucrose. The complexities of these structures differ between the various vascular beds, which allow movement of some substances from one compartment to the other. The two primary barriers within the eye are the blood–aqueous barrier (BAB) and the blood–retinal barrier (BRB). Other lesser barriers of the eye exist as well. The zonula occludens of the corneal epithelium prevents the movement of ions and therefore fluid from the tears into the stroma, prevents some evaporation, and protects the cornea from pathogens. The partial obliteration of the intercellular spaces provided by the macula occludens of the corneal endothelial cells prevents bulk flow of AH into the corneal stroma but allows moderate diffusion of small nutrients and water.

Blood–Aqueous Barrier

The BAB depends primarily on the tight junctions in the nonpigmented ciliary body epithelium, the nonfenestrated iris capillaries, and the posterior iris epithelium. The anterior BAB in the iris allows transcellular transport by means of vesicles. Paracellular transport is controlled by tight junction extensions (Riva et al., 2011). The anterior surface of the iris does not serve as a barrier as it does not have a continuous cellular layer. The epithelial portion of the BAB is the inner, nonpigmented ciliary epithelium, and it controls the flow of fluid into the posterior chamber. The BAB is less effective than the retinal epithelial barrier, because protein can pass into the AH through leakage in other parts of the anterior uvea. Both the ciliary body and choroidal blood vessels are highly fenestrated and thus leak most of their plasma components, including protein, into the stroma.

No barrier is present between the AH and the vitreous humor, which allows the diffusion of solutes from the posterior aqueous into the vitreous humor, or between the anterior uvea and the sclera (Elgin, 1964). Breakdown of the BAB is seen clinically as an aqueous flare in anterior uveitis or secondary to loss of AH, as in anterior chamber paracentesis.

Blood–Retinal Barrier

The tight junctions between the retinal pigmented epithelial cells comprise the epithelial portion of the BRB. The nonfenestrated retinal capillary endothelium with tight junctions between the cells comprises the endothelial portion of the BRB. The most permeable point of the BRB is the optic nerve head, at which substances from the choroid can pass into the nerve (Rodriquez-Peralta, 1975). The choroidal capillaries are highly permeable to permit passage of all low-molecular-weight compounds and proteins. Thus, nutrients from the choroidal blood supply pass readily into the retinal pigment epithelium, where numerous transport systems account for the selectivity of the barrier and elaborate transcellular pathways exist to pass them on into the retina (Mann et al., 2003). This high protein permeability of the choroidal vessels also elevates osmotic pressure, which helps fluid to pass out of the retina. The transport of water from the retina to the choroid is driven by the active transport of chloride to prevent water accumulation in the subretinal space. No significant barrier exists between the vitreous body and the retina.

Aqueous Humor and Intraocular Pressure

In the normal eye, IOP is generated by flow of AH against resistance, and is necessary to maintain the appropriate shape and optical properties of the globe. AH is a clear, colorless liquid that fills the anterior and posterior chambers as well as the pupil. It has a refractive index of 1.335, which

is slightly denser than water, and is a critical constituent of the eye's optical system. As AH is formed by the ciliary body processes, it enters the posterior chamber and flows through the pupil into the anterior chamber, where it leaves the eye through the corneoscleral trabecular and uveoscleral outflow pathways. The rate of AH formation equals the outflow, so the IOP is maintained relatively constant, and the refractive surfaces of the eye are kept in a normal position.

This continuous flow of AH supplies the avascular cornea and lens with nutrients and also removes their waste products. A convection current exists within the anterior chamber whereby AH circulates downward adjacent to the air-cooled cornea and upward near the lens where the temperature is warmer. This thermal circulation is responsible for the deposition of cellular material – termed keratic precipitates – on the inferior aspect of the corneal endothelium.

Aqueous Humor Formation

The ciliary body has several critical functions, including production of AH by active secretion, ultrafiltration, and diffusion; generation of IOP through the aqueous dynamic process; influencing through its musculature the conventional (i.e., corneoscleral trabecular meshwork or pressure-sensitive) AH outflow; provision of blood and nerve supplies for the anterior segment; control of accommodation via its musculature; formation of the BAB; and provision of the entry for nonconventional (i.e., uveoscleral or pressure-insensitive) AH outflow. Furthermore, the ciliary body is also rich in antioxidant systems, with significant concentrations of catalase, superoxide dismutase, and glutathione peroxidase types I and II. In addition, the ciliary body is the major drug detoxification center in the eye, with its microsomes containing the cytochrome P_{450} proteins, which catalyze many drugs. In avian species, the ciliary body musculature is composed of distinct anterior and posterior components that alter the corneal curvature for corneal accommodation and move the ciliary body anteriorly for lenticular accommodation (Glasser & Howland 1996; Murphy et al., 1995).

The bilayered ciliary epithelium, consisting of the outer pigmented epithelium (PE) and inner nonpigmented epithelium (NPE), is the site for AH secretion. At their apical borders, the PE and NPE connect via gap junctions to form an intricate network (Fig. 3.5). Adjacent NPE cells are joined by tight junctions to form a barrier that inhibits paracellular diffusion. AH is formed by three basic mechanisms: diffusion, ultrafiltration, and active secretion by the NPE. The processes of diffusion and ultrafiltration form the "reservoir" of the plasma ultrafiltrate in the stroma of the ciliary body, from which the AH is derived via active secretion by the ciliary epithelium. Diffusion of solutes, such as carbohydrates, occurs from a region of higher concentration to that of lower concentration. By contrast, ultrafiltration occurs when movement of a compound across a cell membrane is increased by a hydrostatic force; in this case, from differences between ciliary body capillary pressure and IOP. Energy-dependent active transport is required to secrete solutes against a concentration gradient across the basolateral membrane of the NPE; it is the most important factor in AH formation (Cole, 1977; Pederson & Green, 1973). Two enzymes critical in this process, Na^+-K^+-ATPase and carbonic anhydrase (CA), are abundantly present in the NPE. The Na^+-K^+-ATPase is membrane-bound and is found in the highest concentrations along the basolateral interdigitation of these cells (Flugel & Lutjen-Drecoll, 1988). Inhibition of the Na^+-K^+-ATPase with cardiac glycosides (e.g., oubain) or vanadate causes a marked decrease in aqueous formation (Bonting & Becker, 1964; Cole, 1977; Garg & Oppelt, 1970) as differences in osmolarity between plasma and AH are small, thereby making the rate of aqueous production dependent on the rate of solute transfer (Maren, 1995).

Due to the primary active secretion of sodium, other molecules and ions cross over the epithelium by secondary active transport. As a consequence, increased concentrations of ascorbate, amino acids, and chloride are observed in AH relative to plasma in most mammalian species (Bito et al., 1965; Blogg & Coles, 1970; Cole, 1974; Gabelt & Kaufman, 2011; Graymore, 1970; McLaughlin & McLaughlin, 1988; Tulamo et al., 1990). Electroneutrality is maintained by anions accompanying the actively transported sodium; channels allow passage of chloride on the basolateral NPE membrane and a passive transporter exchanges bicarbonate for chloride. As a result, high osmolarity is produced on the basolateral aspect of the NPE, thus initiating diffusion of water out of the cells by aquaporins (Frigeri et al., 1995; Verkman, 2003). To continue the process, sodium and chloride constantly enter the PE via Na^+/H^+ and Cl^-/HCO_3^- antiports and a Na-K-2Cl cotransporter. Chloride is just as critical as sodium in driving AH formation, such that A3 adenosine receptor agonists, which enhance chloride release, increase IOP in mice.

CA is abundant in the cytoplasm and on the basal and lateral membranes of the NPE and PE and catalyzes the following reaction:

$$CO_2 + H_2O \leftrightarrow HCO_3^- + H^+.$$

Formation of bicarbonate by CA is essential for secretion of AH, such that inhibition of CA results in decreased active transport of sodium by the NPE; it is unclear how this process occurs, although several hypotheses exist (Gabelt & Kaufman, 2011). Topical and systemic CA inhibitors substantially decrease AH production, therefore reducing IOP, and are thus useful in the management of glaucoma (Higginbotham, 1989; Maslanka, 2015).

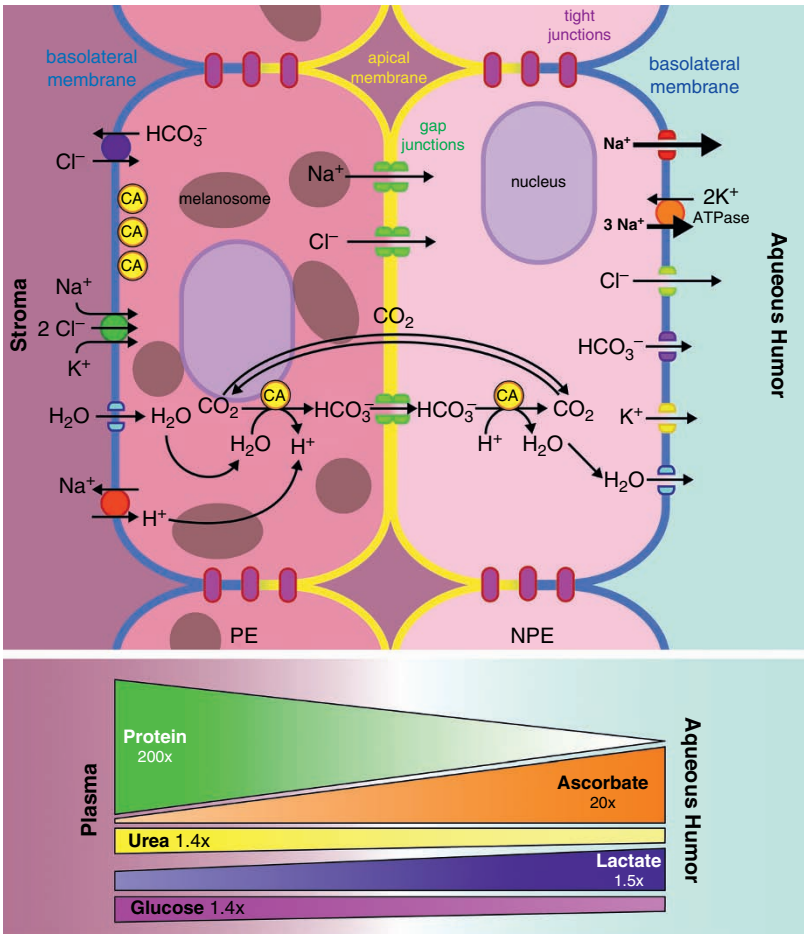

Figure 3.5 Schematic of aqueous humor (AH) production across the pigmented epithelium (PE) and nonpigmented epithelium (NPE) of the ciliary body. Note the position of the critical enzyme, sodium-potassium-activated adenosine triphosphatase (Na^+-K^+-ATPase) on the basolateral enzyme of the NPE. Carbonic anhydrase (CA), also critical to AH formation, is abundant in the cytoplasm of both the NPE and PE. Ion transporters and channels facilitate transfer of Na^+, K^+, chloride (Cl^-) and bicarbonate ($HCO3^-$) into, between, and out of the NPE and PE, while aquaporins enable water movement. Relative solute concentrations that most markedly differ between aqueous humor and plasma can be found at the bottom.

Aqueous Humor Composition

As an ultrafiltrate of plasma, the compositions of AH and plasma are similar, with a few notable exceptions: a low protein concentration, high ascorbate and lactate concentrations, and reduced amounts of urea, glucose, and nonprotein nitrogen occur within AH versus plasma (Fig. 3.5; Blogg & Coles, 1970; Caprioli, 1987; Cole, 1974; Graymore, 1970). Thus, breakdown of the BAB modifies the composition of the AH, primarily by the addition of proteins and prostaglandins, and increases light scattering. The resultant Tyndall effects makes a slit-lamp beam evident within the anterior chamber, an observation clinically known as aqueous flare. With the addition of proteins, the aqueous composition closely approximates that of plasma and is termed *plasmoid aqueous*. Plasmoid aqueous in domestic animals forms fibrin clots easily due to high concentrations of the glycoprotein fibrinogen. Unless treated pharmacologically, these fibrin clots can cause numerous complications, including anterior and/or posterior synechiae or adhesions between the iris and the cornea and/or lens.

Ascorbate concentration in the AH exceeds that in plasma due to an active transport mechanism (Chu & Candia, 1988). This high concentration of ascorbate might assist in protecting the anterior segment structures from oxidative damage induced by ultraviolet radiation. For example, AH ascorbate concentrations are ~35 times greater in diurnal versus nocturnal mammals, suggesting the importance of its role as an antioxidant to prevent photic damage (Koskela et al., 1989). Furthermore, ascorbate is a cofactor in electron transfer reactions, is a reducing agent in hydroxylation reactions, helps regulate production of GAGs in the trabecular meshwork, and might play a role in the storage of iridal catecholamines (Chu & Candia, 1988; DiMattio, 1989).

In addition to protein and ascorbate, other organic compounds constitute the AH, and their concentrations vary relative to plasma. In most mammalian species, the concentration of amino acids in the AH is higher than that in the plasma, suggesting active transport of amino acids is occurring across the ciliary epithelium (Dickinson et al., 1968; Reddy et al., 1977). In the dog, however, amino acid concentrations are less in AH than in plasma (Bito et al., 1965). In this species, the vitreous may act as a "sink" for some of the amino acids, thus causing the deficiency (Dickinson et al., 1968; Reddy et al., 1977). Carbohydrate concentrations in the AH are ~80% of plasma since they enter by diffusion and are subsequently metabolized by the lens and cornea. Thus, the concentration of diffusible substances in blood can impact its amount in the AH. For example, the concentration of glucose in AH is markedly increased in diabetic patients due to elevated plasma concentrations. Urea concentration in the AH is also ~80% that of plasma. Results of previous studies in the dog have indicated that urea penetrates the BAB very slowly; therefore, a steady concentration as compared to that in plasma is never reached, thus resulting in a lower amount of urea in the AH (Davson & Weld, 1941). By contrast, immunoglobulins, enzymes, and lipids are present in much lower concentrations in AH versus plasma due to the BAB.

The major cations in the AH are sodium, potassium, calcium, and magnesium, with sodium comprising 95% of the total cation concentration. Sodium enters the AH via active transport, with a net flow of water into the posterior chamber. The major anions in AH are chloride, bicarbonate, phosphate, ascorbate, and lactate. The chloride and bicarbonate ions enter with sodium, but their concentrations vary among species. For example, in the horse, the aqueous chloride concentration exceeds that of plasma, whereas the amount of bicarbonate in aqueous is less than that of plasma. By contrast, the bicarbonate concentration is higher and the chloride concentration is lower in the AH of the guinea pig (Davson & Weld, 1941; Davson, 1969). Because the total anion and cation concentrations must equal each other, the combined chloride and bicarbonate concentrations equal the sodium concentration. Lactate is found in much higher concentrations in the AH versus plasma likely due to glycolysis by the lens, cornea, ciliary body, and retina, since it does not appear to accumulate in the posterior chamber (Riley, 1972).

The viscosity, or resistance of fluid to flow, of normal AH varies markedly between species, with raptors, particularly barred owls, having a much more viscous AH than dogs, cats, and horses (Davis et al., 2015). Similarly, teleosts, specifically rainbow trout, are reported to have an AH viscosity that is 10 times greater than that of dogs; this difference is due to a high concentration of hyaluronic acid in rainbow trout versus canine AH (Hoffert & Fromm, 1969).

Aqueous Humor Regulation

The rate of aqueous formation by the ciliary epithelium is influenced by sympathetic and parasympathetic innervation as well as humoral mechanisms to maintain a steady-state IOP. Adrenergic regulation of AH formation is complex and the role of some receptor subtypes remains unclear. The β-adrenergic antagonists, such as timolol, lower IOP by decreasing AH production (Coakes & Brubaker, 1978; Schenker et al., 1981; Yablonski et al., 1978); more information on this important drug class for glaucoma management can be found in Chapters 8 and 20. During sleep, AH formation decreases ~50% via modulation of the β-arrestin/cAMP signaling pathway by β-adrenergic receptors in humans (Brubaker, 1991; Reiss et al., 1984; Sit et al., 2008). Thus, IOP exhibits a circadian rhythm, which varies depending on whether animals are nocturnal or diurnal. For example, diurnal species such as dogs and primates (Gelatt et al., 1981; Komaromy et al., 1998) exhibit the greatest IOP during the day, while in nocturnal species such as cats and rats IOP peaks at night (Del Sole et al., 2007; Moore et al., 1996). Consequently, β-antagonists provide little additional reduction in AH production during sleep and may be less effective at controlling IOP during this time period in glaucomatous patients (Sit et al., 2008). The α-2-adrenergic agonists, including brimonidine, markedly lower IOP in humans by decreasing AH formation, but no change in IOP was observed following topical brimonidine administration to glaucomatous Beagles (Gelatt & MacKay, 2001) or normal horses (Von Zup et al., 2017), suggesting that the effects of this drug class vary by species.

Cholinergic regulation of AH formation and composition are similarly ambiguous. For example, parasympathomimetic nerve stimulation or drugs have been demonstrated to increase, decrease, or not change the rate of AH production; these differences are likely due to species and technique-related effects (Berggren, 1970; Bill, 1967a; Chiou et al., 1980; Green & Padgett, 1979; Macri & Cevario, 1974; Stjernschantz, 1976; Uusitalo, 1972). Cholinergic agents may regulate amino acid transport from the blood to the AH as well as modulate inorganic ion concentrations within the AH (Bito et al., 1965; Walinder, 1966; Walinder & Bill, 1969). In aggregate, these studies suggest that the influence of parasympathetic drugs such as pilocarpine is relatively minor in AH formation, and that their efficacy in decreasing IOP is likely due to increased AH outflow.

Other pharmacologic agents as well as local, systemic, and surgical factors can influence AH formation, as reviewed by Gabelt and Kaufman (2011). Importantly, an increase in IOP causes a reduction in AH inflow due to an alteration in the hydrostatic pressure gradient. However, IOP depends on systemic blood pressure to a small degree. For example, marked hypotension reduces blood flow to the eye and concomitantly lowers IOP (Green, 1984; Macri & Cevario, 1975).

In summary, the regulation of AH formation is complex and is influenced by a multitude of factors.

Aqueous Humor Outflow

AH dynamics involve the balance between production (i.e., active secretion) and outflow via the conventional and nonconventional routes (Fig. 3.6). Conventional outflow consists of AH flow through the corneoscleral trabecular meshwork (TM), while the nonconventional route involves uveoscleral outflow (Cruise & McClure, 1981; Samuelson et al., 1985). Depending on the species, ~50–95% of AH drains through the TM via conventional outflow (Table 3.6).

Structural and Biomechanical Attributes

The TM is a complex, three-dimensional structure comprising cells supported by an intricate extracellular matrix (ECM). The TM can be divided into three portions: uveal, the innermost portion; corneoscleral, the middle region; and the juxtacanalicular zone, the outermost section nearest the sclera. The pore size of each TM zone decreases from inward to outward, with the juxtacanalicular zone consisting of several endothelial cell layers that produce a matrix comprising GAGs, collagen, fibronectin, and other glycoproteins in which these cells are embedded. Thus, the juxtacanalicular zone, which is immediately adjacent to Schlemm's canal in primates or the angular aqueous plexus (AAP) in most

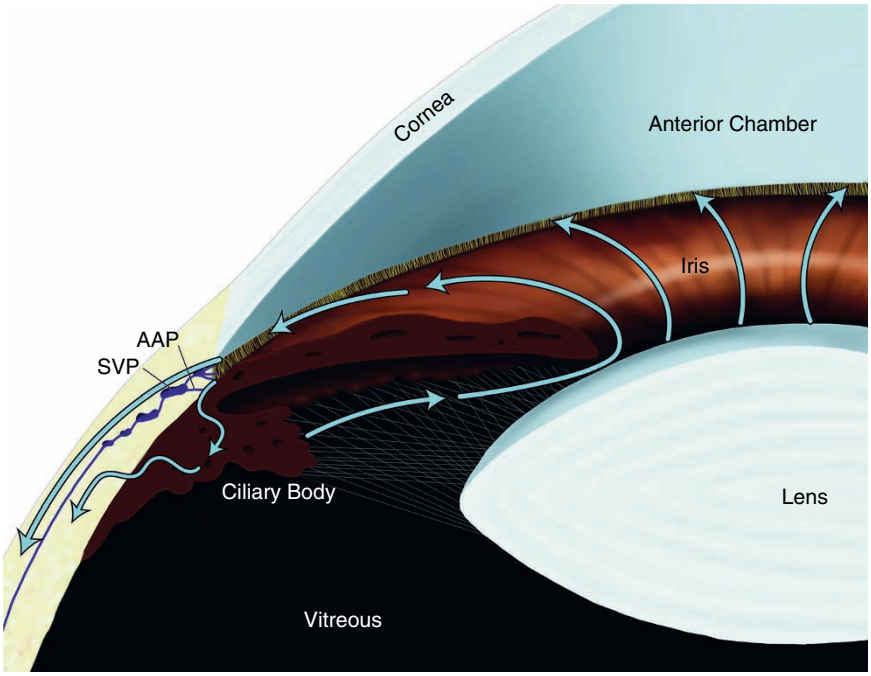

Figure 3.6 Aqueous humor (AH) drainage occurs via the traditional and uveoscleral outflow pathways in the iridocorneal angle of the dog. The ciliary body epithelium produces AH, which flows from the posterior chamber, through the pupil, and into the anterior chamber. Then, AH drains through the pectinate ligament to enter the trabecular meshwork. In the traditional outflow pathway, AH enters the angular aqueous plexus (AAP) to drain anteriorly to the episcleral and conjunctival veins or posteriorly into the scleral venous plexus (SVP) and vortex veins. With uveoscleral outflow, AH flows through the ciliary muscle interstitium to the supraciliary and suprachoroidal spaces to diffuse out the sclera.

Table 3.6 Estimates of aqueous humor dynamics in selected species.

	Dog	Cat	Rabbit	Cow	Horse	Nonhuman Primate
Estimated normal IOP (mmHg)	15–18	17–19	15–20	20–30	17–28	13–15
"C" outflow (μL/mmHg/min by tonography)	0.24–0.30	0.27–0.32	0.22–0.28	—	0.90	0.24–0.28
Uveoscleral outflow (μL/min)	15%	3%	13%	—	—	30%–65%
Episcleral venous pressure (mmHg)	10–12	8	9	—	—	10–11
Aqueous formation (μL/min)	5.22	6.00–7.00	1.84	—	—	2.75

domestic animals, is thought to be the major site of aqueous outflow resistance.

Other studies suggest that the main site of resistance to outflow is the endothelial lining of the AAP and its ECM (Samuelson & Gelatt, 1984a, 1984b; Tripathi & Tripathi, 1972). However, the site of filtration may be different from the site of flow resistance (Johnson et al., 1990). AH transport through the endothelium of the AAP (or Schlemm's canal in nonhuman primates and domestic chickens) is thought to occur via transcellular pores, large vacuoles, or pinocytotic vesicles. However, paracellular routes between the endothelial cells of Schlemm's canal have also been proposed and may be pressure sensitive, particularly at higher IOPs (Epstein & Rohen, 1991; Sabanay et al., 2000; Ye et al., 1997). Nevertheless, disputes regarding juxtacanalicular versus inner wall resistance and transcellular versus paracellular transport are unlikely to translate to major differences in therapeutic approaches from a clinical perspective.

Excessive deposition of ECM and concomitant stiffening of the TM are critical to the pathogenesis of primary open angle glaucoma (POAG) in humans (Chatterjee et al., 2014; Last et al., 2011) and likely dogs with the *ADAMTS10* mutation (Ahonen et al., 2014; Boote et al., 2016; Kuchtey et al., 2011, 2013; Palko et al., 2013, 2016). Thus, phagocytic activity of TM cells and macrophages is important in ECM remodeling and removal of large particulate material (Gasiorowski & Russell, 2009). A malfunction of endothelial phagocytosis and reduced numbers of trabecular endothelial cells may also contribute to the pathogenesis of POAG (Samuelson et al., 1984). The nonfiltering portion of the canine iridocorneal angle (ICA) has been shown to contain Schwalbe's line cells, which have both secretory and epithelial characteristics. Recently, a stem cell niche was identified in Schwalbe's line of cynomolgus macaques, which may serve to repopulate cells in the TM and/or corneal endothelium (Braunger et al., 2014). Changes in the morphology and number of Schwalbe's line cells correlate with disease progression in Beagles with POAG (Samuelson et al., 2001), suggesting that loss of this cell population is important in the pathogenesis of glaucoma.

Fluid Dynamics

As the CB produces AH, the tissues comprising the ICA resist AH outflow, thus generating IOP. Steady-state IOP occurs when the rates of AH inflow and outflow are equivalent. The AH exits the eye by passive bulk flow via two routes in the ICA:

1) The traditional or conventional pathway, which involves passage through the TM, AAP, scleral venous plexus, veins of the episclera and conjunctiva (anterior) or vortex veins (posterior), and systemic venous circulation.
2) The uveoscleral or nonconventional pathway, which involves passage through the iris root, anterior face of the ciliary body muscle, supraciliary or suprachoroidal space, and out through the sclera.

The traditional pathway is dependent on IOP, while the uveoscleral pathway is not, as long as IOP is greater than 7–10 mmHg (Bill, 1966a, 1967b, 1975). At very low IOP, the net pressure gradient across the nonconventional pathway declines, so that uveoscleral outflow subsequently decreases. It is unknown why uveoscleral outflow is largely independent of IOP, but it may relate to complex relationships between pressure and resistance between the fluid compartments and the soft tissues that comprise this route (Bill, 1975). For example, the pressure gradient between the anterior chamber and suprachoroid is independent of IOP, thus fluid flow between these compartments is also IOP independent. Uveoscleral outflow is primarily impacted by the state of the ciliary body and by the hydrostatic pressure difference between the anterior chamber and the suprachoroidal space (Barrie et al., 1985; Bill, 1966a; Emi et al., 1989; Gelatt et al., 1979). Contraction of the ciliary body musculature decreases unconventional outflow, possibly by reducing the extracellular spaces; in turn, relaxation increases outflow via this route. Thus, pilocarpine, a parasympathomimetic, and atropine, a parasympatholytic, will decrease and increase uveoscleral outflow by contracting and relaxing the ciliary body muscle, respectively (Bill, 1967a; Lutjen-Drecoll & Kaufman, 1993; Rohen et al., 1967).

Formulae can be used to describe the formation and drainage of AH (Table 3.7).

Table 3.7 Aqueous humor dynamics formulae.

I	$F_{in} = F_{at} + F_{uf}$ **F = flow (µl/min)** F_{in} = total AH inflow F_{at} = inflow from active transport F_{uf} = inflow from ultrafiltration
II	$F_{out} = F_{trab} + F_{uveo}$ F_{out} = total AH outflow F_{trab} = outflow via the trabecular meshwork F_{uveo} = outflow via uveoscleral pathway
III	$C_{total} = C_{trab} + C_{uv} + C_{pseudo}$ C = facility or conductance of flow (µl/min/mmHg) C_{total} = total AH outflow facility C_{trab} = facility of outflow via the trabecular meshwork C_{uv} = facility of outflow via the uveoscleral pathway C_{pseudo} = pseudofacility
III	At steady state, $F = F_{in} = F_{out}$
IV	$F = C_{trab}(P_i - P_e)$ *Goldmann equation* **P = Pressure (mmHg)** P_i = IOP P_e = episcleral venous pressure
V	$F_{in} = C_{trab}(P_i - P_e) + F_{uveo}$
VI	$P_i = P_e + (F_{in} - F_{uveo}) / C_{trab}$

Episcleral venous pressure or the "backpressure" created by the venous portion of the conventional pathway in the AAP or Schlemm's canal constitutes approximately 50%–75% of the resistance that determines IOP. While minor anatomic variations in the venous system exist between species, results of pressure studies in humans, nonhuman primates, rabbits, and dogs reveal episcleral venous pressure to be between 8 and 12 mmHg (Bill, 1966b; Gelatt et al., 1982b; Maepea & Bill, 1989; Talusan & Schwartz, 1981; Tripathi & Tripathi, 1973). Arteriovenous anastomoses within the episcleral vasculature have been demonstrated in the rabbit, dog, owl monkey, and cynomolgus monkey. These vascular shunts may function in rabbits and dogs, where the episcleral vasculature appears to lack a capillary system, and in the monkey species as an emergency system to elevate IOP after globe perforation or to retrogradely flush the outflow channels (Funk & Rohen, 1996; Rohen & Funk, 1994). Episcleral venous pressure can be measured by direct cannulation (using very fine glass pipettes) or indirect partial to complete compression schemes (using a string-gauge system or a fluid-filled chamber; Gelatt et al., 1982b). The term *pseudofacility* refers to pressure-dependent ultrafiltration formation of AH. It was assumed that any measurement procedure for AH dynamics that temporarily elevated IOP (e.g., perfusion of the anterior chamber, tonography, perilimbal suction cup) would temporarily decrease the rate of humor formation. This slight decrease in the rate of formation would alter the pressure-sensitive outflow measurements obtained by tonography and was termed *false facility*, or *pseudofacility*. Results of studies that involved compressing the episcleral venous pressure of the AH outflow systems in humans and nonhuman primates suggest the pseudofacility to be as high as a 20% error (Brubaker & Kupfer, 1966; Kupfer & Sanderson, 1968). However, fluorophotometric measurements of AH formation rates indicate that these sudden (but limited) increases in IOP do not suppress the rate of AH formation. Indeed, fluorophotometry measurements in both normal and glaucomatous human eyes indicate that rates of AH formation are essentially the same (Beneyto Martin et al., 1995). Thus, the temporary increase in IOP observed in the original experiments by Brubaker and colleagues may be due to immediate dilation of the intraocular blood vessels followed by slow accumulation of AH (Brubaker & Kupfer 1966; Moses et al., 1985).

Results of earlier studies indicated that the volume of the anterior chamber directly relates to the rate of aqueous outflow, so that animals with large eyes have faster outflow rates (Tripathi, 1974; Tripathi & Tripathi, 1972, 1973). The resistance to aqueous outflow is inversely proportional to the facility of outflow (C_{total}).

Regulation of Outflow

Cholinergic agonists such as pilocarpine decrease outflow resistance by contraction of the ciliary muscle and subsequent spreading of the TM. This effect is rapid, such that intravenous administration of pilocarpine to vervet monkeys results in a near-instantaneous decrease in outflow resistance, suggesting that the effect may be mediated by a structure perfused by arteries (Bárány, 1967). Ciliary muscle disinsertion and removal of the iris obliterate this acute response to pilocarpine, suggesting that it is mediated completely by ciliary muscle contraction rather than a direct effect on the TM (Kaufman & Bárány, 1976). The M3 subtype of the muscarinic receptor is strongly expressed in the ciliary muscle and thought to mediate the changes in outflow facility in response to cholinergic agonists (Gabelt, 1994; Gabelt & Kaufman, 1992; Zhang et al., 1995). Because the effect of cholinergic agonists on trabecular outflow (increase) is greater than that on uveoscleral outflow (decrease), the net effect is an increase in AH outflow and concomitant decrease in IOP. As expected, cholinergic antagonists such as atropine decrease traditional outflow and increase nontraditional outflow by similar mechanisms.

Stimulation of adrenergic receptors by nonspecific agonists such as epinephrine increases outflow, but the precise mechanism remains elusive despite extensive study (Ballintine & Garner, 1961; Bárány, 1968; Bill, 1969, 1970; Krill et al., 1965; Sears, 1966). However, it is likely to involve stimulation of β_2 receptors on TM cells and subsequent increased cyclic adenosine monophosphate (AMP) production (Kaufman, 1987; Neufeld et al., 1972, 1975; Neufeld & Sears, 1975; Sears & Neufeld, 1975). Downstream effects may include disruption of actin filaments within TM cells, changes in cell shape, cell–cell and cell–ECM interactions, altered TM structure, and increased hydraulic conductivity within the TM (Kaufman, 1981; Kaufman & Rentzhog, 1981). Epinephrine also increases uveoscleral outflow, likely by stimulation of β-receptors in the ciliary muscle and subsequent relaxation (Bill, 1969; Casey, 1966; Schenker et al., 1981; Tornqvist, 1966; Townsend & Brubaker, 1980; van Alphen et al., 1962, 1965).

Many other influences on the rate of AH formation and regulation of IOP have been proposed. For example, a center in the feline diencephalon has been found that, when stimulated, causes alterations in the IOP (Gloster, 1960). Central nervous system (CNS) regulation of IOP is poorly understood, however, and hormonal control of AH production may be involved (Niederer et al., 1975). The influence of the CNS on AH dynamics was reviewed by Denis and colleagues (1994).

Methods to Measure Aqueous Dynamics

Both invasive and noninvasive methods are used to investigate AH dynamics (Table 3.8), and normative values have been described in domestic and laboratory animal species.

AH formation has been measured using both invasive and noninvasive techniques. As one may anticipate, early methods were invasive and essentially measured the dilution of intracamerally injected substances over short time periods. With the AH volume within the anterior and posterior chambers measured and the amount of dilution of the tracer estimated, the total amount of AH produced per unit of time could be determined. Knowledge of anterior and posterior chamber volumes is critical to determining the rate of AH production (Table 3.9; McLaren et al., 1990; Toris et al., 1995). Unfortunately, a major limitation of these studies is variability in the determination of the anterior and posterior chamber volumes. In glaucomatous animals, these chambers may be altered considerably, and their volumes are subsequently difficult to determine. In response to these invasive experiments, fluorophotometry was developed as both an experimental and a clinical procedure to noninvasively determine the rate of AH formation in many species, including humans.

Fluorophotometry is a noninvasive method for studying AH flow dynamics, for evaluating ocular pharmaceutical agents used to treat glaucoma, and for determining iris permeability in both normal and disease states (Bartels, 1988; Brubaker, 1991; Kurnik et al., 1989; McLaren & Brubaker, 1988). Fluorophotometry of the anterior chamber and vitreous can assess the permeability of the BRB in the normal and diseased eye. Fluorophotometry has been used extensively in humans (Brubaker, 1991), nonhuman primates (Toris et al., 2010), rabbits (Reitsamer et al., 2009; Zhao et al., 2010), cats (Crumley et al., 2012; Lee et al., 1984), dogs (Cawrse et al., 2001; Skorobohach et al., 2003; Ward et al., 2001), and, most recently, the red-tailed hawk (Jones & Ward, 2012). This tool can also be used to assess permeability coefficients of the BAB involved in health and disease, and determine the effects of selected drugs on the BAB.

To determine AH outflow, perfusion of the anterior chamber (AC) of *in vivo* and *ex vivo* eyes has been performed in numerous species. The constant pressure perfusion technique is the most frequently used. It involves maintaining a constant level of IOP with periodic, intermittent, or continuous volumes of perfusate. In the perfusion decay test, either a preselected volume of perfusate is injected or a preselected IOP is achieved. Once the perfusate has been injected, the time for the IOP to regain the baseline or preexisting measurement is obtained. In many ways, the perfusion techniques are similar to the noninvasive tonography methods. The two-step constant perfusion of the anterior chamber, as

Table 3.8 Methods to investigate aqueous humor dynamics.

I	Techniques to investigate the formation of aqueous humor Cannulation of anterior chamber: constant rate/constant pressure perfusion Direct view/measurement of newly formed aqueous humor Use of markers in aqueous humor (radioactive, fluorescein, paraminophippuric acid). Measure the decay rate of intracamerally injected isotopes. Fluorophotometry, a noninvasive method, is primarily used today
II	Procedures to investigate the exit of aqueous humor Ocular perfusion to lower IOP Perilimbic suction cup Tonography (conventional outflow/pressure sensitive) Use of markers (fluorescein, nitrotetrazolin, latex spheres, radioactive tracers). Both conventional and uveoscleral outflow routes are measured
III	Methods to measure the episcleral venous pressure Partial to complete collapse of the episcleral veins to affect alteration in the blood flow Torsion balance Pressure chamber (filled with air or saline) Air jet Ocular compression Direct cannulation and measurement by transducer

Table 3.9 Comparative volumes of the chambers and select structures of the eye.

Species	Anterior Chamber (mL)	Posterior Chamber (mL)	Lens Volume (mL)	Vitreous Volume (mL)
Human	0.2	0.06	0.2	3.9
Rabbit	0.3	0.06	0.2	1.5
Pig	0.3	—	—	3.0
Dog	0.8	0.2	0.5	3.2
Cat	0.8	0.3	0.3	2.8
Cow	1.7	1.5	2.2	20.9
Horse	2.4	1.6	3.1	28.2

reported by Bárány and Scotchbrook (1954), has become the most frequently reported procedure. Briefly, the technique includes constant perfusion of the anterior chamber at two different IOPs (~2–3 and 8–10 mmHg above baseline) for several minutes. The total (i.e., perfusion) facility is determined by dividing the difference in perfusion rates between the two IOPs by the pressure difference between them. Pseudofacility may account for approximately 0.02 μL/min/mmHg with this procedure in humans.

Ample literature is available on anterior chamber perfusion in several species. The type of perfusate, duration of perfusion (i.e., the "washout effect"), eye preparation, IOP during perfusion, addition of certain enzymes, and drugs (including anesthesia and other substances) may directly influence the perfusion rate. If perfusion of the anterior chamber is planned, the literature should be consulted and carefully evaluated. In general, the rates of perfusion obtained in the animals investigated have correlated closely with the values obtained by the noninvasive tonographic and fluorophotometric methods. For more information on tonography to noninvasively measure conventional outflow, see Chapter 10. Several methods have been used to demonstrate anatomic routes and quantity of uveoscleral outflow, as well as of conventional (i.e., corneoscleral) outflow.

The percentages accounted for by uveoscleral outflow range from 30% to 65% in nonhuman primates, 15% in dogs, 13% in rabbits, 4% to 14% in humans, and 3% in cats (Table 3.6; Barrie et al., 1985; Bill, 1966a, 1966b; Bill & Phillips, 1971; Zhan et al., 1998). The horse appears to have an extensive uveoscleral outflow system (Smith et al., 1986), but the volume and percentage of the total outflow system have not been reported. For additional information on unconventional outflow in a variety of species under numerous conditions, the reader is referred to the thorough review by Johnson and colleagues (2017).

Uveoscleral outflow can be demonstrated using observable tracers measuring from 10.0 nm to 1.0 μm in diameter. As one would anticipate, the smaller-diameter (i.e., pore) tracers penetrate the different tissues to greater extents. After perfusion at different IOPs and for different time intervals, the eyes (especially the root of the iris, entire ciliary body, suprachoroidal space, and choroid, even as far posterior as the optic nerve) are examined by light microscopy, scanning electron microscopy, and transmission electron microscopy for these markers. These same methods have also demonstrated the ability of the trabecular endothelium and wandering macrophages to phagocytize particulate material within the outflow pathways. An alternative method to estimate the amount of uveoscleral outflow (either as μL or %) is by using radioactive isotopes injected into the anterior chamber; the time, amount of the isotope, or both is standardized. At the conclusion of perfusion, the ocular tissues are either dissected into the different sections, analyzed for radioactivity, or the entire globe is sectioned, and the radioactivity of each area is measured by scintillation counter. Measurements of tracers in the fluids within the intrascleral veins, episcleral veins, and vortex veins are alternate methods of determining the different routes of AH outflow, but these methods require the anatomy of these venous systems to be determined. There may be mixing between the systems, and the tracer concentrations in the anterior chamber and blood must be established at the same time. Atraumatic entry to the intrascleral or episcleral venous system (or both) must be available.

Ocular Rigidity

Another key concept in the measurement of IOP is ocular rigidity (k), or the resistance offered by the fibrous tunics of the eye (i.e., sclera and cornea) to a change in intraocular volume. Ocular rigidity may also be defined as the change in IOP per incremental change in the intraocular volume; this resistance manifests as a change in IOP. Ocular rigidity is determined by Schiotz tonometry, and it estimates the change in volume (open manometer system) when the instrument is placed on the cornea as well as after injections of exact volumes or preselected elevations in IOP. This logarithmic relationship between IOP and volume of the globe is:

$$\log P_2/P_1 = k\left(V_2 - V_1\right).$$

Ocular rigidity is a constant characteristic of each eye, but it also depends on IOP. Hence, the distensibility of each globe varies among individuals as well as with the IOP. Dogs and cats have greater scleral elasticity than humans, so less resistance is offered with indentation tonometry, and buphthalmia occurs more readily with prolonged, increased IOP (Peiffer et al., 1978; Wyman, 1973). Manometric studies to develop Schiotz tonometer calibration tables for the dog, rabbit, and cat have not been successful clinically and may, perhaps, be associated with different individual rigidities for the cornea and sclera (Miller & Pickett, 1992). Consequently, Schiotz tonometry is rarely performed in animals.

Intraocular Pressure

In many species, IOPs as measured with tonometry in normal animals have been reported (Table 3.10). In humans and animals, fluctuations in IOP occur for a variety of reasons (Table 3.11), and a review of considerations for conducting IOP studies in animals was recently performed (Millar & Pang, 2015). Diurnal IOP variations generally occur in most species; in humans and dogs, the highest pressure occurs in the morning and the lowest in the afternoon (Gelatt et al., 1981). By contrast, the greatest IOPs occur during the day and the lowest IOPs are documented at night in the rabbit, cat, horse, and nonhuman primate (Bertolucci et al., 2009). In glaucomatous canine patients, diurnal IOP fluctuations

Table 3.10 Intraocular pressures in select animal species.

	IOP Results		
Species	**Mean ± SD**	**Tonometer**	**Investigator**
Alligator	23.7 ± 2.1	TonoPen	Whittaker et al. (1995)
Cat	22.6 ± 4.0 19.7 ± 5.6	Mackay-Marg TonoPen	Miller et al. (1991b)
Cow	28.2 ± 4.6 26.9 ± 6.7	Mackay-Marg TonoPen XL	Gum (1990)
Chinchilla	3.0 ± 1.8 9.7 ± 2.5	TonoVet-D TonoVet-D	Müller et al. (2010) Snyder et al. (2018)
Dog	15.7 ± 4.2 16.7 ± 4.0 17.8 ± 0.9 (pm) 21.5 ± 0.8 (am)	Mackay-Marg TonoPen Mackay-Marg	Miller et al. (1991a) Gelatt et al. (1981)
Ferret	22.8 ± 5.5 15.4 ± 1.1 14.1 ± 0.4	TonoPen TonoPen Vet TonoVet	Sapienza et al. (1991) Di Girolamo et al. (2013)
Frog			
White's tree frogs	16.8 ± 3.9 14.7 ± 1.6	TonoLab-R TonoVet-D	Hausmann et al. (2017)
Goat (pygmy)	11.8 ± 1.5 10.8 ± 1.7	TonoVet-D TonoPen XL	Broadwater et al. (2007)
Guinea pig	18.3 ± 4.6 6.1 ± 2.2	TonoPen Vet TonoVet	Coster et al. (2008)
Horse	25.5 ± 4.0 23.5 ± 6.1 23.3 ± 6.9	Mackay-Marg Mackay-Marg TonoPen	Cohen & Reinke (1970) Miller et al. (1990)
Mouse (no anesthetic)	14.6 ± 0.5	TonoLab	Ding et al. (2011)
Nonhuman primate			
Rhesus (ketamine)	14.9 ± 2.1 15.4 ± 2.6	Pneumatonograph TonoPen XL	Bito et al. (1979) Komaromy et al. (1998)
Tibetan monkey	29.3 ± 0.9	TonoVet-P	Liu et al. (2011)
Rabbit	19.5 ± 1.8 17.9 ± 2.1 9.5 ± 2.6 15.4 ± 2.2	Pneumatonograph TonoVet TonoPen Avia	Vareilles et al. (1977a, 1977b) Smith & Gregory (1989) Pereira et al. (2011)
Raptor			
Red-tailed hawk	20.6 ± 3.4	TonoPen	Stiles et al. (1994)
Golden eagle	21.5 ± 3.0		
Great horned owl	10.8 ± 3.6		
White-tailed sea eagle	26.9 ± 5.8	TonoVet	Reuter et al. (2011)
Northern goshawk	18.3 ± 3.8		
Red kite	13.0 ± 5.5		
Eurasian sparrowhawk	15.5 ± 2.5		
Common buzzard	26.9 ± 7.0		
Common kestrel	9.8 ± 2.5		
Peregrine falcon	12.7 ± 5.8		
Tawny owl	9.4 ± 4.1		
Long-eared owl	7.8 ± 3.2		
Barn owl	10.8 ± 3.8		
Rat	17.3 ± 5.3	TonoPen	Mermoud et al. (1994)
	21.4 ± 1.0	TonoPen	Sappington et al. (2010)
Sheep	10.6 ± 1.4	Perkins	Gerometta et al. (2009)

Table 3.11 Factors that cause short- and long-term fluctuations in intraocular pressure.

Short-Term	Long-Term
Diurnal changes	Aging
Forced eyelid closure	Race/breed
Contraction of retactor bulbi muscles	Hormones
Coughing/valsalva maneuver	Glucocorticoids
Abrupt changes in blood pressure	Growth hormone
Pulse	Estrogen
Struggling/electroshock	Progesterone
Changes in body/head position	Obesity
Succinylcholine	Myopia
Acidosis	Gender
	Season

are typically much greater in comparison to normal dogs (Gelatt et al., 1981). Consequently, antiglaucoma medications administered once daily to dogs should be given in the evening to mitigate IOP spikes in the morning, when pressures are typically the greatest (Gelatt & MacKay, 2001).

Lens

The second most powerful refracting structure in the eye is the lens. Like the cornea, the lens is a transparent tissue without a direct blood supply. The lens depends primarily on AH for its metabolic needs. Most of the lens proteins are soluble, with a small amount of glycoproteins, whereas the cornea consists mostly of insoluble collagen and a relatively large amount of glycoproteins.

Lens epithelial cells (LECs) are the progenitors of the lens fibers and transition into lens fiber cells of the cortex at the equator. This process is characterized by distinct biochemical and morphologic changes, such as the synthesis of crystallin proteins, cell elongation, loss of cellular organelles, and disintegration of the nucleus (Ochiai et al., 2014).

Transparency of the lens depends primarily on the highly ordered lens cell arrangement, as well as on the solubility and physical arrangements of its proteins. The lens behaves as a cell syncytium both biochemically and electrically. The lens consists of approximately 68% water, 38% protein, and small amounts of lipids, inorganic ions, carbohydrates, ascorbic acid, glutathione, and amino acids (Viteri et al., 2004). Both the anterior and posterior lens capsules are the lens's extracellular matrix and, like a typical epithelial basement membrane, consist of Type IV collagen and heparan sulfate proteoglycan. The thickness of the anterior lens capsule increases with age because of the anterior location of the lens epithelial cells (Bernays & Peiffer, 2000).

The protein content of the lens is very high in comparison to other organs. Protein synthesis ceases with formation of the lens fiber cells, and all the protein changes that occur after this stage are posttranslational modifications. Lens proteins are divided into water-soluble proteins and water-insoluble proteins. Crystallins comprise 80–90% of the water-soluble lens proteins (Andley, 2007; Piatigorsky, 2003). Most of the insoluble proteins occur in the lens nucleus, whereas the soluble proteins are concentrated in the lens cortex (Harding & Dilley, 1976). The insoluble proteins are associated primarily with membranes of the lens fibers; the soluble proteins comprise the bulk of the refractive fibers of the lens and are considered the structural proteins of the lens. The percentages of soluble and insoluble proteins vary among species and with the pathophysiologic state of the lens. With aging, water-soluble proteins coalesce to make high-molecular-weight aggregates and their hydrophilicity diminishes (Ortwerth & Olesen, 1989). Additionally, when the lens becomes cataractous, the level of water-insoluble proteins increases.

The crystallin proteins are classified as classical or taxon-specific. Crystallins evolved from stress proteins and enzymes (Andley, 2007). Classical crystallins comprise α-crystallins and the β/γ-crystallin superfamily. Crystallins form very stable and durable structures. All vertebrate lenses accumulate large amounts of classical crystallins in their fiber cells. Alpha-crystallins are not only refractive, but as members of the family of small heat shock proteins, they also serve as molecular chaperones that function to protect against physiologic stress. Alpha-crystallins account for almost 50% of the protein mass of the human lens and are thought to bind to partially unfolded β/γ-crystallins and

interact with cytoskeletal proteins, preventing further aggregation, interaction, and precipitation, which would lead to lens opacification (Andley, 2007).

The β/γ-crystallin superfamily is more diverse than the α-crystallins, but its functional role is less evident. Previously the β/γ-crystallins were thought to be two distinct protein families, but protein sequencing has shown that they are closely related. The major difference is that β-crystallins tend to form multimers and γ-crystallins exist as monomers (Driessen et al., 1981).

Taxon-specific crystallins vary between species and provide the lens with transparency and enzymatic capacity. This ability to serve in both capacities is referred to as gene sharing. One example is δ-crystallin, which is a soluble protein that also has argininosuccinate lyase activity and accumulates only in the lenses of birds and reptiles. Delta-crystallin is the first and major crystallin (70%) in the lens of the developing chicken (Das & Piatigorsky, 1988; Piatigorsky & Wistow, 1989). Additionally, these crystallins may have been recruited as lens proteins because of their thermodynamic stability, which is required for the long life of fiber cells (Wistow & Piatigorsky, 1987).

The long prismatic lens fiber cells are organized in tightly packed units with interdigitations that appear as a three-dimensional jigsaw puzzle. The interdigitations stabilize the lateral membranes of the lens fibers, and they are specialized gap junctions that join all the lens cells, thus permitting them to act as a syncytium. Gap junctions mediate cell-to-cell transport of molecules, which is critical since most fibers are distant from their nutrient sources, the aqueous and vitreous humors. Lens fiber cells have a higher concentration of gap junctions than any other cells in the body. The lens fiber cytoskeleton contains micro-filaments and intermediate filaments that are composed of vimentin, filensin, and phakinin. These filaments have a knobby structure leading to the name, beaded filaments, which are only found in lens fiber cells, suggesting a very specialized role. The functions of the beaded filaments probably relate to crystallin packing and density distribution, as well as their being attachment sites for the crystallin molecules (Ireland & Maisel, 1984).

Aquaporins comprise a family of intrinsic membrane proteins involved in water transport in many tissues. Specifically, AQP0 has been localized to the canine lens fibers as well as the lens of other mammals (Karasawa et al., 2011). In rats and most likely other animals, the AQP0 are located on the lens equatorial fiber plasma membranes, both in a diffuse arrangement and in clusters that correspond to specialized junctions between fibers and interact with gap junctions in the apical surface of the fiber. These adaptations are thought to assist the circulating fluxes of ions and water needed to move nutrients into and waste products out of the nucleus. The fluxes are directed from the poles of the lens toward the equator. These adaptations allow the lens to avoid being dependent on the diffusion–consumption equation or capillaries used by other tissues (Zampighi et al., 2002). Homeostasis, especially that associated with solute exchange from the aqueous and vitreous humors to the lens fibers, has been extensively studied. A review by Dahm and colleagues (2011) summarizes current information into four main forms of transport:

1) Paracellular transport via the intercellular spaces between the LECs and the underlying lens fibers is driven by Na^+ leak conductance. This mechanism accounts for the influx of ions, water, and small molecules such as glucose, amino acids, and ascorbic acid.
2) Plasma membrane-based transport of small molecules from the lens's extracellular space into the lens fiber's cytoplasm is via ion and water channels and specific transporters for small molecules.
3) Gap-junctional transport accounts for the flux of ions, water, and small molecules from superficial fibers toward the deep fibers, and also accounts for the efflux of waste products at the epithelial cell lens fiber interface in the equatorial regions.
4) Vesicle-mediated active transport by caveoli accounts for the uptake of macromolecules such as growth factors and other regulatory factors necessary for the normal development and maintenance of lens fibers. Coated vesicles are involved in the uptake of lipoproteins and cholesterol by superficial fibers needed for the biogenesis of new membranes, as lens fiber cells increase their length by up to 1,000-fold (Dahm et al., 2011).

The lens epithelium is the major site of energy production in the lens. Energy is used for active transport of inorganic ions and amino acids and for protein synthesis. Osmoregulation occurs through active transport and involves the action of Na^+-K^+- ATPase to maintain high K^+ and amino acid concentrations and low Na^+, Cl^-, and water concentrations within the lens. The movement of water is passive and occurs with the active cation transport. As the Na^+ ion is transported from the lens, K^+ is transported into the lens (Fig. 3.7) in a manner similar to that in red blood cells. A deficiency of lens Na^+-K^+-ATPase results in cataracts in mice because of the breakdown of this critical pump mechanism (Kinoshita, 1974).

The lens undergoes major oxidative stress due to constant exposure to light and oxidants. Oxidative stress is reduced by radical scavenging antioxidants such as glutathione, carnitine, and ascorbic acid, which are present at high concentrations in the lens. However, some species such as dogs, rabbits, and guinea pigs have lower concentrations of ascorbic acid in the lens than in the AH (Kuck, 1970). The function of lenticular ascorbic acid most likely relates to oxidation–reduction reactions or is coupled to glutathione metabolism (Berger et al., 1988). In humans, the lens epithelium contains transporter molecules for ascorbate, which

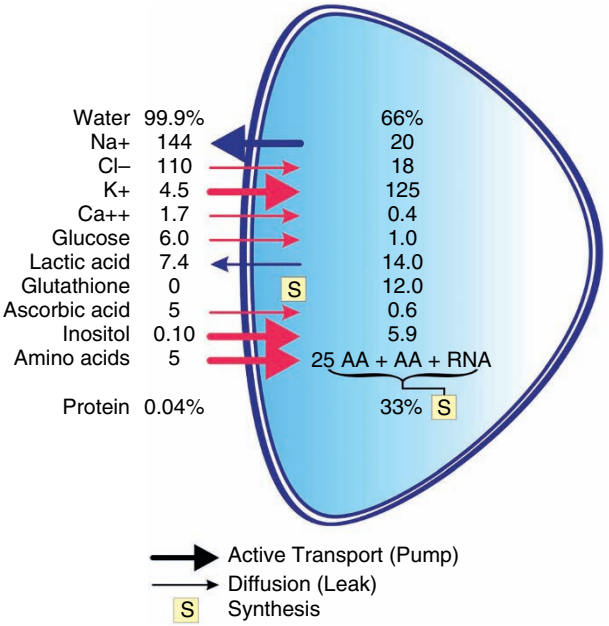

Figure 3.7 Chemical composition of the aqueous humor and lens. Water and protein are expressed as percentages of lens weight. Na+, Cl–, K+, and Ca++ ions are expressed in microequivalent per milliliter of lens water. Other compounds are expressed in micromole per gram of lens weight or micromole per milliliter of aqueous humor. AA, amino acid; RNA, ribonucleic acid.

ensure adequate metabolism and help to protect against damage by free radicals. A deficiency in these protective mechanisms can result in cataractogenic changes (Andley & Clark, 1989). Glutathione is a tripeptide of glutamine, cysteine, and glycine. It is synthesized in the lens epithelial cells and superficial fiber cells and provides most of the protection against oxidative damage in the lens. Glutathione furnishes sulfhydryl groups for the lens proteins, thereby preserving their solubility, and for Na^+-K^+-ATPases, thereby maintaining these transport "pumps." Other biologic functions include participation in amino acid transport with γ-glutamyl transpeptidase and as a substrate for glutathione peroxidase, which destroys cytotoxic lipid hydroperoxides. In a normal lens, glutathione is predominantly in the reduced form (GSH), with the concentration of the oxidized form of glutathione at only 2.1%–2.6% that of the reduced form. Concentrations of both the reduced and the oxidized forms of glutathione are decreased in cataract formation, except in advanced cataract patients, where the amount of the oxidized form is 9% that of the reduced form (Gelatt et al., 1982a). Carnitine is known to have an antioxidative and antiradical role on the ocular surface. The same is suspected to be true in the lens. Recently, the carnitine transporter SLC22A5 was identified in canine lens epithelium and is thought to be responsible for the transport of carnitine to the lens from AH (Ochiai et al., 2014). A major factor involved in cataract formation is oxidative damage caused by O_2 radicals, peroxide (H_2O_2), OH^-, and ultraviolet radiation.

Telomerase is a ribonucleoprotein responsible for maintaining telomere length, preventing chromosomal degradation and recombination, and repairing DNA strand breaks, thereby preventing cell senescence. Telomerase activity has been found in normal canine, feline, and murine lens epithelial cells in the central, germinative, and equatorial regions at equivalent concentrations. Telomerase activity may be in the germinative epithelium to maintain its proliferative potential and prevent cell senescence, whereas it may function in the quiescent, central lens to maintain telomeres damaged by oxidative stress and ultraviolet light exposure, thereby preventing accelerated loss of these elements, which can trigger cell senescence (Colitz et al., 1999).

The lens capsule functions as a semipermeable membrane. It prevents direct contact between the lens and the surrounding ocular environment and protects the lens from the invasion of pathogens. However, the capsule allows water, small solutes, many proteins, and waste to pass, thereby enabling the lens to grow and perform metabolic functions (Danysh & Duncan, 2009). Its mechanical functions include maintaining the shape of the lens in association with accommodating and providing for the attachment of the zonules. Additionally, a contractile system appears to exist in the lens epithelial and cortical cells, and though its physiologic function is not completely understood, it seems to stabilize the shape of the lens (Rafferty et al., 1990).

The primary source of energy for the lens is glucose, which diffuses from the AH. Energy is derived from anaerobic glycolysis and is used for active cation transport and protein synthesis. Oxygen is not necessary for normal lens metabolism, though a small percentage of glucose is metabolized through the Krebs cycle. The hexose monophosphate (i.e., pentose) shunt and the sorbitol pathway are other pathways of glucose metabolism in the lens. The major end product of glucose metabolism in the lens is lactic acid, which diffuses into the AH. The rate of glycolysis is controlled by the amount of hexokinase and the rate of entrance of glucose into the lens. With high concentrations of glucose (>175 mg/dL), the level of glucose-6-phosphate increases, which inhibits hexokinase and limits the rate of glycolysis. This process prevents excessive buildup of lactic acid in the lens, which would lower the pH and activate the lens proteases (Kuck, 1970). With very high blood and AH glucose concentrations, as occur in diabetes mellitus, the enzyme aldose reductase is activated as an alternative route of glucose metabolism in the lens (Sato & Kador, 1989). The result is an accumulation of sorbitol in the lens cells, which causes swelling associated with the increased osmotic pressure. The outcome is a diabetic cataract.

Aging changes in the lens include an increase in insoluble proteins and changes in the cytoskeleton. Normal proteolysis

truncates many of the soluble crystallins and contributes to aging changes. The increase in water-insoluble proteins most likely occurs because of crystallin binding and interactions with the cytoskeletal/membrane components. The chaperone role of α-crystallin, whereby the α-crystallin binds to partially unfolded β/γ-crystallins and interacts with cytoskeletal proteins to prevent uncontrolled aggregation, ultimately increases the amount of insoluble proteins. The increase in insoluble proteins is also secondary to covalent interactions between crystallin fragments (Su et al., 2011). Additionally, with age, the flow of antioxidants from the metabolically active cortex to the lens nucleus decreases, predisposing the lens to cataract development. Iron is also implicated in cataract development, due to its ability to catalyze the formation of free radicals, and aging cataractous lenses have higher concentrations of iron. Normally excess iron is safely stored in ferritin, a ubiquitous protein. One study found that modified fiber cell ferritin L chains are present at the highest amount in the outermost layers of both cataractous and noncataractous canine lenses. They decrease gradually in the inner layers of the fiber mass and are undetectable in the inner two layers of cataractous lenses. By contrast, modified ferritin H chains are ubiquitous throughout noncataractous lens cortex, but are found in decreasing amounts toward the interior of the lens. However, in cataractous lenses, normal-sized ferritin H chains are present in smaller quantities in the outer fiber layers, and increase in quantity and size in the inner layers. These different amounts and types of ferritin may reflect a response of the lens to increased oxidative stress during cataractogenesis (Goralska et al., 2009).

The Vitreous

Vitreal Structure and Aging

Physically, the vitreous is a hydrogel that consists of >98% water and fills the posterior cavity of the eye. Collagen comprises the framework of the vitreous and provides its plasticity. Despite the low protein content, a diverse array of >1,200 soluble proteins have been identified in the vitreous (Murthy et al., 2014). Spaces between the collagen fibers are filled with hyaluronic acid (HA), which provides viscoelasticity to the vitreous (Fig. 3.8). An increase in the collagen content of the vitreous makes it more solid, or gel-like, while a decrease in the collagen content makes its consistency more fluid. Species differ in the collagen content of their vitreous, which accounts for variability in its consistency. Generally, the cortical areas of the vitreous contain more collagen, so they are more rigid than other portions. The vitreous contains few cells, termed hyalocytes. Hyalocytes belong to the monocyte/macrophage lineage and derive from bone marrow. Their origin is not from glial cells or retinal pigment epithelial cells, as previously thought. Hyalocytes are important for extracellular matrix synthesis, vitreous cavity immunology regulation, and modulation of inflammation (Sakamoto & Ishibashi, 2011).

The embryonic vitreous is very dense and therefore translucent. As an individual matures, however, important structural changes occur in the vitreous. The axial length of the vitreous increases, which is critical for growth of the eye (discussed later). The overall collagen content remains unchanged in the adult, but the HA concentration undergoes a fourfold increase in both cattle and humans (Balazs, 1982; Balazs et al., 1959). This change in the HA-to-collagen ratio contributes to greater dispersal of the collagen fibrils, because the newly synthesized HA molecules push the collagen fibril bundles further apart, thus increasing the optical clarity of the vitreous. These changes in HA–collagen interactions as well as in the GAG contents of the vitreous do not cease upon reaching adulthood. Rather, these alterations continue throughout life, and they are believed to be responsible for the vitreal liquefaction observed as part of the aging process in some species (Sebag, 1989). In humans, rheologic (i.e., the gel-liquid state of the vitreous) changes begin in the central vitreous at 5 years of age and continue throughout life, so that in the geriatric patient, more than 50% of the vitreous is eventually liquefied (Balazs, 1982). As liquefaction progresses, the collagen bundles are packed into the remaining gel fraction, whereas HA molecules are redistributed to the liquid fraction. A common complication of this progressive liquefaction is separation of the posterior vitreous cortex from the retinal inner limiting membrane. This detachment, which predisposes to retinal tears, has been implicated as a risk factor in rhegmatogenous retinal detachment in dogs (Hendrix et al., 1993).

Vitreous Functions

The vitreous is the largest structure in the eye, occupying approximately 80% of the globe (Sebag, 1989). It contributes to the development, optics, structure, physiology, and metabolism of the eye. The vitreous plays an important role in the growth of the eye by contributing to the increase in globe size. Inserting a drainage tube into the vitreous cavity of chicken embryos lowers intravitreal pressure and effectively stops the growth of the eye, and vitrectomy of rabbit eyes has a similar inhibitory effect (Arciniegas et al., 1980; Coulombre, 1956). By contrast, vitreal elongation will cause an increase in the axial length of the globe. This lengthens the path of the incoming light, thus providing for greater light refraction. In some aquatic species, such as goldfish, this increased vitreal refractivity is a physiologic mechanism that compensates for the loss of refractive power when the cornea is submerged in water (Seltner et al., 1989). In terrestrial species, the increased refraction by the vitreous leads to myopia. Vitreal elongation resulting in axial myopia has been induced through visual deprivation in a number of species, including

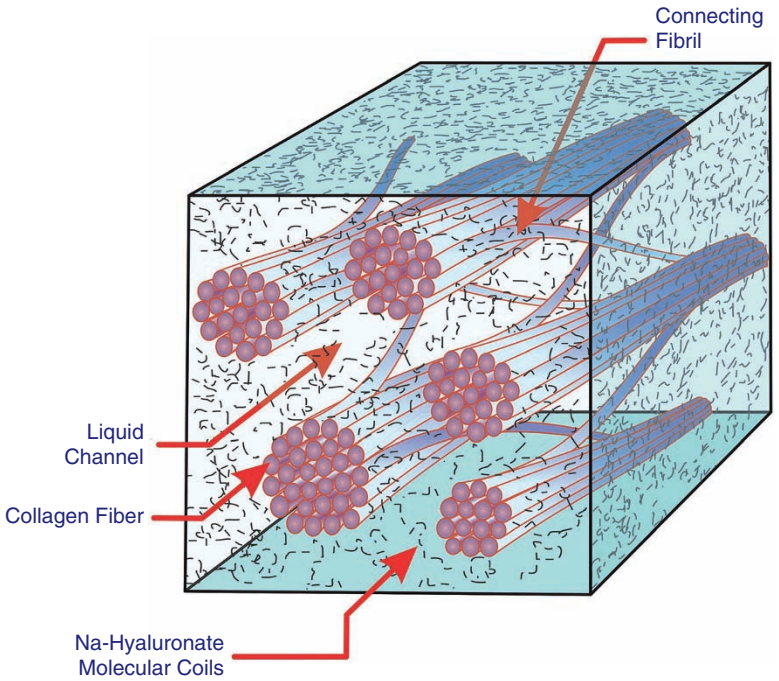

Figure 3.8 Schematic of the vitreal ultrastructure. Parallel collagen fibrils are packed into bundles that aggregate and, ultimately, form visible fibers. Hyaluronic acid and water molecules fill the interfibrillar spaces. (Modified with permission from Sebag, J. & Balazs, E.A. (1989) Morphology and ultrastructure of human vitreous fibers. *Investigative Ophthalmology & Visual Science*, 30, 1867–1873.)

nonhuman primates, chickens, and cats (Belkin et al., 1967; Hodos et al., 1985; Raviola & Wiesel, 1985). This elongation of the vitreous is affected by the synthesis of collagen. Synthesis, molecular reconfiguration, and hydration of HA molecules likewise change the volume of the vitreous and, hence, of the eye (Sebag, 1989).

Diffusion is slow and bulk flow is limited in a gel such as the vitreous. Therefore, topically administered substances are prevented from reaching the retina and optic nerve and systemically administered antimicrobials are unable to reach the center of the vitreous (Lund-Andersen & Sander, 2011). This slow change of substance concentrations has been used in humans to determine time of death and aid in postmortem diagnosis in manatees (Swain et al., 2015; Varela & Bossart, 2005).

The optical transparency of the vitreous is primarily due to a low concentration of structural macromolecules (0.2% w/v) and soluble proteins (Lund-Andersen & Sander, 2011). Additionally, the configuration of highly hydrated glycosaminoglycan chains separating small-diameter collagen fibers aids in the passage of light with minimal scattering (Bettelheim & Balazs, 1968). Another important factor in optical clarity is the blood–vitreous barrier; HA is thought to act as a barrier that prevents diffusion of macromolecules and cells into the vitreous, except in cases of trauma or cortex disruption (Hultsch, 1977). Inflammatory responses, neovascularization, and collagenase activity are likewise suppressed in the vitreous (Hultsch, 1977; Jacobson et al., 1985; Lutty et al., 1983). As a result of these anatomic and physiologic properties, the vitreous transmits 90% of light at wavelengths between 300 and 1400 nm (Boettner & Wolter, 1962).

In addition to its refractive role, the vitreous appears to have additional functions in the process of accommodation. In both humans and monkeys, imaging has revealed that the vitreous bows posteriorly as the ciliary body contracts (Croft et al., 2013). This movement is in proportion to the accommodative amplitude. The vitreous also plays an important role in ocular metabolism. It serves as a storage site for retinal metabolites, including glycogen, amino acids, and potassium (Newman, 1984; Reddy, 1979; Weiss, 1972). Retinal and lenticular waste products, including lactic acid and free radicals, are absorbed by the vitreous, which thus serves to protect the lens and retina from toxic compounds (Sebag, 1989; Ueno et al., 1987). In cattle, these molecules (and water) can diffuse across the vitreous through pores that are 400 nm in diameter (Fatt, 1977). HA serves as a barrier to this diffusion process (Foulds et al., 1985); therefore, molecule size and HA concentration are two of the primary factors affecting the diffusion of molecules through the vitreous. A decrease in HA concentration, which results in vitreous liquefaction, will thus lead to an increase in particle diffusion through the vitreous. Therefore, pathologic or aging processes leading to a decreased HA concentration and vitreal liquefaction will affect the nutrient supply, waste removal, and drug delivery in the posterior segment of the eye (Balazs & Denlinger, 1982).

The vitreous also provides some mechanical and structural support to the lens and retina (Schmidt & Coulter, 1981). Furthermore, its viscoelastic properties protect the internal eye structures from trauma and stress, especially

during rapid eye movement (REM). Concentrations of collagen and HA, as well as the nature of their cross-links, contribute to this viscoelasticity. For example, in humans, the concentration of vitreal HA and collagen is twice as high as in the pig, and this corresponds to a 60% increase in the spring constant of human versus porcine vitreous (Weber et al., 1982). Woodpecker vitreous differs from human vitreous in that it does not have vitreo-retinal attachments. This lack of coupling of the vitreous to the posterior pole, as well as the orientation of the eye with respect to the axis of striking, is thought to reduce relative shearing motions that would be expected to result in ocular trauma from the woodpecker's rapid acceleration–deceleration movements (Wygnanski-Jaffe et al., 2007).

Ocular Mobility

As Chapter 5 discusses, higher-resolution vision is subserved by a small section of the retina termed the *area centralis*. Visual acuity as well as other parameters of vision (e.g., color perception) decrease rapidly in the more peripheral retina outside the area centralis. To keep an object of interest in the center of the visual field, so that its image will stimulate the area centralis (or fovea in birds and primates), vertebrates rely on the actions of six or seven EOM.

Domestic species have four rectus EOM – dorsal (or superior), ventral (inferior), nasal (medial), and temporal (lateral) – all of which move the eye in those respective directions (see Chapter 2). The oculomotor nerve (CN III) innervates the dorsal, ventral, and medial rectus muscles, and the abducens nerve (CN VI) innervates the lateral rectus muscle. Two oblique muscles that work in conjunction with the rectus muscles are also present. The ventral oblique, which is innervated by the oculomotor nerve, rotates the ventral aspect of the eyeball both nasally and dorsally; the dorsal oblique, which is innervated by the trochlear nerve (CN IV), rotates the dorsal aspect of the eyeball both nasally and ventrally. These muscles keep vision horizontally level irrespective of eye position in the orbit. The retractor bulbi, which is present in most species other than primates and birds, is innervated by CN VI and pulls the globe deeper within the orbit. The EOM contain both fast (~85%) and slow (~15%) fibers; however, in contrast to noncranial skeletal muscles, they exhibit both very fast contractility and extreme fatigue resistance. Even among the EOM there is great variation in the composition of each muscle in regard to the myosin heavy chain isoforms that assist with the dynamic physiologic properties and CNS control of eye movements (McLoon, 2011). The EOM are highly aerobic as well as resistant to injury and oxidative stress, with only cardiac muscle having a higher blood flow rate (Wooten & Reis, 1972). Additionally, normal EOM undergo myonuclear addition and subtraction throughout life while maintaining overall size and function, which is not observed in any noncranial muscles (McLoon et al., 2004). A motor axon innervates five to ten muscle fibers in the extrinsic eye muscles, whereas thousands may be innervated by a single axon in skeletal muscles, thus allowing for finer control of eye muscles by the CNS (Gum & MacKay, 2013).

The EOM of the eyes of birds are generally similar to those of mammals, other than the lack of a retractor bulbi muscle. In addition, the rectus muscles are much less robust than in mammals. Globe shape varies considerably among avian species, but the globes are relatively large, such that the two eyes weigh nearly as much as the brain (Martin, 1982). The globe shape and tight fit within the orbit impede globe movement, thus leading to the less robust rectus muscles. Birds compensate for this restricted globe mobility through movement of upper body and neck muscles to obtain a spatial perspective on objects.

Simplistically, two fundamental laws govern eye movements. The first, formulated by Sherrington, states that antagonistic muscles (in the same eye) have reciprocal innervation. In other words, stimulation of an agonistic muscle (e.g., medial rectus) occurs concurrently with inhibition of the antagonistic muscle (e.g., lateral rectus) in the same eye (Sherrington, 1947). The second governs innervation of yoked muscle pairs (i.e., the two muscles responsible for moving both eyes in the same direction). In the 19th century, Hering, (1977) discovered that in mammals, yoked muscle pairs are always equally innervated; therefore, a lateral movement of the left eye will be accompanied by an identical, medial movement of the right eye. Additionally, several EOM pulley systems have been hypothesized but not proven (Miller, 2019).

The seven EOM are responsible for numerous types of eye movements. Saccadic eye movements are very rapid (up to 1000°/s) and very brief (<0.1 second). They are intended for fast correction of eye position to rapidly bring the image of interest onto the area centralis. Thus, saccadic movements are used mostly when tracking a fast-moving object or to begin pursuit of a formerly stationary object.

Once the image of the object has been "captured" by the area centralis, smooth pursuit eye movements are used to match the speed of the object and to maintain its image in the area centralis. Required minor corrections and adjustments are, again, executed by saccadic movements. This combination of alternating rapid and slow eye movements is called optokinetic nystagmus (discussed later), which can be used to track objects moving at speeds <100°/s (Feldon & Burde, 1992). Saccades and smooth pursuit constitute the two types of conjugate (or version) eye movements, in which the two eyes move together without changing the angle between them.

Vergence eye movements, in contrast, change the angle of intersection between the two eyes. These can be either

convergent (i.e., increasing the angle between the visual axes to focus on a near target) or divergent (i.e., decreasing the angle between the visual axes to focus on a far target). Vergence movements are usually slow (<21°/s) and they have two roles. The first is to aid in visualizing nearby objects, which is a process that combines convergent eye movement, accommodation, and miosis. The second is to resolve any small misalignments between the two visual axes that otherwise might result in a disparity between the retinal images of the two eyes.

The afferent stimulus for all these eye movements is the visualized object. If the head is moving, however, eye movement is controlled by a different afferent limb, which allows for a faster tracking response. In this case, the stimulus is the acceleration of the head. Linear acceleration stimulates the otoliths of the vestibular apparatus, and angular acceleration stimulates the hair cells of the semicircular canals. These organs provide the afferent input for the vestibulo-ocular reflex (VOR), the neuronal pathways of which are discussed in detail in Chapter 36. The reflex produces immediate, but slow, eye movements, which compensate for movement of the head and help stabilize the image on the area centralis. Thus, if the head moves up, the VOR moves the eyes down, and if the head moves to the left, the VOR moves the eyes to the right. It appears that the cat makes greater use of the VOR arc than the dog to follow moving objects. Comparison of the dog and cat when visually following a bouncing ball is most dramatic.

Nystagmus is usually characterized by a rapid eye movement in one direction and a slow movement in the opposite direction. Nystagmus can be either horizontal or vertical. The types of nystagmus are categorized on the basis of their causes, and they include optokinetic, rotatory, postrotatory, ocular, caloric, galvanic, anesthetic, brain stem, cerebellar, and vestibular. In optokinetic nystagmus, the eyelids must be open, and the fast phase is opposite in direction to the movement of the visual stimuli. However, the visual stimuli can be moving with the head stationary, or the head and body can be moving with the visual stimuli stationary. In the latter case, the fast phase is in the same direction as the movement of the head. This can be used as an objective means of detecting vision in animals. Optokinetic nystagmus usually occurs in the horizontal plane and is less well substantiated in the vertical plane. In rotatory nystagmus, the fast phase is in the same direction as the rotation of the head. In postrotatory nystagmus, which is seen after rotation stops, the fast phase is opposite to the direction of the rotation of the head. Postrotatory nystagmus lasts approximately 10 seconds after rotation stops. In rotatory and postrotatory nystagmus, the stimuli are acceleration and deceleration, respectively. At a constant rate of rotation, nystagmus does not occur if the lids are closed. Optokinetic nystagmus occurs if the eyelids are open. Ocular nystagmus is associated with congenital blindness and has a wandering or searching movement of the eyes rather than the distinct fast and slow phases (see Chapter 36 for more details).

There are several other types of eye movements. During certain stages of sleep, REM occurs, usually in bursts lasting from 5 to 60 minutes. Numerous REM bursts, which are traditionally associated with dreaming, may occur during a single sleep. Sleep patterns vary with age, however. Discrete eye movement bursts during certain stages of sleep are infrequent in newborn kittens, but after 3 weeks of age adult patterns of sleep develop (Hoppenbrouwers & Sterman, 1975).

Another important class of movements, microsaccades or micronystagmus, are those that maintain eye position while gazing at a stationary target (Alpern, 1982). These movements are required to maintain fixation on the object even when both the observer and the target are immobile. Though slow drifts are also used for this purpose, position maintenance movements are usually characterized by their low magnitude (several minutes/arc) and high frequency (1–50 per second).

Kittens are born with a divergent strabismus that is evident following eyelid opening at approximately 12–14 days postnatally. Normal interocular alignment, which depends on visual stimuli, develops during the second postnatal month (Sherman, 1972). Crossed eyes (i.e., convergent strabismus), which are commonly seen in adult Siamese cats and certain albino mammals, result from a genetic neuroanatomic defect in the primary visual pathway that involves the retinogeniculate and geniculocortical projections (Robertson et al., 1980; Shatz & Levay, 1979).

Oculocardiac Reflex

The oculocardiac reflex can cause reflexive slowing of the heart and can be stimulated by pressure on the globe, tension on the extraocular muscles or iris, or increased intraorbital pressure caused by injection, hemorrhage, or a foreign body. The most common effect of the reflex is bradycardia, but other clinically significant effects are cardiac arrest and ventricular fibrillation. The oculocardiac reflex has been reported in humans, dogs, cats, horses, rabbits, mice, and a cockatiel (Clutton et al., 1988; Panneton & Burton, 1985; Pipo et al., 1996; Rhode et al., 1958; Short & Rebhun, 1980; Walsh & Hoyt, 1969). The afferent arc of the oculocardiac reflex begins with the long and short ciliary nerves to the ciliary ganglion. The ophthalmic division of the trigeminal nerve (CN V) continues to the trigeminal ganglion to its sensory nucleus. The afferent arc continues along short internuncial fibers in the reticular formation to connect with the efferent pathway in the motor nucleus of the vagus nerve (CN X) to the myocardium. Sensory stimulation of the eye and orbital areas results in stimulation of the vagal nucleus

in the brain stem, thus causing a reflexive slowing of the heart. Conscious, healthy rabbits and dogs do not show clinically significant decreases in heart rate with globe compression of 1 minute (Turner-Giannico et al., 2014). Endotracheal intubation can cause vagal stimulation as well, resulting in similar reflexive cardiac alterations (Brunson, 1980). In the dog, as the IOP increases, the heart rate may also increase, thus indicating the possibility of an intraocular-sympathetic-cardiac reflex as well as a trigeminovagal reflex (Howard & Sawyer, 1975).

References

Acosta, M.C., Tan, M.E., Belmonte, C., et al. (2001) Sensation evoked by selective mechanical, chemical and thermal stimulation of the conjunctiva and cornea. *Investigative Ophthalmology & Visual Science*, **42**, 2063–2067.

Ahonen, S.J., Kaukonen, M., Nussdorfer, F.D., et al. (2014) A novel missense mutation in ADAMTS10 in Norwegian Elkhound primary glaucoma. *PLoS One*, **9**, e111941.

Alm, A. & Bill, A. (1972) The oxygen supply to the retina: II. Effects of high intraocular pressure and of increased arterial carbon dioxide tension on uveal and retinal blood flow in cats. *Acta Physiologica Scandinavica*, **84**, 306–319.

Alpern, M. (1982) Eye movements and strabismus. In: *The Senses* (eds Barlow, H.B. & Mollon, J.D.), pp. 201–211. Cambridge: Cambridge University Press.

Andley, U.P. (2007) Crystallins in the eye: Function and pathology. *Progress in Retinal and Eye Research*, **26**, 78–98.

Andley, U.P. & Clark, B.A. (1989) Generation of oxidants in the near-UV photooxidation of human lens α-crystalline. *Investigative Ophthalmology & Visual Science*, **30**, 706–713.

Arciniegas, A., Amaya, L.E., & Ruiz, L.A. (1980) Myopia—a bioengineering approach. *Annals of Ophthalmology*, **12**, 805.

Attariwala, A., Giebs, C., & Glucksberg, M.R. (1994) The influence of elevated intraocular pressure on vascular pressures in the cat retina. *Investigative Ophthalmology & Visual Science*, **35**, 1019–1025.

Balazs, E.A. (1982) Functional anatomy of the vitreous. In: *Ocular Anatomy, Embryology and Tetralogy* (ed. Jakobies, F.A.). Philadelphia, PA: Harper & Row.

Balazs, E.A. & Denlinger, J.L. (1982) Aging changes in the vitreous. In: *Aging and Human Visual Function* (eds. Sekuler, R., Kline, D., & Dismukes, K.), pp. 45–57. New York: Alan R. Liss.

Balazs, E.A., Laurent, T.C., & Larent, U.B.G. (1959) Studies on the structure of the vitreous body: VI. Biochemical changes during development. *Journal of Biological Chemistry*, **234**, 422–430.

Ballintine, E.J. & Garner, L.L. (1961) Improvement of the coefficient of outflow in glaucomatous eyes. Prolonged local treatment with epinephrine. *Archives of Ophthalmology*, **66**, 314.

Banks, M.S., Sprague, W.W., Schmoll, J., et al. (2015) Why do animal eyes have pupils of different shapes? *Science Advances*, **1**, e1500391.

Bárány, E.H. (1967) The immediate effect on outflow resistance of intravenous pilocarpine in the vervet monkey. *Cercopithecus Ethiops. Investigative Ophthalmology & Visual Science*, **6**, 373–380.

Bárány, E.H. (1968) Topical epinephrine effects on true outflow resistance and pseudofacility in vervet monkeys studied by a new anterior chamber perfusion technique. *Investigative Ophthalmology*, **7**, 88–104.

Bárány, E.H. & Scotchbrook, S. (1954) Influence of testicular hyaluronidase on the resistance to flow through the angle of the anterior chamber. *Acta Physiologica Scandinavica*, **30**, 240–248.

Barrett, P.M., Scagliotti, R.H., Merideth, R.E., et al. (1991) Absolute corneal sensitivity and corneal trigeminal nerve anatomy in normal dogs. *Progress in Veterinary & Comparative Ophthalmology*, **1**, 245–254.

Barrie, K.P., Gum, G.G., Samuelson, D.A. & Gelatt, K.N. (1985) Quantitation of uveoscleral outflow in normotensive and glaucomatous Beagles by ^{3}H-labeled dextran. *American Journal of Veterinary Research*, **46**, 84–88.

Bartels, S.P. (1988) Aqueous humor flow measured with fluorophotometery in timolol-treated primates. *Investigative Ophthalmology & Visual Science*, **29**, 1498–1504.

Bartlett, J.D. & Jaanus, S.D. (1989) *Clinical Ocular Pharmacology*, 2nd ed. London: Butterworth-Heinemann.

Beckwith-Cohen, B., Elad, D., Bdolah-Abram, T., & Ofri, R. (2014) Comparison of tear pH in dogs, horses, and cattle. *American Journal of Veterinary Research*, **75**, 494–499.

Belkin, M., Yinon, U., Rose, L., & Reisert, I. (1967) The effect of visual environment on refractive error of cats. *Documenta Ophthalmologica*, **42**, 433–437.

Bellhorn, R.W. & Bellhorn, M.S. (1975) The avian pecten: I. *Fluorescein permeability. Ophthalmic Research*, **7**, 1.

Belmonte, C., Acosta, M.C., & Gallar, J. (2004) Neural basis of sensation in intact and injured corneas. *Experimental Eye Research*, **78**, 513–525.

Belmonte, C., Gallar, J., Pozo, M.A., & Rebollo, I. (1991) Excitation by irritant chemical substances of sensory afferent units in the cat's cornea. *Journal of Physiology*, **437**, 709–725.

Belmonte, C. & Giraldez, F. (1981) Responses of cat corneal sensory receptors to mechanical and thermal stimulation. *Journal of Physiology*, **321**, 355–368.

Beneyto-Martin, P., Fernandez-Vila, P.C., & Perez, T.M. (1995) Determination of the pseudofacility by fluorophotometry in the human eye. *International Ophthalmology*, **19**, 219–223.

Berger, J., Shepard, D., Morrow, F., et al. (1988) Reduced and total ascorbate in guinea pig eye tissues in response to dietary intake. *Current Eye Research*, **7**, 681–686.

Berger, S.L. & King, V.L. (1998) The fluctuation of tear production in the dog. *Journal of the American Animal Hospital Association*, **34**, 79–83.

Berggren, L. (1970) Further studies on the effect of autonomous drugs on in vitro secretory activity of the rabbit eye ciliary processes. A. Inhibition of the pilocarpine effect by isopilocarpine, arecoline, and atropine. B. Influence of isoproterenol and norepinephrine. *Acta Ophthalmologica*, **48**, 293–302.

Bernays, M.E. & Peiffer, R.L. (2000) Morphologic alterations in the anterior lens capsule of canine eyes with cataracts. *American Journal of Veterinary Research*, **61**, 1517–1519.

Bertolucci, C., Giudice, E., Fazio, F., & Piccione, G. (2009) Circadian intraocular pressure rhythms in athletic horses under different lighting regime. *Chronobiology International*, **26**, 348–358.

Best, L.J., Alexiades, V., Hendrix, D.V.H., et al. (2018) Blink patterns and kinematics of eyelid motion in ophthalmologically normal horses. *American Journal of Veterinary Research*, **79**, 650–657.

Best, L.J., Hendrix, D,V., & Ward, D.A. (2015) Tear film osmolality and electrolyte composition in healthy horses. *American Journal of Veterinary Research*, **76**, 1066–1069.

Bettelheim, F.A. & Balazs, E.A. (1968) Light-scattering patterns of the vitreous humor. *Biochimica et Biophysica Acta*, **158**, 309–312.

Beuerman, R.W. & Schimmelpfennig, B. (1980) Sensory denervation of the rabbit cornea affects epithelial properties. *Experimental Neurology*, **69**, 196–201.

Bhattacherjee, P. & Paterson, C.A. (1994) Studies on prostanoid receptors in ocular tissues. *Journal of Ocular Pharmacology*,**10**, 167–175.

Bhattacherjee, P., Smithson, M., & Paterson, C.A. (1997) Generation second messengers by prostanoids in the iris-sphincter and ciliary muscles of cows, cats and humans. *Prostaglandins, Leukotrienes, and Essential Fatty Acids.* **56**, 443–449.

Bill, A. (1962) A method for quantitative determination of blood flow through the cat uvea. *Archives of Ophthalmology*, **67**, 156–162.

Bill, A. (1963) The uveal venous pressure. *Archives of Ophthalmology*, **69**, 780–782.

Bill, A. (1966a) Conventional and uveo-scleral drainage of aqueous humour in the cynomolgus monkey (*Macaca irus*) at normal and high intraocular pressures. *Experimental Eye Research*, **5**, 45–54.

Bill, A. (1966b) Formation and drainage of aqueous humour in cats. *Experimental Eye Research*, **5**, 185–190.

Bill, A. (1967a) Effects of atropine and pilocarpine on aqueous humour dynamics in cynomolgus monkeys (*Macaca irus*). *Experimental Eye Research*, **6**, 120–125.

Bill, A. (1967b) Further studies on the influence of the intraocular pressure on aqueous dynamics in cynomolgus monkeys. *Investigative Ophthalmology & Visual Science*, **6**, 364.

Bill, A. (1969) Early effects of epinephrine on aqueous humor dynamics in vervet monkeys (*Cercopithecus ethiops*). *Experimental Eye Research*, **8**, 35–43.

Bill, A. (1970) Effects of norepinephrine, isoproterenol and sympathetic stimulation on aqueous humour dynamics in vervet monkeys. *Experimental Eye Research*, **10**, 31–46.

Bill, A. (1975) Blood circulation and fluid dynamics in the eye. *Physiological Reviews*, **55**, 383–417.

Bill, A. & Phillips, C.I. (1971) Uveoscleral drainage of aqueous humour in human eyes. *Experimental Eye Research*, **12**, 275–281.

Bito, L.Z., Davson, H., Levin, E., et al. (1965) The relationship between the concentration of amino acids in the ocular fluids and blood plasma of dogs. *Experimental Eye Research*, **4**, 374–380.

Bito, L.Z., Merritt, S.Q., & DeRousseau, C.J. (1979) Intraocular pressure of Rhesus monkeys (*Macaca mulatta*). *Investigative Ophthalmology & Visual Science*, **18**, 785–793.

Blakemore, C. & Cummings, R.M. (1975) Eye-opening in kittens. *Vision Research*, **15**, 1417–1418.

Blocker, T. & van der Woerdt, A. (2001) A comparison of corneal sensitivity between brachycephalic and domestic short-haired cats. *Veterinary Ophthalmology*, **4**, 127–130.

Blogg, J.R. & Coles, E.H. (1970) Aqueous humour proteins—a review. *Veterinary Bulletin*, **40**, 347.

Blount, W.P. (1927) Studies of the movements of the eyelids of animals: Blinking. *Quarterly Journal of Experimental Physiology and Cognate Medical Sciences*, **18**, 112–125.

Boettner, E.A. & Wolter, J.R. (1962) Transmission of the ocular media. *Investigative Ophthalmology*, **1**, 776–783.

Bonanno, J.A. (2012) Molecular mechanisms underlying the corneal endothelial pump. *Experimental Eye Research*, **95**, 2–7.

Bonavida, B., Sapse, A.T., & Sercarz, E.E. (1968) Rabbit tear proteins: I. Detection and quantitation of lysozyme in nonstimulated tears. *Investigative Ophthalmology*, **7**, 435–440.

Bonini, S., Rama, P., Olzi, D., & Lambiase, A. (2003) Neurotrophic keratitis. *Eye*, **17**, 989–995.

Bonting, S.L. & Becker, B. (1964) Studies on Na^+-K^+ activated adenosine triphosphatase. *Investigative Ophthalmology*, **3**, 523–533.

Boote, C., Palko, J.R., Sorensen, T., et al. (2016) Changes in posterior scleral collagen microstructure in canine eyes with an ADAMTS10 mutation. *Molecular Vision*, **22**, 503–517.

Bourges-Abella, N., Raymond-Letron, I., Diquelou, A., et al. (2007) Comparison of cytologic and histologic evaluations of the conjunctiva in the normal equine eye. *Veterinary Ophthalmology.* **10**, 12–18.

Boyce, B., Grazier, J., Jones, R., & Nguyen, T. (2007) *The Mechanics of Soft Biological Composites.* Albuquerque, NM: Sandia National Laboratories.

Brach, V. (1975) The effect of intraocular ablation of the pecten oculi of the chicken. *Investigative Ophthalmology*, **14**, 166–168.

Braunger, B.M., Ademoglu, B., Koschade, S.E., et al. (2014) Identification of adult stem cells in Schwalbes line region of the primate eye. *Investigative Ophthalmology & Visual Science*, **55**, 7499–7507.

Broadwater, J.J., Schorling, J.J., Herring, I.P., et al. (2007) Ophthalmic examination findings in adult pygmy goats (*Capra bicus*). *Veterinary Ophthalmology*, **10**, 269–273.

Bron, A.J. (2001) The architecture of the corneal stroma. *British Journal of Ophthalmology*, **85**, 379–381.

Bron, A.J., Tiffany, J.M., Gouveia, S.M., et al. (2004) Functional aspects of the tear film lipid layer. *Experimental Eye Research*, **78**, 347–360.

Brown, S.A. & Jampol, L.M. (1996) New concepts of regulation of retinal vessel tone. *Archives of Ophthalmology*, **114**, 199–204.

Brubaker, R.F. (1991) Flow of aqueous humor in humans. *Investigative Ophthalmology & Visual Science*, **32**, 3145–3166.

Brubaker, R.F. & Kupfer, C. (1966) Determination of pseudofacility in the eye of the rhesus monkey. *Archives of Ophthalmology*, **75**, 693–697.

Brunson, D.B. (1980) Anesthesia in ophthalmic surgery. Symposium on ophthalmology. *Veterinary Clinics of North America. Small Animal Practice*, **10**, 481–495.

Butovich, I.A., Borowiak, A.M., & Eule, J.C. (2011) Comparative HPLC-MSn analysis of canine and human Meibomian lipidomes: Many similarities, a few differences. *Scientific Reports*, **1**, 24. doi: 10.1038/srep00024.

Butovich, I.A., Millar, T.J., & Ham, B.M. (2008) Understanding and analyzing meibomian lipids—a review. *Current Eye Research*, **33**, 405–420.

Bynke, G., Hakason, R., & Sundler, F. (1984) Is substance P necessary for corneal nociception? *European Journal of Pharmacology*, **101**, 253–258.

Caprioli, J. (1987) The ciliary epithelia and aqueous humor. In: *Adler's Physiology of the Eye* (eds. Moses, R.A. & Hart, W.M.), p. **228**. St. Louis, MO: Mosby.

Carrington, S.D., Bedford, P.G.C., Guillon, J.P., & Woodwards, E.G. (1987a) Polarized light biomicroscopic observations on the precorneal film: 1. The normal tear film of the dog. *Journal of Small Animal Practice*, **28**, 605–622.

Carrington, S.D., Bedford, P.G.C., Guillon, J.P., & Woodward, E.G. (1987b) Polarized light biomicroscopic observations on the precorneal tear film: 2. Keratoconjunctivitis sicca in the dog. *Journal of Small Animal Practice*, **28**, 671–679.

Carrington, S.D., Bedford, P.G.C., Guillon, J.P., & Woodward, E.G. (1987c) Polarized light biomicroscopic observations on the precorneal tear film: 3. The normal tear film of the cat. *Journal of Small Animal Practice*, **28**, 821–826.

Casey, W. J. (1966) Cervical sympathetic stimulation in monkeys and the effects of outflow facility and intraocular volume. A study in the East African vervet (*Cercopithecus aethiops*). *Investigative Ophthalmology*, **5**, 33.

Cawrse, M.A., Ward, D.A., & Hendrix, D.H. (2001) Effects of topical application of a 2.0% solution of dorzolamide on intraocular pressure and aqueous humor flow rate in clinically normal dogs. *American Journal Veterinary Research*, **62**, 859–863.

Chase, J. (1982) The evolution of retinal vascularization in mammals: A comparison of vascular and avascular retinae. *Ophthalmology*, **89**, 1518–1525.

Chatterjee, A., Villarreal, G., Jr., & Rhee, D.J. (2014) Matricellular proteins in the trabecular meshwork, review and update. *Journal of Ocular Pharmacology and Therapeutics*, **30**, 447–463.

Chen, T. & Ward, D.A. (2010) Tear volume, turnover rate, and flow rate in ophthalmologically normal horses. *American Journal of Veterinary Research*, **71**, 671–676.

Chhabra, M., Prausnitz, J.M., & Radke, C.J. (2009) Modeling corneal metabolism and oxygen transport during contact lens wear. *Optometry and Vision Science*, **86**, 454–466.

Chiou, G.C., Liu, H.K., & Trzeciakowski, J. (1980) Studies of action mechanism of antiglaucoma drugs with a newly developed cat model. *Life Sciences*, **27**, 2445–2451.

Chu, T.C. & Candia, O.A. (1988) Active transport of ascorbate across the isolated rabbit ciliary epithelium. *Investigative Ophthalmology & Visual Science*, **29**, 594–599.

Clutton, R.E., Boyd, C., Richards, D.L.S., et al. (1988) Significance of the oculocardiac reflex during ophthalmic surgery in the dog. *Journal of Small Animal Practice*, **29**, 573.

Coakes, R.L. & Brubaker, R.F. (1978) The mechanism of timolol in lowering intraocular pressure: In the normal eye. *Archives of Ophthalmology*, **96**, 2045–2048.

Cohen, C.M. & Reinke, D.A. (1970) Equine tonometry. *Journal of the American Veterinary Medical Association*, **156**, 1884–1887.

Colasabti, B.K. & Trotter, R.R. (1981) Effects of selective beta-1 and beta-2 adrenocepter agonists and antagonists on intraocular pressure in the cat. *Investigative Ophthalmology & Visual Science*, **20**, 69–76.

Cole, D.F. (1974) Comparative aspects of the intra-ocular fluids. In: *The Eye* (eds. Davson, H. & Graham, L.T.), Vol. **5**, p. 71. New York: Academic Press.

Cole, D.F. (1977) Secretion of the aqueous humor. *Experimental Eye Research*, **25**(Suppl.), 161–176.

Colitz, C.M., Davidson, M.G., & McGahan, M.C. (1999) Telomerase activity in lens epithelial cells of normal and cataractous lenses. *Experimental Eye Research*. **69**, 641–649.

Coster, M.E., Stiles, J., Krohne, S.G., & Raskin, R.E. (2008) Results of diagnostic ophthalmic testing in healthy guinea pigs. *Journal of the American Veterinary Medical Association*, **232**, 1825–1833.

Coulombre, A.J. (1956) The role of intraocular pressure in the development of the chicken eye. *Journal of Experimental Zoology*, **133**, 211.

Crawford, M.L. & Marc, R.E. (1976) Light transmission of cat and monkey eyelids. *Vision Research*, **16**, 323–324.

Croft, M.A., Nork, T.M., McDonald, J.P., et al. (2013) Accommodative movements of the vitreous membrane, choroid, and sclera in young and presbyopic human and nonhuman primate eyes. *Investigative Ophthalmology & Vision Science*, **54**, 5049–5058.

Cruise, L.J. & McClure, R. (1981) Posterior pathway for aqueous humor drainage in the dog. *American Journal of Veterinary Research*, **42**, 992–995.

Crumley, W.R., Rankin, A.J., & Allbaugh, R.A. (2012) Evaluation of the aqueous humor flow rate in the eyes of clinically normal cats by use of fluorophotometry. *American Journal of Veterinary Research*, **73**, 704–708.

Dahm, R., van Marle, J., Quinlan, R.A., et al. (2011) Homeostasis in the vertebrate lens: Mechanisms of solute exchange. *Philosophical Transactions of the Royal Society of London. Series B, Biological Sciences*, **366**, 1265–1277.

Danysh, B.P. & Duncan, M.K. (2009) The lens capsule. *Experimental Eye Research*, **88**, 151–164.

Dartt, D.A. (1989) Signal transduction and control of lacrimal gland protein secretion: A review. *Current Eye Research*, **8**, 619–636.

Dartt, D.A. (2011) Formation and function of the tear film. In: *Adler's Physiology of the Eye* (eds. Levin, L.A., Nilsson, S.F.E., Ver Hoeve, J., & Wu, S.M.), 11th ed., pp. 350–362. New York: Elsevier Saunders.

Das, G.C. & Piatigorsky, J. (1988) Promoter activity of the two chicken (delta) ð-crystalline genes in the Hela cell extract. *Current Eye Research*, **7**, 331.

da Silva, E.G., Sandmeyer, L.S., Gionfriddo, J.R., et al. (2013) Tear production in canine neonates: Evaluation using a modified Schirmer tear test. *Veterinary Ophthalmology*, **16**, 175–179.

Daubs, J.G. (1976) A comparison of enzyme reagent strip tests for lacrimal glucose. *American Journal of Optometry and Physiological Optics*, **53**, 232–235.

Davidson, H. & Kuonen, V. (2004) The tear film and ocular mucins. *Veterinary Ophthalmology*, **7**, 71–77.

Davis, K., Carter, R., Tully, T., et al. (2015) Comparative evaluation of aqueous humor viscosity. *Veterinary Ophthalmology*, **18**, 50–58.

Davis, K. & Townsend, W. (2011) Tear-film osmolarity in normal cats and cats with conjunctivitis. *Veterinary Ophthalmology*, **14**(Suppl. 1), 54–59.

Davson, H. (1969) The intraocular fluids. In: *The Eye* (ed. Davson, H.), 2nd ed., Vol. **1**, p. 67. New York: Academic Press.

Davson, H. & Weld, C.B. (1941) Studies on the aqueous humour. *American Journal of Physiology*, **134**, 1.

Dawson, D.G., Ubers, J.L., & Edelhauser, H.F. (2011) Cornea and sclera. In: *Adler's Physiology of the Eye* (eds. Levin, L.A., Nilsson, S.F.E., Ver Hoeve, J., & Wu, S.M.), 11th ed., pp. 71–130. New York: Elsevier Saunders.

Del Sole, M.J., Sande, P.H., Bernades, J.M., et al. (2007) Circadian rhythm of intraocular pressure in cats. *Veterinary Ophthalmology*, **10**, 155–161.

de Moraes, W, Ferreira, T.A.C., Somma, A.T., et al. (2017) Doppler ultrasonography of the pectinis oculi artery in harpy eagles (*Harpia harpyja*). *Open Veterinary Journal*, **7**, 70–74.

Denis, P., Nordmann, J.P., Elena, P.P., et al. (1994) Central nervous system control of intraocular pressure. *Fundamental and Clinical Pharmacology*, **8**, 230–237.

Dickinson, J.C., Durham, D.G., & Hamilton, P.B. (1968) Ion exchange chromatography of free amino acids in aqueous fluids and lens of the human eye. *Investigative Ophthalmology & Visual Science*, **7**, 551–563.

Di Girolamo, N., Andreani, V., Guandalini, A., & Selleri, P. (2013) Evaluation of intraocular pressure in conscious ferrets (*Mustela putorius furo*) by means of rebound tonometry and comparison with applanation tonometry. *Veterinary Record*, **172**, 396.

Dikstein, S. & Maurice, D.M. (1972) The metabolic basis to the fluid pump in the cornea. *Journal of Physiology*, **221**, 29–41.

DiMattio, J. (1989) A comparative study of ascorbic acid entry into aqueous and vitreous humors of the rat and guinea pig. *Investigative Ophthalmology & Visual Science*, **30**, 2320–2331.

Ding, C., Wang, P., & Tian, N. (2011) Effect of general anesthetics on IOP in elevated IOP mouse model. *Experimental Eye Research*, **92**, 512–520.

Dogra, M.R., Katoch, D., & Dogra, M. (2017) An update on retinopathy of prematurity (ROP). *Indian Journal of Pediatrics*, **84**, 930–936.

Driessen, H.P., Herbrink, P., Bloemendal, H., & de Jong, W.W. (1981) Primary structure of the bovine beta-crystallin Bp chain: Internal duplication and homology with gamma-crystallin. *European Journal of Biochemistry*, **121**, 83–91.

Eftimov, P., Yokoi, N., Tonchev, V., et al. (2017) Surface properties and exponential stress relaxations of mammalian meibum films. *European Biophysics Journal*, **46**, 129–140.

Elgin, S.S. (1964) Arteriovenous oxygen difference across the uveal tract of the dog eye. *Investigative Ophthalmology*, **3**, 417–426.

Elsby, J.M. & Wilson, H. (1967) Lacrimal secretion in the cat. *British Journal of Pharmacology and Chemotherapy*, **29**, 1–7.

Elsheikh, A., Alhasso, D., & Rama, P. (2008) Assessment of the epitheliums contribution to corneal biomechanics. *Experimental Eye Research*, **86**, 445–451.

Emi, K., Pederson, J.E., & Toris, C.B. (1989) Hydrostatic pressure of the suprachoroidal space. *Investigative Ophthalmology & Visual Science*, **30**, 233–238.

Eördögh, R., Jakab, C., Papp, R., et al. (2017) Density and distribution of feline conjunctival goblet cells. *Journal of Feline Medicine and Surgery*, **19**, 1048–1054.

Epstein, D.L. & Rohen, J.W. (1991) Morphology of the trabecular meshwork and inner-wall endothelium after cationized ferritin perfusion in the monkey eye. *Investigative Ophthalmology & Visual Science*, **32**, 160–171.

Erickson, O.F., Feeney, L., & McEwen, W.K. (1956) Filter-paper electrophoresis of tears: II. Animal tears and the presence of a "slow-moving lysozyme." *Archives of Ophthalmology*, **55**, 800–806.

Fatt, I. (1977) Hydraulic flow conductivity of the vitreous gel. *Investigative Ophthalmology & Visual Science*, **16**, 565–568.

Feldon, S.E. & Burde, R.M. (1992) The oculomotor system. In: *Adler's Physiology of the Eye* (ed. Hart, W.M., Jr.), pp. 134–183. St. Louis, MO: Mosby–Year Book.

Ferreira, T.A., Turner Giannico, A., & Montiani-Ferreira, F. (2016) Hemodynamics of the pectinis oculi artery in American pekin ducks (*Anas platyrhynchos domestica*). *Veterinary Ophthalmology*, **19**, 409–413.

Flugel, C. & Lutjen-Drecoll, E. (1988) Presence and distribution of Na+/K+-ATPase in the ciliary epithelium of the rabbit. *Histochemistry*, **88**, 613–621.

Forrester, J.V., Dick, A.D., McMenamin, P., & Lee, W.R. (1996) *The Eye: Basic Sciences in Practice*. Philadelphia, PA: W.B. Saunders.

Forster, B.A., Ferrari-Dileo, G., & Anderson, D.R. (1987) Adrenergic alpha 1 and alpha 2 binding sites are present in bovine retinal blood vessels. *Investigative Ophthalmology & Visual Science*, **28**, 1741–1746.

Foulds, W.S., Allan, D., Moseley, H., & Kyle, P.M. (1985) Effect of intravitreal hyaluronidase on the clearance of tritiated water from the vitreous to the choroid. *British Journal of Ophthalmology*, **69**, 529–532.

François, J. & Neetens, A. (1973) Tear flow in man. *American Journal of Ophthalmology*, **76**, 351–358.

Freidman, E. & Smith, T.R. (1965) Estimation of retinal blood flow in animals. *Investigative Ophthalmology*, **4**, 1122–1128.

Frigeri, A., Gropper, M.A., Turck, C.W., & Verkman, A.S. (1995) Immunolocalization of the mercurial-insensitive water channel and glycerol intrinsic protein in epithelial cell plasma membranes. *Proceedings of the National Academy of Science USA*, **92**, 4328–4231.

Fung, Y. (1981) *Biomechanics: Mechanical Properties of Living Tissues*. New York: Springer.

Funk, R.H.W. & Rohen, J.W. (1996) Scanning electron microscopic study of episcleral arteriovenous anastomoses in the owl and cynomolgus monkey. *Current Eye Research*, **15**, 321–327.

Gabelt, B.T. (1994) Inhibition of aceclidine-stimulated outflow facility, accommodation and miosis in rhesus monkeys by muscarinic receptor subtype antagonists. *Experimental Eye Research*, **58**, 623–630.

Gabelt, B.T. & Kaufman, P.L. (2011) Production and flow of aqueous humor. *In: Adler's Physiology of the Eye* (eds. Levin, L.A., Nilsson, S.F.E., ver Hoeve, J., et al.), pp. 274–307. Amsterdam: Elsevier Saunders.

Gabelt, B.T. & Kaufman, P.L. (1992) Inhibition of outflow facility and accommodative and miotic responses to pilocarpine in rhesus monkeys by muscarinic receptor subtype antagonists. *Journal of Ocular Pharmacology & Therapeutics*, **263**, 1133–1139.

Gallar, J., Pozo, M.A., Tuckett, R.P., & Belmonte, C. (1993) Response of sensory units with unmyelinated fibres to mechanical, thermal and chemical stimulation of the cats cornea. *Journal of Physiology*, **468**, 609–622.

Garg, L.C. & Oppelt, W.W. (1970) The effect of ovabain and acetazolamide on transport of sodium and chloride from plasma to aqueous humor. *Journal of Pharmacology and Experimental Therapeutics*, **175**, 237–247.

Gasiorowski, J.Z. & Russell, P. (2009) Biological properties of trabecular meshwork cells. *Experimental Eye Research*, **88**, 671–675.

Gasser, K., Fuchs-Baumgartinger, A., Tichy, A., & Nell, B. (2011) Investigations on the conjunctival goblet cells and on the characteristics of glands associated with the eye in the guinea pig. *Veterinary Ophthalmology*, **14**, 26–40.

Gelatt, K.N., Bruss, M., DeCostanza, S.M., et al. (1982a) Reduced oxidized, and protein-bound glutathione concentrations in normal and cataractous lenses in the dog. *American Journal of Veterinary Research*, **43**, 1215–1217.

Gelatt, K.N., Gum, G.G., Barrie, K.P., & Williams, L.W. (1981) Diurnal variation in intraocular pressure in normotensive and glaucomatous Beagles. *Glaucoma*, **3**, 121–125.

Gelatt, K.N., Gum, G.G., Merideth, R.E., & Bromberg, N. (1982b) Episcleral venous pressure in normotensive and glaucomatous beagles. *Investigative Ophthalmology & Visual Science*, **23**, 131–135.

Gelatt, K.N., Gum, G.G., Williams, L.W., & Barrie, K.P. (1979) Uveoscleral flow of aqueous humor in the normal dog. *American Journal of Veterinary Research*, **40**, 845–848.

Gelatt, K.N. & MacKay, E.O. (2001) Effect of different dose schedules of latanoprost on intraocular pressure and pupil size in the glaucomatous Beagle. *Veterinary Ophthalmology*, **4**, 283–288.

Gelatt, K.N., Peiffer, R.L., Jr., Erickson, J.L., & Gum, G.G. (1975) Evaluation of tear formation in the dog, using a modification of the Schirmer tear test. *Journal of the American Veterinary Medical Association*, **166**, 368–370.

Gerometta, R., Podos, S.M., Danias, J., & Candia, O.A. (2009) Steroid-induced ocular hypertension in normal sheep. *Investigative Ophthalmology & Visual Science*, **50**, 669–673.

Gipson, I.K. and Argüeso, P. (2003) Role of mucins in the function of the corneal and conjunctival epithelia. *International Review of Cytology*, **231**, 1–49.

Glasser, A. & Howland, H.C. (1996) A history of studies of visual accommodation in birds. *Quarterly Review of Biology*, **71**, 475–509.

Gloster, J. (1960) Response of the intraocular pressure to diencephalic stimulation. *British Journal of Ophthalmology*, **44**, 649–664.

Glaze, M.B. (2011) The eye. In: *Small Animal Pediatrics: The First 12 Months of Life* (eds. Peterson, M.E. & Kutzler, M.A.), pp. 461–482. St. Louis, MO: Elsevier.

Good, K.L., Maggs, D.J., Hollingsworth, S.R., et al. (2003) Corneal sensitivity in dogs with diabetes mellitus. *American Journal of Veterinary Research*, **64**, 7–11.

Goralska, M., Nagar, S., Colitz, C.M., et al. (2009) Changes in ferritin H- and L-chains in canine lenses with age-related nuclear cataract. *Investigative Ophthalmology & Visual Science*, **50**, 305–310.

Gornik, K., Moore, P., Figueiredo, M., & Vandenplas, M. (2011) Expression of Toll-like receptors 2, 3, 4, 6, 9, and MD-2 in the normal equine cornea, limbus, and conjunctiva. *Veterinary Ophthalmology*, **14**, 80–85.

Graymore, C.N. (1970) *Biochemistry of the Eye*. New York: Academic Press.

Green, K. (1984) Physiology and pharmacology of aqueous humor inflow. *Survey of Ophthalmology*, **29**, 208–214.

Green, K. & Padgett, D. (1979) Effect of various drugs on pseudofacility and aqueous humor formation in the rabbit eye. *Experimental Eye Research*, **28**, 239–246.

Green, K., Peterson, C.A., & Diddiqui, A. (1985) Ocular blood flow after experimental alkali burns and prostaglandin administration. *Archives of Ophthalmology*, **103**, 569–571.

Gum, G.G. (1990). Unpublished data.
Gum, G.G. (1991) Physiology of the eye. In: *Veterinary Ophthalmology* (ed. Gelatt, K.N.), 2nd ed., pp. 124–161 Philadelphia: Lea & Febiger.
Gum, G.G., Kingsbury, S., Whitley, R.D., et al. (1991) Effect of topical prostaglandin PGA2, PGA2 isopropyl ester, and PGF2 alpha isopropyl ester on intraocular pressure in normotensive and glaucomatous canine eyes. *Journal of Ocular Pharmacology*, **7**, 107–116.
Gum, G.G. & MacKay, E.O. (2013) Physiology of the eye. In: *Veterinary Ophthalmology* (ed. Gelatt, K.N.), 5th ed., pp. 171–207. Ames, IA: Wiley-Blackwell.
Harding, J.J. & Dilley, K.J. (1976) Structural proteins of the mammalian lens: A review with emphasis on changes in development, aging and cataract. *Experimental Eye Research*, **22**, 1–73.
Harmer, E.J. & Williams, D.L. (2003) Blink rate and corneal sensitivity in the dog: Preliminary findings. In: *Proceedings of the Annual Meeting of the British Association, European College, European Society and International Society of Veterinary Ophthalmology*, p. 141. Cambridge, ECVO.
Hausmann, J.C., Krisp, A., Sladky, K., et al. (2017) Measuring intraocular pressure in White's tree frogs (*Litoria caerulea*) by rebound tonometry: Comparing device, time of day, and manual versus chemical restraint methods. *Journal of Zoo and Wildlife Medicine*, **48**, 413–419.
Hayes, S., Boote, C., Lewis, J., et al. (2007) Comparative study of fibrillar collagen arrangement in the corneas of primates and other mammals. *Anatomical Record*, **290**, 1542–1550.
He, J., Pham, T.L., & Bazan, H,E.P. (2019) Mapping the entire nerve architecture of the cat cornea. *Veterinary Ophthalmology*, **22**, 345–352.
Helper, L.C., Magrane, W.G., Koehm, J., & Johnson, R. (1974) Surgical induction of keratoconjunctivitis sicca in the dog. *Journal of the American Veterinary Medical Association*, **165**, 172–174.
Hendrix, D.V., Nasisse, M.P., Cowen, P., & Davidson, M.G. (1993) Clinical signs, concurrent diseases, and risk factors associated with retinal detachment in dogs. *Progress in Veterinary and Comparative Ophthalmology*, **3**, 87–91.
Hering, E. (1977) *The Theory of Binocular Vision*. Trans. Bridgeman, B., eds. Bridgeman, B. & Stark, L. New York: Plenum Press. First published 1879.
Hicks, S.J. & Carrington, S.D. (1997) Demonstration of discrete and membrane-bound ocular mucins in the dog. *Experimental Eye Research*, **64**, 597–607.
Hicks, S.J., Corfield, A.P., Kaswan, R.L., et al. (1998) Biochemical analysis of ocular surface mucin abnormalities in dry eye: The canine model. *Experimental Eye Research*, **67**, 709–718.
Higginbotham, E.J. (1989) Topical carbonic anhydrase inhibitors. In: *Ophthalmology Clinics North America* (ed. Zimmerman, T.J. & Kooner, K.S.), pp. 113–130. Philadelphia, PA: Saunders.
Hodos, W., Fitzke, F.W., Hayes, B.P., & Holden, A.L. (1985) Experimental myopia in chicks: Ocular refraction by electroretinography. *Investigative Ophthalmology & Visual Science*, **26**, 1423–1430.
Hoffert, J.R. & Fromm, P.O. (1969) Viscous properties of teleost aqueous humor. *Comparative Biochemistry & Physiology*, **28**, 1411–1417.
Holmberg, B.J., Maggs, D.J., & Lonnerdal, B.L. (2004) Identification of lactoferrin in canine and feline tears. *Proceedings of the 35th Annual Conference, American College of Veterinary Ophthalmologists*, p. 5. Meridian, ID: ACVO.
Hoppenbrouwers, T. & Sterman, M.B. (1975) Development of sleep state patterns in the kitten. *Experimental Neurology*, **49**, 822–838.
Hoste, A.M., Boels, P.J., Brutsaert, D.L., et al. (1989) Effect of alpha-1 and beta agonists on contraction of bovine retinal resistance arteries *in vitro*. *Investigative Ophthalmology & Visual Science*, **30**, 44–50.
Howard, D.R. & Sawyer, D.C. (1975) Electroretinography of acute hypoxic and increased intraocular pressure status in the dog. *American Journal of Veterinary Research*, **36**, 81–84.
Huang, A.J., Tseng, S.C., & Kenyon, K.R. (1988) Morphogenesis of rat conjunctival goblet cells. *Investigative Ophthalmology & Visual Science*, **29**, 969–975.
Hultsch, E. (1977) Peripheral uveitis in the owl monkey: Experimental model. *Modern Problems in Ophthalmology*, **18**, 247–251.
Ireland, M. & Maisel, H. (1984) A cytoskeletal protein unique to lens fiber cell differentiation. *Experimental Eye Research*, **38**, 637–645.
Jacobson, B., Dorfman, T., Basu, P.K., & Hasany, S.M. (1985) Inhibition of vascular endothelial cell growth and trypsin activity by vitreous. *Experimental Eye Research*, **41**, 581–595.
Jester, J.V. (2008) Corneal crystallins and the development of cellular transparency. *Seminars in Cell & Developmental Biology*, **19**, 82–93.
Jester, J.V., Brown, D., Pappa, A., & Vasiliou, V. (2012) Myofibroblast differentiation modulates keratocyte crystallin protein expression, concentration, and cellular light scattering. *Investigative Ophthalmology & Visual Science*, **53**, 770–778.
Jester, J.V., Moller-Pedersen, T., Huang, J., et al. (1999) The cellular basis of corneal transparency: Evidence for "corneal crystallins." *Journal of Cell Science*, **112**, 613–622.
Johnson, M., Johnson, D.H., Kamm, R.D., et al. (1990b) The filtration characteristics of the aqueous outflow system. *Experimental Eye Research*, **50**, 407–418.
Johnson, M., McLearen, J.W., & Overby, D.R. (2017) Unconventional aqueous humor outflow: A review. *Experimental Eye Research*, **158**, 94–111.
Jones, B.R. & Studdert, V.P. (1975) Horner's syndrome in the dog and cat as an aid to diagnosis. *Australian Veterinary Journal*, **51**, 329–332.
Jones, L.T., Marquis, M.M., & Vincent, N.J. (1972) Lacrimal function. *American Journal of Ophthalmology*, **73**, 658–659.
Jones, M.P. & Ward, D.A. (2012) Fluorophotometric determination of aqueous humor flow rates in red-tailed

hawks (*Buteo jamaicensis*). *American Journal of Veterinary Research*, **73**, 551–555.

Jue, B. & Maurice, D.M. (1986) The mechanical properties of the rabbit and human cornea. *Journal of Biomechanics*, **19**, 847–853.

Karasawa, K., Tanaka, A., Jung, K., et al. (2011) Patterns of aquaporin expression in the canine eye. *Veterinary Journal*, **190**, e72–e77.

Kaufman, P.L. (1981) Adrenergic drug effects on aqueous outflow facility following ciliary muscle retrodisplacement in the cynomolgus monkey. *Investigative Ophthalmology & Visual Science*, **20**, 644–651.

Kaufman, P.L. (1987) Adenosine 3,5-cyclic-monophosphate and outflow facility in monkey eyes with intact and retrodisplaced ciliary muscle. *Experimental Eye Research*, **44**, 415–423.

Kaufman, P.L. & Bárány, E.H. (1976) Loss of acute pilocarpine effect on outflow facility following surgical disinsertion and retrodisplacement of the ciliary muscle from the scleral spur in the cynomolgus monkey. *Investigative Ophthalmology*, **15**, 793–807.

Kaufman, P.L. & Rentzhog, L. (1981) Effect of total iridectomy on outflow facility responses to adrenergic drugs in cynomolgus monkeys. *Experimental Eye Research*, **33**, 65–74.

Keen, P., Tullo, A.B., Blyth, W.A., & Hill, T.J. (1982) Substance P in the mouse cornea: Effects of chemical and surgical denervation. *Neuroscience Letters*, **29**, 231–235.

Kelleher Davis, R., Doane, M.G., Knop, E., et al. (2013) Characterization of ocular gland morphology and tear composition of pinnipeds. *Veterinary Ophthalmology*, **16**, 269–275.

Kiel, J.W. & Shepherd, A.P. (1992) Autoregulation of choroidal blood flow in the rabbit. *Investigative Ophthalmology & Visual Science*, **33**, 2399–2410.

Kiland, J.A., Voss, A.M., & McLellan, G.J. (2016) Effect of timolol maleate gel forming solution on intraocular pressure, pupil diameter, and heart rate in normal and glaucomatous cats. *Veterinary Ophthalmology*, **19**(Suppl. 1), 91–96.

Kinoshita, J.H. (1974) Mechanisms initiating cataract formation. *Investigative Ophthalmology*, **13**, 713–724.

Kirsten, S.J. & Kirsten. E.B. (1983) Spontaneous blink rates of birds. *Condor*, **85**, 92–93.

Kling, S. & Hafezi, F. (2017) Corneal biomechanics: A review. *Ophthalmic and Physiological Optics*, **37**, 240–252.

Komaromy, A.M., Brooks, D.E., Kubilis, P.S., et al. (1998) Diurnal intraocular pressure curves in healthy rhesus macaques (*Macaca mulatta*) and rhesus macaques with normotensive and hypertensive primary open-angle glaucoma. *Journal of Glaucoma*, **7**, 128–131.

Korth, R.M., Romkes, G., & Eule, J.C. (2010) Tear film osmolarity as a diagnostic tool in small animal and equine medicine. *Veterinary Ophthalmology*, **13**, 349.

Koskela, T.K., Reiss, G.R., Brubaker, R.F., & Ellefson, R.D. (1989) Is the high concentration of ascorbic acid in the eye an adaptation to intense solar irradiation? *Investigative Ophthalmology & Visual Science*, **30**, 2265–2267.

Krill, A.E., Newell, F.W., & Novak, M. (1965) Early and long-term effects of levo-epinephrine on ocular tension and outflow. *American Journal of Ophthalmology*, **59**, 833–839.

Kuchtey, J., Kunkel, J., Esson, D., et al. (2013) Screening ADAMTS10 in dog populations supports Gly661Arg as the glaucoma-causing variant in beagles. *Investigative Ophthalmology & Visual Science*, **54**, 1881–1886.

Kuchtey, J., Olson, L.M., Rinkoski, T., et al. (2011) Mapping of the disease locus and identification of ADAMTS10 as a candidate gene in a canine model of primary open angle glaucoma. *PLoS Genetics*, **7**, e1001306.

Kuck, J.F., Jr. (1970) Metabolism of the lens. In: *Biochemistry of the Eye* (ed. Graymore, C.N.), pp. 319–371. New York: Academic Press.

Kumagai, A.K., Glasgow, B.J., & Pardridge, W.M. (1994) GLUT1 glucose transporter expression in the diabetic and nondiabetic human eye. *Investigative Ophthalmology & Visual Science*, **35**, 2887–2894.

Kumar, A. & Yu, F.S. (2006) Toll-like receptors and corneal innate immunity. *Current Molecular Medicine*, **6**, 327–337.

Kupfer, C. & Sanderson, P. (1968) Determination of pseudofacility in the eye of man. *Archives of Ophthalmology*, **80**, 194–196.

Kurnik, R.T., Burde, R.M., & Becker, B. (1989) Breakdown of the blood–aqueous barrier in the rabbit eye by infrared radiation. *Investigative Ophthalmology & Visual Science*, **30**, 717–722.

Laatikairen, L.T. (1976) Regional blood flow in the cat retina. *Experimental Eye Research*, **23**, 47–56.

Last, J.A., Liliensiek, S.J., Nealey, P.F., & Murphy, C.J. (2009) Determining the mechanical properties of human corneal basement membranes with atomic force microscopy. *Journal of Structural Biology*, **167**, 19–24.

Last, J.A., Pan, T., Ding, Y., et al. (2011) Elastic modulus determination of normal and glaucomatous human trabecular meshwork, *Investigative Ophthalmology & Visual Science*, **52**, 2147–2152.

Last, J.A., Thomasy, S.M., Croasdale, C.R., et al. (2012) Compliance profile of the human cornea as measured by atomic force microscopy. *Micron*, **43**, 1293–1298.

Lawrenson, J.G. (1997) Corneal sensitivity in health and disease. *Ophthalmic and Physiological Optics*, **17**(Suppl. 1), S17–S22.

Lee, H.K. & Wang, S.C. (1975) Mechanism of morphine-induced miosis in the dog. *Journal of Pharmacology and Experimental Therapeutics*, **193**, 415–431.

Lee, P.Y., Podos, S.M., & Severin, C. (1984) Effect of prostaglandin F2 alpha on aqueous humor dynamics of rabbit, cat, and monkey. *Investigative Ophthalmology and Visual Science*, **25**, 1087–1093.

Leonard, B.C., Yañez-Soto, B., Raghunathan, V.K., et al. (2016) Species variation and spatial differences in mucin expression from corneal epithelial cells. *Experimental Eye Research*, **152**, 43–48.

Liu, G., Zeng, T., Wenhan, Y., et al. (2011) Characterization of intraocular pressure responses of the Tibetan monkey (*Macaca thibetana*). *Molecular Vision*, **17**, 1405–1413.

Loewy, A.D., Araujo, J.C., & Kerr, F.W. (1973) Pupillodilator pathways in the brain stem of the cat: Anatomical and electrophysiological identification of a central autonomic pathway. *Brain Research*, **60**, 65–91.

Luchter, F.J. & Gurisatti, C. (1974) Queratoconjunctivitis de los bovinos. *Review Medical Veterinaria*, **55**, 139.

Lund-Andersen, H. & Sander, B. (2011) The vitreous. In: *Adler's Physiology of the Eye* (eds. Levin, L.A., Nilsson, S.F.E., Ver Hoeve, J., & Wu, S.M.), 11th ed., pp. 164–180. New York: Elsevier Saunders.

Lutjen-Drecoll, E. & Kaufman, P.L. (1993) Morphological changes in primate aqueous humor formation and drainage tissues after long-term treatment with antiglaucomatous drugs. *Journal of Glaucoma*, **2**, 316–328.

Lutty, G.A., Thompson, D.C., & Gallup, J.Y. (1983) Vitreous—an inhibitor of retinal extract-induced neovascularization. *Investigative Ophthalmology & Visual Science*, **24**, 52–56.

Macri, F.J. & Cevario, S.J. (1974) A pharmacodynamic study of the inhibitory effects of L-norepinephrine, L-epinephrine, and D, L-isoproterenol on aqueous humor formation in the enucleated arterially perfused cat eye. *Investigative Ophthalmology*, **13**, 392–395.

Macri, F.J. & Cevario, S.J. (1975) Ciliary ganglion stimulation: II. Neurogenic intraocular pathway for excitatory effects on aqueous humor production and outflow. *Investigative Ophthalmology*, **14**, 471–476.

Maepea, O. & Bill, A. (1989) The pressure in the episcleral veins, Schlemm's canal and the trabecular meshwork in monkeys: Effects of changes in intraocular pressure. *Experimental Eye Research*, **49**, 645–663.

Maidment, D.C., Kidder, D.E., & Taylor, M.N. (1985) Electrolyte and protein levels in bovine tears. *British Veterinary Journal*, **141**, 169–173.

Mann, G.E., Yudilevich, D.L., & Sobrevia, L. (2003) Regulation of amino acid and glucose transporters in endothelial and smooth muscle cells. *Physiology Review*, **83**, 183–252.

Mann, R.M., Riva, C.E., Stone, R.A., et al. (1995) Nitric oxide and choroidal blood flow regulation. *Investigative Ophthalmology & Visual Science*, **36**, 925–930.

Maren, T.H. (1995) The development of topical carbonic anhydrase inhibitors. *Journal of Glaucoma*, **4**, 49–62.

Marfurt, C., Anokwute, M.C., Fetcko, K., et al. (2019) Comparative anatomy of the mammalian corneal subbasal nerve plexus. *Investigative Ophthalmology & Visual Science*, **60**, 925–930.

Marfurt, C., Murphy, C., & Florczak, J. (2001) Morphology and neurochemistry of canine corneal innervation. *Investigative Ophthalmology & Visual Science*, **42**, 2242–2251.

Marfurt, C.F. (2000) Nervous control of the cornea. In: *Nervous Control of the Eye* (eds. Burnstock, G. & Sillito, A.M.), pp. 41–92. Amsterdam: Harwood Academic.

Marshall, J.M. (1974) Vertebrate smooth muscle. In: *Medical Physiology* (ed. Mountcastle, V.B.), Vol. **1**, p. 133. St. Louis, MO: Mosby.

Martin, G.R. (1982) An owl's eye: Schematic optics and visual performance in *Strix alucol*. *Journal of Comparative Physiology*, **145**, 341.

Marts, B.S., Bryan, G.M., & Prieuo, D.J. (1977) Schirmer tear test measurements and lysozyme concentration of equine tears. *Journal of Equine Medicine and Surgery*, **1**, 427–432.

Maslanka, T. (2015) A review of the pharmacology of carbonic anhydrase inhibitors for the treatment of glaucoma in dogs and cats. *Veterinary Journal*, **203**, 278–284.

Maurice, D.M. (1960) The physics of corneal transparency. In: *Transparency of the Cornea* (ed. Duke-Elder, S.), p. 338. Oxford: Blackwell Scientific.

Maurice, D.M. & Giardini, A.A. (1951) Swelling of the cornea *in vivo* after the destruction of its limiting layers. *British Journal of Ophthalmology*, **35**, 791–797.

McKee, C.T., Last, J.A., Russell, P., & Murphy, C.J. (2011) Indentation versus tensile measurements of Young's modulus for soft biological tissues. *Tissue Engineering. Part B, Reviews*, **17**, 155–164.

McLaren, J.W. & Brubaker, R.F. (1988) A scanning ocular spectro-fluorophotometer. *Investigative Ophthalmology & Visual Science*, **29**, 1285–1293.

McLaren, J.W., Trocme, S.D., Reif, S., & Brubaker, R.F. (1990) Rate of flow of aqueous humor determined from measurements of aqueous fluid. *Investigative Ophthalmology & Visual Science*, **31**, 339–346.

McLaughlin, B.G. & McLaughlin, P.S. (1988) Equine vitreous humor chemical concentrations: Correlation with serum concentrations and postmortem changes with time and temperature. *Canadian Journal of Veterinary Research*, **52**, 476–480.

McLaughlin, S.A., Brightman, A.H., 2nd, Helper, L.C., et al. (1988) Effect of removal of lacrimal and third eyelid glands on Schirmer tear test results in cats. *Journal of the American Veterinary Medical Association*, **193**, 820–822.

McLoon, L. (2011) The extraocular muscles. In: *Adler's Physiology of the Eye* (eds. Levin, L.A., Nilsson, S.F.E., Ver Hoeve, J., & Wu, S.M.), 11th ed., pp. 182–207. New York: Elsevier Saunders.

McLoon, L.K., Rowe, J., Wirtschafter, J., & McCormick, K.M. (2004) Continuous myofiber remodeling in uninjured extraocular myofibers: Myonuclear turnover and evidence for apoptosis. *Muscle & Nerve*, **29**, 707–715.

McMahon, A., Lu, H., & Butovich, I.A. (2013) The spectrophotometric sulfo-phospho-vanillin assessment of total lipids in human meibomian gland secretions. *Lipids*, **48**, 513–525.

Meek, K.M. (2008) The cornea and sclera. In: *Collagen: Structure and Mechanics* (ed. Fratzl, P.), pp. 359–396. Springer: New York.

Meek, K.M. & Newton, R.H. (1999) Organization of collagen fibrils in the corneal stroma in relation to mechanical properties and surgical practice. *Journal of Refractive Surgery*, **15**, 695–699.

Mermoud, A., Baerveldt, G., Minckler, D.S., et al. (1994) Intraocular pressure in Lewis rat. *Investigative Ophthalmology & Visual Science*, **35**, 2455–2460.

Milder, B. & Weil, B.A. (1983) *The Lacrimal System*. Norwalk, CT: Appleton-Century-Crofts.

Millar, J.C. & Pang, I.H. (2015) Non-continuous measurement of intraocular pressure in laboratory animals. *Experimental Eye Research*, **141**, 74–90.

Miller, J.M. (2019) EOM pulleys and sequelae: A critical review. *Investigative Ophthalmology & Visual Science*, **60**, 5052–5058.

Miller, P.E. (1992) Comparison of the human and canine Schiotz tonometry conversion tables in clinically normal dogs. *Journal of the American Veterinary Medical Association*, **201**, 1021–1025.

Miller, P.E. & Pickett, J.P. (1992) Comparison of the human and canine Schiotz tonometry conversion tables in clinically normal cats. *Journal of the American Veterinary Medical Association*, **201**, 1017–1020.

Miller, P.E., Pickett, J.P., & Majors, L.J. (1990) Evaluation of two applanation tonometers in horses. *American Journal of Veterinary Research*, **51**, 935–937.

Miller, P.E., Pickett, J.P., Majors, L.J., & Kurzman, I.D. (1991a) Clinical comparison of the Mackay-Marg and TonoPen applanation tonometers in the dog. *Progress in Veterinary & Comparative Ophthalmology*, **1**, 171–176.

Miller, P.E., Pickett, J.P., Majors, L.J., & Kurzman, I.D. (1991b) Evaluation of two applanation tonometers in cats. *American Journal of Veterinary Research*, **52**, 1917–1921.

Mircheff, A.K. (1989) Lacrimal fluid and electrolyte secretion: A review. *Current Eye Research*, **8**, 607–617.

Mishima, S. (1965) Some physiological aspects of the precorneal tear film. *Archives of Ophthalmology*, **73**, 233–241.

Monk, C.S., Hart, K.A., Berghaus, R.D., et al. (2014) Detection of endogenous cortisol in equine tears and blood at rest and after simulated stress. *Veterinary Ophthalmology*, **17**(Suppl. 1), 53–60.

Moore, C.G., Johnson, E.C., & Morrison, J.C. (1996) Circadian rhythm of intraocular pressure in the rat. *Current Eye Research*, **15**, 185–191.

Moore, C.P., Wilsman, N.J., Nordheim, E.V., et al. (1987) Density and distribution of canine conjunctival goblet cells. *Investigative Ophthalmology & Visual Science*, **28**, 1925–1932.

Morgan, W.H., Yu, D.Y., Cooper, R.L., et al. (1995) The influence of cerebrospinal fluid pressure on the lamina cribrosa tissue pressure gradient. *Investigative Ophthalmology & Visual Science*, **36**, 1163–1172.

Moses, R.A., Grodzki, W.J., Jr., & Carras, P.L. (1985) Pseudofacility: Where did it go? *Archives of Ophthalmology*, **103**, 1653–1655.

Müller, K., Mauler, D.A., & Eule, J.C. (2010) Reference values for selected ophthalmic diagnostic tests and clinical characteristics of chinchilla eyes (*Chinchilla lanigera*). *Veterinary Ophthalmology*, **13**(Suppl. 1), 29–34.

Muller, L.J., Marfurt, C.F., Kruse, F., & Tervo, T.M. (2003) Corneal nerves: Structure, contents and function. *Experimental Eye Research*, **76**, 521–542.

Muller, L.J., Pels, L., & Vrensen, G.F. (1996) Ultrastructural organization of human corneal nerves. *Investigative Ophthalmology & Visual Science*, **37**, 476–488.

Murphy, C.J., Glasser, A., & Howland, H.C. (1995) The anatomy of the ciliary region of the chicken eye. *Investigative Ophthalmology & Visual Science*, **36**, 889–896.

Murphy, C.J. & Howland, H.C. (1986) On the gekko pupil and Scheiner's disc. *Vision Research*, **26**, 815–817.

Murthy, K.R., Goel1, R., Subbannayya, Y., et al. (2014) Proteomic analysis of human vitreous humor. *Clinical Proteomics*, **11**, 29–40.

Neufeld, A.H., Dueker, D.K., Vegge, T., & Sears, M.L. (1975) Adenosine 3,5-monophosphate increases the outflow of aqueous humor from the rabbit eye. *Investigative Ophthalmology*, **14**, 40–42.

Neufeld, A.H., Jampol, L.M., & Sears, M.L. (1972) Cyclic-AMP in the aqueous humor: The effects of adrenergic agents. *Experimental Eye Research*, **14**, 242–250.

Neufeld, A.H. & Sears, M.I. (1974) Cyclic AMP in ocular tissues of the rabbit, monkey, and human. *Investigative Ophthalmology*, **13**, 475–477.

Neufeld, A.H. & Sears, M.L. (1975) Adenosine 3,5-monophosphate analogue increases the outflow facility of the primate eye. *Investigative Ophthalmology*, **14**, 688–689.

Newman, E.A. (1984) Regional specialization of retinal glial cell membrane. *Nature*, **309**, 155–157.

Nicolaides, N. & Santos, E.C. (1985) The di- and triesters of the lipids of steer and human meibomian glands. *Lipids*, **20**, 454–467.

Niederer, W., Richardson, B.P., & Donatsch, P. (1975) Hormonal control of aqueous humor production. *Experimental Eye Research*, **20**, 329–340.

Ninomiya, H. (2017) Microvasculature of the California sea lion (*Zalophus californianus*) eye and its functional significance. *Veterinary Ophthalmology*, **20**, 205–213.

Ninomiya, H., Imamura, E., & Inomata, T. (2014) Comparative anatomy of the ophthalmic rete and its relationship to ocular blood flow in three species of marine mammal. *Veterinary Ophthalmology*, **17**, 100–105.

Nishida, T., Yasumoto, K., Otori, T., & Desaki, J. (1988) The network structure of corneal fibroblasts in the rat as revealed by scanning electron microscopy. *Investigative Ophthalmology & Visual Science*, **29**, 1887–1890.

Nuyttens, J.J. & Simoens, P.J. (1995) Morphologic study of the musculature of the third eyelid in the cat (*Felis catus*). *Laboratory Animal Science*, **45**, 561–563.

Ochiai, H., Kanemaki, N., Sato, R., & Onda, K. (2014) Distribution, molecular structure and functional analysis of carnitine transporter (SLC22A5) in canine lens epithelial cells. *Experimental Animals/ Japanese Association for Laboratory Animal Science*, **63**, 467–473.

Ogidigben, M.J. & Potter, D.E. (1993) Comparative effects of alpha-2 and DA-2 agonists on intraocular pressure in pigmented and nonpigmented rabbits. *Journal of Ocular Pharmacology*, **9**, 187–199.

Ortwerth, B.J. & Olesen, P.R. (1989) Studies on the nature of the water-insoluble fraction from aged bovine lenses. *Experimental Eye Research*, **48**, 605–619.

Palko, J. R., Iwabe, S., Pan, X., et al. (2013) Biomechanical properties and correlation with collagen solubility profile in the posterior sclera of canine eyes with an ADAMTS10 mutation. *Investigative Ophthalmology & Visual Science*, **54**, 2685–2695.

Palko, J.R., Morris, H.J., Pan, X., et al. (2016) Influence of age on ocular biomechanical properties in a canine glaucoma model with adamts10 mutation. *PLoS One*, **11**, e0156466.

Panneton, W.M. & Burton, H. (1985) Projections from the paratrigeminal nucleus and the medullary spinal dorsal horns to the peribrachial area in the cat. *Neuroscience*, **15**, 779–797.

Pederson, J.E. & Green, K. (1973) Aqueous humor dynamics: Experimental studies. *Experimental Eye Research*, **15**, 277–297.

Peiffer, R.L., Gum, G.G., & Gelatt, K.N. (1978) Pressure–volume relationships of the normal canine eye. *American Journal of Veterinary Research*, **39**, 1927–1931.

Pereira, F.Q., Bercht, B.S., Soares, M.G., et al. (2011) Comparison of a rebound and an applanation tonometer for measuring intraocular pressure in normal rabbits. *Veterinary Ophthalmology*, **14**, 321–326.

Petznick, A. Evans, M.D.M., Madigan, M.C., et al. (2012) A preliminary study of changes in tear film proteins in the feline eye following nictitating membrane removal. *Veterinary Ophthalmology*, **15**, 164–171.

Piatigorsky, J. (2003) Crystallin genes: Specialization by changes in gene regulation may precede gene duplication. *Journal of Structural and Functional Genomics*, **3**, 131–137.

Piatigorsky, J. & Wistow, G.J. (1989) Enzyme/crystallins: Gene sharing as an evolutionary strategy. *Cell*, **57**, 197–199.

Piccone, M., Littzi, J., Krupin, T., et al. (1988) Effects of neuropeptide Y on the isolated rabbit iris dilator muscles. *Investigative Ophthalmology & Visual Science*, **29**, 330–332.

Pinero, D.P. & Alcon, N. (2015) Corneal biomechanics: A review. *Clinical and Experimental Optometry*, **98**, 107–116.

Pipo, R.A., Broadstone, R.V., & Murphy, C.J. (1996) Lethal oculocardiac reflex in a cockatiel. *Veterinary & Comparative Ophthalmology*, **6**, 27–29.

Potter, D.E. & Rowland, J.M. (1978) Adrenergic drugs and intraocular pressure: Effects of selective β-adrenergic agonists. *Experimental Eye Research*, **27**, 615–625.

Powell, C.C. & Martin, C.L. (1989) Distribution of cholinergic and adrenergic nerve fibers in the lacrimal glands of dogs. *American Journal of Veterinary Research*, **50**, 2084–2088.

Rafferty, N.S., Scholz, D.L., Goldberg, M., & Lewyckyj, M. (1990) Immunocytochemical evidence for an actinomyosin system in lens epithelial cells. *Experimental Eye Research*, **51**, 591–600.

Raviola, E. & Wiesel, T.N. (1985) An animal model of myopia. *New England Journal of Medicine*, **312**, 1609–1615.

Reddy, V.N. (1979) Dynamics of transport systems in the eye. *Investigative Ophthalmology & Visual Science*, **18**, 1000–1008.

Reddy, V.N., Chakrapani, B., & Lim, C.P. (1977) Amino acid transport across blood–aqueous barrier of mammalian species. *Experimental Eye Research*, **25**, 555–562.

Reiss, G.R., Lee, D.A., Topper, J.E., & Brubaker, R.F. (1984) Aqueous humor flow during sleep. *Investigative Ophthalmology & Visual Science*, **25**, 776–778.

Reitsamer, H.A., Bogner, B., Tockner, B., et al. (2009) Effects of dorzolamide on choroidal blood flow, ciliary blood flow and aqueous production in rabbits. *Investigative Ophthalmology and Visual Science*, **50**, 2301–2307.

Reuter, A., Müller, K., Arndt, G., et al. (2011) Reference intervals for intraocular pressure measured by rebound tonometry in ten raptor species and factors affecting the intraocular pressure. *Journal of Avian Medicine and Surgery*, **25**, 165–172.

Rhode, J., Grom, E., Bajares, A.C., et al. (1958) A study of the electrocardiographic alterations. *American Journal of Ophthalmology*, **46**, 367–382.

Riley, M.V. (1972) Intraocular dynamics of lactic acid in the rabbit. *Investigative Ophthalmology & Visual Science*, **11**, 600–607.

Riva, C.E., Alm, A., & Pournaras, C.J. (2011) Ocular circulation. In: *Adler's Physiology of the Eye* (eds. Levin, L.A., Nilsson, S.F.E., Ver Hoeve, J., & Wu, S.M.), 11th ed., pp. 243–273. New York: Mosby Elsevier.

Roberts, S.R. & Erickson, O.F. (1962) Dog tear secretion and tear proteins. *Journal of Small Animal Practice*, **3**, 1.

Robertson, T.W., Hickey, T.L., & Guillery, R.W. (1980) Development of the dorsal lateral geniculate nucleus in normal and visually deprived Siamese cats. *Journal of Comparative Neurology*, **191**, 573–579.

Rodriquez-Peralta, L. (1975) The blood aqueous barrier in five species. *American Journal of Ophthalmology*, **80**, 713–725.

Rohen, J.W. & Funk, R.H.W. (1994) Functional morphology of the episcleral vasculature in rabbits and dogs: Presence of arteriovenous anastomoses. *Journal of Glaucoma*, **3**, 51–57.

Rohen, J.W., Lutjen, E., & Bárány, E. (1967) The relation between the ciliary muscle and the trabecular meshwork and its importance for the effect of miotics on aqueous outflow resistance: A study in two contrasting monkey species, *Macaca irus* and *Cercopithecus aethiops*. *Albrecht von Graefes Archiv für Klinische und Experimentelle Ophthalmologie*, **172**, 23–47.

Ruberti, J.W., Sinha Roy, A. & Roberts, C.J. (2011) Corneal biomechanics and biomaterials. *Annual Review of Biomedical Engineering*, **13**, 269–295.

Sabanay, I., Gabelt, B. T., Tian, B., et al. (2000) H-7 effects on the structure and fluid conductance of monkey trabecular meshwork. *Archives of Ophthalmology*, **118**, 955–962.

Saito, A., Izumisawa, Y., Yamashita, K., et al. (2001) The effect of third eyelid gland removal on the ocular surface of dogs. *Veterinary Ophthalmology*, **4**, 13–18.

Sakamoto, T. & Ishibashi, T. (2011) Hyalocytes: Essential cells of the vitreous cavity in vitreoretinal pathophysiology? *Retina*, **31**, 222–228.

Samuelson, D.A. & Gelatt, K.N. (1984a) Aqueous outflow in the Beagle: I. Postnatal development of the indocorneal angle: Pectinate ligament and uveal trabecular meshwork. *Current Eye Research*, **3**, 783–794.

Samuelson, D.A. & Gelatt, K.N. (1984b) Aqueous outflow in the Beagle: II. Postnatal morphologic development of the iridocorneal angle: Corneoscleral trabecular meshwork and angular aqueous plexus. *Current Eye Research*, **3**, 795–807.

Samuelson, D.A., Gelatt, K.N., & Gum, G.G. (1984) Kinetics of phagocytosis in the normal canine iridocorneal angle. *American Journal of Veterinary Research*, **45**, 2359–2366.

Samuelson, D.A., Gum, G.G., Gelatt, K.N., & Barrie, K.P. (1985) Aqueous outflow in the Beagle: Unconventional outflow, using different-sized microperes. *American Journal of Veterinary Research*, **46**, 242.

Samuelson, D., Plummer, C., Lewis, P., & Gelatt, K. (2001) Schwalbe line's cell in the normal and glaucomatous dog. *Veterinary Ophthalmology*, **4**, 47–53.

Sapienza, J.S., Porcher, D., Collins, B.R., et al. (1991) Tonometry in clinically normal ferrets (*Mustela putorius furo*). *Progress in Veterinary & Comparative Ophthalmology*, **1**, 291–294.

Sappington, R.M., Carlson, B.J., Crish, S.D., et al. (2010) The microbead occlusion model: A paradigm for induced ocular hypertension in rats and mice. *Investigative Ophthalmology & Visual Science*, **51**, 207–216.

Sasaoka, A., Ishimoto, I., Kuwayama, Y., et al. (1984) Overall distribution of substance P nerves in the rat cornea and their three-dimensional profiles. *Investigative Ophthalmology & Visual Science*, **25**, 351–356.

Sato, S. & Kador, P.F. (1989) Rat lens aldehyde reductase. *Investigative Ophthalmology & Visual Science*, **30**, 1618–1622.

Schenker, H.I., Yablonski, M.E., Podos, S.M., & Linder, L. (1981) Fluorophotometric study of epinephrine and timolol in human subjects. *Archives of Ophthalmology*, **99**, 1212–1216.

Schmidt, G.M. & Coulter, D.B. (1981) Physiology of the eye. In: *Veterinary Ophthalmology* (ed. Gelatt, K.N.), pp. 129–159. Philadelphia, PA: Lea & Febiger.

Scott, D.W. & Bistner, S.I. (1973) Neurotrophic keratitis in a dog, *Veterinary Medicine, Small Animal Clinician*, **68**, 1120–1122.

Sears, M.L. (1966) The mechanism of action of adrenergic drugs in glaucoma. *Investigative Ophthalmology*, **5**, 115.

Sears, M.L. & Neufeld, A.H. (1975) Editorial: Adrenergic modulation of the outflow of aqueous humor. *Investigative Ophthalmology*, **14**, 83–86.

Sebag, J. (1989) *The Vitreous: Structure, Function and Pathology*. New York: Springer.

Sebbag, L., Reilly, C.M., Eid, R., & Maggs, D.J. (2016) Goblet cell density and distribution in cats with clinically and histologically normal conjunctiva. *Veterinary Ophthalmology*, **19**(Suppl. 1), 38–43.

Seltner, R.L., Weerheim, J.A., & Sivak, J.G. (1989) Role of the lens and vitreous humor in the refractive properties of the eyes of three strains of goldfish. *Vision Research*, **29**, 681–685.

Shatz, C.J. & Levay, S. (1979) Siamese cat: Altered connections of visual cortex. *Science*, **204**, 328–330.

Sherman, S.M. (1972) Development of interocular alignment in cats. *Brain Research*, **37**, 187–203.

Sherrington, C. (1947) *The Integrative Action of the Nervous System*, 2nd ed. New Haven, CT: Yale University Press.

Shields, M.B. (1992) *Textbook of Glaucoma*, 3rd ed. Baltimore, MD: Williams & Wilkins.

Shonat, R.D., Wilson, D.F., Riva, C.E., & Cranstoun, S.D. (1992) Effect of acute increases in intraocular pressure on intravascular optic nerve head oxygen tension in cats. *Investigative Ophthalmology & Visual Science*, **33**, 3174–3180.

Short, C.E. & Rebhun, W.C. (1980) Complications caused by the oculocardiac reflex during anesthesia in a foal. *Journal of the American Veterinary Medical Association*, **176**, 630–631.

Silver, F.H., Kato, Y.P., Ohno, M., & Wasserman, A.J. (1992) Analysis of mammalian connective tissue, relationship between hierarchical structures and mechanical properties. *Journal of Long-Term Effects of Medical Implants*, **2**, 165–198.

Sit, A.J., Nau, C.B., McLean, J.W., et al. (2008) Circadian variation of aqueous dynamics in young healthy adults. *Investigative Ophthalmology & Visual Science*, **49**, 1473–1479.

Skorobohach, B.J., Ward, D.A., & Hendrix, D.V. (2003) Effects of oral administration of methazolamide on intraocular pressure and aqueous humor flow rate in clinically normal dogs. *American Journal of Veterinary Research*, **64**, 183–187.

Smith, P.J., Samuelson, D.A., Brooks, D.E., & Whitely, R.D. (1986) Unconventional aqueous humor outflow of microspheres perfused into the equine eye. *American Journal of Veterinary Research*, **47**, 2445–2453.

Smith, S.D. & Gregory, D.S. (1989) A circadian rhythm of aqueous flow underlies the circadian rhythm of IOP in NZW rabbits. *Investigative Ophthalmology & Visual Science*, **30**, 775–778.

Snyder, K.C., Lewin, A.C., Mans, C., & McLellan, G.J. (2018) Tonometer validation and intraocular pressure reference values in the normal chinchilla (*Chinchilla lanigera*). *Veterinary Ophthalmology*, **21**, 4–9.

Stiles, J., Buyukmihci, N.C., & Farver, T.B. (1994) Tonometry of normal eyes in raptors. *American Journal of Veterinary Research*, **55**, 477–479.

Stjernschantz, J. (1976) Effect of parasympathetic stimulation on intraocular pressure, formation of the aqueous humour and outflow facility in rabbits. *Experimental Eye Research*, **22**, 639–645.

Su, S.P., McArthur, J.D., Truscott, R.J., & Aquilina, J.A. (2011) Truncation, cross-linking and interaction of crystallins and intermediate filament proteins in the aging human lens. *Biochimica et Biophysica Acta*, **1814**, 647–656.

Swain, R., Kumar, A., Sahoo, J., et al. (2015) Estimation of post-mortem interval: A comparison between cerebrospinal fluid and vitreous humour chemistry. *Journal of Forensic and Legal Medicine*, **36**, 144–148.

Tada, H., Omori, Y., Hirokawa, K., et al. (2013) Eye-blink behaviors in 71 species of primates. *PLoS One*, **8**, e66018.

Talusan, E.D. & Schwartz, B. (1981) Episcleral venous pressure: Differences between normal, ocular hypertensive, and primary open angle glaucoma. *Archives of Ophthalmology*, **99**, 824–828.

Tanelian, D.L. & Beuerman, R.W. (1984) Responses of rabbit corneal nociceptors to mechanical and thermal stimulation. *Experimental Neurology*, **84**, 165–178.

Thomasy, S.M., Raghunathan, V.K., Winkler, M., et al. (2014) Elastic modulus and collagen organization of the rabbit cornea: Epithelium to endothelium. *Acta Biomaterialia*, **10**, 785–791.

Tomlinson, A., Doane, M.G., & McFadyen, A. (2009) Inputs and outputs of the lacrimal system: Review of production and evaporative loss. *Ocular Surface*, **7**, 186–198.

Toris, C.B., Risma, J.M., Gonzales-Martinez, J., et al. (2010) Aqueous humor dynamics in inbred rhesus monkeys with naturally occurring ocular hypertension. *Experimental Eye Research*, **91**, 860–865.

Toris, C.B., Yablonski, M.E., Wang, Y.L., & Hayaski, M. (1995) Prostaglandin A_2 increases uveoscleral outflow and trabecular outflow facility in the cat. *Experimental Eye Research*, **61**, 649–657.

Tornqvist, G. (1966) Effect of cervical sympathetic stimulation on accommodation in monkeys: An example of a beta-adrenergic, inhibitory effect. *Acta Physiologica Scandinavica*, **67**, 363–372.

Townsend, D.J. & Brubaker, R.F. (1980) Immediate effect of epinephrine on aqueous formation in the normal human eye as measured by fluorophotometry. *Investigative Ophthalmology & Visual Science*, **19**, 256–266.

Toyoshima, K., Kawana, E., & Sakai, H. (1980) On the neuronal origin of the afferents to the ciliary ganglion in cat. *Brain Research*, **185**, 67–76.

Tripathi, R.C. (1974) Comparative physiology and anatomy of the aqueous outflow pathway. In: *Biochemistry of the Eye* (eds. Davson, H. & Graham, L.), Vol. **5**, p. 163. New York: Academic Press.

Tripathi, R.C. & Tripathi, B.J. (1972) The mechanism of aqueous outflow in lower mammals. *Experimental Eye Research*, **14**, 73–79.

Tripathi, R.C. & Tripathi, B.J. (1973) The mechanism of aqueous outflow in primates, lower mammals and birds: A comparative study. *Experimental Eye Research*, **17**, 393–394.

Tulamo, R., Saari, H., & Konttinen, Y.T. (1990) Determination of concentration of hyaluronate in equine serum. *American Journal of Veterinary Research*, **51**, 740–742.

Turner-Giannico, A., de Sampaio, M.O, Lima, L., et al. (2014) Characterization of the oculocardiac reflex during compression of the globe in Beagle dogs and rabbits. *Veterinary Ophthalmology*, **17**, 321–327.

Ueno, N., Sebag, J., Hirokawa, H., & Chakrabarti, B. (1987) Effects of visible light irradiation on vitreous structure in the presence of a photosensitizer. *Experimental Eye Research*, **44**, 863–870.

US Department of Defense (1997) *Composites Materials Handbook, Vol. 3: Polymer Matrix Composites Materials Usage Design and Analysis*. Washington, DC: US Department of Defense.

Uusitalo, R. (1972) Effect of sympathetic and parasympathetic stimulation on the secretion and outflow of aqueous humour in the rabbit eye. *Acta Physiologica Scandinavica*, **86**, 315–326.

van Alphen, G.W., Kern, R., & Robinette, S. (1965) Adrenergic receptors of the intraocular muscles: Comparison to cat, rabbit, and monkey. *Archives of Ophthalmology*, **74**, 253–259.

van Alphen, G.W., Robinette, S.L., & Macri, F.J. (1962) Drug effects on ciliary muscle and choroid preparations in vitro. *Archives of Ophthalmology*, **68**, 81–93.

Van Haeringen, N.J. (1981) Clinical biochemistry of tears. *Survey of Ophthalmology*, **26**, 84–96.

Vareilles, P., Conquet, P., & Ledonarec, J.C. (1977a) A method for the routine extraocular pressure (IOP) measurement in the rabbit: Range of IOP variation in this species. *Experimental Eye Research*, **24**, 369–375.

Vareilles, P., Silverstone, D., Plazonnet, B., et al. (1977b) Comparison of the effects of timolol and other adrenergic agents on intraocular pressure in the rabbit. *Investigative Ophthalmology & Visual Science*, **16**, 987–996.

Varela, R.A. & Bossart, G.D. (2005) Evaluation of biochemical analytes in vitreous humor collected after death in West Indian manatees. *Journal of the American Veterinary Medical Association*, **226**, 88–92.

Verboven, C.A., Djajadiningrat-Laanen, S.C., Teske, E., & Boevé, M.H. (2014) Development of tear production and intraocular pressure in healthy canine neonates. *Veterinary Ophthalmology.* **17**, 426–431.

Verkman, A.S. (2003) Role of aquaporin water channels in eye function. *Experimental Eye Research*, **76**, 137–143.

Viteri, G., Carrard, G., Birlouez-Aragón, I., et al. (2004) Age-dependent protein modifications and declining proteasome activity in the human lens. *Archives of Biochemistry and Biophysiology*, **427**, 97–203.

Voigt, S., Fuchs-Baumgartinger, A., Egerbacher, M., et al. (2012) Investigations on the conjunctival goblet cells and the characteristics of the glands associated with the eye in chinchillas (*Chinchilla laniger*). *Veterinary Ophthalmology*, **15**, 333–344.

Von Zup, M., Lassaline, M., Kass, P.H., et al. (2017) Effects of 0.2% brimonidine and 0.2% brimonidine-0.5% timolol on intraocular pressure and pupil size in normal equine eyes. *Equine Veterinary Journal*, **49**, 810–814.

Walinder, P.E. (1966) Influence of pilocarpine on iodopyracet and iodide accumulation by rabbit ciliary body-iris preparations. *Investigative Ophthalmology*, **5**, 378–385.

Walinder, P.E. & Bill, A. (1969) Aqueous flow and entry of cycloleucine into the aqueous humor of vervet monkeys (*Cercopithecus ethiops*). *Investigative Ophthalmology*, **8**, 434–445.

Wallenstein, M.C. & Wang, S.C. (1979) Mechanism of morphine-induced mydriasis in the cat. *American Journal of Physiology*, **236**, R292–R296.

Walsh, F.B. & Hoyt, W.F., eds. (1969) *Sensory innervation of the eye and orbit. In: Clinical Neuro-Ophthalmology*, 3rd ed. Baltimore, MD: Williams & Wilkins.

Wang, L., Cull, G.A., & Fortune, B. (2015) Optic nerve head blood flow response to reduced ocular perfusion pressure by alteration of either the blood pressure or intraocular pressure. *Current Eye Research*, **40**, 359–637.

Ward, D.A., Cawrse, M.A., & Hendrix, D.V. (2001) Fluorophotometric determination of aqueous humor flow rate in clinically normal dogs. *American Journal of Veterinary Research*, **62**, 853–858.

Weber, H., Landwehr, G., Kilp, H., & Neubauer, H. (1982) Mechanical properties of the vitreous in pig and human donor eyes. *Ophthalmic Research*, **14**, 335–343.

Wei, X.E., Markoulli, M., Millar, T.J., et al. (2012) Divalent cations in tears, and their influence on tear film stability in humans and rabbits. *Investigative Ophthalmology & Visual Science*, **53**, 3280–3285.

Weinstein, J.M., Duckrow, R.B., Beard, D. & Brennant, R.W. (1983) Regional optic nerve blood flow and its autoregulation. *Investigative Ophthalmology & Visual Science*, **24**, 1559–1565.

Weiss, H. (1972) The carbohydrate reserve in the vitreous body and retina of the rabbit eye during and after pressure ischaemia and insulin hypoglycemia. *Ophthalmic Research*, **3**, 360–371.

White, J., Werkmeister, J.A., Ramshaw, J.A., & Birk, D.E. (1997) Organization of fibrillar collagen in the human and bovine cornea: Collagen types V and III. *Connective Tissue Research*, **36**, 165–174.

Whiting, R.E., Yao, G., Narfström, K., et al. (2013) Quantitative assessment of the canine pupillary light reflex. *Investigative Ophthalmology & Visual Science*, **54**, 5432–5440.

Whittaker, C.J., Heaton-Jones, T.G., Kubilis, P.S., et al. (1995) Intraocular pressure variation associated with body length in young American alligators (*Alligator mississippiensis*). *American Journal of Veterinary Research*, **56**, 1380–1383.

Willis, A.M., Diehl, K.A., Hoshaw-Woodard, S., et al. (2001) Effects of topical administration of 0.005% latanoprost solution on eyes of clinically normal horses. *American Journal of Veterinary Research*, **62**, 1945–1951.

Wingstrand, K.G. & Munk, O. (1965) The pectin oculi of the pigeon with regard to its function. *Biologiske Skrifter*, **14**, 5.

Winkler, M., Shoa, G., Tran, S.T., et al. (2015) A comparative study of vertebrate corneal structure: The evolution of a refractive lens. *Investigative Ophthalmology & Visual Science*, **56**, 2764–2772.

Wistow, G.J. & Piatigorsky, J. (1987) Recruitment of enzymes as lens structural proteins. *Science*, **236**, 1554–1556.

Wooten, G.F. & Reis, D.J. (1972) Blood flow in extraocular muscle of cat. *Archives of Neurology*, **26**, 350–352.

Worthington, K.S., Wiley, L.A., Bartlett, A.M., et al. (2014) Mechanical properties of murine and porcine ocular tissues in compression. *Experimental Eye Research*, **121**, 194–199.

Wygnanski-Jaffe, T., Murphy, C.J., Smith, C., et al. (2007) Protective ocular mechanisms in woodpeckers. *Eye*, **21**, 83–89.

Wyman, M. (1973) Applied anatomy and physiology of the anterior chamber angle. *Veterinary Clinics North America*, **3**, 439–451.

Yablonski, M.E., Zimmerman, T.J., Waltman, S.R., & Becker, B. (1978) A fluorophotometric study of the effect of topical timolol on aqueous humor dynamics. *Experimental Eye Research*, **27**, 135–142.

Yang, Q., Shen, J., Guo, W., et al. (2011) Effect of acute intraocular pressure elevation on blood flow velocity and resistance in the rabbit ophthalmic artery. *Veterinary Ophthalmology*, **14**, 353–357.

Ye, W., Gong, H., Sit, A., et al. (1997) Interendothelial junctions in normal human Schlemm's canal respond to changes in pressure. *Investigative Ophthalmology & Visual Science*, **38**, 2460–2468.

Yorzinski, J.L. (2016) Eye blinking in an avian species is associated with gaze shifts. *Scientific Reports*, **6**, 32471. doi: 10.1038/srep32471.

Yoshitomi, T. & Ito, Y. (1986) Double reciprocal innervations in dog iris sphincter and dilator muscles. *Investigative Ophthalmology & Visual Science*, **27**, 83–91.

Yoshitomi, T. & Ito, Y. (1988) Effects of indomethacin and prostaglandins on the dog iris sphincter and dilator muscles. *Investigative Ophthalmology & Visual Science*, **29**, 127–132.

Yu, D.Y., Alder, V.A., Cringle, S.J., & Brown, M.J. (1988) Choroidal blood flow measured in the dog eye *in vivo* and *in vitro* by local hydrogen clearance polarography: Validation of a technique and response to raised intraocular pressure. *Experimental Eye Research*, **46**, 289–303.

Zampighi, G.A., Eskandari, S., Hall, J.E., et al. (2002) Micro-domains of AQP0 in lens equatorial fibers. *Experimental Eye Research*, **75**, 505–519.

Zhan, G.L., Toris, C.B., Camras, C.B., et al. (1998) Bunazosin reduces intraocular pressure in rabbits by increasing uveoscleral outflow. *Journal of Ocular Pharmacology and Therapeutics*, **14**, 217–228.

Zhang, J., Hodge, W., Hutnick, C., et al. (2011) Noninvasive diagnostic devices for diabetes through measuring glucose. *Journal of Diabetes Science and Technology*, **5**, 166–172.

Zhang, X., Hernandez, M.R., Yang, H., & Erickson, K. (1995) Expression of muscarinic receptor subtype mRNA in the human ciliary muscle. *Investigative Ophthalmology & Visual Science*, **36**, 1645–1657.

Zhao, M., Hejkal, J.J., Camras, C.B., et al. (2010) Aqueous humor dynamics during the day and night in juvenile and adult rabbits. *Investigative Ophthalmology & Visual Science*, **51**, 3145–3151.

Zimmerman, T.J. (1993) Topical ophthalmic beta blockers: A comparative review. *Journal of Ocular Pharmacology*, **9**, 373–384.

4

Optics and Physiology of Vision

Ron Ofri[1] *and Björn Ekesten*[2]

[1] *Koret School of Veterinary Medicine, Hebrew University of Jerusalem, Rehovot, Israel*
[2] *Department of Clinical Sciences, Faculty of Veterinary Medicine, Swedish University of Agricultural Science, Uppsala, Sweden*

The aim of this chapter is to describe the physical, anatomic, and physiologic aspects of the process of vision. With this aim in mind, the chapter has been divided into two parts. The first part is devoted to visual optics. It covers the physical changes that light undergoes during its passage from the cornea, through the various structures and tissues of the eye, until it reaches the retina. One may question the amount of text that has been devoted to optical aberrations in the eye and to species not normally seen as patients, such as aquatic animals, chickens, and fish; however, understanding how various species cope with these aberrations, or with their unique habitat, is fundamental to the understanding of visual optics.

The second part of this chapter is devoted to visual processing and describes what happens once light reaches the retina. This part is dedicated to the neuronal processes of vision and describes the generation, processing, and propagation of the visual signal in the retina, the visual pathways, and the cortex. Both these parts lay the foundations for understanding how optical and neuronal processes enable the detection of stimulus movement, details, and color that create the rich experience of vision described in Chapter 5.

Visual Optics

Physical Optics

Light

The nature of light has long been a subject of controversy. Light has alternately been described as a wave (first proposed by Huygens in 1678) or as photon particles (first proposed by Newton in 1672). However, these descriptions are not mutually exclusive. Quantum optics (first proposed by Planck in 1900) integrates both models to explain the dual nature of light and its interaction with matter. Both models also are applicable in the eye: the wave theory explains the physical changes light undergoes during its passage through the eye, and the particle theory explains the energy transformation that occurs when light is absorbed in the outer segments of the photoreceptors. Therefore, the first part of this chapter discusses light as a wave, while the second part discusses it as a particle.

Light behaves like a wave as it passes through transparent media such as air, vacuum, or the visual axis of the eye. Much like a wave of water, a wave of light has two principal characteristics (Fig. 4.1). Its amplitude, A, is the maximum value of the field generated by the propagating wave; it determines the wave's intensity. The wavelength, λ, is the distance between adjacent wave crests; it determines the wave's location in the electromagnetic spectrum. As Fig. 4.2 shows, light, which is the visible portion of the electromagnetic spectrum, occupies a small fraction of that spectrum, which ranges from cosmic and gamma rays ($\lambda < 10^{-10}$ m) to radio transmission ($\lambda > 10^{3}$ m). In humans, visible light ranges in wavelength from approximately 380 (i.e., deep blue) to 780 (i.e., deep red) nm (Wang et al., 2014). However, additional wavelengths, outside the 380–780 nm spectrum, can be seen by other species. For example, many nonmammalian species, and some mammals, possess ultraviolet (UV) vision that allows them to detect light with a wavelength shorter than 380 nm, enabling them to see hues that are not perceived by humans (Odeen et al., 2011). This capability is used in both foraging and courting behavior (Hogg et al., 2011). At the other end of the spectrum, fish living in blackwater rivers, in which the maximally transmitted light is longer than 600 nm, have evolved near-infrared (IR) vision, enabling them to detect light with a wavelength longer than 780 nm that is prevalent in their environment (Shcherbakov et al., 2013). The cat retina has also been shown to respond to IR light (826–875 nm), though the functional and behavioral implications of this capability are not clear (Gekeler et al., 2006). This is not to be confused with the IR "vision"

Veterinary Ophthalmology: Volume I, Sixth Edition. Edited by Kirk N. Gelatt, Gil Ben-Shlomo, Brian C. Gilger, Diane V.H. Hendrix, Thomas J. Kern, and Caryn E. Plummer.

Companion website: www.wiley.com/go/gelatt/veterinary

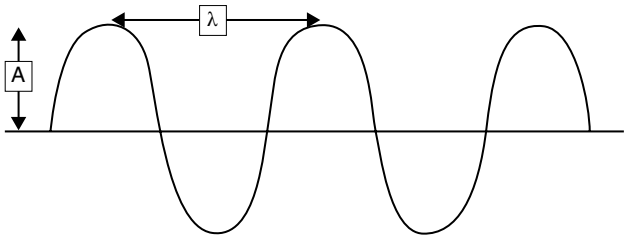

Figure 4.1 Representation of light as a wave, which is characterized by two parameters. Its amplitude (A) is the maximum value the wave obtains as it propagates. Its wavelength (λ) is the distance between two consecutive peaks.

of snakes, which relies on the heat-detection properties of the pit organs (Bolívar-G et al., 2014).

At the same time, light also possesses the properties of particles, termed *photons*, which represent quanta of energy that can be emitted (at the light source) or absorbed (e.g., by retinal photoreceptors). The amount of energy in a given photon is inversely proportional to its wavelength; therefore, blue light possesses more energy than red light, which has a longer wavelength (see Fig. 4.2). An example of the particle nature of light is seen in the use of cobalt blue light to highlight fluorescein staining of corneal ulcers. Fluorescein sodium molecules absorb photons of blue light and reemit photons with a lower energy content, in the yellow-green portion of the spectrum, in a process known as fluorescence (Glasgow, 2016).

As light strikes the photoreceptor outer segments, it is absorbed by a visual photopigment. The function of this two-part molecule reflects the principles of quantum physics, as it utilizes both the wave properties and the particle properties of light. The first part of the molecule, the *opsin*, determines the wavelength of the light that the photopigment will absorb, thus determining color vision. The second part of the molecule, the visual chromophore or *retinal*, uses the energy of the photon particle to undergo isomerization (from 11-*cis*-retinal into all-*trans*-retinal in the case of rhodopsin), thereby initiating conversion of a light stimulus into an electric signal. This process, the *phototransduction process*, which is discussed in detail later in this chapter, is the first step in the initiation and propagation of a visual signal.

Photometry

Photometry is the quantitative measurement of visible light. Photometry measures a number of interrelated properties of light, using a basic unit called a *candela*. Two important characteristics of light are its *luminous intensity*, which describes the intensity of a light source (as measured in candela), and its *luminance*, which describes its brightness reflected from a surface (as measured in foot-Lamberts or *candela/m*^{2}). These two properties are related, but they are not necessarily proportional. A handheld transilluminator is a bright source of light, but it possesses low intensity and therefore cannot be used to illuminate a football stadium. On the other hand, a streetlight provides high-intensity light, which illuminates a large area, but it is not bright and does not provide enough illumination to conduct cataract surgery. Table 4.1 provides the luminances of several common sources of light.

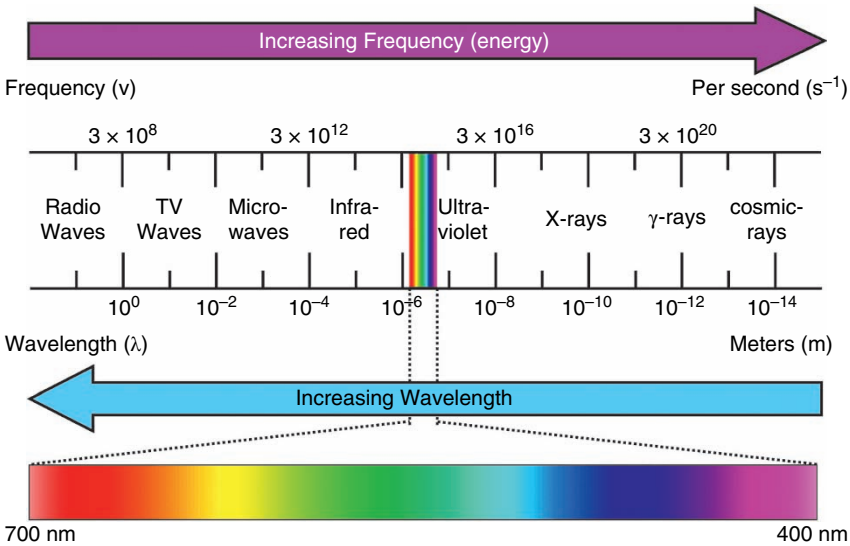

Figure 4.2 Spectrum of electromagnetic radiation. Visible light occupies only a small portion of the spectrum. Most humans can see radiation with a wavelength of approximately between 380 and 780 nm. Some animal species see a more limited part of the spectrum, while others can discern larger portions of the spectrum, as they are also able to perceive shorter (ultraviolet) or longer (infrared) light. Note that the wavelength (blue arrow) of a light wave are inversely related to its energy and frequency (purple arrow). (Reproduced from www.chemicalconnection.org.uk with permission of Dr. Paul Murray.)

Table 4.1 Luminances of natural and artificial light sources[a].

Source	Luminance (cd/m^2)
Sun	10^9
Car light	10^7
Incandescent tungsten lamp	10^6–10^7
Fluorescent lamp	10^4–10^5
Clear sky at noon	10^4
Full moon	10^3
Street lamp	0.1–1.0
Moonless night sky	10^{-3}–10^{-6}

Source: Adapted from Millodot, M. (2018) *Dictionary of Optometry and Visual Science*, 8th ed. St. Louis, MO: Elsevier.
[a] In general, only the *photopic* system is active at a luminance > 3 cd/m^2; at a luminance < 0.03 cd/m^2, the *scotopic* system functions alone. Both systems are active at intermediate luminance values, which are defined as *mesopic* vision.

Luminance is measured using photometers, which are divided into two major classes. Visual photometers provide a subjective reading, because the observer compares the illumination of the measured light with that of a standard light. Photoelectric photometers convert the measured light into an electric current, which is displayed by the instrument. Photometry measurements are extremely important in electroretinographic (ERG) recordings because they are used to describe such variables as threshold, ambient and adapting lights, and stimulus luminance.

Transmission and Reflection

As noted, human vision is limited to a wavelength range of 380–780 nm. This limitation is a result of two factors. The first is the absorption spectrum of the opsin component of the visual photopigment, mentioned previously. The second limiting factor is the transmission, reflection, and attenuation of the various wavelengths by the ocular media, which depend on several properties, the most significant being the wavelength of the light, the angle of incidence, and the clarity of the media.

In humans, radiation wavelengths of 300–2500 nm are transmitted through the cornea (Boettner & Wolter, 1962). Not all wavelengths, however, are transmitted through the cornea equally, as transmission is directly related to wavelength. For example, the human cornea transmits 95% of light with wavelengths of 650 nm or longer, but only 80% of light with a wavelength of 425 nm (Calhoun et al., 2015). In the rabbit, the cornea transmits 89%–93% of the light at 370–500 nm, falling to 50% transmittance at 310 nm and a mere 2% at wavelengths below 290 nm (McLaren & Brubaker, 1996).

Additional attenuation of transmission occurs inside the eye (Fig. 4.3). Even though light with wavelengths of up to 2500 nm passes the cornea, there is barely any transmission of wavelengths greater than 1950 nm through the aqueous humor, and in humans the lens only transmits wavelengths between 390 and 1400 nm (Boettner & Wolter, 1962). A similar range of wavelengths is transmitted through the pig eye (Lei & Yao, 2006). The implication of these numbers is that the aqueous and lens act as color filters, preventing UV and IR light with very short and very long wavelengths (which has passed the cornea) from reaching the retina. The UV filtering by the lens is of particular importance, as UV light is a risk factor in a number of retinal diseases, particularly age-related macular degeneration (Schick et al., 2016). Therefore, intraocular lenses (IOLs) contain chemically-bound UV filters to restore this protection in pseudophakic patients. Consequently, aphakic humans can detect UV radiation following lens extraction, having lost the UV-filtering lens (Li et al., 2017b). In other words, human opsin is capable of absorbing UV light, but these wavelengths do not reach the retina of phakic subjects (Griswold & Stark, 1992). Conversely, transmittance of light by the eye does not automatically result in vision, because transmitted radiation must be absorbed by a photopigment sensitive to that wavelength before the light can be perceived. This is why humans cannot perceive infrared light, even though it reaches the retina (Fig. 4.3).

Additional ocular structures, such as tear film (Choy et al., 2011) and eyelids (Bierman et al., 2011), also act as color filters, causing significant attenuation of short-wavelength

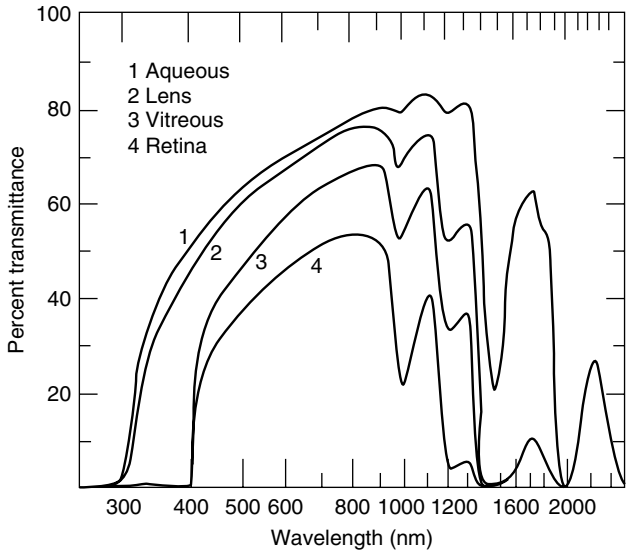

Figure 4.3 Transmittance rates of light through various structures of the human eye, not including light lost due to reflection or scatter, at each wavelength. (Reprinted with permission from Boettner, E.A. & Wolter, J.R. (1962) Transmission of the ocular media. *Investigative Ophthalmology*, **1**, 776–783.)

light. Thus, when cumulative transmittances are calculated for the successive components of the eye, a maximal transmittance rate in humans of 84% is obtained for light between 650 and 850 nm (Boettner & Wolter, 1962), while in rabbits the transmittance rate for light between 370 and 500 nm is 90% (McLaren & Brubaker, 1996). Obviously, transmission will be further reduced by ocular opacities. Grade II nuclear cataracts in rats cause a 50% reduction in transmission of light compared with grade I cataracts (Nishimoto & Sasaki, 1995), and in humans the light scatter index for nuclear cataracts is twice that of cortical cataracts (Siik et al., 1999). Age is another factor affecting transmittance. Transmission of light at 480 nm through the human lens decreases by 72% from the age of 10 years to the age of 80 years (Kessel et al., 2010), thus affecting the color perception of the elderly. Surprisingly, however, studies have failed to demonstrate age-related decline in transmittance in the human cornea (van den Berg & Tan, 1994).

Ocular surfaces can also reflect back incoming light, depending on the angle of incidence. Light that strikes a surface at an oblique angle is reflected back; it is not transmitted into the new medium. The critical angle for reflection is determined by the difference in the indices of refraction between the two media (discussed in the next section). Most of the reflection that takes place in the eye occurs as incoming light strikes the cornea because of the large difference in refraction indices between the cornea and air. Reflection that occurs at the cornea–air interface affects not only incoming light, but also outgoing light. Thus, internal reflection of outgoing light back into the eye prevents the ophthalmologist from examining the iridocorneal angle. Goniolenses filled with fluid are used to decrease the difference in refractive indices between the cornea and air, thus increasing the critical angle and permitting rays emanating from the iridocorneal angle to pass through the cornea (Wilson, 2006).

Light that is not transmitted and not reflected can be either scattered in the eye or absorbed by pigments. Foremost among these pigments are the photopigments of the photoreceptor outer segments, which absorb photons and thus initiate the visual process. Additional absorption processes in the eye may have clinical implications. Cyclophotocoagulation in glaucoma patients is based on the preferential absorbance of 810 and 1064 nm radiation of the diode and Nd : YAG lasers, respectively, by melanin-containing tissue (Bras & Maggio, 2015). In addition, absorption of UV solar radiation has been implicated in diseases such as canine chronic superficial keratitis (Chandler et al., 2008), squamous cell carcinoma in cattle (Pausch et al., 2012), and pterygium (Zhou et al., 2016), cataract, and macular degeneration in humans (Delcourt et al., 2014). The interaction of the cornea with UV light may also hold implications for corneal cross-linking treatment (Lombardo et al., 2015).

Geometric Optics

Refraction

In vacuum, light travels at a constant speed (c) of approximately 3×10^8 m/s. As it strikes denser media, light undergoes three changes:

1) Its velocity is reduced.
2) Its wavelength shortens.
3) It is bent (unless it struck the surface of the medium at a 90° angle).

The first two changes are expressed in the equation

$$n = c/v = \lambda/\lambda_m,$$

where n is the *index of refraction* (or bending) of the new, dense medium; c and λ are the speed and wavelength, respectively, in vacuum; and ν and λ_m are the velocity and wavelength, respectively, in the new, dense medium.

Since the index of refraction of any medium other than vacuum is greater than one ($n > 1$), it follows that $c > \nu$; that is, the speed of light in the new medium (ν) is less than it was in vacuum (c). For the same reason ($n > 1$), it follows that $\lambda > \lambda_m$; that is, the wavelength of light in the new medium (λ_m) is shorter than it was in vacuum (λ).

The third change that occurs when light passes into a dense medium is bending, or refraction. The amount of refraction that occurs as light passes from one medium to another is described by Snell's law (Fig. 4.4) and is determined by the angle of incidence and by the refractive indices

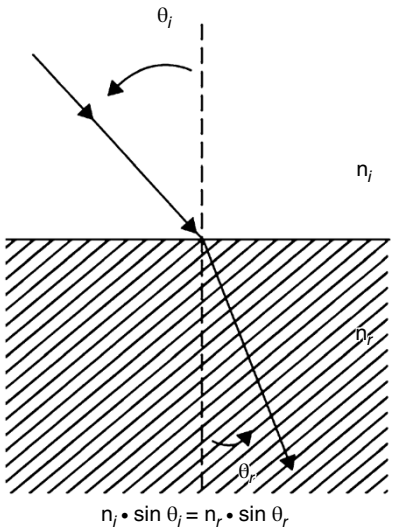

Figure 4.4 Refraction of light as it passes from one medium to another is governed by Snell's law, summarized in the formula below the diagram. The angle of refraction (θ_r) is a function of the angle of incidence (θ_i) and the refractive indices of the two mediums. In this representation, $n_i < n_r$; therefore, $\theta_i > \theta_r$.

of both media. Because various structures of the eye differ in their refraction indices, light is successively refracted (bent) as it passes from air through the precorneal tear film (PTF), cornea, aqueous humor, lens, and vitreous on its way to the retina (see the next section, "Visual Optics").

Vergence

An object that bends (or refracts) light is called a lens. When a single ray of light strikes a lens, the ray undergoes simple refraction, as depicted in Fig. 4.4. Most objects or images, however, generate a pencil of light rays rather than a single ray. When a pencil of rays strikes a lens, they spread apart (i.e., diverge) or come together (i.e., converge). Convergence, or positive vergence, occurs when light strikes a convex lens (Fig. 4.5A, B). Such a lens has a positive power, indicating that it forms a *real image*, which means that incoming rays from the object are converged and focused on the other side of the lens (see Fig. 4.5A, B). On the other hand, divergence, or negative vergence, occurs when light strikes a concave lens (Fig. 4.5C). The negative power of the concave lens indicates that it forms a *virtual* or *aerial* image, which means that the diverging rays are traced, using imaginary extensions, backward to a "focused" virtual image "located" on the same side of the lens as the object (dashed, "imaginary" lines in Fig. 4.5C).

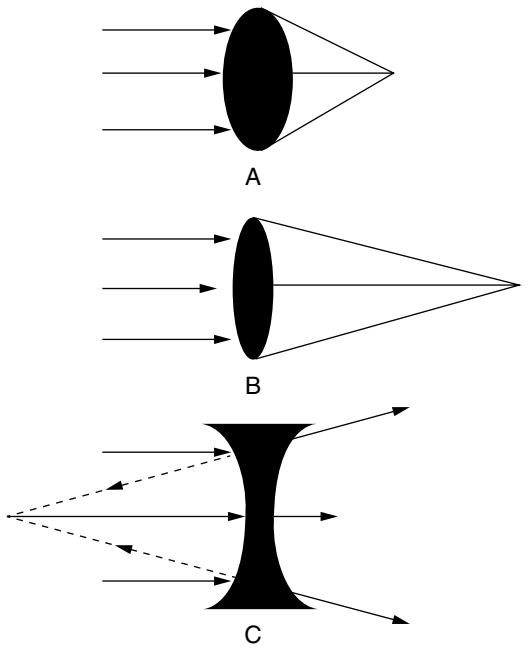

Figure 4.5 Refraction of light through various lenses. **A.** A spherical convex lens with a power of 10 D focuses parallel light rays at a distance of 0.1 m. **B.** A flatter, less spherical convex lens with a power of 5 D focuses parallel rays at a distance of 0.2 m. **C.** Parallel rays passing through a concave spherical lens diverge. A virtual image is formed by tracing back (dashed lines) the diverging rays.

The vergence power (i.e., amount of bending) of a lens is measured in units called *diopters*. One diopter (D) is the vergence power of a lens with a focal length (f) of 1 m when in air. In broader terms,

$$D = 1/f.$$

The focal length of a lens is the distance between the center of the lens and the point at which parallel rays of light are brought into focus by that lens. The focal length of a lens is directly proportional to its curvature radius. Therefore, the vergence power (or the diopter power) of the lens increases as its curvature increases (or its radius of curvature decreases). For example, a convex lens with a focal length of 0.1 m will have a power of +10 D ($D = 1/f = 1/0.1\,m = 10\,D$), while a flatter convex lens with a focal length of 0.2 m will be "weaker," with a power of +5 D ($D = 1/f = 1/0.2\,m = 5\,D$; compare Fig. 4.5A and Fig. 4.5B). On the other hand, a concave lens with a focal length of 0.2 m will have a power of −5 D (Fig. 4.5C).

The vergence powers of lenses in an optical system are additive. Thus, if the lenses in Fig. 4.5A and Fig. 4.5B were placed next to each other, the resulting optical system would have a theoretical power of +15 D. If all three lenses in Fig. 4.5 were combined into one system, it would have a power of +10 D. This principle also holds in the eye, as the refractive contributions of the successive ocular surfaces are added to form a focused or blurred image on the outer segments of the photoreceptors.

As noted, the former formula describes the refractive powers of lenses in air. When placed in a medium with a refractive index n, the refractive power of the lens is described by the formula

$$D = n/f.$$

Since $n > 1$ for any medium other than vacuum, it follows that the refractive power of the lens is reduced in other media. This is what happens to lenses in the eye, an effect that is described in detail in the following section.

Visual Optics

Refractive Structures of the Eye

Precorneal Tear Film and Cornea

As mentioned, light is successively refracted by the various ocular structures as it passes through the eye on its way to the retina. Table 4.2 lists the refractive indices and powers of various ocular surfaces in humans. The most anterior optical surface of the eye is the PTF. By strict definition, it could be argued that the tear film is the most refractive layer of the eye. This is due to the large difference in refractive indices as light passes from air, which has a refractive index of almost 1, into the tear film, which has a refractive index of 1.337 (Barbero, 2006). Factoring the refractive indices of air and the tear film into Snell's law reveals that the human PTF has

Table 4.2 Refraction constants in the human eye.

Structure	Refractive Index	Refractive Power (D)	Reference
Tear film	1.336	43.0[a]	Montes-Mico et al. (2004)
Cornea	1.376	42.3[a]	Duke-Elder (1970); Naeser et al. (2016)
Anterior surface	1.401	48.2	Patel et al. (1995)
Posterior surface	1.373	−5.9	Patel et al. (1995)
Lens	1.41	21.9	Chang et al. (2017); Duke-Elder (1970)
Anterior surface		8.4	Millodot (1982)
Posterior surface		14.0	Millodot (1982)
Vitreous/aqueous	1.336		Duke-Elder (1970)
Retina	1.363		Millodot (1982)

[a] The refractive power of the cornea and tears is not additive. Rather, that of the former arises from the latter, and from its interface with air. The net power of the tears and the anterior and posterior cornea is 43 D.

a refractive power of 43 D (Montes-Mico et al., 2004). Alterations in the composition (Fish et al., 2004) or breakup time (Montes-Mico et al., 2004) of the PTF may change the refractive power of the eye by as much as 1.3 D and may contribute to the blurry vision complaints commonly encountered in (human) dry eye patients (Koh, 2016). Conversely, successful treatment of dry eye can cause a significant improvement in blurred vision (Toshida et al., 2017). The effect of PTF deficiencies on the quality of vision in animal patients has yet to be studied.

The cornea is the next organ through which incoming light passes. As can be seen in Table 4.2, the human corneal stroma has a refractive index of 1.376. Because this value is slightly higher than the refractive index of the tear film, passage of light from the PTF into the anterior layers of the cornea results in an additional 5 D of refractive power (Courville et al., 2004). However, these 5 D are "lost" when light passes from the posterior cornea into the aqueous humor, which has a refractive index nearly identical to that of the PTF. When combined, the PTF and the cornea of humans contribute a net refractive power of 43 D. Strictly speaking, these 43 D are contributed by the tear film, as they are due to the large difference between the refractive indices of air and the PTF. Still, by convention, this power is usually attributed to the cornea (see Table 4.2). Therefore, in humans, for example, the cornea contributes approximately 70% of the total 60 D power of the eye, thus making it our largest refractive organ (Courville et al., 2004).

Another factor affecting the refractive power of the cornea, besides the refractive index, is its curvature. Because the cornea converges light, it acts as a convex lens. As stated earlier, the refractive power of such a lens depends to a large extent on its curvature radius. Therefore, in large eyes, which are characterized by relatively flat corneas, the refractive power of the cornea is reduced. Conversely, in small eyes with more spherical corneas, its power is increased. Table 4.3 shows that the inverse relationship between globe axial length and the refractive power of the cornea is maintained across a large range of species. Furthermore, the central and peripheral corneas have different curvatures and consequently differ in their refractive powers (see "Spherical and Chromatic Aberrations" later in this chapter). It is suggested that evolutionary changes in corneal curvature and shape, especially between mammalian and nonmammalian species, are reflected in collagen lamellar organization in the stroma (Winkler et al., 2015).

Lens

As noted, because of the similar refractive indices of the cornea and aqueous humor, the refraction that occurs as light passes from the former into the latter and during its passage through the aqueous has little overall optical significance. Therefore, the next significant refractive structure through which light passes after the cornea is the lens (see Table 4.2 and Table 4.4). As in the case of the cornea, the refractive power of the lens is determined by both its refractive index and its curvature. In humans and in many nonaquatic species, the refractive index of the lens nucleus is about 1.41; it decreases gradually toward the cortex, forming a bell-shaped refractive index curve known as the *gradient index* (GRIN). In humans, the refractive index in the subcapsular regions is about 1.38 (Piersckionek & Regini, 2012). Since these values are relatively similar to that of the aqueous humor (range, in most species, 1.334–1.338), the lens in these species has a rather low refractive power (Hughes, 1977). In humans, the calculated refractive power of the lens is approximately 22 D (Chang et al., 2017). The implication of this value is that contrary to the popular belief of the general public, the lens is not the main refractive organ of the eye, as its refractive power is less than half of that of the human cornea. The refractive index of the lens increases in aquatic species, where it can be as high as 1.66, resulting in significantly higher refractive power (Sivak, 1978).

Table 4.3 Eye size (ascending order) and corneal power (descending order) in selected animal species.

Species	Axial Length (mm)	Corneal Power (D)	References
Goldfish	4.2	129 (in air)	Hughes (1977)
Rat	6.3	112.7	Hughes (1977)
Chicken	8.9	108	Cohen et al. (2008)
Guinea pig	8.9	83.9	Howlett & McFadden (2007)
Sea otter	14.0	59.2	Murphy et al. (1990)
Rhesus monkey (4 months)	16.3	56	Qiao-Grider et al. (2010)
Rabbit	18.0	44.6	Hughes (1977); Wang et al. (2014)
Cat	21.3	43.0	Habib et al. (1995)
Dog	19.5–21.9	37.8–43.2[a]	Gaiddon et al. (1991); Nelms et al. (1994); Rosolen et al. (1995)
Ostrich	38.0	25.3	Martin et al. (2001)
Elephant	38.8	21.3	Murphy et al. (1992a)
Horse	39.2	16.5 D	McMullen & Gilger (2006)
Horse	43.7	15.7–19.5	Farrall & Handscombe (1990); Miller & Murphy (2017)

[a] The range of values in the dog probably reflects a breed difference, because larger breeds have flatter corneas (Gaiddon et al., 1991).

Table 4.4 Lens power and refractive indices (both in descending order) in selected animal species.

Species	Lens Power (D)	Refractive Index	References
Rat	243.9	1.683	Hughes (1977)
Guinea pig	160.0	1.649	Howlett & McFadden (2007)
Rabbit	75.0	1.6	Hughes (1977)
	58[a]		Sanchez et al. (2017)
Cat	52.9	1.554	Hughes (1977)
Cynomolgus monkey	52.0	1.42	Borja et al. (2010)
Chicken (90 days)	48.1	1.44	Iribarren et al. (2014)
Dog	41.5[b]		Davidson et al. (1993)
Horse	14.9–15.4	1.42	Farrall & Handscombe (1990); Mouney et al. (2012)
Horse	14[b]		Harrington et al. (2013); Townsend et al. (2012)

[a] Calculated value;
[b] Value is based on dioptric strength of intraocular lens needed to regain emmetropia in pseudophakic patients.

The second factor determining lenticular refractivity, the lens curvature, also differs between aquatic and nonaquatic species. Generally, it can be said that the lens is spherical in fish and aquatic mammals, while it is more discoid (i.e., less spherical) in terrestrial species (see Fig. 4.5A and Fig. 4.5B, respectively). Therefore, the lens will have a higher refractive power in the former compared to the latter. The reason for the increased refractive index and lens curvature in aquatic species is the loss of corneal refractive power under water and is discussed later in this chapter. Of course, the curvature (and hence the refractive power) of the lens can also be changed actively through a process termed *accommodation* (see the next section).

Vitreous

The next refractive organ is the vitreous. Though there is little refraction as light passes from the lens into the vitreous (due to their similar refractive indices), the vitreous plays an important role in the refractive development of the eye. Vitreous elongation increases the axial length of the eye, thereby increasing the refractive path of light and inducing myopia, or nearsightedness (Fig. 4.6). In certain fish, this mechanism serves to increase ocular refraction and compensate for loss of corneal refractive power. In different goldfish strains, for example, the vitreous body can contribute anywhere from 37% to 70% of the total axial length of the eye (Seltner et al., 1989). In visual deprivation studies conducted

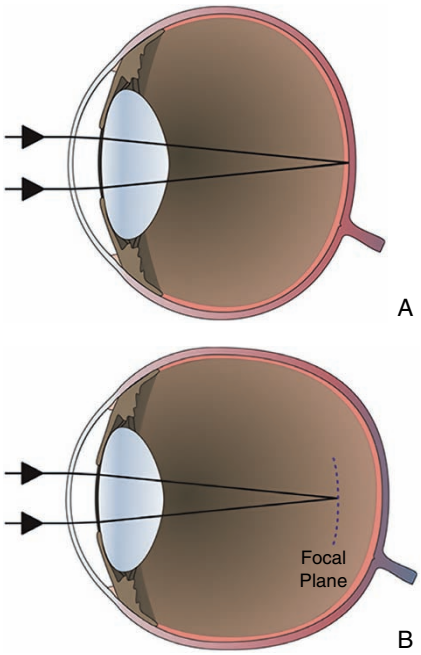

Figure 4.6 The effect of vitreous elongation on ocular refraction. **A.** A focused, emmetropic eye. **B.** The refractive power of the eye has not changed, and the light is focused on the same spot as in panel **A.** However, due to vitreous elongation, the retina has moved posteriorly, and therefore the light is now focused in front of the retina. As a result, the eye is now nearsighted, or myopic.

during critical developmental periods in species as diverse as chickens (Stone et al., 2016), fish (Sivak, 2008), tree shrews (Gawne et al., 2017), and nonhuman primates (Smith et al., 2015), the deprivation-induced myopia was a result of elongation of the vitreous body.

Accommodation

Accommodation is a rapid change in the refractive power of the eye, which is intended to bring the images of objects at different distances into focus on the retina. The stimulus for the accommodative response is a blurred, or defocused, retinal image (Buehren & Collins, 2006). In vertebrates, eyes accommodate by one or more of the following mechanisms (Glasser, 2011):

1) Changing the curvature or position of the lens.
2) Changing the corneal curvature.
3) Changing the distance between the cornea and retina.
4) Having two or more separate optical pathways of different refractive powers (discussed under "Static Accommodation" later in this chapter).

Accommodation is most commonly measured using *infrared photoretinoscopy*, which uses reflection of IR light from the fundus to measure dynamic changes in the refractive error. Since mammalian accommodation is mediated by contraction of the smooth ciliary muscle, it can be stimulated by pilocarpine (Ostrin et al., 2014). For a comprehensive review of comparative accommodation in animals, the reader is referred to Ott (2006).

Humans and other primates accommodate by changing the curvature of the lens (Fig. 4.7). To view distant objects, sympathetic innervation induces relaxation of the ciliary body muscle, which in turn leads to stretching of the lens zonules. The increased tension of the zonules results in a greater pull on the lens capsule, thus causing the lens to become more discoid and decreasing its overall axial thickness and refractive power in a process of *disaccommodation* (see Fig. 4.5B and Fig. 4.7B; Glasser, 2011). To accommodate for near objects, the reverse process takes place. Parasympathetic input induces contraction of the ciliary body muscles, leading to relaxation of the zonular fibers and reduced tension on the lens capsule. In turn, this liberates the inherent elasticity of the lens, resulting in a more spherical lens possessing greater axial thickness and refractive power (Fig. 4.4A and Fig. 4.7A; Glasser, 2011; Hughes, 1977). Consequently, anterior chamber depth decreases and

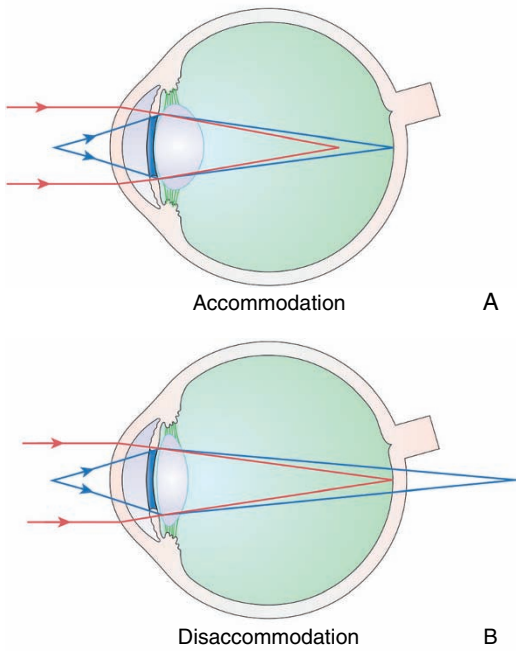

Figure 4.7 Accommodation in the primate lens. **A.** In an accommodated eye, the ciliary muscle contracts, causing the lens to become more spherical, thereby increasing its refractive power. Light from nearby objects (blue lines) is focused on the retina (emmetropia), whereas light from distant objects (parallel red lines) is focused in front of the retina (myopia, or nearsightedness). **B.** At rest the lens is discoid (flat) because of relaxation of the ciliary muscle (disaccommodation). In this state, incoming light from distant objects (parallel red lines) is focused on the retina (emmetropia), whereas light from nearby objects (blue lines) is focused behind the retina (hyperopia, or farsightedness). (Reproduced with permission from Maggs, D.J., Miller, P.E., & Ofri, R. (2018) *Slatter's Fundamentals of Veterinary Ophthalmology*, 6th ed. St Louis, MO: Elsevier.)

increases during accommodation and disaccommodation, respectively. The resulting changes in lenticular curvature allow primates such as the young (< 5 years) rhesus monkey to accommodate by as much as 34 D (Bito et al., 1982). As the animal ages, however, it gradually loses its accommodative capability in a process termed *presbyopia*, and monkeys older than 25 years can accommodate only by an average of 5 D (Bito et al., 1982). A similar and dramatic age-related reduction has been reported in the chicken, as lenticular accommodation decreases from more than 20 D at hatching to less than 5 D at 1 year of age (Choh et al., 2002b). In humans, presbyopia causes a reduction of 0.32 D per year in the refractive power (Croft et al., 2013). Mechanisms proposed for presbyopia include reduction in ciliary muscle contractility, changes in the refractive index of the lens, age-related changes in the relative position of the lens and ciliary body, and loss of the lens capsule and lens fiber elasticity (Charman, 2008; Glasser, 2011; Reilly, 2014).

As with most other aspects of vision research, the mammalian species in which accommodative capabilities have been studied most extensively is the cat. The elasticity of the feline lens capsule is only 5% of the elasticity in humans; thus, the cat is incapable of accommodating by changing its lens curvature (Fisher, 1971). Instead, *translation* (i.e., the anteroposterior movement of the entire lens) is responsible for accommodative changes in the feline eye (Glasser, 2003; Hughes, 1977; Ott, 2006; Sunderland & O'Neil, 1976). This movement is made possible by the relative abundance of meridional (i.e., longitudinal) fibers in the feline ciliary body muscle and by the relative scarcity of circular fibers, which predominate in primates (Ebersberger et al., 1993; Prince et al., 1960). Parasympathetic stimulation of the meridional muscle fibers in the cat results in anterior displacement of the lens by up to 0.6 mm (O'Neill & Brodkey, 1969), thus inducing anywhere between 2 and 4 D of accommodation (Ott, 2006). The dog's accommodative power is reportedly lower, only 1–3 D in range (Hughes, 1977; Miller & Murphy, 1995). Factoring these accommodative powers into the $D = 1/f$ formula reveals that though cats and dogs can focus on distant object (by disaccommodating), their depth of field for nearby objects is 50–25 cm (cats) and 100–33 cm (dogs). Closer objects are usually perceived using the sense of smell.

In other carnivore species, the same translation mechanism is used to achieve a significantly greater magnitude of accommodation. Anterior lens movement in the raccoon induces accommodation of up to 19 D, 6× more than in the dog (Rohen et al., 1989), while the mongoose accommodates up to 13.5 D (Ott, 2006). A similar wide range of accommodative capability also exists in other closely related species. For example, the gray squirrel does not accommodate (McBrien et al., 1993), whereas the California ground squirrel can accommodate up to 6 D (McCourt & Jacobs, 1984). It should be noted that in mammals, translation of the accommodating lens results from ciliary muscle contraction, but in teleost fish, it is affected by a specialized smooth muscle, the *retractor lentis*, which pulls the lens backward to focus on distant objects (Khorramshahi et al., 2008). Snakes also accommodate by moving their lens. However, as snakes lack a ciliary muscle, accommodation is accomplished by contraction of the iris, which causes an increase in vitreous pressure that pushes the lens anteriorly (Fontenot, 2008). And in cetaceans, anterior lens displacement is due to increased intraocular pressure mediated by contraction of the retractor bulbi muscle (Mass & Supin, 2007).

Rodents (Artal et al., 1998) and ruminants (Piggins & Phillips, 1996) are generally described as lacking accommodative capabilities. In the former, this lack of accommodation is explained by the absence of a well-defined ciliary muscle (Samuelson, 1996), though the small pupil size and short axial length in species such as the rat and mouse provide these animals with a significant depth of focus (Geng et al., 2011). Lack of accommodation in ruminants, some of which possess a more developed ciliary muscle (Samuelson, 1996; Samuelson & Lewis, 1995), is more difficult to explain, and may be a consequence of the cytoarchitecture of the lens fibers (Kuszak et al., 2006). Other ungulates also have a very limited accommodative capability. Horses, for example, can accommodate only ±1 D (Miller & Murphy, 2017; Sivak & Allen, 1975).

Another species in which accommodation has been studied extensively is the chicken, which employs several accommodative mechanisms, enabled by the presence of three ciliary muscles: anterior (*Crampton's muscle*), intermediary (*Müller's muscle*), and posterior (*Brücke's muscle*) (Tedesco et al., 2005). Lenticular accommodation in the chicken is mediated by the intermediary and posterior ciliary muscles, which (as in mammals) are parasympathetically innervated by postganglionic ciliary nerves. However, several unique anatomic adaptations combine to significantly increase the lenticular accommodative capability of the chicken compared to that of mammals (Fig. 4.8). These include very large ciliary processes, as well as a ring of columnar epithelial cells at the equatorial periphery of the lens (i.e., the annular pad), which increases the diameter of the lens and its contact area with the processes. Lenses are soft and malleable, and the corneoscleral sulcus, which exists as a consequence of the scleral ossicles, permits a greater range of movement (Choh et al., 2002a). Together, these structures make it possible for contraction of the intermediary and posterior ciliary muscles to directly squeeze the lens, as compared to the indirect effect of the mammalian ciliary muscle, which is transmitted to the lens through the zonules. Contraction of the peripheral iris (Ostrin et al., 2011), as well as the posterior and intermediary ciliary muscles (West et al., 1991), induces thickening of the lens by 0.2 mm, steepening of its curvature, and a bulging of the lens into both the anterior and vitreous chambers (Choh et al., 2002a). The cumulative results of all these mechanisms is 15–19 D of lenticular accommodation (Choh et al., 2002a).

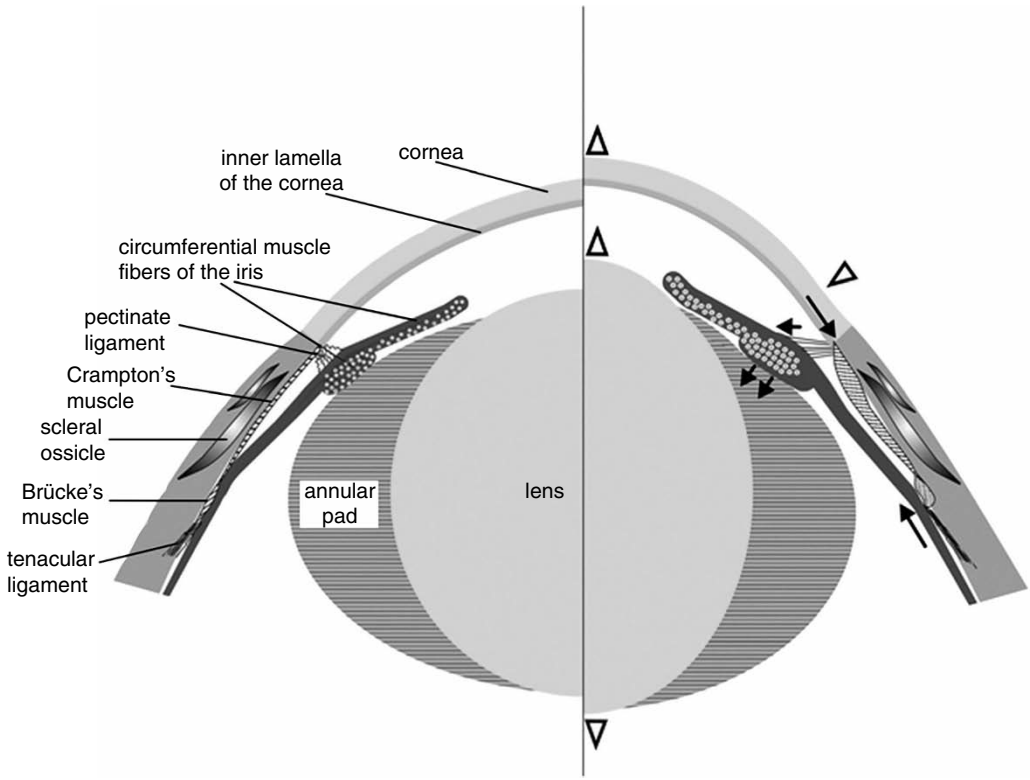

Figure 4.8 A generalized scheme of the mechanism of accommodation in birds. Left side: Relaxed state. Note the deep corneoscleral sulcus, the presence of Brucke's and Crampton's muscle (Müller's muscle not shown), the annular pad, and the lack of zonules, which allows direct contact between the ciliary processes and annular pad. All of these features contribute to the great accommodative power of the chicken eye (see text for details). Right side: An accommodated state. The black arrows show the direction of the contracting muscle forces. The open arrowheads show the resulting deformation of both the cornea and the lens. Similar mechanisms have also been found in lizards, snakes, and turtles. (Reproduced with permission from Ott, M. (2006) Visual accommodation in vertebrates: Mechanisms, physiological response and stimuli. *Journal of Comparative Physiology A*, **192**(2), 97–11.)

Unlike mammals, chickens (and possibly lizards) also accommodate by changing the corneal curvature. Corneal accommodation is mediated by the anterior ciliary muscle. Contraction of Crampton's muscle, which originates in the sclera and inserts in the cornea, flattens the peripheral cornea and increases the curvature of the central cornea (see Fig. 4.8; Chu et al., 2014; Murphy et al., 1995). Corneal accommodation is reported to play an important role in chicken accommodation, contributing 8–9 D (Glasser et al., 1994; Schaeffel & Howland, 1987). Thus, the reported combined (corneal and lenticular) accommodative power of the eye in young chicks is 25 D (Ostrin et al., 2011), compared with a maximal power of 15 D in children (Glasser, 2011). It should be noted that the chicken, as well as other avian (Schaeffel & Wagner, 1992) and reptile (Schmid et al., 1992) species, can accommodate independently in both eyes, potentially resulting in *anisometropia* (i.e., unequal degree of refraction in the two eyes) of up to 6 D. Similar corneal and lenticular mechanisms of accommodation exist in lizards (Ott, 2006).

Finally, in chickens even the choroid plays a role in focusing light on the retina. By changing its choroidal thickness, the chicken changes the distance between the retina and the cornea. The result is that in addition to bringing the focal point of incoming light onto the retina (by lenticular and/or corneal accommodation), chickens can also use "choroidal accommodation" to bring the retina into the focal point of the light (a twist on the proverb "If the mountain will not come to Mohammed, Mohammed will go to the mountain"). Once again, the choroidal "accommodation" is mediated by parasympathetic and sympathetic innervation. Transient thickening of the choroid in response to a blurred image is accomplished by changing either the volume of fluid (blood and aqueous humor) flowing through the choroid, or the tone of the choroidal smooth muscle (Nickla & Wallman, 2010). Long-lasting thickening is due to choroidal and scleral remodeling.

Additional Refraction in the Pupil and Elsewhere

The pupillary aperture is not considered to be a classic refractive structure as it has no refractive index, but it does make an important contribution to the resolving power of the eye. As the pupil dilates in dim light, the number of photons entering the eye increases, resulting in increased retinal illumination.

But there is "a price to be paid" for this increased illumination, as mydriasis also decreases the depth of focus of the eye. This means that as the pupil dilates, the range of distances at which objects remain in focus decreases. For example, in an eye that is focused at a distance of 1 m, objects at a distance of between 0.56 and 5.00 m will be in focus when pupil diameter is 1 mm; the range decreases to between 0.78 and 1.40 m when the pupil dilates to 4 mm (Duke-Elder, 1970). This is especially critical in species that have limited accommodative capability, such as the dog. Furthermore, as the pupil dilates, the relative significance of spherical and chromatic aberrations inherent in the eye increases (see the section on "Spherical and Chromatic Aberrations"), thereby reducing its resolving power. Therefore, the pupillary light reflex is, in effect, a constant balancing of two conflicting requirements for vision: maximal retinal illumination and visual resolution. In a scotopic environment, the pupil dilates to improve retinal illumination at the cost of decreased nighttime resolution (which is further attenuated by cone inactivity). In a photopic environment, pupillary constriction improves visual resolution (which is further enhanced by cone activity). As a rule of thumb, constricting the pupil by half increases visual resolution by a factor of two (Duke-Elder, 1970). The "cost" of miosis in a photopic environment is negligible, as there is sufficient retinal illumination under these conditions. This balancing of retinal illumination and visual resolution is especially dramatic in deep-diving animals, which move rapidly from one environment to another. In the Northern elephant seal (*Mirounga angustirostris*), it has been demonstrated that the pupil constricts from a giant area of 422 mm^2 in dark-adapted conditions (approximately 23 mm in diameter) to a pinhole opening of 0.9 mm^2 in light-adapted conditions; that is, the range of variation is almost 470 times (Levenson & Schusterman, 1997)!

It should be noted that light is also refracted *during* its passage through ocular structures such as the cornea and lens, not just at their interface with other structures. This refraction results from changes in refractive indices in various layers of these structures. Some of these refractive gradients are probably too small to affect the overall optical performance of the eye, however. For example, refractive indices in the various corneal layers range from 1.401 to 1.373 D in humans (Patel et al., 1995), whereas the rat retina has a refractive range of 1.369 to 1.385 D (Chen, 1993). But in other cases, regional differences are significant and must be taken into account; for example, in the goldfish eye, the refractive indices of the lens cortex and nucleus are 1.35 and 1.57 D, respectively (Axelrod et al., 1988).

Abnormal Refractive States and Optical Errors

Emmetropia and Ametropia

The "purpose" the refractive and the accommodative processes described in the previous sections is to focus an image on the outer segments of the photoreceptors. An *emmetropic* eye is one in which parallel light rays (from a distant object) are focused on the outer segments when the eye is disaccommodated. A nonemmetropic, or *ametropic*, eye is one in which the focused image (from a distant object) falls anterior to the retina (i.e., nearsighted or *myopic* eye) or posterior to it (i.e., farsighted, *hyperopic* or *hypermetropic* eye; Fig. 4.9).

Retinoscopy is the most commonly used method to determine the refractive state of the eye. It is based on two assumptions: first, that light emerging from the eye (i.e., emergent rays) follows the same optical path as light entering the eye; and second, that the fundus reflex originates at the level of the outer segments. If those two assumptions hold, then emergent rays exit an emmetropic eye as parallel rays, a hypermetropic eye as diverging rays, and a myopic eye as converging rays (Davidson, 1997). Therefore, the location of the focal point formed by the emergent rays can be used to determine the refractive state of the eye.

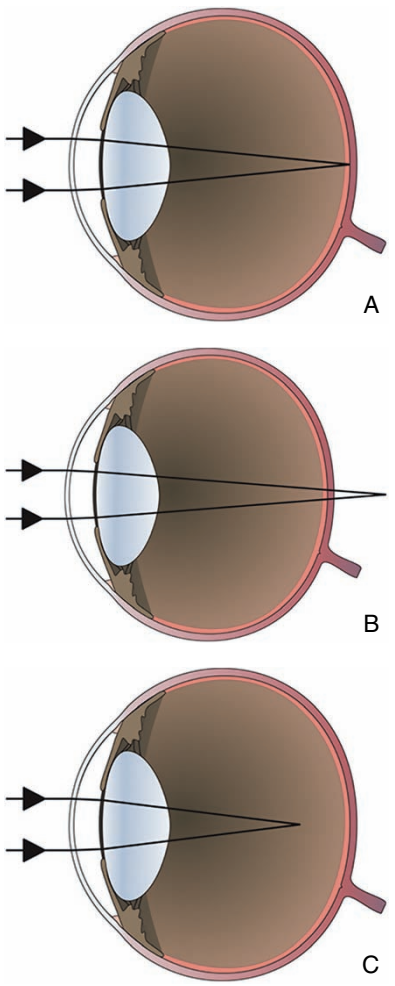

Figure 4.9 **A.** In emmetropia, parallel light rays are focused on the retina. **B.** In a farsighted (hypermetropic or hyperopic) eye, light rays are focused behind the retina. **C.** In a nearsighted (myopic) eye, the light is focused in front of the retina.

However, it should be noted that the second assumption is not completely accurate. The fundus reflex does not originate at the outer segments but closer to the observer, most likely at the level of the inner limiting membrane (Glickstein & Millodot, 1970). Thus, there is a gap (equal to the thickness of the retina) between the point at which the reflected light is actually measured and the point at which it should be measured. This gap, termed the *artifact of retinoscopy*, results in shifting refraction values in the direction of hypermetropia and needs to be corrected using an established formula (Glickstein & Millodot, 1970). This error is relatively minor (+0.25 D) in young humans (Millodot & O'Leary, 1978) and monkeys (+1.4 D; Hung et al., 2012), but it becomes significant in small eyes, reaching values as high as +7 D in tree shrews (Norton et al., 2003). On the other hand, other researchers claim that the fundus reflex originates at the outer limiting membrane, and that the artifact's significance has been overestimated (Mutti et al., 1997).

Table 4.5 lists refractive errors in selected species. Most of these values have been determined using *streak retinoscopy*, though *autorefractors* have also been used in veterinary medicine (Groth et al., 2013; Hernandez et al., 2016; Wang et al., 2016). As can be seen, few species are truly emmetropic, though once the values are corrected for eye size, most mammals are within ±1 D of emmetropia (Hughes, 1977). A large survey found that on average, dogs are indeed emmetropic, with a mean refractive error of −0.05 D (Kubai et al., 2008). Nine dog breeds – English Springer Spaniel, German Shepherd, Golden Retriever, Siberian Husky, Shetland Sheepdog, Labrador Retriever, Border Collie, Samoyed, and "other" terriers – were found to be emmetropic (defined as having a mean refractive error < 0.5 D in either direction). Yet the same study found that 8% of all dogs were hypermetropic, with a refractive error of up to +3.25 D. Three breeds (Australian Shepherd, Alaskan Malamute, and Bouvier des Flandres) were found to have a

Table 4.5 Refractive errors in selected animal species[a]

Species	Refractive Value (D)	References
Cat by habitat		Belkin et al. (1977)
Street cat	−0.8	
Laboratory cats	1.4	
Cat by age		Konrade et al. (2012)
Kitten (≤ 4 months)	−2.45	
Adult (> 1 year)	−0.39	
Cat by coat length		Konrade et al. (2012)
DSH	−1.02	
DLH	−0.13	
Dog – mean value	−0.05 to (−0.39)	Gaiddon et al. (1996); Groth et al. (2013); Kubai et al. (2008); Murphy et al. (1992b)
Dog by habitat		Gaiddon et al. (1996)
Indoor dogs	−0.64	
Outdoor dogs	0.17	
Dog by breed	–1.87 to (+0.98)	For specific breeds see Black et al. (2008); Kubai et al. (2008, 2013); Mutti et al. (1999); Williams et al. (2011)
Horse	–0.17 to (+0.33)	Bracun et al. (2014); Harman et al. (1999); Rull-Cotrina et al. (2013)
Horizontal meridian	−0.06 to (+0.41)	Grinninger et al. (2010); McMullen et al. (2014)
Vertical meridian	0.25 to 0.34	McMullen et al. (2014)
Rabbit (New Zealand White)	1.7	Herse (2005)
Chicken (Cornell-K)	4.1, 3.7 (4 & 17 weeks old, respectively)	Wahl et al. (2015)
Guinea pig (pigmented)	0.7	Howlett & McFadden (2007)
Rat (Norway brown)	4.7, 14.2 (infant & adult, respectively)	Guggenheim et al. (2004)
Mouse (CBL75/6)	–1.5, 4.0 (10 & 102 days old, respectively)	Zhou et al. (2008)

[a] See reference list for additional refractive studies in wildlife and aquatic species.
DSH, Domestic Shorthair; DLH, Domestic Longhair.

mean refractive error that was hypermetropic. Conversely, 25% of all surveyed dogs were myopic, with a refractive error of up to −6.25 D, and four breeds (Rottweiler, Collie, Miniature Schnauzer, and Toy Poodle) had a mean refractive error that was myopic. Even breeds that were on average emmetropic had population clusters and litters that were myopic. This was especially notable in the Labrador Retriever, in which up to 31% of dogs are reportedly myopic, reinforcing the hypothesis that myopia in this breed may be inherited (Black et al., 2008). Myopia in the Labrador Retriever is caused by elongation of the vitreous chamber (Mutti et al., 1999; see Fig. 4.6), while in other breeds, including the Toy Poodle, Collie, and English Springer Spaniel, myopia is due to the presence of a steeper, more powerful lens (Kubai et al., 2013; Williams et al., 2011). The pathogenesis of myopia in the Labrador Retriever, and its mode of inheritance, could make this breed a naturally occurring large animal model for the study of myopia in humans, where vitreous elongation (see Fig. 4.6) and inheritance play a significant role (Black et al., 2008; Mutti et al., 1999).

A study in cats reported that kittens (≤ 4 months) are myopic, with a mean error of −2.45 D, while adult cats are close to emmetropia, with a mean error of −0.39 D, thus demonstrating a significant effect of age (Konrade et al., 2012). It is interesting to note that myopia decreases with age in cats, but in horses and in some dog breeds, notably the English Springer Spaniel and Beagle, it increases with age (Grinninger et al., 2010; Hernandez et al., 2016; Kubai et al., 2008; Maehara et al., 2011). Once again, there was an overall significant positive correlation between feline refractive error and axial globe length, though the correlation was insignificant when only kittens and juvenile cats were examined. Coat length was another significant factor, with domestic shorthair cats more likely to be myopic, and domestic longhair cats more likely to be emmetropic (Konrade et al., 2012). Another study found a significant effect of habitat on the feline refractive error, with hypermetropia (+1.4 D) or myopia (−0.8 D) depending on whether the cats live outdoors or indoors, respectively (Belkin et al., 1977). This is consistent with findings in humans, demonstrating the correlation between time spent outdoors and prevention of myopia (French et al., 2013).

Several large studies have shown horses to be overall emmetropic (Bracun et al., 2014; Grinninger et al., 2010; Rull-Cotrina et al., 2013). However, only 48–68% of horses are emmetropic in both eyes, with hyperopia and myopia reported in equal proportions in the ametropic horses, with errors of up to ±3 D (Bracun et al., 2014; Farrall & Handscombe, 1990; Grinninger et al., 2010). Age and breed may affect the refractive error in horses (Bracun et al., 2014; Rull-Cotrina et al., 2013). Age, habitat, and working environment have also been shown to be significant factors in other species (Belkin et al., 1977; Murphy et al., 1992b; Ofri et al., 2001, 2004). However, because of low accommodative capacity in most veterinary patients, cycloplegia has no significant effect on refraction in patients, including dogs and horses (Groth et al., 2013; McMullen et al., 2014).

A large range of retinoscopy values is reported in species with small eyes. For example, values range from +20 to −13 D in the rat (Guggenheim et al., 2004; Hughes, 1977) and from -0.7 to +13.7 D in C57BL/6J mice (Pardue et al., 2013). Such a range of results may be due to failure to correct for the artifact of retinoscopy, or because of the significant spherical aberrations (see later section) caused by the very high power of the cornea in small eyes, as shown in Table 4.3. It is recommended that retinoscopy in such small eyes be conducted using an artificial pupil, to occlude the corneal periphery.

Ametropia has also been induced in a number of experimental animals, including chickens, fish, and various mammalian species (Schaeffel & Feldkaemper, 2015). Ametropia is usually induced by visual deprivation in young animals, before the eye has completed its development. Initially, eyelid suturing was used to cause visual deprivation, though this has been replaced by exposure to various regimens of ambient light, and the use of pharmacologic agents or refractive contact lenses to degrade the quality of the retinal image. Visual deprivation leads to progressive axial elongation of the vitreous body and the eye, thereby inducing myopia (see Fig. 4.6; Norton, 2016). Additional anatomic changes in the eye induced by visual deprivation include a shallow anterior chamber, thinner lens, and changes in corneal curvature (Choh & Sivak, 2005; Ostrin et al., 2014). On the other hand, removing the lens during the same period retards axial elongation (Lambert, 2016). The aims of these experiments are to develop animal models for the study of the pathogenesis of myopia in humans, to identify molecular and cellular mechanisms controlling emmetropization, and to evaluate new therapeutic approaches (Schaeffel & Feldkaemper, 2015). Identification of genes associated with, or causing, myopia (Guggenheim et al., 2017; Li et al., 2017a) may represent a breakthrough in the prevention and treatment of what is considered to be one of the most prevalent ophthalmic disorders in humans (Morgan et al., 2018).

Aphakic Eyes and Intraocular Lenses

Because of the significant refractive role of the lens, cataract surgery (or any surgical lens extraction) resulting in aphakia leaves the eye severely hypermetropic. The aphakic eye lacks the refractive contribution of the lens; therefore, light is not sufficiently refracted, resulting in image formation "behind" the retina (Pollet, 1982). Since the early 1980s, veterinary ophthalmologists have sought to alleviate this problem by implanting IOLs in dogs' eyes following cataract extraction. The purpose of these implants is to compensate for loss of refraction by the lens, thereby returning the eye to an emmetropic state. Early attempts using 14.5–29.0 D IOLs left the implanted canine eyes hypermetropic (Peiffer & Gaiddon, 1991). Following the results of studies involving large numbers of

dogs of various breeds, it has been determined that the canine IOL should have a power of 40.0–41.5 D (Davidson et al., 1993; Gaiddon et al., 1991, 1996). The 1.5 D range of recommended values probably results from breed differences (Kubai et al., 2008). Indeed, use of 41 D IOLs in 60 dogs resulted in an average refractive error of ≤ 1.2 D (Gift et al., 2009). However, it is important to note that though 41 D IOLs are used to bring aphakic dogs to emmetropia, this does not mean that aphakic dogs suffer from hypermetropia of 41 D. Indeed, the hypermetropia in aphakic dogs has been shown to range from 14.4 to 15.2 D (Davidson et al., 1993; Gaiddon et al., 1991). The reason that a 41 D IOL is needed to correct 15 D of hypermetropia is that an IOL is placed in the capsular bag, surrounded by aqueous humor. This environment results in a reduction of its overall refractive power (due to the small difference in refractive indices between the aqueous humor and the IOL), and therefore this power has to be higher than the aphakia it is intended to resolve. If dogs were to be fitted with spectacles to correct aphakia, then indeed these spectacles would require 15 D lenses!

While canine IOLs are widely used by veterinary ophthalmologists, their development and use in other species is lagging behind. A study in horses concluded that an IOL of 25–30 D overcorrects the aphakic equine eye (McMullen et al., 2010), even though preliminary calculations showed a theoretical power of up to 30 D is required to restore emmetropia (McMullen & Gilger, 2006; Mouney et al., 2012). Subsequent studies, supported by a calculated IOL power of 15.4 D (Mouney et al., 2012), have shown that a 14 D IOL brought five out of six horse eyes to within 0.4 D of emmetropia (Townsend et al., 2012). A 14 D IOL also brought a foal to emmetropia (Harrington et al., 2013), even though calculations showed that adult horses and foals may require different power IOLs (Townsend et al., 2013). Calculated IOL powers for bald eagles and rabbits are 16.4–17.4 and 58 D, respectively (Kuhn et al., 2015; Sanchez et al., 2017).

Studies in the cat indicate that IOLs for this species should have a power of 52–53 D (Gilger et al., 1998). The difference between the canine and feline IOL values stems from differences in the anterior chamber depth of the dog and cat (Fig. 4.10). Though the globe axial length in both species is similar, the cat has a much deeper anterior chamber, which means that the lens (and IOL) is located more posteriorly in the cat. As a result, the distance between the lens and retina in the cat is shorter, and a stronger lens is required to focus the light in the course of such a short optical path. Conversely, humans, who also have a similar size globe, have a much shallower anterior chamber and a more anteriorly located lens. This results in a longer optical path to the retina, and therefore most human IOLs have a power of only 19–22 D. Thus, it is not surprising that a study of pseudophakic dogs found a correlation between the postoperative refractive error and the distance of the IOL from the retina (Gift et al., 2009). Similarly, in Icelandic horses with multiple congenital ocular anomalies, a deeper anterior chamber is associated with myopia in older horses (Johansson et al., 2017).

Besides developing IOLs for additional species, veterinary ophthalmologists could also improve the postoperative refraction of their pseudophakic patients through preoperative calculation of the required IOL power. Such calculations rely on keratometry and intraocular dimension measurements and use established formulas to determine the IOL power (Kuhn et al., 2015; McMullen & Gilger, 2006; Mouney

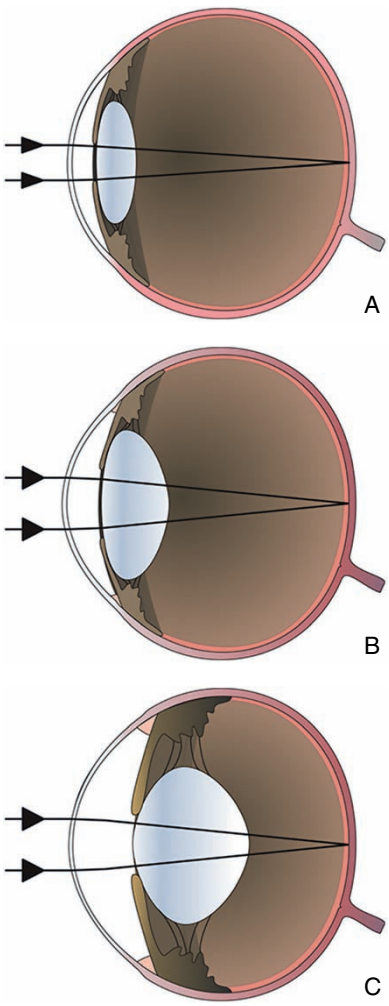

Figure 4.10 The effect of anterior chamber depth on lens curvature in a human (**A**), dog (**B**), and cat (**C**). Though the axial length in the three species is similar, they differ significantly in the depth of their anterior chambers. Humans have the shallowest anterior chamber, and consequently the location of the human lens is relatively anterior. Cats have the deepest anterior chamber, and consequently the location of the feline lens is relatively posterior. As a result, light exiting the lens has a relatively long path before it reaches the retina in a human, and a relatively short path before it reaches the retina in a cat. Therefore, the feline lens needs to have significantly greater power than the human lens, and this is made possible by its greater curvature. The dog has intermediate values in anterior chamber depth, lens location, and lens curvature.

et al., 2012; Sanchez et al., 2017; Townsend et al., 2013). This approach can be especially beneficial in dogs who suffer from vitreous chamber elongation and who may remain ametropic if implanted with a "one size fits all" 41 D IOL. Ideally, such measurements will become part of the routine preoperative evaluation, and every cataractous animal patient will be fitted with an appropriate IOL that will bring its eye to an emmetropic state. Recently introduced Fo-X IOLs with extended depth of focus of ± 1.5 D represent another approach to establishing postoperative emmetropia, but these have yet to be evaluated in clinical studies.

Though veterinary ophthalmologists have made significant progress in restoring emmetropia to pseudophakic patients, little attention has been paid to correcting ametropia in phakic patients. As noted, more than 25% of the canine population has been shown to be significantly myopic (Kubai et al., 2008), and could potentially benefit from such correction through the use of contact lenses or surgery. Indeed, it has been demonstrated that even 1.5–2 D of myopia causes significant deterioration in the visual performance of Labrador Retrievers (Ofri et al., 2012) and in the pattern visual evoked potentials of Beagles (Ito et al., 2016). Various surgical techniques, mostly involving the use of lasers to ablate the cornea, are employed to correct ametropia and astigmatism in humans, and preliminary work shows that some of these techniques are applicable in the dog (Rosolen et al., 1995) and cat (Bühren et al., 2010). Alternatively, lasers have also been used to change the refractive index of the feline cornea (Savage et al., 2014). Interestingly, Wang et al. (2016) have also shown improvement in canine refractive error following 6 months of nutritional antioxidant supplementation.

Astigmatism

Astigmatism is a state of unequal refraction of light along the different meridians of the eye. Normally, a given refractive structure of the eye (e.g., the cornea or lens) has a constant curvature radius in all its meridians (though the cornea may flatten toward the limbus). Astigmatism occurs when the horizontal and vertical meridians of the cornea or lens have different curvature radii. Because of these differing curvatures, light entering the eye through the vertical meridian may be refracted more (i.e., *direct*, or *with-the-rule*, *astigmatism*) or less (i.e., *indirect*, or *against-the-rule*, *astigmatism*) than light entering through the horizontal meridian. There are also cases of *irregular astigmatism* in which the principal meridians are not perpendicular to each other, as in keratoconus, or because of injury. Therefore, light entering along one meridian will be focused on the retina and result in high-resolution vision, whereas light from the other meridian will be unfocused, leading to blurred vision (Fig. 4.11). Such an aberration is corrected with a cylindrical lens rather than with a spherical lens that is used to correct simple ametropia.

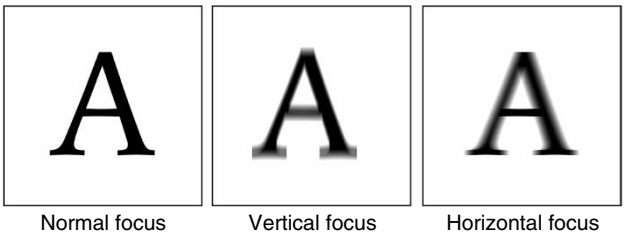

Figure 4.11 A normal eye can see focused horizontal and vertical lines (left). An astigmatic eye will see a focused line in one orientation and a blurred line along the perpendicular axis. **Vertical focus**: The horizontal lines are blurred (center). **Horizontal focus**: The vertical lines are blurred (right).

Astigmatism is diagnosed by refracting the eye in both the horizontal and vertical meridians. A difference of 0.5 D or more in the refractive power of the horizontal and vertical meridians in the same eye is defined as astigmatism. Alternatively, astigmatism can be diagnosed using a keratometer to measure the curvature of the steepest and flattest meridians of the cornea, or by use of a *corneal topographer*, which provides a map based on a large number of photographic sections of the cornea and calibrated into dioptric power (Savini et al., 2017). In humans, most cases of astigmatism result from abnormalities of the anterior surface of the cornea. Only a minority of cases result from lenticular or posterior corneal surface abnormalities (Duke-Elder, 1970). Direct astigmatism accounts for 90% of cases in young eyes, but the proportion of indirect astigmatism increases with age (Nemeth et al., 2013; Xiao et al., 2014). In humans, the prevalence of low-grade astigmatism may be as high as 63% in some populations, but the prevalence of astigmatism > 1.5 D is usually under 5% (Read et al., 2007). The prevalence of significant (> 0.5 D) astigmatism in dogs seems to be equally low, reportedly affecting 1% of all dogs; a higher prevalence of 3.3% was documented in German Shepherds (Kubai et al., 2008). On the other hand, other species are "naturally astigmatic" because of their corneal topography. In the horse, for example, the mean corneal curvature along the horizontal and vertical meridians is 21.6 D and 22.9 D, respectively. Consequently, the horse has a mean degree of 1.3 D direct astigmatism (Grinninger et al., 2010). For the same anatomic reason, 1.75–2.36 D of astigmatism is reported in pig eyes (Sanchez et al., 2011) and 0.4–0.6 D in rabbits (Wang et al., 2014). A high prevalence of astigmatism was also demonstrated in gazelles (Ofri et al., 2004) and elephants (Murphy et al. 1992a). In cows, sheep, and pigs, the lens sutures have been identified as the source of astigmatism and other aberrations (Gargallo et al., 2013).

Some pathologic processes may induce astigmatism. Corneal disease resulting in edema or scarring will inevitably lead to an uneven corneal surface, resulting in irregular astigmatism. Focal cataracts will cause refractive astigmatism

because of variations in refractivity among different lenticular zones (Duke-Elder, 1970). In addition, cataract surgery (Eslami & Mirmohammadsadeghi, 2015), penetrating keratoplasty (Fadlallah et al., 2015), and other procedures that involve incising and suturing of the cornea often result in astigmatism because of imperfect alignment of wound edges; however, such surgically induced astigmatism frequently resolves over time. In dogs undergoing cataract extraction, surgically induced astigmatism was significantly different between right and left eyes, with values of 2.01 and 3.05 D for dorsotemporal and dorsonasal incisions, respectively (Pederson et al., 2019).

Static Accommodation

Several avian (Hodos & Erichsen, 1990), amphibian (Scheaffel et al., 1994), and reptilian (Henze et al., 2004) species possess *lower-field myopia*. The eyes of these animals are emmetropic along the horizontal and in the upper visual field, but they become progressively myopic below the horizontal (Fig. 4.12). In other words, different parts of the eye have a different refractive power because the shape of the eye is more like a flattened circle, so that the posterior focal length differs for different meridians. This adaptation can be regarded as a *static accommodation* mechanism (Ott, 2006). Rather than changing the refractive power of its lens to focus on an object (in dynamic accommodation), the animal shifts its gaze to see the object with the appropriate refractive power. Consequently, the animal can match the average viewing distances of different areas of the visual field (Schaeffel et al., 1994). This allows the animal to keep the ground in focus with relaxed accommodation while foraging for food and, at the same time, monitor the sky for predators while focused at infinity (Hodos & Erichsen, 1990). This may be why predators such as raptors do not possess this adaptation (Murphy et al., 1995). The same principle is also found in the eyes of pinnipeds (Hanke et al., 2006; Mass & Supin, 2007; Miller et al., 2010). Regional changes in the refractive powers of different parts of the cornea allow these animals to maintain high-resolution vision in both water and air (see the section on "Emmetropia and Accommodation Under Water"). Therefore, static accommodation may be an evolutionary mechanism helping animals to improve their spatial resolution capabilities in different environments (Shilo, 1977).

The horse was also believed to possess a similar, static "accommodating" mechanism, resulting from its nonsymmetric eye shape. According to the *ramp retina theory*, the superior retina was believed to be farther from the lens than the inferior retina (Farrall & Handscombe, 1999; Harman et al., 1999; Sivak & Allen, 1975). Therefore, it was argued that the horse raises its head to focus distant objects on the ventral retina and lowers it to focus nearby objects on the dorsal retina. An analogy to this would be a person with bifocal glasses trying to peer through one lens or the other to view objects at different distances, though in this case the person is aided by the different refractive powers

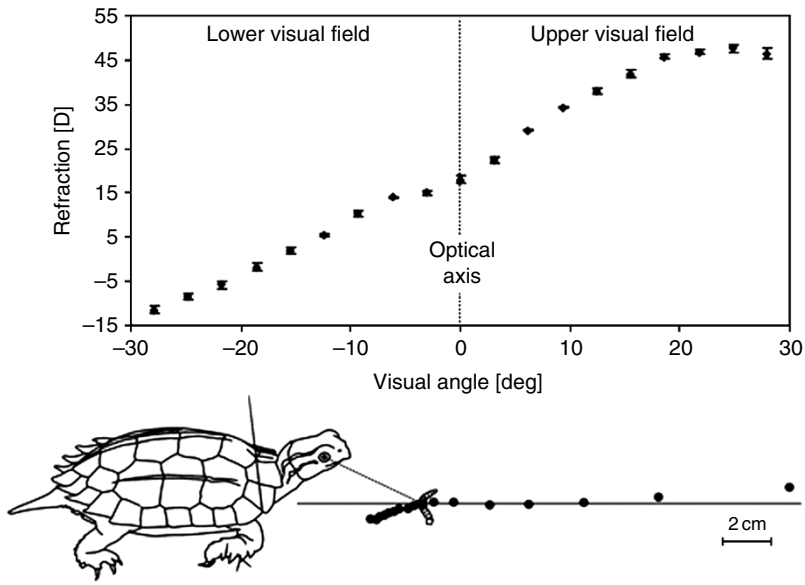

Figure 4.12 Lower-field myopia in the terrestrial turtle *Geoemyda* as an example of static accommodation. Top panel: The refractive state of the unaccommodated eye changes steadily from hyperopic values in the upper visual field to myopic values in the lower visual field. Black dots represent the focal points at various visual angles apart from the optical axis for this state of focus. Lower panel: Because the refractive power changes with the visual angle, the animal can keep the whole ground in focus, and by changing the angle of its gaze focus on its prey no matter how distant it is. (Reprinted with permission from Ott, M. (2006) Visual accommodation in vertebrates: Mechanisms, physiological response and stimuli. *Journal of Comparative Physiology A*, **192**(2), 97–111.)

of the lenses rather than by the varying axial lengths of different meridians. Anatomic measurements have now discredited this theory, and the horse is believed to possess an active (though limited) accommodation mechanism of ±1 D (Harman et al., 1999; Miller & Murphy, 2017; Sivak & Allen, 1975). The head movement previously associated with this behavioral "focusing" is now believed to occur when the horse is interchanging monocular and binocular visual fields (Harman et al., 1999). However, a "ramp retina" has been demonstrated in guinea pigs, with the ventral retina further from the lens center than the dorsal retina as a result of differing globe axial lengths and vitreous chamber depths in different quadrants (Zeng et al., 2013). Consequently, the guinea pig's inferior visual field is –6 D more myopic than the superior field. As in the case of lower-field myopia of nonmammalian species, it is proposed that this adaptation evolved to allow the ground plane to be well focused while maintaining clear vision on the horizon, presumably important to a small creature that needs to detect both food and predators.

Spherical and Chromatic Aberrations

Spherical Aberrations

The eye is not a perfect optical system. Indeed, Duke-Elder (1970) quotes Hermann von Helmholtz, the 19th-century German physicist who invented the ophthalmoscope, as saying that "if an optician should try to sell me an instrument possessing such faults, I would feel justified in using the most severe language with regard to the carelessness of his work and return the instrument under protest." Two of the most significant optical problems that affect the eye are spherical and chromatic aberrations. *Sperical aberrations* occur because in both the cornea and the lens, rays passing through the periphery are refracted more than rays passing through the center. Therefore, rays passing through the periphery are focused closer to the cornea (or lens) than rays passing through its center (Fig. 4.13). Obviously, as the image is not uniformly focused on the retina, the aberration causes blurred vision. In other words, the focusing of rays depicted in Fig. 4.5 and Fig. 4.7 is an "ideal" refraction that in reality does not take place in the eye. The difference between the focal points of the peripheral and central rays, the spherical aberration, is measured in diopters. A comparative study found significant degrees of spherical aberration in the lenses of dogs, cats, and rats, but minimal lenticular aberrations in cows, sheep, and pigs (Sivak & Kreuzer, 1983).

Both the cornea and the lens possess anatomic adaptations that are intended to minimize the extent of their inherent spherical aberrations. In the lens, the higher refractive index of the lenticular nucleus increases the refractive power of the central lens. This results in moving its focal point closer to the lens, nearer to the focal point of the peripheral lens (Fig. 4.14). A gradient variation in the refractive index of the lens would result in the formation of a multifocal lens, with a higher refractive index in the nucleus and a lower refractive index toward the equator, leading to further attenuation of the spherical aberration. Corneal spherical aberrations are minimized because the peripheral cornea is flatter than

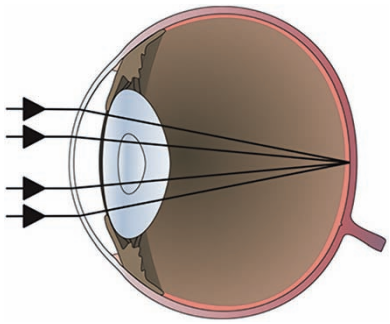

Figure 4.14 Multifocal lenses reduce the amount of spherical aberrations. A higher refractive index of the lens nucleus causes increased refraction of the central light rays (compared to the refraction of the central rays in Fig. 4.13A). Consequently, the focal point of the central rays is shifted closer to the lens and closer to the focal point of the peripheral rays, thus eliminating the spherical aberrations seen in Fig. 4.13A.

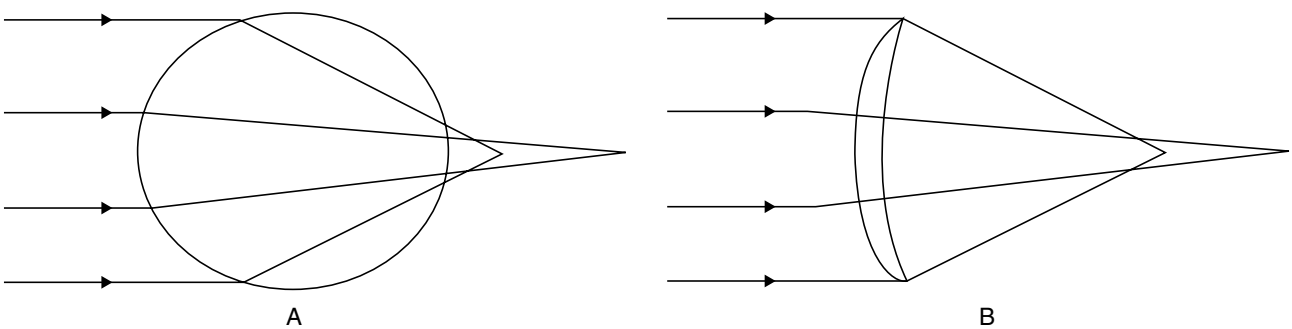

Figure 4.13 Spherical aberrations occur when light passes through the lens (**A**) and cornea (**B**). In both cases, peripheral rays are refracted (bent) more than central rays. Therefore, the focal point of the peripheral rays is closer to the lens/cornea, while the focal point of the central rays is closer to the retina. The result is a blurred image. The distance between the two focal points is called spherical aberration and is measured in diopters (D).

the central (apical) cornea. This decreases the refractive power of the peripheral cornea and moves its focal point toward the retina and closer to that of the central cornea (Millodot & Sivak, 1979). Therefore, refractive surgeons attach great importance to centering the apical cornea so that the aberration-free zone is aligned with the pupil, thereby contributing to a high-quality retinal image (Bühren et al., 2010; Gobbe et al., 2015). A similar problem may arise in corneoscleral transposition in veterinary patients, as the flatter peripheral cornea is transposed into the steeper central cornea, potentially increasing spherical aberrations in the patient. For similar reasons, surgeons performing keratoplasty should strive to collect the donor's cornea from the same region as the intended grafting site. However, the possible effects of corneoscleral transpositions and keratoplasty on visual optics in animal patients have yet to be investigated.

Another structure that plays a critical role in reducing spherical aberrations is the pupil. Contraction of the pupil blocks rays of light that enter the eye through the most peripheral (and refractive) cornea. It also prevents light from passing through the peripheral lens. Thus, miosis allows only rays that pass through the central cornea and lens to reach the retina, thereby contributing to the formation of a well-focused image (Fig. 4.15A). A mydriatic pupil, on the other hand, allows more peripheral rays to enter the eye, and their passage through the peripheral cornea and lens increases the amount of spherical aberrations as well as all the other wavefront aberrations (Fig 4.15B). In humans, an 8 mm pupil induces 1 D of spherical aberrations (Millodot, 2018), which is the reason for the significant blurring of vision that is experienced after pupils have been pharmacologically dilated.

It is worth noting that nowadays the aberrations of the eye are analyzed by assessing the amount of deviation obtained between an output wavefront emanating from it and a theoretical ideal wavefront (Thibos et al., 2002). This stems from the fact that the eye is not a symmetric globe. These aberrations are reported as *Zernike polynomials*, of which there are more than 20 types, including astigmatism, spherical aberration, coma, trefoil, and quatrefoil. They are now routinely measured with various types of commercial *aberrometers*, and a common unit of measurement of all wavefront aberrations is the root mean square (RMS). In a large human survey, Wang and Koch (2003) found that the most significant aberration was spherical aberration, followed by coma.

Chromatic Aberrations

Chromatic aberrations result from the fact that the refractive index n (as in the equation $D = n/f$) is not constant, but rather is wavelength dependent. Once again, therefore, Fig. 4.5 and Fig. 4.7 are somewhat misleading because they portray the ideal situation pertaining to monochromatic light. However, when white light enters a prism (or a lens), each wavelength contained in that light is refracted by a different amount. The n of a given wavelength is inversely proportional to λ. Therefore, waves with a short wavelength (e.g., blue light) have a higher n than waves with a long wavelength (e.g., red light). Consequently, blue light will be more refracted than red light, and its focal point will be closer to the lens (Fig 4.16A). The distance between the focal points of the short and long wavelengths is the chromatic aberration, and once again this distance is measured in diopters. The implication is that when viewing red text on a blue background, for example, the overall image would be blurred, as the text and the background are focused on different planes in the eye. A study comparing chromatic aberrations in different species found that in most animals (including cats, cattle, sheep, pigs, rats, and fish) the amount of chromatic aberration (442–633 nm) of lenses amounts to a relatively constant 4.6% of equivalent focal length; an exception is the dog lens, with 5.7% chromatic aberrations (Kreuzer & Sivak, 1985).

As in the case of spherical aberrations, anatomic adaptations may contribute to a reduction in the effect of the chromatic aberrations. For example, fish have been shown to possess multifocal lenses consisting of concentric rings of differing refractive properties (Kröger, 2013). Thus, red light passing through one ring will be more refracted than blue

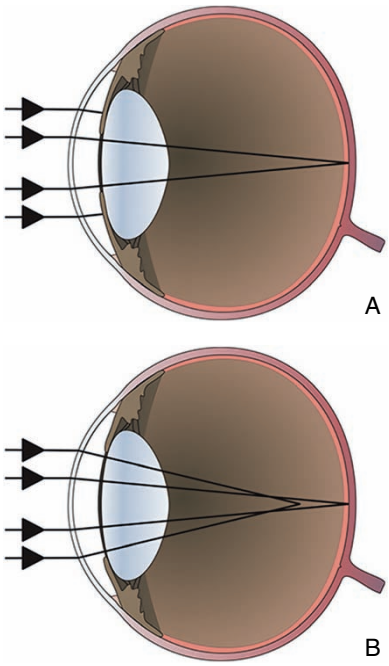

Figure 4.15 Pupillary diameter affects the magnitude of spherical aberrations. A miotic pupil (**A**) blocks the peripheral rays, thereby eliminating the spherical aberrations induced by the peripheral cornea and lens (seen in Fig. 4.13). Only central rays reach the retina, resulting in a focused image. A mydriatic pupil (**B**) admits peripheral rays into the eye, thereby increasing the amount of spherical aberrations. Panel **B** is the basis for the blurred vision experienced following pharmacologic dilation of the pupil.

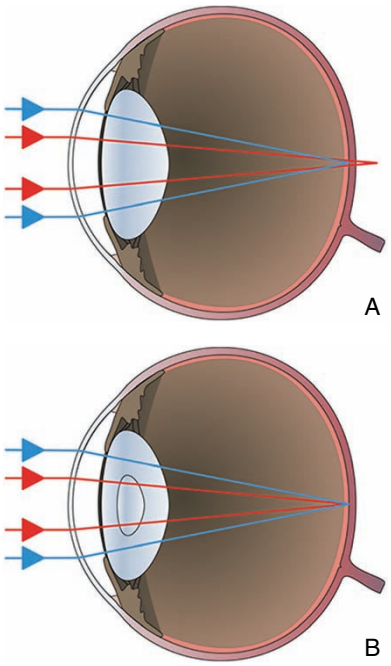

Figure 4.16 Chromatic aberrations in the lens. **A**. White light is composed of numerous wavelengths, each of which is characterized by a different refractive index (*n*). Light with a longer wavelength (e.g., red light) has a lower *n* than light with a shorter wavelength (e.g., blue light). Consequently, red light will be refracted to a lesser degree than blue light. If the blue light is focused on the retina, the red light converges behind the retina. The distance between the focal points of the short and long wavelengths is the chromatic aberration; this distance is measured in diopters. **B**. Multifocal lenses reduce the magnitude of chromatic aberrations. A higher refractive index of the lens nucleus causes increased refraction of the red light (compared to its reduced refraction in panel **A**). Consequently, the focal point of the red light is shifted closer to the lens and closer to the focal point of the blue light, thus eliminating the chromatic aberrations seen in panel **A**.

light passing through another ring, thereby compensating for the blue light's higher *n*. Consequently, the image formed on the retina will be chromatically focused (Fig. 4.16B).

It is interesting to note that in terrestrial species, multifocal lenses consisting of concentric refractive rings can be found in those species in which the miotic pupil is not round (Land, 2006; Malmström & Kröger, 2006). Such a lens has been demonstrated, for example, in the domestic cat. The vertical slit shape of the cat's miotic pupil allows light to pass through both the peripheral and central lens during constriction. Therefore, even during miosis, the cat continues to benefit from the advantage of a multifocal lens (Fig. 4.17). On the other hand, in the closely related tiger, a round pupil is associated with a monofocal lens, so that no optical properties of the lens are "lost" when the pupil constricts (Malmström & Kröger, 2006). Therefore, species with a multifocal lens have a steeper GRIN than species with a monofocal lens. In cats, for example, the refractive indices in the lens nucleus and subcapsular areas are 1.48 and 1.39, respectively; in humans, the respective figures are 1.41 and 1.38 (Pierscionek & Regini, 2012). In this context it is noteworthy that the harbor seal, which is a monochromat, has multifocal lenses; since multifocal lenses have evolved to compensate for chromatic aberrations in animals with color vision, the functional significance of such a lens in a monochromat is not understood (Hanke et al., 2008).

Additional evolutionary adaptations to decrease the detrimental effect of chromatic aberrations on visual resolution can be found in the anatomy of the retina. The human fovea, for example, contains red and green cones, but does not contain any blue cones (Chen et al., 2015). Therefore, red light, which is focused on the fovea, will be absorbed in this region. Blue light, which is not focused on the fovea, will not be absorbed, and therefore not be perceived, thus contributing to the high-resolution vision of the fovea (at the expense of

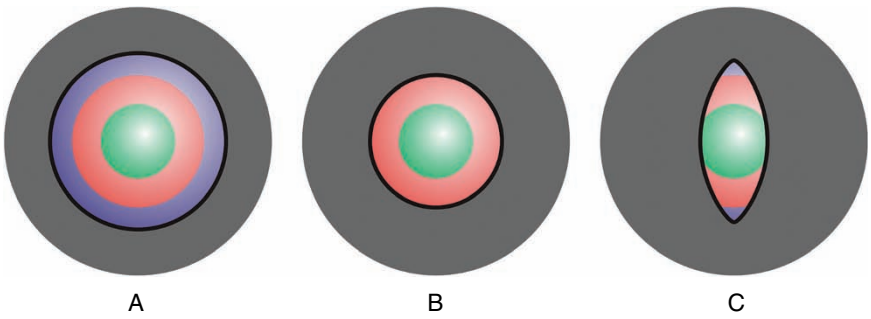

Figure 4.17 The functional significance of the slit pupil in combination with a multifocal lens. In the fully dilated state of the pupil (**A**), all zones of the lens (shown in the colors they are focusing) can be used. A concentrically constricting iris (**B**) would cover the outer zone of the lens, such that a spectral range (blue in this example) could not be focused on the retina. By contrast, all lens zones can be used if the pupil constricts to a slit (**C**). (Reprinted with permission from Malmström, T. & Kröger, R.H. (2006) Pupil shapes and lens optics in the eyes of terrestrial vertebrates. *Journal of Experimental Biology*, **209**, 18–25.)

foveal blue color perception). This is why the fovea has been called the *blue scotoma region* of the retina (Chen et al., 2015). The chromatic aberrations induced by blue light in the macular region are further reduced by the presence of yellow macular pigment, which is abundant in carotenoids, lutein, and zeaxanthin, with a peak absorption of about 460 nm, which absorbs unfocused short wavelengths (Bernstein et al., 2016).

Obviously, chromatic aberrations are less significant in species that have limited color vision, as some of the defocused wavelengths may not be absorbed by the photoreceptors, and hence are not perceived. Thus, in many of our animal patients, who have dichromatic vision, it is possible that this aberration has minor functional implications.

Emmetropia and Accommodation Under Water

In aquatic species, the cornea is in contact with water rather than air. Because of the very small (~0.003) difference between the refractive indices of the cornea and water, the cornea of these species has virtually no refractive power. In fact, because the anterior corneal surface has lower curvature than the posterior surface (Ueno et al., 2015), under water the cornea acts as a weak divergent lens. Fish are forced to compensate for the absence of corneal refraction by increasing the refractive power of other ocular structures, usually the lens. For this reason, as noted earlier, the lenses of fish eyes are very spherical. Their increased curvature results in significantly larger refractive power. Biochemical changes in lenticular proteins also increase the refractive index of the fish lens to up to 1.66, thereby contributing to significant refraction as light passes from the aqueous humor into the lens (Sivak, 1978). In the sandlance fish, these evolutionary adaptations can increase the refractive power of the lens to as much as 500 D (Pettigrew & Collin, 1995). If it were not for these two lenticular adaptations, the absence of corneal refraction would cause fish to be severely hypermetropic under water.

The problem of refraction under water is further complicated in species that move in and out of water because it is physically impossible for an eye to be emmetropic both in air and underwater (Fig. 4.18). Eyes that are emmetropic in the air will be hypermetropic under water because the refractive power of the cornea is lost due to its submersion in water. Conversely, eyes that are emmetropic under water become extremely myopic in the air because now the cornea (due to Snell's law) contributes refraction that the eye did not possess under water. Therefore, species that live and function in both habitats must "choose" whether they will be emmetropic in the air or under water. It is very interesting to observe that both of these evolutionary strategies exist in the animal kingdom. Birds that hunt under water, such as cormorants (Katzir & Howland, 2003), the Australasian gannet (Machovsky-Capuska et al., 2012), and penguins (Sivak et al., 1987), as well as sea otters (Murphy et al., 1990), are emmetropic in the air. These species overcome the resulting underwater hypermetropia by increasing the accommodative power of the lens, thus allowing them to actively hunt and chase their prey under water. During accommodation in the cormorant, for example, the lens bulges through the pupil, forming *anterior lenticonus* that increases the lenticular axial length pathway and consequently its refractive power (Fig. 4.19) (Katzir & Howland, 2003). This combination of forward movement and change in lenticular curvature gives the cormorant lens an accommodative power of 60 D and an incredible accommodation rate of more than 600 D/s, 10 times as fast as nondiving birds (Katzir & Howland, 2003). Sea otters have also been shown to have a similar lenticular accommodative mechanism, combining forward movement and change in the curvature of the lens (Mass & Supin, 2007). As in cormorants, the result is an accommodative power of 55–60 D, which is the highest of any mammal (Murphy et al., 1990). Since the otter loses 59 D of corneal power under water, the equivalent magnitude of lenticular accommodation allows the animal to regain its visual acuity when diving. In penguins, the entire cornea is flat, consequently minimizing the alteration in refractive state when moving from air to water (Sivak et al., 1987).

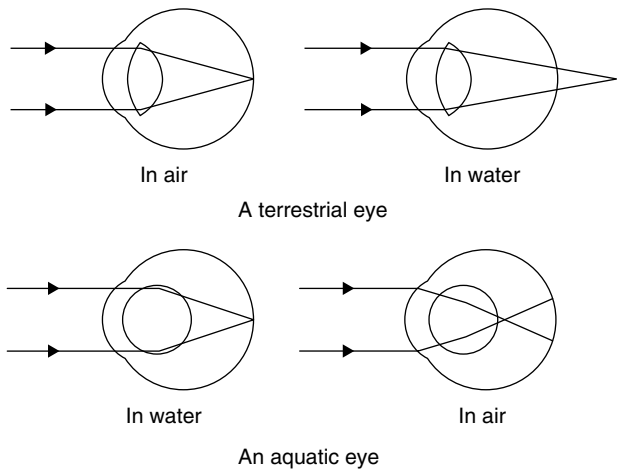

Figure 4.18 No eye can be emmetropic both in air and under water. An eye of terrestrial animals, which is emmetropic in an aerial environment, loses the refractive contribution of the cornea under water and becomes farsighted (top panel). An eye of a fish that is emmetropic under water becomes severely nearsighted (myopic) in the air because it "gained" corneal refraction that it did not possess under water (bottom panel). Note the difference in shapes of the lenses between the two species. The lens of the fish is more spherical in order to increase its refractive power (to compensate for the absence of corneal refraction under water). (Reproduced with permission from Sivak J.G. & Millodot M. (1977) Optical performance of the penguin eye in air and water. *Journal of Comparative Physiology*, **119**, 241–247.)

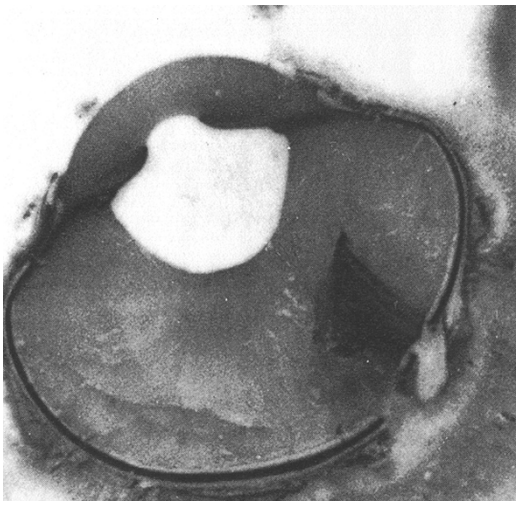

Figure 4.19 A sectioned eye of a cormorant during accommodation. The bulging of the lens through the miotic pupil into the anterior chamber is clearly illustrated. As a result, the axial length of the lens, and its refractive power, increases. This underwater accommodation allows the eye to compensate for the loss of corneal refraction during diving, and the bird can focus on its prey. But if the bird dives into deep, scotopic waters, the inevitable mydriasis will disable this accommodating mechanism. Therefore, the bird is restricted to hunting in shallow, photopic waters. (Courtesy of Gadi Katzir.)

Thus, in cormorants, otters, and penguins, the cornea is the major refractory organ on land, allowing for aerial emmetropia; the lens accommodation provides for underwater refraction. However, as usually happens with evolutionary strategies, there is a price to be paid for this well-developed underwater lenticular accommodative capability. The bulging of the lens through the pupil in these species requires miosis. This, in turn, limits the amount of light entering the eye. Therefore, these species can only hunt to a depth of about 9 m (Boyd et al., 2015). In deeper water, the inevitable mydriasis will not allow them to accommodate and focus on their prey. In this context it is worth noting that other piscivorous (fish-eating) birds, such as osprey, kingfishers, and sea eagles, do not chase their prey under water. Instead, these birds search for their aquatic prey from the air and capture it while plunging into the water, relying on momentum rather than accommodation to catch the fish (Machovsky-Capuska et al., 2012). Therefore, it is not surprising that pursuit-diving ducks accommodate, while nondiving ducks do not (Lisney et al., 2013).

On the other hand, many aquatic mammals developed an opposing evolutionary strategy (Mass & Supin, 2007). Sea lions, harbor seals, and other pinnipeds are emmetropic under water. Consequently, these animals become severely myopic when they come out of the water to breathe. Various mechanisms have evolved to make up for the increased refractive power of the eye in an aerial environment. Harbor seals have one flattened corneal meridian, with a slit-shaped pupil oriented along this flattened meridian (Hanke et al., 2006). When the animal exits the water, the bright light causes pupillary constriction along this meridian, which has minimal refractive power as it is not curved (*stenopaic vision*). Therefore, the resulting aerial myopia along this axis is attenuated significantly. Thus, in the air, the animal suffers from about −20 D myopia along the horizontal meridian, but "only" −7.5 D of myopia in the vertical meridian, the difference in refractive power of the central, flat cornea between water and air (Hanke et al., 2006). The aerial miosis also serves to minimize aberrations and increase the depth of field, thus allowing for further improvement of aerial acuity, which is comparable to the animal's underwater acuity (Hanke & Dehnhardt, 2009). Obviously, aerial visual acuity will deteriorate significantly at night, when mydriasis will allow light to enter through the highly curved and refractive quadrants of the cornea. A similar solution has evolved in the California sea lion, which has a specialized, flattened region with very low refractive power in the ventromedial cornea (Miller et al., 2010), and dolphins, which have a similar region in the medial cornea (Dawson et al., 1987). These regions provide for minimally defocused aerial vision, whereas the rest of the cornea is convex, providing for high underwater acuity. The animal shifts its head as it exits the water to allow light to enter through the flat "window" (Fig. 4.20; Dawson et al., 1987).

In both seals and dolphins, underwater mydriasis enables the eye to benefit from the highly curved and refractive quadrants of the cornea, thus allowing for emmetropia and high-resolution aquatic vision. Therefore, unlike diving birds, these animals can accommodate and hunt in deep water, as they use mydriasis, rather than miosis, for improving underwater acuity. The detrimental effect of the flat window, so beneficial in the air, is probably neutralized by underwater accommodation (Hanke et al., 2006). Therefore, what these animals lose in aerial acuity, they gain in hunting depth. More primitive amphibians (e.g., crocodiles) that lack this compensatory accommodative capability simply cannot focus. These animals are emmetropic in air and are severely hypermetropic under water, forcing them to rely on other senses when hunting under water (Nagloo et al., 2016).

Another interesting adaptation is observed when semi-aquatic garter snakes submerge in water. Contrary to expectations, their pupils constrict under water, rather than dilate. It is suggested that this constriction causes an increase in vitreous pressure in the posterior chamber and pushes the lens forward. The resulting accommodation allows the snake to compensate for the loss of corneal refractive power under water. In other words, aquatic submersion triggers a "pupillary water reflex" that is independent of light intensity; this reflex is intended to prevent hyperopia through lens accommodation, rather than to regulate the amount of light on the retina (Fontenot, 2008).

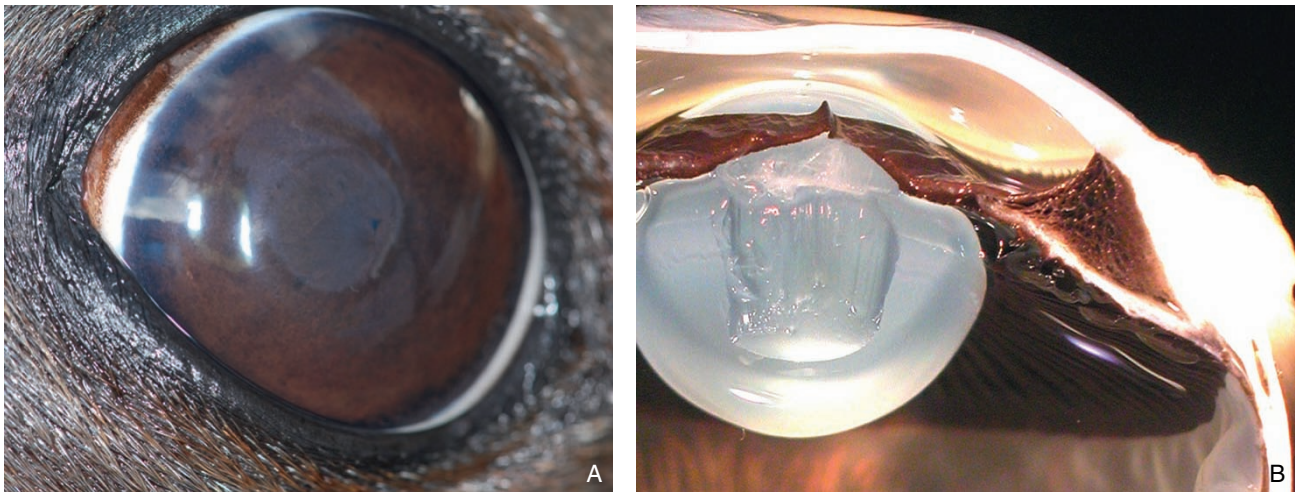

Figure 4.20 A frontal (**A**) and sectioned (**B**) view of the anterior segment of a pinniped eye. Note the flattened central cornea, which minimizes the inevitable myopia that occurs when the animal exits the water to an aerial environment. Note in panel **A** that the pupil constricts around this part of the cornea, so that only light passing through the least refractive part of the cornea will enter the eye. The pinpoint pupil minimizes spherical aberrations and increases depth of focus, further enhancing aerial acuity. (Panel **A** courtesy of Carmen M. Colitz. Panel **B** courtesy of Richard R. Dubielzig.)

Visual Processing: From Photoreceptors to Cortex

The Retina

The optical part of the visual process ends with photons striking the outer segments of the photoreceptors. The neuronal part of the visual process begins with the capture of these photons and absorption of their energy by the photopigments in the outer segments of the cones and rods, where a chain of biochemical reactions starts. In addition to these sensory neurons, the retina also contains secondary and higher-order neurons and an intricate neural circuitry that performs the initial stages of image processing, before trains of electrical impulses are transferred through the axons of the retinal ganglion cells (RGCs) to areas in the brain where secondary processing and eventually visual perception occur. A schematic representation of the retina is shown in Fig. 4.21.

The Photoreceptors

The outermost cells in the neural retina are the photoreceptors, which are divided into two classes: rods and cones. Rods and cones differ from each other in their morphology, function, and retinal distribution. Functionally, cone systems are characterized by high resolution of fine details, rapid responses, color perception, and low sensitivity to small fluctuations in light intensity (Lamb, 2016). Rod systems are characterized by poor visual resolution and no color perception, but they are extremely sensitive to minute changes in light levels and detection of motion. Therefore, cones are particularly suitable for daylight *photopic* vision, whereas rods contribute mostly to dim-light *scotopic* vision (Collin et al., 2009; Lamb, 2013; Lamb et al., 2007, 2016; Mustafi et al., 2009). Hence, a retinal mosaic containing both cone and rod photoreceptors, which appears to be ubiquitous among mammals (Peichl, 2005), forms a duplex retina, which functions in both low and bright light conditions.

These functional differences between rods and cones are partially the result of the morphologic differences discussed in Chapter 2. The rod outer segment is long and thin, about 2 μm in diameter, which permits a high density of rods, thus increasing the probability of absorbing scarce photons at night. Cones are thicker than rods, but both cones and rods in the central part of the retina are thinner than those in the periphery to permit a high photoreceptor density (Mowat et al., 2008). Rod axons are thin, which is consistent with the cell's slow response to light and fewer ribbon synapses, whereas cone axons are thick, enabling transfer of information (signals) at higher rates in multiple synapses (Hsu et al., 1998).

Cones constitute a minority of the photoreceptors in most mammalian retinas, with ranges of 0.5%–3% in nocturnal species and 5%–10% in crepuscular and arrhythmic species, whereas the proportion of cones in diurnal animals ranges from 8% to 95% (Ahnelt & Kolb, 2000). Hence, the cone-to-rod ratio roughly reflects the lifestyle of the species. There are also differences in photoreceptor concentrations in different regions of the retina. A specialized, avascular area with higher cone density providing higher spatial resolution (ability to see finer details) in the corresponding part of the visual field is often present in the retina. In diurnal species possessing high acuity, such as haplorrhine primates and many avian species, this region is called the *fovea centralis*.

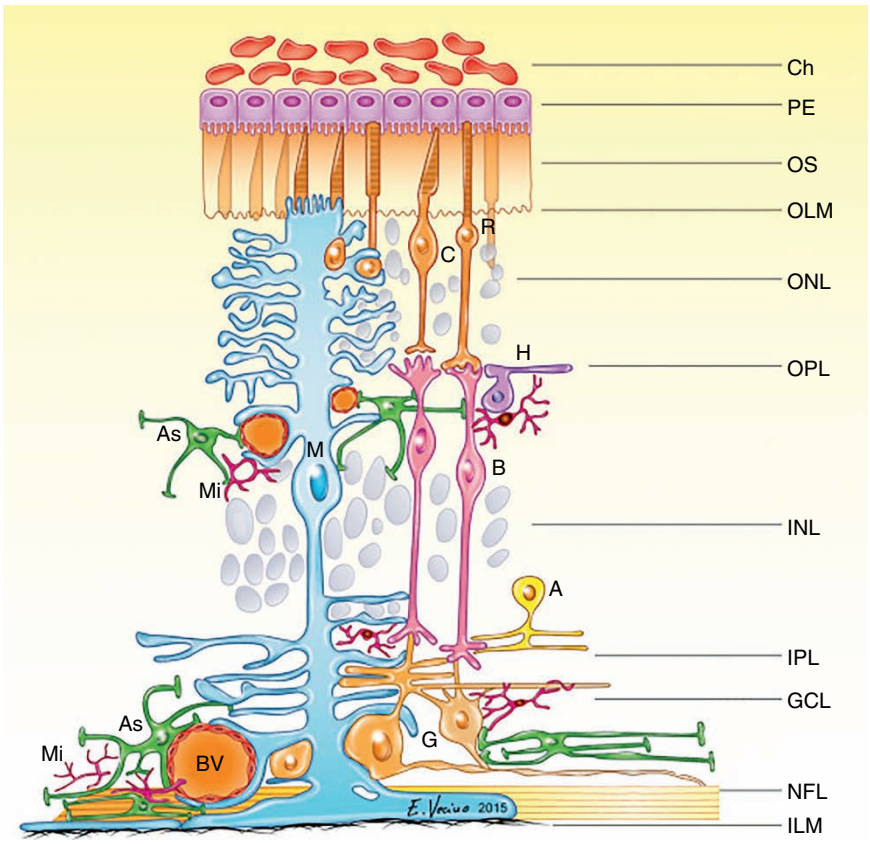

Figure 4.21 Schematic drawing of the mammalian retina with part of the choroid (Ch) on top. Below the retinal pigment epithelium (PE) are the layers of the neuroretina: the outer segments of the photoreceptors (OS), the outer limiting membrane (OLM), the outer nuclear layer with nuclei of cones (C) and rods (R), the neuropil of the outer plexiform layer (OPL), the inner nuclear layer (INL) with nuclei of horizontal (H), bipolar (B), and amacrine (A) cells, the inner plexiform layer with synapses in strata, the ganglion cell layer (G), their axons in the nerve fiber layer, and finally the inner limiting membrane (ILM) facing the vitreous. The glial elements of the retina, Müller cells (M), and microglia (Mi), as well as astrocytes (As) embracing retinal blood vessels, are shown. (Reproduced with permission from Vecino, E., Rodriguez, F.D., Ruzafa, N., et al. (2016) Glia–neuron interactions in the mammalian retina. *Progress in Retinal and Eye Research*, **51**, 1–40. doi: 10.1016/j.preteyeres.2015.06.003.)

The primate and avian fovea is actually a depression (or pit) that contains no rods or retinal capillaries, thus permitting more dense packing of cones almost individually connected to retinal interneurons and ganglion cells (Kolb & Marshak, 2003). This area subserves the highest-resolution vision of the eye. Most other species are devoid of such a highly specialized area, but a *fovea plana*–like area (a fovea without evident foveal pit) temporal to the optic nerve head has recently been identified in the dog (Beltran et al., 2014). A more diffusely outlined region with increased cone density called the *area centralis* surrounds the fovea plana in the dog and is usually seen in other mammals that are currently considered to be afoveate (Beltran et al., 2014; Mowat et al., 2008). Though this area has a higher concentration of cones, rods still outnumber the cones in the area centralis (Table 4.6). Because of their higher rod concentration, these eyes have higher sensitivity under low light conditions, albeit sacrificing visual acuity and richer color vision, as they have fewer cones. The primate fovea and area centralis in lower mammals are surrounded, respectively, by a *macula* and a *visual streak*, which are regions of decreasing cone density. In foveate primates, the macular area appears yellowish because of the macular pigments absorbing blue light and scavenging free radicals, thus protecting the retinal area providing the high visual acuity (Provis et al., 2013). The concentration of cones continues decreasing with retinal eccentricity, and the more peripheral retina is characterized by higher rod-to-cone ratios.

Cones are further subdivided into several types depending on their opsin contents (Hunt et al., 2009). Humans (as well as Old World primates) have three cone classes, with peak sensitivities to either long (552–562 nm, usually called red cones, although they are most sensitive to greenish-yellow), medium (525–533 nm, green), or short (410–450 nm, blue) wavelengths of light (Hofmann & Palczewski, 2015a). These cones, known as *L-*, *M-*, and *S-cones* or *red*, *green*, and *blue cones*, respectively, are the basis of human trichromatic vision. Most New World primates and lower mammals have

Table 4.6 Photoreceptor concentrations in cats, dogs and humans.

	Human (Østerberg, 1935)	Cat (Steinberg et al., 1973)	Dog (Mowat et al., 2008; Beltran et al., 2014*; Yamaue et al., 2015**)
Number of rods ($\times 10^6$)	110–125		
Number of cones ($\times 10^6$)	6.5		
Maximal cone concentration ($\times 10^3$ per mm^2)	199	27	23/127*
Maximal rod concentration ($\times 10^3$ per mm^2)	160	460	501
Cone concentration at ora serrata ($\times 10^3$ per mm^2)	5	<3	7[a]
Rod concentration at ora serrata ($\times 10^3$ per mm^2)	40	250	~200**
Rod-to-cone ratio (area centralis)	No rods	11 : 1	23 : 1[b]
Rod-to-cone ratio (ora serrata)	50 : 1	100 : 1	41 : 1[a]

[a] These numbers were obtained in the periphery by Mowat et al. (2008) and not at the ora serrata;
[b] Data from Beltran et al. (2014) suggest that the rod-to-cone ratio in the area centralis is closer to 1 : 1.

two cone populations (serving dichromatic vision). Some animals have one cone population (monochromatic vision), while others have more than three cone populations (tetrachromatic vision and beyond). Morphologically, the three primate cone populations are almost identical, and immunohistochemistry or another molecular method is needed to distinguish between them. These methods reveal differences in the cone synaptic terminals and in their retinal distribution, such as the absence of S-cones in the fovea. They also reveal a high degree of evolutionary conservation between L- and M-cones. Thus, most dichromatic species will have S- and L/M-cones rather than L- and M-cones, because S- and L/M-cones, whose absorption spectra are further apart, are activated by a wider range of wavelengths and therefore able to detect more of the electromagnetic radiation being reflected off different surfaces in nature. The implications of these properties for color vision are discussed in Chapter 5.

Mammals only have one class of rods, which precludes color vision when light is too dim for cones to be activated. The peak spectral sensitivity of rods is close to 500 nm (cyan-greenish light). In the dog, the highest rod density, almost 540,000 rods/mm^2, is seen dorsal to the area centralis region, whereas the density in the peripheral retina is 2.5–2.7 times lower (Yamaue et al., 2015).

Morphologically, both rods and cones are divided into four parts (Fig. 4.22A):

1) Outer segment
2) Inner segment
3) Nucleus
4) Synaptic terminal.

The *outer segment* is the part of the cell where phototransduction, as well as disc formation and shedding, occurs; for a review see Molday and Moritz (2015). The outer segments are connected by a cilium to the *inner segment*, which is an area rich in mitochondria (ellipsoid), Golgi apparatus, and endoplasmic reticulum (myoid). Opsin is synthesized in the Golgi apparatus of the inner segment and is transported through the cilium to the base of the outer segment, where it is incorporated into the outer segment's plasma membrane, which undergoes evagination and invagination to form a new disc. In rods, the disc detaches from the membrane and the outer segment is filled with a stack of 600–1,600 free-floating discs, similar to a stack of coins (Hofmann & Palczewski, 2015b). In cones, the disc remains part of the membrane, thus exposing it to a greater supply of the recyclable, light-sensitive part of the photopigment (relative to the disconnected rod disc). Thus, the outer segments are in fact tubes full of discs (or tubes made up of discs, in the case of cones) of folded double membranes in which the visual photopigment molecules are embedded.

The outer segments undergo constant destruction due to photo-oxidative damage. The damaged tips of the outer segments are shed and then phagocytized by the retinal pigment epithelium (RPE), where they become phagosomes that are broken down by lysis (Nguyen-Legros & Hicks, 2000). This shedding of outer segments is a diurnal cycle (which takes place following morning light onset in rods, and following night onset in cones), and is *not* to be confused with the intermittent and much more frequent process of chromophore phagocytosis and regeneration. As new discs are formed at the base of the outer segment, older discs are

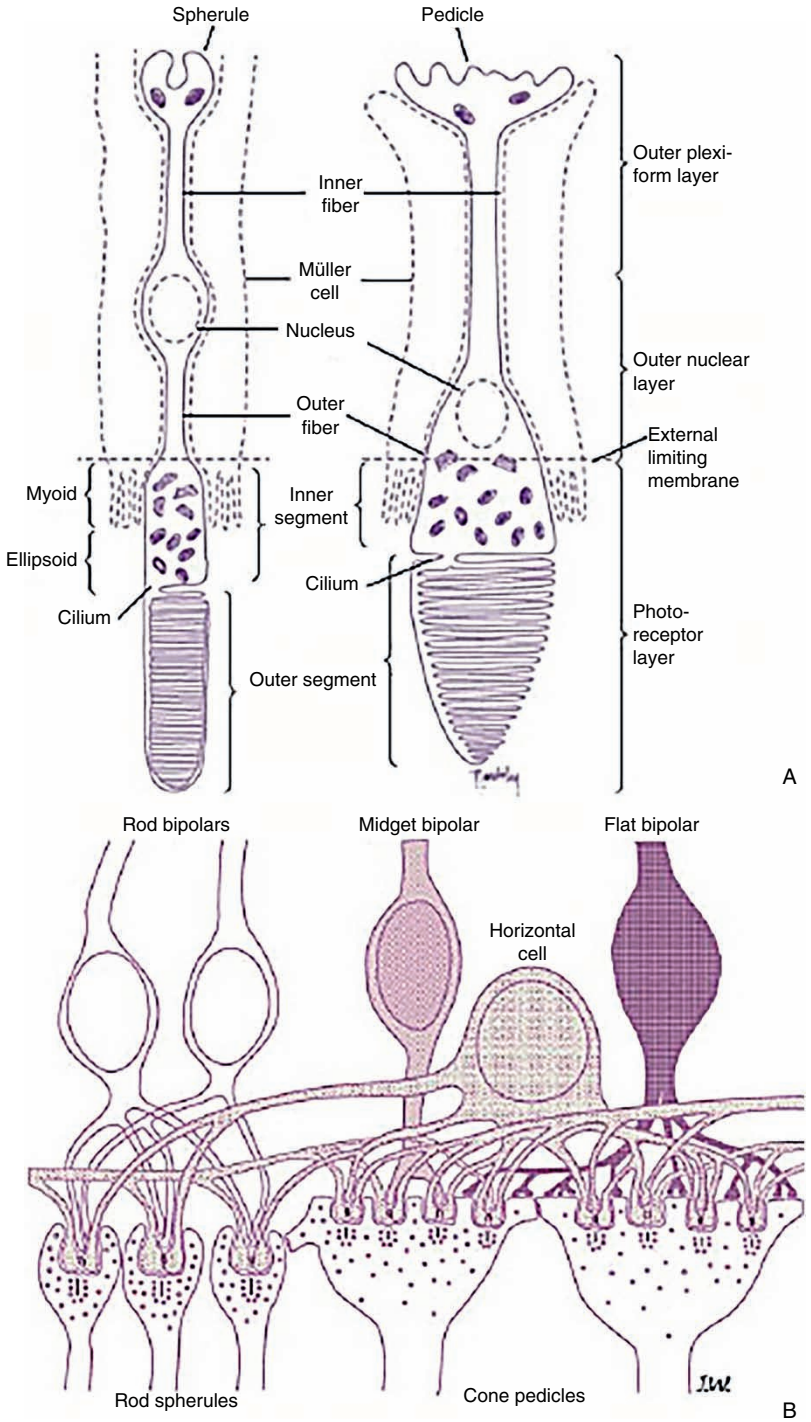

Figure 4.22 **A.** The discs of the outer segments (facing the retinal pigment epithelium) of the photoreceptors contain the photopigment required for vision. The photoreceptors' inner segments contain the mitochondria, and together with the outer segments constitute the photoreceptor layer. The rod spherule and cone pedicle are synaptic expansions where their axons synapse with dendrites of bipolar and horizontal cells in the outer plexiform layer. Portions of Müller's cells (dotted lines) are shown adjoining the rods and cones. **B.** Rod and cone bipolar cells show extensive contacts. Horizontal cells also make synapses with both rods and cones. Interconnections are shown between spherules and pedicles. (Modified and reproduced with permission from Remington, L.A. (2005) *Clinical Anatomy of the Visual System*, 2nd ed. St. Louis, MO: Butterworth-Heinemann.)

displaced toward the distal end. Experiments in which radiolabeled precursors have been injected into the inner segments show that labeled proteins appear at the outer segment base within 2 hours; another 11 days pass before the discs containing these proteins are shed and phagocytized (Anderson et al., 1978).

The *nuclei* of the photoreceptors constitute the outer nuclear layer (ONL) of the retina, which is separated from the inner segments by an outer limiting membrane. Nuclei of cones occupy a single row directly below the membrane, with rod nuclei making up the remainder of the ONL below the cone nuclei. The *synaptic terminals* of the rods and cones synapse with dendritic processes of bipolar and horizontal cells in the outer plexiform layer (OPL; Fig. 4.22B). The synaptic terminal of a mammalian cone, which is large and flat, is called a *pedicle*. The rod terminal, which is rounder and smaller, is called a *spherule*. Both pedicles and spherules contain mitochondria, synaptic vesicles, and synaptic ribbons (Mustafi et al., 2009; Schmitz, 2009).

The Classic Visual Pigments and Phototransduction

Most of our understanding about the processes occurring in the outer segments comes from studying rhodopsin, the rod photopigment. This light-sensitive transmembrane protein comprises more than 90% of the protein content of the discs in the rod outer segments and covers approximately 50% of the disc membrane area (Hargrave, 2001; Hofmann & Palczewski, 2015b; Palczewski, 2006). It is estimated that each human rod has approximately 10^9 rhodopsin molecules (Smith, 2010), whereas the mouse has only about 10^6–10^7 molecules/rod (Palczewski, 2006).

A visual photopigment consists of two components. The first component of the photopigment is the *opsin*, which is an apo-protein that determines the wavelengths of light that the photopigment will absorb. In most mammals studied to date, maximal absorption of rhodopsin, determined by its opsin part (called *scotopsin*), occurs round 500 nm in most species, thus showing a high degree of evolutionary conservation in the molecule (Bowmaker, 1981, 2008; Palczewski, 2006). There is greater evolutionary divergence in the opsin of cones, with most mammalian species possessing at least two classes of cone opsins: those sensitive to one short wavelength (S-cones) and those sensitive to medium to long wavelengths (L/M-cones; Bowmaker, 2008; Imamoto & Shichida, 2014; Lamb, 2013). Although they are more complicated to study because of the smaller number of cones and difficulties in extraction, cone opsins such as iodopsin appear to be similar to scotopsin in both structure and function (Wensel, 2008).

The second component of the photopigment is the *chromophore*, which is the part of the photopigment that is excited when the energy from a photon is absorbed. The chromophore is covalently bound to the opsin. Both rod and cone photopigments use the same excitable chromophore, a vitamin A1 derivative, 11-*cis*-retinal (Wald, 1968). The 11-*cis*-retinal is highly conserved and found in most terrestrial and avian species.

Phototransduction in Image-Forming Photoreceptors

Phototransduction is the process by which light stimulus is converted into a neuronal signal (Fig. 4.23). Photons captured by the photopigment transfer their energy to the chromophore, causing photoisomerization of the 11-*cis*-retinaldehyde, through several intermediate compounds, into all-*trans*-retinal (Hargrave, 2001; Palczewski, 2006). This results in changes in the chromophore conformation that cause a rearrangement of the heptahelical transmembrane opsin molecule, which eventually leads to activation of subsequent steps in the phototransduction cascade (Nakamichi & Okada, 2006). This bleaching process (so called because the rhodopsin loses its purple color when activated) can be recorded as the early receptor potential of the ERG (Müller & Topke, 1987).

Stimulated neurons depolarize, but contrary to intuition, photoreceptors are depolarized in the dark, causing them to release glutamate (an excitatory neurotransmitter). This depolarized state of the photoreceptor is maintained by a *dark current*, which is generated by a constant influx of Na^+ and Ca^{++} (at an 85 : 15 ratio) into the cell and balanced by K^+ outflow. These cations enter the photoreceptor through cyclic guanosine-3,5′-monophosphate (cGMP)-gated cation channels in the outer segment plasma membrane. The end result of the phototransduction process is a decrease in cGMP levels, leading to closure of the ion channels in a millisecond or less (Yau, 1994). Even though only a small fraction of the cation channels is open in the dark, the cessation of Na^+/Ca^{++} influx leads to hyperpolarization of the photoreceptor. This hyperpolarization decreases or terminates the glutamate release at the photoreceptor synaptic terminals, a signal affecting the second-order neurons in the retina (Heidelberger et al., 2005).

The phototransduction cascade, beginning with the absorption of photon energy by the photopigment and ending with closure of the cation channels and photoreceptor hyperpolarization, involves several enzymes. The interactive form of rhodopsin, R*, activates a G-protein in the disc membrane called transducin (T) in rods, which is composed of three subunits (Tα, Tβ, and Tγ). In the dark, transducin is bound to guanosine diphosphate (GDP), but R* binds to transducin, forming a T-GDP-R* complex (see Fig. 4.23). This binding changes the affinity of the complex to GDP, which drops off and is replaced by guanosine triphosphate (GTP), leading to the formation of a T-GTP-R* complex. Additional affinity changes now occur and the complex breaks up. R* falls off and is free to activate additional T-GDP molecules at the rate of one per millisecond. Tβ-Tγ also falls off, thereby removing the inhibitory γ subunit from the Tα-GTP complex (Stryer et al., 1981). Each R*

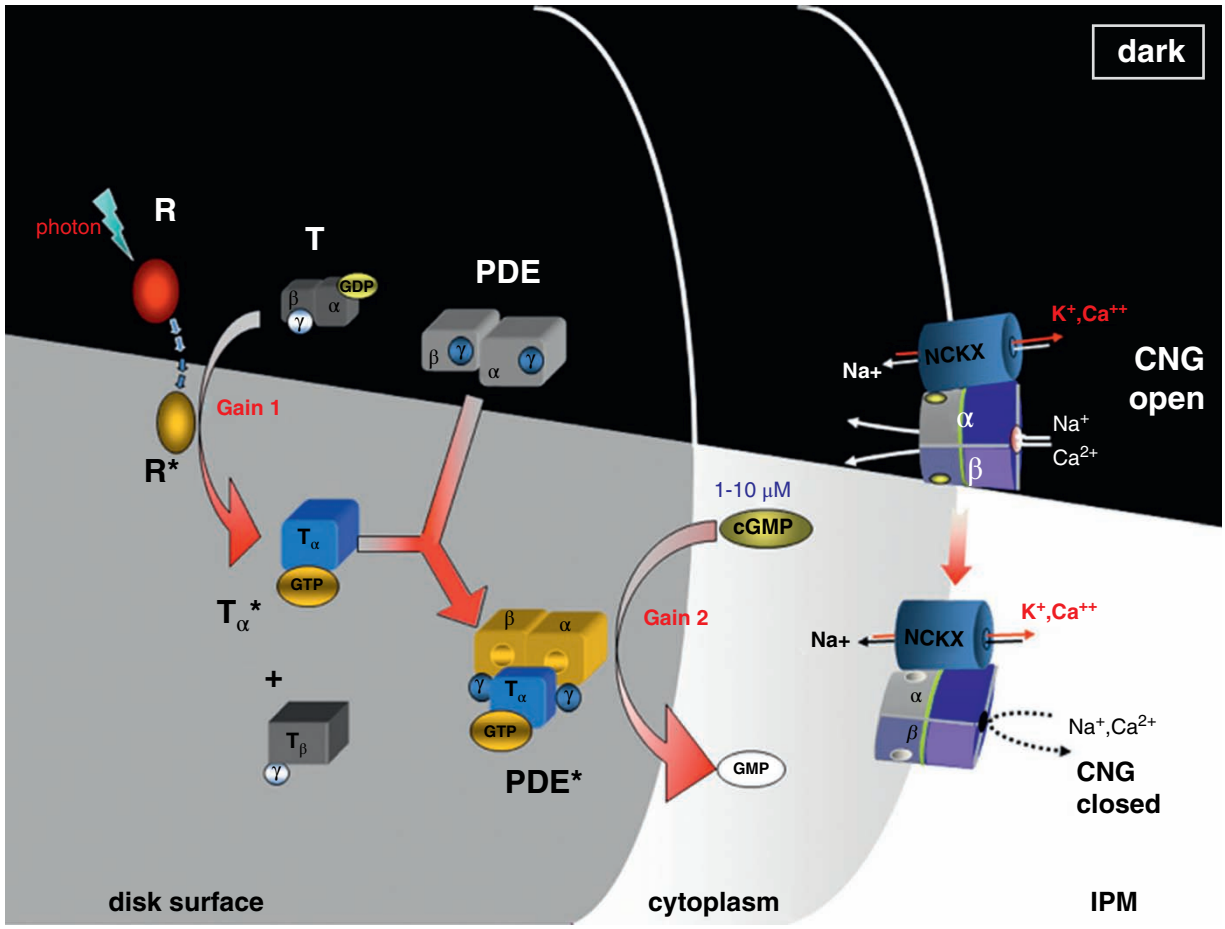

Figure 4.23 Activation of the rod phototransduction cascade. The top of the illustration shows the rod in the dark, where its depolarized state is maintained by influx of sodium and calcium through the open cyclic nucleotide-gated (CNG) cyclic guanosine-3,5′-monophosphate (cGMP)-gated cation channel (α, β). This cation influx is balanced by potassium outflow (through the NCKX Na^+/Ca^{2+}, K^+ exchanger). In the lower part of the figure, a photon has been absorbed by the rhodopsin (R). Activated rhodopsin (R*) now binds to the transducin guanosine diphosphate (T-GDP) complex, leading to reduction in affinity to GDP. GDP is replaced by guanosine triphosphate (GTP), forming an R*-T-GTP complex, leading to dissociation of R* and the transducin Tβ-Tγ subunits. The remaining Tα-GTP complexes remove the inhibitory γ-subunits from the phosphodiesterase (PDE) enzyme. The activated enzyme (PDE*), consisting of its β- and α-subunits, hydrolyzes cGMP into GMP. The reduction in cGMP levels leads to closure of the CNG channels and hyperpolarization. IPM, interphotoreceptor matrix. (Reproduced with permission from *Phototransduction in Rods and Cones*, WebVision, Moran Eye Center (http://webvision.med.utah.edu). Used under CC BY.)

molecule can activate 20 or more T-GDP complexes (Krispel et al., 2006). This is the first step of amplification of the response to the capture of a single photon in the phototransduction cascade.

The activated complex migrates to the disc membrane, where it activates the next enzyme in the cascade, phosphodiesterase (PDE), by removing its inhibitory γ-subunits. Because PDE contains two γ subunits, two Tα-GTP complexes are required for complete PDE activation. However, the density of PDE is lower than that of T in the outer segment. The activated PDE hydrolyzes cytoplasmic cGMP into GMP, resulting in decreased levels of free-floating cGMP. The activation of PDE by Tα-GTP represents no gain *per se*, but the increase in catalytic power of the activated PDE (which hydrolyzes numerous cGMP molecules) is considerable and constitutes the second step of amplification of the response (Lamb & Pugh, 2006).

Multiple cGMP-gated cation channels in the cell's plasma membrane respond by closure to the rapid decrease in cytoplasmic cGMP. Hence, a small relative change in the cGMP concentration produces a threefold larger relative change in the current through the channels. Each photoisomerization interrupts the flow of 10^5 or more cations into the cell (Burns & Baylor, 2001). Therefore, the photoreceptor membrane hyperpolarizes, which generates an electronegative signal that can be recorded at the surface of the eye as the first part of the a-wave of the ERG. The combined amplification for all steps in rods is high, allowing them to detect a single photon.

Cones, on the other hand, need to absorb 10–100 times as many photons to generate the same current, thus accounting for their decreased light sensitivity (Baylor, 1996).

Inactivation of the Phototransduction Cascade

The cascade is eventually quenched by an equally complex chain reaction that leads to inactivation of R*, transducin, and PDE (Fig. 4.24). Initially, the enzyme rhodopsin kinase (regulated by recoverin) phosphorylates R* (Arshavsky & Burns, 2012; Burns & Baylor, 2001). This phosphorylation increases the affinity of rhodopsin to arrestin, and their binding prevents further transducin activation by R*. At the same time, Tα-GTP is hydrolyzed into Tα-GDP, thus freeing up the PDE-inhibitory γ subunit. The γ subunit rebinds to PDE, thus stopping the hydrolysis of cGMP, and Tα-GDP rebinds to Tβ-Tγ, thus deactivating the transducin molecule (Makino et al., 2003). The cessation of cGMP hydrolysis by PDE, together with increased guanylate cyclase activity in the outer segment, results in net synthesis of cGMP (Burns et al., 2002). As cGMP's concentration rises, it eventually causes reopening of the channels and photoreceptor depolarization.

The phototransduction process in rods can be regarded as a G-protein signaling pathway, with rhodopsin as its receptor, transducin as its G protein, and cGMP PDE as its effector. cGMP is the second messenger in this pathway, connecting between the "rhodopsin receptor" in the rod disc membrane and its "target channel," located in the plasma membrane (Luo et al., 2008).

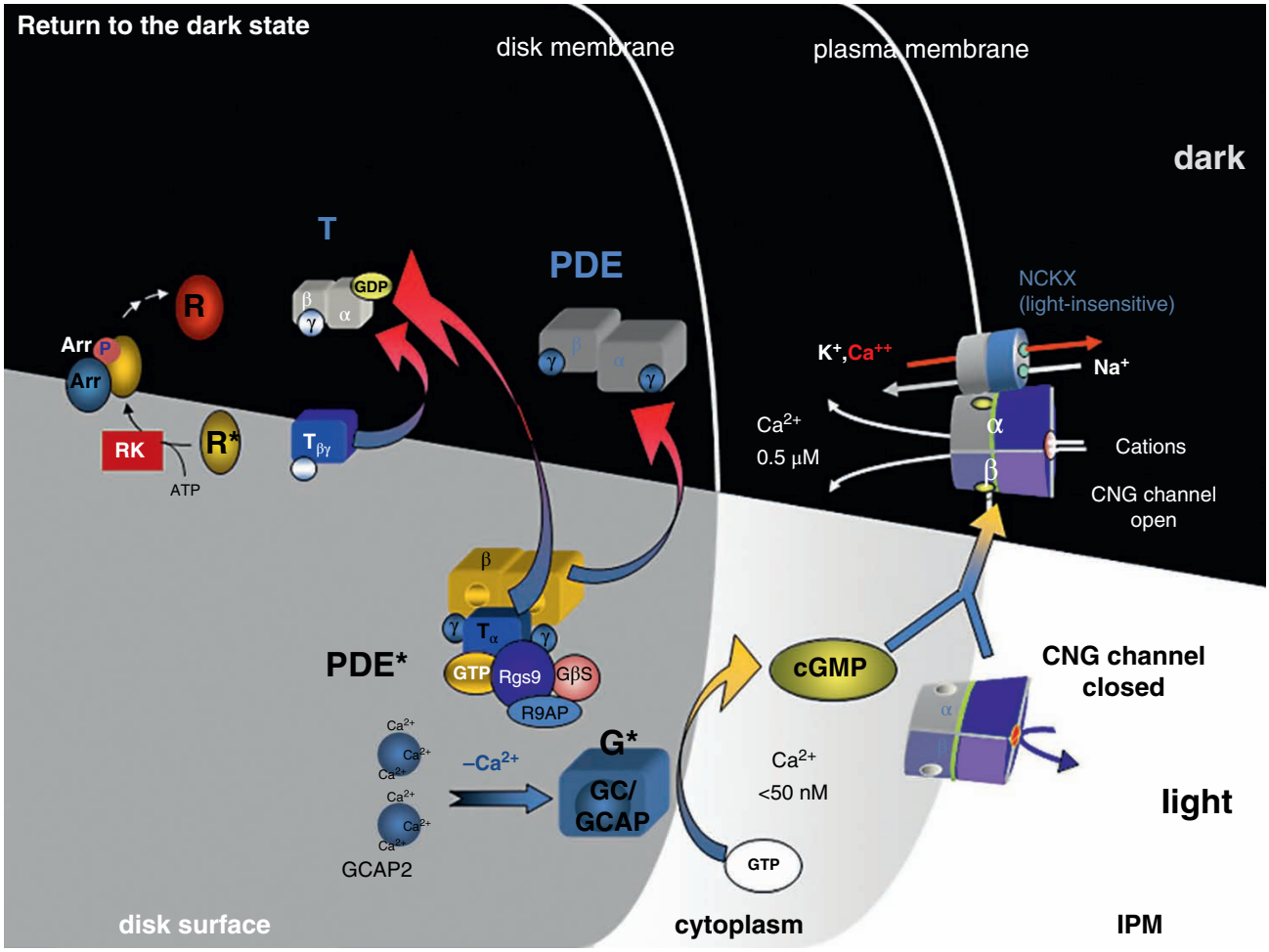

Figure 4.24 Inactivation of the rod phototransduction cascade that results in reopening of the cGMP-gated cation channels on the plasma membrane (from the light-adapted state in the bottom part to the dark-adapted state in the top part of the drawing). Initially, the enzyme rhodopsin kinase (RK, regulated by recoverin) phosphorylates the light-activated rhodopsin (R*). This phosphorylation increases the affinity of rhodopsin to arrestin (Arr), and their binding prevents further transducin activation by R*. At the same time, Tα-GTP is hydrolyzed into Tα-GDP, thus freeing up the PDE inhibitory γ-subunit. The γ-subunit rebinds to PDE, thus stopping the hydrolysis of cGMP, and Tα-GDP rebinds to Tβ-Tγ, thus deactivating the transducin molecule. The cessation of cGMP hydrolysis by PDE, together with increased guanylate cyclase (G*) activity in the outer segment, results in net synthesis of cGMP. As its concentration rises, it eventually causes reopening of the CNG cation channel and photoreceptor depolarization. See Fig. 4.23 for abbreviations. (Reproduced with permission from *Phototransduction in Rods and Cones*, WebVision, Moran Eye Center (http://webvision.med.utah.edu). Used under CC BY.)

Understanding of the molecular biology of phototransduction has led to new insights into the pathogenesis of photoreceptor dysplasias and degenerations, and is leading to new treatments of these diseases (Petersen-Jones & Komaromy, 2015; Scholl et al., 2016).

Synthesis and Regeneration of the Classic Visual Pigments

Regeneration of all-*trans*-retinal to 11-*cis*-retinal is a rather complicated process in vertebrates that mainly takes place in cells adjacent to the photoreceptors. Most of the all-*trans*-retinal is released from the opsin on the cytoplasmic side of the discs in the rod outer segments; however, the portion of the inactive form of the chromophore that enters into the disc lumen has to be transported over to the cytoplasm by an ATP-binding cassette transporter (ABCA4). Because of the reactive aldehyde group on retinal that could potentially damage the photoreceptors, the all-*trans*-retinal is rapidly reduced to all-*trans*-retinol by all-*trans*-retinol dehydrogenase (Fig. 4.25). This is the only step of the regeneration process that occurs in the outer segment of the rods; the rest occurs in the RPE (Kiser et al., 2014; Palczewski, 2014; Saari, 2000).

All-*trans*-retinol diffuses out of the outer segment into the subretinal space and makes its way to the RPE. An interphotoreceptor retinoid-binding protein (IRBP) plays an important role in the movement of all-*trans*-retinol from the photoreceptors through the subretinal space (Wu et al., 2007). Once inside the RPE, all-*trans*-retinol undergoes a three-step transformation reaction to 11-*cis*-retinal. A key enzyme in this reaction is *RPE65* (Redmond, 2009). The 11-*cis*-retinal is then translocated from the RPE back to the outer segment via IRBP, where it binds with opsin (synthesized in the inner segment) to reform the photopigment in both rods and cones (Parker et al., 2011). In addition to the recycling of the chromophore in the RPE, the cones also receive 11-*cis*-retinal through a process involving the Müller cells in the neuroretina (Das et al., 1992). This pathway supports rapid dark adaptation of cones and extends their dynamic range in background light independently of the RPE (Wang et al., 2014). Hence, cones are not completely dependent on the function of the IRBP (Kolesnikov et al., 2011).

Thus, the rods have access to 11-*cis*-retinal from three storage sites in the neuroretina and RPE. When moving abruptly from a scotopic to a photopic environment, the chromophore will be depleted from these three sites in sequential order. The first is the chromophore available in the rod outer segments; the second is the chromophore bound to IRBP in the subretinal space; and the third is the chromophore bound to *RPE65* in the RPE. The cones also have access to a fourth storage site for rapid recovery, the Müller cells. Therefore, *RPE65* plays two vital roles in the visual cycle. In light, it catalyzes the re-isomerization reaction of the chromophore back to 11-*cis*-retinal. In the dark, it serves as a chromophore binding protein and an important reserve pool of 11-*cis*-retinal.

Bleached pigment is not the only source for 11-*cis*-retinal synthesis in the RPE. Dietary uptake remains the main substrate for chromophore synthesis. Carotenoid compounds in food are oxidized into vitamin A (all-*trans*-retinol) in the wall of the small intestine. The vitamin is then esterified and transported to the liver, where it is bound to serum RBP. Retinol-bound RBP is transported through the bloodstream and eventually reaches the choriocapillaris. Specific receptors on the outer aspect of the RPE bind the serum RBP, and the retinol is taken up by the cell for processing, similar to that undergone by all-*trans*-retinol reaching the RPE from the photoreceptor. This dependence on dietary carotenoid compounds is the reason for the nyctalopia and progressive retinal degeneration observed in cases of avitaminosis A in cattle and other species (Millemann et al., 2007).

As indicated earlier, light stimulation causes bleaching of the photopigment; conversely, the pigment undergoes regeneration during darkness (Lamb & Pugh, 2006; Redmond, 2009; Wang & Kefalov, 2011; Wang et al., 2014). Prolonged and intense light stimulation will eventually bleach all of the rod photopigment, resulting in its depletion. Prolonged and total darkness will enable all of the photopigment to regenerate, which is an important part of the dark adaptation process. At intermediate levels of illumination, between these two extremes, a dynamic and continuous process of bleaching and regeneration occurs, leading to equilibrium and contributing to adaptation to existing light levels (see Chapter 5).

Physiology of Retinal Cells

Horizontal and Bipolar Cells

The soma of both the horizontal and bipolar cells are located in the inner nuclear layer (INL). Both cells serve as *second-order* neurons of the retina, connecting, directly or indirectly, the *first-order* (photoreceptors) and *third-order* neurons (RGCs).

Horizontal cells occupy the outermost layer of the INL and synapse almost exclusively in the OPL (Ahnelt et al., 2000; Bloomfield & Xin, 2000; Chapot et al., 2017; Macneil et al., 2009; Marshak & Mills, 2014; Thoreson & Mangel, 2012). They connect photoreceptors laterally across the OPL (see Fig. 4.22), serving to integrate responses from photoreceptors and increase their sensitivity to changes in illumination (i.e., brightness contrast) and color, which is a phenomenon termed *lateral inhibition*. Morphologically, horizontal cells are divided into *HI* or *B*-type cells with axons, and *HII* or *A*-type cells that are axonless. Additional types of horizontal cells are seen in animals, including primates, birds, and reptiles, with more types of cones. The horizontal cells form a mosaic with about six dendritic fields overlapping at any given point in the murine retina (Reese et al., 2005).

The physiologic equivalents of HI/B and HII/A horizontal cells have been characterized as luminosity (L) and color (C) types, respectively. The HI/B- or L-type horizontal cells

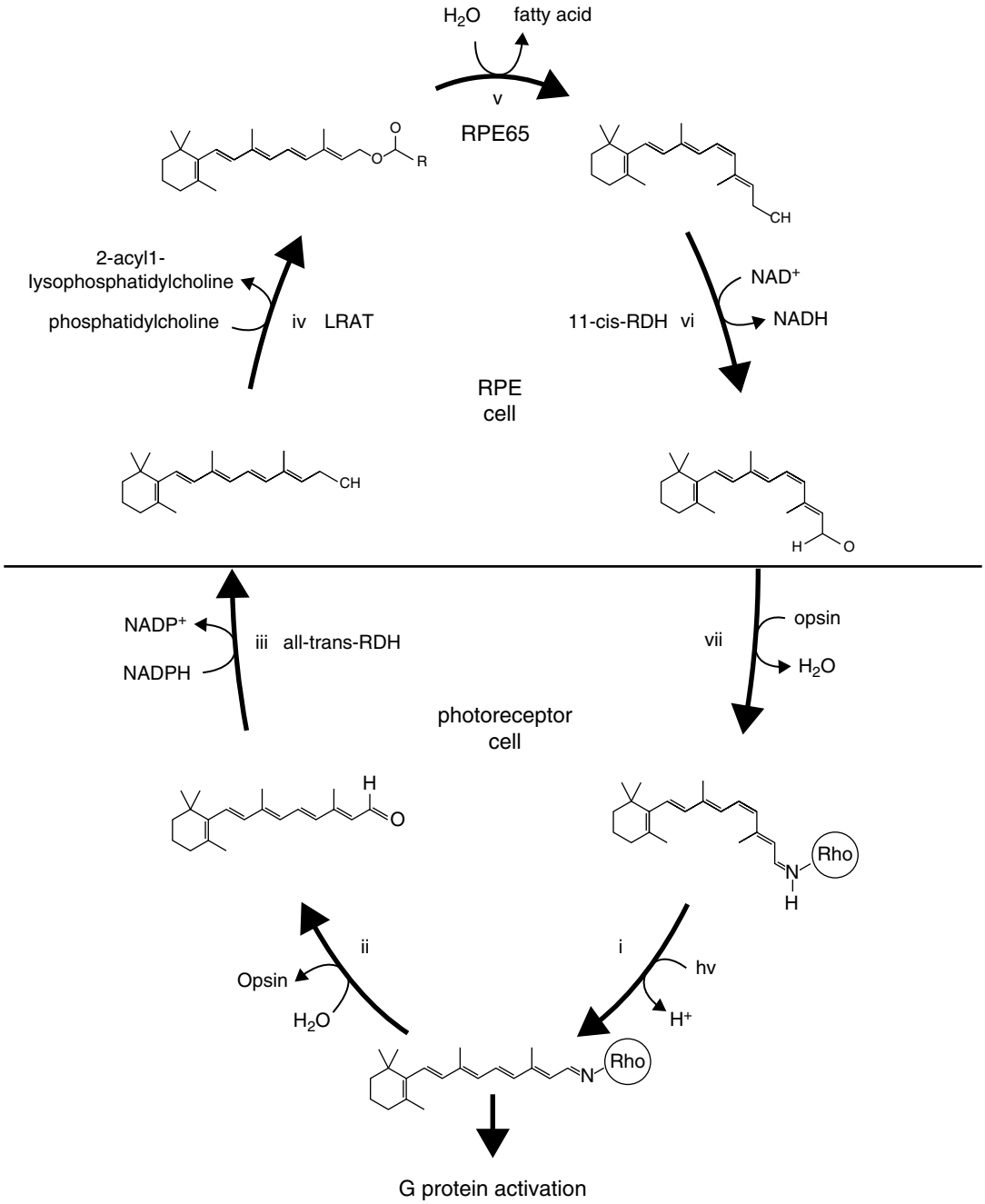

Figure 4.25 The retinoid (visual) cycle, which begins when a photon (hv) causes photoisomerization of the 11-*cis*-retinylidene chromophore of the dark-adapted rhodopsin. Subsequently, a proton is lost and rhodopsin activates G proteins (i). The isomerized chromophore is released via hydrolysis, generating free all-*trans*-retinal and opsin (ii). The all-*trans*-retinal is then enzymatically reduced (iii) to all-*trans*-retinol, which binds to interphotoreceptor retinoid-binding protein (IRBP) and is exported from the outer segment of the rod to the retinal pigment epithelium (RPE). Here all-*trans*-retinol binds to cellular retinaldehyde binding protein (CRALBP) and is metabolized by lecithin retinol acyltransferase (LRAT) to produce all-*trans*-retinyl esters (iv), which can be either stored in retinosomes or further processed. RPE65 is the key enzyme that catalyzes the conversion of all-*trans*-retinyl esters to 11-*cis*-retinol (v). 11-*cis*-retinol is finally enzymatically reduced to 11-*cis*-retinal (vi) and transported back via IRBP to the rod outer segment, where it recombines with opsin to form ground-state rhodopsin (vii). This cycle runs continuously to sustain vision under conditions where rods are primarily active. (Reproduced with permission from Kiser, P.D. & Palczewski, K. (2010) Membrane-binding and enzymatic properties of RPE65. *Progress in Retinal and Eye Research*, **29**, 428–442.)

synapse with both rods and cones. They code changes in ambient light intensity, thus regulating the adaptational and spatial responses of the photoreceptors and bipolar cells. These cells respond with graded hyperpolarizations to light stimuli (regardless of wavelength), with the amplitude and duration of the response depending on the intensity and duration of the stimulus (Svaetichin & MacNichol, 1959). The HII/A- or C-type cells only connect with cones, thus contributing to color and fine detail perception. HII/A- or C-type horizontal cells respond with different polarity to light stimuli of different wavelengths; for example, they may respond with graded depolarization to red light stimuli and with graded hyperpolarization to yellow, green, and blue stimuli. Surprisingly, the HII/A-like cells in the horse seem only to contact S-cones (Sandmann et al., 1996), which precludes color opponency.

Thus, the two types of horizontal cells serve to modulate the antagonistic center-surround receptive fields of bipolar cells, normally contributing to both their spatial and color opponency properties. Furthermore, the receptive field of horizontal cells may extend outside their dendritic fields via electric coupling through gap junctions between horizontal cells (Chapot et al., 2017).

Bipolar cell somata are also located in the INL. Their dendrites synapse with photoreceptors and horizontal cells in the OPL (see Fig. 4.22), and their axons terminate in the inner plexiform layer (IPL), where they synapse with amacrine and ganglion cells. There are several ways to classify bipolar cells. Anatomically, bipolar cells (bipolars) are divided based on whether they synapse with rods or with cones. Because most species have more rods, *rod bipolars* are numerically superior to *cone bipolars*. Only one type of rod bipolar has been described in mammals. As each rod bipolar cell can receive input from numerous rods, the rod pathway has been described as a *convergent pathway* with large receptive fields (the *receptive field* of a bipolar cell is the sum of the receptive fields of the photoreceptors from which it receives input; Fig. 4.26). Such a pathway enhances scotopic vision, because the absorption of just one photon anywhere in the receptive field is sufficient to stimulate the rod bipolar pathway.

The number of cone bipolar types in species carefully studied, such as the macaque, mouse, and rabbit, seems to be about 11–12 (Euler et al., 2014; Tsukamoto & Omi, 2016; Wässle et al., 2009). In the primate fovea, *midget bipolars* typically synapse only with one M- or L-cone in a one-to-one relationship (Jusuf et al., 2006; Wässle et al., 1994). Since each midget bipolar cell receives input from just one cone, it will have a much smaller receptive field, and form a *nonconvergent pathway* (Fig. 4.27). This feature, combined with the antagonistic center-surround properties of the receptive fields that is thought to be established at the bipolar cell level (Dacey et al., 2000), contributes to the higher visual resolution that characterizes the cone system. *Diffuse cone bipolars* receive input from as few as a handful of cones in the central retina, and as many as 20 cones in the peripheral retina. Thus, diffuse cone bipolars function much like rod bipolars, converging input from several cones, but their role in retinal processing is still largely elusive, although progress has been made (Hoon et al., 2014).

Bipolar cells are the first visual neurons exhibiting spatial organization of their receptive fields. The cells respond with opposite-voltage polarity to light stimuli illuminating either the center or the surround of the receptive field. The interactions between horizontal cells and photoreceptors that underlie this organization of spatial opponency organization are illustrated in Fig. 4.28. Specifically, direct input from photoreceptors is believed to contribute to the central response of bipolar cells, while the horizontal cells form the antagonistic surround component through modulation of photoreceptor synaptic output.

Therefore, another way of classifying bipolar cells is on the basis of the response generated by light stimulation of their central receptive field. "ON-center" cells are activated (depolarized) when their center is stimulated by light, whereas "OFF-center" cells are inhibited (hyperpolarized) in response to light stimulation in the central field.

The peripheral (i.e., toroidal) receptive field of these cells is antagonistic to the center. Thus, for example, an ON-center bipolar cell will also have OFF-surround properties and will activate (depolarize) when light is turned off in the surrounding field. Therefore, when both the central and peripheral fields of an ON-center–OFF-surround bipolar cell are stimulated by light, the central field will depolarize, and the peripheral field will hyperpolarize. The result is decreased responsiveness by the cell, because the response of the periphery will inhibit the response of the center.

However, if an OFF-field is inhibited (hyperpolarized) by light, it follows that it is activated (depolarized) by darkness. Therefore, if the same ON-center–OFF-surround bipolar cell was presented with a small light stimulus in its central field and an adjacent dark stimulus in its peripheral field, the net result would be an enhanced response, as both fields respond with activation and depolarization to their respective stimuli. This enhanced responsiveness to small, adjacent light and dark stimuli is the cornerstone of high-resolution vision.

In addition to enabling spatial center-surround antagonism, horizontal cell modulation also allows chromatic antagonism. For example, based on horizontal cell feedback, it is possible to have a red-OFF green-ON bipolar cell. Such a cell responds with hyperpolarization to red stimuli and with depolarization to green stimuli. This color opponency is generated by different types of inputs from different types of cones, in this case excitatory input from the red cones and inhibitory input from the green cones, forming the first step in chromatic visual processing.

Other Inner Nuclear Layer Cells

The INL is populated by three more types of cells, in addition to some displaced RGCs. Little is known about the *interplexiform cells*, which are neurons with processes in both the

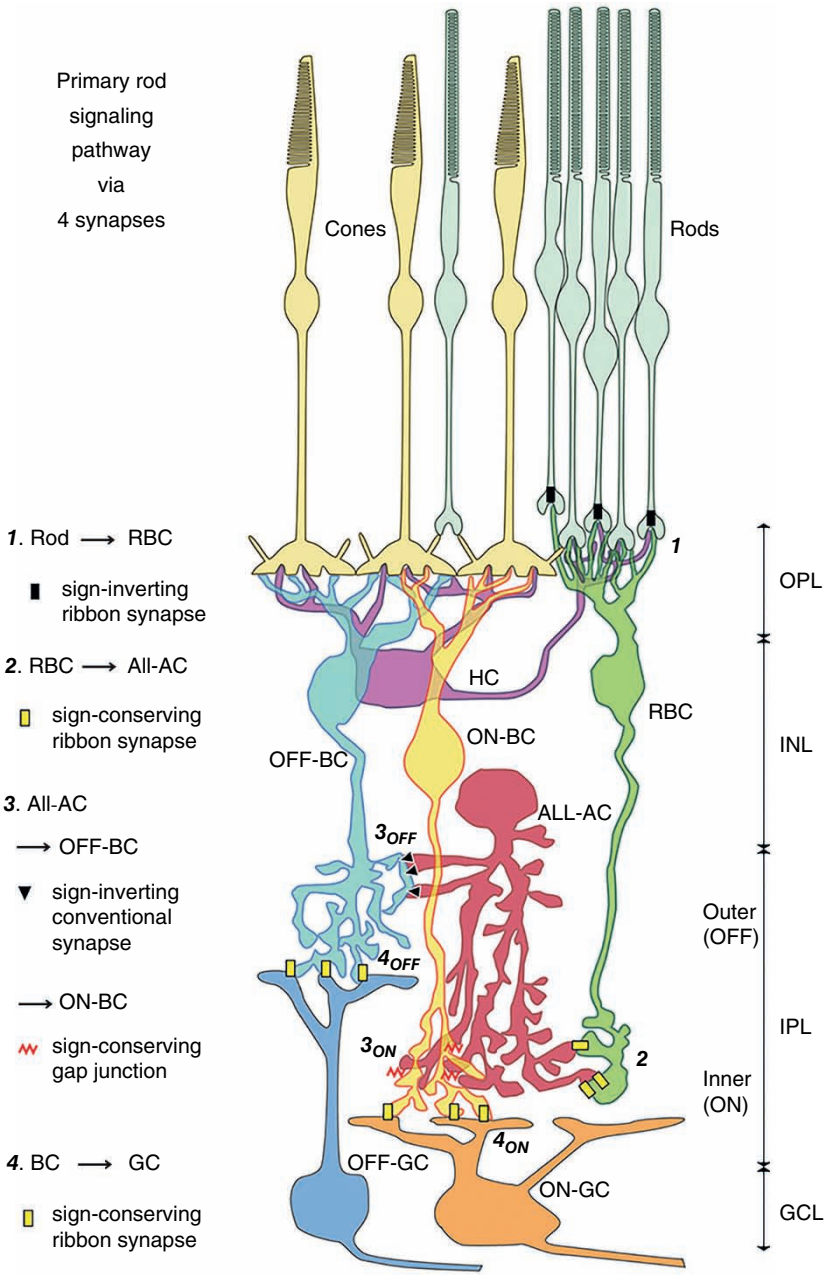

Figure 4.26 The primary rod pathway is indirect and more convergent than that of cones. A group of rods connect to a rod bipolar cell (RBC), whereas the cones connect to both ON- and OFF-cone bipolars. Furthermore, the rod signal has to pass via the amacrine and cone bipolar cells before reaching the ON-ganglion cell, whereas the cone bipolar cells synapse directly to the ganglion cells. GCL, ganglion cell layer; INL, inner nuclear layer; IPL, inner plexiform layer; OPL, outer plexiform layer. (Reproduced with permission from Tsukamoto, Y. & Omi, N. (2017) Classification of mouse retinal bipolar cells: Type-specific connectivity with special reference to rod-driven AII amacrine pathways. *Frontiers in Neuroanatomy*, **11**, 92. doi: 10.3389/fnana.2017.00092. Licensed under CC BY 4.0.)

OPL and the IPL. In the OPL, they are presynaptic to bipolar cells. In the IPL, they are pre- and postsynaptic to amacrine cells, and presynaptic to bipolar cells. Thus, it believed that they may modulate the synaptic gain between photoreceptors and their second-order neurons (Jiang et al., 2014).

Müller cells are another class of cells found in the INL, and they are the main glial cells of the retina (de Melo Reis et al., 2008; Kofuji et al., 2000; Vecino et al., 2016). Müller cells are ependymoglial cells, meaning they have both a structural support and a metabolic role. Their perikarya are located in the INL, but they extend long processes toward the inner and outer retina, where they join to form both the inner and outer limiting membranes. Therefore, the Müller cells can be regarded as retinal radial cells, extending

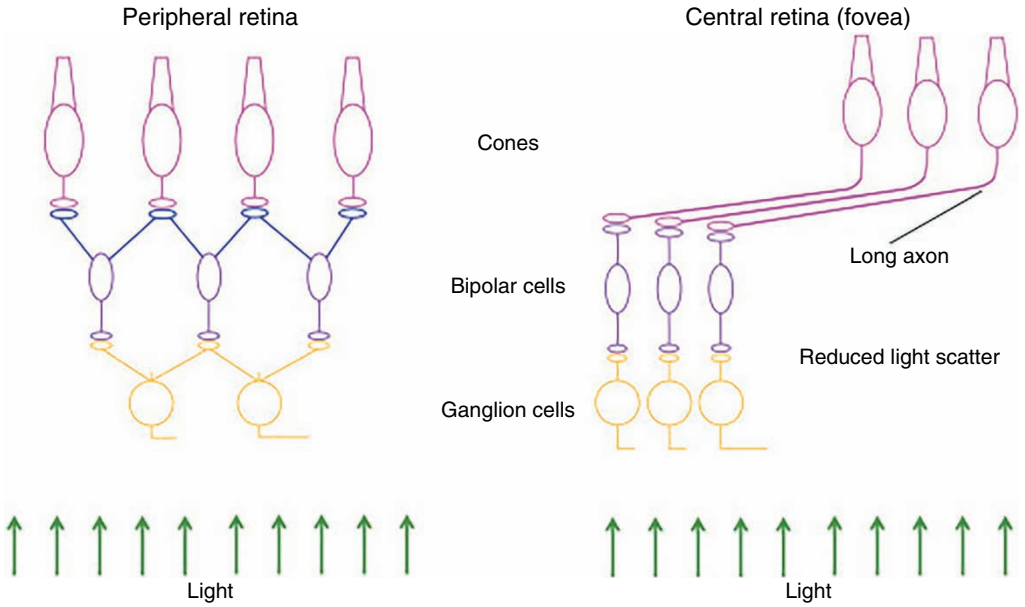

Figure 4.27 Cone pathways in the central (foveal) and in the peripheral primate retina. In the fovea, each cone photoreceptor has a private line to one retinal ganglion cell. In the peripheral retina, there is progressive convergence of several cones onto a bipolar cell. Furthermore, the long axons of the foveal cones allow light to reach the outer segment without having to pass through the neurons of the inner retina. Both of these specializations increase the resolution of details. (Reproduced with permission from Masland, R.H. (2017) Vision: Two speeds in the retina. *Current Biology*, **27**(8), R303–R305. doi.org/10.1016/j.cub.2017.02.056.)

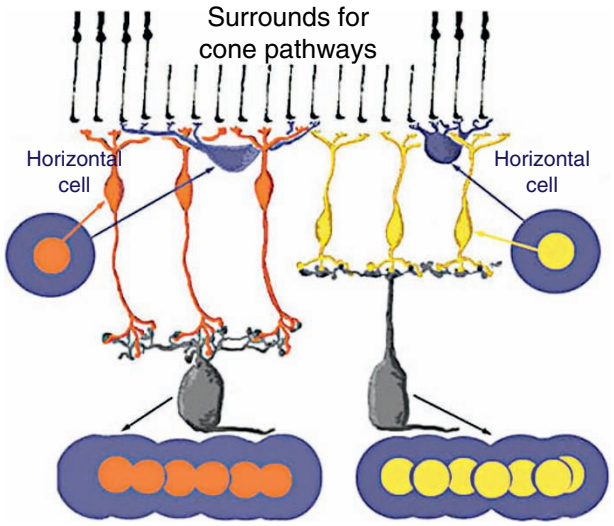

Figure 4.28 Center-surround antagonism of bipolar (and consequently ganglion) cells is due to modulation by horizontal cells. A central stimulus is relayed directly from cones (in black), through a yellow or orange bipolar cell onto a gray ganglion cell. A peripheral stimulus is relayed through an inhibitory horizontal cell (in purple). The resulting receptive fields are depicted at the bottom, with stimulated centers (yellow or orange) and inhibited surround (bluish-violet). (Reproduced from *Cone Pathways through the Retina*, WebVision, Moran Eye Center (http://webvision.med.utah.edu) with permission of Dr. Helga Kolb. Used under CC BY.)

through the retina's entire thickness and lending it architectural support. Müller cells also fill in all gaps in the neuroretina not occupied by other elements. Thus, their processes encircle intraretinal blood vessels and RGC axons in the nerve fiber layer. They also sheath dendritic processes, isolating them chemically and electrically, and surround the individual photoreceptors, insulating them from each other and keeping them properly aligned. Recently, it has also been shown that Müller cells have a circadian clock function (Xu et al., 2016).

Metabolically, Müller cells synthesize and store glycogen, which helps protect the retina from fluctuations in systemic glucose levels. These cells also help to maintain the anionic balance in the retina by taking up the K^+ secreted by the photoreceptors. Müller cells remove the excess K^+ from the retina, thus acting as a "K^+ sink" and contributing to the generation of the ERG b-wave. Müller cells are also active in uptake and metabolism of neurotransmitters, including γ-aminobutyric acid (GABA), dopamine, and glutamate (Bringmann et al., 2013). In pathophysiologic conditions, they can become activated by inflammatory mediators, and contribute to the immune response of the retina following injury (Bringmann et al., 2009). In mammals, their ability to reacquire a retinal progenitor state and regenerate neurons after retinal damage is very limited (Hamon et al., 2016).

Amacrine cells, which are the last type of INL cells, occupy the innermost tier of this layer, though displaced amacrine cells are also found in the ganglion cell layer (Klump et al., 2009; Lee et al., 2016b; Masland, 2012; Weltzien et al., 2015). Morphologically, more than 30 types of amacrine cells have been identified in the mammalian retina. They are characterized by the fact that they do not possess any recognizable axons, and they are classified by the size (i.e., narrow, small, medium, and wide) and shape of their dendritic tree (e.g., linear, beads, starburst), or by the neurotransmitter they release (e.g., acetylcholine, serotonin, dopamine). However, as the IPL is traditionally divided into five strata, the most widely used classification of amacrine cells is based on the IPL strata in which their dendritic tree is found.

Amacrine cells are known to be inhibitory neurons containing the common inhibitory neurotransmitters GABA or glycine, but they also excite bipolar and ganglion cells through gap junctions and possibly glutamate release (Marshak, 2016; Nath & Schwartz, 2017; Roy et al., 2017). The cells form very complex networks of connections with bipolar axon terminals, with RGC dendrites, and with other types of amacrine cells (Fig. 4.29). Each type of amacrine cell seems to be functionally charged with specific tasks in the retina. The amacrine cells create contextual effects for the responses of RGCs, including the center-surround antagonism enhancing motion detection relative to a background, but also mediate gain control (Grimes et al., 2010) and alter the kinetics of the bipolar cell output (Sagdullaev et al., 2011). Some of them also exchange information between the layers of the IPL, thus sending signals between the ON- and OFF-strata. Hence, amacrine cells such as the AII cell contribute to both lateral and vertical communications in the retina (Fig. 4.30).

Amacrine cells are the target cells of centrifugal fibers from higher cortical centers, which further modulate the retinal responsiveness in birds and nonmammalian species. It is still unknown whether amacrine cells also are targeted in mammals.

Ganglion Cells

All information processed by the retina eventually converges on the RGCs, the innermost cell layer in the retina, and its final-order output neuron. Though much signal processing has already occurred in the vertical (photoreceptor to bipolar to RGC) and in the lateral (photoreceptor to horizontal cell to bipolar to amacrine to RGC) pathways, the RGCs are the most complex information processing cells in the retina (Schiller, 2010). To date, more than 30 functionally-distinct classes of RGCs have been described in the mouse (Baden et al., 2016). This means that even in the mouse, the data obtained and processed in the retina is sent to the brain in a rather large number of parallel output channels providing information about different features of the visual scene.

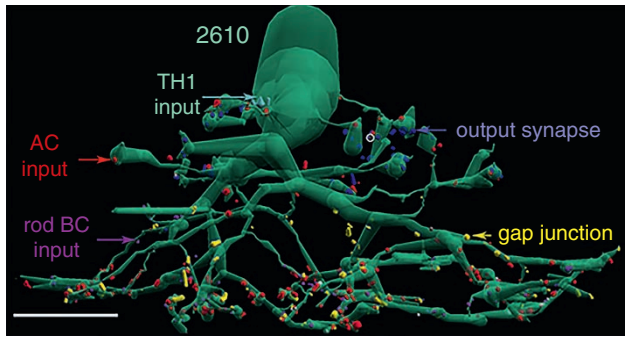

Figure 4.29 Amacrine cells (AC) form complex networks with other retinal neurons. Each colored dot represents a contact between this AII cell (labeled no. 2610) and other cells. Synapses with its rod bipolar are shown in magenta. Yellow gap junctions form electrical contacts with adjacent cells, such as cone bipolar cells (BC). A single ribbon synapse with a cone OFF-bipolar cell is marked with a white circle. Inputs from other amacrine cells are shown in red and the cyan inputs come from a tyrosine hydroxylase (TH-1) immunopositive interneuron. Glycinergic synaptic outputs from this AII cell are labeled blue. Scale bar: 10 µm. (Reproduced with permission from Marc, R.E., Anderson, J.R., Jones, B.W., et al. (2014) The AII amacrine cell connectome: A dense network hub. *Frontiers in Neural Circuits*, **8**, 104. doi: 10.3389/fncir.2014.00104. Used under CC BY.)

Traditionally, ganglion cells have been classified in three ways:

1) *Morphology*. Morphologic classification schemes have been used extensively. RGCs have been subdivided into classes such as the α-, β-, and γ-cells in cats (Boycott & Wässle, 1974). Later these classes have been further subdivided according to more detailed analysis of the cell's microcircuitry (Kolb et al., 1981; Masri et al., 2019; Rockhill et al., 2002). Midget ganglion cells in primates (corresponding to β-cells in the cat) are located in the central retina, and the small size of these cells permits denser packing, thus allowing each to receive input from fewer cones and bipolars. In species with high-resolution vision, the functional ratio of cones and bipolar cells to β-ganglion cells approaches 1:1:1 in the foveal region. Larger (α) ganglion cells are found in the more peripheral retina, and their large size permits convergence of input from many amacrine cells. Axonal diameter is proportional to the somata size; therefore, central β-cells possess smaller-diameter axons than peripheral α-cells. More recently, specific markers for individual RGC classes and molecular genetic techniques have been employed to characterize and subdivide the RGCs (Badea & Nathans, 2011; Kim et al., 2010; Siegert et al., 2009; Sweeney et al., 2019).
2) *Physiologic responses*. Physiologic classifications according to the responses generated by the RGC, which of course depend on the input the cell receives, have also been elaborated (Enroth-Cugell & Robson, 1984; Zeck &

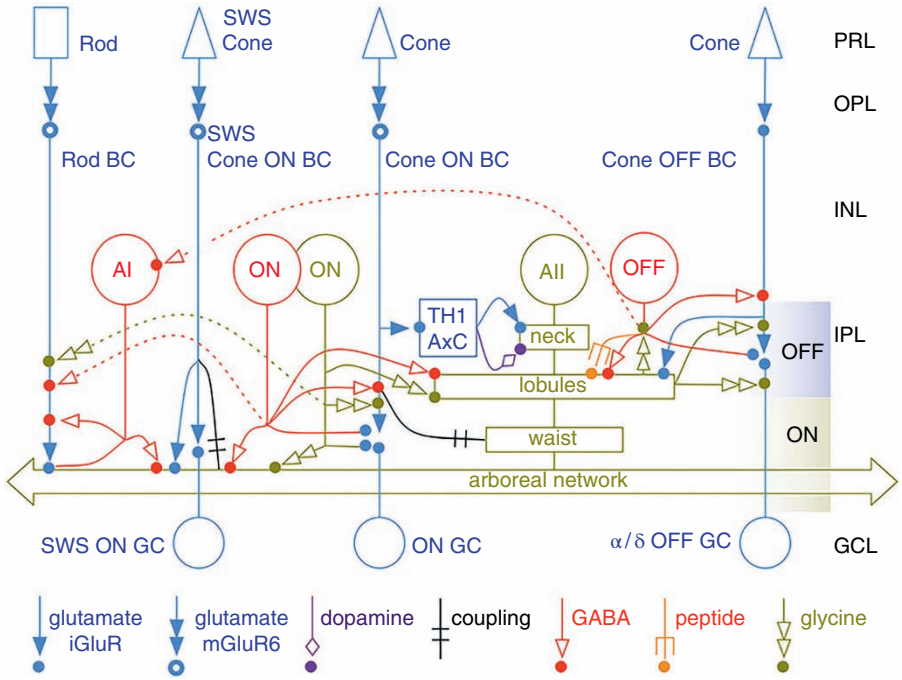

Figure 4.30 The intricate amacrine AII network contributes to both horizontal and vertical communication in the retina. The AII cell is subdivided into five parts, with the nucleus in the inner nuclear layer (INL) and the lower four representing the dendritic tree in different strata of the inner plexiform layer (IPL). The neck and lobule in the OFF-layer of the IPL do not overlap with neighboring AII cells, whereas the waist and arboreal network in the ON-layers do. The inputs to this AII cell include four types of excitatory glutamate inputs: gap junctions (electrical coupling) between cells, dopaminergic and peptide modulation, inputs from three types of wide-field GABAergic cells, and glycinergic inputs from narrow-field cells. The AII cell outputs to OFF-bipolar cells and OFF-inhibitory neurons and two types of OFF retinal ganglion cells (RGCs). Different types of pure cone bipolar cells (CBs) are lumped into single ON- and OFF-channels, as well as multiple types of ON- and OFF-amacrine cells lumped into single representative classes in the drawing. The dashed lines show cone -> rod suppressive crossover pathways. TH_1AxC shows a glutamate/dopaminergic wide-field axonal cell. GCL, ganglion cell layer; OPL, outer plexiform layer; PRL, photoreceptor layer; SWS cone, short wavelength-sensitive (blue) cone. (Reproduced with permission from Marc, R.E., Anderson, J.R., Jones, B.W., et al. (2014) The AII amacrine cell connectome: A dense network hub. *Frontiers in Neural Circuits*, **8**, 104. doi: 10.3389/fncir.2014.00104. Used under CC BY.)

Masland, 2007). Most RGCs receive input directly from bipolar cells. Therefore, the receptive fields of these cells function in a manner similar to those of their associated bipolar cells (i.e., ON-center–OFF-surround, or vice versa). These cells are called X-cells and correspond to the cat β-cells. Other RGCs (i.e., Y-type) receive input mainly from amacrine cells. RGCs are also subdivided according to their ability to detect motion in a certain direction or respond better to elongated stimuli that have a certain orientation. Motion-responsive RGCs that are directionally selective respond to stimuli moving in a preferred direction and may be completely inhibited by movement in other directions (Fig. 4.31; Borst & Euler, 2011; Fried et al., 2002). Some cells respond better to bar-shaped stimuli that have a certain angular orientation (pointing in a particular direction like a hand on a clock) and are consequently called orientation selective (Antinucci et al., 2016; Levick, 1967). RGCs are also classified on the basis of the cell to which they output. M-ganglion cells synapse in the magnocellular layers of the lateral geniculate nucleus (LGN), and P-ganglion cells terminate in the parvocellular layers. The function of the heterogenous group of K-cells synapsing in the koniocellular layer is less well understood, but the K-ganglion cells are reported to convey blue color signals and respond to rapid movements (Percival et al., 2014).

3) *Information processing*. The luminance (magnocellular) pathway both processes and relays information regarding changes in light levels and motion. The resolution (parvocellular) pathway processes information pertaining to fine details and the color of the stimulus.

Obviously, these classifications are not exclusive; rather, they constitute different descriptions of the same cells. The β-, X-, or parvo-cells are numerous, small cells that receive input from cone systems and bipolar cells. They can further be subdivided into additional types, but all have a small diameter in common, and therefore the slower-conducting axons of these cells transmit information on stimulus wavelength (color) and fine detail. The different types of RGCs

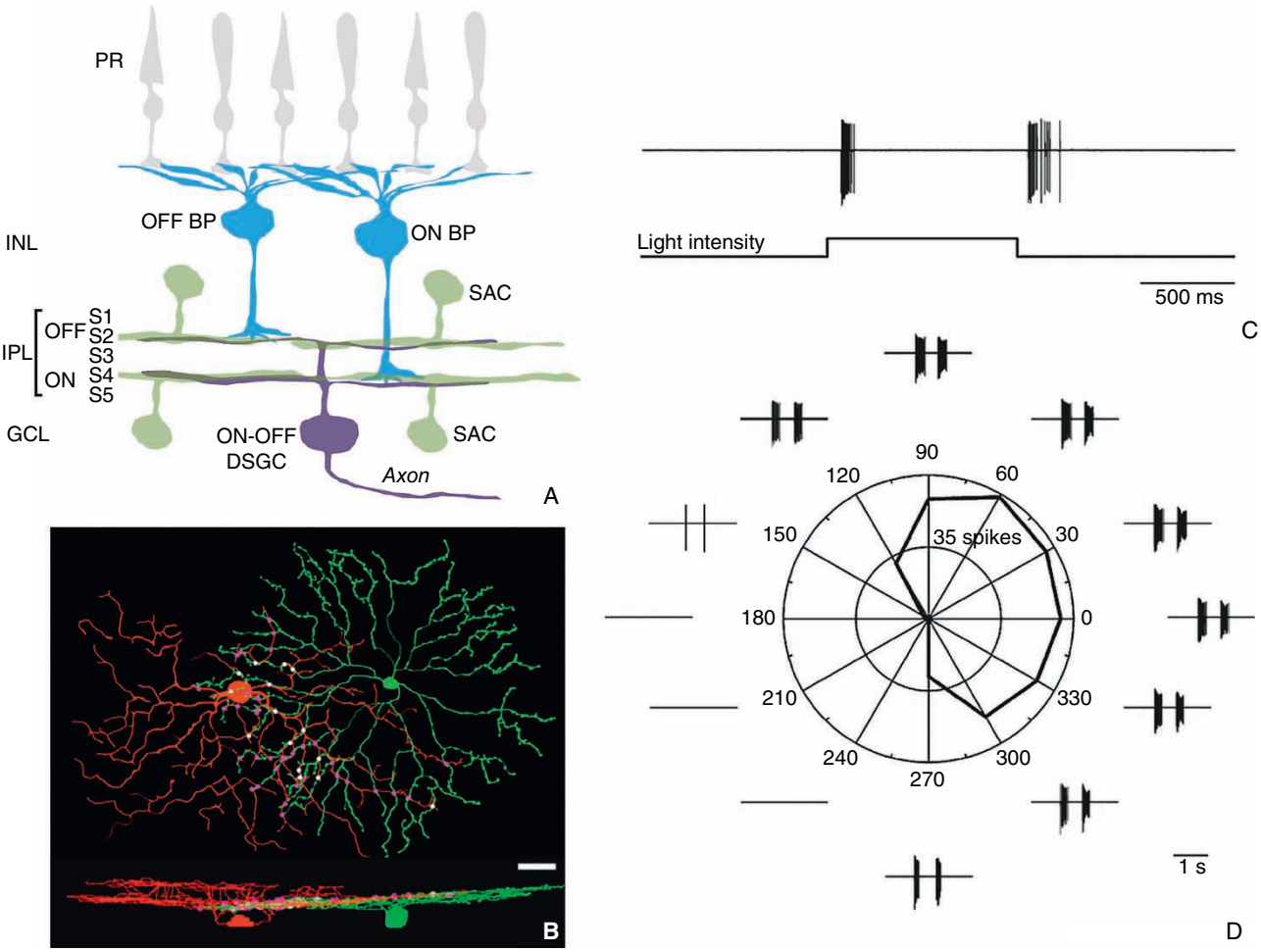

Figure 4.31 **A**. A mammalian ON–OFF direction-selective ganglion cell (DSGC) fed by ON- and OFF-bipolar cells (BP) that relay signals from photoreceptors (PR). The DSGC has a bistratified dendritic arbor in sublaminae (S) 2 and 4 of the inner plexiform layer (IPL). Two mirror symmetric populations of starburst amacrine cells (SAC) with their nuclei in the inner nuclear layer (INL) and ganglion cell layer (GCL, where they are often termed "displaced amacrine cells") modulate the signals to the DSGC. **B**. Reconstruction of contacts between a DSGC (red) and an SAC (green). Dots show dendritic contacts with putative GABAergic contacts (cofasciculation segments) on the null side in white and the rest in purple (scale bar 25 μm). **C**. Responses from recordings of an ON–OFF DSGC to a flashing spot of light. Both the onset of the light stimulus and the cessation of the stimulus trigger short bursts of spikes in this phasic cell. **D**. Recordings from the same ON–OFF DSGC in response to a bar moving in 12 different directions. Movement in the preferred directions elicits brisk bursts of spikes, whereas the cell is silent or responds very weakly when the bar is moved in nonpreferred directions. (Reproduced with permission from Wei, W. & Feller, M.B. (2011) Organization and development of direction-selective circuits in the retina. *Trends in Neuroscience*, **34**, 638–645. doi: 10.1016/j.tins.2011.08.002.)

lumped together as α-, Y-, or magno-cells are fewer in number and larger in size; these cells receive input from rod systems and amacrine cells. Their larger-diameter and faster-conducting axons relay information on subtle changes in illumination levels (i.e., contrast) and stimulus motion (i.e., temporal resolution). These cells are characterized by transient (phasic) responses, as compared to the more sustained (tonic) responses of the β-cells.

About 3%–5% and 45%–50% of the feline RGCs can be classified as α- and β-cells, respectively. They are arranged in regular, superimposed mosaics across the entire retina. Both OFF-center and ON-center classes of α- and β-cells are arranged in a paired manner, so that an ON/OFF pair receives inputs from almost the same retinal region. Naturally, both cell types have their smallest dendritic tree sizes at the area centralis. The dendritic tree size increases (and RGC density decreases) with retinal eccentricity, and consequently peripheral RGCs extend over 10× larger areas than those in the area centralis. Most of the axons of both types of cells terminate in the LGN, with only a few collateral fibers synapsing in the superior colliculus.

The remaining balance of the feline RGCs is classified morphologically as γ- (gamma) or δ- (delta). The γ-cells, also classified as W-cells, have small somata and axons, but their

response to light can be either sustained or transient. They serve in cone systems and contribute to high-resolution photopic vision. There are more than 20 types of δ-cells, classified as G4—G23 based on their size. Half of these cells project to the superior colliculus rather than to the LGN.

RGCs usually have an intrinsic, basal firing rate in darkness. Changes in the number of spikes in response to light or darkness are similar to those of the associated ON- or OFF-bipolar cells, and amacrine cells, with which they synapse in the IPL. Thus, an ON-center–OFF-surround RGC will respond to a light stimulus in the center of its receptive field with depolarization and a vigorous train of impulses due to input from its associated ON-bipolar cells (see Fig. 4.32A–C). On the other hand, a stimulus in the surround will actively inhibit the same RGC by hyperpolarizing its membrane based on input from its associated OFF-bipolar and amacrine cells (see Fig. 4.32). Conversely, OFF-center cells, which are excited at light offset in their center, have regions in the peripheral receptive field where ON excitation is evoked by light onset. As in the case of the bipolar cells, the result is a high degree of contrast perception between central and peripheral stimuli.

This antagonistic center–surround receptive field organization of RGCs is also used to code additional information about the stimulus. For example, amacrine cell modulation allows direction-selective RGCs to respond to stimuli moving in a preferred direction (see Fig. 4.31). Color opponent RGCs will change their firing rate in response to different colors. For example, in a red-OFF–green-ON center RGC, green light will excite the cell and evoke impulses, while red light will inhibit discharges (Fig. 4.33). The same cell will also have reciprocal red-ON–green-OFF surround properties. At the same time, additional RGCs code other features about the stimulus, including its size, contrast, orientation, and speed of movement.

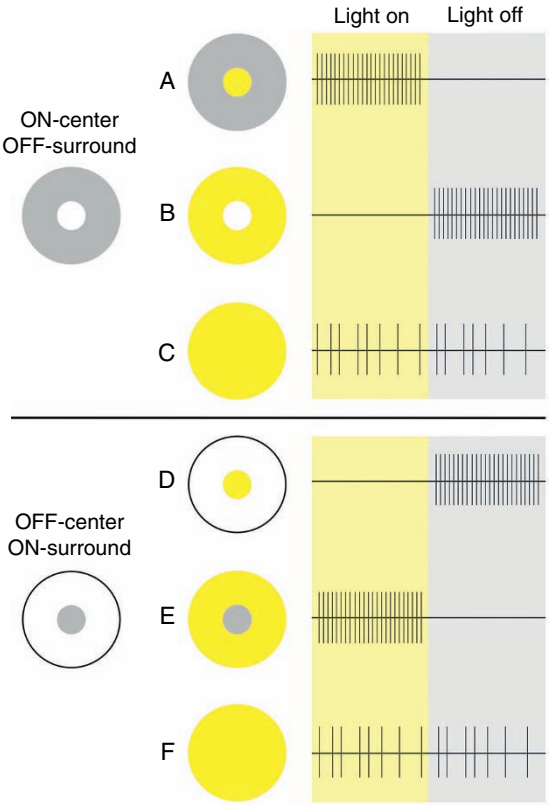

Figure 4.32 The upper half shows responses of an ON-center OFF-surround retinal ganglion cell (RGC). In (**A**), only the ON-center is stimulated by light (yellow) and a tonic train of spikes is seen throughout the stimulus. When the center is in the dark (gray) and only the surround is stimulated by an annulus of light, the cell is inhibited and starts firing first at the cessation of the annular stimulus (**B**). When both the center and surround are stimulated by light simultaneously (**C**), the RGC is spiking much less frequently because the excitatory signals from the center are counteracted by the inhibitory ones from the surround. Panels (**D**) through (**F**) show responses from an OFF-center ON-surround RGC.

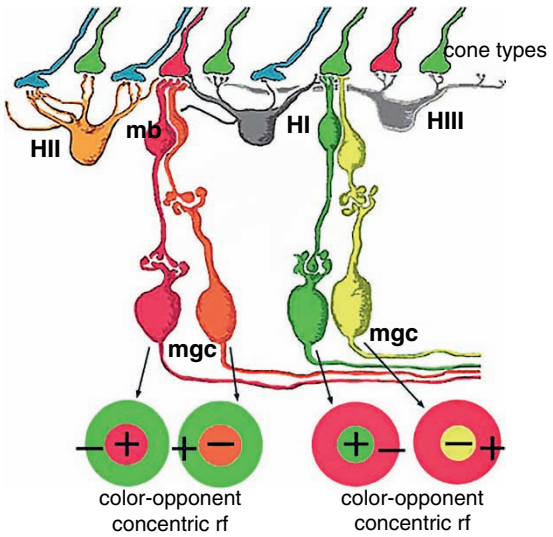

Figure 4.33 Schematic drawing of color opponent circuits in the primate fovea. A long wavelength-sensitive cone (in red; L) contacts an ON-midget bipolar cell (red mb), which connects to a L-cone midget RGC (red mgc). The same L-cone also connects to an OFF-midget bipolar cell and RGC (both in orange). Thus, an L-cone ON- (red center and green surround) and an L-cone OFF-center receptive field ganglion cell (orange center and green surround) are generated. Further to the right, a middle wavelength-sensitive cone (in green; M) is connected in a similar manner creating green ON- and OFF-receptive fields, respectively. Horizontal cells (HI through HIII) can contribute the surrounds to the L-cone center bipolar cells. (Reproduced from *Midget Pathways of the Primate Retina Underlie Resolution and Red Green Color Opponency*, WebVision, Moran Eye Center (http://webvision.med.utah.edu) with permission of Dr. Helga Kolb. Used under CC BY.)

Intrinsically Photosensitive/Melanopsin-Expressing Retinal Ganglion Cells

In 1998, a high level of expression of another vitamin A-based opsin, melanopsin, was identified in non-photoreceptor cells in the frog retina (Provencio et al., 1998). Later, it was found that the melanopsin was expressed in a subset of RGCs with small somata, but large, sparsely branching dendritic fields (Nasir-Ahmad et al., 2019). These intrinsically photosensitive RGCs (ipRGCs) were mainly projecting to the hypothalamic suprachiasmatic nucleus (SCN), but also targeting the geniculate and the olivary pretectal nuclei (Hattar et al., 2002). Axons reaching other centers in the brain, including the superior colliculus, have been described more recently. The ipRGCs constitute up to 3% of the total RGC count. To date, six classes of ipRGCs have been identified in the mouse, whereas primates are considered to have three classes (Fig. 4.34; Hughes et al., 2016; Quattrochi et al., 2019; Sexton et al., 2012). Different types of ipRGCs appear to have both different response characteristics and, at least in part, project to different areas in the brain.

Melanopsin uses the same chromophore as cones and rods, 11-*cis*-retinal, and has a peak absorbance in the blue part of the spectrum at about 480 nm. Phylogenetic analysis indicates that mammalian melanopsin is more closely related to the invertebrate opsins than the classical vertebrate visual opsins (Provencio et al., 1998). The phototransduction cascade driven by photoactivation of melanopsin is also different from that of cones and rods (Hughes et al.,

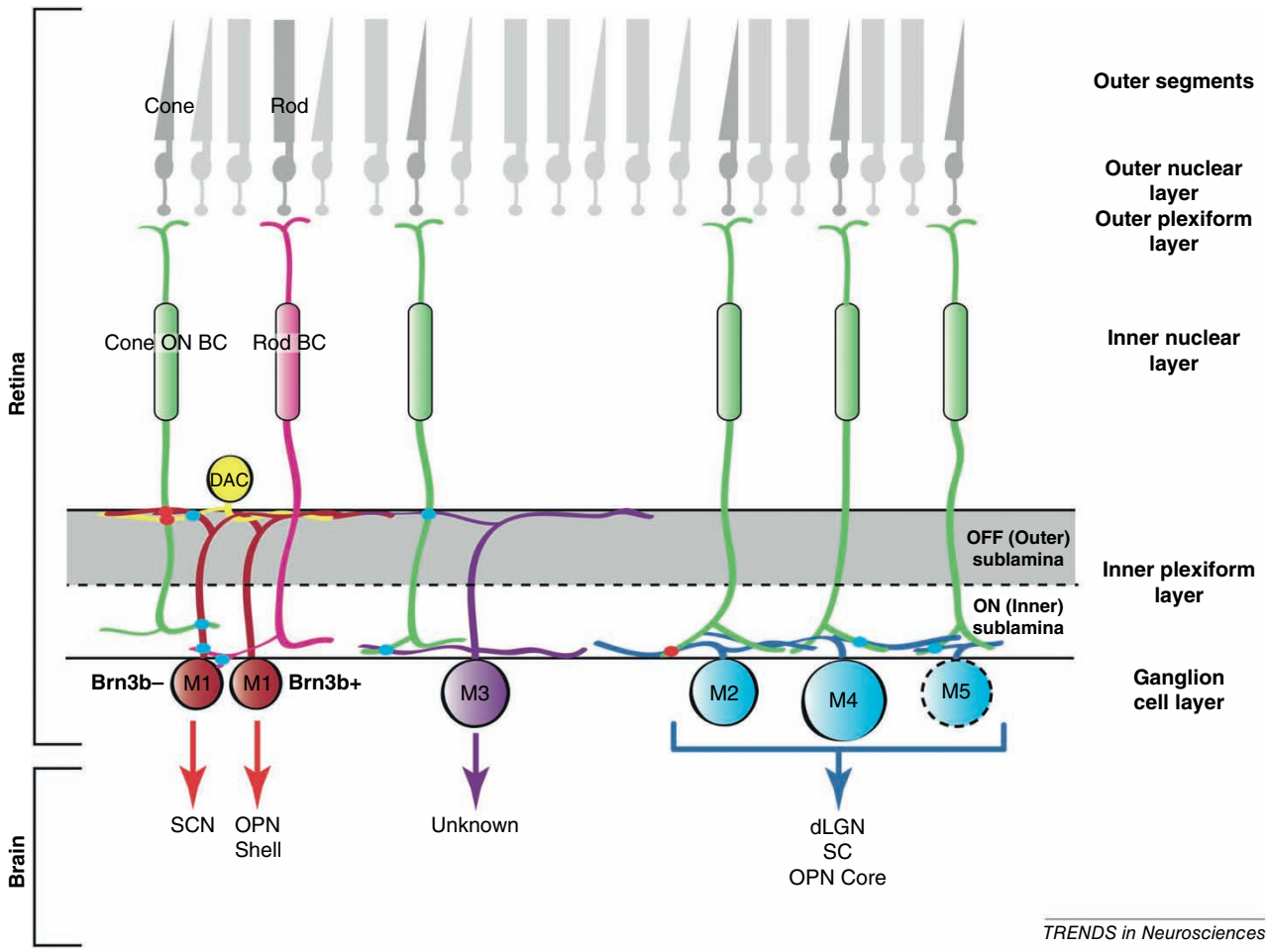

Figure 4.34 So far six distinct subtypes of intrinsically photosensitive retinal ganglion cells (ipRGCs) have been identified in the mouse (M1–M6). This figure briefly outlines the input to and targets of the first five ipRGCs. Their nuclei make up a small fraction of those seen in the ganglion cell layer of the retina (and occasionally displaced into the inner nuclear layer) and subtypes have different dendritic patterns and primary nonimage or image-forming targets in the brain. They also differ in size, with the M1 being small and the M4 having large soma. Dots indicate synapses with other retinal cells. BC, bipolar cell; DAC, dopaminergic amacrine cell; dLGN, dorso-lateral geniculate nucleus; OPN, olivary pretectal nucleus (for pupillary light reflexes); SC, superior colliculus; SCN, suprachiasmatic nucleus (for circadian photoentrainment). It has been suggested that M1 cells can be further subdivided according to their expression of the transcription factor Brn3b. (Reproduced with permission from Schmidt, T.M., Chen, S.K., & Hattar, S. (2011) Intrinsically photosensitive retinal ganglion cells: Many subtypes, diverse functions. *Trends in Neuroscience*, **34**, 572–580. doi: 10.1016/j.tins.2011.07.001.)

2012). It seems to start with activation of special G-proteins that in turn activate the enzyme phospholipase C (PLC), which leads to an influx of Ca^{2+} through transient receptor potential (TRP) channels in the cell membrane of the ipRGCs and generation of action potentials. However, the melanopsin density in ipRGCs is about 10^4 less than that of cone and rod opsins (Do et al., 2009). This implies a low probability of photon catch, which is why the phototransduction in ipRGCs mainly plays a role in relatively bright light. However, ipRGCs are not only depolarized by the activation of melanopsin by light, but also by input from circuits driven by cones and rods (Fig. 4.35; Weng et al., 2013). This expands the dynamic range and spectral sensitivity of responses driven by or through ipRGCs.

IpRGCs may play a role in image-forming vision, but most of their important functions are non-image-forming (Feigl & Zele, 2014). Their input to the SCN is essential for the body's circadian clock, whereas ipRGC axons to the intergeniculate leaflets contribute to the entrainment of the circadian rhythm. Projections to the ventrolateral preoptic nucleus are likely to play a role in the control of sleep, and ipRGCs' signals to the pretectal olivary nucleus contribute to the pupillary light reflexes (PLRs) and the sustained constriction after offset of bright, short-wavelength lights. This is why Keeler could detect PLRs in blind mice (Keeler, 1927). Furthermore, ipRGCs have been reported to be less vulnerable than other RGCs in some diseases (such as Leber's hereditary optic neuropathy), but are susceptible to other neurodegenerative diseases, such as glaucoma (Georg et al., 2017).

Retinal Synapses and Neurotransmitters

Obviously, with so many different types and classes of retinal cells, there are numerous potential pathways for transferring a signal from the photoreceptors to the RGC axons. Furthermore, new cell types, projections, and synapses are constantly being discovered.

The rod spherules and cone pedicles contain *synaptic invaginations*, in which one bipolar and two horizontal cells synapse and together form the *synaptic triad* (see Fig. 4.22). Photoreceptors usually have more than one synaptic invagination. A typical rod synapses with two triads, and a cone may have multiple contacts with three or more bipolar cells. The cone pedicle with its 20–50 presynaptic ribbons and up

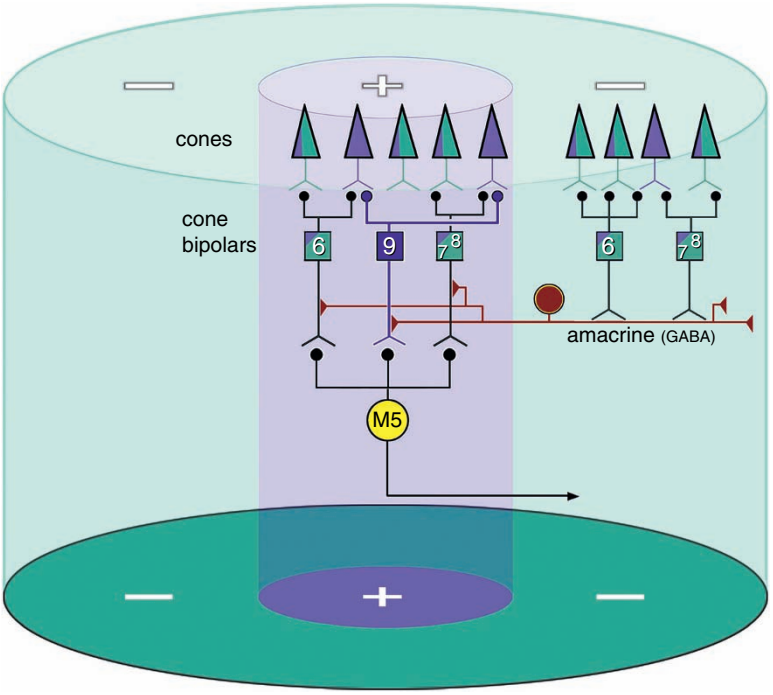

Figure 4.35 The M5 intrinsically photosensitive retinal ganglion cell (ipRGC; yellow) contains light-sensitive melanopsin, but can also be driven by the ultraviolet (UV-; violet) and M-cone (green) opsin in murine cones. In the mouse, most cones coexpress both opsins, but some only one opsin. Cone signals are relayed to the M5 cell through different subtypes of cone bipolar cells (numbered 6 through 9). In the center, the M5 cell receives input through all bipolar cell subtypes, including type 9, which contact pure UV-cones. A wide-field GABAergic amacrine cell (red) selectively samples type 6–8 bipolar cells and can thus create surround with cones relatively better driven by green light than the more UV-sensitive center. Hence, the M5 cell can send both chromatic opponent signals to the latero-dorsal geniculate nucleus of the mouse and signals driven by activation of the melanopsin in the ganglion cell itself. (Reproduced with permission from Stabio, M.E., Sabbah, S., Quattrochi, L.E., et al. (2018) The M5 cell: A color-opponent intrinsically photosensitive retinal ganglion cell. *Neuron*, **97**, 150–163.e4. doi: 10.1016/j.neuron.2017.11.030.)

to 500 contacts to postsynaptic cells is considered to be the most complex synapse in the central nervous system (CNS; Haverkamp et al., 2000). In addition, photoreceptors send out processes to neighboring spherules and pedicles, thus providing for direct electrical junctions between photoreceptors. Because of these couplings, current can spread between adjacent photoreceptors. Therefore, the stimulation of a single rod can activate other photoreceptors, resulting (once again) in the large receptive field that converges on the bipolar cell. These junctions also allow rod signals to be transmitted through cone pathways when the light is so dim that the cones are unable to respond (see Fig. 4.26).

Traditionally, the retina has been considered to have two pathways conveying signals from the photoreceptors: the cone pathway and the rod pathway (see Fig. 4.26). The *cone pathway* typically is short, involving only two types of synapses: cone to bipolar cell to RGC, lateral processing provided by horizontal and amacrine cells in the OPL. Even though it is shorter than the rod pathway, the cone pathway is also complex, as it provides two parallel channels of processing, ON- and OFF-center (Wässle, 2004). This dichotomy is made possible by the fact that bipolar cells can respond to light and subsequent cone hyperpolarization with either depolarization (ON-center bipolar cell) or hyperpolarization (OFF-center bipolar cell; see Fig. 4.30). However, it is clear that the cone and rod pathways are more complex than outlined above and not as distinctly separated as previously believed (Pang et al., 2010; Strettoi et al., 2010). Hence, some rods contact cone bipolars and cones synapse with rod bipolars, but for enhancing the basic understanding of the retinal circuitry, the presentation has been restricted to the more traditional pathways of cone and rod signals.

OFF-center bipolar cells have excitatory, ionotropic (AMPA kainate) glutamate receptors (Puller et al., 2013). Therefore, these cells are excited (depolarized) in the dark when cone glutamate release is high. Light stimulation decreases the amount of excitatory glutamate released from the cone and consequently the OFF-center bipolar is inhibited and hyperpolarizes. This is called a *sign-conserving synapse*, as both the photoreceptor and the bipolar cell respond with hyperpolarization to light.

ON-type bipolar cells have inhibitory, metabotropic glutamate receptors (Gerber, 2003). As a result, the cells are inhibited (hyperpolarized) in the dark due to glutamate release by cones. Light stimulation and the consequent decrease in glutamate release remove the inhibition, allowing the cell to be excited and depolarize. The result is a *sign-reversing synapse*, because the response of the bipolar cell is opposite to that of the photoreceptor. Hence, the separation of signals for dark and light in the cone pathway is initiated by different glutamate receptors present in the first synapse in the retina.

The ON- and OFF-center dichotomy of cone bipolar cells is further enhanced by horizontal cell modulation in the OPL. In other words, the negative feedback signals of horizontal cells to the synaptic terminals of a cone provide lateral inhibition from surrounding cones (which are also stimulated), creating an antagonistic surround to the response in the center. This is considered to enhance the detection of edges in visual stimuli. This concentric organization is maintained in the inner retina, as ON- and OFF-center bipolar cells synapse exclusively with ON- and OFF-center RGCs, respectively. The antagonistic effect of the surrounding receptive field (OFF- and ON-surround, respectively) is once again enhanced by amacrine cell modulation and lateral inhibition in the INL (see Fig. 4.30). This arrangement improves contrast and, in combination with the dense packing of cones in the central retina, the low cone–bipolar–ganglion cell ratio, and the small size of the cone receptive fields, contributes to high spatial resolution and detection of fine details.

The traditional *rod pathway* differs from the cone pathway in several important features (Tsukamoto et al., 2001). First, there is only one type of rod bipolar cell. It has metabotropic, inhibitory glutamate receptors, similar to those of the ON-bipolar cells. Therefore, light stimulation and the consequent decrease in the amount of glutamate released by rods will remove the neurotransmitter's inhibitory effect on these receptors, leading to depolarization of rod bipolars, as it does in ON-bipolar cells.

Another significant difference between the two pathways is that rod ON-bipolar cells synapse with RGCs indirectly, through amacrine cells (see Fig. 4.26). This allows further convergence and processing of rod output, and its channeling to both ON- and OFF-center RGCs. Summation and convergence of the rod pathway are much greater than those of the cone pathway. It has been demonstrated that in the ON-pathway of the cat, about 1,500 rods synapse with 100 rod bipolars and 5 AII amacrine cells that converge on one small, β-ganglion cell. In the OFF-pathway, 75,000 rods synapse with 5,000 rod bipolars and 250 AII amacrine cells that converge on a single, large α RGC. This contrasts with the feline cone pathway, where each small, β-ganglion cell in the area centralis receives inputs from 3–4 cone bipolars, each of which, in turn, receives input from 4–8 cones (Kolb, 1979; Wässle et al., 1981). These figures further demonstrate the low visual acuity of the rod pathway compared to that of the cone pathway. When a rod RGC fires, there is no way of knowing which of the thousands of rods in its receptive field was hyperpolarized by light. Therefore, its activation provides little information about the location of the stimulus. This contrasts with the cone pathway in the central retina, where the RGC has a much smaller receptive field, and therefore its firing provides more accurate stimulus localization. Still, it is important to note that the feline cone pathway has some convergence, as opposed to the non-convergent nature of the primate, foveal cone pathway (Kolb & Marshak, 2003). This is one reason why feline visual acuity is lower than that of primates.

Several neurotransmitters are involved in lateral and vertical communication in the neuroretina. Glutamate is an excitatory, mainly "vertical" neurotransmitter relaying information from the photoreceptors, via the bipolars, to the RGCs (Wan & Heidelberger, 2011), but a subset of amacrine cells also uses glutamate to excite RGCs and contrast-sensitive circuits (Lee et al., 2016a). Acetylcholine is another excitatory transmitter released by cholinergic amacrine cells; it binds to muscarinic and nicotinic receptors in different types of amacrine cells in the mature retina (Gleason, 2012). Starburst amacrine cells are known to use acetylcholine to depolarize RGCs, although the function of these cholinergic circuits is still unclear (Taylor & Smith, 2012). Prior to the maturation of the photoreceptors, the primary source of previsional neural activity is cholinergic retinal waves (Ackman et al., 2012).

The main inhibitory neurotransmitter in the retina is GABA (Hoon et al., 2014; Wu, 2010). As such, it is used mainly for lateral processing of the signal by both horizontal and amacrine cells, which have an inhibitory function in the OPL and IPL, respectively. Together with glycine, GABA acts to inhibit RGCs by opening their Cl^- channels (Lynch, 2009)

Dopamine and serotonin are two more neurotransmitters found in amacrine cells. They probably play an important role in retinal signal processing but may also have other functions (Brandies & Yehuda, 2008; Trakhtenberg et al., 2017). Dopamine is only released from one class of amacrine cells that is driven by both cones and rods, as well as ipRGCs (Qiao et al., 2016). Dopamine can bind to D_1 and D_2 receptors, thus enabling further signal refinements. Many aspects of the role of the dopaminergic cells in the retina are still unclear or subject to contradictory reports.

Additional neurotransmitters, including substance P, adenosine, nitric oxide, somatostatin, neuropeptide Y, vasoactive intestinal peptide, corticotropin-releasing factor, and cholecystokinin, have also been described in various types of amacrine cells.

From Retina to Visual Cortex

Optic Nerve

RGC axons constitute the optic nerve fibers. These axons converge at the optic disc, where they are joined in bundles to form the nerve. As the nerve contains RGC axons but no other neuronal cell body, it can be considered a pure white matter tract. But the nerve does contain several important glial cell populations (Butt et al., 2004). These include oligodendrocytes, which contribute to its myelin sheath and formation of nodes of Ranvier, and astrocytes, which have several functions, including K^+ homeostasis and transportation and storage of metabolites (mainly glycogen) used by the axons. Microglia are CNS-specific macrophages that are smaller than the other glial cells and scan the tissues for signs of damage or distress (MacNair & Nickells, 2015). Once activated in inflamed or degenerating tissue, they can perform several tasks including phagocytosis of cellular debris, antigen presentation, and cytokine production.

RGCs (and some subtypes of amacrine cells) are the only retinal neurons that generate *action potentials*. Unlike the graded hyperpolarizing or depolarizing responses of other retinal neurons, action potentials are all-or-nothing spikes of electrical activity. This means that all of the neuronal processing of the visual signal that has taken place in the retina so far, including information about stimulus size, contrast, color, movement, and location, is coded as alterations in the firing pattern (e.g., short bursts or sustained episodes of firing) and firing rates of the RGCs (Meister et al., 1995).

In their resting state, optic nerve axons are hyperpolarized, maintaining a negative resting potential due to outflow of K^+ cations, balanced by inflow of Na^+ cations. Opening of voltage-sensitive sodium channels increases the inflow of Na^+ into the axon and causes rapid depolarization. The increased potential within the axon will cause adjacent sodium channels to open, propagating the action potential further downstream. Myelination of the optic nerve, provided by oligodendrocytes, allows for decreased capacitance and increased resistance of the nerve, as well as clustering of sodium channels in the nodes of Ranvier, providing for efficient and rapid saltatory conduction of the electrical signal (Kaplan et al., 2001).

A target anywhere in the visual field will elicit a cohort of signals generated by multiple RGCs representing different points in that particular part of the visual field. Consequently, arrangement of the axons within the optic nerve is not random. Instead, the fibers are arranged in a *retinotopic* manner, meaning that the precise spatial arrangement of the retina is maintained within the nerve. Through a carefully controlled process during development, fibers from the superior retina are made to arrive at the superior half of the optic nerve head, and those from the inferior retina form the inferior half. Fibers from the peripheral RGCs are peripheral within the nerve, and those from RGCs in the area centralis are located centrally within the nerve. This precise arrangement is a condition for the subsequent accurate projection of the visual field in both the LGN and the visual cortex (Herrera et al., 2019; Reese, 2011). However, the fibers do not necessarily work as parallel channels sending independent information about the visual scene, but may also be part of a multineural signaling system sending more complexly coded information to the brain (Ala-Laurila et al., 2011; Meister et al., 1995).

Optic Chiasm and Optic Tract

As the optic nerve approaches the optic chiasm, the location of fibers within the nerve gradually shifts in preparation for decussation at the optic chiasm (Neveu & Jeffery, 2007; Reese, 2011; see Fig. 4.36). Generally, fibers from the temporal retina remain in the ipsilateral hemisphere, and fibers

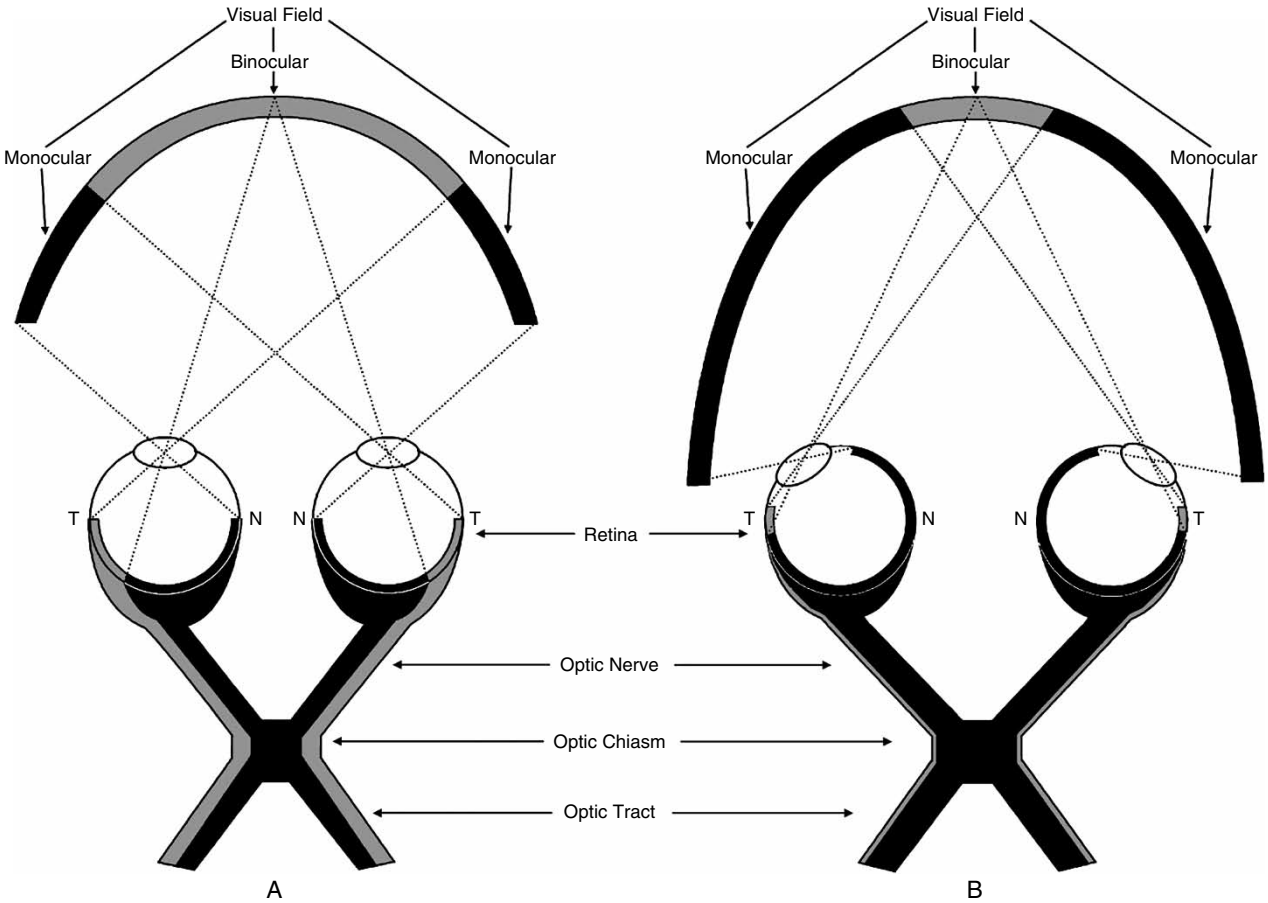

Figure 4.36 In animals with more frontally positioned eyes, such as several predatory mammals, the binocular overlap is large and consequently a large portion of the axons in the optic nerve project ipsilaterally at the optic chiasm (**A**). Animals with more laterally positioned eyes have a larger visual field, although the area of binocular overlap is smaller, resulting in fewer axons projecting ipsilaterally at the chiasm (**B**). N, nasal; T, temporal. (Reproduced with permission from Jeffery, G. & Erskine, L. (2005) Variations in the architecture and development of the vertebrate optic chiasm. *Progress in Retinal and Eye Research*, **24**, 721–753. doi: 10.1016/j.preteyeres.2005.04.005.)

from the nasal retina cross over to the contralateral side. The amount of decussation varies between species, perhaps representing a broad evolutionary scale. Birds, as well as many amphibian and reptilian species, have complete crossover of fibers to the contralateral side. A greater proportion of fibers remains on the ipsilateral side in mammals that have developed binocular vision. In the horse, 15% of the fibers stay on the ipsilateral side, as do 25% in the dog and 33% in the cat. In humans, only 50% of the fibers cross over. Partial crossover of fibers allows both hemispheres to continue receiving visual input even when one retina or optic nerve has been completely destroyed, thus enabling the animal to maintain better physiologic function and correlation with other sensory input (Fraser et al., 2011). Because the topography of decussating fibers is characterized by spatial precision in primates (Jeffery et al., 2008), lesions in different areas of the chiasm (or the optic nerve) will cause specific visual deficits.

The optic tract runs from the optic chiasm to the LGN. Because of decussation at the chiasm, fibers of the optic tract conduct information from the opposite visual field of both eyes. In humans, where roughly 50% of the axons decussate in the chiasm, the left optic tract relays the right visual hemifield of both eyes, and the right optic tract relays both left visual hemifields. In animals, where a greater percentage of fibers cross over, the left optic tract will relay a greater proportion of the right visual field from the right eye and a smaller proportion of the right visual field from the left eye.

It is important to remember that the optic tract carries only 80%–90% of the RGC axons to the LGN. The rest of the RGC axons, including those of the ipRGCs, exit the optic tract before it reaches the LGN and relay visual information to several other areas in the thalamus, midbrain, hypothalamus, and amygdala/pallidum (Martersteck et al., 2017; Morin & Studholme, 2014). In total, RGCs project to more than 50 regions in the brain of a tiny mouse. Best known are

the fibers that relay information to the pretectal olivary nucleus, and through it to the parasympathetic oculomotor nucleus, providing afferent input to the PLR. Other optic tract fibers synapse in the superior colliculus, which controls saccadic eye movement and also receives information from other sensory organs (i.e., ears and spinal cord) and is therefore involved in the correlation of sensory information. In addition, information from the retina reaches additional nuclei involved in controlling optokinetic reflexes, circadian rhythms, and endocrine activity of the hypothalamus.

Lateral Geniculate Nucleus

For most RGC axons, the first synapse occurs in the LGN, which is one of about ten targets of RGCs in the thalamus (Monavarfeshani et al., 2017). The axons maintain their retinotopic arrangement through the optic nerves, chiasm, and tracts and as they enter the LGN. Here, the RGC axons synapse with dendrites of LGN *interneurons* (which provide for signal processing) and *projecting cells* in synaptic glomeruli.

In the LGN, RGC axons segregate by eye and functional group, usually forming layers where they terminate in discrete clusters, generating a retinotopic map of the contralateral visual hemifield (with receptive fields similar in size and response properties to the retinal receptive fields). Furthermore, the somata of the projecting cells, classically subdivided into magnocellular (M), parvocellular (P), and koniocellular (K) cells, are also segregated into the same distinct LGN layers as the RGC axons (Fig. 4.37). Traditionally, it has been considered that P-cells process form information (visual acuity and contrast), while M-cells process motion and K-cells process colors. Although these descriptions are oversimplifications, corticogeniculate neurons can be segregated according to their konio-, magno-, and parvocellular properties (Briggs & Usrey, 2009).

Thus, in primates where the decussation is about 50%, three of the six LGN layers receive input from the ipsilateral visual hemifield, and three alternating layers receive their input from the corresponding contralateral hemifield. Furthermore, the six resulting monocular maps are in register, which means that an electrode vertically penetrating through the six layers would record information about the same point in the visual field in each of the layers.

The maps of the LGN also reflect the physiologic processing of the signal that has occurred in the retina. Thus, cells in the magno-layer receive input from Y- or α-type RGCs, while cells in the parvo-layers receive input from X- or β-type RGCs. Therefore, the six cells through which the abovementioned line of projection passes receive both X- and Y-type data about an identical receptive field in both eyes. Furthermore, the LGN cells also maintain the center-surround antagonism of the RGC receptive fields. This provides the basis for the additional merging of visual information that occurs in the cortex.

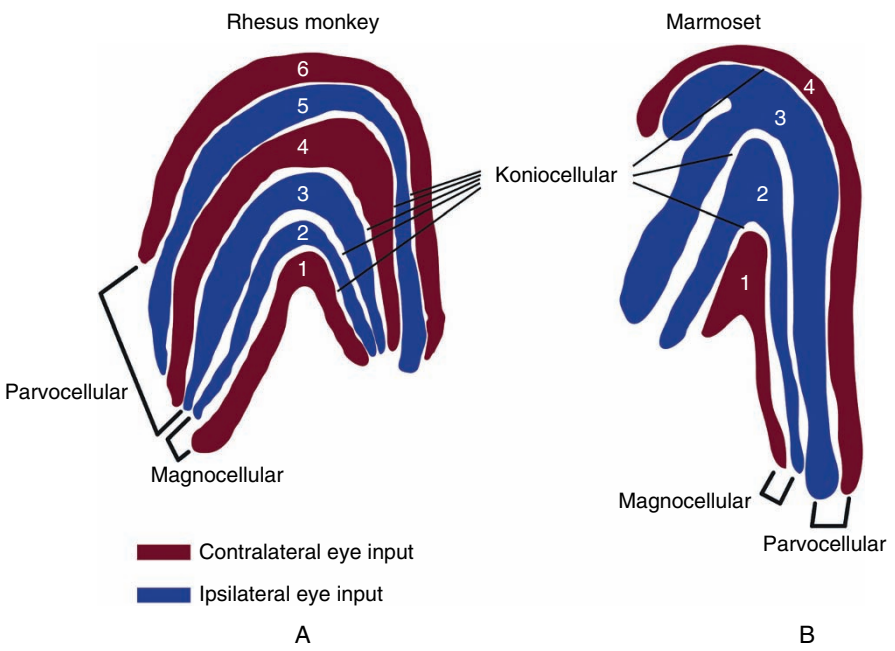

Figure 4.37 In the lateral geniculate nucleus (LGN), the parvo- and magnocellular layers are separated by thinner koniocellular layers. Each LGN receives input from the part of the retina looking at the contralateral visual field in both eyes. In contrast to humans and rhesus monkeys (**A**), the marmoset (**B**) has fewer parvocellular layers and a large proportion of binocular cells in the koniocellular layers. (Reproduced with permission from Wallace, D.J., Fitzpatrick, D., & Kerr, J.N. (2016) Primate thalamus: More than meets an eye. *Current Biology*, **26**, R60–R61. doi: 10.1016/j.cub.2015.11.025.)

In recent years, it has been shown that rather than being a simple relay station conveying signals from the RGCs to the visual cortex, the LGN is actually a complex and multifunctional center. In fact, signals from the RGCs account only for 5%–10% of the input to projecting cells, and the LGN receives large amounts of feedback from the visual cortex and other areas. Weyand (2016) lists a multitude of putative functions of the LGN, including parsing retinal inputs for selective access for non-retinal inputs; amplifying and integrating retinal inputs; controlling contrast (luminance) gain; controlling retinogeniculate gain by state, level of arousal, and attention; implementing pattern-recognition algorithms; synchronizing saccades and retinogeniculate signaling; enhancing temporal diversity, thus potentially improving coding of natural scenes; and generating signals that are used by directionally selective cortical neurons.

Axons of projecting cells exit the LGN and form the *optic radiations*. These axons relay the visual signal from the LGN to the primary visual cortex, as well as to other visual centers, where they synapse.

The Primary Visual Cortex

Location

Brodmann (1909) demonstrated that the primary visual cortex (i.e., *area 17*) receiving the input from the LGN is located in the posterior part of the occipital lobe in a number of species. This area is now usually called *V1* (visual area 1) or the *striate cortex*, after the striae of Gennari. In contrast, all other visual areas in the cortex lacking the stria (which is a myelinated stripe where the LGN axons enter the gray matter of the V1) are termed *extrastriate*.

V1 has been mapped in several species. In the cat, it occupies the posteromedial portion of the cortex, extending from the crown of the lateral gyrus on the dorsal surface to the superior bank of the splenial sulcus on the medial surface (Tusa et al., 1978). In the dog, it is located at the junction of the marginal and endomarginal gyri (Ofri et al., 1994). The striate cortex has also been identified in the horse (Ström and Ekesten, 2016).

Neuronal Organization

Like the rest of the cerebral cortex, cells of V1 are orderly arranged in six layers. The incoming thalamic (LGN) axons synapse with cortical neurons, glutamate-containing *simple cells*, in layer 4. More precisely, magno-, parvo-, and koniocellular projections synapse in layers 4Ca, 4Cb, and 4A, respectively, thus maintaining the segregation of visual information that characterizes the visual system to this point. More superficial layers (layers 1–3) contain excitatory neurons that project to each other and to extrastriate visual areas; these layers also receive feedback from the same extrastriate visual areas (Binzegger et al., 2009). Layers 5 and 6 communicate with the superficial layers and feed back to the LGN.

The simple cells in layer 4 maintain the functional center-surround orientation of their afferent RGCs and LGN layers, but they are monocular in nature (Lehky et al., 2005). Complex cells in other layers of V1 receive binocular input from several simple cells, making them (in some species) the first neuron where input from both eyes is fused. Surprisingly, the incoming thalamic fibers provide just 5% of the excitatory synapses in layer 4 (Douglas & Martin, 2007). This small fraction of sensory input from the retina, compared to the huge number of synapses made by cortical and subcortical neurons in V1, is testimony to the complexity of the processing of the image by local and long-distance circuits in the brain (Iacaruso et al., 2017; Stepanyants et al., 2009).

Functional Architecture of the Striate Cortex

The functional architecture of the striate cortex was extensively studied by Nobel prize winners David Hubel and Torsten Wiesel (Wurtz, 2009). Here we present the organization they originally proposed. The basic cortical unit that processes an incoming signal is termed a *cortical column*, which extends through all six layers of V1. As in the LGN, vertical penetration through the six cortical layers of the column will result in passage through cells with almost identical receptive fields. Therefore, adjacent retinal receptive fields project onto adjacent columns in V1. Consequently, the entire contralateral visual hemifield, as projected on both retinas, is mapped on the surface of the cortex retinotopically, meaning that adjacent loci of the contralateral visual hemifield are projected onto adjacent loci of the cortex in a point-to-point manner (Schira et al., 2007; Wandell & Winawer, 2011). There is no difference in size between columns serving the central and the peripheral retina; rather, more columns are used to process visual input from the central retina.

There are several functional types of columns in V1. These are devoted to stimulus size, color, orientation, and ocular dominance (Fig. 4.38). In an orientation column, all the cells respond best only to one stimulus orientation; in other words, cells in a given column may fire in response to a horizontal bar, but not to a vertical or diagonal bar. Movement of 50 μm along one axis of the cortical surface will bring a shift of 10° in the orientation preference of the cells. Movement of 0.1 mm along the same axis will shift the orientation preference by 20°. Therefore, a column 0.9 mm wide will contain cells responding to a 180° change in orientation, thus containing all the possible permutations.

Movement along another axis of the cortical surface will result in movement across ocular dominance columns. A dominance column is an area approximately 0.4 mm wide in which input from one eye is dominant over that of the other eye. The dominance is strongest at the center of the column and decreases gradually, so that input is almost equally binocular at the column periphery. As movement continues into the adjacent column, there is a gradual buildup of dominance by the other eye, which, again, will be most dominant at the adjacent column's center.

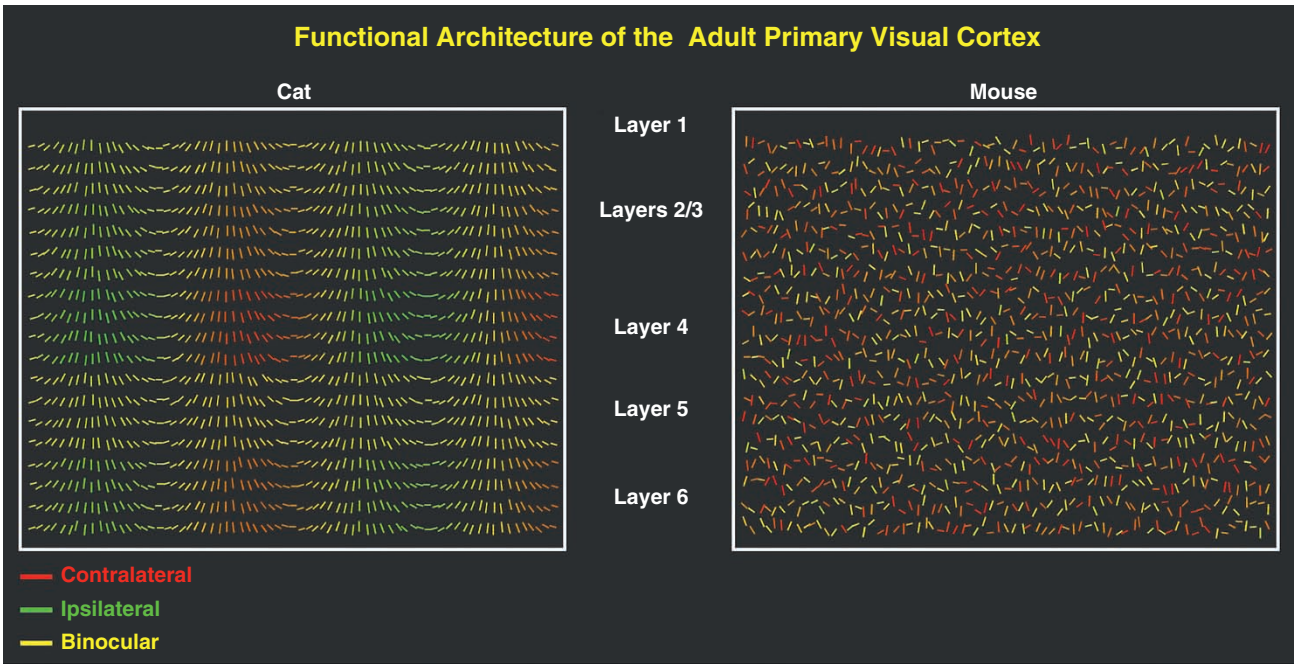

Figure 4.38 The functional architecture of the cat visual area 1 (V1) is highly structured and the neurons are highly specialized. Both specific orientation (shown by the angle of the lines) and ocular dominance properties (indicated by the color of each line) are organized into columns. The columnar organization of preferred orientation of the stimulus spans all layers, from the most superficial layer 1 to the deepest layer 6. The ocular dominance columns are not as clearly outlined throughout the layers and are most pronounced in layer 4, where many cells are driven monocularly from the lateral geniculate nucleus. The mouse also has specialized neurons in V1, but neither preferred orientation nor ocular dominance properties are organized in columns. Furthermore, in this species, where the vast majority of the axons of the retinal ganglion cells decussate at the optic chiasm, a bias in ocular dominance is seen toward the contralateral retina. (Reproduced with permission from Espinosa, J.S. & Stryker, M.P. (2012) Development and plasticity of the primary visual cortex. *Neuron*, **75**, 230–249, doi: 10.1016/j.neuron.2012.06.009.)

A *hypercolumn* is a complete set of both column types. It contains, along one axis 0.9 mm in length, all possible permutations of orientation preferences. Along a different axis 0.8 mm in length, it contains all possible ocular dominance combinations. Therefore, every given cell in a hypercolumn will respond best just to one stimulus orientation from one eye. Such a response of a given cell provides information regarding stimulus orientation, movement, direction, and binocularity.

Subsequently, it was discovered that interspaced between the hypercolumn's columns is another system responsible for processing color information. Cells belonging to this system are arranged in "blobs" (so named because of their appearance after staining for cytochrome oxidase) and respond selectively to different combinations of stimulus wavelength (Economides et al., 2011; Livingstone & Hubel, 1984). These *color opponent cells* display antagonistic center-surround properties (similar to those of bipolar and ganglion cells) regarding color.

Despite the knowledge about this basic organization of cells in V1, still little is known about the connections individual neurons make. In the mouse, a local cortical circuit (encompassing about 0.25 mm^3) contains approximately 25,000 neurons and 250 million synapses (Reid, 2012). Local signals from different types of neurons in V1 must be integrated to create a unified visual percept and the extensive interconnections between visual areas provide almost countless pathways along which signals can travel. V1 outputs to higher visual areas, where more specialized neurons respond to more complex stimuli. Both hierarchic and parallel processing are used in the visual areas and contribute different information (Ponce et al., 2008). At the same time, there is also extensive feedback activity from extrastriate areas to V1 and from there back to the LGN.

Para- and Extrastriate Visual Areas

Visual area 2 (V2) or the parastriate cortex (Brodmann's area 18) forms a concentric crescent around V1. V2 can be separated from V1 based on histologic appearance, connectivity pattern, response properties, and reversal of the retinotopic map at the border between V1 and V2 (Buckner & Yeo, 2014).

Another well-defined, more anterior area that has a binocular visual field map is the MT (middle temporal). MT is important for processing information about the motion, speed, and binocular disparity of moving stimuli (Maunsell & Van Essen, 1983a, 1983b).

There are additional maps and representations of the visual field in other extrastriate areas. Furthermore, some higher-order extrastriate areas are not as distinctly defined

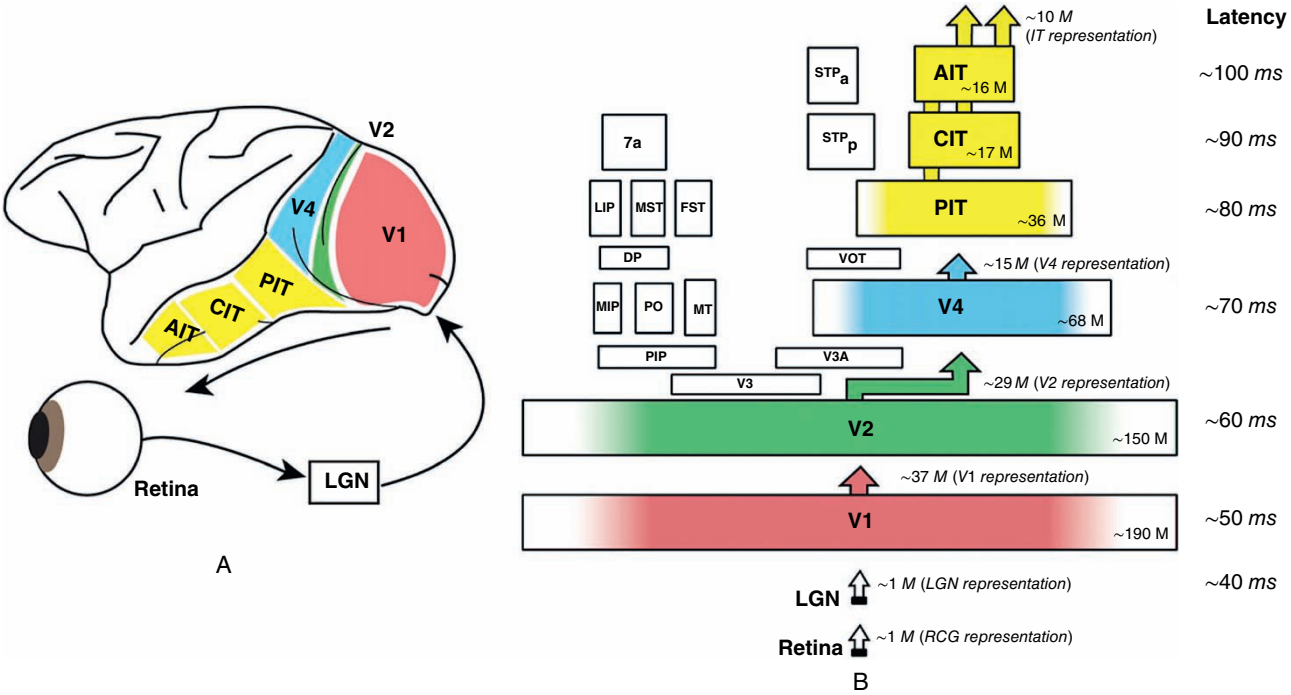

Figure 4.39 **A**. The flow of visual information from the retina to ventral stream area locations in the macaque brain. **B**. The areas plotted to their cortical surface areas; numbers in the lower right corners indicate the number of neurons in millions (M) in each area. The approximate number of neurons projecting from one area to the next is shown above each rectangle. Approximate median response latencies are listed to the right. PIT, CIT, and AIT indicate posterior, central, and anterior inferotemporal cortex (areas essential for object recognition), respectively. LGN, lateral geniculate nucleus; RCG, retinal ganglion cell. All other abbreviations refer to specific visual areas in the macaque monkey cortex. (Reproduced with permission from DiCarlo, J.J., Zoccolan, D., & Rust, N.C. (2012) How does the brain solve visual object recognition? *Neuron*, **73**, 415–434. doi: 10.1016/j.neuron.2012.01.010.)

as V1, V2, and MT, neither anatomically nor functionally, and their exact number and boundaries are still controversial (Angelucci & Rosa, 2015). This uncertainty is no surprise, because the visual input is widely spread in the brain. Even in a tiny mouse, 50 or more areas receive input from the retina (Martersteck et al., 2017).

After V2, the visual pathways diverge into two functional streams. Broadly speaking, these two pathways process information about *where* and *how* (the *dorsal pathway* or *stream* in the parietal cortex) and *what* (the *ventral pathway* or *stream* in the inferotemporal cortex) a certain visual stimulus is (Conway, 2014; Kravitz et al., 2011). The dorsal pathway is devoted to object localization, processing motion, direction, and stereoscopic depth perception, but also to unconscious visually guided behavior (like grasping a cup on a table when you are drinking coffee). It receives mostly magnocellular input from V1 and V2, relaying it through areas usually termed V3 and V5 to even higher visual areas. The ventral pathway deals with object recognition (Fig. 4.39), processing details such as form, color, orientation, and shape. It receives both magno- and parvocellular input from V1 and V2, relaying it through V4 to higher processing in several visual areas.

The complexity of the stimulus selectivity increases step by step when ascending the hierarchy of the extrastriate areas. Eventually, high-order neurons are driven only if the visual stimulus has a certain shape or other properties that contribute to object recognition. Lesions in higher visual areas can cause deficits in spatial or motion perception and visuomotor control (dorsal pathway disorders) or in color processing and object recognition (ventral pathway disorders; Barton, 2011).

References

Ackman, J.B., Burbridge, T.J., & Crair, M.C. (2012) Retinal waves coordinate patterned activity throughout the developing visual system. *Nature*, **490**, 219–225.

Ahnelt, P.K., Fernandez, E., Martinez, O., et al. (2000) Irregular S-cone mosaics in felid retinas: Spatial interaction with axonless horizontal cells, revealed by cross correlation. *Journal of the Optical Society of America. A, Optics, Image Science, and Vision*, **17**, 580–588.

Ahnelt, P.K. & Kolb, H. (2000) The mammalian photoreceptor mosaic-adaptive design. *Progress in Retinal and Eye Research*, **19**, 711–777.

Ala-Laurila, P., Greschner, M., Chichilnisky, E.J., et al. (2011) Cone photoreceptor contributions to noise and correlations in the retinal output. *Nature Neuroscience*, **14**, 1309–1316.

Anderson, D.H., Fisher, S.K., & Steinberg, R.H. (1978) Mammalian cones: Disc shedding, phagocytosis, and renewal. *Investigative Ophthalmology & Visual Science*, **17**, 117–133.

Angelucci, A. & Rosa, M.G. (2015) Resolving the organization of the third tier visual cortex in primates: A hypothesis-based approach. *Visual Neuroscience*, **32**, E010.

Antinucci, P., Abbas, F., & Hunter, P.R. (2016) Orientation selectivity in the retina: ON cell types and mechanisms. *Journal of Neuroscience*, **36**, 8064–8066.

Arshavsky, V.Y. & Burns, M.E. (2012) Photoreceptor signaling: Supporting vision across a wide range of light intensities. *Journal of Biological Chemistry*, **287**, 1620–1626.

Artal, P., Herreros de Tejada, P., Muñoz Tedó, C., et al. (1998) Retinal image quality in the rodent eye. *Visual Neuroscience*, **15**, 597–605.

Axelrod, D., Lerner, D., & Sands, P.J. (1988) Refractive index within the lens of a goldfish eye determined from the paths of thin laser beams. *Vision Research*, **28**, 57–65.

Badea, T.C. & Nathans, J. (2011) Morphologies of mouse retinal ganglion cells expressing transcription factors Brn3a, Brn3b, and Brn3c: Analysis of wild type and mutant cells using genetically-directed sparse labeling. *Vision Research*, **51**, 269–279.

Baden, T., Berens, P., Franke, K., et al. (2016) The functional diversity of retinal ganglion cells in the mouse. *Nature*, **529**, 345–350.

Barbero, S. (2006) Refractive power of a multilayer rotationally symmetric model of the human cornea and tear film. *Journal of the Optical Society of America*, **23**, 1578–1585.

Barton, J.J. (2011) Disorders of higher visual processing. *Handbook of Clinical Neurology*, **102**, 223–261.

Baylor, D. (1996) How photons start vision. *Proceedings of the National Academy of Sciences of the USA*, **93**, 560–565.

Belkin, M., Yinon, U., Rose, L., et al. (1977) Effects of visual environment on refractive error of cats. *Documenta Ophthalmologica*, **42**, 433–437.

Beltran, W.A., Cideciyan, A.V., Guziewicz, K.E., et al. (2014) Canine retina has a primate fovea-like bouquet of cone photoreceptors which is affected by inherited macular degenerations. *PLoS One*, **9**, e90390.

Bernstein, P.S., Li, B, Vachali, P.P., et al. (2016) Lutein, zeaxanthin, and meso-zeaxanthin: The basic and clinical science underlying carotenoid-based nutritional interventions against ocular disease. *Progress in Retinal and Eye Research*, **50**, 34–66.

Bierman, A., Figueiro, M.G., & Rea, M.S. (2011) Measuring and predicting eyelid spectral transmittance. *Journal of Biomedical Optics*, **16**, 067011.

Binzegger, T., Douglas, R.J., & Martin, K.A. (2009) Topology and dynamics of the canonical circuit of cat V1. *Neural Network*, **22**, 1071–1078.

Bito, L.Z., DeRousseau, C.J., Kaufman, P.L., et al. (1982) Age-dependent loss of accommodative amplitude in rhesus monkeys: An animal model for presbyopia. *Investigative Ophthalmology & Visual Science*, **23**, 23–31.

Black, J., Browning, S.R., Collins, A.V., et al. (2008) A canine model of inherited myopia: Familial aggregation of refractive error in Labrador Retrievers. *Investigative Ophthalmology & Visual Science*, **49**, 4784–4789.

Bloomfield, S.A. & Xin, D. (2000) Surround inhibition of mammalian AII amacrine cells is generated in the proximal retina. *Journal of Physiology*, **523(**Pt. 3), 771–783.

Boettner, E.A. & Wolter, J.R. (1962) Transmission of the ocular media. *Investigative Ophthalmology*, **1**, 776–783.

Bolívar-G, W., Antoniazzi, M.M., Grant, T., et al. (2014) Discovery of a novel accessory structure of the pitviper infrared receptor organ (serpentes: viperidae). *PLoS One*, **9**, e90622.

Borja, D., Manns, F., Ho, A., et al. (2010) Refractive power and biometric properties of the nonhuman primate isolated crystalline lens. *Investigative Ophthalmology & Visual Science*, **51**, 2118–2125.

Borst, A. & Euler, T. (2011) Seeing things in motion: Models, circuits, and mechanisms. *Neuron*, **71**, 974–994.

Bowmaker, J.K. (1981) Visual pigments and colour vision in man and monkeys. *Journal of the Royal Society of Medicine*, **74**, 348–356.

Bowmaker, J.K. (2008) Evolution of vertebrate visual pigments. *Vision Research*, **48**, 2022–2041.

Boycott, B.B. & Wässle, H. (1974) The morphological types of ganglion cells of the domestic cat's retina. *Journal of Physiology*, **240**, 397–419.

Boyd, C., Castillo, R., Hunt, G.L., et al. (2015) Predictive modelling of habitat selection by marine predators with respect to the abundance and depth distribution of pelagic prey. *Journal of Animal Ecology*, **84**, 1575–1588.

Bracun, A., Ellis, A.D., & Hall, C. (2014) A retinoscopic survey of 333 horses and ponies in the UK. *Veterinary Ophthalmology*, **17(**Suppl. 1), 90–96.

Brandies, R. & Yehuda, S. (2008) The possible role of retinal dopaminergic system in visual performance. *Neuroscience and Biobehavioral Reviews*, **32**, 611–656.

Bras, D. & Maggio, F. (2015) Surgical treatment of canine glaucoma: Cyclodestructive techniques. *Veterinary Clinics of North America, Small Animal Practice*, **45**, 1283–1305.

Briggs, F. & Usrey, W.M. (2009) Parallel processing in the corticogeniculate pathway of the Macaque monkey. *Neuron*, **62**, 135–146.

Bringmann, A., Grosche, A., Pannicke, T., et al. (2013) GABA and glutamate uptake and metabolism in retinal glial (Müller) cells. *Frontiers in Endocrinology*, **4**, 48.

Bringmann, A., Iandiev, I., Pannicke, T., et al. (2009) Cellular signaling and factors involved in Müller cell gliosis: Neuroprotective and detrimental effects. *Progress in Retinal and Eye Research*, **28**, 423–451.

Brodmann, K. (1909) *Vergleichende Lokalisationslehre der Grosshirnrinde in ihren Prinziepien auf Grund des Zellbaues*, Leipzig: J. A. Barth.

Buckner, R.L. & Yeo, B.T. (2014) Borders, map clusters, and supra-areal organization in visual cortex. *Neuroimage*, **93(**Pt. 2), 292–297.

Buehren, T. & Collins, M.J. (2006) Accommodation stimulus-response function and retinal image quality. *Vision Research*, **46**, 1633–1645.

Bühren, J., Yoon, G., MacRae, S., et al. (2010) Contribution of optical zone decentration and pupil dilation on the change of optical quality after myopic photorefractive keratectomy in a cat model. *Journal of Refractive Surgery*, **26**, 183–190.

Burns, M.E. & Baylor, D.A. (2001) Activation, deactivation, and adaptation in vertebrate photoreceptor cells. *Annual Review of Neuroscience*, **24**, 779–805.

Burns, M.E., Mendez, A., Chen, J., et al. (2002) Dynamics of cyclic GMP synthesis in retinal rods. *Neuron*, **36**, 81–91.

Butt, A.M., Pugh, M., Hubbard, P., et al. (2004) Functions of optic nerve glia: Axoglial signalling in physiology and pathology. *Eye*, **18**, 1110–1121.

Calhoun, W.R., Akpek, E.K., Weiblinger, R., et al. (2015) Evaluation of broadband spectral transmission characteristics of fresh and gamma-irradiated corneal tissues. *Cornea*, **34**, 228–234.

Chandler, H.L., Kusewitt, D.L., & Colitz, C.M. (2008) Modulation of matrix metalloproteinases by ultraviolet radiation in the canine cornea. *Veterinary Ophthalmology*, **11**, 135–144.

Chang, C.K., Lin, J.T., & Zhang, Y. (2017) Human eye ocular component analysis for refractive state and refractive surgery. *International Journal of Ophthalmology*, **10**, 1076–1080.

Chapot, C.A., Euler, T., & Schubert, T. (2017) How do horizontal cells "talk" to cone photoreceptors? Different levels of complexity at the cone–horizontal cell synapse. *Journal of Physiology*, **595**, 5495–5506.

Charman, W.N. (2008) The eye in focus: Accommodation and presbyopia. *Clinical and Experimental Optometry*, **91**, 207–225.

Chen, E. (1993) Refractive indices of the rat retinal layers. *Ophthalmic Research*, **25**, 65–68.

Chen, Y., Lan, W., & Schaeffel, F. (2015) Size of the foveal blue scotoma related to the shape of the foveal pit but not to macular pigment. *Vision Research*, **106**, 81–89.

Choh, V. & Sivak, J.G. (2005) Lenticular accommodation in relation to ametropia: The chick model. *Journal of Visualization*, **5**, 165–176.

Choh, V., Sivak, J.G., Irving, E.L., et al. (2002a) Ultrasound biomicroscopy of the anterior segment of the enucleated chicken eye during accommodation. *Ophthalmic and Physiological Optics*, **22**, 401–408.

Choh, V., Sivak, J.G., & Meriney, S.D. (2002b) A physiological model to measure effects of age on lenticular accommodation and spherical aberration in chickens. *Investigative Ophthalmology & Visual Science*, **43**, 92–98.

Choy, C.K., Cho, P., & Benzie, I.F. (2011) Antioxidant content and ultraviolet absorption characteristics of human tears. *Optometry and Vision Science*, **8**, 507–511.

Chu, C.H., Zhou, Y., Zheng, Y., et al. (2014) Bi-directional corneal accommodation in alert chicks with experimentally-induced astigmatism. *Vision Research*, **98**, 26–34.

Cohen, Y., Belkin, M., Yehezkel, O., et al. (2008) Light intensity modulates corneal power and refraction in the chick eye exposed to continuous light. *Vision Research*, **48**, 2329–2335.

Collin, S.P., Davies, W.L., Hart, N.S., et al. (2009) The evolution of early vertebrate photoreceptors. *Philosophical Transactions of the Royal Society of London. Series B, Biological Sciences*, **364**, 2925–2940.

Conway, B.R. (2014) Color signals through dorsal and ventral visual pathways. *Visual Neuroscience*, **31**, 197–209.

Courville, C.B., Smolek, M.K., & Klyce, S.D. (2004) Contribution of the ocular surface to visual optics. *Experimental Eye Research*, **78**, 417–425.

Croft, M.A., McDonald, J.P., Katz, A., et al. (2013) Extralenticular and lenticular aspects of accommodation and presbyopia in human versus monkey eyes. *Investigative Ophthalmology & Visual Science*, **54**, 5035–5048.

Dacey, D., Packer, O.S., Diller, L., et al. (2000) Center surround receptive field structure of cone bipolar cells in primate retina. *Vision Research*, **40**, 1801–1811.

Das, S.R., Bhardwaj, N., Kjeldbye, H., et al. (1992) Müller cells of chicken retina synthesize 11-cis-retinol. *Biochemical Journal*, **285**(Pt. 3), 907–913.

Davidson, M.G. (1997) Clinical retinoscopy for the veterinary ophthalmologist. *Veterinary & Comparative Ophthalmology*, **7**, 128–137.

Davidson, M.G., Murphy, C.J., Nasisse, M.P., et al. (1993) Refractive state of aphakic and pseudophakic eyes of dogs. *American Journal of Veterinary Research*, **54**, 174–177.

Dawson, W.W., Schroeder, J.P., & Sharpe, S.N. (1987) Corneal surface properties of two marine mammal species. *Marine Mammal Science*, **3**, 186–197.

Delcourt, C., Cougnard-Grégoire, A., Boniol, M. et al. (2014) Lifetime exposure to ambient ultraviolet radiation and the risk for cataract extraction and age-related macular degeneration: The Alienor Study. *Investigative Ophthalmology & Visual Science*, **55**, 7619–7627.

de Melo Reis, R.A., Ventura, A.L., Schitine, C.S., et al. (2008) Müller glia as an active compartment modulating nervous activity in the vertebrate retina: Neurotransmitters and trophic factors. *Neurochemical Research*, **33**, 1466–1474.

Do, M.T., Kang, S.H., Xue, T., et al. (2009) Photon capture and signalling by melanopsin retinal ganglion cells. *Nature*, **457**, 281–287.

Douglas, R.J. & Martin, K.A. (2007) Mapping the matrix: The ways of neocortex. *Neuron*, **56**, 226–238.

Duke-Elder, S. (1970) The dioptric imagery of the eye. In: *System of Ophthalmology: Vol. V. Ophthalmic Optics and Refraction* (eds. Duke-Elder, S. & Weale, R.A.), pp. 93–152. London: Henry Kimpton.

Ebersberger, A., Flügel, C., & Lütjen-Drecoll, E. (1993) [Ultrastructural and enzyme histochemical studies of regional structural differences within the ciliary muscle in

various species]. *Klinische Monatsblätter für Augenheilkunde*, **203**, 53–58.
Economides, J.R., Sincich, L.C., Adams, D.L., et al. (2011) Orientation tuning of cytochrome oxidase patches in macaque primary visual cortex. *Nature Neuroscience*, **14**, 1574–1580.
Enroth-Cugell, C. & Robson, J.G. (1984) Functional characteristics and diversity of cat retinal ganglion cells: Basic characteristics and quantitative description. *Investigative Ophthalmology & Visual Science*, **25**, 250–267.
Eslami, Y. & Mirmohammadsadeghi, A. (2015) Comparison of surgically induced astigmatism between horizontal and X-pattern sutures in the scleral tunnel incisions for manual small incision cataract surgery. *Indian Journal of Ophthalmology*, **63**, 606–610.
Euler, T., Haverkamp, S., Schubert, T., et al. (2014) Retinal bipolar cells: Elementary building blocks of vision. *Neuroscience*, **15**, 507–519.
Fadlallah, A., Mehanna, C., Saragoussi, J.J., et al. (2015) Safety and efficacy of femtosecond laser-assisted arcuate keratotomy to treat irregular astigmatism after penetrating keratoplasty. *Journal of Cataract and Refractive Surgery*, **41**, 1168–1175.
Farrall, H. & Handscombe, M.C. (1990) Follow-up report of a case of surgical aphakia with an analysis of equine visual function. *Equine Veterinary Journal Supplement*, **10**, 91–93.
Farrall, H. & Handscombe, M.C. (1999) Equine vision. *Equine Veterinary Journal*, **31**, 354–355.
Feigl, B. & Zele, A.J. (2014) Melanopsin-expressing intrinsically photosensitive retinal ganglion cells in retinal disease. *Optometry and Vision Science*, **91**, 894–903.
Fish, S.K., Pflugfelder, S.C., & de Paiva, C.S. (2004) The effect of tear film composition on refraction. *Investigative Ophthalmology & Visual Science*, **45**, ARVO abstract 3887.
Fisher, R.F. (1971) The elastic constants of the human lens. *Journal of Physiology*, **212**, 147–180.
Fontenot, C.L. (2008) Variation in pupil diameter in North American Gartersnakes (*Thamnophis*) is regulated by immersion in water, not by light intensity. *Vision Research*, **48**, 1663–1669.
Fraser, J.A., Newman, N.J., & Biousse, V. (2011) Disorders of the optic tract, radiation, and occipital lobe. *Handbook of Clinical Neurology*, **102**, 205–221.
French, A.N., Ashby, R.S., Morgan, I.G., et al. (2013) Time outdoors and the prevention of myopia. *Experimental Eye Research*, **114**, 58–68.
Fried, S.I., Munch, T.A., & Werblin, F.S. (2002) Mechanisms and circuitry underlying directional selectivity in the retina. *Nature*, **420**, 411–414.
Gaiddon, J., Bouhana, N., & Lallement, P.E. (1996) Refraction by retinoscopy of normal, aphakic and pseudophakic canine eyes: Advantage of a 41-diopter intraocular lens? *Veterinary & Comparative Ophthalmology*, **6**, 121–124.
Gaiddon, J., Rosolen, S.G., Steru, L., et al. (1991) Use of biometry and keratometry for determining optimal power for intraocular lens implants in dogs. *American Journal of Veterinary Research*, **52**, 781–783.
Gargallo, A., Arines, J., & Acosta, E. (2013) Lens aberrations and their relationship with lens sutures for species with Y-suture branches. *Journal of Biomedical Optics*, **18**, 25003.
Gawne, T.J., Siegwart, J.T., Ward, A.H., et al. (2017) The wavelength composition and temporal modulation of ambient lighting strongly affect refractive development in young tree shrews. *Experimental Eye Research*, **155**, 75–84.
Gekeler, F., Shinoda, K., Blatsios, G., et al. (2006) Scotopic threshold responses to infrared irradiation in cats. *Vision Research*, **46**, 357–364.
Geng, Y., Schery, L.A., Sharma, R., et al. (2011) Optical properties of the mouse eye. *Biomedical Optics Express*, **2**, 717–738.
Georg, B., Ghelli, A., Giordano, C., et al. (2017) Melanopsin-expressing retinal ganglion cells are resistant to cell injury, but not always. *Mitochondrion*, **36**, 77–84.
Gerber, U. (2003) Metabotropic glutamate receptors in vertebrate retina. *Documenta Ophthalmologica*, **106**, 83–87.
Gift, B.W., English, R.V., Nadelstein, B., et al. (2009) Comparison of capsular opacification and refractive status after placement of three different intraocular lens implants following phacoemulsification and aspiration of cataracts in dogs. *Veterinary Ophthalmology*, **12**, 13–21.
Gilger, B.C., Davidson, M.G., & Colitz, C.M. (1998) Experimental implantation of posterior chamber prototype intraocular lenses for the feline eye. *American Journal of Veterinary Research*, **59**, 1339–1343.
Glasgow, B.J. (2016) Fluorescence lifetime imaging microscopy reveals quenching of fluorescein within corneal epithelium. *Experimental Eye Research*, **147**, 12–19.
Glasser, A. (2003) How other species accommodate. In: *Current Aspects of Human Accommodation, Vol. II* (eds. Guthoff, R. & Ludwig, K.), pp. 13–38. Heidelberg: Kaden.
Glasser, A. (2011) Accommodation. In: *Adler's Physiology of the Eye* (eds. Levin, L.A., Nilsson, S.F.E., ver Hoeve, J.N., et al.), 11th ed., pp. 40–70. St. Louis, MO: Elsevier Saunders.
Glasser, A., Troilo, D., & Howland, H.C. (1994) The mechanism of corneal accommodation in chicks. *Vision Research*, **34**, 1549–1566.
Gleason, E. (2012) The influences of metabotropic receptor activation on cellular signaling and synaptic function in amacrine cells. *Visual Neuroscience*, **29**, 31–39.
Glickstein, M. & Millodot, M. (1970) Retinoscopy and eye size. *Science*, **168**, 605–606.
Gobbe, M., Reinstein, D.Z., & Archer, T.J. (2015) LASIK-induced aberrations: Comparing corneal and whole-eye measurements. *Optometry and Vision Science*, **92**, 447–455.
Grimes, W.N., Zhang, J., Graydon, C.W., et al. (2010) Retinal parallel processors: More than 100 independent microcircuits operate within a single interneuron. *Neuron*, **65**, 873–885.
Grinninger, P., Skalicky, M., & Nell, B. (2010) Evaluation of healthy equine eyes by use of retinoscopy, keratometry, and ultrasonographic biometry. *American Journal of Veterinary Research*, **71**, 677–681.
Griswold, M.S. & Stark, W.S. (1992) Scotopic spectral sensitivity of phakic and aphakic observers extending into the near ultraviolet. *Vision Research*, **32**, 1739–1743.

Groth, A.D., Hollingsworth, S.R., Ofri, R., et al. (2013) Clinical comparison of the Welch Allyn SureSight™ handheld autorefractor vs. streak retinoscopy in dogs. *Veterinary Ophthalmology*, **16**, 319–323.

Guggenheim, J.A., Creer, R.C., & Qin, X.J. (2004) Postnatal refractive development in the Brown Norway rat: Limitations of standard refractive and ocular component dimension measurement techniques. *Current Eye Research*, **29**, 369–376.

Guggenheim, J.A., Ghorbani Mojarrad, N., Williams, C., et al. (2017) Genetic prediction of myopia: Prospects and challenges. *Ophthalmic and Physiological Optics*, **37**, 549–556.

Habib, M.S., Speaker, M.G., Tello, C., et al. (1995) Ultrasound biomicroscopy of intrastromal photorefractive keratectomy with the Nd:YLF picosecond laser. *Journal of Refractive Surgery*, **11**, 448–452.

Hamon, A., Roger, J.E., Yang, X.J., et al. (2016) Müller glial cell-dependent regeneration of the neural retina: An overview across vertebrate model systems. *Developmental Dynamics*, **245**, 727–738.

Hanke, F.D. & Dehnhardt, G. (2009) Aerial visual acuity in harbor seals (*Phoca vitulina*) as a function of luminance. *Journal of Comparative Physiology A: Neuroethology, Sensory, Neural, and Behavioral Physiology*, **195**, 643–650.

Hanke, F.D., Dehnhardt, G., Schaeffel, F., & Hanke, W. (2006) Corneal topography, refractive state, and accommodation in harbor seals (*Phoca vitulina*). *Vision Research*, **46**, 837–847.

Hanke, F.D., Kröger, R.H., Siebert, U., et al. (2008) Multifocal lenses in a monochromat: The harbour seal. *Journal of Experimental Biology*, **211**, 3315–3322.

Hargrave, P.A. (2001) Rhodopsin structure, function, and topography. The Friedenwald lecture. *Investigative Ophthalmology & Visual Science*, **42**, 3–9.

Harman, A.M., Moore, S., Hoskins, R., et al. (1999) Horse vision and an explanation for the visual behaviour originally explained by the "ramp retina." *Equine Veterinary Journal*, **31**, 384–390.

Harrington, J.T., McMullen, R.J., Clode, A.B., et al. (2013) Phacoemulsification and +14 diopter intraocular lens placement in a Saddlebred foal. *Veterinary Ophthalmology*, **16**, 140–148.

Hattar, S., Liao, H.W., Takao, M., et al. (2002) Melanopsin-containing retinal ganglion cells: Architecture, projections, and intrinsic photosensitivity. *Science*, **295**, 1065–1070.

Haverkamp, S., Grunert, U., & Wässle, H. (2000) The cone pedicle, a complex synapse in the retina. *Neuron*, **27**, 85–95.

Heidelberger, R., Thoreson, W.B., & Witkovsky, P. (2005) Synaptic transmission at retinal ribbon synapses. *Progress in Retinal and Eye Research*, **24**, 682–720.

Henze, M.J., Schaeffel, F., & Ott, M. (2004) Variations in the off-axis refractive state in the eye of the Vietnamese Leaf turtle (*Geoemyda spengleri*). *Journal of Comparative Physiology A*, **190**, 131–137.

Hernandez, J., Moore, C., Si, X., et al. (2016) Aging dogs manifest myopia as measured by autorefractor. *PLoS One*, **11**, e0148436.

Herrera, E., Erskine, L., & Morenilla-Palao, C. (2019) Guidance of retinal axons in mammals. *Seminars in Cell and Developmental Biology*, **85**, 48–59. doi: 10.1016/j.semcdb.2017.11.027.

Herse, P. (2005) Effects of hyperglycaemia on ocular development in rabbit: Refraction and biometric changes. *Ophthalmic and Physiological Optics*, **25**, 97–104.

Hodos, W. & Erichsen, J.T. (1990) Lower-field myopia in birds: An adaptation that keeps the ground in focus. *Vision Research*, **30**, 653–657.

Hofmann, L. & Palczewski, K. (2015a) Advances in understanding the molecular basis of the first steps in color vision. *Progress in Retinal and Eye Research*, **49**, 46–66.

Hofmann, L. & Palczewski, K. (2015b) The G protein-coupled receptor rhodopsin: A historical perspective. *Methods in Molecular Biology*, **1271**, 3–18.

Hogg, C., Neveu, M., Stokkan, K.A., et al. (2011) Arctic reindeer extend their visual range into the ultraviolet. *Journal of Experimental Biology*, **214**, 2014–2019.

Hoon, M., Okawa, H., Della Santina, L., et al. (2014) Functional architecture of the retina: Development and disease. *Progress in Retinal and Eye Research*, **42**, 44–84.

Howlett, M.H. & McFadden, S.A. (2007) Emmetropization and schematic eye models in developing pigmented Guinea pigs. *Vision Research*, **47**, 1178–1190.

Hsu, A., Tsukamoto, Y., Smith, R.G., et al. (1998) Functional architecture of primate cone and rod axons. *Vision Research*, **38**, 2539–2549.

Hughes, A. (1977) The topography of vision in mammals of contrasting life style: Comparative optics and retinal organization. In: *The Visual System in Vertebrates: Handbook of Sensory Physiology VII* (ed. Crescitelli, F.), pp. 86–195. Berlin: Springer.

Hughes, S., Hankins, M.W., Foster, R.G., et al. (2012) Melanopsin phototransduction: Slowly emerging from the dark. *Progress in Brain Research*, **199**, 19–40.

Hughes, S., Jagannath, A., Rodgers, J., et al. (2016) Signalling by melanopsin (OPN4) expressing photosensitive retinal ganglion cells. *Eye*, **30**, 247–254.

Hung, L.F., Ramamirtham, R., Wensveen, J.M., et al. (2012) Objective and subjective refractive error measurements in monkeys. *Optometry and Vision Science*, **89**, 168–177.

Hunt, D.M., Carvalho, L.S., Cowing, J.A., et al. (2009) Evolution and spectral tuning of visual pigments in birds and mammals. *Philosophical Transactions of the Royal Society of London. Series B, Biological Sciences*, **364**, 2941–2955.

Iacaruso, M.F., Gasler, I.T., & Hofer, S.B. (2017) Synaptic organization of visual space in primary visual cortex. *Nature*, **547**, 449–452.

Imamoto, Y. & Shichida, Y. (2014) Cone visual pigments. *Biochimica et Biophysica Acta*, **1837**, 664–673.

Iribarren, R., Rozema, J.J., Schaeffel, F., et al. (2014) Calculation of crystalline lens power in chickens with a customized version of Bennett's equation. *Vision Research*, **96**, 33–38.

Ito, Y., Maehara, S., Itoh, Y., et al. (2016) Effect of refractive error on visual evoked potentials with pattern stimulation in dogs. *Journal of Veterinary Medical Science*, **78**, 505–508.

Jeffery, G., Levitt, J.B., & Cooper, H.M. (2008) Segregated hemispheric pathways through the optic chiasm distinguish primates from rodents. *Neuroscience*, **157**, 637–643.

Jiang, Z., Yang, J., Purpura, L.A., et al. (2014) Glycinergic feedback enhances synaptic gain in the distal retina. *Journal of Physiology*, **592**, 1479–1492.

Johansson, M.K., Jäderkvist Fegraeus, K., Lindgren, G., et al. (2017) The refractive state of the eye in Icelandic horses with the silver mutation. *BMC Veterinary Research*, **13**, 153.

Jusuf, P.R., Martin, P.R., & Grunert, U. (2006) Synaptic connectivity in the midget-parvocellular pathway of primate central retina. *Journal of Comparative Neurology*, **494**, 260–274.

Kaplan, M.R., Cho, M.H., Ullian, E.M., et al. (2001) Differential control of clustering of the sodium channels Na(v)1.2 and Na(v)1.6 at developing CNS nodes of Ranvier. *Neuron*, **30**, 105–119.

Katzir, G. & Howland, H.C. (2003) Corneal power and underwater accommodation in great cormorants (*Phalacrocorax carbo sinensis*). *Journal of Experimental Biology*, **206**, 833–841.

Keeler, C.E. (1927) Iris movements in blind mice. *American Journal of Physiology*, **81**, 107–112.

Kessel, L., Lundeman, J.H., Herbst, K., et al. (2010) Age-related changes in the transmission properties of the human lens and their relevance to circadian entrainment. *Journal of Cataract and Refractive Surgery*, **36**, 308–312.

Khorramshahi, O., Schartau, J.M., & Kröger, R.H. (2008) A complex system of ligaments and a muscle keep the crystalline lens in place in the eyes of bony fishes (teleosts). *Vision Research*, **48**, 1503–1508.

Kim, I.J., Zhang, Y., Meister, M., et al. (2010) Laminar restriction of retinal ganglion cell dendrites and axons, subtype-specific developmental patterns revealed with transgenic markers. *Journal of Neuroscience*, **30**, 1452–1462.

Kiser, P.D., Golczak, M., & Palczewski, K. (2014) Chemistry of the retinoid (visual) cycle. *Chemical Reviews*, **114**, 194–232.

Klump, K.E., Zhang, A.J., Wu, S.M., et al. (2009) Parvalbumin-immunoreactive amacrine cells of macaque retina. *Visual Neuroscience*, **26**, 287–296.

Kofuji, P., Ceelen, P., Zahs, K.R., et al. (2000) Genetic inactivation of an inwardly rectifying potassium channel (Kir4.1 subunit) in mice: Phenotypic impact in retina. *Journal of Neuroscience*, **20**, 5733–5740.

Koh, S. (2016) Mechanisms of visual disturbance in dry eye. *Cornea*, **35(**Suppl. 1), S83–S88.

Kolb, H. (1979) The inner plexiform layer in the retina of the cat: Electron microscopic observations. *Journal of Neurocytology*, **8**, 295–329.

Kolb, H. & Marshak D. (2003) The midget pathways of the primate retina. *Documenta Ophthalmologica*, **106**, 67–81.

Kolb, H., Nelson, R., & Mariani, A. (1981) Amacrine cells, bipolar cells and ganglion cells of the cat retina: A Golgi study. *Vision Research*, **21**, 1081–1114.

Kolesnikov, A.V., Tang, P.H., Parker, R.O., et al. (2011) The mammalian cone visual cycle promotes rapid M/L-cone pigment regeneration independently of the interphotoreceptor retinoid-binding protein. *Journal of Neuroscience*, **31**, 7900–7909.

Konrade, K.A., Hoffmam, A.R., Ramey, K.L., et al. (2012) Refractive states of eyes and associations between ametropia and age, breed, and axial globe length in domestic cats. *American Journal of Veterinary Research*, **73**, 279–284.

Kravitz, D.J., Saleem, K.S., Baker, C.I., et al. (2011) A new neural framework for visuospatial processing. *Neuroscience*, **12**, 217–230.

Kreuzer, R.O. & Sivak, J.G. (1985) Chromatic aberration of the vertebrate lens. *Ophthalmic and Physiological Optics*, **5**, 33–41.

Krispel, C.M., Chen, D., Melling, N., et al. (2006) RGS expression rate-limits recovery of rod photoresponses. *Neuron*, **51**, 409–416.

Kröger, R.H. (2013) Optical plasticity in fish lenses. *Progress in Retinal and Eye Research*, **34**, 78–88.

Kubai, M.A., Bentley, E., Miller, P.E., et al. (2008) Refractive states of eyes and association between ametropia and breed in dogs. *American Journal of Veterinary Research*, **69**, 946–951.

Kubai, M.A., Labelle, A.L., Hamor, R.E., et al. (2013) Heritability of lenticular myopia in English Springer Spaniels. *Investigative Ophthalmology & Visual Science*, **54**, 7324–7328.

Kuhn, S.E., Hendrix, D.V., Jones, M.P., et al. (2015) Biometry, keratometry, and calculation of intraocular lens power for the bald eagle (*Haliaeetus leucocephalus*). *Veterinary Ophthalmology*, **18(**Suppl. 1), 106–112.

Kuszak, J.R., Mazurkiewicz, M., Jison, L., et al. (2006) Quantitative analysis of animal model lens anatomy: Accommodative range is related to fiber structure and organization. *Veterinary Ophthalmology*, **9**, 266–280.

Lamb, T.D. (2013) Evolution of phototransduction, vertebrate photoreceptors and retina. *Progress in Retinal and Eye Research*, **36**, 52–119.

Lamb, T.D. (2016) Why rods and cones? *Eye*, **30**, 179–185.

Lamb, T.D., Collin, S.P., & Pugh, E.N., Jr. (2007) Evolution of the vertebrate eye: Opsins, photoreceptors, retina and eye cup. *Neuroscience*, **8**, 960–976.

Lamb, T.D., Patel, H., Chuah, A., et al. (2016) Evolution of vertebrate phototransduction: Cascade activation. *Molecular Biology and Evolution*, **33**, 2064–2087.

Lamb, T.D. & Pugh, E.N., Jr. (2006) Phototransduction, dark adaptation, and rhodopsin regeneration. *The Proctor lecture. Investigative Ophthalmology & Visual Science*, **47**, 5137–5152.

Lambert, S.R. (2016) Changes in ocular growth after pediatric cataract surgery. *Developments in Ophthalmology*, **57**, 29–39.

Land, M.F. (2006) Visual optics: The shapes of pupils. *Current Biology*, **16**, R167–R168.

Lee, S., Zhang, Y., Chen, M., et al. (2016a) Segregated glycine-glutamate co-transmission from vglut3 amacrine cells to contrast-suppressed and contrast-enhanced retinal circuits. *Neuron*, **90**, 27–34.

Lee, S.C., Weltzien, F., Madigan, M.C., et al. (2016b) Identification of A amacrine, displaced amacrine, and bistratified ganglion cell types in human retina with antibodies against calretinin. *Journal of Comparative Neurology*, **524**, 39–53.

Lehky, S.R., Sejnowski, T.J., & Desimone, R. (2005) Selectivity and sparseness in the responses of striate complex cells. *Vision Research*, **45**, 57–73.

Lei, B. & Yao, G. (2006) Spectral attenuation of the mouse, rat, pig and human lenses from wavelengths 360 nm to 1020 nm. *Experimental Eye Research*, **83**, 610–614.

Levenson, D.H. & Schusterman, R.J. (1997) Pupillometry in seals and sea lions: Ecological implications. *Canadian Journal of Zoology*, **75**, 2050–2057.

Levick, W.R. (1967) Receptive fields and trigger features of ganglion cells in the visual streak of the rabbits retina. *Journal of Physiology*, **188**, 285–307.

Li, J., Jiao, X., Zhang, Q., et al. (2017a) Association and interaction of myopia with SNP markers rs13382811 and rs6469937 at ZFHX1B and SNTB1 in Han Chinese and European populations. *Molecular Vision*, **23**, 588–604.

Li, X., Kelly, D., Nolan, J.M., et al. (2017b) The evidence informing the surgeon's selection of intraocular lens on the basis of light transmittance properties. *Eye*, **31**, 258–272.

Lisney, T.J., Stecyk, K., Kolominsky, J., et al. (2013) Ecomorphology of eye shape and retinal topography in waterfowl (Aves: Anseriformes: Anatidae) with different foraging modes. *Journal of Comparative Physiology A, Neuroethology, Sensory, Neural, and Behavioral Physiology*, **199**, 385–402.

Livingstone, M.S. & Hubel, D.H. (1984) Anatomy and physiology of a color system in the primate visual cortex. *Journal of Neuroscience*, **4**, 309–356.

Lombardo, M., Pucci, G., Barberi, R., et al. (2015) Interaction of ultraviolet light with the cornea: Clinical implications for corneal crosslinking. *Journal of Cataract and Refractive Surgery*, **41**, 446–459.

Luo, D.G., Xue, T., & Yau, K.W. (2008) How vision begins: An odyssey. *Proceedings of the National Academy of Sciences of the USA*, **105**, 9855–9862.

Lynch, J.W. (2009) Native glycine receptor subtypes and their physiological roles. *Neuropharmacology*, **56**, 303–309.

MacNair, C.E. & Nickells, R.W. (2015) Neuroinflammation in glaucoma and optic nerve damage. *Progress in Molecular Biology and Translational Science*, **134**, 343–363.

Machovsky-Capuska, G.E., Howland, H.C., Raubenheimer, D., et al. (2012) Visual accommodation and active pursuit of prey underwater in a plunge-diving bird: The Australasian gannet. *Proceedings of the Royal Society B: Biological Sciences*, **279**, 4118–4125.

Macneil, M.A., Purrier, S., & Rushmore, R.J. (2009) The composition of the inner nuclear layer of the cat retina. *Visual Neuroscience*, **26**, 365–374.

Maehara, S., Itoh, Y., Higashinozono, K., et al. (2011) Evaluation of refractive value by skiascopy in healthy Beagles. *Journal of Veterinary Medical Science*, **73**, 927–929.

Makino, C.L., Wen, X.H., & Lem, J. (2003) Piecing together the timetable for visual transduction with transgenic animals. *Current Opinions in Neurobiology*, **13**, 404–412.

Malmström, T. & Kröger, R.H. (2006) Pupil shapes and lens optics in the eyes of terrestrial vertebrates. *Journal of Experimental Biology*, **209**, 18–25.

Marshak, D.W. (2016) A tale of two neurotransmitters. *Visual Neuroscience*, **33**, E017.

Marshak, D.W. & Mills, S.L. (2014) Short-wavelength cone-opponent retinal ganglion cells in mammals. *Visual Neuroscience*, **31**, 165–175.

Martersteck, E.M., Hirokawa, K.E., Evarts, M., et al. (2017) Diverse central projection patterns of retinal ganglion cells. *Cell Reports*, **18**, 2058–2072.

Martin, G.R., Ashash, U., & Katzir, G. (2001) Ostrich ocular optics. *Brain, Behavior and Evolution*, **58**, 115–120.

Masland, R.H. (2012) The neuronal organization of the retina. *Neuron*, **76**, 266–280.

Masri, R.A., Percival, K.A., Koizumi, A., et al. (2019) Survey of retinal ganglion cell morphology in marmoset. *Journal of Comparative Neurology*, **527**, 236–258. doi: 10.1002/cne.24157.

Mass, A.M. & Supin, A.Y. (2007) Adaptive features of aquatic mammals' eye. *Anatomical Record*, **290**, 701–715.

Maunsell, J.H. & Van Essen, D.C. (1983a) Functional properties of neurons in middle temporal visual area of the macaque monkey. I. Selectivity for stimulus direction, speed, and orientation. *Journal of Neurophysiology*, **49**, 1127–1147.

Maunsell, J.H. & Van Essen, D.C. (1983b) Functional properties of neurons in middle temporal visual area of the macaque monkey. II. Binocular interactions and sensitivity to binocular disparity. *Journal of Neurophysiology*, **49**, 1148–1167.

McBrien, N.A., Moghaddam, H.O., New, R., et al. (1993) Experimental myopia in a diurnal mammal (*Sciurus carolinensis*) with no accommodative ability. *Journal of Physiology*, **469**, 427–441.

McCourt, M.E. & Jacobs, G.H. (1984) Refractive state, depth of focus and accommodation of the eye of the California ground squirrel (*Spermophilus beecheyi*). *Vision Research*, **24**, 1261–1266.

McLaren, J.W. & Brubaker, R.F. (1996) Measurement of transmission of ultraviolet and visible light in the living rabbit cornea. *Current Eye Research*, **15**, 411–421.

McMullen, R.J., Davidson, M.G., Campbell, N.B., et al. (2010) Evaluation of 30- and 25-diopter intraocular lens implants in equine eyes after surgical extraction of the lens. *American Journal of Veterinary Research*, **71**, 809–816.

McMullen, R.J., Davidson, M.G., & Gilger, B.C. (2014) The effect of 1% tropicamide-induced mydriasis and cycloplegia on spherical refraction of the adult horse. *Veterinary Ophthalmology*, **17**, 120–125.

McMullen, R.J. & Gilger, B.C. (2006) Keratometry, biometry and prediction of intraocular lens power in the equine eye. *Veterinary Ophthalmology*, **9**, 357–360.

Meister, M., Lagnado, L., & Baylor, D.A. (1995) Concerted signaling by retinal ganglion cells. *Science*, **270**, 1207–1210.

Millemann, Y., Benoit-Valiergue, H., Bonnin, J.P., et al. (2007) Ocular and cardiac malformations associated with maternal hypovitaminosis A in cattle. *Veterinary Record*, **160**, 441–443.

Miller, P.E. & Murphy, C.J. (1995) Vision in dogs. *Journal of the American Veterinary Medical Association*, **207**, 1623–1634.

Miller, P.E. & Murphy, C.J. (2017) Equine vision. In: *Equine Ophthalmology* (ed. Gilger, B.C.), 3rd ed., pp. 508–544. Ames: Wiley-Blackwell.

Miller, S.N., Colitz, C.M., & Dubielzig, R.R. (2010) Anatomy of the California sea lion globe. *Veterinary Ophthalmology*, **13(**Suppl.), 63–71.

Millodot, M. (1982) Image formation in the eye. In: *The Senses* (eds. Barlow, H.B. & Mollon, J.D.), pp. 46–61. Cambridge: Cambridge University Press.

Millodot, M. (2018) *Dictionary of Optometry and Visual Science*, 8th ed. St. Louis, MO: Elsevier.

Millodot, M. & O'Leary, D. (1978) The discrepancy between retinoscopic and subjective measurements: Effect of age. *American Journal of Optometry and Physiological Optics*, **55**, 309–316.

Millodot, M. & Sivak, J. (1979) Contribution of the cornea and lens to the spherical aberration of the eye. *Vision Research*, **19**, 685–687.

Molday, R.S. & Moritz, O.L. (2015) Photoreceptors at a glance. *Journal of Cell Science*, **128**, 4039–4045.

Monavarfeshani, A., Sabbagh, U., & Fox, M.A. (2017) Not a one-trick pony: Diverse connectivity and functions of the rodent lateral geniculate complex. *Visual Neuroscience*, **34**, E012.

Montes-Mico, R., Alio, J.L., Munoz, G., et al. (2004) Postblink changes in total and corneal ocular aberrations. *Ophthalmology*, **111**, 758–767.

Morgan, I.G., French, A.N., Ashby, R.S., et al. (2018) The epidemics of myopia: Aetiology and prevention. *Progress in Retinal and Eye Research*, **62**, 134–149.

Morin, L.P. & Studholme, K.M. (2014) Retinofugal projections in the mouse. *Journal of Comparative Neurology*, **522**, 3733–3753.

Mouney, M.C., Townsend, W.M., & Moore, G.E. (2012) Association of height, body weight, age, and corneal diameter with calculated intraocular lens strength of adult horses. *American Journal of Veterinary Research*, **73**, 1977–1982.

Mowat, F.M., Petersen-Jones, S.M., Williamson, H., et al. (2008) Topographical characterization of cone photoreceptors and the area centralis of the canine retina. *Molecular Vision*, **14**, 2518–2527.

Müller, W. & Topke, H. (1987) The early receptor potential (ERP). *Documenta Ophthalmologica*, **66**, 35–74.

Murphy, C.J., Bellhorn, R.W., Williams, T., et al. (1990) Refractive state, ocular anatomy, and accommodative range of the sea otter (*Enhydra lutris*). *Vision Research*, **30**, 23–32.

Murphy, C.J., Howland, M., & Howland, H.C. (1995) Raptors lack lower-field myopia. *Vision Research*, **35**, 1153–1155.

Murphy, C.J., Kern, T.J., & Howland, H.C. (1992a) Refractive state, corneal curvature, accommodative range and ocular anatomy of the Asian elephant (*Elephas maximus*). *Vision Research*, **32**, 2021.

Murphy, C.J., Zadnik, K., & Mannis, M.J. (1992b) Myopia and refractive error in dogs. *Investigative Ophthalmology & Visual Science*, **33**, 2459–2463.

Mustafi, D., Engel, A.H., & Palczewski, K. (2009) Structure of cone photoreceptors. *Progress in Retinal and Eye Research*, **28**, 289–302.

Mutti, D.O., ver Hoeve, J.N., Zadnik, K., et al. (1997) The artifact of retinoscopy revisited: Comparison of refractive error measured by retinoscopy and visual evoked potential in the rat. *Optometry and Vision Science*, **74**, 483–488.

Mutti, D.O., Zadnik, K., & Murphy, C.J. (1999) Naturally occurring vitreous chamber-based myopia in the Labrador Retriever. *Investigative Ophthalmology & Visual Science*, **40**, 1577–1584.

Næser, K., Savini, G., & Bregnhøj, J.F. (2016) Corneal powers measured with a rotating Scheimpflug camera. *British Journal of Ophthalmology*, **100**, 1196–1200.

Nagloo, N., Collin, S.P., Hemmi, J.M., et al. (2016) Spatial resolving power and spectral sensitivity of the saltwater crocodile, *Crocodylus porosus*, and the freshwater crocodile, *Crocodylus johnstoni*. *Journal of Experimental Biology*, **219**, 1394–1404.

Nakamichi, H. & Okada, T. (2006) Local peptide movement in the photoreaction intermediate of rhodopsin. *Proceedings of the National Academy of Sciences of the USA*, **103**, 12729–12734.

Nasir-Ahmad, S., Lee, S.C., Martin, P.R., et al. (2019) Melanopsin-expressing ganglion cells in human retina: Morphology, distribution, and synaptic connections. *Journal of Comparative Neurology*, **527**, 312–327. doi: 10.1002/cne.24176.

Nath, A. & Schwartz, G.W. (2017) Electrical synapses convey orientation selectivity in the mouse retina. *Nature Communications*, **8**, 2025.

Nelms, S.R., Davidson, M.G., Nasisse, M.P., et al. (1994) Comparison of corneal and scleral surgical approaches for cataract extraction by phacoemulsification and intraocular lens implantation in normal dogs. *Veterinary and Comparative Ophthalmology*, **4**, 53–60.

Nemeth, G., Szalai, E., Berta, A., et al. (2013) Astigmatism prevalence and biometric analysis in normal population. *European Journal of Ophthalmology*, **23**, 779–783.

Neveu, M.M. & Jeffery, G. (2007) Chiasm formation in man is fundamentally different from that in the mouse. *Eye*, **21**, 1264–1270.

Nguyen-Legros, J. & Hicks, D. (2000) Renewal of photoreceptor outer segments and their phagocytosis by the retinal pigment epithelium. *International Review of Cytology*, **196**, 245–313.

Nickla, D.L. & Wallman, J. (2010) The multifunctional choroid. *Progress in Retinal and Eye Research*, **29**, 144–168.

Nishimoto, K. & Sasaki, K. (1995) *In vivo* light scattering intensity in the lens versus *in vitro* spectral transmission in the nuclear region. *Ophthalmic Research*, **27**, 1–11.

Norton, T.T. (2016) What do animal studies tell us about the mechanism of myopia-protection by light? *Optometry and Vision Science*, **93**, 1049–1051.

Norton, T.T., Wu, W.W., & Siegwart, J.T. (2003) Refractive state of tree shrew eyes measured with cortical visual evoked potentials. *Optometry and Vision Science*, **80**, 623–631.

Odeen, A., Hastad, O., & Alstrom, P. (2011) Evolution of ultraviolet vision in the largest avian radiation—the passerines. *BMC Evolutionary Biology*, **11**, 313.

Ofri, R., Dawson, W.W., & Samuelson, D.A. (1994) Mapping of the cortical area of central vision in two dog breeds. *Veterinary and Comparative Ophthalmology*, **4**, 172–178.

Ofri, R., Hollingsworth, S.R., Groth, A., et al. (2012) Effect of optical defocus on performance of dogs involved in field trial competition. *American Journal of Veterinary Research*, **73**, 546–550.

Ofri, R., Millodot, S., Shimoni, R., et al. (2001) Development of the refractive state in eyes of Ostrich chicks (*Struthio camelus*). *American Journal of Veterinary Research*, **62**, 812–815.

Ofri, R., Millodot, S., Tadmor, Y., et al. (2004) The development of the refractive state in the newborn Thomson gazelle. *Journal of Comparative Physiology A*, **190**, 831–835.

O'Neill, W.D. & Brodkey, J.S. (1969) Linear regression of lens movement with refractive state using ciliary ganglion stimulation in the cat. *Archives of Ophthalmology*, **82**, 795–799.

Osterberg, G. (1935) Topography of the layer of rods and cones in the human retina. *Acta Ophthalmologica (Suppl.)*, **6**, 1–103.

Ostrin, L.A., Garcia, M.B., Choh, V., et al. (2014) Pharmacologically stimulated pupil and accommodative changes in guinea pigs. *Investigative Ophthalmology & Visual Science*, **55**, 5456–5465.

Ostrin, L.A., Liu, Y., Choh, V., et al. (2011) The role of the iris in chick accommodation. *Investigative Ophthalmology & Visual Science*, **52**, 4710–4716.

Ott, M. (2006) Visual accommodation in vertebrates: Mechanisms, physiological response and stimuli. *Journal of Comparative Physiology A*, **192**, 97–111.

Palczewski, K. (2006) G protein-coupled receptor rhodopsin. *Annual Review of Biochemistry*, **75**, 743–767.

Palczewski, K. (2014) Chemistry and biology of the initial steps in vision. *The Friedenwald lecture. Investigative Ophthalmology & Visual Science*, **55**, 6651–6672.

Pang, J.J., Gao, F., Lem, J., et al. (2010) Direct rod input to cone BCs and direct cone input to rod BCs challenge the traditional view of mammalian BC circuitry. *Proceedings of the National Academy of Sciences of the USA*, **107**, 395–400.

Pardue, M.T., Stone, R.A., & Iuvone, P.M. (2013) Investigating mechanisms of myopia in mice. *Experimental Eye Research*, **114**, 96–105.

Parker, R., Wang, J.S., Kefalov, V.J., et al. (2011) Interphotoreceptor retinoid-binding protein as the physiologically relevant carrier of 11-cis-retinol in the cone visual cycle. *Journal of Neuroscience*, **31**, 4714–4719.

Patel, S., Marshall, J., & Fitzke, F.W., 3rd (1995) Refractive index of the human corneal epithelium and stroma. *Journal of Refractive Surgery*, **11**, 100–105.

Pausch, H., Wang, X., Jung, S., et al. (2012) Identification of QTL for UV-protective eye area pigmentation in cattle by progeny phenotyping and genome-wide association analysis. *PLoS One*, **7**, e36346.

Pederson, S.L., Cleymaet, A.M., Hess, A.M., et al. (2019) Surgically induced astigmatism in canines following sutured dorsonasal vs dorsotemporal clear corneal incisions. *Veterinary Ophthalmology*, **22**, 799–806.

Peichl, L. (2005) Diversity of mammalian photoreceptor properties: Adaptations to habitat and lifestyle? *Anatomical Record. Part A, Discoveries in Molecular, Cellular, and Evolutionary Biology*, **287**, 1001–1012.

Peiffer, R.L., Jr. & Gaiddon, J. (1991) Posterior chamber intraocular lens implantation in the dog: Results of 65 implants in 61 patients. *Journal of the American Animal Hospital Association*, **27**, 453–462.

Percival, K.A., Koizumi, A., Masri, R.A., et al. (2014) Identification of a pathway from the retina to koniocellular layer K1 in the lateral geniculate nucleus of marmoset. *Journal of Neuroscience*, **34**, 3821–3825.

Petersen-Jones, S.M. & Komaromy, A.M. (2015) Dog models for blinding inherited retinal dystrophies. *Human Gene Therapy, Clinical Development*, **26**, 15–26.

Pettigrew, J.D. & Collin, S.P. (1995) Terrestrial optics in an aquatic eye: The sandlance, *Limnichthytes fasciatus* (Creediidae, Teleostei). *Journal of Comparative Physiology A*, **177**, 397–408.

Pierscionek, B.K. & Regini, J.W. (2012) The gradient index lens of the eye: An opto-biological synchrony. *Progress in Retinal and Eye Research*, **31**, 332–349.

Piggins, D. & Phillips, C.J.C. (1996) The eye of the domesticated sheep with implications for vision. *Animal Science*, **62**, 301–308.

Pollet, L. (1982) Refraction of normal and aphakic canine eyes. *Journal of the American Animal Hospital Association*, **18**, 323–326.

Ponce, C.R., Lomber, S.G., & Born, R.T. (2008) Integrating motion and depth via parallel pathways. *Nature Neuroscience*, **11**, 216–223.

Prince, J.H., Diesem, C.D., Eglitis, I., et al. (1960) *Anatomy and Histology of the Eye and Orbit in Domestic Animals*. Springfield, IL: Charles C. Thomas.

Provencio, I., Jiang, G., De Grip, W.J., et al. (1998) Melanopsin: An opsin in melanophores, brain, and eye. *Proceedings of the National Academy of Sciences of the USA*, **95**, 340–345.

Provis, J.M., Dubis, A.M., Maddess, T., et al. (2013) Adaptation of the central retina for high acuity vision: Cones, the fovea and the avascular zone. *Progress in Retinal and Eye Research*, **35**, 63–81.

Puller, C., Ivanova, E., Euler, T., et al. (2013) OFF bipolar cells express distinct types of dendritic glutamate receptors in the mouse retina. *Neuroscience*, **243**, 136–148.

Qiao, S.N., Zhang, Z., Ribelayga, C.P., et al. (2016) Multiple cone pathways are involved in photic regulation of retinal dopamine. *Scientific Reports*, **6**, 28916.

Qiao-Grider, Y., Hung, L.F., Kee, C.S., et al. (2010) Nature of the refractive errors in rhesus monkeys (*Macaca mulatta*) with experimentally induced ametropias. *Vision Research*, **50**, 1867–1881.

Quattrochi L.E., Stabio M.E., Kim I., et al. (2019) The M6 cell: A small-field bistratified photosensitive retinal ganglion cell. *J Comp Neurol* 527, 297–311.

Read, S.A., Collins, M.J., & Carney, L.G. (2007) A review of astigmatism and its possible genesis. *Clinical and Experimental Optometry*, **90**, 5–19.

Redmond, T.M. (2009) Focus on molecules: RPE65, the visual cycle retinol isomerase. *Experimental Eye Research*, **88**, 846–847.

Reese, B.E. (2011) Development of the retina and optic pathway. *Vision Research*, **51**, 613–632.

Reese, B.E., Raven, M.A., & Stagg, S.B. (2005) Afferents and homotypic neighbors regulate horizontal cell morphology, connectivity, and retinal coverage. *Journal of Neuroscience*, **25**, 2167–2175.

Reid, R.C. (2012) From functional architecture to functional connectomics. *Neuron*, **75**, 209–217.

Reilly, M.A. (2014) A quantitative geometric mechanics lens model: Insights into the mechanisms of accommodation and presbyopia. *Vision Research*, **103**, 20–31.

Rockhill, R.L., Daly, F.J., MacNeil, M.A., et al. (2002) The diversity of ganglion cells in a mammalian retina. *Journal of Neuroscience*, **22**, 3831–3843.

Rohen, J.W., Kaufman, P.L., Eichhorn, M., et al. (1989) Functional morphology of accommodation in the raccoon. *Experimental Eye Research*, **48**, 523–527.

Rosolen, S.G., Ganem, S., Gross, M., et al. (1995) Refractive corneal surgery on dogs: Preliminary results of keratomileusis using a 193 nanometer excimer laser. *Veterinary and Comparative Ophthalmology*, **5**, 18–24.

Roy, K., Kumar, S., & Bloomfield, S.A. (2017) Gap junctional coupling between retinal amacrine and ganglion cells underlies coherent activity integral to global object perception. *Proceedings of the National Academy of Sciences of the USA*, **114**, E10484–E10493.

Rull-Cotrina, J., Molleda, J.M., Gallardo, J., et al. (2013) Refractive state of the Spanish Thoroughbred horse: A comparison with the Crossbred horse. *Veterinary Ophthalmology*, **16**, 25–28.

Saari, J.C. (2000) Biochemistry of visual pigment regeneration. The Friedenwald lecture. *Investigative Ophthalmology & Visual Science*, **41**, 337–348.

Sagdullaev, B.T., Eggers, E.D., Purgert, R., et al. (2011) Nonlinear interactions between excitatory and inhibitory retinal synapses control visual output. *Journal of Neuroscience*, **31**, 15102–15112.

Samuelson, D.A. (1996) A reevaluation of the comparative anatomy of the eutherian iridocorneal angle and associated ciliary body musculature. *Veterinary and Comparative Ophthalmology*, **6**, 153–172.

Samuelson, D.A. & Lewis, P.A. (1995) Comparative morphology of the iridocorneal angle among selected atriodactyls (ungulates). *Veterinary and Comparative Ophthalmology*, **5**, 89–103.

Sanchez, I., Martin, R., Ussa, F., et al. (2011) The parameters of the porcine eyeball. *Graefe's Archives of Clinical and Experimental Ophthalmology*, **249**, 475–482.

Sanchez, R.F., Becker, R., Dawson, C., et al. (2017) Calculation of posterior chamber intraocular lens (IOL) size and dioptric power for use in pet rabbits undergoing phacoemulsification. *Veterinary Ophthalmology*, **20**, 242–249.

Sandmann, D., Boycott, B.B., & Peichl, L. (1996) Blue-cone horizontal cells in the retinae of horses and other equidae. *Journal of Neuroscience*, **16**, 3381–3396.

Savage, D.E., Brooks, D.R., DeMagistris, M., et al. (2014) First demonstration of ocular refractive change using blue-IRIS in live cats. *Investigative Ophthalmology & Visual Science*, **55**, 4603–4612.

Savini, G., Næser, K., Schiano-Lomoriello, D., et al. (2017) Optimized keratometry and total corneal astigmatism for toric intraocular lens calculation. *Journal of Cataract and Refractive Surgery*, **43**, 1140–1148.

Schaeffel, F. & Feldkaemper, M. (2015) Animal models in myopia research. *Clinical and Experimental Optometry*, **98**, 507–517.

Schaeffel, F., Hagel, G., Eikermann, J., et al. (1994) Lower-field myopia and astigmatism in amphibians and chickens. *Journal of the Optical Society of America A*, **11**, 487–495.

Schaeffel, F. & Howland, H.C. (1987) Corneal accommodation in chick and pigeon. *Journal of Comparative Physiology A*, **160**, 375–384.

Schaeffel, F. & Wagner, H. (1992) Barn owls have symmetrical accommodation in both eyes, but independent pupillary responses to light. *Vision Research*, **32**, 1149–1155.

Schick, T., Ersoy, L., Lechanteur, Y.T., et al. (2016) History of sunlight exposure is a risk factor for age-related macular degeneration. *Retina*, **36**, 787–790.

Schiller, P.H. (2010) Parallel information processing channels created in the retina. *Proceedings of the National Academy of Sciences of the USA*, **107**, 17087–17094.

Schira, M.M., Wade, A.R., & Tyler, C.W. (2007) Two-dimensional mapping of the central and parafoveal visual field to human visual cortex. *Journal of Neurophysiology*, **97**, 4284–4295.

Schmid, K.L., Howland, H.C., & Howland, M.J. (1992) Focusing and accommodation in Tuatara (*Sphenodon punctatus*). *Journal of Comparative Physiology A*, **170**, 263–266.

Schmitz, F. (2009) The making of synaptic ribbons: How they are built and what they do. *Neuroscientist*, **15**, 611–624.

Scholl, H.P., Strauss, R.W., Singh, M.S., et al. (2016) Emerging therapies for inherited retinal degeneration. *Science Translational Medicine*, **8**, 368rv6.

Seltner, R.L., Weerheim, J.A, & Sivak, J.G. (1989) Role of the lens and vitreous humor in the refractive properties of the eyes of three strains of goldfish. *Vision Research*, **29**, 681–685.

Sexton, T., Buhr, E., & Van Gelder, R.N. (2012) Melanopsin and mechanisms of non-visual ocular photoreception. *Journal of Biological Chemistry*, **287**, 1649–1656.

Shcherbakov, D., Knörzer, A., Espenhahn, S., et al. (2013) Sensitivity differences in fish offer near-infrared vision as an adaptable evolutionary trait. *PLoS One*, **8**, e64429.

Shilo, S. (1977) Astigmatism of the mammalian cornea: Evolutionary and perceptive significance. *Documenta Ophthalmologica*, **44**, 403–419.

Siegert, S., Scherf, B.G., Del Punta, K., et al. (2009) Genetic address book for retinal cell types. *Nature Neuroscience*, **12**, 1197–1204.

Siik, S., Chylack, L.T., Friend, J., et al. (1999) Lens autofluorescence and light scatter in relation to the lens opacities classification system, LOCS III. *Acta Ophthalmologica Scandinavica*, **77**, 509–514.

Sivak, J.G. (1978) Optical characteristics of the eye of the spiny dogfish (*Squalus acanthias*). *Revue Canadienne de Biologie*, **37**, 209–217.

Sivak, J.G. (2008) The role of the lens in refractive development of the eye: Animal models of ametropia. *Experimental Eye Research*, **87**, 3–8.

Sivak, J.G. & Allen, D.B. (1975) An evaluation of the "ramp" retina of the horse eye. *Vision Research*, **15**, 1353–1356.

Sivak, J.G., Howland, H.C., & McGill-Harelstad, P. (1987) Vision of the Humboldt penguin (*Spheniscus humboldti*) in air and water. *Proceedings of the Royal Society B: Biological Sciences*, **229**, 467–472.

Sivak, J.G. & Kreuzer, R.O. (1983) Spherical aberration of the crystalline lens. *Vision Research*, **23**, 59–70.

Smith, E.L., Hung, L.F., Arumugam, B., et al. (2015) Effects of long-wavelength lighting on refractive development in infant rhesus monkeys. *Investigative Ophthalmology & Visual Science*, **56**, 6490–6500.

Smith, S.O. (2010) Structure and activation of the visual pigment rhodopsin. *Annual Review of Biophysics*, **39**, 309–328.

Steinberg, R.H., Reid, M., & Lacy, P.L. (1973) The distribution of rods and cones in the retina of the cat (*Felis domesticus*). *Journal of Comparative Neurology*, **148**, 229–248.

Stepanyants, A., Martinez, L.M., Ferecsko, A.S., et al. (2009) The fractions of short- and long-range connections in the visual cortex. *Proceedings of the National Academy of Sciences of the USA*, **106**, 3555–3560.

Stone, R.A., Cohen, Y., McGlinn, A.M., et al. (2016) Development of experimental myopia in chicks in a natural environment. *Investigative Ophthalmology & Visual Science*, **57**, 4779–4789.

Strettoi, E., Novelli, E., Mazzoni, F., et al. (2010) Complexity of retinal cone bipolar cells. *Progress in Retinal and Eye Research*, **29**, 272–283.

Ström, L. & Ekesten, B. (2016) Visual evoked potentials in the horse. *BMC Veterinary Research*, **12**, 120.

Stryer, L., Hurley, J.B., & Fung, B.K.K. (1981) Transducin – an amplifier protein in vision. *Trends in Biochemical Sciences*, **6**, 245–247.

Sunderland, H.R. & O'Neill, W.D. (1976) Functional dependence of optical parameters on circumferential forces in the cat lens. *Vision Research*, **16**, 1151–1158.

Svaetichin, G. & MacNichol, E.F., Jr. (1959) Retinal mechanisms for chromatic and achromatic vision. *Annals of the New York Academy of Sciences*, **74**, 385–404.

Sweeney, N.T., James, K.N., Nistorica, A., et al. (2019) Expression of transcription factors divides retinal ganglion cells into distinct classes. *Journal of Comparative Neurology*, **527**, 225–235. doi: 10.1002/cne.24172.

Taylor, W.R. & Smith, R.G. (2012) The role of starburst amacrine cells in visual signal processing. *Visual Neuroscience*, **29**, 73–81.

Tedesco, R.C., Calabrese, K.S., & Smith, R.L. (2005) Architecture of the ciliary muscle of *Gallus domesticus*. *The Anatomical Record. Part A, Discoveries in Molecular, Cellular, and Evolutionary Biology*, **284**, 544–549.

Thibos, L.N., Applegate, R.A., Schwiegerling, J.T., et al. (2002) Standards for reporting the optical aberrations of eyes. *Journal of Refractive Surgery*, **18**, S652–S660.

Thoreson, W.B. & Mangel, S.C. (2012) Lateral interactions in the outer retina. *Progress in Retinal and Eye Research*, **31**, 407–441.

Toshida, H., Funaki, T., Ono, K., et al. (2017) Efficacy and safety of retinol palmitate ophthalmic solution in the treatment of dry eye: A Japanese Phase II clinical trial. *Drug Design, Development and Therapy*, **11**, 1871–1879.

Townsend, W.M., Jacobi, S., & Bartoe, J.T. (2012) Phacoemulsification and implantation of foldable +14 diopter intraocular lenses in five mature horses. *Equine Veterinary Journal*, **44**, 238–243.

Townsend, W.M., Wasserman, N., & Jacobi, S. (2013) A pilot study on the corneal curvatures and ocular dimensions of horses less than one year of age. *Equine Veterinary Journal*, **45**, 256–258.

Trakhtenberg, E.F., Pita-Thomas, W., Fernandez, S.G., et al. (2017) Serotonin receptor 2C regulates neurite growth and is necessary for normal retinal processing of visual information. *Developmental Neurobiology*, **77**, 419–437.

Tsukamoto, Y., Morigiwa, K., Ueda, M., et al. (2001) Microcircuits for night vision in mouse retina. *Journal of Neuroscience*, **21**, 8616–8623.

Tsukamoto, Y. & Omi, N. (2016) ON bipolar cells in macaque retina: Type-specific synaptic connectivity with special reference to OFF counterparts. *Frontiers in Neuroanatomy*, **10**, 104.

Tusa, R.J., Palmer, L.A., & Rosenquist, A.C. (1978) The retinotopic organization of area 17 (striate cortex) in the cat. *Journal of Comparative Neurology*, **177**, 213–235.

Ueno, Y., Hiraoka, T., Miyazaki, M., et al. (2015) Corneal thickness profile and posterior corneal astigmatism in normal corneas. *Ophthalmology*, **122**, 1072–1078.

van den Berg, T.J. & Tan, K.E. (1994) Light transmittance of the human cornea from 320 to 700 nm for different ages. *Vision Research*, **34**, 1453–1456.

Vecino, E., Rodriguez, F.D., Ruzafa, N., et al. (2016) Glia-neuron interactions in the mammalian retina. *Progress in Retinal and Eye Research*, **51**, 1–40.

Wahl, C., Li, T., & Howland, H. (2015) Plasticity in the growth of the chick eye: Emmetropization achieved by alternate morphologies. *Vision Research*, **110**, 15–22.

Wald, G. (1968) Molecular basis of visual excitation. *Science*, **162**, 230–239.

Wan, Q.F. & Heidelberger, R. (2011) Synaptic release at mammalian bipolar cell terminals. *Visual Neuroscience*, **28**, 109–119.

Wandell, B.A. & Winawer, J. (2011) Imaging retinotopic maps in the human brain. *Vision Research*, **51**, 718–737.

Wang, J.S. & Kefalov, V.J. (2011) The cone-specific visual cycle. *Progress in Retinal and Eye Research*, **30**, 115–128.

Wang, J.S., Nymark, S., Frederiksen, R., et al. (2014) Chromophore supply rate-limits mammalian photoreceptor dark adaptation. *Journal of Neuroscience*, **34**, 11212–11221.

Wang, L. & Koch, D.D. (2003) Ocular higher-order aberrations in individuals screened for refractive surgery. *Journal of Cataract and Refractive Surgery*, **29**, 1896–1903.

Wang, W., Geiger, J.H., & Borhan, B. (2014) The photochemical determinants of color vision: Revealing how opsins tune their chromophore's absorption wavelength. *Bioessays*, **36**, 65–74.

Wang, W., Hernandez, J., Moore, C., et al. (2016) Antioxidant supplementation increases retinal responses and decreases refractive error changes in dogs. *Journal of Nutritional Science*, **5**, e18.

Wang, X., Dong, J., & Wu, Q. (2014) Mean central corneal thickness and corneal power measurements in pigmented and white rabbits using Visante optical coherence tomography and ATLAS corneal topography. *Veterinary Ophthalmology*, **17**, 87–90.

Wässle, H. (2004) Parallel processing in the mammalian retina. *Neuroscience*, **5**, 747–757.

Wässle, H., Boycott, B.B., & Illing, R.B. (1981) Morphology and mosaic of on- and off-beta cells in the cat retina and some functional considerations. *Proceedings of the Royal Society of London. Series B*, **212**, 177–195.

Wässle, H., Grunert, U., Martin, P.R., et al. (1994) Immunocytochemical characterization and spatial distribution of midget bipolar cells in the macaque monkey retina. *Vision Research*, **34**, 561–579.

Wässle, H., Puller, C., Müller, F., et al. (2009) Cone contacts, mosaics, and territories of bipolar cells in the mouse retina. *Journal of Neuroscience*, **29**, 106–117.

Weltzien, F., Percival, K.A., Martin, P.R., et al. (2015) Analysis of bipolar and amacrine populations in marmoset retina. *Journal of Comparative Neurology*, **523**, 313–334.

Weng, S., Estevez, M.E., & Berson, D.M. (2013) Mouse ganglion-cell photoreceptors are driven by the most sensitive rod pathway and by both types of cones. *PLoS One*, **8**, e66480.

Wensel, T.G. (2008) Signal transducing membrane complexes of photoreceptor outer segments. *Vision Research*, **48**, 2052–2061.

West, J.A., Sivak, J.G., & Doughty, M.J. (1991) Role of accommodation in experimental myopia in chicks. *Optometry and Visual Science*, **68**, 847–852.

Weyand, T.G. (2016) The multifunctional lateral geniculate nucleus. *Reviews in Neuroscience*, **27**, 135–157.

Williams, L.A., Kubai, M.A., Murphy, C.J., et al. (2011) Ocular components in three breeds of dogs with high prevalence of myopia. *Optometry and Vision Science*, **88**, 269–274.

Wilson, F.M. (2006) *Basic and Clinical Science Course, Section 3: Optics, Refraction, and Contact Lenses*. San Francisco, CA: American Academy of Ophthalmology.

Winkler, M., Shoa, G., Tran, S.T., et al. (2015) A comparative study of vertebrate corneal structure: The evolution of a refractive lens. *Investigative Ophthalmology & Visual Science*, **56**, 2764–2772.

Wu, Q., Blakeley, L.R., Cornwall, M.C., et al. (2007) Interphotoreceptor retinoid-binding protein is the physiologically relevant carrier that removes retinol from rod photoreceptor outer segments. *Biochemistry*, **46**, 8669–8679.

Wu, S.M. (2010) Synaptic organization of the vertebrate retina: General principles and species-specific variations. The Friedenwald lecture. *Investigative Ophthalmology & Visual Science*, **51**, 1263–1274.

Wurtz, R.H. (2009) Recounting the impact of Hubel and Wiesel. *Journal of Physiology*, **587**, 2817–2823.

Xiao, X., Liu, W.M., Ye, Y.J., et al. (2014) Prevalence of high astigmatism in children aged 3 to 6 years in Guangxi, China. *Optometry and Vision Science*, **91**, 390–396.

Xu, L., Ruan, G., Dai, H., et al. (2016) Mammalian retinal Müller cells have circadian clock function. *Molecular Vision*, **22**, 275–283.

Yamaue, Y., Hosaka, Y.Z., & Uehara, M. (2015) Spatial relationships among the cellular tapetum, visual streak and rod density in dogs. *Journal of Veterinary Medical Science*, **77**, 175–179.

Yau, K.W. (1994) Phototransduction mechanism in retinal rods and cones. The Friedenwald lecture. *Investigative Ophthalmology & Visual Science*, **35**, 9–32.

Zeck, G.M. & Masland, R.H. (2007) Spike train signatures of retinal ganglion cell types. *European Journal of Neuroscience*, **26**, 367–380.

Zeng, G., Bowrey, H.E., Fang, J., et al. (2013) The development of eye shape and the origin of lower field myopia in the guinea pig eye. *Vision Research*, **76**, 77–88.

Zhou, W.P., Zhu, Y.F., Zhang, B., et al. (2016) The role of ultraviolet radiation in the pathogenesis of pterygia. *Molecular Medicine Reports*, **14**, 3–15.

Zhou, X., Shen, M., Xie, J., et al. (2008) The development of the refractive status and ocular growth in C57BL/6 mice. *Investigative Ophthalmology & Visual Science*, **49**, 5208–5214.

5

Fundamentals of Animal Vision

Björn Ekesten[1] *and Ron Ofri*[2]

[1] *Department of Clinical Sciences, Faculty of Veterinary Medicine, Swedish University of Agricultural Science, Uppsala, Sweden*
[2] *Koret School of Veterinary Medicine, Hebrew University of Jerusalem, Rehovot, Israel*

Ability to detect light is, of course, fundamental for vision, but other aspects, such as detection of motion or determining other qualities of an object, including shape and details, color, size, and distance, help to form our visual percept. The processing of the output from the photoreceptors starts in the retina (Fig. 5.1), but countless neurons in the brain finally shape and interpret the final perceived image of the world around us.

Animal visual perception is a subject of great fascination to researchers, clinicians, and animal owners. Unfortunately, we can know neither exactly what an animal sees because they usually cannot tell us, nor precisely what there is to see because of the limitations of our own visual system. Still, understanding the physiologic basis of animal vision and what different species can potentially perceive helps both to satisfy our curiosity and to better judge the impact of an ocular condition on an animal's welfare, performance, and safety. While we often generalize about canine, feline, or equine vision, one should remember that an Irish Wolfhound, for example, may depend to a much greater extent on its vision than a typical scent hound, such as a Dachshund. Hence, individual and breed differences must also be recognized. In this context, owners may be able to help assess the quality of their animal's vision just as parents can aid in assessing the vision of their child using standardized questionnaires (Miller & Parisi, 2018), thus providing raw data for research that will improve our ability to establish better-substantiated prognoses for various conditions and treatments.

Scotopic and Photopic Vision

We have all experienced temporary loss of vision when moving from a dark room into a brightly lit outdoor environment, or vice versa. This is because at any given moment photoreceptors have a narrow operating range: they do not respond to light that is too dim, and they are saturated by light that is too bright. However, photoreceptors can respond to changes in levels of background luminance by processes of *adaptation* (Demb, 2008; Kelber & Lind, 2010; Reuter, 2011; Rieke & Rudd, 2009). The adaptation results in an extended operating range, allowing the eye optimal performance at a given illumination level. A decrease in background illumination to below 0.03 cd/m^2 will deactivate the cone system, resulting in increased light *sensitivity* (i.e., a lower *threshold*) and *scotopic* rod vision. An increase in background illumination, to 0.03–3 cd/m^2, will lead to *mesopic* vision in which both the rod and cone systems are active, for example before dawn or after sunset. A further increase in background illumination above 3 cd/m^2, to *photopic* levels, will result in rod saturation. In such an environment, cones will continue to function, albeit with a higher threshold, or with lower sensitivity.

The implication of this higher threshold is that in a bright environment, higher-stimulus intensities are required to stimulate cones. The "price" of adaptation to a bright environment, a lower sensitivity, means that the eye will not be able to detect miniscule changes in stimulus intensity, a task that is easily performed by rods in darkness. The inverse relationship between retinal sensitivity and threshold is depicted in Fig. 5.2. For example, because of light adaptation, we are able to see the glaring sand on a sunny day at the beach (high threshold), but we are unable to detect the small luminance change caused by the glow of a distant cigarette on the beach (low sensitivity). As noted in the following sections, however, what is lost in low photopic sensitivity is gained in higher visual acuity and faster responsiveness, both of which characterize cone function and output. Furthermore, a retina with more than one type of photoreceptor is a prerequisite for color vision. Because we have both rods and cones, and thanks to the adaptation of their

Veterinary Ophthalmology: Volume I, Sixth Edition. Edited by Kirk N. Gelatt, Gil Ben-Shlomo, Brian C. Gilger, Diane V.H. Hendrix, Thomas J. Kern, and Caryn E. Plummer.

Companion website: www.wiley.com/go/gelatt/veterinary

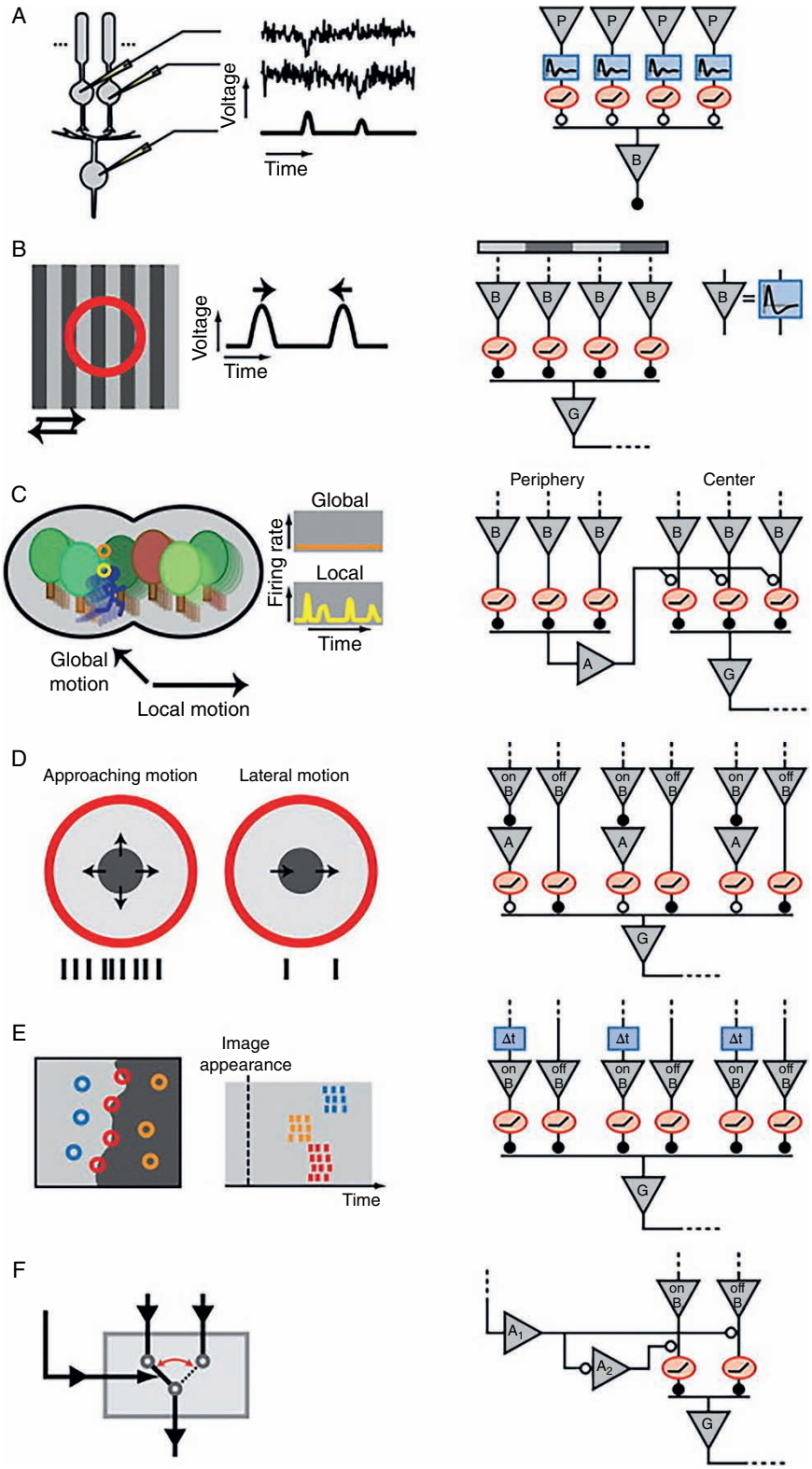

Figure 5.1 A considerable amount of processing of data from the photoreceptors is performed in the neuroretina. The left-hand panels briefly describe the purpose of the computations performed, and the right-hand column illustrates important elements of the underlying circuits schematically (triangle – neuron; A – amacrine cell; B – bipolar cell; G – retinal ganglion cell (RGC); P – photoreceptor; rectangle – temporal filter function; oval – instantaneous rectifier; closed/open circle – sign-preserving/sign-inverting synapse). **A**. The rod-to-rod pathway detects single photons. The output of each rod (noisy tracings) is sent through a band-pass temporal filter followed

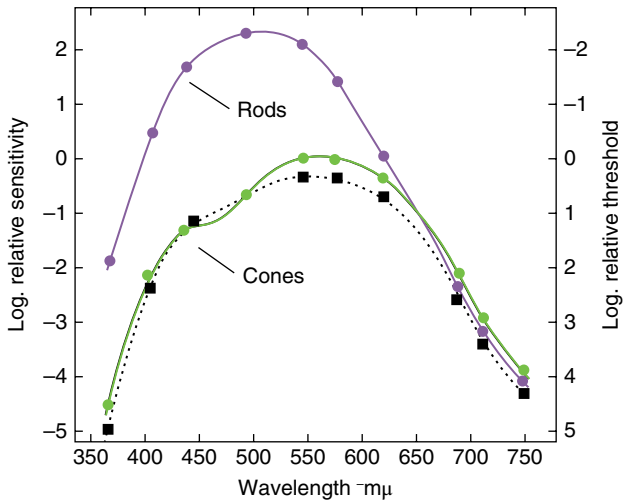

Figure 5.2 The inverse relationship between retinal threshold (right Y-axis) and retinal sensitivity (left Y-axis). Note that the units of the left Y-axis (sensitivity) are increasing, while those of the right Y-axis (threshold) are decreasing. Sensitivities and thresholds of rods (purple) and cones (foveal - green, peripheral - black) are shown as a function of wavelengths. Note that for wavelengths < 650 nm, rods are much more sensitive, and have a lower threshold, than cones (keeping in mind the logarithmic scales of both Y-axes). (Reproduced with permission from Kalloniatis, M. & Luu, C. (1995–) Psychophysics of vision. In *Webvision: The Organization of the Retina and Visual System* (eds., Kolb, H., Nelson, R., Fernandez, E., & Jones, B.), http://webvision.med.utah.edu.)

pathways described next, we are able to see on a moonless, starry night (~10^{-4} cd/m^2) as well as on a sun-drenched sandy beach (~10^5 cd/m^2), a 10^9-fold (one billion) change in illumination (see Chapter 4, Table 4.1).

Scotopic Vision

Rods and Rod Pathways

Cones are inactive in scotopic conditions, and in such an environment our fovea becomes a relative blind spot (Records & Brown, 1999). Instead, scotopic vision is possible because of the molecular and anatomic characteristics of both rods and the rod pathway. The unique features that make an individual rod more sensitive than an individual cone have been recently reviewed by Ingram et al. (2016) and are described in Chapter 4. Even though rods and cones share many proteins involved in the activation and termination of the phototransduction cascade, because of a number of differences in isoforms and/or levels of expression of certain proteins, rods both have greater gain and close the sodium channels more rapidly. Consequently their responses rise much faster per photon absorbed. For the same reasons, the responses of rods decay much more slowly than those of cones, allowing the former to process incoming photons for longer. In addition, the volume of the outer segments is much larger in rods than in cones, increasing the probability of absorption of a photon by rhodopsin (Ingram et al., 2016). All these factors contribute to significant differences in the activation and inactivation of rods and cones (Fig. 5.3). For example, in mice the response per activated photopigment molecule (R^*) is 20–30 times larger in rods than in cones (Cao et al., 2014; Reingruber et al., 2015). In cats, rods are about 200 times more sensitive than cones (Enroth-Cugell et al., 1977).

Another important feature that enables sensitive scotopic vision is the *converging* nature of the rod pathway (see Chapter 4, Fig. 4.26). In cats, it has been estimated that in the peripheral retina, the output of approximately 75,000 rod photoreceptors converges on about 5,000 rod bipolar cells, which output to 250 amacrine cells, which converge on one ganglion cell (Sharma & Ehinger, 2003). The resulting spatial (and temporal) summation of signals from numerous rods increases scotopic retinal sensitivity, as numerous responses are summed to generate a stronger signal and brighten the projected retinal image (Lamb, 2011; Taylor & Smith, 2004). At the same time, the rod pathway also has *diverging* features, with one feline rod synapsing with two rod bipolar cells that diverge to five amacrine cells and eight cone bipolar cells. Therefore, hyperpolarization of a single

Figure 5.1 (Continued) by a thresholding operation. Signals from several rods are then pooled to and summed by one rod bipolar cell, which shows distinct activations (tracings without noise). **B**. The Y-RGC is activated by texture motion in either direction over its receptive field (red circle). Each movement elicits either transient ON- or OFF-responses in the bipolar cells, but only the depolarized bipolar cells signal to the ganglion cell that fires transiently to each shift in the grating. **C**. An RGC sensitive to local motion fires when the object in its central receptive field moves in different direction than that from the background, thus detecting differential motion. This RGC is silent when the object in the center moves in the same direction as the background, because the excitatory input in the center is counteracted by inhibitory input from the surround via the amacrine cell. **D**. An RGC responds strongly (several spikes) to an approaching dark object, but only weakly to lateral motion. More OFF-bipolar cells are excited when a larger part of the receptive field is dark. When the object only moves laterally, the RGC receives both excitatory signals from the OFF-bipolars and inhibitory signals from amacrine cells activated by ON-bipolar cells. **E**. Specific RGCs use differences in spike latencies to rapidly encode the structure of an image. RGCs with receptive fields (circles) in the dark part of the image have short latencies, those in the light have long. RGCs with receptive fields containing both dark and light areas fire in between, thus indicating the position of the border. Here signals from both ON- and OFF-bipolar cells are individually rectified, and the timing difference follows from a delay (Δt) in the ON-pathway. **F**. Wide-field amacrine cells (A1) are activated during rapid shifts of the image in the retinal periphery, which suppresses the OFF-bipolar cell signal and disinhibits the ON-bipolar cell through a local amacrine cell (A2). Hence, this circuit acts like a switch, in this case enabling a signal in the more central part of the retina. (Reproduced with permission from Gollisch, T. & Meister, M. (2010) Eye smarter than scientists believe: Neural computations in circuits of the retina. *Neuron*, **65**, 150–164.

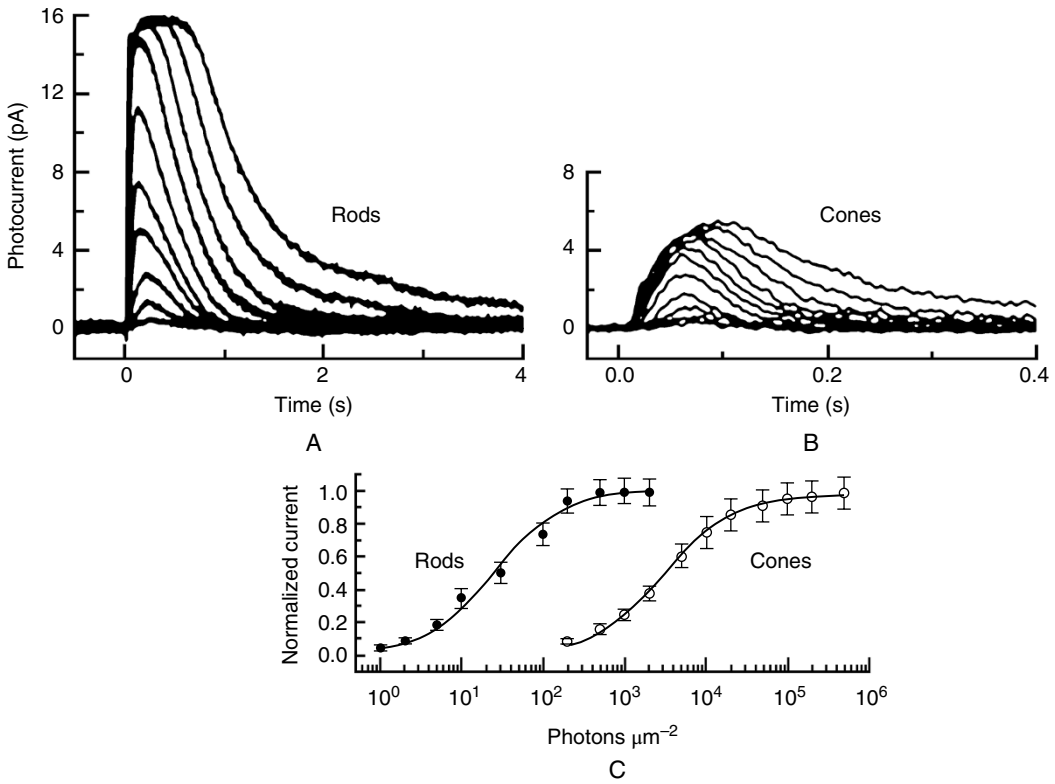

Figure 5.3 Responses of mouse rods and cones. **A**. Mean responses of mouse rods to illumination from 0.5 to 2000 photons. **B**. Mean responses of mouse cones to illumination from 200 to 500,000 photons. Note the significantly lower responses of cones, even though they are illuminated by many more photons. **C**. Mean peak amplitudes of responses of mouse rods (left, •) and cones (right, °) to increasing illumination. Note that there is only a small mesopic range of illumination where both systems are active. (Reproduced with permission from Ingram, N.T., Sampath, A.P., & Fain, G.L. (2016) Why are rods more sensitive than cones? *Journal of Physiology*, **594**, 5415–5426.)

rod in a cat can activate several retinal ganglion cells (RGCs), resulting in increased responsiveness (Sterling et al., 1988). Because of the increased sensitivity afforded by these features of the rods and rod pathway, our scotopic vision can detect small changes in light intensity that would be invisible in daytime, such as dim stars uncovered by moving clouds. In fact, the rod pathway is so sensitive that it is able to detect just a single photon (Takeshita et al., 2017).

In many animal species, the increased number and density of rods enhances scotopic vision. As can be seen in Chapter 4, Table 4.6, the maximal rod concentration in humans (found about 15° away from the fovea) is about one-third of the maximal rod concentration in cats; in the ora serrata (or ora ciliaris retinae), the ratio between the two species is 1:6. It can also be appreciated that dogs have a higher maximal rod concentration than cats, even though most people associate the latter with greater scotopic sensitivity. This discrepancy may be explained by the structure of the tapetum, which is less reflective in dogs than in cats. Nonetheless, the high concentration of rods, which evolved to allow the retina to capture every available photon at night, endows both these species with enhanced scotopic vision.

The advantages conferred by a high rod density in certain environments have resulted in some extreme evolutionary adaptations. Thus, it is not surprising that some deep-sea fish which inhabit a scotopic environment (Hirt & Wagner, 2005), and some nocturnal species such as the nocturnal gecko (Yokoyama & Blow, 2001), have a pure-rod retina. However, these are rare examples, and most nocturnal species, including mice, have cones (Musser & Arendt, 2017). Indeed, many species that were formerly believed to have a pure-rod retina, such as seals and whales (Peichl et al., 2001) and chinchillas (Sandalon et al., 2018), have been shown to be cone mono- and dichromats, respectively.

The Tapetum

One of the most fascinating adaptations for enhanced scotopic vision is the evolution of a reflective tapetum in the choroid (Fig. 5.4). Light photons striking this layer bounce back onto the retina, thus giving them a second chance to be absorbed by the photoreceptors. This second opportunity is not significant in daytime, as cones absorb enough photons during their "first pass" through the retina. In fact, the tapetum has a detrimental effect on visual acuity in broad daylight, as the light is reflected onto a photoreceptor different from the one in the original trajectory (Ofri, 2018b). However, at night this detrimental effect on visual resolution is insignificant since cones are inactive. Instead, the retina benefits from the increased probability that rods will absorb the few

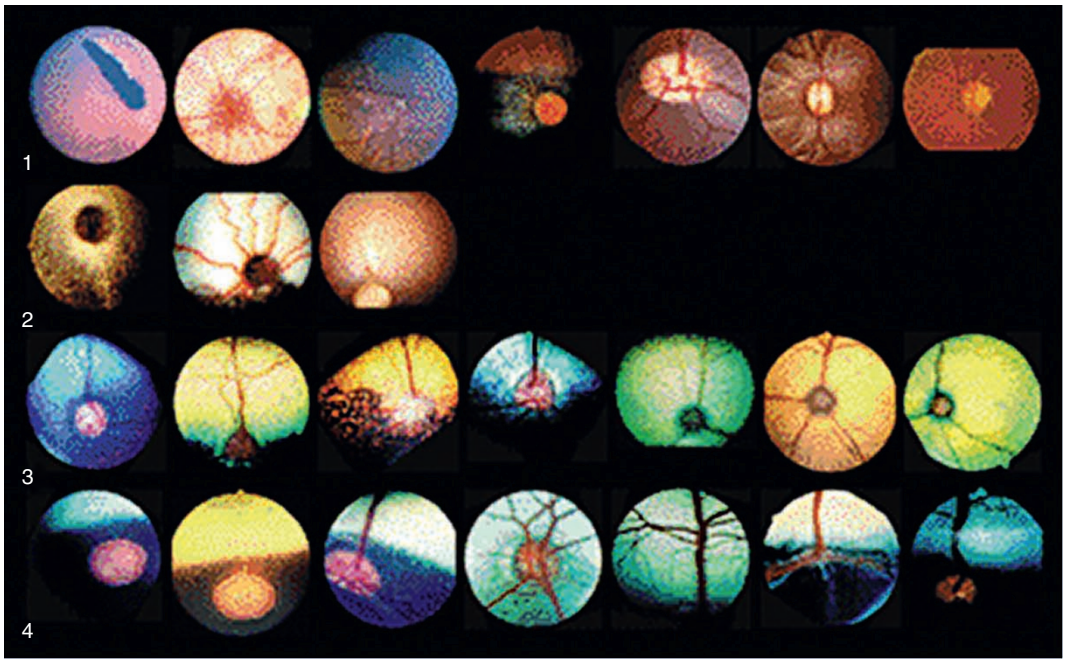

Figure 5.4 Ocular fundus of various species showing the absence or presence of a tapetum lucidum that can exhibit various colors. From right to left: Lane 1: absence of tapetum: bird, albino rat, hooded rat, red kangaroo, pig, rhesus monkey, human. Lane 2: retinal tapeta: alligator, opossum, fruit bat. Lane 3: Choroidal tapeta cellulosa: puppy, dog, cat, jaguar, leopard. Lane 4: choroidal tapeta fibrosa: foal, horse, sheep, goat, cow, deer, mouflon. (Reproduced with permission from Ollivier, F.J., Samuelson, D.A., Brooks, D.E., et al. (2004) Comparative morphology of the tapetum lucidum (among selected species). *Veterinary Ophthalmology*, **7**, 11–22.)

photons entering the eye in a dim environment, thus enhancing scotopic vision.

The composition of the tapetum varies between species, depending on the habitat and ecologic requirements of the animal. The feline tapetum, for example, is 15–20 layers thick (Ollivier et al., 2004), giving it a reflectance rate of almost 100% (Land, 1972). Indeed, the cat's eye reflects about 130 times more light than the human eye (Rodieck, 1973). However, not all wavelengths are reflected equally, as reflectivity is also affected by the dimensions and packing of the reflecting tapetal fibrils or rodlets (Ollivier et al., 2004). As noted previously, the canine tapetum is less reflective than the feline one as it has fewer layers (Yamaue et al., 2015) and suboptimal packing of the reflecting rodlets (Ollivier et al., 2004), which certainly contributes to cats having higher scotopic sensitivity than dogs.

The horse tapetum is only 4–5 layers thick, thus significantly reducing its reflectivity (Ollivier et al., 2004), but the diameter and interfibrous distance of the tapetal collagen fibrils are such that they reflect light at about 468 nm; this wavelength is more effectively absorbed by rods than by cones, minimizing the detrimental effect of tapetal scatter on equine photopic vision (Shinozaki et al., 2013). In contrast, the tapetal reflectance of the diving hooded seal selectively increases the relative ultraviolet (UV)/blue components to more than 10 times those of other wavelengths, which may have advantages in the dim, blue light-shifted environment experienced by submerged marine mammals (Hogg et al., 2015). The most dramatic example of the adaptability of the tapetum to the animal's environment is probably that of the Arctic Reindeer, which changes its tapetal reflectivity with the seasons! The reindeer tapetum is golden and less reflective in summer to enable high visual acuity during the long and bright Arctic days, but turns blue and more reflective in winter, when higher retinal sensitivity is required to detect predators in the dark Arctic night (Stokkan et al., 2013).

Globe Size

The dimensions of the ocular tissues also contribute to improved scotopic sensitivity in many species. For example, the mean diameter of the cornea in cats and humans is 16.5 and 11.7 mm, respectively (Carrington & Woodward, 1986; Rüfer et al., 2005). Consequently, much more light enters the cat's eye. Next, light must pass through the pupil. The diameter of a mydriatic pupil in cats and humans is about 12 and 8 mm, respectively (Hammond & Mouat, 1985; Gilmartin et al., 1995), translating into a pupillary aperture of 113 and 50 mm^2, respectively. As a result, far more light passes through the cornea and pupil to reach the feline retina at night, when the pupil is fully dilated. Indeed, it has been calculated that a fully dilated pupil increases the amount of light reaching the retina by 135-fold in the cat, compared to an 80-fold increase in humans (Hughes, 1977; Records & Brown, 1999). When all of these factors – a large aperture for light to enter the eye, a high concentration of rods, and a

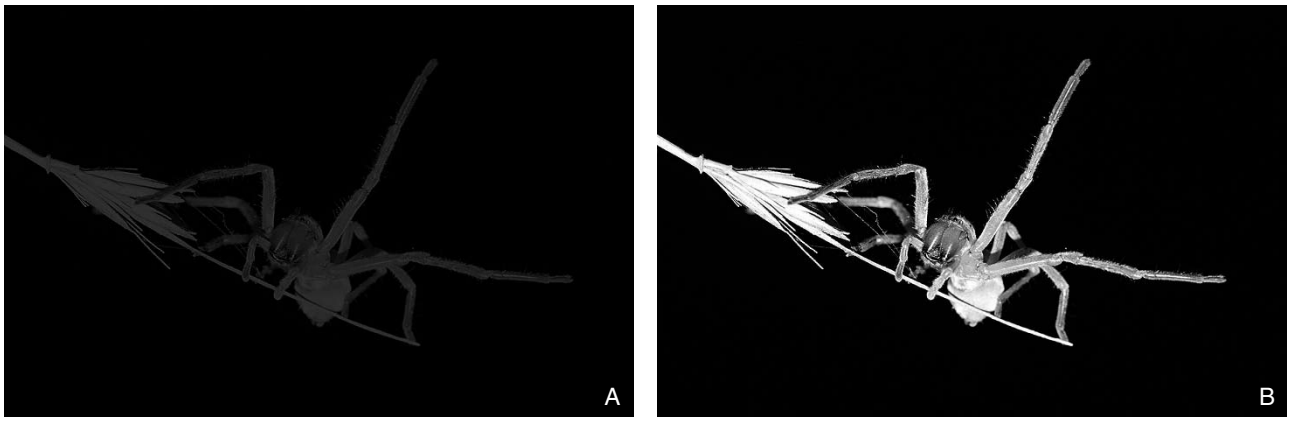

Figure 5.5 Increased scotopic sensitivity of a cat. The same spider is seen at night, under identical scotopic conditions, by a human (**A**) and a cat (**B**). Even though both are viewing the spider under the same conditions, the cat sees a much brighter image because of its greater retinal sensitivity. The spider is seen by both observers in black and white, as no cones are active at these low intensities. (Courtesy of Dr. Shlomi Levi.)

highly reflective tapetum – are considered, it is not surprising that the scotopic threshold of cats (1.6×10^{-7} cd/m^2) is 5.5 times lower than that of humans (7.6×10^{-7} cd/m^2); that is, cats can detect light that is 5.5 times dimmer (Harmening & Wagner, 2011; Weale, 1953; Fig. 5.5).

These species differences obviously become even more dramatic in larger eyes, such as in horses. The horizontal and vertical diameters of the equine cornea are 30.3 and 21.2 mm, respectively (Badial et al., 2015). The respective diameters of the equine pupil, dilated with tropicamide, are about 22 and 25 mm (McMullen et al., 2014), giving it a surface area of approximately 430 mm^2. Consequently, a greater number of photons can enter the dilated horse pupil and reach its retina, and though data regarding rod density in the horse are lacking, it is safe to assume that the large area of the equine retina allows it to pack more rods and to capture more light, compared to other species. However, as in the case of dogs, the scotopic sensitivity of the equine eye may be affected by a suboptimal tapetum. Nonetheless, Hanggi and Ingersoll (2009) report that horses could recognize shapes when the ambient light intensity was as low as 3.4×10^{-5} cd/m^2, so dim that the researchers were stumbling into objects and their cameras were unable to capture any images!

Dark Adaptation

Dark adaptation is a process in which sensitivity of photoreceptors increases, and their threshold decreases (see Fig. 5.2). It takes place in darkness following prolonged exposure to bright light, which causes bleaching of a substantial portion of the photopigment and includes several components.

One mechanism of dark adaptation is biochemical and revolves around the resynthesis of rhodopsin from free opsin and from recycled (or newly available) 11-*cis*-retinal. Consequently, the amount of unbleached photopigment increases in the dark, and in a totally dark-adapted eye, 100% of the rhodopsin is in an unbleached form (Rushton, 1965). The rate-limiting and time-consuming step of the process is the supply and transport of 11-*cis*-retinal from the retinal pigment epithelium back to the outer segments, where it binds with opsin to reform unbleached rhodopsin (see Chapter 4, Fig. 4.25; Wang et al., 2014). Therefore, the time required for dark adaptation and photopigment regeneration is largely determined by the duration, intensity, and wavelength of the preadapting light, which dictates how much of the photopigment has been bleached, and how much remains unbleached.

Postreceptoral neuronal processes make an equally important contribution to dark adaptation (Lamb, 2011). Reciprocal synapses between bipolar and amacrine cells may regulate retinal sensitivity through feedback mechanisms (see Fig. 5.1) (Dowling, 1967; Reuter, 2011) and reorganization of RGC-receptive fields also enhances dark adaptation (Puell et al., 2014; Troy et al., 1993). Together, the biochemical and neuronal adaptation processes increase the retinal sensitivity so that light that is about 10,000× dimmer (4 log units) can be detected.

The third mechanism that plays a role in dark adaptation is pupil dilation. Mydriasis contributes about 1 log unit of adaptation in humans and most terrestrial species (Dowling, 1987). However, in diving pinnipeds, such as seals, where very fast adaptation is needed, very large pupils may contribute 2 log units of dark adaptation (Hanke & Dehnhardt, 2009). In fact, the pupillary range of three pinniped species studied correlates with the range of light levels over which their visual system has to operate during diving (Levenson & Schusterman, 1999).

Dark adaptation is a biphasic process (Fig. 5.6). Cones (and cone pathways) dark-adapt too, as their stores of unbleached photopigment also increase in darkness. This first phase is relatively fast, and cones completely dark-adapt in 5–8 minutes (Reuter, 2011). Since rod rhodopsin regenerates much

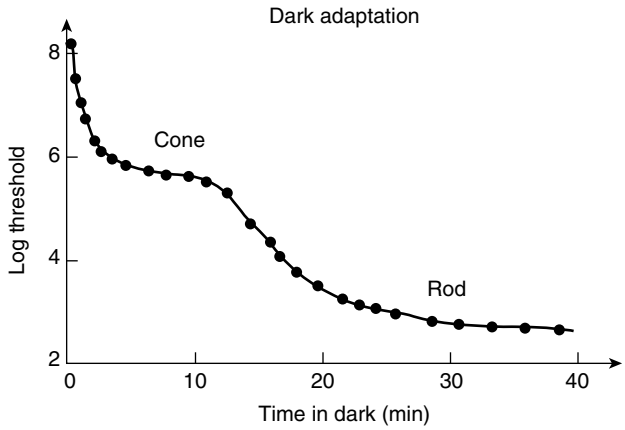

Figure 5.6 The processes of dark adaptation in humans. Cones dark-adapt for the first 5–8 minutes, increasing their sensitivity (lowering their threshold) by about 2.5 log units. Dark adaptation of rods is a much slower process, which increases retinal sensitivity by another 3–4 log units. (Reproduced with permission from Goldstein, E. B. (2005) *Blackwell Handbook of Sensation and Perception*, 2nd ed. Malden, MA: Blackwell.)

more slowly than the cone iodopsin (Wald, 1955), rod dark adaptation is a longer process, usually lasting 30–40 minutes in humans (Lamb & Pugh, 2006).

In animals, in which it is difficult to conduct psychophysical studies, dark adaptation is most often determined through electroretinographic (ERG) recordings. The aim is to establish the amount of time needed, following exposure to strong ambient light, for the scotopic b-wave to return to its maximal response to a dim stimulus. Such studies have shown that 100 minutes are needed for complete dark adaptation in albino rats (Dowling, 1960). During this time, rod sensitivity increased by 3.5 log units, while the amount of rhodopsin increased from 4% (in the light-adapted state) to about 100%, reflecting a logarithmic relation between these two parameters. In horses, scotopic b-wave amplitude reaches maximal amplitude after 20 minutes of dark adaptation (Ben-Shlomo et al., 2012). In dogs, the dark-adapted b-wave reaches maximal amplitude after 20 minutes in alert subjects (Yu et al., 2007) and after 30 minutes in sedated animals (Maehara et al., 2015). These species differences may be due to evolutionary differences in the speed at which retinal is released by the bleached photopigment (Bickelmann et al., 2015). Electroretinographic recordings of the dark adaptation process can be used for early diagnosis of outer retinal diseases in patients (Ekesten et al., 2013; Narfström et al., 2002; Fig. 5.7).

Photopic Vision

Light Adaptation

Light adaptation is a process in which cone (and rod) sensitivity decreases, and threshold increases, in response to increased background light intensity and the resulting

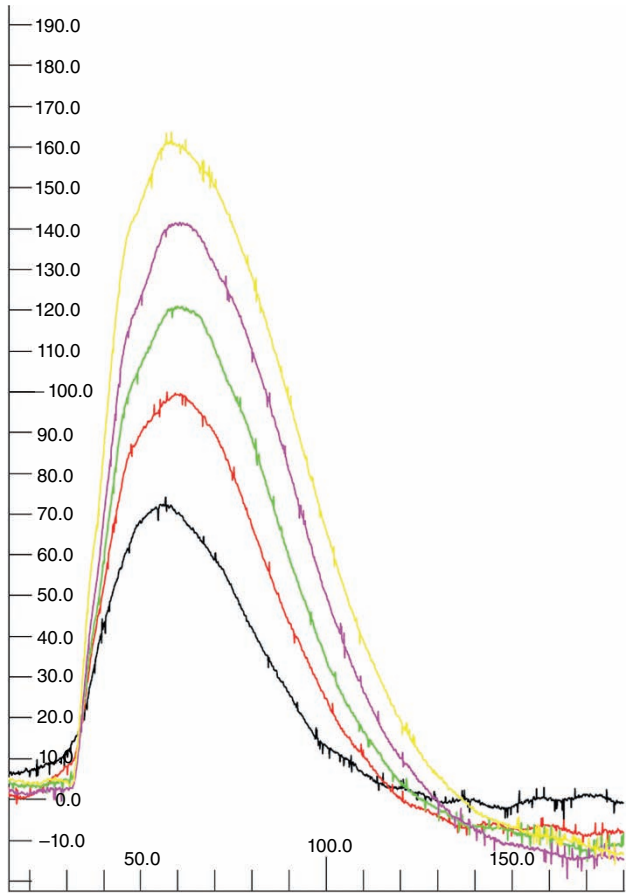

Figure 5.7 In a comprehensive canine electroretinographic (ERG) protocol, following preparation of the animal in ambient light, the light is turned off. During the next 20 minutes, the retina is stimulated with a dim flash every 4 minutes, thus generating a dark adaptation curve (Narfström et al., 2002; Ekesten et al., 2013). In a normal animal, signal amplitude will increase from one flash to the next as the retina dark-adapts (black, red, green, pink, and yellow traces represent the respective responses recorded after 4, 8, 12, 16, and 20 minutes in the dark). Failure of the signal to increase with time in the dark may be an early sign of rod dysfunction.

increased photopigment bleaching. This is a much faster process than dark adaptation. Our eyes begin light adapting within seconds to a sudden increase in background light intensity, such as that experienced when exiting a dark room. Indeed, it is suggested that the reason for the initial *photophobia* exhibited when exiting a dark room is an attempt by the eye to preserve the dark-adapted state of the retina (Records & Brown, 1999).

Several mechanisms account for light adaptation (see Chapter 4). One is the increased activity of phosphodiesterase, resulting in a shorter turnover time for cyclic guanosine-3,5′-monophosphate (cGMP) and accelerating the response kinetics of cones. Another factor contributing to light adaptation is a drop in cytoplasmic Ca^{2+} concentration. This leads to activation of guanylyl cyclase, recoverin (which

phosphorylates R^*), and calmodulin (responsible for channel reactivation), all resulting in increased opening of cGMP-gated sodium channels (Lamb, 2011; see Chapter 4, Fig. 4.24). Generally, eyes are fully light-adapted within 5 minutes, in contrast to the 30 minutes or more required for complete dark adaptation (Records & Brown, 1999).

These adaptation processes take place in both rods and cones. However, the former reach saturation at moderate levels of background light, as all the rhodopsin is bleached, thus making rods unresponsive in saturating light levels. In contrast, cones can continue functioning over an extended range of photopic intensities, albeit at a lower sensitivity (see Fig. 5.3C), and actually they never reach saturation in steady light (Lamb, 2016). Indeed, over 8 log units of background light, cone sensitivity is inversely correlated with background intensity (Burkhardt, 1994; see Fig. 5.2). This is because bleaching (and depletion) of the photopigment results in a proportional increase in the amount of light required for photoreceptor hyperpolarization. In fact, for each 1 log unit increase in light intensity there will be a 1 log unit decrease in the amount of unbleached photopigment available to absorb light, resulting in a 1 log unit reduction in photoreceptor sensitivity (Lamb, 2011).

The Pupil

As with scotopic vision, the pupil also contributes to photopic vision because miosis protects the retina from excessive and harmful amounts of light (Fig. 5.8). It is proposed that the large corpora nigra found on the superior border of the pupil in some species (and often the inferior pupil also) provides additional protection. This is because the corpora nigra supposedly decreases the amount of light entering the eye from the superior visual field (where the sun is located), further reducing glare and improving vision in bright light (Miller & Murphy, 2017). Moreover, because a miotic slit pupil can block light more efficiently than a miotic circular one, it is suggested that slit pupils have evolved in nocturnal or crepuscular species such as cats and geckos that need to function in daytime (Brischoux et al., 2010; Murphy & Howland, 1986). However, this view is challenged by others who note that some species (such as the tarsier) have round pupils that constrict very effectively, to a diameter of about 0.5 mm, while many ungulate species have rather rectangular pupils that do not close to a narrow slit in photopic conditions (Land, 2006). Instead, it is possible that slit pupils have evolved to decrease the detrimental effects of chromatic aberrations (see Chapter 4, Fig. 4.17) (González-Martín-Moro et al., 2014; Malmström & Kröger, 2006).

Flicker Detection

The temporal responsiveness of the retina has two aspects: motion detection and flicker detection. The retina responds to flashes of light as long as there is a sufficient interval between two consecutive flashes, allowing the retina to recover from one response before the next flash is presented. But as the frequency of these flashes increases, a point is reached at which the retina does not have enough time to recover between flashes, and therefore it can no longer distinguish the individual flashes. At this point, which is termed the critical flicker frequency (CFF) or flicker fusion frequency (FFF), the eye perceives a steady light even though this light is made up of numerous flickers (Ezra-Elia et al., 2014; Lisney et al., 2012). There are separate CFFs for rod-driven responses and signals generated from the different cone types, just as there are separate adaptation mechanisms for the rod and cone systems. Therefore, CFF is a function of

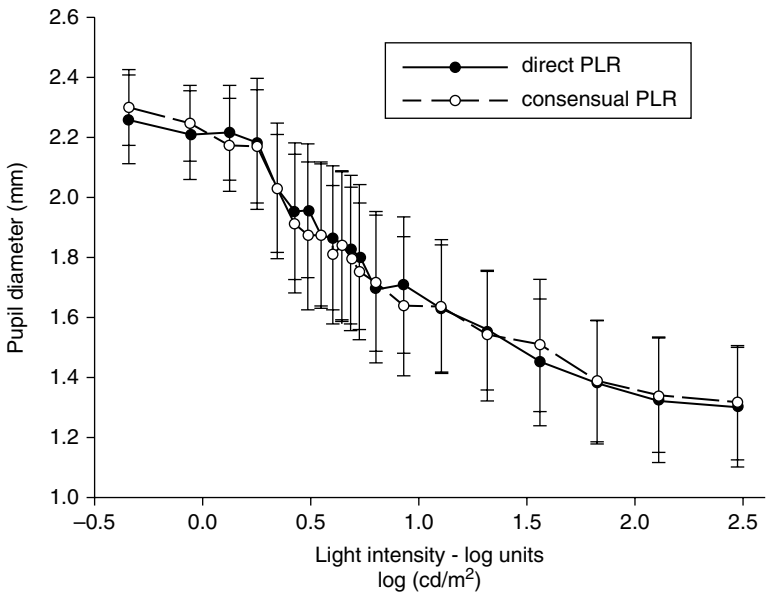

Figure 5.8 The direct and consensual pupillary light reflex in mice as a function of stimulating light intensity. (Reproduced with permission from Grozdanic, S., Betts, D.M., Allbaugh, R.A., et al. (2003) Characterization of the pupil light reflex, electroretinogram and tonometric parameters in healthy mouse eyes. *Current Eye Research*, **26**, 371–378.)

stimulus intensity, wavelength, background light, adaptation levels, and retinal eccentricity. Figure 5.9 shows the effect of the last two variables on CFF. It can be appreciated that flickers of low-intensity light projected on the peripheral retina, and consequently stimulating the rod pathway, "fuse" at a frequency of approximately 10–20 Hz. Flickers characterized by high illumination projected onto the central retina will activate the cone pathway and therefore fuse at much higher frequencies. CFF is also determined by the location in the visual pathways at which it is measured. The CFF of the cone ERG is higher than the more processed signal detected in the visual cortex; similarly, the CFFs of channels delivering either luminance or chromatic information will also differ (Bowles & Kraft, 2012; Spitschan et al., 2016).

As noted, CFF is affected by numerous factors, and therefore it is difficult to make interspecies comparisons. However, in general, the CFF for the canine rod system is similar to that of humans (10–20 Hz). CFFs of 60 Hz or more have been reported for the feline and canine cone systems (Coile et al., 1989), whereas birds can reach values close to 150 Hz (Bostrom et al., 2016). The ability to resolve very rapid changes in luminance allows these species to view their surroundings in "slow motion" (compared to the temporal resolution of humans) and more easily to follow rapidly moving objects (such as prey) or avoid stationary obstacles (such as tree trunks and branches in a dense forest) while running or flying at high speed.

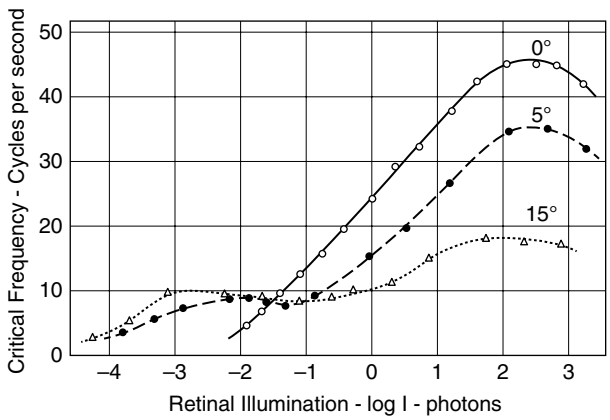

Figure 5.9 Critical flicker frequency (CFF) as a function of retinal illumination for light projected at the fovea (0°), as well as 5 and 15° above the fovea. As can be seen, the highest CFF values are attained for light flashing at the fovea, whereas the lowest values were obtained when stimulating the most peripheral location (15°). CFF values also increase with illumination (moving to the right along the X-axis). Both of these characteristics illustrate that the CFF of cones is higher than that of rods. In the foveal region of this test person (who was also the first author of the original article), using high illumination, responses of cones fuse at about 45 Hz. (Reproduced with permission from Hecht, S. & Verrijp, C.D. (1933) The influence of intensity, color and retinal location on the fusion frequency of intermittent illumination. *Proceedings of the National Academy of Science*, **19**, 522–535.)

Motion Perception

Moving through the environment produces a flow of images projected onto the photoreceptors, resulting in huge amounts of visual information necessary for navigating through a complex environment (Lee, 1980). Perception of motion is required for both directing visual attention to a certain location in the visual field and for segmenting moving objects from their background. Psychophysically, there are three ways of discerning motion (Burr & Thompson, 2011). Movement can be perceived if an object is moving across our visual field while our eyes and head are stationary. Motion can also be perceived when either the head or the eyes are moved to pursue a moving object. It is interesting to note that even though each of these perceptual mechanisms involves the use of different pathways, all three result in similar sensations and experiences.

Processing of motion across the visual field starts in the retina, typically enabled through lateral inhibition by large-field starburst amacrine cells that contribute to motion discrimination and direction detection. Directionally selective RGCs, firing robustly in response to motion in a certain direction and weakly or not at all in response to motion in other directions, make specialized synapses with these amacrine cells. However, it seems that the inhibitory amacrine cell circuits are the primary source of the directional selectivity, which is then amplified by the RGCs (Vaney et al., 2012). Signals from the RGCs, providing information about more rapidly moving targets, are relayed through the magnocellular pathway to the striate cortex, whereas the parvocellular pathway may contribute to the transfer of signals triggered by relatively slow motions (Gilaie-Dotan et al., 2013). Visual area 1 (V1) relays information about motion hierarchically to extrastriate areas, such as the middle temporal area (MT/V5) in primates and to similar areas in lower mammals, mainly through the dorsal stream. Information about fast motion is also conveyed in parallel pathways bypassing V1, thus enhancing vision of rapidly moving objects (Juavinett & Callaway, 2015; Zeki, 2015).

Subtle movement of objects with relatively high luminance is best detected by the central retina, which has a lower threshold and higher sensitivity for motion detection. Therefore, motion sensitivity is directly correlated with visual acuity. Thus, in bright light a human can detect moving objects that are 10 times slower than can a cat (Pasternak & Merigan, 1980). However, in dim light the cat's more efficient scotopic vision makes it superior to humans in detecting slow motion, though even in these conditions humans have an advantage when spatial frequencies exceed 0.5 cycles/degree (Kang et al., 2009). Furthermore, the peripheral retina perceives motion and may be more sensitive to certain speeds, directions, or objects that function as "attention-grabbing" stimuli. For example, it has been shown that the ferret's chase behavior is reflexively triggered by objects

moving at the speed of a running mouse, but not by faster or slower objects (Apfelbach & Wester, 1977).

Different gaze behaviors, including fixations on objects, gaze shifts, and constant gaze, have developed to guide animals during locomotion (Rivers et al., 2014). Fixations occur when head and/or eye movements temporarily stabilize the image of an object moving relative to the observer on the retina, thereby projecting it onto the area with best acuity and allowing more time for visual processing of its properties. Here, the optokinetic reflex allows the eye to follow objects in motion when the head remains stationary. Gaze shifts or saccades are rapid movements between fixations and episodes of constant gaze when sampling of visual information is suppressed to avoid blurring the image (Kowler, 2011). Saccades are exploratory movements used by a wide range of species, where selected locations of the visual scene are brought to the area of best vision and the visual environment is sampled during a brief period of relative image stability in between these small eye movements. Finally, constant gaze occurs when the animal looks at a fixed distance ahead, thus probably extracting visual clues from the information flow about both its own movements and objects in the environment.

Visual Fields, Binocular Vision, and Depth Perception

It is rather extraordinary to note that all vertebrate species, and many invertebrates, have two eyes. Having more than one eye is required for a large visual field, virtually 360° in some species, and for *stereopsis*, or depth perception. However, no more than two eyes are required to achieve these aims (Tyler & Scott, 1994).

Visual Fields

The extent of the visual field depends largely on the placement of the orbits within the skull (Fig. 5.10). Many mammalian prey species, as well as avian and fish species, have lateral eyes, providing almost a 360° field of view. These animals have a small, frontal *binocular* field; two large, peripheral *monocular* fields; and a small blind spot behind their head. On the other hand, most primate and predator species have frontal eyes. In these species, most of the frontal visual field is covered by extensive binocular vision; there are two small, peripheral monocular fields and a large blind spot behind the skull (Fig. 5.10). Therefore, enucleation will cause a cat, for example, to lose approximately 30° of one visual field, while in a horse the same procedure will cause a loss of about 145°.

While the two lateral (monocular) visual fields are equal in size, they may differ in their importance, a phenomenon known as *visual lateralization*. In dogs, for example, it has been shown that the right side of the brain, and subsequently the left lateral visual field, is more responsive to threatening and alarming stimuli (Siniscalchi et al., 2018). This may explain why canine left eyes were 5.3 times more likely to sustain snake-induced trauma compared to right eyes (Scott et al., 2019).

Large (monocular) visual fields are typically associated with prey species that need to detect predators. This is why these species usually have a pupil and a visual streak whose shapes are aligned with the horizon, allowing them to identify predators and conspecifics (Pettigrew et al., 2010). The horizontal visual streak in species such as the horse is augmented by a relatively high RGC concentration both temporally and nasally (Evans & McGreevy, 2007). The former serves the frontal binocular visual field of the animal, while the latter improves vision in the posterior visual field that may harbor predators (Land, 2017; Pettigrew et al., 2010). In fact, horses can detect the appearance of objects within almost 360°, and Hanggi and Ingersoll (2012) suggest that the high acuity of the posterior field (provided by the high concentration of nasal RGCs) may explain how horses can defend themselves with such well-aimed hind-leg kicks.

Obviously, in addition to horizontal visual fields, we also have vertical visual fields. The vertical visual field of horses and humans is 178° and 135°, respectively (Harwerth & Schor, 2011; Miller & Murphy, 2017). The latter is divided into 60° superiorly and 75° inferiorly, though naturally the visual perspective changes when the head is raised or lowered. In fact, in some species these vertical fields, and their enhancement by eye movement, are more important than the horizontal visual fields. In rats, for example, eye movements are mostly disconjugate, impeding horizontal binocular vision; instead, the eyes have a large area of binocular vision above the head, most likely to detect raptors overhead (Land, 2013).

Stereopsis

Many people associate stereopsis with predatory behavior, as depth vision is required to pounce on prey with precision. However, stereopsis is just as important for the prey that uses it to distinguish between a camouflaged predator and its surroundings. Though monocular stereopsis is possible thanks to various visual cues including grain, texture, brightness, contour, size, and relative motion (Ono & Steinbach, 1990), in most cases stereopsis is the result of binocular vision, and the extent to which the visual fields of the two eyes overlap. In addition, optimal stereopsis requires normal visual function and refraction, oculomotor control to maintain fixation, and sensory and neuronal mechanisms to extract and process important visual cues (Harwerth & Schor, 2011).

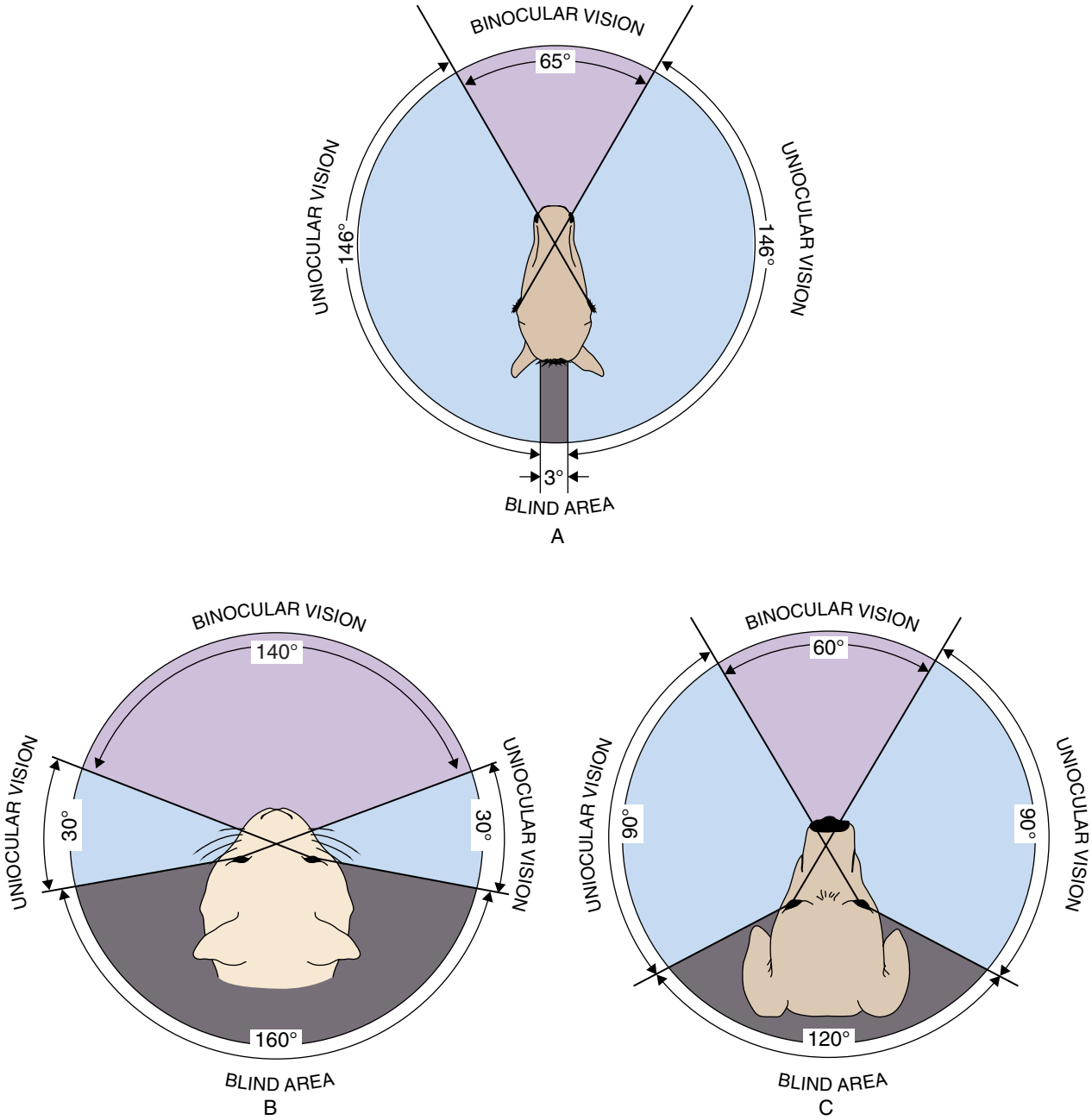

Figure 5.10 **A**. The visual field of a horse showing a frontal binocular field (65°) comparable to that of a dog, but with much larger panoramic monocular fields (each spanning 146°) and a very small posterior blind area (3°). **B**. The visual field of a cat showing a large frontal binocular field (140°) with relatively small monocular fields (each 30°) and a relatively large posterior blind area (160°). **C**. Monocular and binocular visual fields in a typical mesocephalic dog. The dog has a modest frontal binocular visual field (60°) with relatively large monocular visual fields (each 90°) and a posterior blind area of approximately 120°. (Reproduced with permission from Maggs, D.J., Miller, P.E., & Ofri, R., eds. (2018) *Slatter's Fundamentals of Veterinary Ophthalmology*, 6th ed. St. Louis, MO: Elsevier.)

Geometry and Retinal Disparity

If an object is located in the plane of fixation of both eyes, it is viewed with the same angle by both eyes (Fig. 5.11). However, objects outside the binocular plane of fixation are viewed with a slightly different angle by each eye, resulting in *disparate images*. The visual angle can serve as a "range finder." An object is deemed close if the projection lines from both eyes intersect before the plane of fixation, thus triggering a converging oculomotor response; for a distant object the projection lines intersect beyond the plane of fixation, serving as an oculomotor stimulus for divergence (see Fig 5.11). Therefore, range detection requires highly coordinated

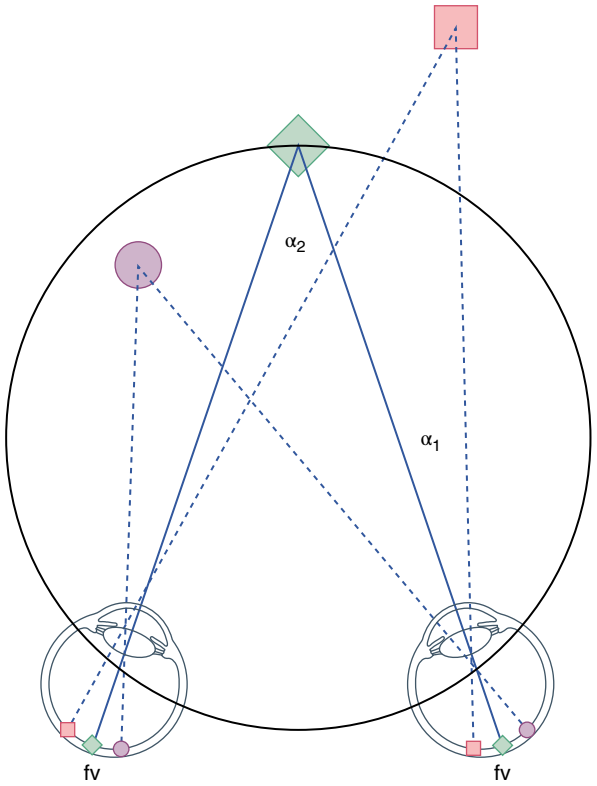

Figure 5.11 Binocular disparity and the perception of stereoscopic depth. The green diamond is on the plane of fixation of both eyes. It is therefore seen at the same angle by both eyes and projected onto both foveas (*fv*). Both the purple circle and red square are outside the plane of fixation. Therefore, they are viewed at different angles by both eyes, and projected onto disparate (but corresponding) retinal regions. The purple circle is closer than the object of fixation (the green diamond) and therefore the projection lines from both eyes intersect before the plane of fixation. The red square is further away, and the projection lines from both eyes intersect after the plane of fixation. The α angles of these projection lines, and their intersection, serve as range finders in stereoscopic depth detection. (Modified with permission from Levin, L.A., Nilsson, S.F.E., ver Hoeve, J., et al., eds. (2011) *Adler's Physiology of the Eye*, 11th ed. St. Louis, MO: Saunders Elsevier.)

movements by both eyes. However, one should remember that many species have limited eye movement and convergence, in which case head or trunk movements supply the required cues. In barn owls, for example, eye movement is limited to only 2°, but the head can turn up to 270°, thus compensating for the immobile eyes (Harmening & Wagner, 2011).

The implication of the geometric angles depicted in Fig. 5.11 is that an object in the binocular plane of fixation will be projected on both foveas (or on the same spot of both areas centralis), resulting in *haplopia*, or a single image. However, because of the disparate viewing angles, objects outside the binocular plane of fixation will be projected on two different (but corresponding) retinal areas in both eyes (see Chapter 4, Fig. 4.36). The result is two disparate retinal images. This disparity increases with the distance of the object from the plane of fixation and allows accurate determination of this distance (Wilcox & Allison, 2009). It is important to note that stereopsis is the result of horizontal (mediolateral) disparity, which allows for perceiving the relative distance, or depth, of an object. Obviously, objects may also trigger vertical (ventrodorsal) disparity, which is important in estimating elevation and height, but this does not contribute to stereopsis in humans (Duke et al., 2006; Fig. 5.12).

Processing Retinal Disparity

Retinal disparity is resolved in the visual cortex, which has the unenviable task of reconstructing a three-dimensional image from the projection of this image on two two-dimensional retinas (Tsutsui et al., 2005). As discussed in Chapter 4, the first synapse of the RGC axons occurs at the lateral geniculate nucleus (LGN); yet, though each LGN receives input from both eyes, binocular interaction typically commences in the visual cortex. The segregation between the outputs of the two eyes is still maintained at the first cortical synapse; that is, the simple cells populating layer 4 of the striate cortex. Binocular interaction begins when these cells output to adjacent layers of the striate cortex and to extrastriate visual areas, where many of the neurons receive binocular input and act as *disparity detectors* (Bridge & Cumming, 2008; Tong et al., 2006). The disparity-sensitive neurons of the occipital cortex act as "low-level" detectors of spatial disparity and process stereopsis; additional neurons in the parietal lobe, inferotemporal cortex, and other cortical areas process "high-level" cues such as texture, shading, and motion to construct a three-dimensional image of the visual field (Tsutsui et al., 2005). Thus, it can be said that some cortical neurons act to integrate disparate binocular inputs and fuse them into one image, while others use the same disparity as a stereoptic cue to process depth perception and three-dimensional vision (Backus et al., 2001; Poggio & Talbot, 1981; Read & Cumming, 2005). Disparity-selective neurons have been described in the cortices of a number of species with laterally placed eyes, including sheep, goats, and rabbits (Clarke et al., 1976; Swadlow, 1988).

However, disparity cannot always be resolved by cortical integration and fusion of two images into haplopia. Sometimes the disparity is so significant that the fusion mechanism "breaks" and normal binocular input must be suppressed. For example, such suppression may occur due to anisometropia or unilateral aphakia that produces unequal contrast perception in both eyes. The consequence of the suppression is functional loss of visual input from the eye that cannot fixate (Harwerth & Schor, 2011). In this context, it is worth remembering that Kubai et al. (2008) demonstrated anisometropia in 6% of dogs surveyed, raising questions about the potential degradation of binocular cortical vision in some veterinary patients. Failure of the

Figure 5.12 The effect of visual perspective on vision. The same scene as viewed by a small dog with eyes located 8 inches above the ground (**A**), a tall dog with eyes 34 inches above the ground (**B**), and a person with eyes 66 inches above the ground (**C**). (Reproduced with permission from Maggs, D.J., Miller, P.E., & Ofri, R., eds. (2018) *Slatter's Fundamentals of Veterinary Ophthalmology*, 6th ed. St. Louis, MO: Elsevier.)

suppression mechanism will result in *diplopia* (i.e., double vision) or *visual rivalry* (i.e., visual confusion; Fig. 5.13).

Another form of suppression occurs when the two eyes see differing images due to a partial obstruction in the near visual field. Humans experience this when the view of a distant object is partially obstructed by the nose (Harwerth & Schor, 2011). The effect this suppression has on vision in canine, equine, bovine, and other long-nosed patients is unknown, though it probably accounts for the *anterior blind spot* that horses have below their nose (Miller & Murphy, 2017). Similarly, in birds the beak falls in the anterior blind spot. Therefore, birds that eat immobile food usually have shorter beaks, while birds that need to capture moving food require a longer beak that extends beyond the blind spot and can be seen (Lisney et al., 2013; Tyrrell & Fernández-Juricic, 2017). The former are also often characterized by lower visual acuity, a larger (monocular) visual field, and just one fovea, whereas the latter have higher acuity, a larger binocular field, and two foveas (Potier et al., 2016).

Another prerequisite for binocular vision is optic nerve decussation, which allows cortical neurons to receive input

Figure 5.13 Diplopia, or double vision, is the simultaneous perception of two images of a single object. These images may be displaced vertically, horizontally (shown in this figure), diagonally, or rotationally in relation to each other. Diplopia may be the result of failure of cortical centers responsible for suppressing disparate input, or from dysfunction of the extraocular muscles that disrupts binocular convergence. (Courtesy of Dr. Shlomi Levi.)

from corresponding areas of the retinas of both eyes. Consequently, Siamese cats and albino animals with congenital misrouting of optic nerve fibers and abnormal decussation patterns suffer from deficits in their binocular vision (Di Stefano et al., 1984). Similarly, species with no decussation at the optic chiasm, such as birds, lack the input required to generate the binocular maps in the striate and extrastriate cortex. Instead, these species rely on cerebral commissures connecting the two hemispheres to make stereopsis possible.

However, as noted earlier, various visual cues make stereopsis possible in monocular visual fields, which is why humans have depth perception even when closing one eye (Fig. 5.14). Such cues have long been thought to play a central role in providing stereopsis for animals with laterally placed eyes. Nonetheless, it has been shown that even species with lateral orbits (such as the horse) rely on binocular rather than monocular stereopsis, as the former is about 5× superior to the latter (Timney & Keil, 1999). An interesting question that remains unstudied in veterinary medicine is the effect of enucleation on stereopsis, and the extent to which one-eyed animals can learn to use such monocular visual cues (Steeves et al., 2008). The story of Patch, a one-eyed Thoroughbred who ran the 2017 Kentucky Derby (he finished 14th in a field of 20 horses), suggests that such compensation occurs.

Of course, the world is not static and therefore stereopsis is not restricted to stationary objects such as those depicted in Fig. 5.11. *Motion-in-depth* processing is necessary to catch moving prey or to avoid colliding with obstacles while running. Such processing may be facilitated by changes over time in the retinal disparity of a moving object, or by differential velocities of the retinal images (Harwerth & Schor, 2011). The cortex also processes motion-in-depth (Kim et al., 2016). This is why the segregation into magnocellular and parvocellular pathways (see Chapter 4) is also maintained in regard to stereopsis. The parvocellular pathway is associated with static stereopsis and fine disparities, and the magnocellular pathway is associated with motion stereopsis and coarse disparities (Mansilla et al., 1995). Nonetheless, motion-in-depth stereopsis is rather poor, and in humans it has only one-sixth the resolution of static stereopsis (Brooks & Stone, 2006).

Stereoacuity

Stereoacuity is the measurement of the smallest detectable stereoscopic depth. Just like visual acuity, it is measured in arc minutes or arc seconds (see the later section on "Visual Acuity"). It is largely determined by the distance of the object, as obviously smaller disparities can be detected for nearby objects than for distant objects. For example, at a distance of 25 cm some humans can detect a depth of 25 µm (Tyler & Scott, 1994). Of course, such fine discrimination is not possible for objects 100 m away. However, stereoacuity is also determined by other stimulus parameters such as color, contrast, orientation, size, duration of exposure, location (central or peripheral), and luminance (Chima et al., 2016; Harwerth et al., 2003; Simmons & Kingdom, 2002). Stereoacuity is also affected by ocular parameters such as eccentricity and by interpupillary distance, which determines the disparity of the viewing angles. And finally, it is determined by the refractive error and visual acuity, as poor acuity and optical defocusing obviously have a negative impact on stereoacuity (Nabie et al., 2017). Low visual acuity

Figure 5.14 Even though this picture is two-dimensional, various visual cues including relative size, perspective, partial obstruction, and texture gradient provide depth perception of the scene.

may explain why horses and cats have only 5% and 10%, respectively, of the stereoacuity of humans (Miller & Murphy, 2017). However, in nearly all species stereoacuity is much finer than visual acuity, and therefore stereoacuity is also called *hyperacuity* (Harwerth & Schor, 2011). In barn owls, for example, stereoacuity is about three times higher than visual acuity (Harmening & Wagner, 2011).

Stereoacuity is also affected by ocular pathologies. For example, strabismus increases disparity and reduces stereoacuity, an effect that persists even after surgical correction (Chang et al., 2017). Lack of visual input during the critical developmental period (e.g., due to congenital cataracts or corneal opacities) also degrades stereoacuity (Jeffrey et al., 2001). Nobel Prize–winning work by Hubel and Wiesel (1970) showed that in cats, the sensitive developmental period is through 3 months of age; during this time, even one week of monocular deprivation will result in *amblyopia* and cause irreversible deficits in binocular function (Timney, 1990). The implication is that congenital ocular opacities in veterinary patients should be treated as soon as possible. Indeed, humans undergoing surgery for congenital cataract after 2 years of age (which is the critical developmental period in infants; Harwerth et al., 1990) will have visual acuity < 20/200 for the rest of their lives (Tyler & Scott, 1994).

Color Vision

Prerequisites for color vision are that the retina has both photoreceptors with different spectral sensitivities that are active under the same background light conditions, as well as circuits where signals from the different photoreceptors are compared (Kelber, 2016). In most mammals, two or three types of cones with different opsins provide the first step in color vision in daylight, but some amphibians have more than one type of rod and are therefore likely to distinguish between hues at night too (Yovanovich et al., 2017). The central part of the absorption curve of a photopigment is bell shaped, and the overlap of different photopigments' absorption curves will allow perception of intermediate hues.

Photopigments are classified according to the wavelength at which the opsin molecule has its peak absorption. As noted in Chapter 4, the most common opsin molecules of cones are the L-, M-, and S-opsins, most sensitive to either long (~560 nm, greenish-yellow light, but by convention called the L- or red opsin), medium (~530 nm, green light), or short (~420 nm, blue light) wavelengths, respectively. This means that even though peak absorbance (or maximum sensitivity) occurs at a primary wavelength, the photoreceptor can also be hyperpolarized by a relatively broad range of wavelengths. However, wavelengths further away from the absorbance peak will be weaker stimuli for the photoreceptor. In species with an overlap of two or more absorbance curves, a given light stimulus will stimulate cones of different classes. The extent of stimulation of the various cone classes will determine the color perceived. For example, the dashed vertical line seen in Fig. 5.15 would describe a yellow color, because this light stimulates green and red cones equally. A light source containing longer wavelengths would stimulate the red cones more strongly and the green (and blue) cones less, and would therefore be perceived as more orange-red by a normal human subject. In summary, the number of hues that can be perceived is a function of the number of cone classes and the degree of their overlap.

Perception of color also depends on the luminosity of the light source. Colors are best perceived in bright light, when the cone system is fully active. Under optimal conditions, humans can detect wavelength (color) differences as subtle as 1–2 nm. As the source luminosity decreases, so does the perception of color. At low illumination, when only the rod system is functional, the observer can see only varying shades of gray.

Humans and Old World primates possess three opsins, thus allowing them *trichromatic vision*. The green photopigment is the most abundant in the human retina, while the blue is the scarcest. Total color blindness, which is very rare, usually refers to *rod monochromacy* (or *achromatopsia*), where the patient has no cones at all and no color vision. Cone monochromats potentially have limited color vision under lighting conditions where both the rods and their single type of cones are active (Joesch & Meister, 2016). Most color vision–deficient human subjects have *dichromatic*

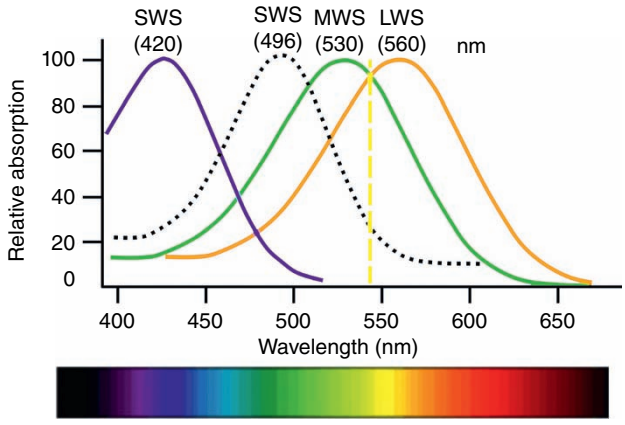

Figure 5.15 Approximate absorption spectra of human rhodopsin (rods) and cone opsins. The wavelength where each opsin has its maximal sensitivity is indicated above each curve. SWS, short-wavelength-sensitive (blue) opsin; MWS, middle-wavelength-sensitive (green) opsin; LWS, long-wavelength-sensitive (blue) opsin. The dashed, yellowish, vertical line indicates the hue detected when the green and red opsins are equally stimulated (see text for additional explanation). The colors of the visible spectrum, as perceived by a normal trichromat, are shown below the diagram. (Modified and reproduced with permission from Deeb, S.S. & Motulsky, A.G. (2013) Color vision defects. In: *Emery and Rimoin's Principles and Practice of Medical Genetics* (eds. Rimoine, D.L., Pyeritz, R.E., & Korf, B.), 6th ed., Fig. 133-1. St. Louis, MO: Elsevier.)

vision, either missing or having a mutated form of the red (*protanopia* or *protanomaly*, most frequent), green (*deuteranopia* or *deuteranomaly*), or blue opsin (*tritanopia* or *tritanomaly*, least frequent). Hence, they perceive colors but, for example, a protanope will perceive red and green objects to have very similar colors, but will readily discriminate between isoluminant blue and green (or red) objects.

Some species are monochromats. Rod monochromacy is mainly found in some fish species, whereas marine mammal species and a few terrestrial mammalian species, including the owl monkey, are cone monochromats (Hunt & Peichl, 2014; Jacobs et al., 1993b; Levenson et al., 2006).

Most mammals, including cats, dogs, horses, cattle, goats, sheep, and swine, are dichromats, just like human protanopes or deuteranopes (Jacobs, 2018; Table 5.1). Horses, for example, have cone opsins with peak absorbance in the blue and green parts of the spectrum, making their color vision comparable to human protanopes. Dogs (and cats), on the other hand, have cone opsins most sensitive to blue and greenish-yellow, making their color vision more similar to that of human deuteranopes (Siniscalchi et al., 2017; Fig. 5.16). When light stimulates the two opsins in a dichromat equally (a monochromatic light of a wavelength that coincides with the intersection of the absorption curves), the retina will not be able to distinguish this wavelength from an achromatic stimulus. This neutral point is reported at about 505 nm in the cat, and 480 nm in the dog and horse (Clark & Clark, 2016; Geisbauer et al., 2004; Neitz et al., 1989). Despite their having fewer cones than humans and being dichromats, for dogs color vision cues seem to be important during daylight conditions (Kasparson et al., 2013), and it is likely that other mammalian species also take advantage of their ability to discriminate between different wavelengths to enhance their daily lives, and particularly their sexual and feeding behavior.

Table 5.1 Cone opsin peak sensitivities in selected species.

	Cone Peak Sensitivity (nm)		
Species	**S-opsin**	**M/L-opsin**	**References**
Cat	454	561	Loop et al. (1987)
	450	550	Guenther & Zrenner (1993)
Dog[a]	429–435	555	Neitz et al. (1989); Jacobs et al. (1993a)
Horse	428	539	Carroll et al. (2001); Timney & Macuda (2001)
Pig	439	556	Neitz & Jacobs (1989)
Cow	451	555	Jacobs et al. (1998)
Sheep and goat	445	552	Jacobs et al. (1998)
Syrian gold hamster	—	508	Williams & Jacobs (2008)
Rat	358[b]	510	Jacobs et al. (2001)
Mouse	360[c]	510	Jacobs et al. (2004)
Guinea pig	429	529	Jacobs & Deegan (1994)

[a] Three species of foxes also have similar values. [b] Ultraviolet light sensitivity.

Some dichromats, including many rodents, such as the mouse, rat, gerbil, and Siberian hamster, have a specialized short-wavelength opsin that peaks in the UV range of the spectrum rather than in the blue (Peichl, 2005). Hence, they have extended the spectral range of the electromagnetic radiation that they can perceive (Gouras & Ekesten, 2004). Furthermore, some dichromats that have "regular" S- and M/L-cone pigments, such as the reindeer and dog (and most likely the cat, too), have lenses transmitting UV light, which enables them to see in the UV part of the spectrum using their regular cone pigments (Ekesten et al., 2014; Hogg et al., 2011).

Many modern-day reptilian, avian, and fish species still have all four ancestral photopigments, including an additional short-wavelength opsin with peak absorbance in the UV or violet range (355–450 nm) that humans and most domestic mammals have lost, and have thus *tetrachromatic vision* (Bowmaker, 2008).

Birds have developed additional unique mechanisms for color vision. Their *double cones* are used for fine spatial discrimination (visual acuity), while *single cones* are used for color vision. *Oil droplets* found in the cones of birds contribute to color perception by filtering out different wavelengths of incoming light and shifting the wavelength sensitivity of the photoreceptor (Toomey et al., 2015).

Although not using such a sophisticated system as a palette of oil droplets, incident light is in fact filtered in most species before reaching the photoreceptors. Transmission of UV light is profoundly reduced or blocked by the lens in several species, and the yellow macular pigment in haplorrhine primates filters out short-wavelength light. Furthermore, the yellowing of the lens in some species, such as the horse, may have a similar function, as it filters out the blue wavelengths of incoming light, although several other factors associated with aging may also contribute to age-related changes in color vision (Beirne et al., 2008).

Another extraretinal factor that determines color perception is the architecture of the LGN and visual cortex. Both areas are populated by color-sensitive cells, termed *color opponent cells*. These cells are activated in response to a given color but are inhibited by another, in a manner similar to the on–off responses characterizing the retinal bipolar and ganglion cells. For example, blue-yellow cells respond to blue light, but they are inhibited by yellow light. Other cells

Figure 5.16 A colorful dog, as seen by a normal trichromat (**A**). In (**B**), the color information from the photograph has been extracted. The photograph has been filtered to mimic how a protanope (**C**), a deuteranope (**D**), a tritanope (**E**), and a cone monochromat (**F**) would perceive the same scene. The protanope and deuteranope can distinguish between short and long wavelengths, whereas the tritanope can subdivide the middle to long wavelengths into different hues.

may be triggered by red light and inhibited by green. *Double opponent cells* will respond in an antagonistic manner to both spatial and spectral stimuli. Thus, some cells may be "red-ON-center, green-OFF-surround," or "blue-ON-center, yellow-OFF-surround." Obviously, the number of possible double opponent cell types is potentially very large, depending on the number of cone classes (Conway, 2009; Shapley & Hawken, 2011).

Visual Acuity

Visual Acuity in the Animal Kingdom

Visual acuity is the minimal detection power of the eye, or the minimal angle that can be resolved by the eye. There are a number of ways to express visual acuity, but the best-known method is based on the Snellen chart (Fig. 5.17). This is determined by the size of letters that a subject can read at a distance of 20 ft, or 6 m. Obviously, determination of Snellen acuity requires verbal cooperation by the test subject and therefore is not applicable in veterinary medicine. In animals, visual acuity can be determined using behavioral discrimination tests (Hanggi & Ingersoll, 2009), by electrophysiologic recordings to determine the smallest pattern that elicits an ERG or cortical response (Ofri et al., 1993), or by pursuit (i.e., optokinetic) eye responses to determine the smallest stimulus that elicits a tracking eye movement (Ryan et al., 2016). Acuity is also often determined by theoretical calculations based on cone or RGC density (Coimbra et al., 2013, 2015, 2017; Pettigrew et al., 2010), though the results of these calculations may differ from those of behavioral tests (Clark & Clark, 2013; Mitkus et al., 2014).

There are two ways to express the results of such tests and calculations. Minutes of arc (MAR) describes the angle (in minutes) subtended by the narrowest bar that can be discriminated, keeping in mind that 60 MAR make up a 1° visual angle. Alternatively, cycles per degree (cpd) is the number of cycles (a dark and a white bar) that can be seen within a field subtended by a 1° visual angle. These values are inversely related (Fig. 5.18). A subject with high visual acuity can resolve very narrow bars, resulting in a low MAR value; therefore, in 1° this subject will be able to see many bars, resulting in a high cpd value. Published charts can be used to convert between MAR, cpd, and Snellen acuity units (Miller & Murphy, 1995). A human adult typically has a Snellen acuity of 20/20 or 6/6, depending on whether the nonmetric or metric system is used, respectively. These fraction values represent the size of the object that should be seen at a distance of 20 ft, or 6 m, by a person with normal vision. At this distance, the dimensions of this "gold standard" target are 1 MAR or 30 cpd. In the decimal system, a visual acuity of 20/20 or 6/6 corresponds to 1.0, whereas 20/80 equals 0.25.

Snellen acuity values for selected species are provided in Table 5.2. Fractional values < 1 represent visual acuity that is lower than that of a gold standard human. The value of 20/50 reported for the dog, for example, roughly means that a dog and a human who stand 20 and 50 ft away from a visual target, respectively, would both have the same resolution for that target. The general implication is that the resolution of the human is 2.5 times better than that of the dog, as both will be resolving and detecting the same target, even though the human is 2.5 times further away from it. In a metric system, these results are reported as 6/15, with the dog and the human standing 6 and 15 m away, respectively, from the target. Figure 5.19 shows the optical quality of the images formed by a dog's eye with 20/50 (or 6/15) vision.

As can be seen in Table 5.2 and Fig. 5.17, due to the presence of a fovea and macula, humans and nonhuman primates have the highest visual acuity among mammalian species. However, it can also be appreciated that raptors have even

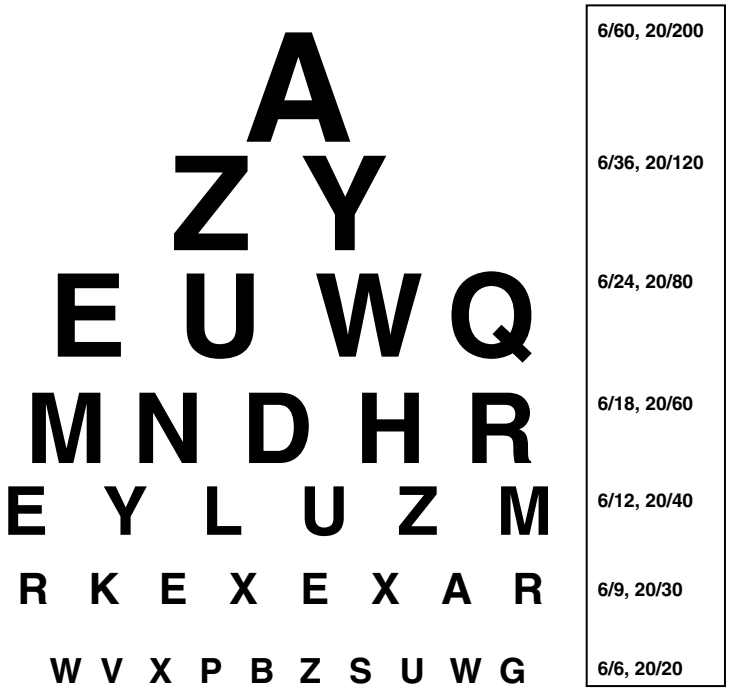

Figure 5.17 Snellen acuity chart. A normal human with 6/6 or 20/20 vision should be able to read the bottom line at a distance of 6 m or 20 ft. Humans and animals with lower acuity, as indicated by the figures on the right, can only detect larger letters at the same distance. Based on the values in Table 5.2, horses, for example, should be able to see the second line from the bottom, while rabbits can only detect the top letter.

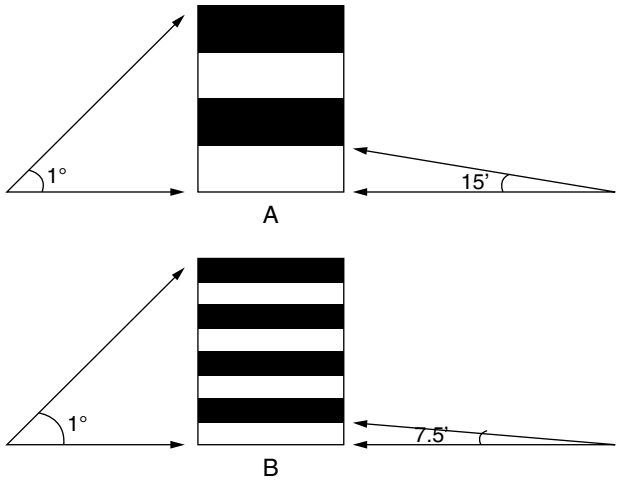

Figure 5.18 Visual acuity expressed in cycles per degree (cpd) and minutes of arc (MAR). The acuity of the observer on the left is denoted in cpd, which expresses the number of cycles (each cycle consisting of a dark and a light bar) seen within a 1° visual field. The observer on the right has an identical visual acuity, but it is denoted in MAR, which expresses the angle (in minutes) subtended by a single bar. **A.** The acuity of the observer on the left is 2 cpd (two pairs of light and dark bars). Because there are four bars in a degree, each is 15' wide; therefore, the acuity of the observer on the right is 15 MAR. **B.** The observer on the left can discriminate four pairs of dark and light bars in a 1° field and, therefore, has an acuity of 4 cpd. The width of each bar is now 7.5', however, and the acuity of the observer on the right is therefore 7.5 MAR.

higher visual resolution, with Snellen fractions > 1. The 20/5 resolution of the eagle, for example, implies that an eagle can be 4x further from a visual target than a human (20 and 5 ft, respectively), yet both species will equally resolve this target. On the other hand, it can be seen that contrary to common perception, the domestic cat has very low visual acuity, perhaps as low as 50% of the canine visual acuity. The popular belief that cats have high visual acuity may stem from the superior scotopic sensitivity of this species; however, this high scotopic sensitivity of the cat is enabled by the presence of a tapetum lucidum (which scatters light) and a rod-rich retina, two factors that have detrimental effects on visual acuity.

When looking at Table 5.2, one should keep in mind that the legal definition of blindness in humans is 20/200 (or 6/60). This means that by human standards rabbits, cows, rats, and mice are legally blind. Furthermore, the menace response requires a visual acuity of only 20/20,000, far below the threshold of legal blindness, thus casting doubts on the usefulness of this commonly used method to assess vision (Miller, 2018).

Factors Affecting Visual Acuity

Numerous factors affect visual acuity. These include both visual system- and stimulus-dependent factors. Visual system factors are further subdivided into optical, retinal, and cortical features.

Optics of the Visual System

Refractive Error

Many of the optical factors affecting visual acuity were discussed in Chapter 4. Foremost among these is the refractive error of the eye. The values presented in Table 5.2 are for an emmetropic eye, when the image is focused on the retina. Obviously, ametropia results in a blurred image on the retina, and leads to degradation of acuity. In the dog, 1.5 D (diopters) of myopia reduces visual acuity from 20/50 to 20/92, and 3 D myopia reduces it further, to 20/120 (Fig. 5.20). Such defocusing had a significant negative impact on retrieval times and performance scores of trained Labrador Retrievers (Ofri et al., 2012).

A large survey of over 1,400 dogs found that the average canine refractive error is −0.05 D, and that two-thirds of the study population was emmetropic, defined as a refractive error of <0.5 D in either direction (Kubai et al., 2008). Therefore, two-thirds of canine patients have the visual acuity values presented in Table 5.2. Yet the same study found that 8% of all dogs were hypermetropic, with a refractive error of up to +3.25 D, and three breeds (Australian Shepherd, Alaskan Malamute, and Bouvier des Flandres) had a mean refractive error that was hypermetropic. Conversely, 25% of all surveyed dogs were myopic, with a refractive error of up to −6.25 D, and four breeds (Rottweiler, Collie, Miniature Schnauzer, and Toy Poodle) had a mean refractive error that was myopic. Other researchers also confirmed a high prevalence of myopia in Toy Poodles (63.9%), English Springer Spaniels (36.4%), and Collies (35.7%; Williams et al., 2011). Thus, it would seem that a high proportion of dogs suffer from the adverse behavioral effects described for canine myopia (Ofri et al., 2012; see Fig. 5.20). Furthermore, it should be noted that if an intraocular lens is not implanted in a canine patient undergoing cataract surgery, the aphakic eye will have 14.5 D of hyperopia (Davidson et al., 1993), resulting in visual acuity of 20/800, which is well below the 20/200 legal definition of blindness in humans.

Other species may also suffer from a high prevalence of ametropia. Only 48%–68% of horses are emmetropic in both eyes, with hyperopia and myopia reported in equal proportions in the ametropic horses (Bracun et al., 2014; Grinninger et al., 2010), with errors of up to ±3 D (Farrall & Handscombe, 1990; Grinninger et al., 2010). In Icelandic horses, a mutation causing silver coat color and multiple ocular anomalies is associated with myopia (Johansson et al., 2017). Though there are no studies documenting the behavioral consequences of equine ametropia, the condition has been associated with nervousness in affected horses (Miller & Murphy, 2017).

In a survey of 98 cats, only 30% were emmetropic; 54% and 16% of the study population were myopic and hyperopic, respectively (Konrade et al., 2012). However, the results may have been skewed by the fact that only 58% of the study

Table 5.2 Visual acuity in select species.*

Species	Snellen Resolution**	Spatial Frequency (Cycles/Degree)**	Method***	References
Eagle (*Aquila audax*)	20/4	140	Behavioral and anatomic	Reymond (1985)
Falcon (*Falco berigora*)	20/8	73	Behavioral and anatomic	Reymond (1987)
Macaque monkey	20/16	38	Behavioral	Merigan & Katz (1990)
Human	20/20	30		Ravikumar et al. (2011)
Horse	20/26	23	Behavioral	Timney & Keil (1992)
	20/36	16.5	Anatomic	Harman et al. (1999)
King penguin			Anatomic	Coimbra et al. (2012)
Under water	20/30	20.4		
In air	20/40	15.3		
Alpaca	20/45	13.4	Anatomic	Wang et al. (2015)
Sheep	20/51–20/43	11.7–14	Behavioral	Sugnaseelan et al. (2013)
	20/86–20/60	7–10	Anatomic	Hughes (1977)
Camel	20/60	10	Anatomic	Harman et al. (2001)
Dog	20/140–20/52	4.3–11.6	Electrophysiologic	Odom et al. (1983); Ofri et al. (1993); Murphy et al. (1997)
	20/110–20/31	5.5–19.5	Behavioral	Lind et al. (2017)
Cat	20/190	3.2	Behavioral	Jarvis & Wathes (2007)
	20/90	6.5	Electrophysiologic	Berkley & Watkins (1971)
	20/33	18	Anatomic	Steinberg et al. (1973); Clark & Clark (2013)
Barn owl			Behavioral	Orlowski et al. (2012)
	20/190	3.2 (Mesopic)		
	20/500	1.2 (Scotopic)		
Rabbit	20/200	3	Electrophysiologic	Pak (1984)
Cow	20/460–20/230	1.3–2.6	Behavioral	Rehkämper & Görlach (1998); Rehkämper et al. (2000)
Rat			Behavioral	Prusky et al. (2002)
Pigmented	20/600–20/400	1–1.5		
Albino	20/1200	0.5		
Mouse	20/1000	0.58	Behavioral	Lehmann et al. (2012)
	20/1500	0.39	Optokinetic	Lehmann et al. (2012)

* This table mostly contains data for species commonly seen by veterinary ophthalmologists in clinical and research settings. Avian species have been included to demonstrate their high acuity (eagle, falcon) or the effects of aquatic vision (penguin) and light conditions (owl). The scientific literature reports visual acuity values for numerous other species, such as giraffes (Coimbra et al., 2013), elephants (Pettigrew et al., 2010), rhinoceros (Pettigrew & Manger, 2008), and marsupials (Dooley et al., 2012), that are beyond the scope of this book.
** Most articles report visual acuity in cycles/degree. These values have been converted to Snellen units by the author (R.O.) as most readers are more familiar with this latter scale. Values for Snellen acuity < 20/200 have been rounded.
*** Anatomic methods of assessment include counting the density or cones and/or retinal ganglion cells; electrophysiologic methods are based on recordings of the pattern electroretinogram or pattern visual evoked potentials.

population were adults. Indeed, in dogs (Kubai et al., 2008), horses (Grinninger et al., 2010), and cats (Konrade et al., 2012) as well as in wildlife species (Ofri et al., 2001, 2004), it has been shown that refractive error changes with age. Therefore, ametropia should be considered a differential diagnosis for age-related deterioration in the visual performance of animals with an unremarkable ophthalmic examination, and refraction should be added to the list of diagnostic tests performed in such patients.

Accommodation

Accommodation is another optical factor that may affect visual acuity, as it brings the images of nearby objects into focus on the retina. The process is described in detail in

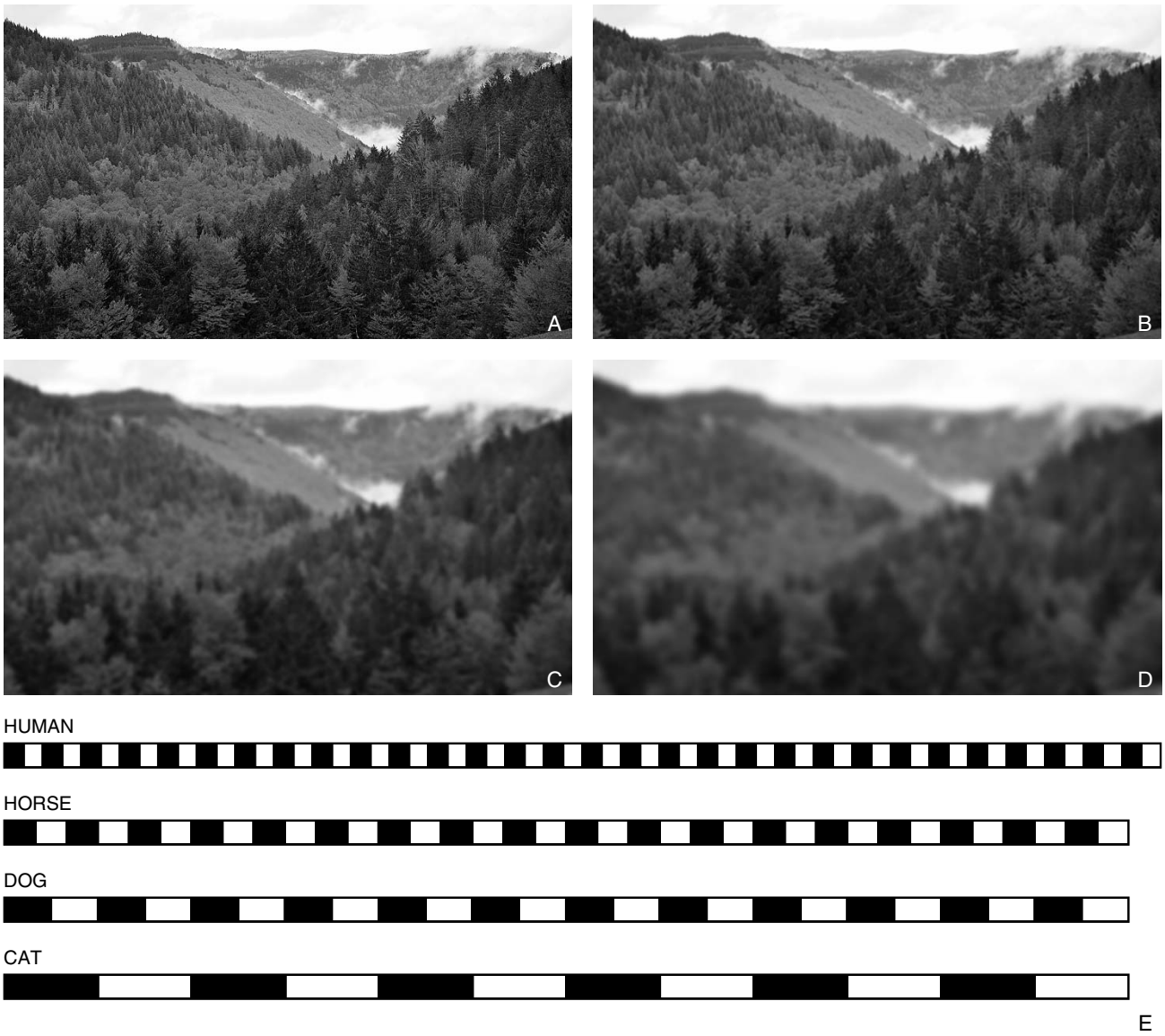

Figure 5.19 Comparative visual resolution. The same landscape is seen by (**A**) a human, (**B**) a horse, (**C**) a dog, and (**D**) a cat. The landscape is presented in black and white to avoid the confounding factor of differences in color vision between species. Differences in visual field size have also been ignored. **E**. Visual acuity depicted as cycles per degree, which means how many lines one can distinguish as being separate in 1 degree of the visual field. A cycle is a pair of a black and a white bar. Humans see 30 cycles per degree, horses 18, dogs 12, and cats 6. Therefore, acuity in cats is 0.2 times that of humans, 0.33 times that of horses, and 0.5 times that of dogs. (Panels A–D courtesy of Dr. Shlomi Levi.)

Chapter 4 (see Fig. 4.7). Briefly, during accommodation parasympathetic stimulation leads to contraction of the ciliary body muscle, allowing the eye to focus on nearby objects. In primates and birds this contraction leads to an increase in the curvature of the lens, while in carnivores it results in anterior movement of the lens in the eye. In disaccommodation, sympathetic stimulation leads to relaxation of the ciliary body muscle, allowing the eye to view distant objects. In primates and birds the relaxation results in a flatter lens with reduced refractive power, while in carnivores it results in posterior movement of the lens in the eye (Ofri, 2018b).

Children have a powerful accommodating capability, perhaps as high as 15 D, which means that they can focus on objects as close as 6–7 cm; unfortunately, humans gradually lose this capacity with age, in a process called *presbyopia*, and by 50–55 years of age they are left with virtually no accommodative power (Glasser, 2011). As detailed in Chapter 4, in diving birds and otters the accommodative power can be as high as 60 D, and accommodative powers of 10–20 D have been demonstrated in other avian species, as well as some mammals such as raccoons and mongooses. However, most mammalian species that are commonly seen

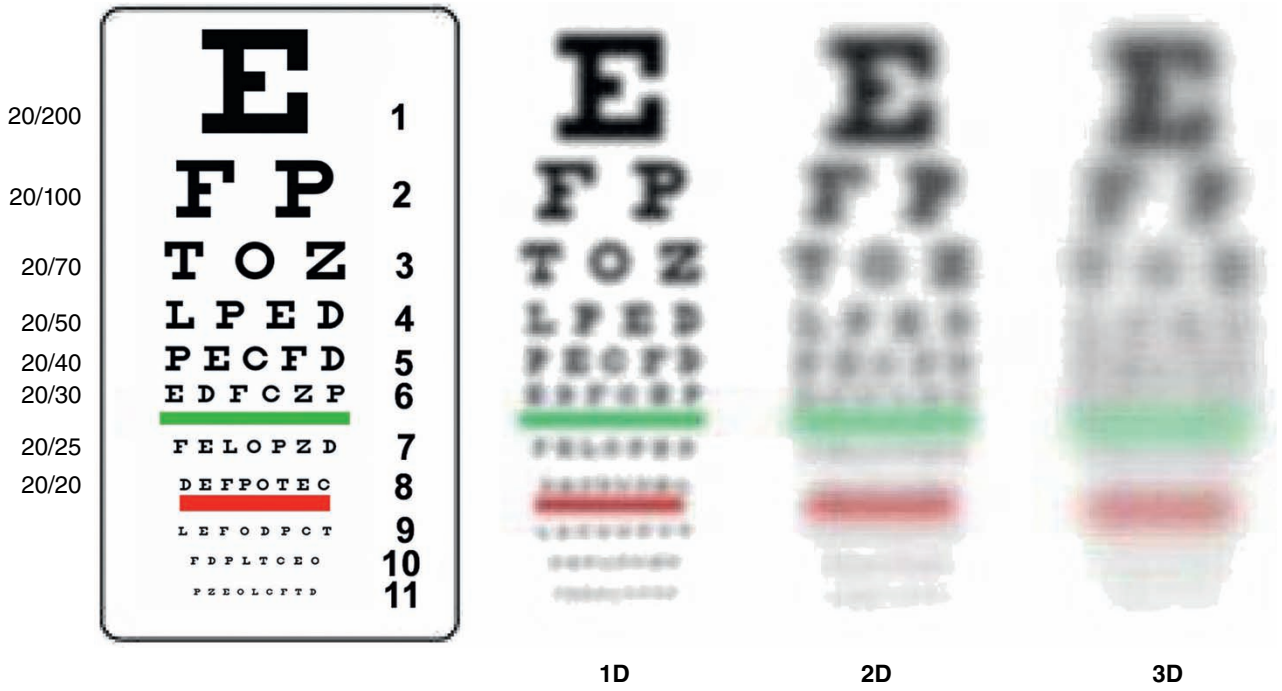

Figure 5.20 Simulated blurred vision due to myopia. 1–3 D (diopter) defocus can result in blurry vision simulated based on human subject experience. Similar blurry vision can be expected for dogs that have −1 to −3 D myopia. (Reproduced with permission from Hernandez, J., Moore, C., Si, X., et al. (2016) Aging dogs manifest myopia as measured by autorefractor. *Plos One*, **11**, e0148436.)

by veterinary ophthalmologists have very low, or no, accommodative power. Dogs and cats have accommodative power of just 1–3 D (Hughes, 1977) and 2–4 D (Ott, 2006), respectively. The implications of these numbers are that though dogs and cats can focus on distant objects (by disaccommodating), their depth of field for nearby objects is just 100–33 cm (dogs) and 50–25 cm (cats). Closer objects are very blurred and are usually perceived using the sense of smell, rather than vision. Horses can accommodate only ±1 D in either direction (Sivak & Allen, 1975), while rodents (Artal et al., 1998) and ruminants (Piggins & Phillips, 1996) generally lack accommodative capabilities. Thus, it would seem that in most veterinary patients, accommodation does not make a significant contribution to visual acuity.

The Pupil

Unlike accommodation, the pupil has a great impact on the visual acuity of many veterinary patients. As described in Chapter 4, the peripheral cornea and lens introduce significant spherical (and chromatic) aberrations into the eye. Therefore, mydriasis results in reduced visual acuity as peripheral rays reach the retina (Fig. 5.21). In humans, dilating the pupil with 1% tropicamide will decrease acuity to about 20/30 (Chew et al., 2007; Montgomery & MacEwan, 1989). While similar studies are unavailable in animals, one can assume that due to the large pupil size in some veterinary

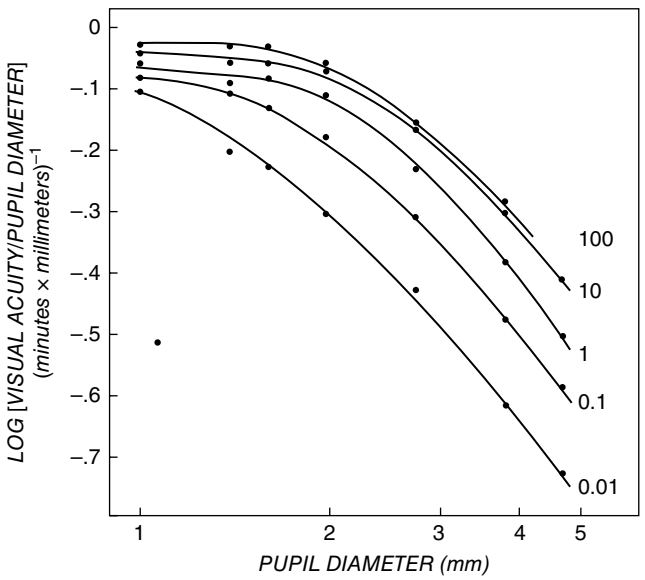

Figure 5.21 The effect of pupil diameter on visual acuity. Luminance values of the reference field are indicated at the right of the curves. Note how acuity decreases with decreasing luminance (compare top curve to bottom curve) and how it also decreases with increasing pupil diameter due to increased spherical aberrations. (Reproduced with permission from Leibowitz, H. (1952) The effect of pupil size on visual acuity for photometrically equated test fields at various levels of luminance. *Journal of the Optical Society of America*, **42**, 416–422.)

patients, the effect of mydriasis on visual acuity could be even more detrimental. The area of a mydriatic human and feline pupil is 50 mm^2 (Gilmartin et al., 1995) and 113 mm^2 (Hammond & Mouat, 1985), respectively, allowing significant spherical aberrations and visual degradation in cats.

Conversely, miosis decreases spherical aberrations and improves visual acuity. For example, treatment with carbachol causes significant improvement in the visual acuity of human patients (Abdelkader, 2015). This is why miosis is a component in the *near reflex* triad, which also includes ocular convergence and lens accommodation, as these three mechanisms allow humans to view nearby objects of interest with high resolution (Kardon, 2011). Another beneficial effect of miosis is that it increases the depth of field of the eye; that is, the distance between the nearest and farthest objects on which the eye can focus. With a 4 mm pupil, the depth of field of the human eye is 0.78–1.40 m; constricting the pupil to a 1 mm pupil will increase it to 0.56–5.0 m (Wang & Ciuffreda, 2006). This is one instance where the eye may be compared to a camera, as miosis may be compared to the pinhole effect attained when the lens aperture is decreased, thereby increasing the photographer's depth of field, or f-stop (Harmening & Wagner, 2011).

However, there is a limit to the beneficial effects of miosis. As the pupil constricts, the diffraction of light, or its bending and scattering as it passes through the pupillary aperture, becomes more noticeable (Fig. 5.22). This has a detrimental effect on visual acuity, similar to that of the spherical aberrations associated with mydriasis. In humans, the ideal pupil size, which balances diffraction (enabled by miosis) and aberrations (enabled by mydriasis), is 3–5 mm (Smith & Atchison, 1997). Furthermore, miosis reduces the amount of light reaching the retina. Due to the stenopaeic (slit-shaped) feline pupil, miosis in cats decreases retinal illumination by 3 log units (Hammond & Mouat, 1985), compared to the 1.5 log units decrease in miotic humans (Kardon, 2011). Depending on the prevailing conditions, this decrease may result in suboptimal retinal illumination, thus affecting retinal factors that determine visual acuity, as discussed in the next section.

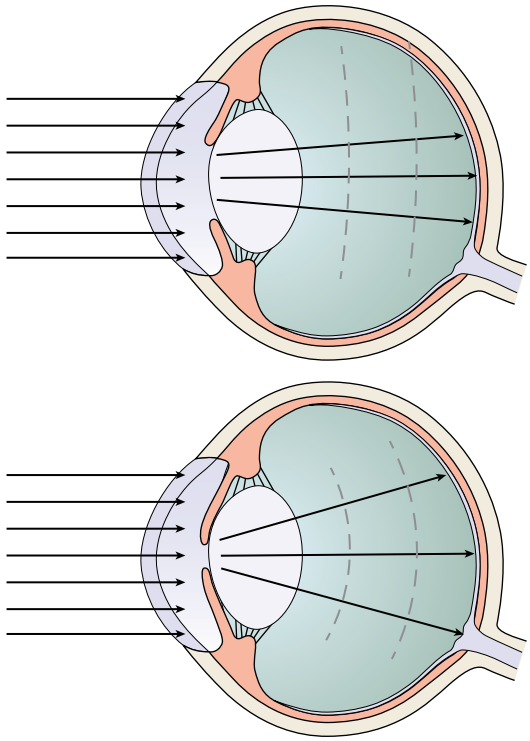

Figure 5.22 The effect of pupil size on light diffraction. Note that with the smaller pupil (bottom) light passing through the pupil is more scattered. Though miosis can improve visual resolution as it decreases spherical aberrations (see Fig. 5.21), beyond a certain threshold it can have a detrimental effect on resolution due to increased light diffraction.

Globe Size

Another optical factor influencing visual acuity is the size of the eye. A comparative study of 91 mammalian species shows that axial length and visual acuity are significantly and positively correlated (Veilleux & Kirk, 2014). This is because an increase in axial length produces a longer posterior focal distance (between the lens and the retina; Fig. 5.23). Consequently, as axial length increases a larger image is formed on the retina, an image that can be sampled by more photoreceptors and RGCs, as discussed next. Interestingly, large eyes and high visual acuity are also correlated with large semicircular canals in the inner ear; it is suggested that high acuity requires precise gaze stabilization, which is enabled by a vestibular system possessing canals with large radii and the resulting high vestibular sensitivity (Kemp & Kirk, 2014).

Retinal Factors Affecting Visual Acuity

Visual acuity is also determined, largely, by anatomic and functional differences between the rod and cone pathways (see Chapter 4). In the retina, visual acuity decreases as a function of increased eccentricity because of the decreased number of cones and RGCs in the peripheral retina (see Chapter 4, Table 4.6). This decline in the peripheral RGC population has been described in the dog (Gonzalez-Soriano et al., 1995), horse (Evans & McGreevy, 2007; Guo & Sugita, 2000), and cat (Stein & Berson, 1995; Stein et al., 1996). In the latter, the ratio of RGCs in the central and peripheral retina is 20:1 (Miller, 2018). Additionally, the peripheral retina is populated mostly by α- or Y-type ganglion cells, which are characterized by large dendritic trees (Li & Da Costa 2002; Stein & Berson, 1995; Stein et al., 1996), further contributing to the low acuity of this region. Thus, it is not surprising that dogs and horses have low visual resolution in the peripheral retina, where most information is processed by the converging rod pathway (Harman et al., 1999; Ofri et al., 1993).

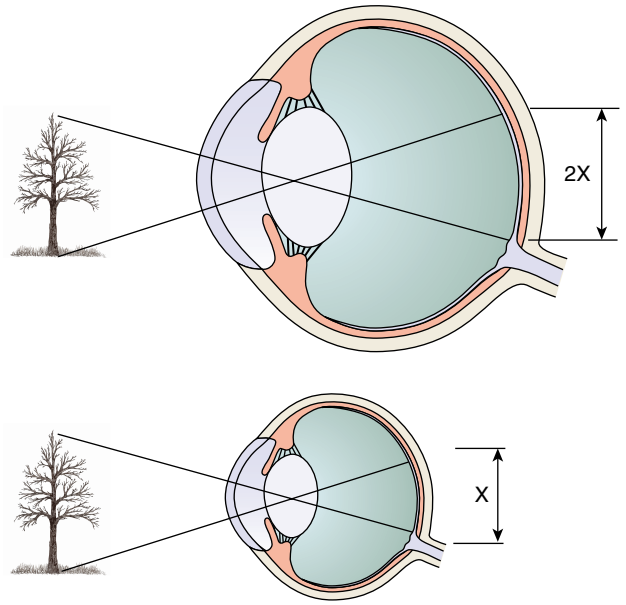

Figure 5.23 The effect of globe size on the image projected on the retina. The larger globe (top) has a longer posterior focal distance (between the lens and the retina), resulting in a larger retinal image. This results in higher visual resolution for this eye, as the image can be sampled and processed by more photoreceptors and ganglion cells than the bottom image.

Conversely, the architecture of the central retina has evolved to provide high visual acuity. It is characterized by a high density of cones and RGCs, by a low photoreceptor-to-RGC ratio, and by RGCs with small dendritic trees. In primates and some avian species, the evolution of this arrangement has culminated in the formation of an anatomic pit called the *fovea*. The central fovea contains no rods, and cones are tightly packed in a regular arrangement for maximal density (Levi, 2011). Each of these cones outputs, through a single midget bipolar cell, to a single midget RGC (Provis et al., 2013). This pathway ensures maximal resolution, as there is no convergence or summation of the cone output, and each cell projects its signal directly to the brain, providing pinpoint localization of the visual stimulus. The high density of photoreceptors, particularly the cones, and their associated bipolar and RGCs in the central retina, compared with peripheral retina, explains why the central canine retina is thicker than the retinal periphery (Ofri & Ekesten, 2020).

Though a fovea-like bouquet of cones has recently been described in dogs (Beltran et al., 2014), in other (nonprimate) mammals central vision is subserved by an *area centralis*, rather than a fovea. The principles of area centralis architecture are similar to those of the fovea: it is the retinal region containing the highest concentration of cones and associated RGCs, with small dendritic trees and minimal convergence. However, in the area centralis these principles are not as refined as they are in the fovea. Thus, even though it contains the highest concentration of cones, the area centralis is not rod free, and the presence of rods results in a lower cone density than in the fovea. Furthermore, the area centralis does not have the midget circuitry that characterizes the fovea, resulting, once again, in cellular packaging that is not as dense as in the fovea. In the cat, for example, midget RGCs are replaced by β-RGCs; though their dendritic tree is smaller than that of other feline RGCs, it is larger than the dendritic trees of the primate foveal midget RGCs (Stein et al., 1996). Just as importantly, even in the area centralis the output of several feline cones converges on a single β-RGC (Cohen & Sterling, 1992). The result is summation of cone output in the cat's area centralis, compared to the "private line" that conveys the output of each primate foveal cone to the brain.

Obviously, differences in cone-to-rod ratios and variations in RGC types are not limited to regional retinal variations in eccentricity. Such differences are also found between species, depending on their environment (diurnal vs. nocturnal), life style (herbivorous vs. carnivorous), and other evolutionary factors (see Chapter 4, Table 4.6). For example, barn owls are unique in that they have a fovea that is rod dominant, to facilitate scotopic hunting by this nocturnal raptor (Harmening & Wagner, 2011). On the other hand, other avian species, including diurnal raptors and passerines, have evolved bifoveate retinas, containing both a shallow temporal and a deeper nasal/central fovea (Coimbra et al., 2015; Inzunza & Bravo, 1993; Fig. 5.24), contributing to their high visual acuity (see Table 5.2). In diurnal raptors, the nasal/central fovea (which has a higher acuity) is used to identify distant objects during flight, while the temporal one is used to fixate on nearby prey (González-Martín-Moro et al., 2017).

In general, after controlling for eye size and phylogeny, visual acuity in mammals is associated with diurnality, even in closely related species (Veilleux & Kirk, 2014). For example, megabat species that roost outdoors and have a carnivorous diet possess a pronounced visual streak (analogous to the area centralis) of high RGC density, whereas cave-dwelling megabat species with a herbivorous diet have a less pronounced streak with lower RGC concentration. Consequently, the visual resolution of the former is twice as high as that of the latter (Coimbra et al., 2017).

Another feature of retinal anatomy that affects visual acuity is the presence of a tapetum lucidum, though its effect is negative (Fig. 5.25). Light striking the tapetum is reflected back onto the retina at various angles, resulting in light scatter and diminished acuity (Ofri, 2018a; Schwab et al., 2002). Since in most species the tapetum underlies the area centralis, this scatter occurs in a region where it would have the most detrimental effect on the animal's visual acuity. This may be why elephants have a heterogenous structure of a tapetum lucidum, with its least dense and least reflective area located behind the horizontal visual streak (Pettigrew

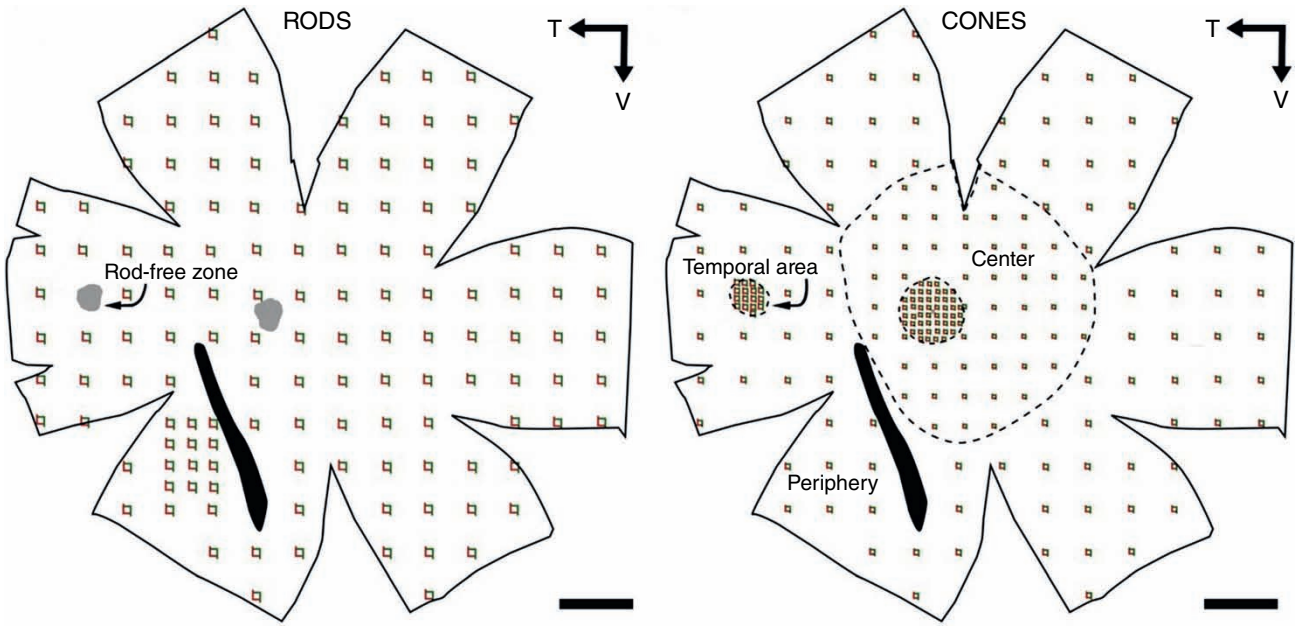

Figure 5.24 Stereologic sampling scheme used to map the topographic distribution of rods and cones in the retinal wholemounts of passerines. **A**. Rod density. The gray shaded areas mark the location of the rod-free zones in this representative retina. **B**. Cone density. The two rod-free areas in panel A are actually a central and a temporal fovea. The thick, dark diagonal line represents the pecten. T, temporal; V, ventral. Scale bars = 1 mm. (Modified with permission from Coimbra, J.P., Collin, S.P., & Hart, N.S. (2015) Variations in retinal photoreceptor topography and the organization of the rod-free zone reflect behavioral diversity in Australian passerines. *Journal of Comparative Neurology*, **523**, 1073–1094.)

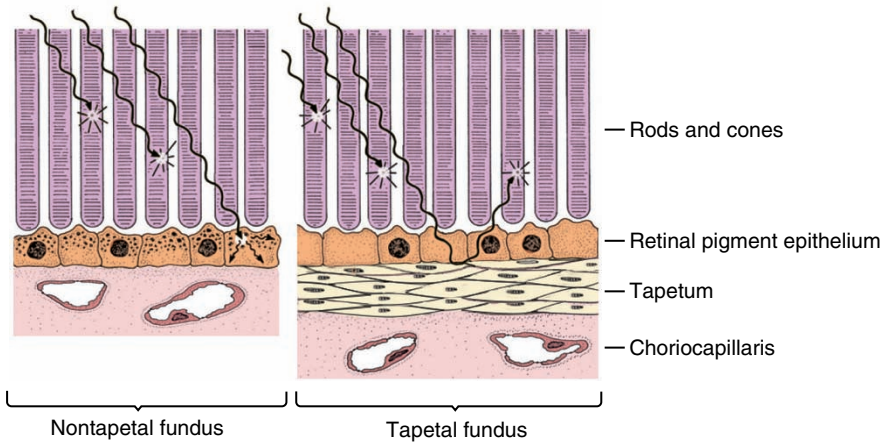

Figure 5.25 Light scatter by the tapetum. The left side of this figure represents a nontapetal section of the fundus, the right half a tapetal region. On both sides of the figure, three incoming photons are shown. Two are absorbed by the photoreceptors and contribute to visual sensation, and the third passes through the retina without being absorbed. In the nontapetal fundus (left), this photon's energy dissipates in the pigment epithelium and does not contribute to visual sensation. By comparison, in the tapetal fundus (right), this third photon is reflected back onto the photoreceptors, where it is absorbed and contributes to vision, thereby enhancing scotopic sensitivity. However, note that in this region the photon is eventually absorbed by a photoreceptor that is not in its original trajectory, and therefore the resulting image is blurred. Consequently, tapetalized eyes have low visual acuity but great scotopic sensitivity. (Reproduced with permission from Maggs, D.J., Miller, P.E., & Ofri, R., eds. (2018) *Slatter's Fundamentals of Veterinary Ophthalmology*, 6th ed. St. Louis, MO: Elsevier.)

et al., 2010). Such an anatomic arrangement would minimize the negative effect that the tapetum has on the elephant's visual acuity.

Of course, features that are a disadvantage in daytime, when the photopic cone system is active, become advantageous in dim light, when the scotopic rod system takes over (see "Scotopic and Photopic Vision"). Cats have low visual resolution because of a large pupil (and the consequent spherical aberrations) and a reflective tapetum, combined with an afoveate retina characterized by a low concentration

of cones, converging cone output, and RGCs with large dendritic trees. Because of these anatomic constraints, the low acuity values of cats can never be improved by visual aids such as glasses or LASIK surgery, contrary to suggestions by the public. After all, the feline visual resolution is poor even though the cat eye is close to emmetropia (Konrade et al., 2012). However, what cats lack in cone function they gain in rod function. The same factors – a large pupil, a reflective tapetum, and photoreceptor pathways that converge on RGCs with large dendritic trees – afford cats superior scotopic vision. Furthermore, the maximal rod concentration in cats and humans is 460,000/mm^2 and 160,000/mm^2, respectively (see Chapter 4, Table 4.6). Therefore, though their view of the world may not be as colored or as detailed as ours, cats continue to see at night, while humans are left groping in the dark (see Fig. 5.5)!

The Visual Cortex and Visual Acuity

Just like the central retina, the architecture of the visual cortex devoted to the central visual field has also evolved to enable high-resolution vision. However, there is a fundamental difference in the anatomic features that have evolved to process high-resolution vision in the retina and cortex. In the retina, each degree of the visual field is projected onto a similar-size retinal area, regardless of whether it is peripheral or central. The increased visual resolution of the central retina is obtained by increasing the density of the cones and their associated RGCs, as described in Chapter 4. In the cortex, on the other hand, the density of neurons serving the peripheral and central visual fields is identical. The increased detail with which visual input from the fovea or area centralis is analyzed by the cortex is not a result of thicker neuronal layers and increased cell density, as in the retina. Rather, this increased cortical visual discrimination is a result of the increased cortical area devoted to representing the fovea or area centralis. In other words, because of the importance of the visual input from the area centralis or fovea, large cortical areas are devoted to processing the signals originating from these regions.

The larger area devoted to processing information from the central retina results in magnification of its cortical representation. *Magnification factor* is a term coined by Daniel and Whitteridge (1961) to quantify the disproportionate amount of cortical area devoted to processing the high-resolution vision of the central visual field. In the cat, for example, the surface area of the visual cortex is 380 mm^2, 50% of which is devoted to the central 20° of the visual field (Tusa et al., 1978). Consequently, half the visual cortex is devoted to the central 20° of the feline retina, and half of it is devoted to the rest of the visual field (Fig. 5.26). In humans, the disproportionate cortical representation of the central visual field is even more striking. The fovea occupies only 0.01% of

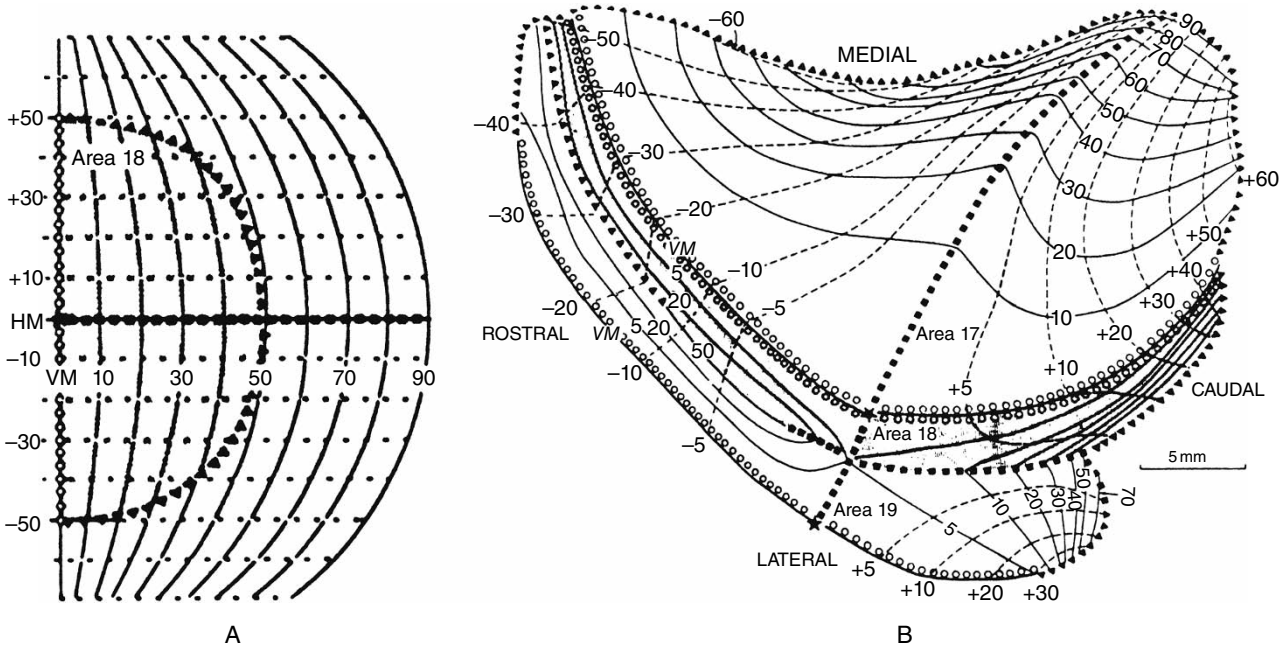

Figure 5.26 The projection of the visual field on the cat cortex. **A.** Perimeter chart showing the extent of the visual hemifield. Azimuths and elevations are illustrated by solid and dashed lines, respectively. **B.** Visual hemifield projection in areas 17 (V I), 18 (V II), and 19 of the unfolded cat cortex. Note the disproportionate large amount of cortical area devoted to processing the central 5° of the visual field, at the expense of the small areas devoted to processing input from the peripheral visual field. (Reproduced with permission from Tusa, R.J., Rosenquist, A.C., & Palmer, L.A. (1979) Retinotopic organization of areas 18 and 19 in the cat. *Journal of Comparative Neurology*, **185**, 657–678.)

the human retina, yet its representation takes up 8% of the visual cortex (Azzopardi & Cowey, 1993). Furthermore, in primates the density of neurons in this cortical area is 2.5× greater than in nonprimates, reflecting the high acuity of the fovea that it serves (Srinivasan et al., 2015). The increased cortical "machinery" devoted to processing the output of the area centralis and fovea is another reason for the significant difference between central and peripheral acuity, and contributes a critical element to the actual perception of high-resolution vision.

Stimulus-Dependent Factors Affecting Visual Acuity

The two most important stimulus parameters affecting visual acuity are its luminance and contrast (Fig. 5.27). Visual acuity is high in photopic conditions, when the cone system is active, and decreases in scotopic conditions, when the rod system is active. In dogs, for example, behavioral studies have shown that it decreases from an average of 20/70 in the former to 20/225 in the latter. Even in the barn owl, a nocturnal raptor highly adapted to night vision, acuity decreases by 75% when transitioning from photopic to scotopic conditions (Orlowski et al., 2012). This is because of the functional and anatomic differences between the cone and rod systems (high density of cones in the fovea or area centralis, the synaptic connection of one cone to one midget bipolar cell and one midget RGC, versus the convergence and low photoreceptor and RGC density of the rod pathway).

Likewise, a high degree of stimulus contrast is required for high acuity. On a sunny day, humans can easily see dark power lines at a distance, as they sharply contrast with the blue sky, but the same lines would not be easily seen if they were blue. As with luminance, acuity decreases with log contrast (Legge et al., 1987). In harbor seals, for example, behavioral testing demonstrated a linear decrease of acuity with increased water turbidity, potentially affecting the animals' foraging ability (Weiffen et al., 2006). However, as noted earlier, contrast and luminance sensitivities are not only dictated by retinal anatomy and physiology; the visual cortex also contributes to these functions, as it has functional contrast- and luminance-modulating units (Dai & Wang, 2012).

The texture of the stimulus (De Weerd et al., 1992; Wilkinson, 1995) – that is, the density and size of its constitutive elements – and its shape are also important in determining visual perception (Fig. 5.28). For example, horses are better than chimpanzees at perceiving shapes with diagonal lines, but are worse at perceiving shapes with right angles (Tomonaga et al., 2015). Similarly, young kittens react

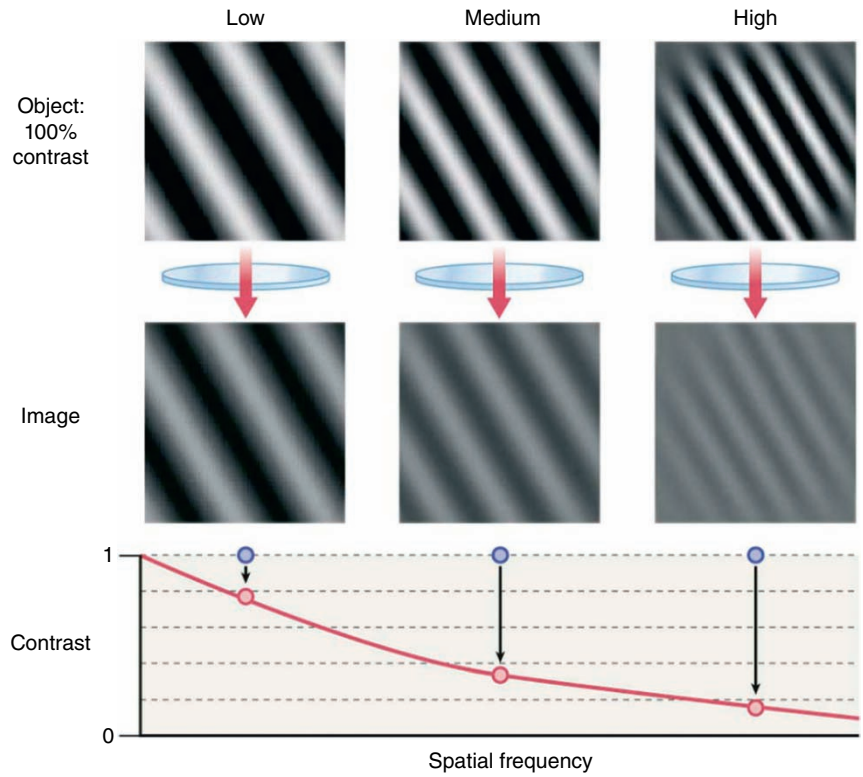

Figure 5.27 Visual acuity increases with contrast. With high contrast (top row), high visual resolution is possible (top right image). With lower contrast (middle row), the object on the right can barely be seen, and only low visual resolution is possible (middle row, left image). The linear relationship is shown in the bottom graph. (Reproduced with permission from Levin, L.A., Nilsson, S.F.E., ver Hoeve, J., et al., eds. (2011) *Adler's Physiology of the Eye*, 11th ed. St. Louis, MO: Saunders Elsevier.)

Figure 5.28 Visual texture allows the viewer to differentiate an object from its surroundings. In this image, a barn owl can be distinguished from the surrounding vegetation based on differences in the texture of the feathers, which are more homogenous and smooth than the tree trunk on the left.

strongly to horizontal lines, but not to dots (Wilkinson, 1995). Additional stimulus parameters influencing visual acuity include stimulus duration (acuity declines for brief stimuli because of insufficient retinal exposure) and stimulus movement (movement faster than the tracking response will also result in insufficient retinal exposure).

Other factors also become important when conducting behavioral tests to determine visual discrimination in animals. For example, in horses, visual discrimination is enhanced when the target is at ground level and poorer when it is at a height of 70 cm, or about 2 ft (Hall et al., 2003). In addition, the examiner should recall that most nonprimates have minimal accommodative ability, and therefore test objects should not be placed too close to the animal (Clark & Clark, 2013). For example, since horses can accommodate by only 1 D, they will fail a behavioral test if the target is closer than 1 m.

References

Abdelkader, A. (2015) Improved presbyopic vision with miotics. *Eye & Contact Lens*, **41**, 323–327.

Apfelbach, R. & Wester, U. (1977) The quantitative effect of visual and tactile stimuli on the prey-catching behaviour of ferrets (*Putorius furo* L.). *Behavioural Processes*, **2**, 187–200.

Artal, P., Herreros de Tejada, P., Muñoz Tedó, C., et al. (1998) Retinal image quality in the rodent eye. *Visual Neuroscience*, **15**, 597–605.

Azzopardi, P. & Cowey, A. (1993) Preferential representation of the fovea in the primary visual cortex. *Nature*, **361**, 719–721.

Backus, B.T., Fleet, D.J., Parker, A.J., et al. (2001) Human cortical activity correlates with stereoscopic depth perception. *Journal of Neurophysiology*, **86**, 2054–2068.

Badial, P.R., Cisneros-Àlvarez, L.E., Brandão, C.V., et al. (2015) Ocular dimensions, corneal thickness, and corneal curvature in Quarter Horses with hereditary equine regional dermal asthenia. *Veterinary Ophthalmology*, **18**, 385–392.

Beirne, R.O., McIlreavy, L., & Zlatkova, M.B. (2008) The effect of age-related lens yellowing on Farnsworth-Munsell 100 hue error score. *Ophthalmic and Physiological Optics*, **28**, 448–456.

Beltran, W.A., Cideciyan, A.V., Guziewicz, K.E., et al. (2014) Canine retina has a primate fovea-like bouquet of cone photoreceptors which is affected by inherited macular degenerations. *PLoS One*, **9**, e90390.

Ben-Shlomo, G., Plummer, C., Barrie, K., et al. (2012) Characterization of the normal dark adaptation curve of the horse. *Veterinary Ophthalmology*, **15**, 42–45.

Berkley, M.A. & Watkins, D.W. (1971) Visual acuity of the cat estimated from evoked cerebral potentials. *Nature: New Biology*, **234**, 91–92.